



6p1723

IN THE UNITED STATES PATENT AND TRADEMARK OFFICE

January 22, 2001

Invention: A NEW PROCESS AND APPARATUS FOR RAPID AND
HOMOGENEOUS MIXING OF FLUIDS IN CONTINUOUS
OPERATIONS
Application No.: 09/283,198
Filed: April 1, 1999
Country: United States
Inventor: Fielder et al.
Examiner: David L. Sorkin
Art Unit: 1723
Due Date: February 3, 2001

The Commissioner of Patents and Trademarks
WASHINGTON, D.C.
U.S.A. 20231

TECHNOLOGY CENTER 1100
JAN 29 2001
JAN 29 2001

Dear Dr. D. L. Sorkin and W. L. Walker,

Applicant respectfully acknowledges receipt of office DETAILED ACTION dated December 5, 2000.

Applicant hereby revokes all previous appointments of agents and representatives of Eugene J. A. Gierczak (Registration No. 31,690), c/o KEYSER MASON BALL, Barristers & Solicitors, 201 City Centre Drive, Suite 701, Mississauga, Ontario Canada L5B 2T4 as my attorney in respect of the above-referenced patent. (The reason is that I have been unemployed for many years and can not offer them to work for me even if I have sold my car this month. I have two very young daughters (one 4 and the other 2 years old, very expensive). Therefore, from now on I will apply the patent myself.)

Applicant hereby also revokes Farkas & Manelli, whose full post office address is 2000 M Street, N.W., Suite 700, Washington, D.C., 20036-3307, U. S.A., as my representative. No notices or process in proceedings affecting the patent application may be served upon them.

Enclosed are also the copies of the references. I have marked the most important relevant topics in each paper respectively to save examiner's time. May I ask Professor I.



Wyganski to explain to you the difference between the two inventions to save your time, so that I may not pay the possible cost associated with the government filing fee?

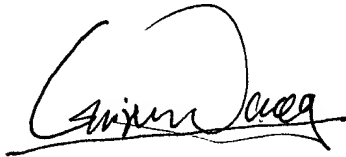
Enclosed is also a response to the DETAILED ACTION dated December 5, 2000.

Due to variety of reasons I received your detailed action very late, i.e. on Jan. 15, 2001. I am very sorry for the very late response.

If you have any question, please let me know. Please be noticed that my present address is changed as shown in the end of the letter.

Thank you very much for your help!

Your faithfully,

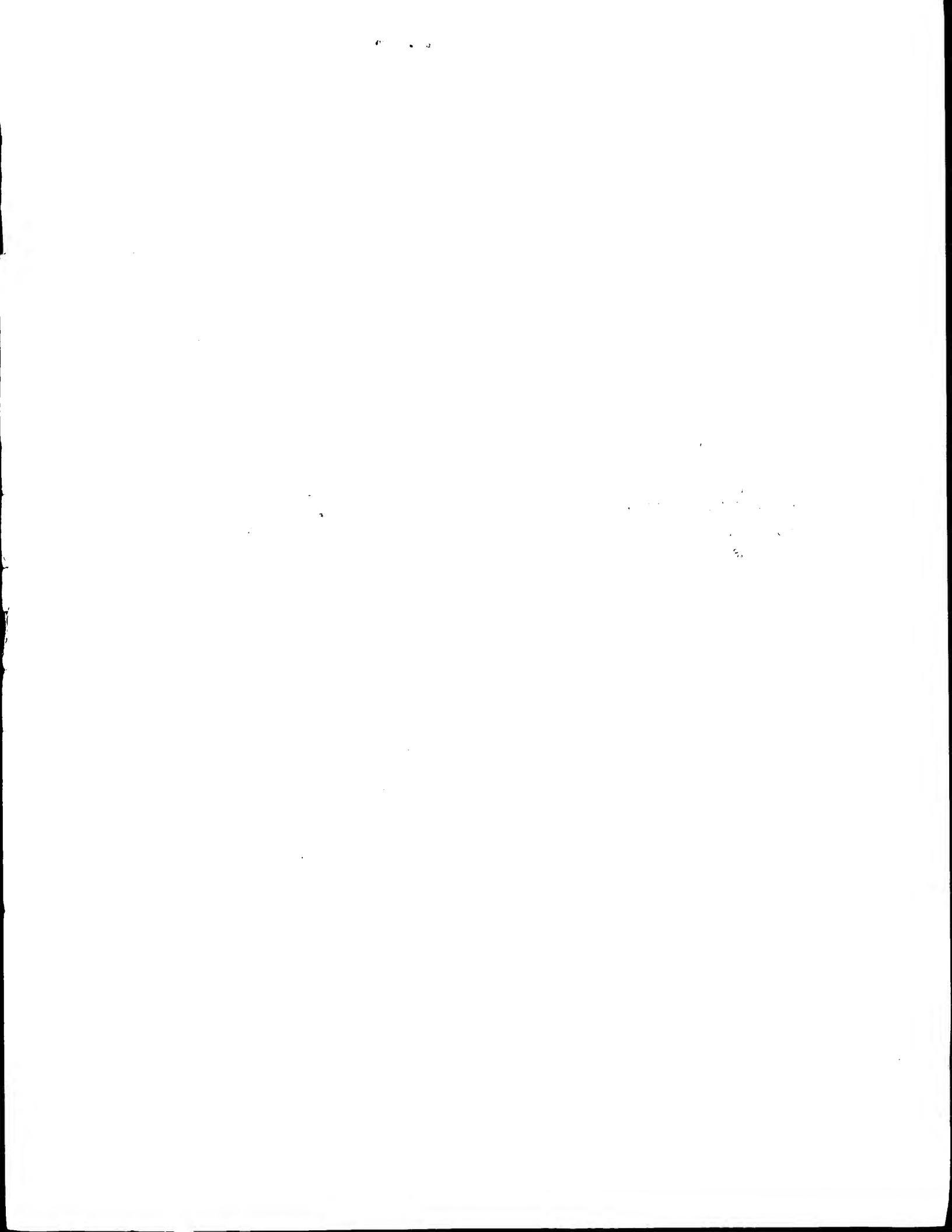
A handwritten signature in black ink, appearing to read 'Guiren Wang', with a large, stylized initial 'G' and 'W'.

Guiren Wang c/o Esther Feder
455 Grant Ave., Apt. 7
Palo Alto, CA 94306-1817
USA

Tel: (650) 322-5371
(650) 723-1295

Fax: (208) 279-0304

Email: mrgrwang@yahoo.com





Response to the DETAILED ACTION

Here is the response to the DETAILED ACTION dated December 5, 2000.

1 The required legible copies of publications are enclosed. The main relevant topics from papers of H. E. Fiedler & H. H. Fernholtz (1990), C. -M. Ho & P. Huerre (1984) and H. E. Fiedler & P. Mensing (1985), and the dissertation from G.R. Wang (1999), are marked by yellow color. The whole manuscript from G.R. Wang (2000) is dedicated to show that a new receptivity for mixing control is discovered, which is related to the new invention.

2 I regret that the copies of the references mentioned in the last application were not enclosed. These references might help you to understand that no new issue has actually been added. The word "a narrow frequency band" in the last application's claim is used to help the examiner to understand better the difference between the new invention and the one of Wygnanski & Fiedler. It is the same meaning as the one used in the claim of the original patent application (page 4, line 17-21), where the word "by a frequency" and "under this suitable frequency" are used.

The word "the interaction between corner vortices and primary vortices" are also the same meaning with the word "The flow becomes three dimensional due to the secondary vortices, two kinds of which are produced....." in the original claim (page 4, line 25-29). There are several different kinds of secondary vortices (you can simply call all of them ~~secondary-vortices-or-streamwise-vortices~~). ~~Corner-vortices-belong-to-the-secondary-vortices~~. The primary vortices (or spanwise structure or spanwise vortices) always exist when there are corner vortices in the shear flows. These primary vortices can approximately be regarded as two-dimensional flow. The control in the invention enhances the corner vortices creation and their interaction with the primary of vortices. This results in the corresponding three-dimensional flow, and thus enhances the fluids mixing.

The uses of these new words have actually reduced the scope of the new invention. However, to make the difference between the two inventions more distinguished for the examiner, these words in the claim of the last application are used.

3 I am deeply sorry for the mistake. The symbol "ooooin" should be replaced by "flow in". Should I send the whole claim again to you?



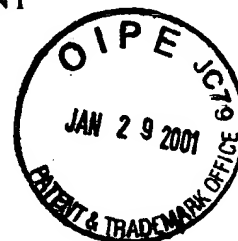
wing

ON MANAGEMENT AND CONTROL OF TURBULENT SHEAR FLOWS

H. E. FIEDLER and H.-H. FERNHOLZ

Hermann-Föttinger-Institut, Technische Universität Berlin, F.R.G.

(Received 24 August 1990)



Abstract—Concepts of turbulent flow control have become of growing importance during the last few years, following increased interest in the detailed structural scenario of turbulence—in particular our improved understanding of coherent structures on the one hand (the prerequisite), and a need for improvement of technological processes on the other (the goal). These considerations have mainly been followed by engineers and physicists concerned with problems in aerodynamics. It is our aim to draw the attention of a wider group of engineers to turbulent flow control in order to speed up the transfer of knowledge from aerodynamics to applications in other fields of engineering.

In this paper an attempt is made to compile a major body of the available knowledge on flow control in separated and wall bounded turbulent flows. After a brief introduction of the basics of control theory (Section 2) and of the major flow structures and their stability characteristics (Section 3) free and wall bounded turbulent shear flows are discussed (Sections 4 and 5). This discussion summarizes the main relationships between structure and flow behaviour and shows possibilities of influencing properties of these flows such as increasing mixing or avoiding separation.

CONTENTS

1. INTRODUCTION	306
1.1. General remarks	306
1.2. Technological and scientific interests	307
2. THE PRINCIPLE OF THE MATTER	307
2.1. Basics of control theory	307
2.2. Control, management and optimized design	309
2.3. Goals and gains	310
3. WHAT MEANS 'DO WE COMMAND?'—STRUCTURES AND THEIR 'SOFT SPOTS'	311
3.1. Major structures and what they stand for	311
3.2. Structures and stability	312
4. FREE TURBULENT SHEAR FLOWS	313
4.1. Principles and methods of control	316
4.2. Jets	319
4.2.1. Major configurations	321
4.2.2. Periodic forcing—the established method of active control	321
4.2.3. Passive control	325
4.3. Wakes	331
4.3.1. Configurations	331
4.3.2. Stability, structures and control	331
4.3.3. Jets and wakes—their different control behaviour	333
4.4. Mixing layers	333
4.4.1. Configurations	334
4.4.2. Structures and stability	334
4.4.3. Active control	335
4.4.4. Possibilities of passive control	336
4.5. Mixed configurations of free- and wall-bounded flows	341
5. WALL-BOUNDED TURBULENT SHEAR FLOWS	341
5.1. Introductory remarks	341
5.2. Manipulation of turbulence by boundary conditions	342
5.2.1. Introductory remarks	342
5.2.2. Separation control by manipulation of the pressure distribution	342
5.2.3. Manipulation of the turbulence structure due to control mechanisms originating at the wall	344
5.2.3.1. Suction and blowing	344
5.2.3.2. Control of the near-wall and the large eddy structures	345
5.2.3.3. Riblets	346
5.2.3.4. Compliant walls	346
5.2.3.5. Curved walls	347
5.3. Manipulation by free-stream turbulence or by upstream flow unsteadiness	347
5.3.1. Introductory remarks	347

TECHNOLOGY CENTER 1708

5.3.2. Free-stream turbulence	348
5.3.2.1. Free-stream turbulence interacting with turbulent boundary layers	348
5.3.2.2. Free-stream turbulence interacting with separated boundary layers	350
5.3.3. Perforated obstacles	351
5.3.3.1. Perforated obstacles with a free wake	351
5.3.3.2. Perforated obstacles with a splitter plate	352
5.3.4. Upstream flow unsteadiness or wake	353
5.3.4.1. Turbulence manipulators inside the boundary layer	353
5.3.4.2. Turbulence manipulators outside the boundary layer	355
5.3.5. Longitudinal vortices imbedded in a boundary layer	355
5.3.6. Leading-edge vortices	356
5.4. Manipulation and control of separation and reattachment	357
5.4.1. Introductory remarks	357
5.4.2. Manipulation of separation bubbles	359
5.4.2.1. Separation bubbles near the leading edge of aerofoils	359
5.4.2.2. Separation bubbles near the front edge of blunt bodies	359
5.4.3. Control of leading-edge separation	361
5.4.3.1. Vibrating ribbon or oscillating flap	361
5.4.3.2. Acoustic excitation	363
5.4.3.3. Suction or blowing	366
5.4.4. Manipulation of base-drag flow	366
5.4.4.1. Open base-drag regions	366
5.4.4.2. Base-drag regions with reattachment	368
6. GLOBAL FLOW MANAGEMENT	372
7. SUMMARIZING REMARKS	372
ACKNOWLEDGEMENTS	373
REFERENCES	373

1. INTRODUCTION

"it is my intention first to cite experience, then to demonstrate through reasoning why experience must operate in a given way"

Leonardo da Vinci

1.1. GENERAL REMARKS

Animals are the result of millennia of optimization in natural 'design'. What makes them so perfectly adapted to their specific need is often a highly sophisticated control scheme, as we find it of equally high standard in birds as well as in fish—where the 'compliant wall'—skin of the dolphin is a typical if popular example (Nachtigall, 1974).

In fluid flows we distinguish between laminar and turbulent motion. Practically all technical and natural flows are turbulent, when exceeding a critical value of the characterizing Reynolds number $Re = cl/v$, where c denotes a characteristic velocity, l stands for a characteristic dimension and v is the kinematic viscosity of the fluid. Natural flows range over many decades of scale in their Reynolds number. The turbulent flows of primary interest in this paper are flows with mean velocity gradients: the 'turbulent shear flows'.

In the past decade the concept of turbulence had its 100th anniversary (Reynolds, 1883; Boussinesq, 1879): Osborne Reynolds provided the scientific basis for what he himself did not yet call 'turbulence' and gave us a powerful tool to handle it: the treatment of the averaged quantities. Reynolds-averaging has since then dominated the way turbulence is looked at and as a negative consequence many features—most notably the coherent structures—have simply not been recognized as individual entities—a weakness of all statistical approaches.

Present day knowledge about the origin, dynamics and topology of coherent structures—albeit still incomplete—provides a basis for their efficient and specific management and control. Earlier attempts on controlling certain flows—observed and reported already in the last century—remained incompletely understood and therefore failed to provide a 'recipe' as to a general and applicable procedure. Only when Prandtl had presented his boundary layer theory at the beginning of this century was it possible to control separation and to explain the underlying mechanism.

1.2. TECHNOLOGICAL AND SCIENTIFIC INTERESTS

To explore the possibilities of flow control has for a long time inspired and challenged the engineer as much as the scientist, and many classical examples may be quoted. The topic has lately received increased attention both because of technological demands—e.g. the control of separation, the improvement of combustion processes or suppression of aerodynamic noise—and also as the outcome and side benefit of the study of coherent structures, the stability of which appears to provide the most efficient handle for turbulence control.

There is a large amount of literature dealing with specific control methods and experiments, among which there are a few surveys of a broader scope (e.g. Husain *et al.*, 1987; Fiedler *et al.*, 1988; Hussain and Husain, 1988; Zhou Ming De, 1988; Kibens, 1989). A general and comprehensive compilation and survey seems to be, however, so far missing.

2. THE PRINCIPLE OF THE MATTER

2.1. BASICS OF CONTROL THEORY

For a clear semantic distinction 'management and control' seems to be a more adequate title for this survey instead of just 'control', which is generally understood to be related to a dynamic process. Thus a splitter plate in the wake of a cylinder (to suppress vortex shedding) or a geometric constraint of a mixing layer flow may not be properly described by the term 'control' but rather by 'management'.

Whatever name is chosen, however, there is no doubt as to the major issue: how to gain a lot from as little (input) as possible.

According to the systematics of control theory we distinguish between two control principles (see e.g. DiStefano *et al.*, 1976):

- (a) *open loop or 'feedback' control*, a method of control, which necessitates external adjustments based on measurements of any kind, and
- (b) *closed loop control*, where the continuous adjustment is provided by an 'internal' control loop.

In a closed loop or feedback control system the difference between the actual value of the controlled output and the desired value of that output is used to change the value of the input to the system in such a manner as to maintain the output as close as possible to a desired value. A special situation of (b) is when this control loop is 'unstable', i.e. when any deviation is amplified (a situation which in common understanding is known as a feedback). A feedback situation, which may be external or internal, is characterized by threshold- and saturation-levels and is—in general—a non-linear phenomenon. In more specific terms we call a situation where feedback signal and input signal are of opposite phase a negative (or degenerative) feedback. If both signals are of equal phase the feedback is positive (or regenerative).

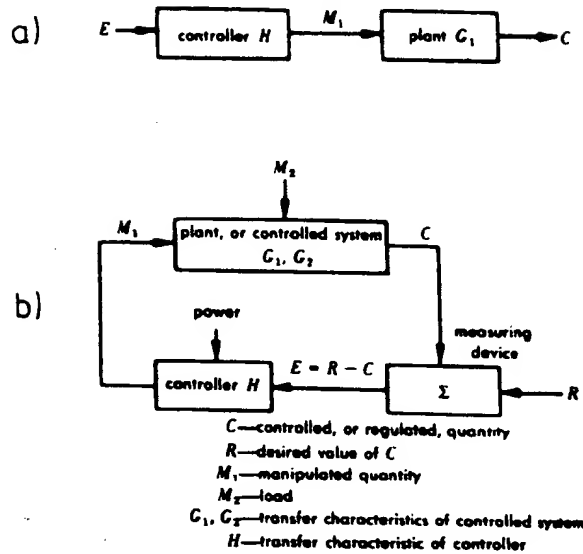
According to the terminology of control theory the system consists of the plant (the controlled system), a measuring or monitoring system and a controller. Figure 1 shows block diagrams of the different control systems.

Let us consider a plane mixing layer (the PLANT), which—as is well known (see Section 5)—is easily controlled by periodic perturbations of appropriate frequency and amplitude.

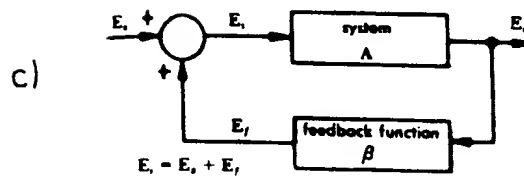
Open loop control is then applied by forcing the flow (via loudspeaker or other appropriate means = the CONTROLLER) with an independently adjusted external periodic signal from, say, a frequency generator.

Closed loop control has various possibilities:

- (1) the frequency generator is controlled by some characteristic amplitude (e.g. the RMS-output) as obtained from the periodic fluctuations, measured at some station in the flow, or,



$$E = \frac{R - G_2 M_2}{1 + H G_1}$$



$$\frac{E_o}{E_s} = \frac{A}{1 - A\beta}$$

FIG. 1. Principles of control loops. (a) Open loop; (b) closed loop with characteristic equation for linear (feedback) system; (c) general feedback loop with gain relation.

(2) the (filtered) output signal is directly used to drive (via amplifier) the forcing unit (the CONTROLLER). Adjustment is possible via the amplifier, by a time shift of the feedback signal, or by spatial shift of the location where the control signal is obtained. This is the case of an external direct feedback loop.

Internal feedback can be provided by pressure waves or mechanical vibrations of the system. An obvious model relation then is—as has been proposed by various authors (e.g. Tam, 1974; Laufer and Monkewitz, 1980; Rockwell, 1982; see also Raghu, 1987):

$$\frac{L}{U_p} + \frac{L}{a} = \frac{n}{f}$$

where L is a 'feedback-characteristic' length, U_p = phase velocity of the feedback wave in the flow (the 'structure'), f = feedback frequency, a = velocity of sound (by which the wave is transported upstream) and $n = 1, 2, 3, \dots$ representing the state of oscillation.

This can be expressed as a feedback Strouhal number

$$S_F = n/(U_0/U_p + Ma)$$

with Ma = Mach number and U_0 = velocity of the basic flow.

Of particular importance in turbulent flow control is the dispersion relation: If we consider a wave-train or -packet, the propagation- or phase velocity of the individual components is not necessarily the same. In a general way the wave frequency

$$\omega = kc_r = \Omega^r(k)$$

is related to the wave number k by the dispersion relation

$$\omega + i\gamma = \Omega(k) = \Omega^r + i\Omega^i$$

with $\gamma = \Omega^i(k) = kc_i$ as the temporal growth rate of the wave train.

Energy can be exchanged between those components as long as their phase velocities are equal. If this is the case we observe the phenomenon of 'resonance' between harmonic components. In most flows the phase velocities are a function of frequency, becoming constant and equal only at the higher frequency end (Cohen and Wygnanski, 1987).

2.2. CONTROL, MANAGEMENT AND OPTIMIZED DESIGN

Turbulent flow control describes a mechanism by which specific turbulent or overall characteristics of a given flow are modified to change certain characteristics of technological interest.

If this is done by a geometrical modification of some sort (stationary boundary condition), then we shall consider only those cases of essentially unaltered basic geometry. Otherwise we have a case of design optimization, which is not the subject of this study ('form follows function'—this famous and often quoted truism by Sullivan being the key issue for this problem as much as for any other technical applications issue). This may often be a difficult and certainly subtle distinction and in many cases far from clear cut. In addition, one might have to consider facility effects, when e.g. by a certain (minor) modification of the flow's geometry the test-section should become a resonator or a vibration transmitter (feedback).

There are then two different kinds of control according to the goal to be achieved: the 'overall' control, with the general purpose of managing—reducing (e.g. Windtunnel-) or enhancing (e.g. mixing-) turbulence with its many facets and problems, and—the 'tailored' control aiming at specifically influencing certain characteristic of flow structures and their development, which obviously requires detailed knowledge of the latter.

Specific control may again be sub-divided, according to the physical principle involved, into an 'external' (= open loop-) and an 'adaptive' (= closed loop-) control.

Often a distinction between 'active-' and 'passive-' control is made in the pertinent literature, where the basis of distinction is the source of the energy needed to activate the control mechanism. A controlling method is considered 'passive' when by means of special circumstances, e.g. boundary conditions, feedback loops or mechanical devices, the controlling energy is drawn directly from the flow to be controlled. Controlling the flow with external energy then constitutes the 'active' case.

Passive methods are often of technical simplicity and practicability, whereas active control serves most conveniently (being itself easily controllable) a systematic and scientific study of turbulent phenomena.

The major question to be asked at this point is: What and how do we control? Figure 2 outlines essential paths and ways.

From this picture it is inferred that control of sub-structures might possibly provide a way of controlling the primary structures and thereby the overall flow behaviour. While this may be so in principle, its practical realization appears to be much more difficult if not impossible. This is illustrated by an example: The large structures in a plane mixing layer—displaying, when periodically excited, perfectly rolled up two-dimensional vortices—are

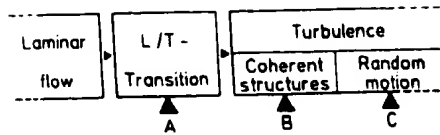


FIG. 2. Simplified scheme of turbulent flow development and ways of control. (A) Delay or initiation of transition (pressure gradient, surface roughness, trip wire, adaptive methods etc.); (B/C) Simplified general picture. Energy goes essentially from mean flow to coherent structures and from there to random small scale motion. Control goes the other way: Coherent structures control mean flow. CS are controlled either via random (small scale) motion or directly.

composed of thin (stretched) sheared layers. One might then think of exciting those wrapped layers with a frequency of, say, an order of magnitude above the basic excitation frequency, thereby enhancing the diffusion and the dissipation of the primary structures. Since, however, these smaller layers are curved and their convection velocity is a function of their position, it is not possible by simple means to impress on to them a constant frequency with constant wavelength, a necessary condition for receptivity. In addition these rolled up layers are stabilized by their curvature (higher velocity at larger radii of curvature). Thus no receptivity of the plane mixing layer of this kind is observed when forced at appropriately higher frequencies.

2.3. GOALS AND GAINS

The purpose of control is two-fold:

- (1) it is a means to systematically analyze a given flow and its structures (i.e. to provide a better understanding), and
- (2) to achieve—and this is the major goal—improvement of technical or technological processes or characteristics.

The latter are readily summed up as:

- increasing lift, reducing drag and avoiding separation—as in many engineering, particularly aeronautical or naval problems,
- increasing or reducing turbulent mixing—of paramount importance for all kinds of environmental aerodynamics, for heat and mass transfer (chemical engineering), and foremost for combustion in burners for heating, in aircraft jet engines and other internal combustion engines,
- influencing pressure fluctuations, which is of importance in architectural and environmental aerodynamics, particularly with respect to reducing aerodynamic noise (aircraft-jet- and fan-noise)
- in flow control devices, of necessity in fluidic applications.

Since control of turbulent flow is often synonymous with control of turbulent structures, the question as to its efficiency may best be answered by looking at the major structural constituents and their specific role in the flow—e.g. large scale for noise production and small scale for mixing. Thus the problem reduces to the question of possible minimum and maximum states (saturation values of those structures), their specific stability (receptivity) and their interaction. What can be accomplished depends on the role of the structure under control in the physical process. Thus mixing, being mainly influenced by small scale turbulence, may be increased by, say, 100% or more by destruction or deformation of the large coherent structures. At the same time effects of comparable magnitude are observed in noise reduction, which is a direct consequence of the large scales and their amalgamations. Major limitations are provided by the fact that most control mechanisms affect the flow only in a limited spatial range, which is particularly true for evolving configurations like e.g. the turbulent jet, which develops from a wall boundary layer first into a mixing layer and then into its final state.

3. WHAT MEANS DO WE COMMAND?—STRUCTURES AND THEIR SOFT SPOTS

3.1. MAJOR STRUCTURES AND WHAT THEY STAND FOR

Up to the time when coherent structures were finally recognized the major problem in turbulence research was the definition of turbulence itself, which did not seem to permit a simple and unique answer. It was then superseded by a new (pseudo-) problem concerning the essence of coherent structures. The very core of the problem is the impossibility of defining uniquely and stringently a varying, metamorphic object—such as an evolving structure. Therefore a vague description as “the transient yet repetitive manifestation (in concentrated vorticity) of an instability mode” will have to do. To make matters worse there is usually more than just one structure which deserves the ‘title’ coherent. Turbulent flows may instead be characterized by coherent scenarios.

It has been accepted that coherent structures are responsible for many characteristics of turbulent flow. They seem to be—on the other hand—easily influenced by outside conditions, thus lending themselves willingly to flow control. Indeed this is one of the most fascinating and complex aspects of the coherence-phenomenon. In view of the above ‘problem’ we first have to ask ourselves, however, as to which of the recognizable coherent structures (or structural manifestations) are the important ones concerning a specific control aspect. Having decided this, the next question follows automatically: How can one influence, i.e. control it?

Coherent structures and in particular their amalgamations have been recognized as principal sources of flow noise (large scale), in affecting chemical engineering processes, in mixing and combustion (small scale) and in influencing drag and lift of airborne vehicles. Their effects have been a central object of research and increasing interest in recent years. However, it must be established that the structures to be influenced have a sufficient bearing on the dynamics of the flow considered.

What fraction E_C/E_T of the total turbulent energy E_T is then to be attributed to the major (coherent) structures? An exact assessment of this quantity is practically impossible and estimates will have to suffice. Table 1 presents typical values.

On the basis of these data (for wall bounded flow we may assume fractions of the order of 10%) the idea of controlling turbulent flows via influencing their coherent structures seems promising. Are, however, these values as such meaningful? Indeed it is not primarily the energy of the coherent structure that determines its importance, but rather its distributive actions and in particular the ratio of the Reynolds-shear-stresses $(u'v')_{\text{coherent}}/(u'v')_{\text{total}}$, which may reach values of up to 95% in the region of maximum structural organization of an excited mixing layer (region II according to Oster and Wygnanski, 1982).

Still, those figures seem to be of importance only in an indirect way. We find that a jet flow in still ambient fluid with relatively weak coherent content is—owing to its configuration—easily controlled by periodic excitation in most spectacular ways (see Lee and Reynolds, 1985). A wake on the other hand has a notably higher CS energy content, yet its controllability is—by comparison—limited. The major difference between those two flows is in its convective characteristics. In a jet the convection is of the same order as its diffusion and highly dependent on the state of excitation. In the wake on the other hand, being a flow deficit, the convection velocity of its structures in the far region is almost constant and large in comparison with its diffusion, which reduces its controllability.

TABLE 1. COHERENT ENERGY CONTENTS OF BASIC FREE SHEAR FLOWS

plane mixing layer	20% Ho and Huerre, 1984; Fiedler and Mensing, 1985
accelerated mixing layer	≥ 25% Fiedler <i>et al.</i> , 1990
near jet	50% Kibens, 1980
axisymmetric far-jet	10% Nieberle, 1985; Mumford, 1982
near wake	25% Scholz, 1985
plane far-wake	20% other sources

From Fiedler, 1988.

3.2. STRUCTURES AND STABILITY

Flow stability—and in particular the stability of the coherent structures—is obviously the key to control. It is responsible for such mechanisms as the laminar/turbulent transition, as well as for the origin (the creation) and to some extent the decay of structures by creation of smaller structures as a consequence of the instability of the former. We therefore distinguish between primary and secondary instability, which can manifest in various modes (denoted by numbers 0, 1, 2, ...).

While the basic mechanism that leads to growth of perturbations may be one of many, a major and more general distinction in stability behaviour, of particular importance for controllability, is provided by the temporal and spatial growth behaviour of the initial disturbances. We define (see also Drazin and Reid, 1981; Huerre and Monkewitz, 1985):

A flow is considered *absolutely unstable* if the group velocity of any one perturbation frequency is less or equal to zero. In this case the amplitude of a given perturbation grows with time at any x -position in the flow. For *convectively unstable* flows all perturbation frequencies have positive group velocity.

Thus, at a given $x > x_p$, where x_p defines the position where the perturbation is introduced, the perturbation wave will reach a finite amplitude for a finite time only. The following diagram—Fig. 3—gives a graphical explanation.

Huerre and Monkewitz (1990) have extended the scope of stability behaviour by introducing a distinction between local and global instability:

Local instability denotes the situation of instability of a local velocity profile (being usually a function of x), while in *global instability* the entire flow field is concerned.

There are basic differences between those four conditions with respect to their control behaviour: Convectively unstable flows are characteristic of a frequency selective, non-linear amplifier. Accordingly they are sensitive to external forcing at a given frequency, while the amplifier characteristics themselves are modified by stationary boundary conditions. Absolutely unstable flows, which have an oscillator characteristic, are on the other hand comparatively resistant against external (periodic) forcing, being "self-excited flows" according to Koch (1985). Flows of this kind may be effectively influenced by minor changes introduced into the unstable flow regimes, as was demonstrated by Strykowski and Sreenivasan (1989) in the near wake behind a cylinder.

Locally unstable flows may—by modifications of their boundary conditions—become globally unstable. Global instabilities are often indicative of a feedback situation. A control-relevant distinction in this context is whether the flow system behaves as an externally excitable amplifier or as an oscillator with characteristic global response. This question was looked into in detail by Monkewitz and Sohn (1986).

Finally there are 'mixed' situations, where a flow has locally limited regions of absolute instability. Those may lead to a self excited global response in a way similar to that of feedback mechanisms.

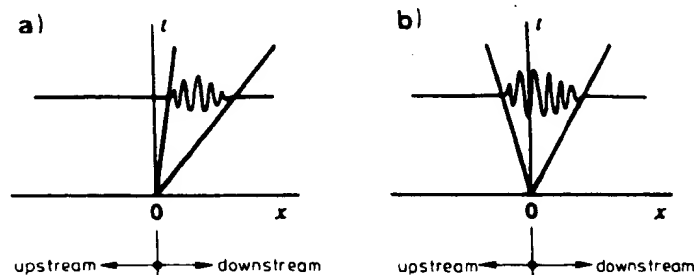


FIG. 3. Characteristics of wave propagation for absolute and convective instability. (a) Convective instability. (b) absolute instability.

A comprehensive summary of stability results as known for different kinds of shear flows is provided by Huerre and Monkewitz (1990)—see also Bechert (1985). Some of their results, being fundamental to the discussion of turbulence control, are presented in Table 2.

Temporal development of the perturbation frequency amplitude is found in absolutely and in globally unstable flows. There is a more than superficial similarity between the behaviour of absolutely unstable flow scenarios and flows with (natural) feedback, as observed by Hilberg and Fiedler (1989)—see Section 4.3.3. Both situations show the characteristic transient behaviour as described below. However, transient times in true feedback cases are apparently shorter and the flow is more easily influenced by external forcing.

In real flows the initially exponential growth is limited by non-linearities and a saturation amplitude is reached. This behaviour was first described by Landau (1966). For small times the complex amplitude of a given perturbation of frequency ω is described by

$$A(t) \sim e^{\gamma_1 t} \cdot e^{-i\omega_1 t}, \quad \text{or} \quad \frac{d|A|^2}{dt} = 2\gamma_1 |A|^2,$$

which obviously is only the first term of a series. Expansion leads to

$$\frac{d|A|^2}{dt} = 2\gamma_1 |A|^2 - \alpha |A|^4.$$

This formula takes care of the characteristic saturation behaviour, where the asymptotic limiting value for the amplitude—reached after a characteristic transient time—is given by

$$|A|_{\max}^2 = 2\gamma_1 / \alpha.$$

While α is assumed to be a constant, γ is—in the case of laminar/turbulent transition—a function of the Reynolds number:

$$\gamma_1 \sim (Re - Re_{\text{crit}}).$$

When this relation is applied to a turbulent flow to describe the mechanism of a coherent structure formation we might write (with ε = eddy viscosity):

$$\gamma_1 \sim (Re_\varepsilon - Re_{\varepsilon, \text{crit}}), \quad \text{which is constant for most flows.}$$

4. FREE TURBULENT SHEAR FLOWS

We know of a few quite spectacular examples of dynamic flow control from the last century. The famous description by Tyndall (1864) relates to the observation by Leconte (1858) and extends it to show a multitude of surprising possibilities of acoustically influencing and modifying gaseous and liquid jets alike. Some examples are shown in Fig. 4.

It was only after many years that the topic was then taken up again by Brown (1935), who undertook a thorough study of jet flow and its sensitivity to sound, observing, describing

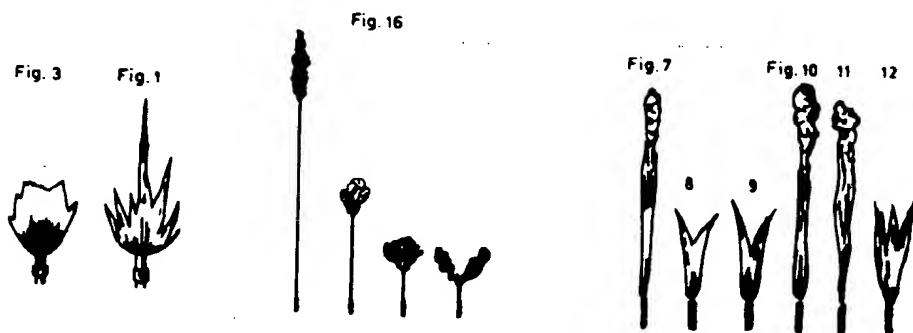


FIG. 4. Examples from Tyndall's (1867) investigation of jets exposed to a sound field.

A comprehensive summary of stability results as known for different kinds of shear flows is provided by Huerre and Monkewitz (1990)—see also Bechert (1985). Some of their results, being fundamental to the discussion of turbulence control, are presented in Table 2.

Temporal development of the perturbation frequency amplitude is found in absolutely and in globally unstable flows. There is a more than superficial similarity between the behaviour of absolutely unstable flow scenarios and flows with (natural) feedback, as observed by Hilberg and Fiedler (1989)—see Section 4.3.3. Both situations show the characteristic transient behaviour as described below. However, transient times in true feedback cases are apparently shorter and the flow is more easily influenced by external forcing.

In real flows the initially exponential growth is limited by non-linearities and a saturation amplitude is reached. This behaviour was first described by Landau (1966): For small times t the complex amplitude of a given perturbation of frequency ω is described by

$$A(t) \sim e^{\gamma_1 t} \cdot e^{-i\omega_1 t}, \quad \text{or} \quad \frac{d|A|^2}{dt} = 2\gamma_1 |A|^2,$$

which obviously is only the first term of a series. Expansion leads to

$$\frac{d|A|^2}{dt} = 2\gamma_1 |A|^2 - \alpha |A|^4.$$

This formula takes care of the characteristic saturation behaviour, where the asymptotic limiting value for the amplitude—reached after a characteristic transient time—is given by

$$|A|_{\max}^2 = 2\gamma_1 / \alpha.$$

While α is assumed to be a constant, γ is—in the case of laminar/turbulent transition—a function of the Reynolds number:

$$\gamma_1 \sim (Re - Re_{crit}).$$

When this relation is applied to a turbulent flow to describe the mechanism of a coherent structure formation we might write (with ε = eddy viscosity):

$$\gamma_1 \sim (Re_e - Re_{e,crit}), \text{ which is constant for most flows.}$$

4. FREE TURBULENT SHEAR FLOWS

We know of a few quite spectacular examples of dynamic flow control from the last century. The famous description by Tyndall (1864) relates to the observation by Leconte (1858) and extends it to show a multitude of surprising possibilities of acoustically influencing and modifying gaseous and liquid jets alike. Some examples are shown in Fig. 4.

It was only after many years that the topic was then taken up again by Brown (1935), who undertook a thorough study of jet flow and its sensitivity to sound, observing, describing

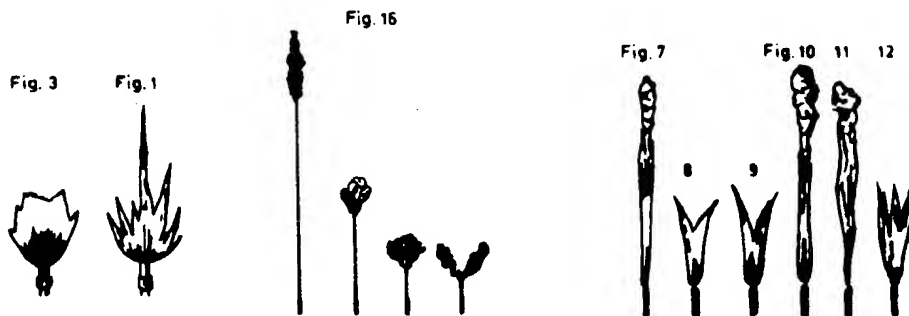


FIG. 4. Examples from Tyndall's (1867) investigation of jets exposed to a sound field.

TABLE 2. STABILITY BEHAVIOUR OF SOME BASIC FLOWS

System	Characteristic parameters	Type of investigation	Results and references
Axisymmetric jet	Family of velocity and density profiles, $R = \infty$, $F = \infty$, variable M , Λ , and S	Local LS	<ul style="list-style-type: none"> Spatial stability, implying AI for $S = 0.5$ (Michalke, 1971, 1984) Boundary of AI in (M, Λ, S) profile shape parameter-space, $S_{\text{min}} = 0.72$ for AI at $M = 0$ (Monkewitz and Sohn 1986, 1988) Demonstration of GLI as function of S and R (or M), and presence of Hopf bifurcation (Monkewitz <i>et al.</i> 1989)
Heated axisymmetric jet	$5 \times 10^3 < R < 5 \times 10^4$ $0.03 < M < 0.3$, $\Lambda = 1$, variable S	Global behavior by LE	<ul style="list-style-type: none"> Implications for entrainment (Monkewitz <i>et al.</i>, 1989) Demonstration of GLI as function of S and M, lock-on to forcing, and effect on spreading (Kyle 1988, Sreenivasan <i>et al.</i>, 1989a; Kyle and Sreenivasan, 1989; Guyon, 1988) Indication of GLI in dump combustor (Subbarao, 1987)
Inhomogeneous axisymmetric jet	$0.02 < M < 0.5$, $\Lambda = 1$, variable S (He-N ₂ mixture)	Global behavior by LE	<ul style="list-style-type: none"> Demonstration of GLI for feedback gains $G > G_{\text{crit}}$ (Reisenthel, 1988; generic modelling by Monkewitz, 1989a)
Axisymmetric jet with feedback	$3.9 \times 10^4 < R < 8.5 \times 10^4$, $M \approx 0$, $\Lambda = 1$, $S = 1$, feedback from hot wire to acoustic driver	Global LS (model)	<ul style="list-style-type: none"> Association of jet-column mode with excited global mode for marginal global stability (Monkewitz <i>et al.</i>, 1987)
2-D jet	Family of velocity profiles fitted to experiment, $R = \infty$, $M = 0$, $\Lambda = 1$, $S = 1$	Global LS (model)	<ul style="list-style-type: none"> Boundary of AI in (S) profile shape parameter-space, $S_{\text{min}} = 0.90$ for AI (Monkewitz, 1988, Yu and Monkewitz, 1988)
2-D inhomogeneous jet	Family of velocity and density profiles, $R = \infty$, $M = 0$, $\Lambda = 1$, $F = \infty$, variable S	Local LS	<ul style="list-style-type: none"> AI for $R > \text{approx. } 45$ in the $\text{sech}^2(y)$ wake with $\Lambda = -1$ (Nakaya, 1976)
2-D wake	Family of velocity profiles and computed profiles, finite R , $M = 0$, $S = 1$, variable Λ	Local LS	<ul style="list-style-type: none"> Boundary of AI in (Λ, R)-space for Gaussian wake (Hultgren and Aggarwal, 1987) Boundary of AI in (Λ, R) profile shape parameter-space. Evidence of AI region before GLI by comparison with measured profiles (Monkewitz, 1988a) Evidence of AI region before GLI by comparison with computed profiles (Hannemann, 1988; Hannemann and Oertel 1989; Yang and Zebib, 1989)
2-D heated-cylinder wake	$M \approx 0$, $S \neq 1$, variable R mostly near the onset of von Kármán shedding	Global behavior by LE	<ul style="list-style-type: none"> Suppression of vortex shedding by heating (Noto <i>et al.</i>, 1985; Mori <i>et al.</i>, 1986; Strykowski, 1986; Strykowski and Sreenivasan, 1989; Berger and Schumm, 1988; Le-cordier <i>et al.</i>, 1988)

2-D inhomogeneous (heated) wake	Family of velocity profiles, $M = 0$, $S \neq 1$, $F = \tau$, variable R and Λ	Local LS	<ul style="list-style-type: none"> Boundary of AI in (S, R, Λ)-plane with CI for sufficiently low S (Monkewitz, 1988c)
2-D cylinder wake with control cylinder	$46 < R < 100$, $M \approx 0$, $S = 1$	Global behavior by LE and NE	<ul style="list-style-type: none"> Suppression of GLI by presence of small cylinder in near wake (Strykowski, 1986; Strykowski and Sreenivasan, 1989)
2-D wake	Family of velocity profiles pertinent to wake of blunt trailing edge, $R = x$, $S = 1$, $M = 0$, variable Λ	Local LS	<ul style="list-style-type: none"> AI in the near wake (Koch, 1985) Postulate of global frequency-selection criterion $u_0 = \omega_0(X_1)$, where $\omega_0(X_1) = 0$
2-D wake of blunt trailing edge	$M \approx 0$, R near the onset of von Kármán vortex shedding, variable base blowing/suction	Global behaviour by transient LE (step change of base bleed)	<ul style="list-style-type: none"> Suppression of von Kármán vortex shedding by steady base bleed at high R (Wood, 1964)
Asymmetric wake	Family of velocity profiles, $M = 0$, $S = 1$, variable R and Λ	Local LS	<ul style="list-style-type: none"> Demonstration of GLI (Berger 1989) AI for first helical mode only Boundary of AI in (R, Λ), profile shape parameter-space (Monkewitz, 1988b) Lock-on of helical vortex shedding, suggesting GLI (Schoiz, 1985)
Wake of axisymmetric disk	$1.5 \times 10^4 < R < 3.5 \times 10^5$, $M \approx 0$, $S = 1$	Global behavior by LE	
Plane mixing layer	$\tanh(\tau)$ velocity profile, $R = \infty$, $S = 1$, $M = 0$, variable Λ	Local LS	<ul style="list-style-type: none"> AI for $\Lambda \geq 1.315$ (Huerre and Monkewitz, 1985)
Plane mixing layer	$M = 0$	Global behavior by NE	<ul style="list-style-type: none"> Discovery of self-excited global modes due to feedback from downstream to upstream end of computational box (Lowery and Reynolds, 1986; Buell and Huerre, 1988)*
Inhomogeneous plane mixing layer with wake component	$\tanh(\tau)$ velocity profile plus Gaussian wake, $\tanh(\tau)$ density profile, $R = \tau$, $M = 0$, variable S , variable Λ	Local LS (spatial)	<ul style="list-style-type: none"> Probable AI for $\Lambda = 0.45$ and $S < \text{approx. } 0.12$ Direct resonance between shear layer and wake mode (Koochesfahani and Friefer, 1987)
Inhomogeneous plane mixing layer	$\tanh(\tau)$ velocity profile, $R = x$, $M \neq 0$, variable S , variable Λ	Local LS	<ul style="list-style-type: none"> Boundary between CI and AI in (M, S, Λ) parameter space (Pavithran and Redekopp, 1989; Djordjevic et al., 1989; Jackson and Grosch, 1989)
Flat plate boundary-layer	Blasius boundary-layer profile, $M \approx 0$	Local LS	<ul style="list-style-type: none"> CI, focus on signaling problem (receptivity to sound) (Tam, 1981)
Boundary-layer over compliant wall	$M = 0$, $R = \tau$, and finite	Local LS	<ul style="list-style-type: none"> AI above critical freestream velocity (Brazier-Smith and Scott, 1984; Carpenter and Garrard 1986)

* Experimental verification of self excited global instability for one-stream layer in 'narrow' test section (Fiedler and Hilberg, 1990).
 The following acronyms and parameters are used: LS: linear stability analysis; LE: laboratory experiment; NE: numerical experiment; CI: convective instability; AI: absolute instability; GLI: global instability; A: velocity ratio; S: density ratio; R: Reynolds number; M: Mach number; F: Froude number; W: Weber number.
 After Huerre and Monkewitz, 1990.

and explaining many of the spectacular consequences of sinusoidal excitation on jet flow, that were then again revisited and expanded upon some thirty years later.

Early examples of control of wall bounded flows are Dubuat's (1779) paradox, Prandtl's (1914) trip wire, and the Coanda (1934) effect.

Observation of nature may provide valuable inspiration and insight into flow control mechanisms. Nature has—over many millenia of optimization—achieved and developed some amazingly elegant and efficient ways of flow control, the most widely known ones being the control of wing-flow of birds and the drag reduction mechanisms found with aquatic animals—particularly the dolphin and the shark. Some of the underlying principles are as yet still incompletely investigated and understood.

In recent years the topic has again been revived for two reasons: It is on the one hand a scientifically logical extension of the coherent structures research of the last two decades, and on the other hand the economically driven need for improved technical processes wherever a turbulent flow is involved, as well as the ubiquitous necessity for reduced energy consumption (e.g. drag reduction—see Section 5), which has economical as much as ecological implications.

In the following we shall discuss major developments of recent years in some depth. We shall—after a general introduction of the physical phenomena and principles involved—discuss specific flow scenarios in the light of their susceptibility to certain ways of control.

4.1. PRINCIPLES AND METHODS OF CONTROL

A principal distinction regarding the controllability of free- and wall-bounded flows is derived from their different stability characteristics. While wall-bounded flows are Orr-Sommerfeld unstable, with viscosity playing a crucial role, free flows are in essence Rayleigh- (inflexion point-) unstable. There the (largely negligible) effect of viscosity is only of damping influence and the prime instability mechanism is by vortical induction. Flows dominated by this kind of instability tend to develop comparatively 'simple' instability modes which to a considerable extent persist in the random-turbulent ambience, becoming prey of either mutual interaction or of secondary instabilities (pairing, tearing, wearing).

The primary instability modes of the turbulent flow are, in a convectively unstable situation, highly receptive to (external) periodic forcing, according to the individual growth rate vs Strouhal-number curves. This is the basis for dynamic control, leading to a Strouhal number classification, or characterization. Two kinds of Strouhal number are mostly used:

- (1) a local Strouhal number, and
- (2) an initial Strouhal number, used for describing special, locally limited, phenomena as e.g. the preferred mode.

Examples for (1) as found in the literature are $S_\theta = \Theta / U$, which is based on the momentum thickness of the local velocity profile Θ . The Strouhal number most often used for characterizing and scaling the frequency selectivity with downstream position is, however, $S_x = x / U$, being typically of the order 1. It is proportional to S_θ , since $\Theta = \Theta(x)$. The reader is referred to Section 5.4.3. Initial Strouhal numbers are based on e.g. the initial momentum thickness of the velocity profile forming from the separated nozzle boundary layer Θ_0 . These Strouhal numbers are typically of the order 10^{-2} to 10^{-1} . Relevant (equivalent-) diameter-based Strouhal numbers S_d are typically of the order 1 or less. For a given geometry and Reynolds number $S_{\theta,0} \sim S_d$.

Growth-rate characteristics on the other hand depend strongly on boundary conditions—a fact which accounts for certain aspects of static or stationary control.

Classical treatment of free shear flow of the boundary layer type is based on the phenomenological distinction between jet, wake and mixing layer flow. Jet and wake may, however, be considered as being of one family, distinguished only by different ratios of volume flux as is outlined in Fig. 5. Mixing layers, being the most basic configuration, are a transient state for both jet and wake flows near their origin.

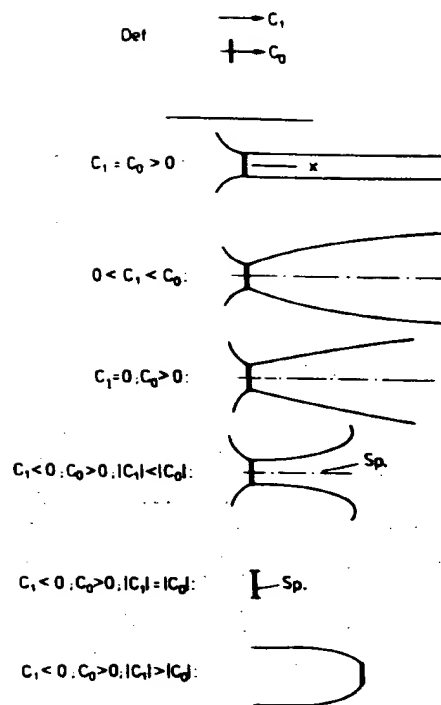


FIG. 5. A metamorphosis of jet and wake configurations based on the velocity (momentum-flux) ratio. First four configurations from top: jets; bottom: wake.

Characteristic structural modules of all three flows are line-vortices in the plane configurations and ring-vortices in axisymmetric cases, with their characteristic secondary instabilities (Weske and Rankin, 1960; Widnall and Sullivan, 1973; Widnall *et al.*, 1974; Schneider, 1980; Glezer, 1981). A module common to both configurations are longitudinal helices (Levich and Tsinober, 1983).

As suggested above, we shall distinguish between dynamic and static control according to the following scheme:

(a) Dynamic control of a turbulent flow is possible by periodic excitation at one or more frequencies with positive (amplitude) growth rate. The control behaviour is determined and characterized by the frequency(s), the amplitude(s), the phase position(s) and the waveform(s), which controls the content of higher harmonics.

In his investigation of control possibilities of combustion and other related processes, Raghu (1987) suggests the following systematic: Control by periodic heat addition, by periodic momentum addition, by periodic mass addition and by combinations thereof.

The physical mechanism of excitation is in the modification of the coherent structures. Thus excitation at 'low' frequencies (near the local characteristic passage frequency of the coherent structures) acts directly on their strengthening and stabilization, causing local increase and spread in the region of their formation and decrease in the stabilization range.

Conversely, 'high' frequency forcing acts on the coherent structures of higher frequency and small dimension—i.e. those near the trailing edge (in any case upstream of the region to be influenced). There it causes either premature transition or at least fast growth with subsequent decay and only asymptotic recovery. High frequency excitation is often applied where suppression of turbulence activity is asked for.

The technical principle of producing and introducing periodic excitation (see Fig. 6) is based on the modification of the concentrated vorticity sheet near the trailing edge, where

at the same time

□

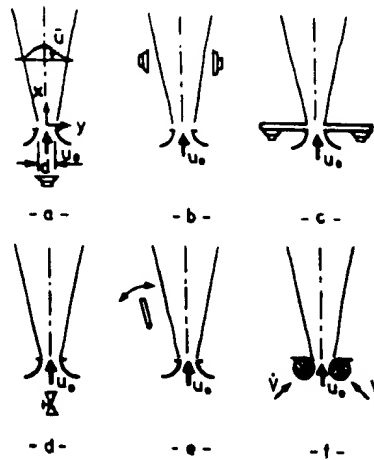


FIG. 6. Methods of jet excitation. (a) Speaker in plenum (0th mode); (b) speakers at outside locations; (c) speakers at nozzle exit (various modes); (d) valve (0th mode); (e) outside flap; (f) side jets.

the receptivity of the flow is at its maximum. This is possibly done either by an active or passive mechanism. Active ways of excitation include

- pressure waves by (i) acoustic means, e.g. a loudspeaker, which may be driven externally by a frequency generator, or by the flow itself, providing an external feedback loop (Fiedler *et al.*, 1978), or (ii) by a resonance mechanism within or outside of the flow regime (e.g. the test section). The important parameter here is the fluctuating pressure gradient at the trailing edge, as was shown by Bechert and Michel (1975) (see also Morkovin and Paranjape, 1971). This investigation may serve as a basis for the proper setup of a loudspeaker-excitation-system. Self-sustained oscillations of impinging flows—jets and mixing layers of various geometries—have been extensively discussed by Rockwell and Naudascher (1979);
- shedding/modulating of vorticity (mechanically activated ribbon or flap (see also Section 5.4.3), vibration (or rotation) of the trailing edge (nozzle);
- Tollmien/Schlichting (TS)—waves in the boundary layer of the splitter plate (nozzle). This constitutes an indirect method as was recently developed by Glezer (1986)—see also Neuwald (1990).

Passive ways of excitation are by

- feedback or resonance (e.g. Hussain *et al.* 1987; Monkewitz 1988);
- mechanical means which are activated by the flow itself—e.g. a self-oscillated vane as described by Fiedler and Korschelt (1979).

The efficiency of excitation:

- It is locally determined and limited by the saturation behaviour of the structures to be influenced, depending essentially on the amplitude and the mode of excitation frequency.
- The location of maximum excitation effect depends on the frequency (usually at larger x for lower frequencies), being a function of the characteristic frequency of the neutral flow.
- The—generally limited—local extent of the controlled region may be extended by excitation of more than one frequency. The effect depends then on the individual amplitudes of the two frequencies and on their phase relation.
- Exciting a flow at certain (instability) modes or their combinations may produce special effects.

Dynamic schemes appear to be the classics in flow control. However, static methods have also become known, and the Dubuat's paradox was nothing else but the poorly understood consequence of a static control mechanism. Prandtl's trip wire and Coanda's jet deflection (following a modified boundary condition) are two other prominent examples.

if I want to control small scale, must then

(b) *Static ('passive') control* is achieved by

- modification of structural stability by stationary boundary conditions, e.g.
 - pressure gradients (transverse, longitudinal—see also Sections 5.2.2 and 5.2.3),
 - geometric distortion (continuous variation of the flow cross-section in downstream direction),
 - side and bottom walls (proximity of walls);
- by introducing or causing structural instability and disruption of structures either by directly introducing three-dimensional vorticity at the trailing edge (upstream boundary conditions), or by selecting a trailing edge geometry whereby undulations of the dominant structures are triggered (see also Section 5.4.4). In both cases the production of streamwise vorticity is enhanced. Disruption or destruction of large scale structures is also possible directly by screens or gauzes in the flow. This possibility has been examined by—among others—Yajnik and Acharya (1988), Nieberle (1985) and Wygnanski *et al.* (1979); a special case is the influencing of the laminar-turbulent transition, as e.g. by a trip-wire (Wygnanski and Fiedler, 1970).
- by entrainment: direct influence is executed via the Coanda effect, i.e. when the entrainment is obstructed by the proximity of adjacent walls (this is not to be confused with the stability-modification due to wall proximity as noted above). Indirect influence ('internal control') is provided by background turbulence according to its intensity and scale etc. (e.g. Symes and Fink, 1978; Dziomba, 1981; Tavoularis and Corrsin, 1981; Chandrusda *et al.*, 1978; Tanner, 1989). Increased turbulence level in the entrainment stream acts primarily as a destabilizing agent (= noise) for the organized structures, causing overall increase of spread. Related is the aspect of
- fluid characteristics, which in most applications will be introduced via entrainment. Here we might think of density or viscosity inhomogeneity (temperature, species), and finally of additives (polymers).

The overall efficiency of static control methods is comparable to that of the dynamic methods, since in both cases the coherent structures are controlled and thereby modified. The spatial extent of control depends on the method applied: side-wall boundary conditions control most of the flow exposed to them. Entrainment and fluid characteristics provide comparable (overall) effects. Upstream boundary conditions have a more limited, local effect. Often a combination of methods is successfully employed (as e.g. the periodic forcing of a three-dimensional jet or a distorted mixing layer. In this way it is often possible to increase the effect considerably.

The above list might be further extended to include stratification and field forces (temperature, immiscible media, magnetic fields) and the like. We shall, however, restrict this survey to the more practical cases, where a sufficient body of information is already available.

4.2. JETS

Jet flow has probably been most studied as a ready object of control by external stimulation or manipulation (Kibens, 1989; Hussain and Husain, 1988). Like the wake, it is a flow of evolving characteristics, developing first into a mixing layer (from the boundary layer of the nozzle wall)—and after the eventual merging of the mixing layer(s) the true jet flow develops into its final state. It is then that for certain configurations (ambient flow at rest or with 'tailored' pressure gradient) self similarity develops. This is the case after, say, 70 nozzle diameters in the axisymmetric configuration, and around 120 in the plane jet in still surroundings. As a consequence we find the flow to be dominated by different structures or structural modes, depending on the axial position we are looking at.

Susceptibility for control depends also on the ratio of jet velocity to ambient velocity, and the self-similar jet in still surroundings provides the most convenient special case of highest instability and of highest priority for research.

Traditional distinction in jet flow is made according to geometrical characteristics.

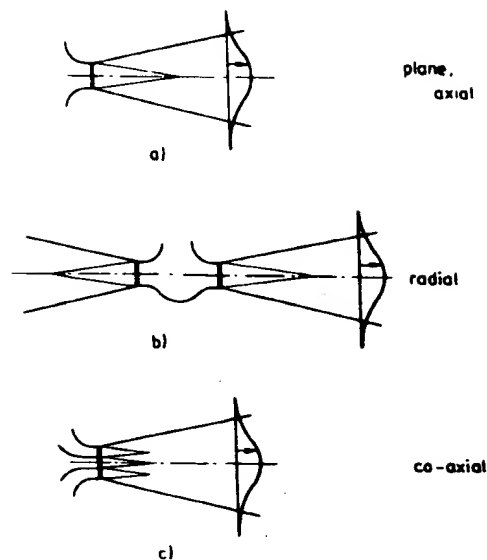


FIG. 7. Some basic jet configurations.

In rising degree of complexity basic configurations are: plane-, radial-, axisymmetric-, co-axial-, three-dimensional- and confined jets, as depicted in Fig. 7.

Jets can easily be controlled over a limited downstream length by various methods, e.g. by dynamic control, as by periodic forcing at one or more frequencies of the flow near the nozzle exit—with its characteristic manifestations of 'flapping', 'blooming' and 'pulsating'; and by static control, which is essentially imposed onto the flow by the nozzle geometry.

Another possibility of exerting some influence on the flow behaviour is provided by the turbulence level of the primary stream. There are yet other possibilities of controlling the jet via its entrainment flow e.g. by a different density of the entrained medium. Jet development may be also influenced by a 'tailored' external flow (e.g. for a jet in a diffuser flow). Finally there is the control mechanism of additives, particularly in the primary stream.

Many of these aspects have been investigated and a host of information is available. Essential for understanding of the observed phenomena are the basic stability characteristics, leading to the dominant structures—vortex rings, line vortices, single- and multi-helices etc., e.g. see Fiedler (1988). A great number of investigations, reported in the recent, say, two decades, have provided us with a relatively detailed picture of the coherent structures in the near-jet and in particular the characteristic phenomenon of the preferred mode (e.g. Crow and Champagne, 1971; Armstrong *et al.*, 1977; Peterson, 1978; Armstrong, 1981; Eickhoff, 1982; Peterson and Samet, 1988; Gutmark and Ho, 1983; Nieberle, 1985).

Owing to a higher degree of complexity and weaker structures, the picture is considerably less clear and detailed for the far-field of turbulent jets, as we find from the few investigations known (e.g. Tso, 1984; Tso *et al.*, 1980; Kumori and Ueda, 1985; Nieberle, 1985; Dimotakis *et al.*, 1982).

Most studies were concerned with the axisymmetric jet. Less is known about the plane and little about the coaxial jet (Bremhorst and Watson, 1981; Szajner and Turner, 1987). No structural investigation seems to have been devoted to the radial jet since Heskestad's (1966) work.

There is, on the other hand, increasing interest in three dimensional configurations, some of their characteristic structures and global manifestations will be discussed below in some depth.

The primary stability behaviour of jets, as summarized by Michalke (1984), has been studied by a number of authors (e.g. Lessen and Paillet, 1976; Morris, 1976; Haertig, 1979; Plaschko, 1979; Bejan, 1981; Michalke and Hermann, 1982; Morris, 1983).

A homogeneous jet is a purely convectively unstable flow (see Table 2). Exceptions, where absolute instability is observed, may, however, turn up in the presence of density inhomogeneities (when the jet has lower density than the ambient fluid—see Monkewitz *et al.* (1989) and Raghu *et al.* (1990)).

Special stability aspects of wave interaction and resonance were investigated and discussed by Kelly (1967), Cohen and Wygnanski (1987a,b), Mankbady (1984) and Paschereit and Wygnanski (1989); of absolute instability by Huerre and Monkewitz (1985, 1990), of secondary instability of large structures by Widnall and Sullivan (1973), Schneider (1980) and Glezer (1981), and of feedback by Fiedler *et al.* (1978), Laufer and Monkewitz (1980), Koch (1985), Reisenthel (1988) and Monkewitz (1989).

Basic and general aspects of jet flow were discussed e.g. by Wille (1963), and—summarizing—by Abramovich (1963) and by Rajaratnam (1976).

4.2.1. Major Configurations

The jet is—as has already been pointed out—an evolving flow. Of dominant practical relevance and interest for most cases is the region near the nozzle exit (the 'near region'), and the majority of investigations have indeed been devoted to this part of the flow, which is strictly not a jet but a mixing layer.

Discussions of non-stationary jets of a more general kind have been presented by e.g. Binder *et al.* (1971), Borisov and Gynkina (1975), Bremhorst (1979), Favre-Marinet *et al.* (1981), Hussain and Husain (1988), Kato *et al.* (1987), Kozlov *et al.* (1989), Stone and McKinzie (1984), Kibens (1989), Gutmark *et al.* (1986), McCormack and Cochran (1966), McCrosbey (1977), Platzer *et al.* (1978) and Hill and Jenkins (1976).

There are many applications of jet control, the most obvious ones are in combustion, fluidics, noise control, thrust control, mixing and entrainment enhancement (ejectors) and for continuous lasers. Some of them are discussed by Peters and Williams (1981), Ramachandran *et al.* (1989), Crighton (1981), Michalke (1978), Mollo-Christensen (1967), Bechert and Pfizenmaier (1976), Kibens (1980), Laufer and Ta-Chun (1983), Roffman and Toda (1969), Norum (1982), Guicking (1988) and Gutmark *et al.* (1986).

Specific investigations and their major outcome are summarized in the following, where distinction is drawn according to the control method employed.

4.2.2. Periodic Forcing—the Established Method of Active Control

Jets of various configuration have been exposed to periodic forcing of a single frequency or multiple frequencies with obvious manifestations. As was mentioned earlier, the first scientifically documented research in this subject was by Tyndall (1867) (see Fig. 4). He described a host of spectacular phenomena for gaseous and liquid jets of various configurations with mostly axisymmetric or three-dimensional jet geometry. Later, Brown in 1935 investigated the excited plane jet, and already by then most phenomena which we know today were observed and documented.

The topic was re-visited in the late 1960s and since then a large number of detailed results have been uncovered for two-dimensional, three-dimensional and co-axial jets under single- and (later) multiple-frequency excitation (e.g. Goldschmidt and Kaiser, 1971; Korschelt, 1980; Fiedler and Korschelt, 1979; Favre-Marinet *et al.*, 1981; Morkovin and Paranjape, 1971; Rockwell, 1971; Bradshaw, 1972; Bernal and Sarohia, 1984; Binder and Favre-Marinet, 1981; Binder *et al.*, 1971; Rockwell, 1972; Goldschmidt and Bradshaw, 1972; Weir and Bradshaw, 1975; Lee and Reynolds, 1985; Vlasov and Ginevsky, 1967, 1976; Nieberle, 1987; Paschereit and Wygnanski, 1989; Monkewitz *et al.*, 1989; Raghu *et al.*, 1990; Vlasov, 1965; Breidenthal, 1986; Roffmann and Toda, 1969; Ahuja *et al.*, 1982; Bremhorst and Harch, 1979; Bremhorst and Hollis, 1988; Hasan and Hussain, 1982; Hussain and Zaman, 1977; Kondratiev and Rimski-Korsakov, 1971; Lee and Reynolds, 1985; Lepicowsky *et al.*, 1984; Vlasov and Ginevskiy, 1967, 1976; Zaman and Hussain, 1982; Szajner and Turner,

1986; Wille, 1963; Vagt, 1969; Platzer *et al.*, 1978; Reisentel, 1988; Wille, 1963; Raman, 1976).

The strongest effect of periodic excitation is in the region where the forcing frequency is equal to (or slightly upstream of) the natural (characteristic) frequency of the neutral flow. In the near (core-) region two modes dominate the flow: the mixing layer mode—with $f_{ML} \sim 1/x$ —and the 'preferred mode' with $f_{PM} = \text{const.}$

The particular aspect of the preferred mode was introduced by Crow and Champagne (1971) and later reviewed by Gutmark and Ho (1983), who compiled results from many authors for plane and axisymmetric flows. This mode, which is observed over the full length of the core region is characterized by a Strouhal number of

$$0.25 \leq St_d = f_{PM} d / U_0 \leq 0.5, \quad (\text{for elliptic jets } d = d_{\text{equivalent, hydraulic}}).$$

It was only recently again discussed and explained by Wygnanski and Petersen (1987) and Petersen and Samet (1988), who suggest the preferred mode to be simply the characteristic instability frequency at the end of the core, i.e. at the merging of the mixing layer(s). Two possible explanations for the disturbing wide variation of the values as obtained by several authors are offered: (1) The confidence interval of the spectral estimate and (2) the effect of initial (i.e. upstream boundary-) conditions. But there might even be a third possibility: The various measurements reported have been done in different velocities and geometries. Assuming the preferred mode to be a feedback effect of (a multiple of) the shear layer mode at the end of the core, then this feedback frequency would have to depend also on the flow's (usually neglected) Mach number, which then might account for part of the scatter.

The major points of periodic control are summarized in the following. Most of the more general aspects are equally valid for wake- and mixing layer control as discussed below.

Choice of frequency (range): Free turbulent flows at high Reynolds number are characterized by the so called Reynolds similarity, i.e. their dependence on a characteristic length l^* and a characteristic velocity c^* only, which may be obtained from the local velocity profile (e.g. its width and its maximum velocity). Those two parameters define a characteristic frequency $f_c \sim c^*/l^*$, the true value of which is usually determined from the frequency maximum of the lateral fluctuations (preferably).

The jet is—as are all developing flows—frequency selective and maximum excitation effect is near (usually 10–20% downstream of) the x -position, where the characteristic frequency (maximum) of the flow corresponds to the frequency of excitation. For the near region this corresponds to a Strouhal number range of $0.2 \leq S_d = fd/U_0 \leq 0.6$. In decaying flows the characteristic frequency decreases downstream, typically as $f_c \sim 1/x$ for the near region (mixing layer) and for the axisymmetric far-jet, and as $f_c \sim 1/\sqrt{x}$ for the plane far-jet. Excitation at high frequencies (in the range of $1 \leq S \leq 5$, or—as suggested by Zaman and Hussain (1981)— $S_\theta = \Theta/f/U_0 \approx 0.017$, where Θ = local momentum thickness of the mean velocity profile) therefore causes structural stabilization near the nozzle—or premature transition in the case of laminar flow—with little local effect, but which is followed, however, by a region of reduced turbulence intensity of long persistence. This "dual nature of acoustic effect on free turbulent jets" as described by Vlasov and Ginevsky (1967 and 1976) was not confirmed, however, by Goldschmidt and Kaiser (1971).

Choice of amplitude: Apparently the mean velocity profile of a turbulent flow follows similar stability criteria as does the laminar one. In most cases low amplitudes (order $\leq 1\%$) are usually needed to achieve stabilization of the structures together with appreciable local increase in mixing and spread. With further increase of driving amplitudes the flow reacts in a non-linear way, reaching a saturation value for the periodic constituent, which is accompanied by reduction of the stochastic fluctuation intensity, the amplitude of which is correlated with the phase position of the periodic. The x -position of the locus of maximum energy of the periodic fluctuation content is weakly influenced by the excitation amplitude, reaching its highest upstream position at saturation. Situations with extreme amplitudes are described by Bernal and Sarohia (1984), Bremhorst and Harch (1979) and Bremhorst and Hollis (1988).

Location of maximum receptivity: Maximum receptivity for periodic excitation is determined by two parameters: (1) The position where the mean velocity profile is most unstable. The mean velocity profile of a separating flow immediately at or downstream of the trailing edge (nozzle) is still very much a wall boundary layer profile. It needs a certain time to develop into the more unstable 'free' profile (see Michalke (1970) and (2) where a given (absolute) perturbation provides maximum relative perturbation. This is the case for minimum profile thickness as compared to the amplitude of forcing.

It is for these two reasons that maximum receptivity of a separating flow is always near (order of the boundary layer thickness) to the trailing edge.

Waveform: The specific waveform chosen for excitation (sinusoidal wave, square wave etc.) determines the content of higher harmonics. No systematic investigation of the effects involved seem to have been done on a general scale. Investigations of two-frequency forcing are discussed under *resonance and feedback* (below).

Modes: Jet flow is unstable for different instability modes (see e.g. Michalke, 1984; Michalke and Hermann, 1982). Excitation of those modes has different consequences for the (local) flow development, both in amplitude and in appearance. In a plane jet the sinuous mode—leading to jet 'flapping'—is considerably more dominant than the varicose one. In the axisymmetric jet on the other hand the development of an infinite number of azimuthal modes is possible (with dominating 0' and—further downstream—1st mode), permitting a much greater variety of control (Wynanski and Petersen, 1985).

Mach number: While some authors claim that there is negligible influence of Mach number on the development of coherent structures in an axisymmetric jet (e.g. Armstrong, 1981), the high speed jet appears to be somewhat less excitable than low Mach number jets. This peculiar behaviour seems to be unresolved as of yet (Ahuja *et al.* (1986)).

Let us look at some typical manifestations of active control. Major effects of jet-flow excitation with a single frequency are a notable increase of the *overall spread*, the extent of which is locally limited, depending on the variation of the characteristic frequency $f_c \sim (U_{\max} + U_{\min})/\Theta$ with x and on the excitation amplitude. Thus the range of influence will strongly depend on the external flow condition and may indeed stretch over a long distance. This distance can be effectively extended by double-frequency forcing. Associated with the widening of the flow are a high coherence of the large scale structures and an increase of the overall turbulence intensity, which is primarily a consequence of the large periodic signal content. Under certain circumstances, broadband amplification of the radiated noise from a round jet is found as a consequence of pure tone excitation (Bechert and Pfizenmaier, 1976). Cancellation of pure tones in excited jets is on the other hand also possible, as was shown by Arbey and Ffowcs-Williams (1984) (see also Hussain and Zaman, 1980). According to Crighton (1981) there are two different kinds of jet response to periodic forcing at a Strouhal number of $S_d \approx 0.5$, depending on the value of the Reynolds number $Re_d = U_0 d/\nu$. Amplification at the excitation frequency is accompanied by suppression of the broad band spectrum for $Re_d < 10^5$ and an initially laminar mixing layer. Broad band excitation is, on the other hand, observed for $Re_d > 10^5$ and an initially turbulent mixing layer.

Forcing the jet in certain mode combinations (Wynanski and Petersen, 1985; Paschereit *et al.*, 1989) or introducing the perturbation in a three-dimensional configuration (Glezer, 1990) may cause a local *re-shaping* (e.g. *squaring*) of the jet's cross section, resulting in local enhancement of small scale mixing and then to tilting of the jet's axis (see under *upstream boundary conditions*). Modification of the mean flow of a jet by excitation in two modes was first shown and theoretically proven by Cohen and Wynanski (1987). They showed how to produce elliptical or triangular jets out of circular nozzles. Paschereit *et al.* (1990) have demonstrated that by exciting the axisymmetrical jet with modes 1 and 2 a triangular deformation of the cross section can be achieved, where small scale- (high diffusive-) turbulence is particularly produced in the corners. This is clearly obvious from the schlieren photograph shown in Fig. 8, which was obtained in a jet with exit velocity of 1.5 m/sec and excitation frequency of 32 Hz, corresponding to a Strouhal number of $S_d \approx 1$.

Certainly the most spectacular effects of periodic excitation on axisymmetric jets were reported by Lee and Reynolds (1985)—some characteristic examples are shown in Fig. 9.

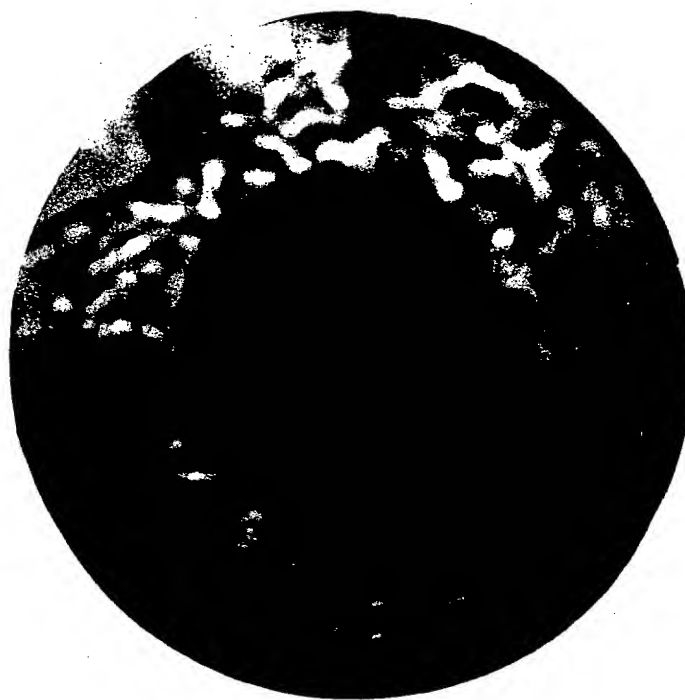


FIG. 8. Schlieren photograph of axisymmetric jet cross section near the nozzle exit. Excitation by the two frequency modes 1 and 2.

When the flow was forced by a combination of (fixed amplitude) axial (17%) and orbital (4% nozzle tilt) excitation, they observed two different developments, depending on the ratio F of axial and orbital frequency. Bifurcation (i.e. splitting into two individual jets) of the flow was found for $F = 2$, trifurcation for $F = 3$ etc., while for non-integer ratios of F the jet was aptly described as blooming (see also Fig. 4). In all cases molecular mixing was found to be enhanced. Bi- or trifurcating jets eventually develop as individual jets in the far field, their enclosed angle (as for the blooming configuration), depending on the axial Strouhal number, was found to reach values of 80 (see also Parekh *et al.*, 1988). Complete termination of a round jet by axisymmetric deflection jet can be achieved by specially shaped nozzles with boundary layer injection causing strong Coanda effect (see Reynolds and Juvet, 1990).

Compared to this multitude of control possibilities in axisymmetric turbulence—owing to the multitude of instability modes—there is only the modest choice between the varicose and the sinuous modes for plane jet control, of which only the latter shows sufficient receptivity. Local increase of spread by up to around 100% was observed for relatively high excitation amplitudes of $\sim 2.5\%$ by Korschelt (1980). The situation is characterized by a stepwise widening of the jet over a relatively short downstream region $\Delta x \approx x_i$ (x_i defines the beginning of the excited region). The position of maximum periodicity in the excited jet follows the Strouhal relation $S_{AS} = f_e (x_p - x_0) u_m \approx 1$, where f_e = excitation frequency and the Strouhal index x_s stands for 'saturation position'.

Another interesting phenomenon is the different location of maximum periodicity (different values for the Strouhal number), as determined by the correlation between the driving signal and the local flow signal for the lateral fluctuation (r') and the (passive scalar-) temperature signal (T'), as shown in Fig. 10 together with the longitudinal development of Reynolds stress maxima.

Other efficient ways and methods of influencing the behaviour of a turbulent jet are provided by passive control.

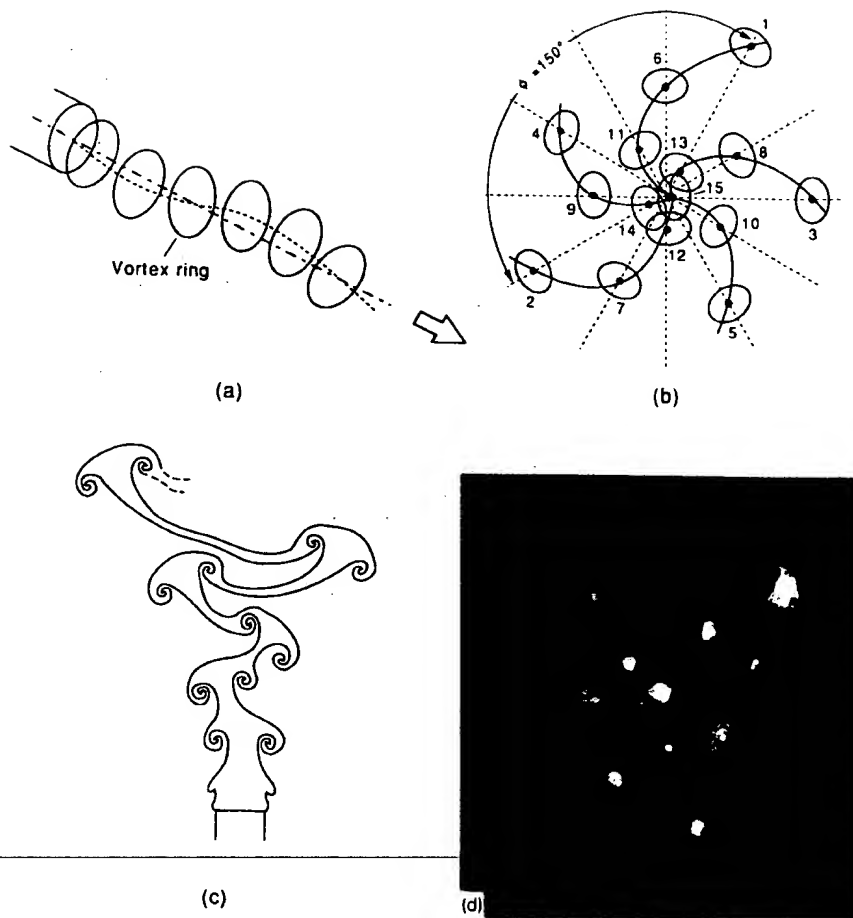


FIG. 9. Manifestations of axisymmetric jet forcing (after Lee and Reynolds, 1985). (a) Succession of ring vortices near nozzle in double mode excitation; (b) locations of vortices in the blooming jet; (c) vortex arrangement in the bifurcating jet; (d) a smoke photograph of the bifurcating jet.

4.2.3. Passive Control

Upstream boundary conditions: Modifying the upstream boundary conditions of a jet provides the easiest way to passive flow control (see e.g. Schneider, 1979; Kuznetsov and Munin, 1982). Significant effects are by necessity limited to the near jet region, i.e. the first, say 10 (equivalent) diameters (geometrically equivalent diameters are defined by expressing the nozzle exit area by an equivalent circular area).

The most fundamental control item is the state of the separating nozzle-wall boundary layer. Its influence was first investigated by Bradshaw (1966) and later by Hill and Jenkins (1976), Hussain and Clark (1977) and Hussain and Hussain (1979). They found its influence restricted to the range of the mixing layer (i.e. the jet's core region), accompanied by a shift of the virtual origin.

Earliest attempts to interfere with the jet's dynamics in the near region were made nearly 40 years ago, when lobed jet-engine nozzles were first used in the attempt to suppress or reduce jet noise. The underlying physical idea was that this corrugation may lead to an early breakup of the large scale (ring-) vortices—the major sources of aerodynamic noise. Since

有实验证明
1979年

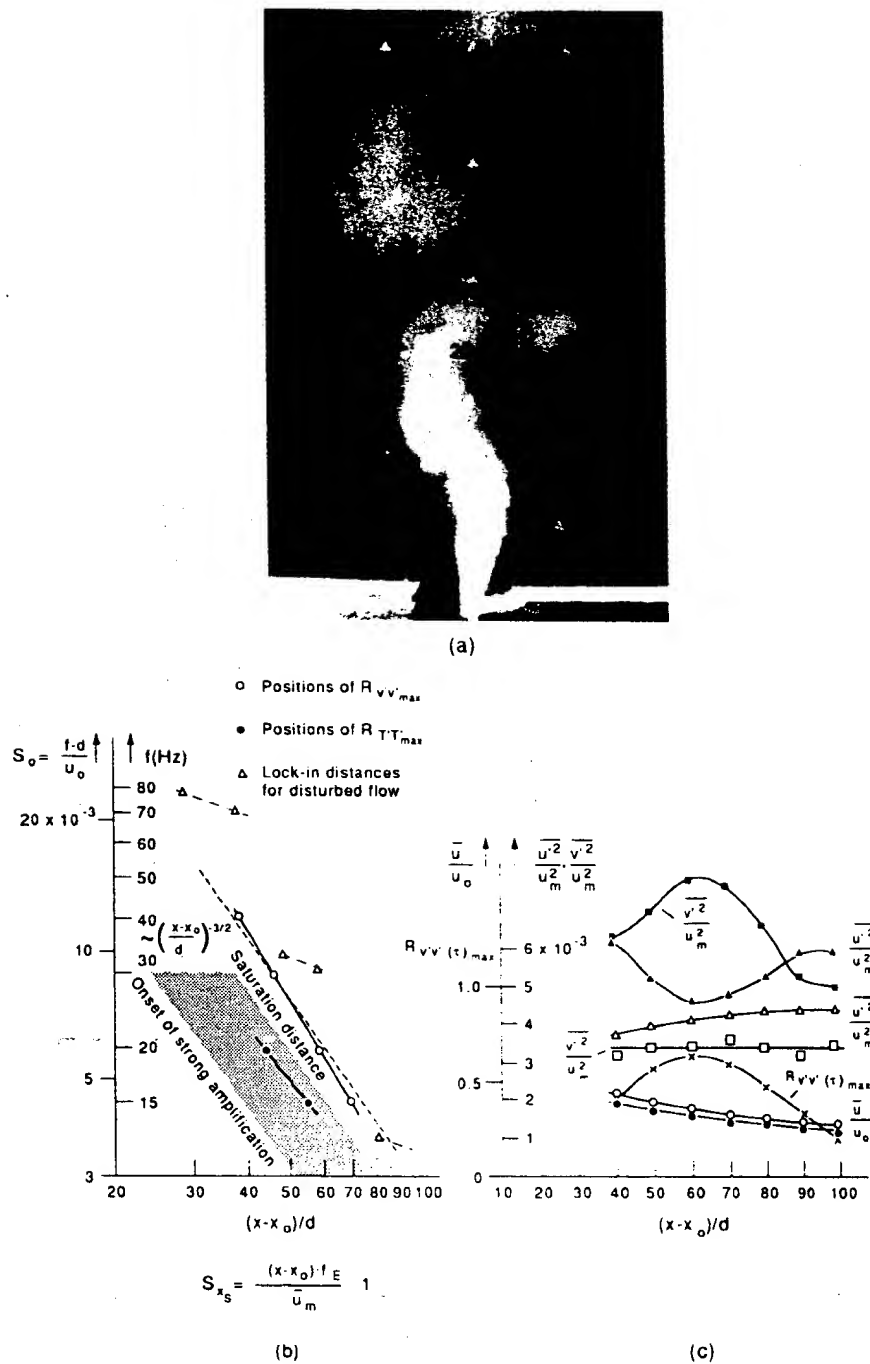


FIG. 10. Characteristics of plane jet forcing (after Korschelt, 1981). (a) Smoke photograph of the excited jet; (b) characteristics of excitation; (c) axial development of velocity parameters in excited jet.

this concept appeared to be successful to some extent, a number of basic investigations on three dimensional jet configurations were carried out with the aims somewhat shifted, particularly towards increasing small scale mixing for improved combustion.

A major body of investigations were reported on jets from elliptic nozzles (Fujii *et al.*, 1981; Gutmark and Ho, 1986; Ho and Gutmark, 1982, 1987; Husain and Hussain, 1983;

Schadow *et al.*, 1986), on triangular jets (Schadow *et al.*, 1988), on square- (Quinn *et al.*, 1985; Quinn and Militzer, 1988), on rectangular jets (Ukhanova and Voitovich, 1984; Krothapalli *et al.*, 1981; Trentacoste and Sforza, 1967), and finally on multiple nozzle-jets (Krothapalli *et al.*, 1979).

The essence of all findings is that the large (coherent) scales are broken up owing to their self induction, which—being inversely proportional to the radius of curvature of the vortex filament—in any non-circular geometry causes a non-planar, i.e. three-dimensional, development, followed by locally increased mixing and frequent break-up and re-connection of the vortex filaments (the so called “cut and connect” phenomenon—as described by Hussain *et al.* (1986)). What leads to the production of small scales from large scale vortices is—in a generic sequence—(1) perturbation of the basic vortex (wave), (2) corner formation, and (3) filamentation, which is finally responsible for the small scale mixing. Mixing is therefore controlled by any kind of perturbation of the basic wave, as was numerically investigated by Zabusky *et al.* (1990).

A particularly clear situation is found with the small-aspect ratio elliptic jet. This provides an effective way to increase the overall entrainment as compared with the circular jet by factors in excess of two, where the major increase is on the ‘long’ sides of the elliptic cross section of the flow. Optimum values of nozzle aspect ratios are between 2:1 and 3:1. Elliptic ring vortices, as they form near the nozzle exit (0 mode) are an unstable configuration. They deform by auto-induction, thereby switching their major axes consecutively, as was theoretically shown by Dhanak and De Bernardinis (1981). As a consequence the elliptical jet’s cross section also switches axes, becoming only gradually axisymmetric (for $x/d \geq 50$)—a fate which all three-dimensional configurations eventually share.

Three-dimensionalization is particularly strong in jets issuing from cornered (polygonal) nozzles. High instability modes are introduced in those corners, leading to early vortex

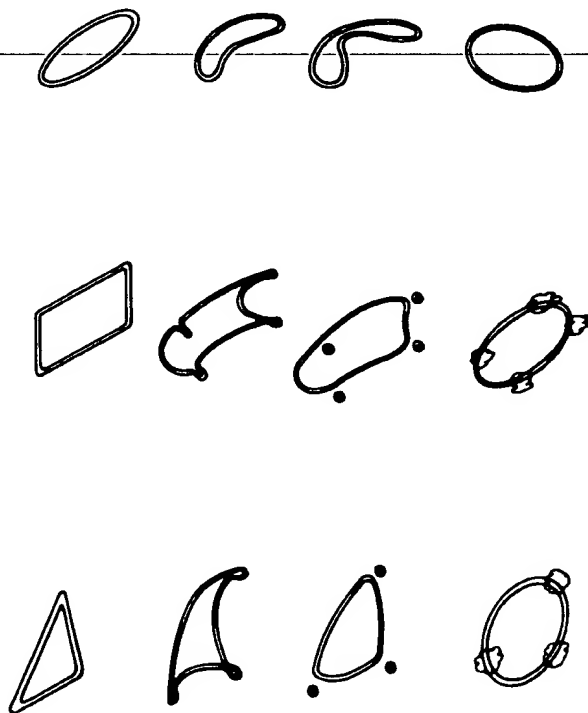


FIG. 11. Ring-vortex development from three-dimensional nozzles: Top: from an elliptical nozzle; middle: from a rectangular nozzle—showing cut and connect behaviour at the corners, leading to rapid diffusion; bottom: from triangular nozzle.

breakup and increase of highly turbulent small scale eddies. In this way selective control of flow coherence is possible and thereby enhancement of fine scale mixing at pre-determined locations. Characteristic three-dimensional vortex developments are sketched in Fig. 11 together with the cut and connect mechanism.

Wlezien and Kibens (1984) looked into the particularly interesting configuration of jets with indeterminate origins, which are produced by round nozzles with exit sections which are either stepped or at an angle less than 90° to the flow direction. It was found that the mean flowfield is significantly modified for the case where the shear layer thicknesses are large compared to the nozzle diameter. The dominant shear layer scales are determined by the local distance from the nozzle lip. The phenomenon of self excitation is also observed, resulting in augmentation of shear layer growth. This is achieved by excitation of the instabilities of those parts of the shear layer which begin further downstream by those which have developed earlier. Control is thus established by modifying the azimuthal distribution of energy in the shear layer instability modes. The directional nature of mixing augmentation may have an application to jet noise and combustion alike.

The response of three-dimensional jets to periodic excitation was found to be even stronger than in the axisymmetric case. This situation has been looked into by Gutmark and Ho (1986) for high forcing amplitudes of 5% U_0 (0 mode) of a 2:1 aspect ratio jet. The initial, most amplified, frequency f_0 was—as in the axisymmetric case—determined by a Strouhal number $S = d_e f_0 / U_0 \approx 0.8$, with d_e the equivalent nozzle diameter (see also Husain and Hussain, 1983). Vortex merging, which is observed in the potential core region at high forcing frequencies ($f_e = 0.65 f_0$) can be suppressed by low frequency forcing ($f_e = 0.45 f_0$). Thus the degree of deformation of the coherent vortices may indeed be effectively controlled. Husain and Hussain (1983) presented measurements of the excited elliptical jet with aspect ratios of 2:1 and 4:1. They measured suppression of axial fluctuations in the Strouhal range of $0.01 \leq S \leq 0.02$ (S_0 = Strouhal number based on the exit boundary layer momentum thickness Θ). Maximum increases of the jet cross-sectional area were found to be around 150% for the 2:1 nozzle and as much as 190% for the 4:1 nozzle at x/d_e when (high amplitude-) forcing at the preferred mode ($S_{de} \approx 0.4$) was applied.

Controlled excitation of non-circular jets of geometries other than elliptic (e.g. square, triangle, rectangle with two aspect ratios) was also studied by Toyoda (1990), who applied preferred-mode- (Strouhal-number $S = 0.4$) and pairing-mode- (Strouhal-number $S = 0.85$) excitation from a loudspeaker in the plenum chamber. Most significant enhancement of mixing was observed for the rectangular jet of aspect ratio 2 at pairing excitation. Glezer (1990) on the other hand applied different forcing modes and different (high) amplitude ratios at the exit of a square jet, using piezo-electrically driven 'flappers'. This opens possibilities to almost shape the jet's cross section and thereby its local diffusivity to any measure desired as well as to bend the jet axis by local modification of the entrainment flux.

Finally we must mention the non-stationary jet described by Breidenthal (1986). It shows reduced entrainment as compared with the stationary jet (see also Kato *et al.*, 1987; Bremhorst and Hollis, 1988).

(Side-) boundary conditions, pressure gradients: Boundary conditions and their effect on turbulent jets do not seem to have attracted many researchers for systematic investigations. The same appears to be true for distortion of the jet's cross section, as e.g. for jets in a finite space of varying geometry. There is, however, one observation of importance: Giger (1987) described the amazing two-dimensionalization of the large coherent structures in a plane jet of small aspect ratio (plane jet in shallow water) as a consequence of secondary motions induced by the (limiting) side walls. This situation is often found in river junctions. Given a jet of transverse width H (= water depth), he defines a near field $x/H \leq 2$, a central field $2 \leq x/H \leq 13$ and a far field beyond. While the near field is characterized by the classical jet behaviour, the central field is dominated by three-dimensional small scale turbulence. The far field finally shows strong meandering of the flow, caused by alternating, two-dimensional vortices, which are described by a Strouhal number $S = fb/U_m \approx 0.1$, where b = local half velocity width and U_m = mean velocity on the jet axis.

Questions of resonance and feedback have only recently attracted scientific curiosity: The term 'resonance' is often used in two different contexts with different meanings: The classical

this maybe useful
for suppression of back-mixing
in reactor

use of the resonance concept implies the existence of an elastic system, capable of performing vibrations when continuously 'driven'. Jets displaying resonant phenomena of this kind are usually of the confined or impinging kind (Gutmark *et al.*, 1978; Rockwell and Schachenmann, 1980; Rockwell and Naudascher, 1979).

In most cases, the phenomenon can be re-traced to a feedback mechanism, which seems to occur also in infinite jet flow (Laufer and Monkewitz, 1980; Hasan and Hussain, 1982). In the latter work it was shown that the self excited axisymmetric jet, driven by a whistler nozzle, has considerably larger fluctuation intensities in the near field than are common for the natural jet (up to about 50%—depending on the whistler geometry). This is also true for the spread and the mean velocity decay, which was observed even as far downstream as $x/d = 50$.

The resonant flapping of the plane jet in the initial region, as reported by Goldschmidt and Bradshaw (1972) and Weir and Bradshaw (1975) on the other hand appears to be a consequence of unintentional, spurious forcing from the facility or the blower, as could be shown by Fiedler and Korschelt (1979).

The other meaning of 'resonance' refers to the energy transfer between the basic and the subharmonic waves in a jet. This may occur whenever the excited waves are non-dispersive. Depending on the overall forcing level the initial phase difference between the two waves may either suppress the resonance mechanism or have no influence. The phenomenon of subharmonic resonance may considerably increase the control range (Cohen and Wygnanski, 1987; Paschereit and Wygnanski, 1989; Mankbadi, 1984; Husain and Hussain, 1989).

Field effects/initial turbulence: Vagt (1969) has investigated the influence of turbulence in the primary flow on the development of a jet (see also Wille, 1963). He found the jet's development essentially unchanged, the only significant effect appeared to be a reduction of core length (i.e. an upstream shift of the virtual origin) with increased turbulence level, owing to the typical increase of shear layer spread for turbulent entrained flow. Virtually the same observations were made by Kleis and Foss (1974) and by Flora and Goldschmidt (1969). No substantial effect of the scale of the initial turbulence was observed. Investigations on the influence of external turbulence for jets in moving streams are not known to the authors. We may assume that again the turbulence in the entrained fluid accounts for an increase of spread (see also Tanner, 1989).

Field effects/density inhomogeneities: The effect of density inhomogeneities in turbulent shear flows is of some technical significance, particularly for heated jets, or jets of gases different from their ambient gas (e.g. in burners). Early studies have provided certain 'recipes' to handle the effects in a global way, e.g. by defining an equivalent, density-ratio dependent nozzle diameter $d_e = d(\rho_j/\rho_0)^{1/2}$ as suggested by Thring and Newby (1952). Other investigations are by Corrsin and Uberoi (1949), v. Ohain (1944) and Eickhoff (1982), the latter being particularly concerned with the jet flame, where, as a consequence of the strong heat release, the coherent structures appear to be noticeably strengthened.

Because of the strong entrainment in a jet, density differences are fast equalized, being of significance only in the near flow field, i.e. in the core region.

Density inhomogeneities may, however, give rise to yet another, much more dramatic, effect: under certain conditions inhomogeneous or heated jet flow may develop a region of global instability (see Section 3.2), as was investigated by Monkewitz *et al.* (1989). Theoretically this condition is expected for density ratios $\rho_{jet}/\rho_{ambient} \leq 0.72$ (under conditions of zero Mach number and infinite Froude number); in the experiment it occurs at a value of 0.69. In the absolutely unstable flow the near region is dominated by a single, self sustained frequency, corresponding to a Strouhal number of $S = 0.44-0.47$. This is accompanied by strong non-linear local growth of the flow. Closer (stroboscopic) inspection then revealed the formation of single ring vortices of high instability, shooting as it were side jets in a radial direction, which accounts for the apparent step-like growth of the flow as seen from visualization. Those side jets were conjectured by the first author to be the consequence of self propelled small secondary ring vortices having separated from the highly distorted primary ring vortices ("cut and connect mechanism"). Proof for this model was indeed only recently provided by Lasheras *et al.* (1990) on the basis of flow visualization.

This growth is found in the temperature profiles, but not, however, in the velocity profiles, which show only a modest variation of growth when compared to the cold jet. Two characteristic smoke photographs—a longitudinal section and a cross section—and the two growth rates for the velocity profile (δ_v/D) and the temperature profile (δ_T/D) versus x/D are shown in Fig. 12. The following symbols are used: D = nozzle diameter, $\delta_{q,T}$ = width of velocity and temperature profile as determined from the intersection of the steepest tangent to the profile with the minimum and the maximum values.

Phenomena of this nature were recently investigated by Sreenivasan *et al.* (1989), Subbarao (1987) and Monkewitz *et al.* (1989, 1990). Raghu (1990), in studying this specific phenomenon, found the side jets to occur also in the convectively unstable homogeneous jet at unusually high forcing amplitudes.

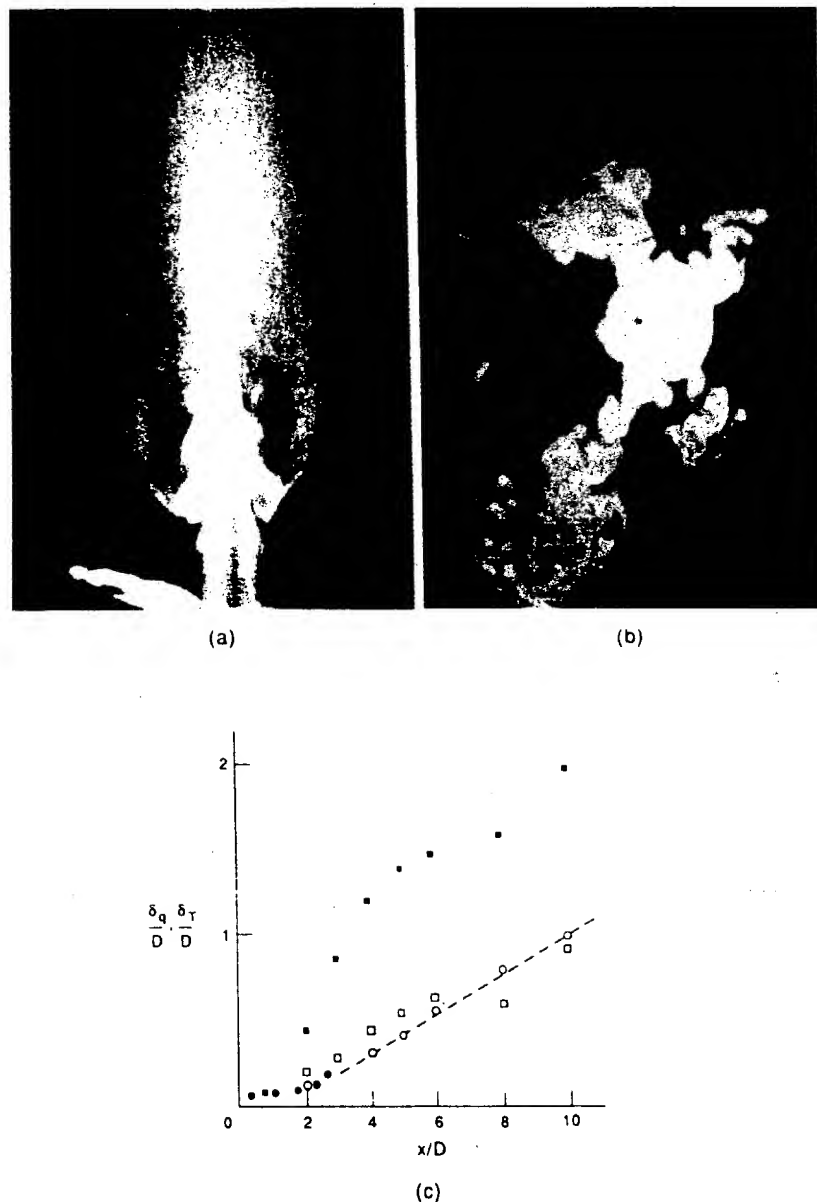


FIG. 12. Jet structures at absolute instability condition as observed in a heated jet (after Monkewitz *et al.*, 1990). (a) Longitudinal cross section; (b) cross section, showing side jets; (c) axial development of spread parameters.

Additives: Other than the characteristic phenomena of reducing small scale structure and thereby increasing the coherence in a turbulent jet in the presence of additives, no details of jet flow structure when treated with additives are known in the literature. This may be a consequence of the fact that most jet flow investigations as well as most practical applications are with gaseous jets, where additives are not applicable. Only quite recently Eriksson and Karlson (1990) have provided us with some insight into the effects of Cationic Surfactant Solutions (CTAB and NaSal) on turbulence and global characteristics of the first few diameters of a confined axisymmetric jet (see also Edberg, 1989).

The following observations are reported: (a) the growth of the jet is smaller in the presence of surfactants, (b) turbulence intensities and shear stress are reduced in the outer part of the jet (i.e. for $y/R > 1$).

A somewhat exotic application—in the context of this review—is the use of additives as spray suppression agents in certain two-phase jet flows (Hoyt *et al.* (1980)—‘antimisting additives’).

4.3. WAKES

Wakes in a stream of constant velocity are only asymptotically self-preserving. In addition they do not seem to reach a universal equilibrium state, developing instead in a way which depends on characteristics of the wake producing body: e.g. its shape and solidity, as was shown by Wagnanski *et al.* (1983). Wake flow is characterized by periodicity (Berger and Wille, 1972), where typical (coherent) structures are similar to those in the jet, with a multitude of modal development in the axisymmetric case. In the two-dimensional case the two dominating modes—the sinusoidal and the varicose—are of comparable strength and probability, showing a tendency towards early developing of three dimensionalities.

4.3.1. Configurations

Again—as in jet flow—we distinguish between two-dimensional, axisymmetric and three-dimensional wake configurations. In all cases, distinction is made between the near region and the far wake. The near region—being of practical interest particularly in structural (environmental) aerodynamics—is essentially dominated by absolute instability of the flow. Accordingly control of the near region requires specific influencing of the flow field to block the feedback mechanism of the fluid mechanical resonance, as was discussed and/or demonstrated by e.g. Berger *et al.* (1990), Strykowski (1986) and Koch (1985).

The far wake is convectively unstable. It can, as was only recently shown by Marasli *et al.* (1990), be dynamically controlled to the same degree as the mixing layer, showing again the characteristic three regions (I, II, III) as described by Oster and Wagnanski (1982). An obvious practical aspect to this is the inherent possibility of changing the signature of wake producing vehicles. The forcing can be applied by either vibrating the wake producing body itself or by an external acoustic field.

The near wake region of plane and axisymmetric configurations, its stability, its structures, and their controllability have been thoroughly studied in recent years by Scholz (1985) for neutral as well as excited conditions, e.g. ‘pumping’ and ‘tumbling’ modes.

Only little is known about the near region of three-dimensional wakes. In their far region they asymptotically approach the axisymmetric case. Specifically for wakes behind bodies with two axes of symmetry—e.g. ellipsoids, elliptic disks, cubes, rectangular disks etc.—the phenomenon of successive switching of the major axes—as in jet flows—is observed.

Control of wake flow has its practical importance particularly in the suppression of the inherent periodicity, which may give rise to unwanted aerodynamic sound (the aeolian phenomenon) as well as to structural vibrations.

4.3.2. Stability, Structures and Control

Wakes can be both absolutely and convectively unstable, depending on the region under consideration. The near wake with its characteristic recirculation is clearly absolutely

in clear jet
maybe it is
worth research

Bräidenthal
& mine shows
side - wake is
another effect

1. 1000
P

1000
1000

unstable unless recirculation is suppressed as might be the case for a porous wake producing body.

Near wake control seems to be possible by some of the following principal ways:

Passively by

- geometrical modifications (two-dimensional: splitter plates (see also Section 5.4.4); three-dimensional: 'Scruton-helix')
- flow alterations (two- and three-dimensional: base bleeding/suction)
- entrainment.

Actively by

- periodic excitation (acoustical/mechanical)
- adaptive techniques with feedback.

Major investigations of the near wake, its turbulent structure and stability behaviour were done by Fuchs *et al.* (1979), Scholz (1985), Berger *et al.* (1990) and by Strykowski (1986). Scholz found the axisymmetric near wake behind a circular disk to be dominated by three instability mechanisms: a high frequency 'shear layer mode' as characterized by the Strouhal number $S_{SL} = f_{SL} D/U_0 \approx 1.62$, a low frequency 'pumping mode' (0 mode) of $S_p = 0.05$, and a (first) 'helical mode' of typically $S_h = 0.135$. Of those three modes only the helical was susceptible for external excitation by tumbling the disk. The pumping mode remained stable to external forcing, which is a clear indication of its absolute instability. The shear layer mode was not investigated.

Thorough studies of stability characteristics in the near wake have been made only for the plane wake configuration (e.g. Berger *et al.*, 1990; Strykowski, 1986; Strykowski and Sreenivasan, 1989). This flow was found to be absolutely unstable (which is also assumed to be the case for the axisymmetric near wake). Consequently, control, i.e. suppression of periodicity, is possible only via modification of the velocity profile. This can be accomplished in various ways, as was demonstrated by Berger *et al.* (1967, 1990), who used base bleeding or high frequency, low amplitude forced oscillation of the cylinder. Suppression of vortex shedding, as accomplished by the latter, is demonstrated in Fig. 13. This figure shows the local amplification of the perturbation amplitude at the most unstable frequency versus time as typically found in absolutely unstable flows, after suppression is released (see discussion in Section 3.2).

The other, well known, possibility of suppression of two-dimensional vortex shedding is by means of a 'control wire' as proposed by Strykowski and Sreenivasan (1989, 1985). These authors proved, that by placing a small cylinder in a certain, well defined region downstream sideways near a vortex shedding cylinder the periodicity in the latter's wake can be completely suppressed and thereby its drag modified.

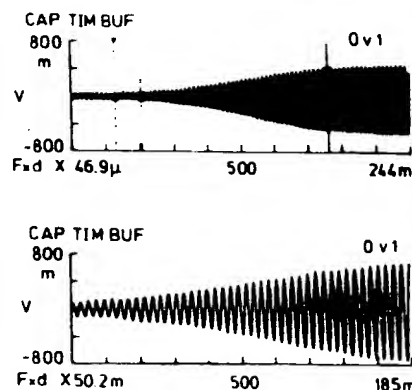


FIG. 13. Characteristic absolute instability behaviour in the plane near wake-onset of vortex shedding after suppression by high frequency vibration of the cylinder (bimorph transducer)—Berger (1989). The lower picture is a time expansion of the upper one.

The intermediate and far plane wake, its stability and structure was studied by Wygnanski *et al.* (1983), by Cimbala *et al.* (1988) and by Hayakawa and Hussain (1989). Possibilities of control of the vortex street of larger scale, which develops in the far wake ($x/d > 100$) at low Reynolds number wakes, as was first observed by Taneda 1959, was recently investigated by Cimbala *et al.* (1989). Other investigations concerned with dynamic wake control were reported by Wehrmann (1967) and Ericsson (1989). Passive (static) control is possible via boundary conditions. Takeuchi and Okamoto (1983) showed, that periodic vortex shedding is suppressed by quenching the flow below a ratio of $c/H = 0.3$ —here c = width of the two-dimensional bluff body (plate) behind which the turbulent wake is produced and H = distance between limiting tunnel sidewalls.

Only limited information is available about field effects. Nakamura and Tomonari (1976) investigated the influence of turbulence on the drag of prismatic bodies. According to their measurements increased turbulence level in the free stream results in increase of drag and base pressure coefficients, while little, if any, effect was found on the Strouhal number. Symes and Fink (1978) have studied the influence of turbulence in the free stream on the overall development of wakes past cylinders. They found the influences on the spread and on the Reynolds stresses strongly dependent on the ratio between the integral scales of the external turbulence and of the wake, with appreciable effects only for ratios > 1 , with maximum effects for scale ratios around 10. 11

4.3.4. Jets and Wakes—their Different Control Behaviour

It is interesting and revealing to compare and juxtapose the different behaviour of jet and wake when exposed to periodic excitations of, say, the 0-th, or the 1st mode as was discussed above.

Obviously, the effect of forcing a structure must depend to a large extent on the ratio between vortex velocity and the velocity by which the structures are transported (other than by their own induction). Or, to be more specific: the velocity field of the jet in quiescent surroundings is a consequence of the induction of the dominating vortices. Perturbation of the latter is therefore directly reflected in the flowfield. Consequently, excitation of a jet structure is of strong and far reaching effect. 10

In a wake, with its prevailing memory of the initial condition, the vortices themselves constitute only a perturbation of the basic convective flow. Their perturbation is therefore only of secondary effect—except for the near-wake region, where the flow is dominated by the large structures and their motion, and where the 'external' flowfield is then of reduced influence. It is for this reason that spectacular effects as e.g. observed by Lee and Reynolds (1985) in the excited jet in quiescent surroundings—will not be found in wake flows, nor can they be expected for jets in a moving stream. The generic picture of jet and wake flow as shown in Fig. 5 may serve to support this explanation.

A special jet-wake combination of some technological relevance is provided by the jet in a counter-stream (König and Fiedler, 1990). Depending on the ratio of the jet velocity over the ambient (counterstream) velocity $R = U_j/U_0$ we observe two different flow situations. A highly unstable flow for $R > 1.4$ where control by periodic forcing is of no visible effect. This may be understood in view of the fact that the random motion of the flow in the stagnation region is of high amplitude, thereby causing phase scrambling of any periodic wave imposed onto the flow. However $R < 1.4$ the jet immediately wraps around the nozzle and creates a wake of some receptivity to periodic excitation in different modes as is observed in the true wake. 10 11

4.4. MIXING LAYERS

Mixing layers have for a long time been favourite 'pets' for turbulence researchers, surpassed in the number of papers devoted to them only by those on the wall boundary layer. This is easily understood since the mixing layer represents the 'cleanest and clearest'

scenario for a free turbulent, non-decaying flow, being somewhat of a hybrid between jet and wake. For both flows the mixing layer provides the first—transient—configuration. General introductions and surveys on this flow are provided by Birch and Eggers (1972), Ho (1981), Fiedler *et al.* (1981), Browand and Ho (1983), Ho and Huerre (1984) and by Fiedler *et al.* (1989).

4.4.1. Configurations

Classical objects of research are the plane mixing layer between parallel streams of 'infinite' extent and the axisymmetric layer (which was dealt with in Section 4.2)—two flows of limited self similarity.

In the general case the layer is formed between two streams of different velocity U_1 and U_2 ($< U_1$). There is sufficient experimental support for the general validity of a transformation—usually known as the 'Abramovich–Sabin rule'—by which the results for mixing layers between streams of different ratios U_2/U_1 can be reduced and generalized. Introducing a velocity parameter $\lambda = (U_1 - U_2)/(U_1 + U_2) = \Delta U/\Sigma U$ we find for the ratio of the local width b : $b(\lambda, x)/b(\lambda = 1, x) = \lambda = b/b_0$, and, correspondingly, $f/f_0 = 1/\lambda$ etc., where the index 0 defines the case of the one-stream layer. The relation between local width—as defined by the momentum thickness

$$\Theta = \int \frac{(U - U_1)}{(U_2 - U_1)} \left(1 - \frac{U - U_1}{U_2 - U_1} \right) dy$$

and downstream position x is given by $\Theta/\lambda x \approx 0.032$.

In recent years this group of basic flow geometries was extended, following a growing interest in controlling the flow via boundary conditions. Thus constraining and distorting geometries were looked into and finally the study of the general three-dimensional mixing layer between two non-parallel streams in a parallel plane was taken up by the first author.

4.4.2. Structures and Stability

We shall restrict ourselves to discussing only the plane flow. In the parallel case there is a relatively simple picture of a coherent structure to start with: the line vortex with its axis parallel to the trailing edge as a consequence of Rayleigh instability. After its creation, secondary instability soon sets in, resulting in a deformation and spanwise undulation of those vortices. The evolving pictures of the complete structural scenario as suggested by Bernal (1981), and by Hussain (1986) are shown in Fig. 14. A general survey on the structure of the two-dimensional mixing layer is given by Browand and Ho (1983)—see also Browand and Weidman (1976).

Streakline visualizations—e.g. by Konrad (1976)—have revealed the typical spanwise (large scale) structures and the superimposed longitudinal vortices (the streaks), where the latter are usually triggered and their spacing determined by minute upstream irregularities in the flow. Only the complete three-dimensional structure provides for turbulent (small scale-) mixing, the enhancement of which therefore requires the production of three-dimensionalities.

Although beyond an overall Reynolds number of $Re_x \approx 10^5$ the global rate of spread of the flows seems to be constant (Birch and Eggers, 1972) there is a so called 'diffusion critical Reynolds number' (defined by Konrad, 1976)

$$Re_{\delta, crit} = (\Delta U)^2 / \nu (dU/dy)_{max} \approx 10^4$$

below which turbulent mixing is at a very low level. This critical Reynolds number was determined e.g. from the 'unmixedness' (see again Konrad, 1976).

First theoretical investigations of the spatial development of laminar free boundary-layer flow stability were made by Gaster (1962), Michalke (1965) and Kelly (1967a, b). Experimental corroboration was provided by Freymuth (1966). The applicability of the laminar

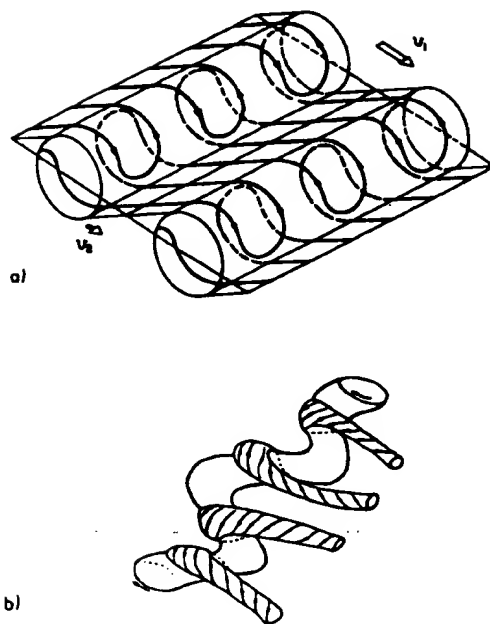


FIG. 14. Structures in a plane mixing layer. (a) According to Bernal (1981); (b) according to Hussain (1986).

instability concept to turbulent flow and the subsequent creation of coherent structures was probably first suggested by Fiedler *et al.* (1981). The idea was further developed and established by Ho and Huerre (1984) and by Gaster *et al.* (1985). Monkewitz and Huerre (1982) showed that instability is strongest for a velocity parameter $\lambda = \Delta U / \Sigma U = 1$ (the one-stream layer), reducing with reducing velocity parameter. Koochesfahani and Frierer (1987) and Lummer (1989) obtained stability results for shear layers separating fluids of different density, and finally Cohen and Wygnanski (1987a, b), and Wygnanski and Weisbrot (1988) investigated questions of wave dispersion and subharmonic resonance as well as the phenomenon of pairing.

4.4.3. Active Control

Dynamic control/periodic excitation: This was probably the first conscious application of mixing layer control and an excellent survey is given by Ho and Huerre (1984). Some early investigations of the axisymmetric case date back to the 1950s (e.g. Wehrmann, 1957; Michalke and Wehrmann, 1962). Yet only in the 1970s did this technique (adopted primarily as a means to stabilize the structural flow pattern for easier experimentation) become of serious interest and detailed investigation in plane flow undertaken (Bechert and Michel, 1975; Oster *et al.*, 1976; Oster *et al.*, 1978; Fiedler *et al.*, 1978). Many aspects were further clarified by a host of investigations to follow, the major results of which are summarized by Ho and Huerre (1984). Here we can only mention a selected number of those papers: Bechert (1982), Bechert and Stahl (1984), Dziomba and Fiedler (1985), Fiedler and Mensing (1985), Fiedler and Thies (1978), Oster and Wygnanski (1982), Morkovin and Paranjape (1971), Weisbrot and Wygnanski (1988), Wygnanski and Peterson (1985).

The basic and obvious achievement of single-frequency forcing is a local widening of the flow of order 100%, accompanied by an increase of the Reynolds stresses and the coherence (stabilization) of the dominating structures. For very high excitation amplitudes we find regions of negative spread rate and negative production. The entrainment flux undergoes a maximum, followed by a minimum, after which the flow only gradually and asymptotically returns to its neutral state. The essence of this is sketched in Fig. 15.

useful for later

what is the curve compared with no excitation?

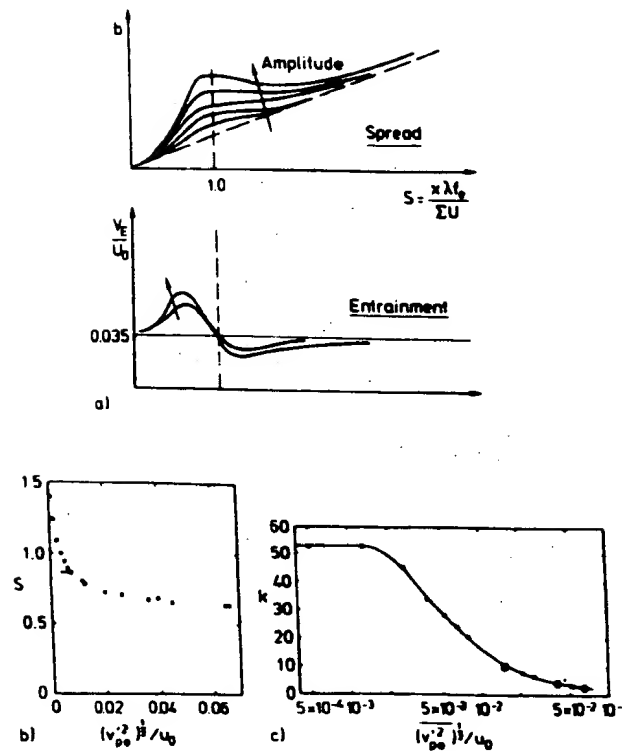


FIG. 15. Characteristics of excited plane mixing layer (after Mensing, 1981). (a) Top: local non-linear spread Θ , depending on excitation amplitude, vs generalized Strouhal number S ; below: typical variation of the normalized entrainment velocity V_E/U_0 ; (b) generalized Strouhal number for excitation frequency f_e and location of maximum periodic signal content in the excited flow vs relative excitation amplitude at trailing edge; (c) amplification k of excitation signal in the flow vs relative excitation amplitude at trailing edge.

Recent investigations concentrate on rather more elaborate excitation schemes, for example by multiple frequency forcing (Ho and Huang, 1982), wave packets, amplitude modulated excitation, three-dimensional forcing etc. (Fiedler *et al.*, 1989; Nygaard and Glezer, 1989), by which specific influences—particularly on small scale mixing—can be exerted.

4.4.4. Possibilities of Passive Control

Static—upstream boundary conditions (splitter plate, boundary layer(s)): Probably surprised by the unexpectedly high spread rate of a one-stream mixing layer, as was reported by Wygnanski and Fiedler (1970)—who had investigated the mixing layer developing from a tripped boundary layer—Batt (1975) and Foss (1977) investigated the different developments of turbulent mixing layers starting from laminar and from turbulent (tripped) wall boundary layers. Later investigations concerning the effect of splitter plate geometry and the boundary layer(s) were made by Hussain and Zedan (1978), Husain and Hussain (1979), Dziomba (1981), Gurecki (1981), Dziomba and Fiedler (1985), Roberts (1985) and Mehta (1990).

According to most investigations the length of the development region from the boundary layer state to the final asymptotic mixing layer state is

$$400 \leq x_{\text{asymptotic}} \lambda / \Sigma \Theta \leq 600,$$

where $\Sigma \Theta = \Theta_1 + \Theta_2 + h_{TE}$ = sum of the momentum thicknesses of the two boundary layers at the trailing edge plus the thickness of the trailing edge itself. In the case of a one-stream layer $\Sigma \Theta = \Theta$. This is (fortunately) clearly less than the conservative value of 1000,

which was proposed for the first time by Bradshaw (1966) and has been taken as a standard since then.

In the transition region the spread rate and the turbulence level is generally below the asymptotic for the turbulent boundary layer, while the mixing layer, developing from a laminar boundary layer experiences an overshoot of spread rate and turbulence intensity (owing to the highly agitated flow during the L/T transitional process), before reaching asymptotic values. For equal momentum thicknesses the tripped flow—while providing a better defined upstream condition—needs slightly longer to reach the asymptotic condition.

Again—as in the case of dynamic control—later works were more concerned with three dimensional aspects. Lasheras and coworkers (Lasheras and Choi, 1986; Lasheras *et al.*, 1986) investigated the (low Reynolds number) flow behind sinusoidally indented and corrugated splitter plates. Three-dimensionality was introduced by Nygaard and Glezer (1989) by most elaborate heating schemes on the splitter plate of a two stream water tunnel, whereby almost any conceivable two- and three-dimensional static and dynamic forcing condition at the splitter plate can be adjusted. This scheme permits the introduction of longitudinal vorticity in a predetermined way and thus for selective control of small scale mixing enhancement.

Changing the geometry of the test section of a given flow—i.e. its 'ambient'—offers a variety of simple and at the same time amazingly efficient possibilities to influence and manipulate the turbulence structure, and in turn the integral development of a mixing layer over a longer range. Some possible influences of boundary conditions—static and dynamic—have been discussed by Fiedler *et al.* (1981, 1989). The following cases may serve as examples.

Pressure gradients: Small, inadvertent pressure gradients from the growing wall boundary layers in a closed test section are often responsible for discrepancies in the spread rate of otherwise identical mixing layers. This question was looked into by Dziomba (1981). Fiedler (1984, 1989) and Fiedler *et al.* (1990) studied the plane mixing layer between two convectively accelerated parallel streams of different velocities $U_1(x)$ and $U_2(x)$, where the (negative) longitudinal pressure gradient was tailored for constant characteristic frequency $f_c \sim \Sigma U/b$ (we recall that in the parallel mixing layer $f_c \sim 1/x$). This specific flow provides for extreme structural simplicity, showing a quasi frozen pattern of a certain structural manifestation which does not—or scarcely—include evolutionary phenomena such as pairing. Still, the spread of the mixing region, being $b \sim (x - x_0)^{1/3}$ is found to follow the Abramovich-Sabin rule as applied to local values, although being in essence a sole consequence of coherent vortex decay. Periodic excitation of this flow has—contrary to what is typical for the layer in zero pressure gradient—an overall effect in x , where again increases of the order 100% are found possible.

The opposite of this apparent stabilization (and thus 'deactivation' of structures and of mixing) in the accelerated flow is to be expected for decelerated mixing layers, where coherent structures experience reduced life-times, i.e. accelerated dynamic evolution, followed then by an increase of the small scale constituents. A numerical analysis by discrete vortex simulation was only recently presented by Böttcher (1990), where accelerated, neutral, and decelerated mixing layers are studied and juxtaposed. Figure 16 demonstrates reduced mixing activity in the accelerated flow and enhanced mixing (and spread) in the presence of a positive pressure gradient (decelerated flow) as compared to the neutral case.

Aspect ratio and feedback: Growth and structure of a free mixing layer are found to be considerably influenced by the lateral extent of the flow at reduced relative side wall distance. First investigations of this condition in a one stream layer ($\lambda = 1$) were reported by Hilberg and Fiedler (1989): with increasing aspect ratio $\Lambda = L/h$ (where h is the sidewall distance and L the length of the test section—see Fig. 17) a periodicity develops in the fluctuation spectrum, accompanied by considerable increase of spread. The amplitude of this periodicity reaches saturation for around $\Lambda \geq 40$, corresponding to a ratio of $h/\Theta_L \approx 1$ (Θ_L = momentum thickness of the mixing layer at the test section exit).

This effect, which appears quite spectacular in flow visualization and less so in the measurements, is demonstrated in Fig. 17. Here we have a clear case of feedback of pressure

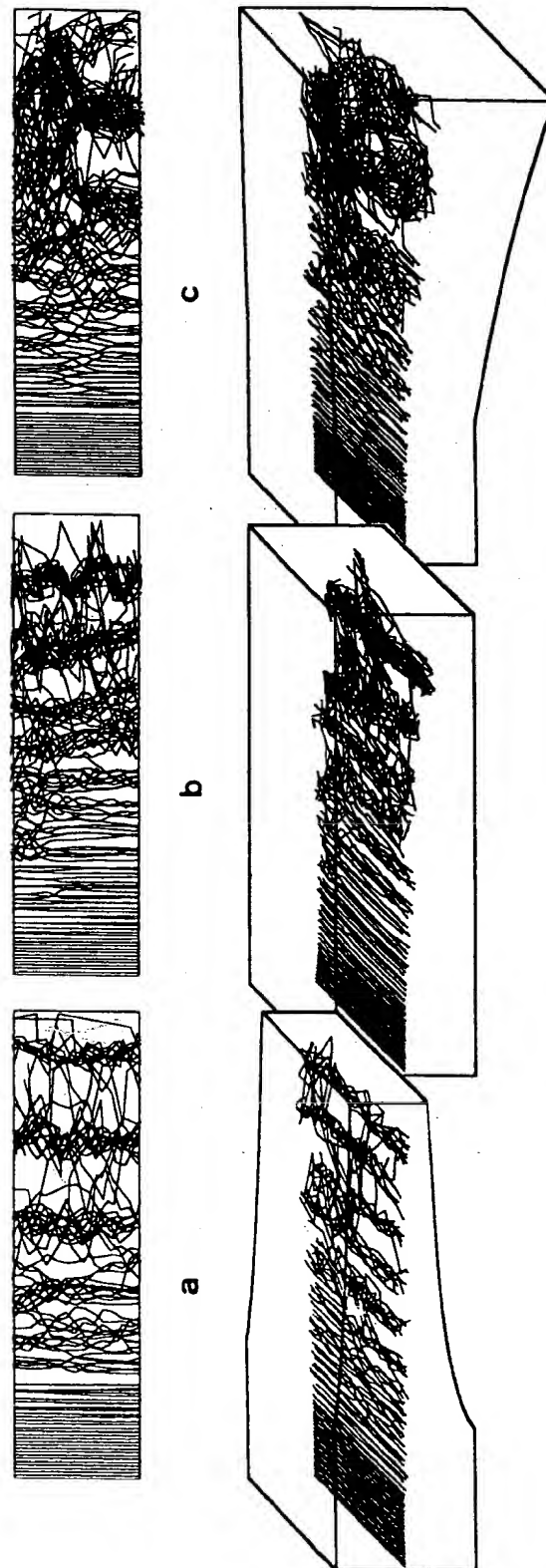


FIG. 16. Discrete vortex simulation of mixing layer flows (Böttcher, 1990). (a) Accelerated flow; (b) parallel flow; (c) decelerated flow.

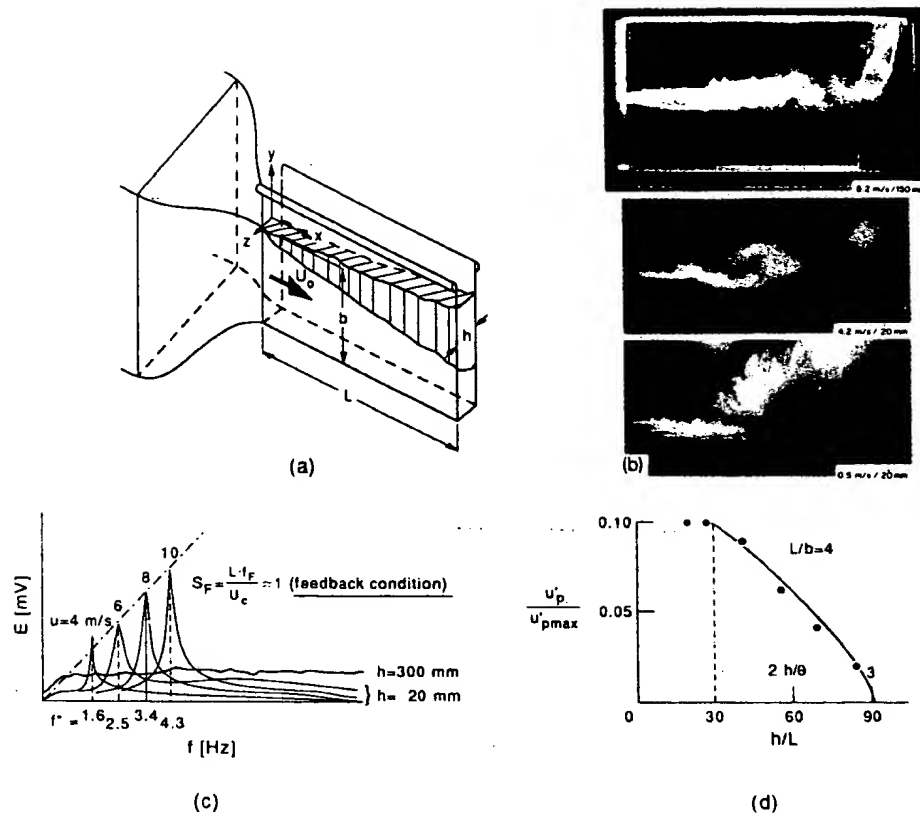


FIG. 17. Narrow mixing layer with feedback manifestations. (a) Experimental configuration; (b) juxtaposition of smoke pictures for different aspect ratios; (c) spectra; (d) relative periodic signal content (measured at $x = L$) vs aspect ratio. Saturation condition at $h/\theta \approx 1$ (θ = momentum thickness of mixing layer at $x = L$).

waves from the two trailing edges of the test section side walls to the trailing edge of the mixing layer (a feedback effect of this kind was conjectured already by Dimotakis and Brown (1976)). Those pressure waves are uncorrelated at large values of h , and then unable to maintain a feedback cycle. According to the discussion in Section 2.1 the feedback frequency scales with a Strouhal number of $S_F = fL/U_p \approx 1.0$ (as compared to the ordinary mixing layer mode with its typical scaling law $S_{ML} = fx/\Sigma U \approx 0.80-0.85$).

Suppression or attenuation of the feedback loop is possible by modification of the sources of the feedback signal, i.e. the sidewall trailing edges by short flexible (energy absorbing) or by indented (scrambling) trailing edge extensions. Reduction of the feedback effect is also provided by increased turbulence level of the basic flow and by reducing the relative distance b of the bottom wall of the test section from the mixing layer. This is a consequence of flow stabilization, as was only recently shown by Michalke (1990).

Only during the final preparation of this manuscript an investigation by Buell and Huerre (1988) became known to the first author, in which on the basis of a numerical simulation global resonances of the kind observed in the experiment are conjectured.

Phenomenologically similar observations of developing strong periodicity, which are, however, caused by different physical mechanisms, were reported by Giger (1987) for two-dimensional jets in shallow water (e.g. river inlets). Active feedback interaction experiments in a shear layer have recently been reported by Dimotakis and Koochesfahani (1987)—see also Fiedler *et al.* (1978).

Flow distortion: Another passive/static tool for controlling the development of a mixing layer is provided by flow distortion: this phenomenon was first investigated by Keffer *et al.* (1978) and later by Paschereit *et al.* (1989) in a test section, the cross section of which

gradually changed from a square of 0.3×0.3 m to a rectangle of equal area with dimensions 0.15×0.60 m over a length of 1.2 m (i.e. no longitudinal pressure gradient). This test section could be rotated around its longitudinal axis. Control of the flow was thus achieved by imposing axial strain on the coherent structures. Compression destabilizes these structures, causing increase of spread, accompanied by appropriate reduction of the Reynolds stresses, proportional to the maximum gradient of the mean velocity distribution. Stretching of the dominating vortices has the opposite effect. This behaviour is approximately described by rapid distortion theory (see Sreenivasan and Narashima, 1974; Takaki, 1975).

Curvature: Limited experiments on the influence of curvature on a two stream mixing layer were done by Dziomba and Fiedler (1979) in a test section with flexible walls. In this case one has to distinguish between stabilizing (towards the low velocity side) and destabilizing curvature. Accordingly increased spread was measured in the destabilizing configuration and vice versa.

Additives: This important aspect (Toms' (1948) effect) was—among others—studied by Kwade (1982) and by Riediger (1989), who found the effect of small amounts of long chained high-polymers (e.g. Separan) to be a significant reduction of small scale turbulence (corresponding in effect to a laminarization, i.e. suppression of dissipation), which in turn strengthens and stabilizes the coherent transverse vortices. The total spread was found to be smaller in the presence of additives—owing to different initial behaviours of the two flows—yet the spread rate was higher by more than 40%.

Turbulence level: The rather disturbing so-called Dubuat's (1779) paradox, according to which the drag of a body at rest in a moving fluid by far exceeds that of a moving body in a fluid at rest turned out to be on closer inspection an early example of flow control by disturbed flow conditions (high turbulence level).

Dziomba (1981), Tavoularis and Corrsin (1981), Chandrsuda *et al.* (1978) and Tanner (1989) have invested some effort in the study of the consequences of turbulence in the primary streams on the flow development. Dziomba found the flow to reach an early self similar state for initial (but decaying) turbulence levels of approximately 2%, exceeding the rate of spread for low turbulence levels at otherwise the same conditions by approximately 10%. While this is in agreement with expectation, the reduced turbulence level (by again 10%) is yet to be explained. Tavoularis and Corrsin and Chandrsuda *et al.* were rather concerned with questions of structures. Particularly in the work of Tavoularis and Corrsin it was shown that the turbulence level does not seem to interfere with the (spontaneous) creation and development of coherent structures, which appears contradictory to the findings reported by Chandrsuda *et al.* Tanner gives spread rates for different external turbulence levels, which he finds strictly on theoretical grounds. His results (which need experimental corroboration) show, that in any case—according to expectation—increased external turbulence levels give rise to increased spread. The overall effect depends on the velocity parameter λ . It is almost negligible for $\lambda \approx 1$, becoming, however, significant for small values of λ , e.g. 100% spread increase for, say, $\lambda = 0.14$ and a turbulence level of (only) 3%. Tanner's results may be approximately described by the relation $b_T/b_0 \approx (Tu_1^2 + Tu_2^2)60/\lambda + 1$, where b_T = flow width in the presence of external turbulence, b_0 = flow width at negligible external turbulence, and $Tu_{1,2}$ = Turbulence intensity of streams 1 and 2 respectively.

Taking a 1% increase of the spread as a critical value we find—on the basis of the above—a critical value for external turbulence to be $Tu_{\max} \approx 0.002 \sqrt{\lambda_u}$, or—more generally—external turbulence ought to be two orders of magnitude below the maximum level produced in the mixing layer itself. Thus, for flows with low λ_u , external turbulence may be highly influential, which, by usual standards, is considered 'innocent' (see also Mehta (1990)).

Density inhomogeneities: Influences of density differences of the two streams on the strength of coherent structures have been investigated by Rebollo (1972) and Brown and Roshko (1974)—amongst others. This problem has only recently been revisited by numerical (direct simulation) and experimental methods (Lummer, 1989; Fiedler *et al.*, 1990; Nottmeyer, 1990). It was found that the influence of density ratio on the formation of

coherent structures and mean spread is well described by stability theory. Coherent structures are stabilized (and thereby the spread reduced) in a situation where the higher density is on the high velocity side and vice versa ('co-gradient' and 'counter-gradient' configuration). The quantity most sensitive to the density ratio is the ρ - u correlation, while the ρ - v correlation remains largely indifferent to the inhomogeneity. Clearly the overall spread is a function of the density ratio, being larger in the counter-gradient case, with pronounced effects on the low density side of the flow. On the basis of his measurements Nottmeyer suggests an extended 'Abramovich-Sabin rule' for the spread of the density field:

$$b/b_{00} = \lambda_u(1 - 0.627 \tan h(2\lambda_\rho)), \quad \text{where } \lambda_\rho = (\rho_2 - \rho_1)/(\rho_2 + \rho_1).$$

Interactions: Various cases of flow interaction and self sustained oscillation are described by Rockwell and Naudascher (1979). Wood and Bradshaw (1982), Bradshaw and Weir (1974), Ziada and Rockwell (1981) and Wygnanski *et al.* (1979). The influence of the system response on the coherent structures in a confined shear layer was studied by Veynante *et al.* (1986).

4.5. MIXED CONFIGURATIONS OF FREE- AND WALL-BOUNDED FLOWS

A flow of high practical appeal and value is the boundary layer at incipient separation. Given the possibility to control this kind of flow, thereby preventing or delaying separation, we would have an instrument to control the aerodynamic performance—and in particular the lift—of an airfoil. Again such a separating boundary layer may be influenced by passive or by active means. Separation on an airfoil may be caused by genuine separation of the boundary layer itself or by bursting of the leading edge separation bubble. In both cases the wall boundary layer leaves the wall and develops into a free shear layer, though still influenced on one side by the wall. Since the free shear layer is by far more susceptible to control than the boundary layer it is the former which can be influenced most easily. Control and manipulation of these phenomena are discussed in Sections 5.4.2 and 5.4.3 below.

5. WALL-BOUNDED TURBULENT SHEAR FLOWS

5.1. INTRODUCTORY REMARKS

Betz (1961) reports that Prandtl controlled the separation of a boundary layer on a cylinder by suction as early as 1904 and reduced the drag of a blunt body by two counter-rotating cylinders at the trailing edge in 1910, modelling a "ship of zero 'drag' resistance". So boundary layer control was a method developed together with boundary layer theory itself. As so often before, progress in these two fields has come on a large scale from efforts to increase the efficiency of aircraft. The history of flow control and management up through the 1950s is well documented in the two volumes *Boundary Layer and Flow Control*, edited by G. Lachmann (1961). With the enormous increase in fuel costs during the oil crisis of the 1970s, increased efforts have been undertaken to increase lift and to reduce drag for all kinds of aircraft configurations. The recent host of investigations has been initiated and guided by NASA Langley with very interesting results in the fields of drag reduction and separation control. Separation, which more often than not has a detrimental effect on a flow configuration is of course no prerogative of aerodynamics. Its control also concerns, for example, fluid machinery and the chemical process industry. Typical applications of turbulence control in wall flows, as listed by Bushnell and Mc Ginley (1989) are heat- and mass-transfer augmentation/minimization, combustion optimization, control of pressure fluctuations, and increased propulsor efficiency. The same authors have also compiled a list of the more obvious control parameters which opens up many alleys for as yet unexplored possibilities of control.

Turbulent wall-bounded shear flows can be manipulated and eventually controlled by influencing upstream and boundary conditions which affect the physical processes in the

shear layer as expressed by the conservation laws and the transport equations, e.g. for the kinetic turbulent energy where we find terms which characterize convection, production, diffusion and dissipation. Influencing these terms may lead to a manipulation of the turbulence in various ways:

- increasing the small fluctuations inherent in a flow triggers the flow to become transitional and fully turbulent,
- maintaining or increasing the turbulent energy prevents separation or decreases form drag,
- decreasing or minimizing turbulent energy reduces viscous drag.

We intend to deal with the last option only briefly, except as coupled with the prevention of separation. For an extensive discussion of the effects of (a) riblets (longitudinal grooves in the wall) attention is drawn e.g. to Section 5.2.3.3 and to review papers by Wilkinson *et al.* (1988) and Bechert (1990), of (b) LEBUs (large eddy breakup devices) to an investigation by Sahlin *et al.* (1988), and of (c) polymer additives, to Hoyt (1979). These are by no means the only important methods to reduce the viscous drag of a surface but probably the three most common ones. Furthermore it should be noted that viscous drag reduction does not necessarily require a reduction in the overall turbulent energy level of the flow; it suffices to change some flow characteristics in the vicinity of the wall which affect the skin friction. On the other hand, in a re-laminarizing boundary layer the integral of the turbulent kinetic energy normal to the wall remains approximately constant while the skin friction rises (Blackwelder and Kovasznay, 1972). So the ultimate in turbulence suppression is not relaminarization but any successful attempt to preserve laminar flow by delaying transition.

It is also obvious that intrinsically unstable flows, such as free shear layers or separated boundary layers, lend themselves more easily to manipulation and control than intrinsically stable flows, such as boundary layers far from separation.

5.2. MANIPULATION OF TURBULENCE BY BOUNDARY CONDITIONS

5.2.1. Introductory Remarks

The importance of boundary conditions is evident from Prandtl's paper (1904) in which he showed that an adverse pressure gradient can lead to separation of the boundary layer from the wall and that suction at the wall can delay separation (Betz, 1961). Both boundary conditions change the turbulence structure of the boundary layer, suction in the near-wall region and the pressure gradient both in the inner and outer layer. As far as boundary conditions at the outer edge of the boundary layer are concerned we deal here with the influence of the pressure distribution (Section 5.2.2), and the free-stream turbulence (Section 5.3.2), and with vorticity effects (Section 5.3.4). Wall boundary conditions may be divided into two groups, direct and indirect ones. Direct ones, such as the normal component \bar{v} (suction or blowing) and the wall temperature T_w (heating or cooling), enter the boundary layer equations directly, whereas the inclusion of the effects of riblets and of compliant walls need additional considerations. Here we shall describe only the physical mechanisms and their effects on the structure of turbulence with the main emphasis on separation.

5.2.2. Separation Control by Manipulation of the Pressure Distribution

① In a boundary layer an increase of the static pressure in the streamwise direction leads to a decrease of the skin friction and, often, to separation of the flow from the wall. Since the pressure distribution is dependent on the shape of the body, the surface of the body can be tailored such that the flow is kept close to separation along a fixed distance with skin friction nominally zero. To prevent separation and yet obtain a large pressure rise, the pressure should increase sharply where the boundary layer is thin and then flatten off as

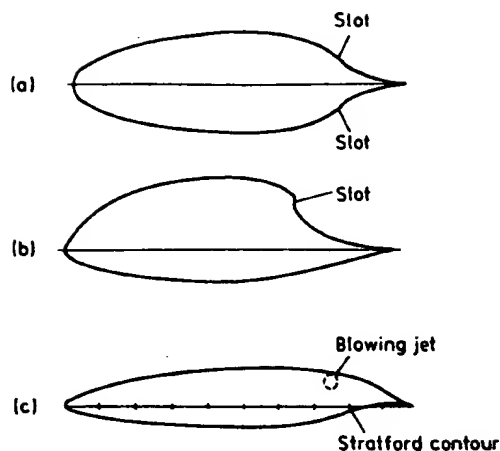


FIG. 18. (a, b) Suction aerofoils of Griffith type from Head (1961); (c) antiseparation tailored contour laminar aerofoil from Mask (1980).

separation threatens. Prandtl (1935) appears to have been the first to solve this inverse boundary layer problem. He calculated the pressure distribution for a laminar boundary layer which remained on the verge of separation (zero skin friction), thus allowing a maximum pressure recovery. It is possible that such a contour was used for the rear part of laminar aerofoils of the Griffith type as early as 1943* (Fig. 18a and b, taken from Head, 1961). The idea was definitely used, now called a 'Stratford diffusion contour' (Stratford, 1959a) for an antiseparation tailored contour (ATC) laminar aerofoil design (Fig. 18c, taken from Mask, 1980) at the rear of the pressure side of the aerofoil.

In 1959 Stratford (1959b) published the results of an experiment in which he proved that a stable turbulent boundary layer with "near zero skin friction" could be generated. At the time and even later in the investigations of Spangenberg *et al.* (1967) and Fernholz (1968) measurement techniques were not sophisticated enough to perform measurements of skin friction near incipient separation and of velocity profiles with instantaneous or mean reverse flow. Only by using a wall pulsed-wire probe to determine accurately the occurrence of zero skin friction was it possible to achieve the matching pressure distribution (Dengel and Fernholz, 1990). The pressure distribution generating zero skin friction along a prescribed distance also generates a larger boundary layer thickness than for a pressure distribution where skin friction is still positive and thus a higher momentum loss in the wake of the body. Winter and East (1982) showed that for a diffuser with the velocity distribution $u \sim x^m$ (where m is -0.3) the loss of mechanical energy is about half that for a flow with incipient separation. The 'limit approach' (nearly separating condition) has been applied to the design of diffusers at low and high subsonic flows (e.g. Stratford and Tubbs (1965) and Fernholz (1966), respectively, and more recently Strawn and Kline (1983) and Härtl (1989)) and of aerofoils (e.g. Liebeck (1973) and Mask (1980)).

As pointed out by Bushnell (1983) there is, however, the off-design sensitivity which may cause difficulties, i.e. separation may occur on an aerofoil due to small angle-of-incidence excursions with a consequently large drag increase. This sensitivity problem was addressed by Dengel and Fernholz (1990) who studied three boundary layers in which the skin friction was either approximately zero, slightly negative or slightly positive along a fixed length. These three different skin-friction distributions were generated from slight variations in the upstream pressure distribution. A survey of the distributions of three boundary layer wall

* A. D. Young kindly informed the authors that according to his recollection separation was controlled by slot suction on this type of aerofoil.

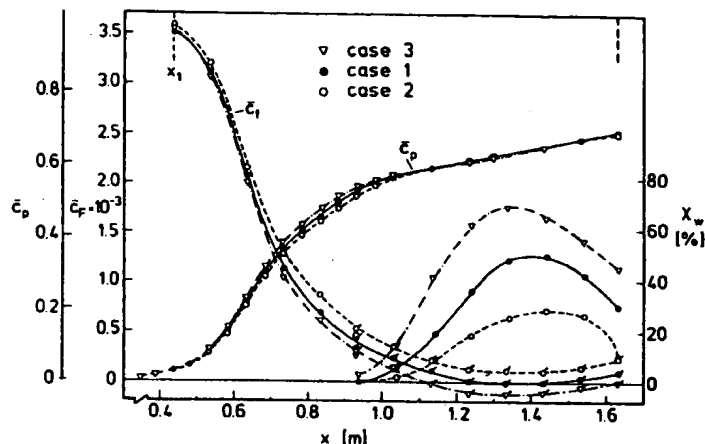


FIG. 19. Distributions of pressure coefficients \bar{c}_p , skin-friction coefficient \bar{c}_f , and reverse-flow parameter χ_w for three 'near zero skin-friction' boundary layers from Dengel and Fernholz (1990).

parameters is shown in Fig. 19. \bar{c}_p is the pressure coefficient $(\bar{p}(x) - p(\text{ref})/(0.5\rho u_0^2))$, where \bar{p} is the static pressure, $p(\text{ref})$ the static pressure at the position where the reference velocity u_0 is measured, and ρ the density; \bar{c}_f is the skin-friction coefficient $(\bar{\tau}_w/(0.5\rho u_0^2))$, with $\bar{\tau}_w$ as the mean value of the skin friction; and χ_w is the wall value of the reverse-flow parameter. χ_w is defined as the fraction of time the flow travels in the upstream direction as measured by the wall pulsed-wire probe and it shows distinct differences between the three cases. The deviation of χ_w from zero is indicative of a change of the turbulence structure from its typical adverse pressure gradient behaviour even well upstream of separation.

Stratford's separation criterion was adapted to axially-symmetric flow by Smith (1977) and used to design optimum tail shapes for bodies of revolution (Smith *et al.*, 1981). Here 'optimum' means to generate the shortest tail shape. The length of the afterbody is not known a priori because it is a function of Reynolds number, boundary layer state, forebody geometry, and the momentum loss thickness at the beginning of the pressure recovery section. One significant conclusion from this investigation is that tail shapes in fully turbulent flow are relatively insensitive to Reynolds numbers over a wide range (see also Hess, 1976).

5.2.3. Manipulation of the Turbulence Structure due to Control Mechanisms Originating at the Wall

5.2.3.1. Suction and blowing

This section can be dealt with rather briefly since good survey papers exist. There are chapters on suction research in Lachmann's *Boundary Layer and Flow Control* (1961), a survey on slot injection for skin-friction drag reduction by Cary, Bushnell and Hefner (1977), and a section on blowing and suction in *Viscous Flow Drag Reduction* (Hough, 1980).

Probably the first control mechanism to influence a boundary layer and to delay separation was suggested by Prandtl in 1904 when the boundary layer was removed by means of a slot at the rear surface of a circular cylinder (Betz, 1961). Since then boundary-layer suction has been used to increase the lift of aerofoils, to prevent transition of a laminar boundary layer (e.g. Lachmann, 1961; Reynolds and Saric, 1982) and to relaminarize turbulent boundary layers (Pfenninger, 1977; Pfenninger *et al.*, 1988). Boundary-layer suction has been applied mainly to aerofoils and applications to other areas of fluid mechanics are scarce, largely because of the danger that the suction holes or slots are blocked by dirt in many industrial applications. With increasing suction the velocity profile

becomes fuller near the wall and skin friction should increase accordingly. Savas and Haritonidis (1989) found experimentally a noticeable change in the near wall turbulence structure of a boundary layer with zero pressure gradient (ZPG), resulting in a 20–30% reduction in the Reynolds shear stress (they do not mention, however, an increase of $\bar{\tau}_w$ as one would expect) and a comparable reduction in the turbulence production. This is complementary to results in turbulent pipe flow reported by Elena (1984), who noticed that the maximum of the production was shifted further away from the wall and that the flatness factor F_w , which may be interpreted as a measure of the intermittent structure of the viscous sublayer, is reduced by suction.

Mass may be added to a boundary layer using a porous or slotted wall, where the latter is mainly used to protect the wall from excessive heat transfer (for a survey see Goldstein, 1971). Aspects of turbulence control and drag reduction were emphasized in a review paper by Cary *et al.* (1977) providing a description and analysis of slot injection in low-speed and high-speed flows. They define slot injection as the process of injecting a gas from a slot such that the injected gas lowers the downstream surface temperature and, if of sufficiently low momentum, reduces the downstream skin-friction drag. To increase the length of the low-drag region downstream of the slot, it is necessary to retard mixing between the slot flow and the external boundary-layer flow. Retarded mixing increases, however, the base drag penalty of the slot which can only be reduced by an increase in mixing downstream from the slot, and these two requirements are contradictory. Cary *et al.* conclude the survey by stating that much experimental research is needed to determine methods to reduce slot base drag, decrease downstream mixing, and reduce collection and ducting losses for slot air on conventional aircraft. A more optimistic opinion is expressed by Wilkinson *et al.* (1988), who state that porous wall injection will in fact provide large skin-friction reduction and an alternative to slot injection if a low-loss source of injectant is available.

5.2.3.2. Control of the near-wall and the large eddy structures

The direct control of near-wall and large eddy structures is a straightforward idea to manipulate turbulence but so far there are only a few investigations.

Assuming that the modification of the large eddies can lead to a reduction in skin friction and that the large eddy structure of a turbulent boundary layer is produced by the Emmons spot generation process (confirmed for $Re_{\delta_2} < 5 \times 10^3$ by Zilberman *et al.*, 1977), then we can infer that a manipulation, i.e. a close spacing and triggering of the spots, should lead to a reduction in skin friction. Goodman (1985) reported a reduction of the order of 15% for certain combinations of triggering frequency and amplitude and spacing of the holes, which permitted the connection between the sound source and the flow, but no net drag reduction was obtained since the energy required to force the spots was too large (Wilkinson *et al.*, 1988).

Gad-el-Hak and Blackwelder (1987) investigated large-scale periodic structures which were generated by cyclically injecting secondary fluid from a spanwise slot. The aim was to remove the inherent randomness of the large-eddy structures and, since these eddies seemed to trigger bursting events in the near-wall region, to make these inner layer structures periodic, too. Although periodic structures could be generated by this process both in the inner and the outer layer, it is not clear whether, for example, the skin friction can be changed by changing the bursting rate.

Since, however, Reynolds shear stress is associated with the bursting process (it is primarily produced by the ejection of low speed streaks from the wall region), it is important to manipulate these events, decrease the Reynolds shear stress, and interrupt the turbulence production. Gad-el-Hak and Blackwelder (1989) suggested two possible mechanisms to influence the near-wall structure: (1) to withdraw fluid from under the low-speed streaks through a streamwise suction slot to inhibit the ejection process; (2) to inject fluid selectively under the high-speed regions with the immediate effect of decreasing the viscous shear at the wall. They found that when continuous suction was applied optimally from a streamwise

slot, the natural bursting frequency as computed from the VITA algorithmus was reduced by as much as 50%.

Choi *et al.* (1989) explored another mechanism by numerically testing a change in wall-boundary conditions and found that significant net drag reduction was obtained when the normal velocity at the wall was prescribed to be 180° out of phase with the normal velocity at $y^+ \approx 10$. This was accompanied by a significant change in the intensity of the wall-layer structures.

5.2.3.3. Riblets

After polymer additives (e.g. Hough, 1980; Gyr, 1990), riblets (for a review see Wilkinson *et al.*, 1988) have been the most successful drag-reduction device to lower skin friction. They have been used both on ship hulls (cf. Eilers *et al.*, 1985) and on aircraft in flight (e.g. Nagel *et al.*, 1985; Walsh *et al.*, 1988). Riblets are small longitudinal grooves in the surface, aligned in the flow direction, with typically sharp ridges separating the valleys. Of the many possible geometries (see for example Bushnell, 1983) the optimal drag reducing surface appears to be the sawtooth arrangement, which resulted in a 4–7% skin-friction reduction compared to an aerodynamically smooth flat plate. An optimization of riblets for turbulent drag reduction was performed by Walsh and Lindemann (1984). They showed that the riblet drag reduction is insensitive to yaw angles up to 15° but that drag is no longer reduced at 30° . Height and spacing of the grooves should be about 30 wall units which is smaller than the spacing of the streaks observed in the viscous sublayer. In comparison Wilkinson *et al.*, 1988 give a symmetric v-groove design as optimal with $h^+ = s^+ \approx 15$. Here $h^+ = hu_\tau/\nu$ and $s^+ = su_\tau/\nu$ where u_τ is the skin friction velocity, ν the kinematic viscosity, and h and s the height and width of the groove. This means that high Reynolds number flow requires very small grooves. Bechert and Bartenwerfer (1989) suggest guidelines for an optimal riblet geometry: (i) a sharp wedge for the rib, preferably with a radius of curvature smaller than 0.5–1% of the lateral rib spacing; (ii) a rib wedge angle as small as possible; and (iii) a valley depth of about 60% of the lateral rib spacing. The same authors state as their basic hypothesis for the drag reduction mechanism "that sharp ribs impede the instantaneous crossflow in the viscous sublayer which is generated by the turbulent motion. In this way the whole turbulent momentum exchange in the boundary layer is reduced, which is equivalent to a shear stress reduction". According to Walsh (1982) the turbulence intensity near the surface is reduced—in agreement with the above hypothesis—but burst frequency is not. Riblets appear to function in moderate adverse and favourable pressure gradients (Walsh and Anders, 1985). So far there are no investigations of the interaction of riblets with severe adverse pressure gradients but one must assume that separation will occur earlier due to the lower level of skin friction.

5.2.3.4. Compliant walls

It has now been established that compliant walls can be used to stabilize a laminar boundary layer but it has taken a long time to prove this, and it is probably a typical 'Freudian slip' if it is spelt twice as 'complaint wall' (Bandyopadhyay, 1986; Wilkinson *et al.*, 1988). The number of references is extensive; see for example Carpenter and Garrad (1985) for a listing of many difficult and often non-repeatable experiments and complicated theoretical models. Experiments dealt with both turbulent and laminar boundary layers. A careful experiment in a fully developed ZPG turbulent boundary layer in air was performed by McMichael *et al.* (1980), using a membranous surface backed by a thin cavity containing a layer of polyurethane foam. No significant change from the rigid surface skin-friction coefficient was observed (for a survey see Bushnell *et al.* (1977) and a more recent investigation Gad-el-Hak (1984)). There appears to be more hope to keep skin-friction drag low by delaying transition in a laminar boundary layer. In this respect a breakthrough, at least for water, was achieved by Gaster (1985, 1988) experimentally and by Carpenter and

Garrad (1985, 1986) theoretically. The former showed that the best surface tested allowed an increase in transition Reynolds number of 30% over that of a rigid surface (Gaster 1988), but the surfaces tested were probably not optimum for promoting a delay in transition. Multi-layer and non-isotropic coatings are expected to offer much more promise, at least theoretically (see Carpenter, 1988).

5.2.3.5. Curved walls

The flow along a curved wall can either follow a convex or a concave contour. Prandtl (1935) showed that the turbulence in a flow along a convex wall is attenuated whereas it is known that Taylor-Görtler vortices are formed in a laminar boundary layer on a concave wall, an effect which is destabilizing for the flow and even leads to a completely different flow structure. Bradshaw and co-workers (Muck *et al.*, 1985; Hoffmann *et al.*, 1985) and others investigated the effects of mild convex and concave surface curvature on turbulent boundary layers. The flow responded very rapidly to the application or removal of stabilizing (convex) curvature and slowly to concave (destabilizing) curvature, the latter due to the forced change in the flow structure which needs time for the change. If convex curvature is sufficiently large (δ/R larger than about 0.05 with R as the radius of curvature) Gillis and Johnston (1983) noticed that the Reynolds normal stresses were greatly attenuated and the Reynolds shear stress was reduced almost to zero. This apparently affects also the mean velocity distribution and reduces skin friction. Since regions of convex curvature are normally short in comparison to the total length of a flow configuration the relaxation behaviour determines how far downstream the drag reduction can be expected to continue, and this was investigated by Alving *et al.* (1990). They found that the level of the skin friction in the relaxing boundary layer appears to be independent of the skin friction level at the end of the bend, except in the initial recovery region. More important, however, there is no lasting benefit for drag reduction with a zero pressure-gradient region downstream. These results cast doubts on the usefulness of the viscous drag reduction concept suggested by Bushnell (1983) which implies that the reduction in skin friction due to convex curvature of the wall is persisting—even after the curvature is removed—far enough downstream to obtain a net gain in drag reduction. Model calculations for single and three-stage nose bodies with convex curvature were performed by Bandyopadhyay (1989). Although separation could be avoided in the latter configuration the drag coefficient was lower only by about 1.6%.

5.3. MANIPULATION BY FREE-STREAM TURBULENCE OR BY UPSTREAM FLOW UNSTEADINESS

5.3.1. Introductory Remarks

In principle, every boundary layer is affected by its upstream history but the effects depend on the type and position of the disturbance, the memory of the boundary layer (higher or lower viscosity, for example), the boundary conditions, and the distance downstream from the location of the disturbance. If a perturbation affects mainly the outer part of the layer its effects are more long-lived than if the inner layer is perturbed. This is due to the shear-stress distribution in a boundary layer where the larger shear stresses close to the wall affect a disturbance more strongly than in the outer layer and make it abate more quickly. Coherent structures in the outer layer generally live longer than in the inner layer. In this review interest is not focussed, however, on the response of a turbulent boundary layer to a sudden perturbation, as introduced by a rough or curved wall, for example. For a discussion of such effects and their relaxation process the reader is referred to Smits and Wood (1985). Here we are more interested in the effects of perturbations in the potential flow upstream of a boundary layer which is liable to separate. These perturbations may be generated by:

— grid-generated freestream turbulence,

- a perforated fence or gauze fixed to a wall on which the boundary layer develops,
- interaction of a vortex street shed by a bluff body with a reattaching shear layer,
- longitudinal vortices interacting with a downstream boundary layer,
- vortex/vortex-boundary-layer interaction as in a canard/delta-wing configuration.

These effects will be discussed in the following subsections.

5.3.2. Free-Stream Turbulence

The interaction of free-stream turbulence (FST) or upstream flow unsteadiness with boundary layers, wall bounded shear flows, or separated shear layers is a very important problem in the investigation of turbulent flows. It is not surprising, therefore, that there is a vast number of experimental and theoretical papers, see for example the surveys by Bearman and Morel (1983) and by Bushnell (1984), the latter containing no less than 334 references.

Following Bearman and Morel (1983): "free-stream turbulence is the name given to the background level of random, three-dimensional velocity fluctuations present in every fluid. Its characteristics at a given position e.g. its intensity and spectral composition, depend on how the FST was generated and on the history of the flow. Since the power spectra of grid turbulence tend to have a well defined shape, it follows that the longitudinal component of turbulence produced by grids can be described by a single velocity scale (u') and a single length scale (L_x)."

Other upstream turbulence effects may be (1) flow unsteadiness due to vortex shedding or due to blade wakes (ordered unsteadiness) and (2) steady wakes and longitudinal vortices. These effects may or may not be combined with FST, which is here considered to be "nearly homogeneous and nearly isotropic turbulence" (Hancock and Bradshaw, 1983). The dominance of FST or of turbulence caused by flow unsteadiness may be determined by investigating the ratio of the length scales, i.e. integral length scale of the outer flow, say L_x or L_y , to the thickness of the shear layer δ . If $L_x/\delta \gg 1$ FST will appear to the local flow as a correlated unsteady mean flow of varying magnitude and direction. According to Bearman and Morel (1983) the two turbulent fields will not interact and the gross effects of FST can be estimated using the quasi-steady assumption.

5.3.2.1. Free-stream turbulence interacting with turbulent boundary layers

The interaction of FST with a zero pressure gradient turbulent boundary layer was investigated experimentally by Hancock (1980) and Castro (1984), for example, and reviewed by Bradshaw (1981) and Hancock and Bradshaw (1989).

In general, there are two basic mechanisms by which FST interacts with boundary layers or with separated shear layers (1) accelerated transition to turbulence and (2) enhanced mixing and entrainment. In separated shear layers the overall effect of FST is often the result of both mechanisms. Both the laminar shear layer and the laminar boundary layer are affected by the excitation of the FST introducing disturbances and leading to an earlier instability of the velocity profiles than in a low turbulence free stream. This results in very much higher skin friction due to the turbulent boundary layer and in an increase in heat transfer (McDonald and Kreskowsky, 1974). In addition there is a further increase in skin friction if the FST level is changed outside a fully turbulent boundary layer. Both the free-stream turbulence length scale $L_s^{(u)}$ (FST L) or the dissipation length scale, since it is characteristic of the decay of the FST, and the intensity play a rôle. Hancock and Bradshaw (1983) suggested a plot of the fractional change $(c_f - c_{f0})/c_{f0}$ of the skin friction parameter c_f due to FST, where c_{f0} is the coefficient with minimal FST, against a purely empirical parameter $\beta = [(u'^2/u_s^2)^{1/2}/((L_s^{(u)}/\delta) + 2)]$. They could show that at least for $Re_{\delta 2} > 2000$ their data collapsed within a small band (Fig. 20). Castro (1984) on the other hand displayed that such a correlation does not hold for boundary layers with $Re_{\delta 2}$ approximately smaller

meaning

different?

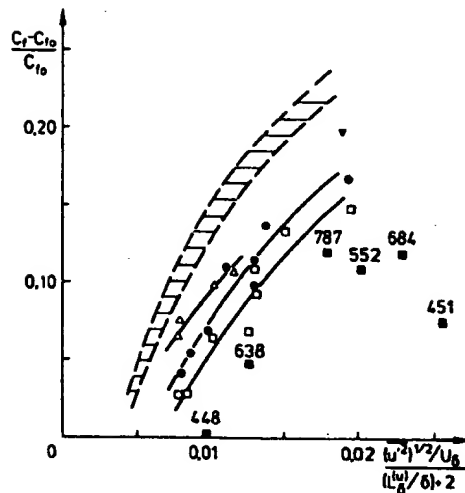


FIG. 20. Fractional increase in skin friction vs Hancock's 'Free stream turbulence parameter'. Shaded region is Hancock's data with ∇ showing his $Re_{\delta_1} = 1830$ result. $Re_{\delta_1} \pm 5\%$; Δ , 2400; \bullet , 1350; \square , 920. Other points (\blacksquare) with Re_{δ_1} shown. From Castro (1984).

than 2×10^3 . The parameter ranges for the three relevant investigations are given in Table 3.

It should be noted here that the majority of the experiments were performed with a FST lengthscale in the order of the boundary-layer thickness for which the interaction with the boundary-layer properties is felt to be strongest.

Results of the three investigations may be summarized as follows:

- (1) The logarithmic law was found to be extraordinarily insensitive to the variations of turbulence intensity (Hancock and Bradshaw, 1983).
- (2) The shape parameter H_{12} is decreased with increasing $\Delta c_f/c_{f0}$ (Hancock and Bradshaw, 1983).
- (3) The wake component of the velocity profile is reduced (Hancock and Bradshaw, 1983).
- (4) For approximately $Re_{\delta_2} < 1000$ the free-stream turbulence level shows a greater effect on H_{12} than on c_f , increases in skin friction are lower than those that would occur at higher Reynolds number, and the wake component does not fall so rapidly with decreasing Re_{δ_2} (Castro 1984).
- (5) Larger free-stream length scales penetrate further into the boundary layer but have a smaller effect on the mean flow (Hancock and Bradshaw, 1989).
- (6) The v -component intensity is attenuated by the surface constraint at distances from the surface less than about L_δ^w . Both the u - and w -components are increased in the same region (Hancock and Bradshaw, 1989).

There is only one investigation (Hopfeniz, 1984) of the effect of the FST level ($0.2\% \leq T_{\delta_1} \leq 8\%$, no length-scale data given) on an adverse pressure gradient boundary layer at low Reynolds numbers ($Re_{\delta_1} < 5000$). Here Reynolds number effects still play an important

TABLE 3

Author	$Re_{\delta_1} \times 10^{-3}$	L_δ^w/δ	$(\bar{u}^2)^{1/2}/u_\infty$
Hancock and Bradshaw (1983)	1.6-6.0	0.67-4.94	0.018-0.06
Castro (1984)	0.45-2.4	0.80-2.90	0.023-0.07
Hancock and Bradshaw (1989)	2.8-5.2	0.67-2.23	0.02-0.058

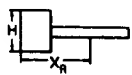
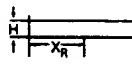
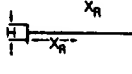
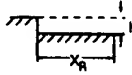
rôle. If the pressure distribution was kept the same for various FST levels, an increase in T_{u_0} shifted the maximum of the Reynolds shear stress $\overline{u'v'}$ closer to the wall and increased the skin friction at a fixed position. A shift of the separation point in the downstream direction was observed only for values of T_{u_0} larger than 4% and at most by about 10% for $T_{u_0} = 8\%$. For further investigations see Arnal (1977) and Hoffmann and Gonzales (1984).

5.3.2.2. Free-stream turbulence interacting with separated boundary layers

In the case of a separating boundary layer three mechanisms due to FST may be of importance, the first two of which affect laminar boundary layers: (1) Disturbances introduced by FST lead to an earlier instability of the velocity profile than in a low turbulence free stream and possibly to reattachment of the separated boundary layer. (2) The interaction of FST with the separated shear layer originating at the leading edge of a body generates vorticity fluctuations into the shear layer which amplify downstream and affect the mixing process (this was discussed first by Bearman and Morel (1983) for trailing edge interaction). (3) In fully turbulent shear flows FST leads to an augmentation of turbulent mixing and an increase of entrainment. Both effects are more pronounced in separated shear layers than in wall bounded flows, since a wall attenuates the fluctuation velocity component normal to the wall. The interaction of the FST with the shear layer includes interaction with the coherent structures of the shear layer. Bearman and Morel (1983) suggest "that it is likely that the presence of a random turbulence field will reduce the spanwise coherence of the structures and this may in some way enhance the shear layer growth. Another possibility may be that the presence of fluctuations in the stream, feeding into the shear layer both at its origin and along its length, may modulate the strength of the coherent structures such that the pairing process is perhaps accelerated and shear layer growth enhanced". The second effect is a typical free shear-layer phenomenon whereas a reduction of the spanwise coherence to more three-dimensional structures could also occur in the outer region of boundary layers or in 'near-wall' shear layers.

Whatever the effect of FST on the coherent structures may be, its main effect is to increase the entrainment in the separated shear layer which curves the shear layer inwards towards the wall and reduces the length of the separation region. There are at least four interesting geometries with reverse flow where the shortening of the reverse-flow region in at least nominally two-dimensional flows were investigated (Table 4). There are three relevant

TABLE 4

Author	Configuration	Reynolds number	L_s^*/H	$(u'^2)^{1/2}/u_\infty^*$	X_R/H	Comments
Bearman (1978)				≤ 0.07	8.5-5	
Hillier (1976)				≤ 0.12	3.5-1.5	
Hillier and Cherry (1981)		$(2.7-8) \times 10^4$ Re_H	0.64-1.95	≤ 0.0935	data not given in figures	Effect of length scale negligible
Nakamura and Ozono (1987)		$(1.4-4.2) \times 10^4$	0.5-24	0.069-0.128	—	Effect of length scale negligible up to $L_s/H \approx 2$.
Castro (1988)		$Re_H > 2 \times 10^4$	≈ 0.8	≤ 0.087	8.75-6	
Castro and Haque (1988)						
Scott (1980)						
Isomoto and Honami (1989)		$Re_H = 3.2 \times 10^4$	not given			Not enough information given

* At leading edge.

studies of reattachment on the side face of a long plate of rectangular cross-section, one on a long splitter plate preceded by a square section cylinder, one on a long splitter plate in the wake of a normal plate, and two on a backward facing step.

Up to ratios of $L_s^{(u)}/H \leq 2$ the statement of Bearman and Morel (1983) holds that the reattachment length is decreased with increasing turbulence intensity and there is no significant effect of turbulence scale. Nakamura and Ozono (1987) found that with a further increase in the scale ratio, the mean pressure distribution asymptotes towards the low FST, meaning that turbulence of very large scale is equivalent to a flow with slowly fluctuating velocity so that it can no longer influence the mean flow. Thus we expect the length of the reverse-flow region to increase again when the length scale ratio becomes larger than two.

Castro & Haque (1988) claim that FST leads to an increased flapping motion of the shear layer just after separation, giving higher axial Reynolds stresses across the whole layer and that the turbulence structure of the flow around reattachment is different with and without FST.

In these cases the separating shear layer leaves the body at an angle 90° to the approaching flow, and the initial part of the shear layer is highly curved. Bearman and Morel (1983) think that there is evidence to suggest that the sensitivity of a shear layer to FST is dependent on this separation angle. The effect of FST on the reattaching flow downstream from a backward facing step, where the shear layer separates parallel to the free-stream direction was investigated by Scott (1980), Westphal (1983), and Isomoto and Honami (1989). The latter authors used different kinds of grids, a two-dimensional rod on or above the wall, and a transverse cavity as turbulence generators near the step. The reattachment length was decreased by 25% if the FST level was increased from 0.25 to 7.4%. Since the largest reduction occurred for the grid-rod combination (AO-R2 and FO-R2, see authors for notation), it is probable that in this case the structure of the turbulence, as expressed by a length scale, must have been changed.

5.3.3. Perforated Obstacles

Perforated obstacles in the free stream of a wind tunnel flow are usually screens or honeycombs. They are used to increase or decrease the turbulence level or to destroy swirl in the turbulence field downstream, and their properties were reviewed, for example, by Laws and Livesey (1978), Durbonovich *et al.* (1981), Tan-Atichat *et al.* (1982), Wigeland *et al.* (1978) and Mehta (1984). There is a large number of references given by Bushnell (1984) on the flow through perforated fences or screens situated in wall boundary layers which were often investigated in connection with windbreakers. In the latter type of obstacle both boundary-layer thickness in relation to fence height and free-stream turbulence play an important rôle. Here we are not interested in either of the two types of perforated obstacles described above but in the downstream turbulence and drag of perforated blunt bodies with and without a splitter plate. A strong influence of the open area ratio on the separated flow region was found in the case of a perforated normal plate with a long splitter plate (Ruderich, 1985). The control of drag and turbulence properties of the flow downstream from the obstacle shows features which are similar to those described in Section 5.4.4. Besides this there are two interesting phenomena: (i) a distinct change in the flow properties if the porosity exceeds a certain limit and (ii) the memory of the flow downstream of its wake-generating mechanism.

5.3.3.1. Perforated obstacles with a free wake

The drag of perforated plates normal to an airstream was investigated by Castro (1971) with β as the ratio of open to total plate area. The drag coefficient c_D plotted against $1/\beta^2$ shows a sharp increase up to about $\beta = 0.2$, followed by a kink and a further increase towards the limiting value $c_D \approx 1.86$ for an impermeable plate. Correspondingly, the Strouhal number $S = f \cdot c/u_\infty$ (c is the plate chord width and u_∞ the corrected freestream velocity) increases gradually with rising β until $\beta = 0.2$, where an abrupt reversal of slope

occurs, followed by a further steep increase of S . Pulsed-wire measurements of the mean flow velocity downstream from the perforated plate showed that the reverse-flow region behind the impermeable plate had detached and moved downstream. Its average position was now characterized by two free stagnation points. With increasing porosity the fluid through the plate separates the two shear layers originating at the upper and lower plate edge and moves the reverse-flow region and the location of the formation of the vortex street downstream until finally, at $\beta = 0.2$, the vortex street ceases to exist. It is not clear for which value of β the reverse-flow region disappears. Gray and Sheldon (1982) complemented some of Castro's experiments and found that the normalized wake growth behind the solid plate is much faster than behind a perforated plate with $\beta = 0.425$. They conclude that the different growth rate is due to the lack of a vortex street in the latter case. The same strong influence of the wake-generating mechanism on the downstream turbulence was found earlier by Bevilacqua and Lykoudis (1978), who compared the wakes of a sphere and a perforated disc ($\beta = 0.82$) of the same diameter.

5.3.3.2. Perforated obstacles with a splitter plate

The shear layers which originate at the edges of a plate normal to an airstream can be separated by bleed air through the plate, by a splitter plate in the plane of symmetry of the

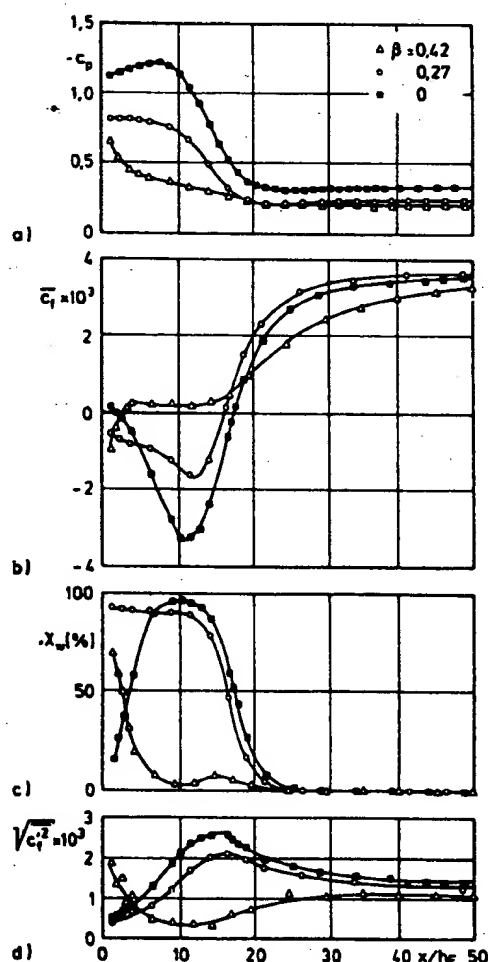


FIG. 21. Distributions of pressure coefficient \bar{c}_p , mean and fluctuating (r.m.s.) skin friction coefficients \bar{c}_f and c_f' , and reverse-flow parameter vs x/h_f (where h_f is the fence height). From Ruderich (1985).

plate, or by both. The latter flow configuration was investigated by Ruderich (1985), and his wall data, plotted against the distance x made dimensionless by the fence height h_F , are presented in Fig. 21 for three values of the permeability ratio β (0; 0.27; 0.42). Even without a detailed account of the experiment the reader will note that the two cases $\beta = 0$ and 0.27 show overall similar trends for all four wall parameters, pressure coefficient c_p , mean skin-friction coefficient \bar{c}_f , reverse-flow parameter χ_w , and fluctuating skin-friction coefficient c'_f . The case $\beta = 0.42$, however, displays a completely different behaviour in that the reverse flow region is very short, followed by a region of almost constant positive skin friction, and a much reduced level of c'_f . The respective pressure distribution is on a much lower level, too, indicating a decrease of drag as compared with the less permeable plates. The changes in the structure of the turbulence are discussed by Ruderich; suffice it to mention here the decrease in the level of $\overline{u'^2_{\max}}$ by a factor of about 3 and of $\overline{u'v'}$ by a factor of about 2. This configuration has still considerable potential for influencing both turbulence structure and heat and mass transfer.

5.3.4. Upstream Flow Unsteadiness or Wake

There are many flow configurations where an upstream wake or an unsteady vortex street interacts with a boundary layer, and the interaction is quite different if the wake generator is inside or outside the boundary layer. Two-dimensional generators are mainly situated normal to the flow and parallel to the wall and consist of circular or rectangular cylinders, thin plates, or aerofoils, in single or tandem array (Fig. 22). The most important case for an obstacle generating a wake or a "vorticity trail" outside a boundary layer are multi-element aerofoils, as exemplified by the investigation of Zhou and Squire (1985) and Squire (review paper 1989), and the interaction of a circular cylinder or blade wake with a boundary layer, as in a turbomachine.

5.3.4.1. Turbulence manipulators inside the boundary layer

Turbulence manipulators of the type defined above may be divided into two groups according to the main effects by which they influence the boundary layer: (i) those which cause reverse-flow by touching the wall or are so deeply immersed in the boundary layer that vortex shedding has ceased, or both; (ii) those which still show vortex shedding or achieve a sustained lowering in skin friction, such as large eddy break-up devices (LEBUs). Coverage here of LEBUs is confined to a few remarks only.

Bearman and Zdravkovich (1978) investigated the flow around a cylinder near to a wall in a turbulent boundary layer. They varied the following parameters: Reynolds number, based on the diameter D of the cylinder and the freestream velocity u_∞ , the ratio of D to the

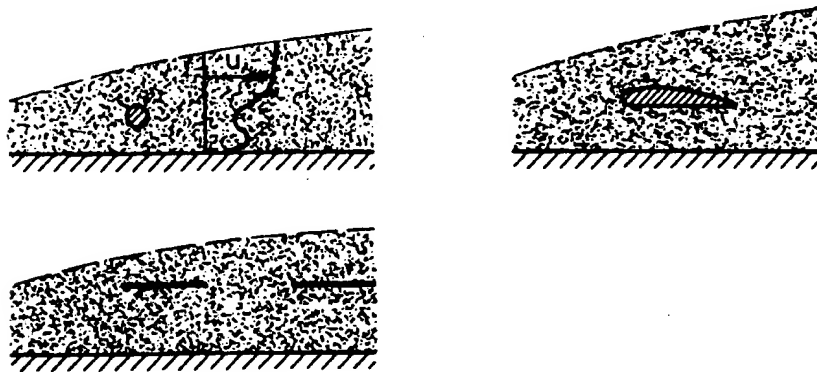


FIG. 22. Wake generators inside a boundary layer.

TABLE 5

Author	$Re_D \times 10^{-4}$	δ/D	G/D	$S = \frac{f \cdot D}{u_\infty}$	Remarks
Bearman and Zdravkovich (1978)	4.5 2.5	0.8	0-0.2	—	regular vortex shedding suppressed
Marumo <i>et al.</i> (1978)	4.5 0.75	0.8 3.3	≥ 0.2 1.37; 3.69	≈ 0.20 —	constant Strouhal number of 10 high periodic fluctuations in one case
Tsiolakis <i>et al.</i> (1983)	1.8	2.6	0.8; 4.7	—	Extensive measurements of downstream flow
Müller (1985)	$Re_{\delta_0} = 3700$	2.6	0.8	—	

boundary layer thickness δ , and the ratio of D to the gap width G between the cylinder and the wall (see Table 5).

Pressure distributions around the cylinder showed that as G/D was reduced, there was always a mean force on the cylinder repelling it from the wall. This force falls very rapidly as the cylinder is moved away from the wall. The base pressure increased rapidly between $G/D = 0.6$ and 0.3 with no change of the Strouhal number. Shedding of vortices disappeared at G/D just less than 0.3 and separation bubbles formed on the plate upstream and downstream of the cylinder, attaching themselves to the cylinder when it touched the wall. Vortex shedding and a suction peak on the plate situated half a diameter downstream of the cylinder axis existed side by side. This brief summary probably displays all the main features of this type of wake/vortex/wall-bounded shear layer interaction.

In the 'vortex-shedding parameter space' measurements were performed by Tsiolakis *et al.* (1983) and Müller (1985) of the relaxing boundary-layer downstream and the changes of the turbulence structure on its way to equilibrium. At $x/D = 70$, the measuring station furthest downstream, the balance of the kinetic turbulent energy in the outer layer still differed from that in a flat-plate boundary layer. This confirms results obtained by Marumo *et al.* (1978) who found that the near-wall region recovered much more quickly than the outer region. Preston-tube data showed that the skin friction was hardly changed from the undisturbed flow for $G/D = 3.69$, was reduced by about 30% before increasing again to the undisturbed level for $G/D = 1.37$ (middle of the outer layer), and increased from separation just downstream from the cylinder to the undisturbed level for $G/D = 0.250$. An exploratory investigation on vortex generators submerged in a turbulent boundary layer was performed by Rao and Kariya (1988) and showed some potential of exceeding the performance of conventional vane-type vortex generators (see Section 5.3.4.2).

Large eddy break-up devices (Fig. 22) are preferably situated in the outer 30% of the boundary layer and consist mainly of tandem configurations of aerofoils, thin plates, or flat ribbons of chord δ_0 (with δ_0 being the undisturbed boundary-layer thickness at the position of the device) spanning the entire width of the wind tunnel, and having a spacing of about $8 \delta_0$ between the devices. They change the structure of the turbulence in the boundary layer considerably resulting in a reduction of the skin friction (see for example reviews by Anders and Watson (1985) and Wilkinson *et al.* (1988)). There appears to be no net drag reduction, however, after the device drag penalty is taken into account (Sahlin *et al.*, 1988; Lynn *et al.*, 1989).

Another turbulence manipulator was investigated by Roth and Leehey (1989). They optimized a honeycomb LEBU with a height slightly larger than the thickness of the undisturbed boundary layer, achieving a reduction in c_f of almost 55%, greater in both magnitude and duration than that of aerofoil LEBUs. Although nothing was said about a net drag reduction, these authors suggest the possibility of a reduction in the fluctuating wall pressure which in some cases of acoustical applications is more interesting than a net drag reduction.

5.3.4.2. Turbulence manipulators outside the boundary layer

Among the many flow configurations where an upstream wake interacts with a boundary layer there is the case where the wake of one blunt body interacts with the boundary layer on another blunt body downstream, or the case where a vortex sheet from the trailing edge of a body merges with the boundary layer on a body downstream (as for a multi-element aerofoil), or the case of a blade which passes continually through the individual wakes from upstream rows of blades.

Zdravkovich (1977) has reviewed experiments in the flow around two parallel cylinders in tandem arrangement positioned at right angles to the approaching flow. He found that the interaction between two closely spaced cylinders drastically changed the flow around them, produced unexpected forces and pressure distributions, and intensified or suppressed vortex shedding. Zdravkovich concluded his review by stating that the flow patterns provided phenomenological explanations but that their intrinsic nature remained a mystery. Here is apparently still a wide range of possibilities that can be explored for drag reduction.

It is somewhat puzzling to note that most of the information on the flow interaction between a single wake and a boundary layer is buried in internal reports or conference proceedings. Squire (1989) displayed the experimental evidence in a survey in which he also discussed the phenomena causing separation on the main wing, for example the too early merging of the slat wake with the wing boundary layer or the too large increase of the suction peak at the leading edge caused by too large a gap between the slat and the wing. For a detailed discussion of the multi-parameter problem of the interaction of a wake which is initially above the boundary layer and the boundary layer in zero and adverse pressure gradients the reader is referred to Squire's survey.

Squire (1989) addressed also the flow configuration of a wake originating from a blade in a turbomachine and affecting the boundary layer on the blade downstream. He points out two important effects: "In the first place the flow is unsteady, however, more important is the fact that the blades normally operate in the Reynolds number range where there would be considerable regions of laminar flow on the blade surface in a clean flow. Clearly the upstream wakes increase the overall turbulence level in the flow and thus bring transition forward. . . . The situation is further complicated if a laminar separation bubble occurs on part of the blade surface. In this case the turbulent patches passing back over the surface periodically suppress this bubble." The main difference between this type of flow and those discussed in this review is the flow unsteadiness which is mentioned as an important phenomenon of separation control but will not be discussed here any further.

5.3.5. Longitudinal Vortices Imbedded in a Boundary Layer

The effects of longitudinal vortices on skin friction and turbulence structure of nominally two-dimensional boundary layers have been investigated for flows with and without separation. According to Bradshaw (see Shabaka *et al.*, 1985) "longitudinal vortices in turbulent boundary layers belong to the class of 'slender' turbulent flows, in which velocity gradients in the y and z directions are much larger than longitudinal gradients. Once formed, the angular momentum of a single longitudinal imbedded vortex is reduced only by the spanwise component of surface shear stress, which is usually very small. Therefore, isolated vortices in boundary layers tend to persist for very long distances downstream. Vortex pairs which are close enough to exchange angular momentum by mixing decay more rapidly". These remarks set the pattern for many possibilities. 16 different vortex-pair configurations were studied by Pauley and Eaton (1988), for example. The case which was investigated most extensively was that of vortex interaction with common flow between the vortices directed towards the wall (common-flow-down). This flow caused the strongest distortion of the boundary layer over the widest streamwise extent. Such a vortex pair moves apart as it develops, producing a thinning of the boundary layer between the vortices (see also Bradshaw and Cutler, 1987). Both the spacing between the vortices and the vortex

strength influence this process and can be used to delay separation of the boundary layer due to the increased skin friction. Pauley and Eaton also observed that the spanwise component of the skin friction was much larger in the common-flow-down case, resulting in a stronger diffusion of vorticity and a shorter lifetime. In the common-flow-up case the spanwise skin friction decreases as the vortices lift each other away from the wall causing a thickening of the boundary layer. To establish an effective vortex pattern requires the correct choice of the vortex strength, of the spacing of adjacent vortices, and of their sense of rotation. Pearcey (1961) reports that an effective spacing is achieved only if the initial spacing of the vortices is greater than about three times their height. For a smaller spacing than this, the vortices (co-rotating) tend to damp one another and fail to maintain high velocities at the surface at any point in the cross-section of the boundary layer and the vortex flow. Counter-rotating vortex systems are effective in delaying separation (Pearcey) when they have extensive high energy regions in which the boundary layer is kept thin between alternate pairs of vortices.

Single longitudinal vortices were investigated in ZPG boundary layers by Shabaka *et al.* (1985) and Westphal *et al.* (1987) and in APG boundary layers by Westphal *et al.* (1985) and Mehta (1988). The latter author studied experimentally the interaction between a longitudinal vortex and a separated boundary layer at three transonic Mach numbers. At a Mach number of 0.7, the effect of the vortex was to delay boundary-layer separation on the downwash side and move it forward on the upwash side, with the distorted separation line forming a focus on the surface. Reattachment moved upstream in the region of the vortex. The main effect of the vortex was to transform a nominally two-dimensional separation region into a three-dimensional one.

The effects of vortex generators and of the ensuing vortices on APG boundary layers were investigated by Schubauer and Spangenberg (1960) and on turbulent separated flow associated with a curved rearward-facing ramp by Selby *et al.* (1989).

5.3.6. Leading-Edge Vortices

Vortical flow fields are generated, for example, due to separation at the leeward side of flow configurations, such as circular or conical bodies or delta wings at moderate and high angles of incidence. For delta wings Gad-el-Hak and Blackwelder (1987) have listed some perturbation methods which can be used to control the separated shear layer at the leading edge:

- a passive cavity system tuned to a frequency range corresponding to the natural frequency of vortex shedding,
- acoustical means, such as the use of an array of loudspeakers along the leading edge of a wing,
- a piezo electric array embedded near the leading edge,
- a heating element to provide an unsteady perturbation to the flow before separation,
- blowing or suction through slots near the leading edge,
- mechanical devices, such as vibrating ribbons, fences etc.

This list should be supplemented by the effect of the vortex generated at the canard wing on the vortex of the delta wing (e.g. Hummel, 1988).

Only a few investigations using these control mechanisms have apparently been published so far and four of them are listed in Table 6. All investigations aim at influencing the two large bound vortices on the suction side of a delta wing which result from the separating flow along the entire leading edge forming a strong shear layer. Gad-el-Hak and Blackwelder (1985) noticed by flow visualization that the separated shear layer develops due to instability mechanisms into a series of discrete longitudinal vortices which are shed parallel to the leading edge at a repeatable frequency. The discrete vortices appear to merge and finally form the large bound vortex on each side of the wing. Gad-el-Hak and Blackwelder (1985) perturbed the flow at the leading edge by impulsively injecting at

TABLE 6

Author	$Re_\infty \times 10^{-3}$	Sweep angle of Δ -wing ^(a)	Angle of incidence ^(a)	Perturbation
Rao and Johnston (1980)	20	60	0-28	Vortex plate, slots, fences, pylon vortex generators
Gad-el-Hak and Blackwelder (1987)	1-4	60	10, 28	Periodic blowing or suction through leading edge slot
Lowson (1989)	0.05-0.5	70, 80	20, 30	Acoustic forcing

constant frequency a secondary fluid from a slot along that edge. By this mechanism the flowfield was altered significantly when the amplitude was relatively low and when the injection frequency was chosen to be a subharmonic of the shedding frequency of the discrete vortices. This procedure resulted in a more repeatable pairing of the discrete vortices and a more organized large vortex. Effects on the secondary separation on the wing and on vortex bursting are not known. One should also note that Payne *et al.* (1986) did not confirm the results of Gad-el-Hak and Blackwelder (1985). P

Two further control mechanisms may be addressed briefly: Rao and Johnston (1980) investigated four different leading-edge flow manipulators on delta wings. They found the 'vortex plate' to be the most efficient device which utilizes the suction effect of a vortex produced by controlled separation in front of the leading edge. Lowson (1989) applied acoustic forcing to the separated vortex flow over a delta wing and found an interesting but as yet unexplained effect that at higher sound levels the effect of acoustic forcing caused large scale breakdown of the flow.

5.4. MANIPULATION AND CONTROL OF SEPARATION AND REATTACHMENT

5.4.1. Introductory Remarks

In external flows separation occurs either at fixed positions, for example at the leading or trailing edge of a blunt body (fixed separation), or it moves from the trailing edge of a slender body or aerofoil upstream when the angle of incidence is increased until it reaches the leading edge (free separation). In some cases the separation region will be open in the downstream direction and in other cases it will end in a reattachment line forming a closed reverse-flow region or a separation bubble. Appropriate to the position on a body where separation occurs methods of controlling and manipulating separation have been described for the leading edge, the main body, and the trailing edge. 5.4.1.1

Separation at the leading edge may be caused by a blunt leading edge, by the upstream movement of the separation position in a turbulent boundary (mainly at high Reynolds numbers and large angles of incidence), or by the so called burst of the laminar separation bubble present on the airfoil nose (mainly in low Reynolds number flows). Separation from the leading edge is also called 'stall' whereas 'pre-stall' denotes separation downstream from the leading edge and 'post-stall' characterizes flow conditions at angles of incidence of an airfoil beyond the stall angle.

Separation in the region near the leading edge is crucial in determining the lift at large angles of incidence. To influence this separation region it is necessary to influence the separated shear layer which forms downstream from the separation point and to force it to reattach to the aerofoil surface. That the spreading rate in a free mixing layer can be influenced by controlled periodic oscillations at the beginning of the layer (Oster *et al.*, 1978), suggests that a separated laminar or turbulent boundary layer may be manipulated in a similar way. This manipulation can be achieved by suction or blowing, by a vibrating ribbon, by an oscillating flap, or by acoustic excitation, and will be discussed in Sections 5.4.3.1 to 5.4.3.3. □

Another important phenomenon connected with separation near the leading edge is a separation bubble which occurs almost always on wings of low Reynolds number vehicles

(e.g. Mueller, 1985) but has been observed anywhere in the range $Re_c \leq 10^6$, where Re_c is the chord Reynolds number. Separation bubbles are formed when the boundary layer separates from the surface of an aerofoil in a laminar condition, with transition following in the separated shear layer. A short bubble produces a relatively small effect on the pressure distribution and the resulting effects on the lift and drag of the aerofoil are usually negligible. For a large enough angle of incidence and a low Reynolds number the short separation bubble may either burst and reattach, leading to a long bubble (Young, 1977), or burst without reattachment, leading to open separation. In both cases the pressure distribution is changed significantly, the lift is reduced, and the drag is increased. A criterion for bubble burst with reattachment depending on the pressure rise over the bubble length and the Reynolds number Re_{δ_2} (where δ_2 is the momentum loss thickness at separation) was given by Gaster (1966). For a discussion of two-dimensional (unswept) and swept bubbles the reader is referred to Young (1977), for example. The manipulation of bursts leading to open separation bubbles will be dealt with in Section 5.4.2. In many cases it does not appear to be clear, however, whether leading edge stall is caused by the separation of the turbulent boundary layer or by the burst of the separation bubble. Van den Berg (1981) showed in a theoretical analysis that turbulent boundary-layer separation in the nose region may well be the dominant cause, especially at higher Reynolds numbers.

Methods of controlling and manipulating separation along the main body surface have been discussed in Sections 5.2 and 5.3 so that the final part of this section can be confined to the manipulation of base drag flows (Section 5.4.4).

Drag resulting from separation regions at the trailing edge of a flow configuration is a pressure or form drag, since the base flow has a lower pressure than it would have if the flow were inviscid. At the trailing edge separation may occur at a fixed position, such as at a sharp edge, or may vary its position, as in a diffuser or on the rear part of an airfoil. As mentioned earlier, Prandtl (see Betz, 1961) recognized the importance of increasing the base pressure by delaying separation at the trailing edge of a blunt body, by replacing parts of the wall by two counter-rotating cylinders (moving the wall in the flow direction) or by forcing transition on a sphere and thus reducing the size of the separation region (Prandtl, 1914). In this latter case the turbulence increased the friction drag but, by decreasing the form drag, decreased the total drag.

The form drag differs considerably between different flow configurations and Mair (1978) explains how this can happen: "A two-dimensional bluff body in a stream at low Mach number generates a wake in the form of a Kármán vortex street, a regular array of vortices with circulation of alternate sign. This vortex wake is known to be associated with a large drag force on the body, and any device that causes the vortices to form further away from the body gives a reduction of drag." This has been achieved by splitter plates. Roshko (1954) and Bearman (1965), for example, have shown that a splitter plate with a length equal to only one base height can in some cases reduce base drag by as much as 50%. The vortex street is suppressed entirely with a longer splitter plate and the base drag may be reduced by 60% or more. Splitter plates in the wake of a normal flat plate modify the drag and the vortex shedding monotonically as L/H increases from 0 to 3 (here L denotes the length of the splitter plate and H the height of the normal plate). For longer splitter plates the drag coefficient remains constant at 1.84 and vortex shedding has ceased (Apelt and West, 1975). Unfortunately other important information is missing in this latter investigation, such as upstream turbulence level and structure or blockage in the wind tunnel, both of which affect the separation region (Smits, 1982) and thus c_D ; this confines the generality of the statement.

Mair (1978) states furthermore that "some three-dimensional bodies generate wakes in which there is noticeable periodicity, indicating some regular pattern of vortex shedding, but for axisymmetric bodies any regular vortex shedding is only a minor feature of the flow. Correspondingly, the drag coefficients of axisymmetric bluff bodies, based on their frontal areas, are usually considerably smaller than those of the related two-dimensional bodies."

These observations refer mainly to 'open' base drag regions, meaning regions where the wake or the vortex street are not influenced by a wall downstream of the generating body. This case is discussed first, followed by a discussion of the control of base drag in flows

where a wall plays an important rôle, acting as a splitter plate with or without reattachment or, permitting the growth of a new boundary layer which then interacts with the reattached shear layer.

At the end of this introductory section one may mention a study by Ludwig (1982) attempting to minimize drag for a motor-car-like configuration where suggestions were made to reduce both leading and trailing edge separation.

5.4.2. Manipulation of Separation Bubbles

5.4.2.1. Separation bubbles near the leading edge of aerofoils

Depending on the strength and structure of ambient disturbances laminar separation bubbles on airfoils have been observed anywhere in the range $Re_c \leq 10^6$, where Re_c is the chord Reynolds number. Even at low angles of incidence the laminar boundary layer on the upper surface of an aerofoil encounters an adverse pressure gradient which can cause separation. The shear layer may never reattach to the aerofoil or may go through transition, in which case it may reattach, creating a closed bubble. The formation of a laminar separation bubble can be controlled actively (see Section 5.4.3.) or the bubble as such may be prevented by passive means, such as by roughness elements or spoilers which force transition. However, such manipulation must be tailored to the operating conditions and can easily cause drag penalties (e.g. Carmichael, 1981; Lissaman, 1983; Mangalam and Pfenniger, 1984). It is also well known that laminar separation bubbles are easily affected by the disturbance environment, such as the acoustic or turbulence level in a test section (e.g. Marchman, 1987; Marchman *et al.*, 1987; O'Meara and Mueller, 1987). These parameters of influence would have to be incorporated into calculation methods for laminar separation bubbles, such as into that of van Ingen (1975) which takes into account only Reynolds number and a mean velocity gradient parameter.

O'Meara and Mueller (1987) varied chord Reynolds number, freestream disturbance, and angle of incidence. They found the pressure distribution upstream of the separation bubble to be highly dependent not only on the angle of incidence but also on the chord Reynolds number and the disturbance environment. As the chord Reynolds number or the upstream turbulence level are increased, the bubble decreased in length and thickness, decreasing the pressure plateau near separation and increasing the suction peak.

5.4.2.2. Separation bubbles near the front edge of blunt bodies

A flow approaching a blunt body is decelerated in the region of the stagnation point, accelerated in the boundary layer on the blunt face, and separates near the sharp front edge of the body forming a separation bubble or an open separation region according to the length of the body in the main-stream direction. Since the separation bubble and the open separation region increase the total drag of a blunt body, it is necessary to control them. As was shown by Hoerner (1965) the drag coefficient of a two-dimensional square cylinder can be reduced from $c_D = 2$ to close to 1 if the corners are rounded so that the square cylinder becomes cylindrical. The drag of a flat faced circular cylinder (Fig. 23) aligned coaxially with the freestream can be reduced passively in at least four ways all of which have in common that the separation bubble near the front edge of the cylinder is reduced or even eliminated: firstly, by rounding the edge of the front face, secondly by fixing a hemispherical forebody, thirdly by fixing strakes to the front face, and finally by shielding the cylinder face by a disc placed coaxially upstream. This shielding effect is brought about by the interaction of two bluff bodies. Koenig and Roshko (1985) distinguish two cases: "(1) If one body is far downstream in the wake of another one, the drag of the downstream body is reduced owing to the reduced dynamic pressure in the wake in which it is immersed, while the drag of the first body is unaffected. This may be called a weak interaction." (See also Section 5.3.4.2.) "(2) When the downstream body is brought close to the base of the first one, the drag of the

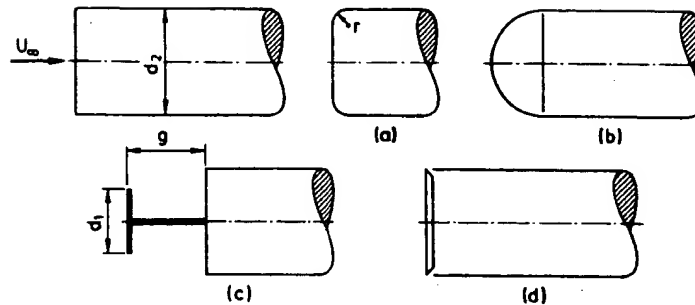


FIG. 23. A coaxial semi-infinite cylinder with (a) rounded edges, (b) a hemispherical nose cone, (c) a coaxial disc upstream, and (d) with sound excitation emanating from a gap at the leading edge. From Koenig and Roshko (1985) and Sigurdson and Roshko (1988).

former may be significantly reduced. In addition, the drag of the first body may be strongly affected; this would be a strong interaction."

Koenig and Roshko (1985) investigated the reduction of drag and the elimination of the separation bubble near the front edge of a flat axisymmetric cylinder by placing a sharp edged disc connected to the cylinder coaxially upstream, varying the diameter ratio d_1/d_2 of the disc and the cylinder and the gap ratio g/d_2 (Fig. 23). There was no interference between the leading edge flow and the base flow downstream. Drag reduction was measured for the forebody system only which consisted of the disc, the sting forming the connection to the cylinder, and a short segment of the cylinder downstream of its face. The Reynolds number based on the diameter of the cylinder d_2 was 5×10^5 . The drag coefficient (blockage correction applied) was found to be reduced from 0.75 for the flat-faced cylinder without a forebody to 0.03 with the forebody as the 'absolute' minimum. In the (d_1, d_2, g) space this value was found to characterize two stable minimum regions (Table 7).

Under these conditions, the disc is in a range where the separation streamline springing from the disc can reattach at or near the shoulder, in a cavity configuration close to the free streamline ideal. Turbulence measurements show that compared with higher drag cases the low-drag case (II) displays some distinct features: the turbulence is quite small midway into the cavity, the Reynolds shear stress $-\overline{u'v'}$ is very small except for a narrow peak in the shear layer ($-\rho \overline{u'v'}/(\rho u_\infty^2) = 0.004$), the separated shear layer spanning the cavity is thin, and the flow within the cavity appears to be a fairly well defined and steady vortex with a fairly high level of Reynolds stress deep in the cavity. It is interesting to note that case II (disc ahead of body) is practically identical to the optimum geometry found by Mair (1965) for a disc behind a body (see Section 5.4.4.1).

Morel and Bohn (1980) investigated the interaction of two discs placed normal to the flow in tandem. For the single disc (diameter d_2) the drag coefficient c_D was 1.15. If a second disc with a diameter $0.8 d_2$ and a gap ratio $g/d_2 = 0.54$ was placed ahead of the first disc c_D reduced to a value of 0.21.

The drag on the blunt faced circular cylinder (Koenig and Roshko, 1985) can, of course, be drastically reduced by rounding the corners. With a corner radius equal to one-eighth the cylinder diameter, and with a roughness on the face (to make the boundary layer turbulent and thus to prevent premature laminar separation) the drag coefficient was less than 0.01 for

TABLE 7

	I	II
d_1/d_2	0.875	0.75
g/d_2	0.094	0.25-0.50

$Re > 4 \times 10^5$. The drag coefficient could be reduced further by replacing the frontbody (disc) by a hemispherical nose with the same radius as the cylinder. For zero gap the forebody drag coefficient was of the order $c_D = 0.005$. As the gap is increased from zero the drag coefficient increased and in the range $0.25 \leq g/d_2 \leq 1.5$ the forebody system with the disc had less drag than the one with the hemisphere.

In potential flow in an infinite stream such a cylinder, assuming it to be an infinite half body, would have zero drag, the high pressure near the centre of the face being balanced by the suction near the edge. The drag is then due to the loss of suction near the edge of the front face as a consequence of separation from the edge. Pamadi *et al.* (1988) have attempted to increase suction near the edge of a square faced cylinder by fitting two strakes on the front face. By optimizing the height and position of these strakes drag reduction of about 80% was achieved for Reynolds numbers up to 1.1×10^5 . A second effect to reduce drag in addition to the increased negative pressure region on the windward face was the smooth reattachment of the separated shear layer close to the corners of the blunt body.

Sigurdson and Roshko (1988) extended the experiment of Koenig and Roshko (1985) using *active* control. They investigated the effect of a periodic velocity perturbation on the separation bubble downstream of the sharp-edged blunt face of a circular cylinder. The forcing technique used was to generate acoustic waves inside the cylinder by oscillation of a loudspeaker located there. Via a small circumferential gap just downstream of the separation line communication to the external flow was possible and velocity fluctuations could be superimposed. The Strouhal number ($St = F_{ex} D / u_\infty$) of excitation was 3.1—being in the range where the drag was a minimum—the amplitudes of excitation (as measured in the gap) were $u'/u_\infty = 3.9\%$ and 7.8% , and the Reynolds number was 1.32×10^5 . The reattachment length was reduced a maximum of 10% and 31% for the respective forcing amplitudes. The authors conclude: "The flow is considerably modified when forced at frequencies for which associated wave lengths are comparable to bubble height. At high Reynolds numbers these wave lengths are greater and the forcing frequencies are lower than those of the initial Kelvin-Helmholtz frequencies of the separating free shear layer. Forcing then increases entrainment in the early part of the shear layer; as a result, reattachment length, bubble height, pressure at separation and drag on the face, are all reduced." □

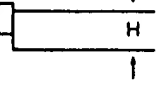
For a further discussion of separation control by acoustic forcing the reader is referred to section 5.4.3.2.

5.4.3. Control of Leading-Edge Separation

5.4.3.1. Vibrating ribbon or oscillating flap

Vibrating ribbons are used extensively to generate small amplitude disturbances in laminar boundary layers and to start the transition process. Turbulence-generating wires can also be placed parallel to the leading edge of a low Reynolds-number airfoil with the purpose of influencing the laminar separation bubble. In both cases velocity perturbations are imparted to the flow by active control and may affect the separated flow in three ways: (1) they may shorten or even avoid the laminar separation bubble at low Reynolds numbers and high angles of incidence, (2) they may force the ~~separated~~ laminar or turbulent boundary layer to reattach or (3) they may eliminate the hysteresis loop, which is a result of laminar bubble breakdown and reformation during stall and stall recovery resulting in severe control problems. For a Wortmann FX 63-137 aerofoil, Neuburger and Wygnanski (1987) found that if a typical inception of stall at a prescribed Reynolds number occurred at an angle of incidence $\alpha = 18^\circ$, the recovery from stall might occur at $\alpha = 10^\circ$. Placing a vibrating ribbon at the position of the origin of the separation bubble eliminated the hysteresis loop and increased the stall angle from 15° to 18° (see Table 8). The hysteresis phenomenon depends on the surface smoothness, the Reynolds number, the noise level and its frequency content, as well as on the turbulence level in the free stream (Marchman *et al.*, 1987). 483

TABLE 8

Author	Configuration	Re_δ	$f^+ = \frac{f \cdot c}{u_0}$	$A \cdot \omega / u_0$	Position/chord of oscillator
Koga (1983)	ZPG + APG	$Re_{\delta_2} = 500-3500$	0.075	—	Downstream from wedge flow separation
spoiler-like flap	boundary layer				
Neuburger and Wygnanski (1987)	NACA 0015	4×10^5	0.9		0.1
vibrating ribbon	FX-63-137	2×10^5	0.9	3×10^{-3}	0.1
Nakamura and Ozono (1987)	flat blunt plate	$Re_H = 1.4-4.2 \times 10^4$	0.12	—	at blunt leading edge
oscillating leading edge spoiler					
Katz <i>et al.</i> (1989)	P 255	3×10^5	1.6	—	0.14
flaperon					
Bar-Sever (1989)	LRN (I) 1010	1.5×10^5	1	—	— 0.01
oscillating wire					

Bar-Sever (1989) investigated the effects of periodic forcing of the separated shear layer for a range of post-stall angles of incidence of an aerofoil. He forced a 0.1 mm tungsten wire to oscillate at its fundamental natural frequency by passing an oscillating electrical current through it. The wire was located about 1.5 mm upstream from and parallel to the leading edge of the aerofoil. Forcing increased the maximum lift coefficient from 1.43 to 1.60 and shifted the angle of incidence at which it occurred from about 11° to 20° with separation moving from about 70% to 80% chord (for the 20° case from the leading edge to 80% chord). The wire oscillation amplitude was kept constant at all forcing frequencies (no value given) and the dimensionless frequency f^+ is of the order of one (see Table 8). Hot-wire data given do not appear to be very reliable, since no information is provided on the degree of instantaneous reverse flow.

Small amplitude oscillatory motions may also be introduced by small flaps or flaperons near the leading edge. Katz *et al.* (1989) investigated the influence of an oscillating flap (height 10 mm, oscillation amplitude ± 1 mm) on a separating turbulent boundary layer along an inclined flat wall. Activating the flap at frequencies corresponding to Strouhal numbers based on initial momentum thickness ($St = f \delta_2 / u_{init}$), which are smaller than 0.01, and at reference amplitudes $u'/u_{init} > 0.25\%$ resulted in a complete reattachment of the flow to the surface. It was found that the proportions of the 'wall' and wake functions in the reattached boundary layer were changed and that the large scale coherent structures had a greater spanwise extent near the solid surface in the forced case.

Nakamura and Ozono (1987) investigated the effect of a spoiler oscillating vertically at the blunt leading edge of a rectangular flat plate with amplitudes of 0.05 H and 0.1 H and found from the mean pressure distribution that the main effect of the spoiler oscillation was to shorten the leading edge separation bubble; it shortened as the flow velocity decreased. The effects of an oscillating spoiler-like flap in zero and adverse pressure gradient flows were investigated by Koga (1983) and Chen and Shiyng (1989). The former author showed that a two-dimensional separated flow region can be controlled by the generation of vortices of size of the order of the separation height and that the most effective reattachment control occurs near f^+ of about 0.075. The latter authors used a 'flapping spoiler' on the straight wall to control separation in an asymmetric 15° diffuser so that the position of the separation region was changed in a flip-flop-like manner between the two walls. The optimum position for the spoiler was found to be on the straight wall opposite the locus of separation on the inclined wall.

Work on closed loop control of a round jet/diffuser is in progress (Koch *et al.*, 1989). The diffuser flow exhibits transitory stall, and eight radial on/off jets are used as the actuators

and four hot-wire probes as the sensors to attempt to stabilize the jet in the centre of the diffuser.

As may be seen from the scanty results presented above, the control and manipulation of separated flows by means of oscillating spoiler-like devices and control jets is still in its infancy and needs further investigation. Table 8 shows, however, for the Reynolds number range of the experiments on aerofoils, $10^5 \leq Re_c \leq 10^6$, that the effective dimensionless frequency $f^+ = f \cdot c/u_\infty$ lies between 0.9 and 1.6, and that the position of an effective oscillator should be very close to the leading edge.

5.4.3.2. Acoustic excitation

It is well known that sound of particular frequencies and intensities can influence the transition process, and that both 'external' sound and sound emitted 'internally' through openings in the body surface will initiate transition.

The bulk of the investigations discussed below (see Table 9) is concerned with the control of pre-stall, stall and post-stall flows over aerofoils and thus goes beyond leading-edge separation (stall) discussed in Section 5.4.3. The control of flow separation by sound was investigated by Collins and Zelenevitz (1975) and later more extensively by Ahuja and Burrin (1984). A survey of some investigations is given in Table 9. Besides this, there are two papers which deal with circular cylinder flow (Hsiao *et al.*, 1989) and with a backward facing step (Bhattacharjee *et al.*, 1986), respectively. The important question is the sound pressure level (SPL) required to fully or partially attach the flow around an aerofoil as a function of sound frequency, chord Reynolds number, and angle of incidence in order to increase the lift coefficient, decrease the drag coefficient, and extend the operating range of the aerofoil (Collins and Zelenevitz, 1975). Some answers were provided for specific aerofoils in the chord Reynolds number range 6.3×10^3 to 5.4×10^5 , but even for these cases many questions concerning, for example, the flow quality, the two-dimensionality of the flow, the turbulence level, and the acoustic background remain open. The latter two parameters are of special importance (see Marchman *et al.*, 1987), since investigations of the same aerofoil showed different results in different wind tunnels, raising the question whether these wind tunnel data can be applied in free flight. A catalogue of questions concerning the mechanisms of sound interaction was prepared by Zaman *et al.* (1987) and is reproduced and extended here:

- How does the observed effect depend on the chord Reynolds number ($Re_c = u_\infty \cdot c/\nu$) and on the angle of incidence α ?
- How critical is the intensity of the incident sound wave?
- Is stall suppression a continuous function of frequency or effective only at certain frequencies? What is the envelope of the effective excitation frequencies?
- How does the effective excitation frequency f_{exc} scale?
- Which component of the velocity fluctuations is most effective for excitation?
- How does wind-tunnel resonance affect the flow?
- Does a specific sound field influence the transition process in the laminar boundary layer or in the separated shear layer or both?
- What is the receptivity process through which vortical disturbances are excited by sound waves?
- How does tunnel noise and/or turbulence level influence separation control and possibly hysteresis effects?

Answers to these questions are definitely always of academic interest but would be of minor practical importance, especially at higher Reynolds numbers, say 10^6 , if separation control by oscillating flaps, for example, were to turn out to be more effective and less dependent on wind-tunnel conditions, thus easier to transfer to free flight. Bearing in mind that results quoted below may refer only to one specific aerofoil under specific wind-tunnel conditions, the following preliminary answers may at least give some guidance. Acoustic excitation is

TABLE 9

Author Type of separation	Aerofoil	Source of sound	$Re_c \times 10^{-3}$	$f^+ = \frac{f \cdot c}{u_0}$	SPL dB	b/c	$7u_{rms}(\%)$	frequency range (kHz)	Optimum $St/Re_c^{1/2}$	α° -range
Collins and Zelenevitz (1975) Laminar separation Collins (1981)	NACA 2412	External	2.5-5.3	—	88-134	3 (end-plates)	0.5	0.7-4.0	—	-24
	NACA 2412	Internal and external open tunnel	3.3-5.4	—	—	—	—	—	—	-24
	NACA 0015	External	—	—	—	—	—	—	—	—
Ahuja and Burtin (1984)	NACA 65(1)-213 3 chord lengths GA(W)-1	External	≈ 4	≈ 4	-143	2, 3, 5	0.1%	0.45-6	≈ 0.006	-24
Marchman <i>et al.</i> (1987)		Internal, slot near the leading edge	≈ 2.3	≈ 11	—	—	0.3%	0.92	≈ 0.023	-28
	Wortmann FX 63-137	External, VPI-tunnel	1	—	95-110	8	0.02 to 0.3	0.5-5.5	—	-18°
	LRN(1)-1007	External	0.4-1.4	1-5	87-127	3	0.25	0.1-10	—	-18
Zaman, Bar-Sever and Mangalam (1987) Laminar separation pre-stall and post-stall	High performance, low Re —no airfoil, no hysteresis									
Huang <i>et al.</i> (1987) Stall and post-stall	Symmetric airfoil with 18% thickness ratio	Internal, gap near the leading edge	0.35	(0.19/sin α)	115	—	—	Twice the shedding frequency reduces the re- gion of separa- tion 100 Hz	—	-30
Zaman and Mc Kinzie (1989) Laminar separation	LRN(1)-1007 Wortmann FX 63-137	External	0.25-1	1-25	90-130	6 and 3	< 0.1	0.1-1.2	0.025	-20
Niakioka <i>et al.</i> (1989)	Flat plate at incid- ence with knife edge	External, open tunnel	0.4	7.5	—	1.3 (end-plates)	0.3	0.2-1.0	0.035	-14
Hsiao <i>et al.</i> (1989) Pre-stall and post-stall Shearin and Jones (1989)	NACA 63,018	Internal	0.063-3	2	95 at slot exit 110-136	—	0.25	0.1-0.7	0.0034 -0.015	-24 0
	NACA 0009	External, anechoic flow facility NASA Langley	15-30	—	—	0.51 (side-plates)	0.5	1.4-6	—	0
Bhattacharjee <i>et al.</i> , (1986) Laminar and turbulent separation	Backward facing step	External	$Re_w \times 10^{-4} = 2.6-7.6$	0.2	92	16.2 b/H	2.3%	< 0.2	—	0

found to significantly influence the flow separation over an aerofoil for chord Reynolds numbers Re_c below approximately 10^5 but the strength of the effect changes with the state of separation (pre-stall, stall, post-stall). For example Zaman *et al.* (1987) found the following:

(1) For a chord Reynolds number $Re_c = 4 \times 10^4$ and an angle of incidence $\alpha = 8^\circ$, laminar separation (low pre-stall) could be removed and the lift coefficient c_L increased by as much as 50% compared with when the separation region was furthest upstream. The corresponding Strouhal number ($St = f_{exc} \cdot c/u_\infty$) ranged from 5 to 1 and the amplitudes were at most 10 dB higher than the background level. Excitation at higher frequencies was ineffective.

(2) For the same chord Reynolds number and amplitude (SPL) but at angles of incidence in the range $10^\circ \leq \alpha \leq 15^\circ$, i.e. at high pre-stall, practically no improvement in c_L could be achieved. Instead, for certain high f_{exc} a decrease in c_L was found.

(3) For post-stall conditions (here $\alpha = 18^\circ$)—other parameters unchanged—the Strouhal number range was larger (4–25) and c_L could be increased if the amplitude of excitation was increased.

If acoustic excitation was effective a narrower wake was observed yielding a drop in the drag.

At higher Reynolds numbers ($Re_c = 10^5$) and post-stall conditions ($\alpha = 18^\circ$), the effective Strouhal-number range shifted to 6–60 and the amplitude had to be increased by 8 dB. For each specific aerofoil there is, of course, a limiting angle of incidence where excitation does no longer affect the separated flow.

Zaman and McKinzie (1989) found that for pre-stall conditions and a Reynolds number range $2.5 \times 10^4 < Re_c < 10^5$ the most effective frequency for separation control scales with $U_\infty^3/2$ which corresponds with the parameter $St_c/Re_c^{1/2}$ falling in the range 0.02–0.03. A value of 0.035 can be calculated from the experimental results of Nishioka *et al.* (1989), and this value is close to the above range.

Little is known about the velocity fluctuations causing the most effective excitation and the available data is slightly contradictory. Zaman *et al.* (1987) indicated that the effect was strongest whenever a large v' fluctuation was induced, and this could be enhanced by tunnel cross-resonances, especially when large amplitudes were required. Zaman and McKinzie (1989) showed that u' and v' fluctuations were equally effective in the excitation of the flow, however at different frequencies. The amplification of the imposed perturbation took place primarily in the downstream shear layer rather than in the upstream boundary layer which, as shown by stability analysis (Zaman *et al.*, 1987), is insensitive to the imposed perturbations. Nishioka *et al.* (1989) confirmed that the receptivity and instability of the separated shear layer are the important properties. The shear layer rolls up into discrete vortices right at the leading edge almost without a stage of growing travelling waves. These vortices enhance entrainment leading to reattachment as long as their scale (thickness of the separated shear layer) is matched to that of the separation bubble. Huang *et al.* (1987) showed that with the injection of sound emanating from a narrow gap in the vicinity of the leading edge of a symmetrical aerofoil ($Re_c = 3.5 \times 10^4$) at or above the shedding frequency of the shear layer the separation region was drastically reduced. For a recent review on boundary-layer receptivity to unsteady pressure gradients the reader is referred to Nishioka and Morkovin (1986).

All the above investigations were performed in flows where the turbulence level in the freestream was 0.25% or larger, with the exception of Zaman and McKinzie (1989) where Tu was 0.1%. Such a relatively high turbulence level causes additional difficulties in separating aerodynamic from sound-excited effects. Marchman *et al.* (1987) therefore performed experiments in a low turbulence wind tunnel ($Tu \approx 0.02\%$) with no measurable standing waves. The ambient turbulence of the wind tunnel was most pronounced in magnitude in the 10–20 Hz range, and this part of the spectrum was amplified by a turbulence grid. An increase from 0.02 to 0.2% almost eliminated the hysteresis loop. The additional turbulence (see Section 5.3.2) was capable of restoring attached flow over the rear

half of the wing, but not full suction around the leading edge of the aerofoil. The effect decreases with increasing Reynolds number ($Re_c > 10^5$). Acoustic disturbances increased the angle of incidence at which initial stall occurred, a phenomenon that is highly frequency dependent (here at $\alpha = 10^\circ$ and with an SPL of 110 dB, f_{exc} was 4830 Hz) and not seen with the increase in free-stream turbulence. Furthermore tests showed that a disturbance of the proper frequency and pressure level can often completely restore a fully separated flow to a fully attached state, which remains stable and attached after the disturbance signal is removed. That the influence of an acoustic disturbance is so frequency-dependent emphasizes the importance of knowing the frequency spectrum of any disturbance.

Experiments in a backward-facing step flow (Bhattacharjee *et al.*, 1986) showed that the spreading rate of the separated shear layer increases and the reattachment length decreases when acoustic forcing is applied in a Strouhal number of 0.2–0.4 ($St = fH/u_\infty$ where H is the step height and u_∞ the freestream velocity prior to the step edge). The controlled forcing apparently affects the separated flow by enhancing the vortex merging process and by increasing the spanwise extent of the resulting structures. The effects of the forcing were found to be relatively independent of flow conditions and upstream boundary layer properties within the range $2.6 \times 10^4 \leq Re_H \leq 7.6 \times 10^4$.

The trailing-edge flow of a LEBU, where acoustic waves phase-locked to the large scale structure interacted with a large-eddy break-up device was investigated by Nagel (1988). Both turbulent mixing and skin friction were reduced.

5.4.3.3. Suction or blowing

To control separation in the leading edge region suction and slot blowing have also been investigated (e.g. McLachlan, 1987) but have not been used in many practical applications. Suction could become important, however, in minimizing cross-flow instability on swept wings. The suction orifices at the leading edge could also double as a leading-edge cleanser discharge system to prevent accumulation of dirt and insects during the low-altitude climbout (Thomas, 1984). Slot blowing at the leading edge of turbine blades has been used mostly for cooling purposes and will not be discussed here.

5.4.4. Manipulation of Base-Drag Flow

5.4.4.1. Open base-drag regions

Mair (1978) presented an extensive discussion on drag-reducing techniques for the subsonic flow around blunt based bodies (see also Tanner (1975) for compressible and incompressible flow and Heffner *et al.* (1977)). One special configuration is a boat-tailed afterbody terminating in a blunt base with a smaller area than that of the main body. The addition of a conical body to match the shape of the boat tail would give the 'streamline' tail piece (Fig. 24a).

In the case of blunt-based bodies of revolution Mair concluded that a boat-tailed afterbody is much more effective than any other device that had been tried. This conclusion was based on experimental results obtained from bodies aligned with the flow direction, with small overall length (here $L/D \approx 3$, where L is the length of the cylindrical body and D its diameter) and thus a thin upstream boundary layer, with fairly large cone angles 2β of the boat tail (between 40° and 50°) and a smooth transition of the contour between boat tail and main body, and with a turbulent boundary layer without separation ahead of the base. The best boat-tailed afterbody found by Mair (1969) was a cone with $\beta = 22^\circ$, joined by a curved fairing of length $0.5 D$ to the cylindrical body at A (see Fig. 24a). The position shown for B corresponds to $L/D = 0.76$.

All design measures discussed by Mair (1969) were aimed at keeping the boundary layer attached down to plane B and at increasing the pressure recovery. The philosophy can be taken further by designing a short tailed body with optimum pressure recovery which

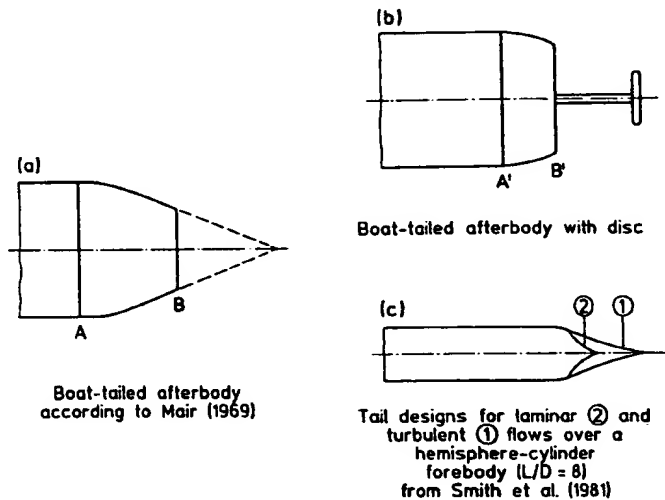


FIG. 24. Various afterbody shapes, (a) and (b) from Mair (1969) and (c) from Smith *et al.* (1981).

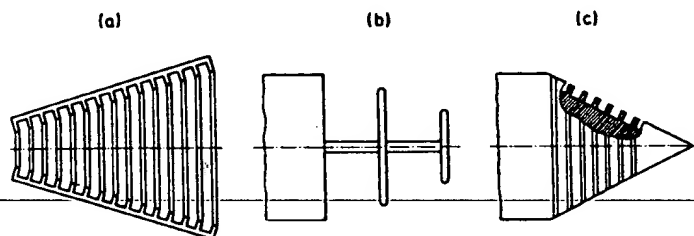


FIG. 25. Various devices for reducing base drag.

avoids separation (Smith *et al.* (1981), see Fig. 24c and Section 5.2.2) or by increasing the pressure downstream of B by mounting a disc behind the base (Fig. 24b). The latter was first suggested by Mair (1965) who gives credit for the physical effect to Migay (1962) who applied it to the ribbed diffuser (see Fig. 25a). He introduced the 'roller bearing' effect of certain cavity flows, which ensures that the flow outside the cavities follows the ribs fairly closely, resulting in a good pressure recovery even for large cone angles (up to 40°). Migay's and Mair's suggestions were combined in circumferentially-grooved afterbodies (Howard *et al.*, 1981, 1983; Fig. 25c). Discs or ridges between the grooves may have edges which are rounded or sharp, the former showing slightly better results for drag reduction (see Mair, 1965, Figs 4 and 5).

Returning to the afterbody with one or two discs mounted downstream we find several interesting results (Fig. 26a): (i) the greatest drag reduction obtainable by adding a disc to the short body (rounded nose with cylindrical body ($L/D = 4.69$)) is $\Delta c_D = 0.053$, which is 35% of the base drag of the simple body. For the long body ($L/D = 10$) the drag reduction was always less (here 30%). (ii) 'Drag reducing devices' can also lead to drag increases which can be much larger than the drag decrease. In the high drag regime ($x/D \approx 0.3$ of Fig. 26a) low frequency oscillations were observed connected with an inward and outward movement of the shear layer. This implies that in this regime the usual balance between air flow entrained and diverted back into the cavity by the disc is unstable (Mair, 1965), (for a more detailed investigation see Little and Whipkey (1979)). The disc configuration was therefore replaced by a solid boat-tailed afterbody as sketched in Fig. (24a) with a diameter of $0.795 D$ at its downstream end and an axial length of $0.5D$. This configuration gave a Δc_D of -0.099 , i.e. about twice that of the optimum disc. Figure 26b shows a parametric study of the double disc configuration including the greatest observed drag reduction

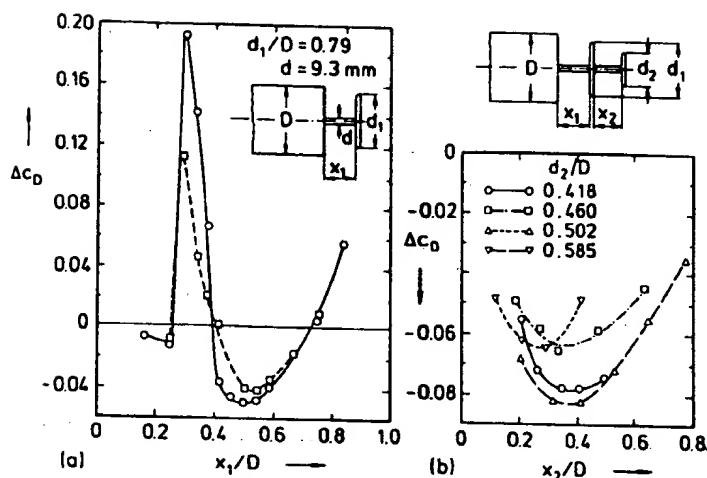


FIG. 26. (a) Drag due to 3 mm thick disc with rounded edge on short (○) and long (□) bodies from Mair (1965). (b) Drag reduction due to two discs; short body $x_1/D = d_2/D = 0.5$; $d_1/D = 0.79$. Discs 3.2 mm thick, rounded edges.

$\Delta c_D = -0.082$ amounting to 55% of the base drag of the simple body. This is still not the drag reduction obtained by the solid body alone but is encouraging in that it suggests a further possible improvement by combining the solid boat-tailed afterbody with an additional disc. Such a combination will be less dependent on Reynolds number effects than a tail fairing and will probably be more docile to changes of the body axis with yaw.

For subsonic 'locked-vortex-afterbody configurations' (single disc) Little and Whipkey (1979) found from drag measurements and flow visualization that the minimum-drag condition is obtained if the cavity vortex centres itself fairly well in the cavity and produces a smooth cavity flow and does not disturb the external flow. Mass transfer into and out of the cavity is minimized with a balance between vortex size and cavity size. This occurs at some combination of disc diameter, disc position, and spindle diameter (d) and shows that separation control in this case consists of preventing separation on the solid body and of tuning the separated shear layer with the flow in the axisymmetric cavity.

The trailing-disc concept was also successfully tested in flight experiments at higher Reynolds numbers than those of Mair and at Mach numbers up to 0.93 by Powers (1988).

Mair noted the importance of the smooth fairing between the contours of the main body and the afterbody. A smooth contour avoids a suction peak at the junction and thus an additional pressure rise leading to premature separation. A turbulent and even more a laminar boundary layer are strongly Reynolds number dependent in such a flow configuration. Therefore Howard *et al.* (1983) investigated the effectiveness of shoulder 'radiusing' and circumferential 'grooving' (Fig. 25c) to reduce the base drag for a range of Reynolds numbers based on body diameter ($2 \times 10^4 \leq Re_D \leq 2 \times 10^5$). For $Re_D > 10^5$ shoulder 'radiusing' relative to body diameter of $R_s/D = 2.75$ was found to reduce the body drag to levels equivalent to a streamline body having 67% greater fineness ratio. Circumferential grooves cut perpendicular to the local surface were found to provide on the order of 50% net body drag reduction with zero shoulder radius for both laminar and tripped boundary layers approaching the shoulder. An earlier study covering longitudinal V-grooves by Howard *et al.* (1981) had shown that afterbody shoulder radiusing is a more efficient technique for reducing bluff-body base drag than longitudinal 'grooving' which need not be discussed here.

5.4.4.2. Base-drag regions with reattachment

The classical case of a base drag region with reattachment is found downstream of a backward facing step followed by a wall or a long splitter plate where the step may be

normal or oblique to the oncoming flow. Interesting features of the subsonic flow are the distance of the reattachment line from the step, the structure of the shear layer turbulence, the spreading rate of the shear layer, the properties of the flow in the reverse-flow region, heat and mass transfer, and the downstream recovery of the attached flow. Several of these features are conducive to control or manipulation. Control parameters are, for example, tunnel blockage, area ratio, streamwise pressure gradient, turbulence level and structure of the upstream flow, state (laminar or turbulent), and thickness of the upstream boundary layer. There is also mass addition by injection of fluid into the reverse-flow region and passive separation-control techniques, such as transverse cavities, longitudinal grooves, porous surfaces, and vortex generators (e.g. Lin *et al.*, 1989). Active control has been achieved by using periodic oscillations of a spoiler or a flap at separation or inside the separated zone (Reisenthel *et al.* 1984; Roos and Kegelmann, 1986). There is no systematic investigation of the effects of these flow parameters and control devices on the flow downstream of the straight backward facing step, let alone of other step configurations. As one example, the length X_R of the reattachment region was found to be in the range of five to nine step heights H (Eaton and Johnston, 1981). The most extensive studies into the influence of some of the above mentioned flow parameters on the reattachment length were performed by Westphal and Johnston (1984) and by Adams and Johnston (1988). Reattachment was defined in their investigations as $\chi_w = 0.5$, where χ_w denotes the probability of forward flow close to the wall.

Adams and Johnston (1988) plotted the dimensionless reattachment distance x_R/H (where H is the step height) against expansion ratio $ER = (W_1 + H)/W_1$ (W_1 is the duct height upstream of the step) and against Reynolds number Re_H using up to 20 experimental investigations. In the former diagram x_R/H increased from about 5 to 8.7 with a scatter of 20–50% with ER increasing from 1.1 to 2.9, probably at Reynolds numbers larger than 1.5×10^4 . In the range $1.5 \times 10^4 \leq Re_H \leq 2 \times 10^5$ variations of x_R/H lie in a range approximately 6.5 to 8 even in experiments performed in the same laboratory (Fig. 2 of Adams and Johnston, 1988). It is possible to attribute this variation not to a Reynolds number effect but to that of a thin laminar boundary layer for $x_R/H = 6.5$ and a thicker ($\delta/H = 0.2$) turbulent boundary layer for the higher value (Westphal and Johnston, 1984). This was confirmed by measurements of Adams and Johnston (1988) who showed a $\Delta(x_R/H) \approx 2$ between a very thin laminar and a thick turbulent boundary layer ($\delta/H \sim 1.1$). The same difference in reattachment length was obtained when—all other parameters equal—large triangular vortex generators were installed upstream of the step. They generated an array of counterrotating vortices imbedded in the separating turbulent boundary layer.

The influence of an adverse pressure gradient caused by the divergence of the wall on the flow downstream of a backward-facing step was investigated by Driver and Seegmiller (1982, 1985). The spreading rate of the shear layer was increased and the reattachment distance was lengthened from x_R/H of about 6 to about 10 for a deflection angle varying between 0° and 9° at an inlet Reynolds number Re_{δ_2} of approximately 5000 (here δ_2 is the momentum loss thickness and u_∞ the velocity at the boundary-layer edge).

Finally one should mention the effect of the boundary-layer thickness upstream of the step on the heat transfer downstream.

Vogel and Eaton (1984) found that the heat-transfer coefficient, which had its maximum value just upstream of reattachment, decreased by about 25% with an increase of δ/H from 0.15 to 1.6. They also noticed that the r.m.s. value of the skin friction increased by 25% when the boundary layer thickness ratio was reduced from 1.1 to 0.2 which led to the conclusion that the turbulence levels near the wall and the heat transfer increases with a thinning of the inlet boundary layer.

Passive control of the flow through changes in the geometry of the backward facing step was applied by using longitudinal grooves mitigating the imposed adverse pressure gradient, transverse and swept grooves, different kinds of segmented blunt edges, and passive bleed through porous surfaces. Lin *et al.* (1989) claim a reduction of more than 50% of the reattachment length by transverse grooves in the region of the maximum adverse pressure gradient using a height to width ratio greater than 2.5. Some control devices

TABLE 10. COMPILATION OF CHARACTERISTIC STROUHAL NUMBERS RELATING TO PERIODIC FORCING OF BASIC FREE SHEAR FLOWS (COMPILED BY R. HAGEN, F. MICHAEL AND C. WOLFFSTIEG)

Flow	f (Hz)	Ma	St_r, St_v	Re_δ, Re_θ	Result	Ref.
jet, 2-D	500 ... 5000			6000 (d)	decrease in turbulent scale	Kaiser and Goldschmidt (1971)
jet, 2-D	500 ... 5000			6000 (d)	increase in turb. intensity	Kaiser and Goldschmidt (1971)
jet, 2-D	500 ... 5000			6000 (d)	increase in spreading of jet	Kaiser and Goldschmidt (1971)
jet, elliptic			0.4 (d)		preferred mode (incr. jet cross-sect)	Hussain <i>et al.</i> (1987)
jet, elliptic			0.85 (d)		stable pairing mode	Hussain <i>et al.</i> (1987)
jet, elliptic			0 ... 0.9 (d)/0.01 ... 0.02	$1 \cdot 10^3$ (d)	turbulence suppression	Hussain (1983)
jet, elliptic			0.4 (d)	$1 \cdot 10^3$ (d)	preferred mode (incr. jet cross-sect)	Hussain and Hussain (1983)
jet, free			0.25 ... 0.5 (d)		preferred mode	Ho and Gutmark (1982)
jet, free	56	0.15	0.0028	$0.84 \cdot 10^{-4}$	mean mass flow constant	Bernal and Sarohia (1984)
jet, free	326	0.15	0.016	$0.84 \cdot 10^{-4}$	mean mass flow constant	Bernal and Sarohia (1984)
jet, free	900	0.15	0.045	$0.84 \cdot 10^{-4}$	mean mass flow constant	Bernal and Sarohia (1984)
jet, free	900	0.5	0.013	$2.8 \cdot 10^{-4}$	mean mass flow constant	Bernal and Sarohia (1984)
jet, free	326	0.5	0.0048	$2.8 \cdot 10^{-4}$	mean mass flow constant	Bernal and Sarohia (1984)
jet, free	56	0.5	0.00084	$2.8 \cdot 10^{-4}$	mean mass flow constant	Bernal and Sarohia (1984)
jet, free	326	0.8	0.00032	$4.5 \cdot 10^{-4}$	mean mass flow constant	Bernal and Sarohia (1984)
jet, free	326	0.8	0.0032	$4.5 \cdot 10^{-4}$	mean mass flow constant	Bernal and Sarohia (1984)
jet, free	900	0.8	0.0084	$4.5 \cdot 10^{-4}$	mean mass flow constant	Bernal and Sarohia (1984)
jet, plane	112 ... 420		3.1 (d)	$5.9 \cdot 10^3$ (d)		Bechert (1976)
jet, plane	76 ... 660		0.01 ... 6 (d)	$1 \cdot 10^3$ (d)		Brown (1973)
jet, plane	500 ... 5000		0.42 (d)	$6.1 \cdot 10^3$ (d)		Goldschmidt and Kaiser (1971)
jet, plane	10 ... 150		$5.9 \cdot 10^{-3}$ (d)	$1.4 \cdot 10^3$ (d)		Korczak (1980)
jet, plane	300 ... 425		0.14 (d)	$4 \cdot 10^3$ (d)		Morkovin (1971)
jet, plane	1500 ... 4500		0.01 ... 0.48 (d)	$4.4 \cdot 8 \cdot 10^3$ (d)		Roffmann (1969)
jet, plane	240 ... 800		0.2 ... 0.5 (d)	$4 \cdot 10^3$ (d)		Sato (1960)
jet, plane	100 ... 6400		600 ... 7200 (d)	$6.5 \cdot 520 \cdot 10^3$ (d)		Vlasov and Ginevskiy (1968)
jet, plane	3 ... 12		0.33 ... 2 (d)	$1.8 \cdot 10.8 \cdot 10^3$ (d)		Rockwell (1972)
jet, plane	10 ... 30		$1.6 \cdot 5 \cdot 10^{-3}$ (d)	$1.4 \cdot 10^4$ (d)		Simons <i>et al.</i> (1979)
jet, plane	100		0.01 (d)	$1 \cdot 10^4$ (d)		Soult (1977)
jet, plane	0 ... 1600				vorticity production	Brown (1935)
jet, plane	0 ... 30		0.005 (d)	$1.4 \cdot 10^4$ (d)	increase of entrainment	Simmons <i>et al.</i> (1979)
jet, plane	930 ... 26800		0.018 (e)	$4.9 \cdot 10^4$ (d)	maximum of turbulences	Zaman and Hussain (1981)
jet, plane			0.03 ... 2 (d)	1860 ... 10800 (d)	5 regimes of exciting jets	Rockwell (1972)
jet, plane			0.14 (wide)	200 ... 9000 (wide)	change jet velocity (sound)	Roffmann and Toda (1969)
jet, rectangular	50 ... 4500		0.46 ... 1.69 (d)	$1.5 \cdot 20 \cdot 10^3$ (d)		Bechert (1968)
jet, round	103 ... 5700		0.15 ... 0.6 (d)	$7.8 \cdot 13.4 \cdot 10^4$ (d)		Crow <i>et al.</i> (1971)
jet, round	70 ... 337		0.01 ... 1.6 (d)	$1.1 \cdot 11.3 \cdot 10^4$ (d)		Hussain <i>et al.</i> (1977)
jet, round	40 ... 2500		600 ... 7200 (d)	$1.3 \cdot 250 \cdot 10^3$ (d)		Wehrmann (1957)
jet, round	10 ... 25		0.01 ... 0.02 (d)	$6.2 \cdot 10^4$ (d)		Brenthorst (1979)

jet, round	27	0.04 ... 2	0.11 (d)	$8.1 \cdot 10^3$ (d)	mixing enhancement	Curtet and Girard (1973)
jet, round		0.2 ... 1.3	0.2 ... 0.62 (d)	$5 \cdot 10^3$... $2 \cdot 10^4$ (d)	noise amplification	Stone and Mc Kinzie (1984)
jet, round		0.04 ... 0.8	0.2 ... 1.4 (d)	$2 \cdot 10^3$... $2 \cdot 10^4$ (d)	mixing suppression	Stone and Mc Kinzie (1984)
jet, round		0.2 ... 1	0.5 ... 4 (d)	$5 \cdot 10^3$... $1 \cdot 10^4$ (d)	noise suppression	Stone and Mc Kinzie (1984)
jet, round		0 ... 0.3	1.7 ... 4.2 (d)	$1.5 \cdot 10^3$... $9 \cdot 10^3$ (d)	mixing enhancement	Vlasov and Ginevskiy (1967)
jet, round		< 0.15	0.2 ... 0.6 (d)	$1 \cdot 10^3$... $2.5 \cdot 10^3$ (d)	mixing suppression	Vlasov and Ginevskiy (1967)
jet, round	308 ... 2480		0.017 (e)	$3 \cdot 10^3$ (d)	max. of turbulence suppression	Zaman and Hussain (1981)
jet, round			0.005 ... 0.009 (e)	$2.1 \cdot 10^3$... $20 \cdot 10^3$ (d)	noise amplification + 3.5 dB	Hussain <i>et al.</i> (1987)
jet, round			0.009 ... 0.017 (e)		noise suppression - 2.5 dB	Hussain <i>et al.</i> (1987)
jet, round			0.01 ... 0.02 (e)		noise suppression	Hussain <i>et al.</i> (1987)
jet, round			0.35 ... 0.75 (axial)		Blooming jet	Hussain <i>et al.</i> (1987)
jet, round				2800 ... 1000	bifurcating jet	Lee and Reynolds (1985)
jet, round				2800 ... 1000	trifurcating jet	Lee and Reynolds (1985)
jet, round				4300	self-excitation	Lee and Reynolds (1985)
jet, round			0.5 ... 0.69 (d)	$7.5 \cdot 10^3$ (d)	$n = 1$: increase with temperature	Monkewitz (1990)
jet, round			0.3	7500 (d)	$n = 1$: increase with temperature	Monkewitz (1990)
jet, round			0.45	7500 (d)	amplific. of u_r reach. maximum	Monkewitz (1990)
jet, round			0.85 (d)		decrease average speed, increase	Hussain (1978)
jet, round			0.2 ... 1 (d)		pulsation	Vlasov and Ginevskiy (1967)
jet, round			1 ... 5 (d)	$6.5 \cdot 10^3$ (d)	increase average speed, decrease	Vlasov and Ginevskiy (1967)
jet, wall			0.012/0.017 (e)		pulsations	Hussain <i>et al.</i> (1987)
jet, whistler			1.47 (d)	$5 \cdot 10^3$ (d)	under investigation	Hussain <i>et al.</i> (1987)
mix. layer, plane	21		1 (d)	$3.7 \cdot 10^3$ (d)	self excitation, mix enhancement	Fiedler <i>et al.</i> (1977)
mix. layer, plane	20		2.4 (d)	$1.5 \cdot 10^3$ (d)		Mensing <i>et al.</i> (1979)
mix. layer, plane	20 ... 60		0.017 (e)	269 (e)		Oster <i>et al.</i> (1977)
mix. layer, plane	600/1680		0.075		maximum of turb. suppressions	Zaman and Hussain (1981)
mix. layer, plane	90		0.3 (d)		saturation of mixing layer	Oster and Wagnansky (1984)
mix. layer, impinging	21		0.09 (d)	$12 \cdot 60 \cdot 10^3$	increase in mean velocity	Gutmark <i>et al.</i> (1978)
mix. lay., impinging			0.012 (e)	$12 \cdot 60 \cdot 10^3$	stable pairing	Gutmark <i>et al.</i> (1978)
shear lay.,			0.017 (e)		suppression of pairing	Hussain <i>et al.</i> (1987)
shear layer,			0.004		acoustic excitation	Hussain <i>et al.</i> (1987)
wake, round	63		0.05 (d)	155 (d)	amplitude of perturbation 0.8 dB/d	Bechert (1982)
wake, round	20 ... 100				$n = 0$: vortex	Clembala <i>et al.</i> (1989)
wake, round	3 ... 5				$n = 1$: helical vortex	Scholz (1985)
wake, round	12 ... 15				$n = 0, 1, 2$: shear layer instab.	Scholz (1985)
wake, round	190	0.135			stochastic appearance of coherent structure	Scholz (1985)
wake, round		1.1 ... 1.2 (d)			$n = 1$: stable helix, 3-D coherent	Scholz (1985)

introduce three-dimensional disturbances which distort the starting region of the separated shear layer and decrease the reattachment length, though not much (Gai and Sharma, 1987). Selby (1989) investigated a swept (30°) rearward-facing step with 'V-shaped' streamwise grooves. A pair of streamwise vortices is generated in each groove, energizing the separated flow region and resulting in almost a 30% reduction of the maximum value of the reattachment distance x_R/H .

Active control of the separated shear layer and thus of the reattachment length was achieved by localized excitation of the shear layer using an oscillating flap at the point of separation (Roos and Kegelmann, 1986). Low amplitude flap oscillations at Strouhal numbers fH/u_0 smaller than 0.3 show both a remarkable organizing influence on the large structures in the shear layer and a reduction in the reattachment length by approximately two step heights. The enhanced vortical structure formation which results produces a higher Reynolds stress (a measure of the more intense mixing) and increased entrainment. Reisenthel *et al.* (1984) discovered two regions of optimum reattachment control and their relation to three different mechanisms: "At reduced frequencies less than 0.03, the primary mechanism is that of induced shear layer vortex control. Up to frequencies of 0.08 control is achieved primarily through the vortex formed by the motion of the flap. At higher frequencies multiple reattachment and reseparation lead to a deterioration of the control."

Further work is needed to study the receptivity of the shear layer to frequency and amplitude of the excitation.

6. GLOBAL FLOW MANAGEMENT

This is an altogether different story that we encounter particularly in wind tunnel problems. It encompasses all means and technique to suppress wind tunnel turbulence, and also to create certain flow configurations of high fluctuation level and a prescribed structure—as needed e.g. in environmental wind tunnels. Some of the possibilities and limitations of turbulence management are discussed by Loehrke and Nagib (1976), Nagib and Corke (1984), Nagib and Marion (1984), Way *et al.* (1973) and Wigeland *et al.* (1977).

7. SUMMARIZING REMARKS

In trying to reduce the problem to its essentials all of the above can be retraced to two key phenomena: (a) turbulent mixing (redistribution/diffusion) and—even more fundamentally, (b) turbulence creation/destruction, with its three aspects: (i) laminar/turbulent transition, (ii) production, and (iii) dissipation.

What can be accomplished depends exclusively on the stability behaviour of the flow, on the efficiency of the control method and on the interaction of the scales and energy mechanisms. Thus increasing the spread of a given free flow by 100% is a comparatively easy task if one uses the proper 'tool': periodic excitation—thereby controlling the (creation of) coherent structures directly. This may provide the best results; and indeed also the mixing process, which is primarily related to the smaller eddies, 'trapped' as it were in the large coherent ones, may be controlled by controlling the large ones.

Indirect control, e.g. via entrainment (turbulence level) is, by comparison, only of small effect. The situation may be inverted for flows of strongly reduced instability, e.g. for mixing layers with low values of λ .

Another parameter of influence is the ratio of convection and diffusion in a flow as discussed in the comparison of jet and wake flow.

Reductions on the other hand seem to be more limited. This is equally true for free flows and even more so for wall bounded flows, where the achievable reduction in frictional drag is clearly below 10%. What is of importance in any case is how, i.e. to what extent, the quality to be controlled depends on the quality which is (most easily and effectively) controllable.

Ways and stratagems to influence a given flow and achieving useful results in comparison with the efforts needed, necessitate a clear knowledge about turbulent structural interplay,

stability behaviour and amplification rates. Apart from the direct control of flow instability by one or more frequencies, we have a number of passive mechanisms of influencing turbulent structures, as e.g. by

- influencing the stability of the basic flow (walls, field effects),
- influencing the stability of the basic coherent structure (wall geometry, field effects, upstream boundary conditions), thereby—in certain cases
- influencing the feedback characteristics of the flow.

It seems that by now a reasonable body of knowledge is available to provide a solid basis for control of a great number of flows to achieve various goals. This is particularly true for the aspect of active control by periodic forcing, for which Table 10 provides comprehensive compilation of characteristic Strouhal numbers.

All available information is, however, limited to 'clean' and relatively simple configurations and considerable work is still needed to extend our knowledge far enough to enable extrapolations to more complex scenarios.

ACKNOWLEDGEMENTS

Some of the results presented were obtained in our laboratory. Financial support for most of those investigations was provided by Deutsche Forschungsgemeinschaft (DFG). Pictures, diagrams and other results from other publications used herein are reproduced with kind permission. The second author acknowledges the critical comments on Section 6 by Dr A. Alving. The compilation of Strouhal numbers in Table 10 was prepared by R. Hagen, F. Michael and C. Wolfstieg. Valuable comments by I. Wygnanski are gratefully acknowledged. Ms L. Lindemann, S. Nordt and E. Kulzer took perfect care of the manuscript and the figures. We wish to express our gratitude to all contributors.

REFERENCES

- ABRAMOVICH, G. N. (1963) *The Theory of turbulent jets*, MIT Press, Cambridge MA.
- ADAMS, E. W. and JOHNSTON, J. P. (1988) Effects of the separating shear layer on the reattachment flow structure. Pt. 2: Reattachment length and wall shear stress, *Expt Fluids* 6, 492–499.
- AHUJA, K. K. and BURRIN, R. H. (1984) Control of flow separation by sound. *AIAA Pap.* 84-2298.
- AHUJA, K. K., LEPICOVSKI, J., TAM, C. K. W., MORRIS, P. J. and BURRIN, R. H. (1982) Tone excited jets—theory and experiments. NASA CR-3538.
- AHUJA, K. K., WHIPKEY, R. R. and JONES, G. S. (1983) Control of turbulent boundary layers by excitation. *AIAA Pap.* 83-0726.
- AHUJA, K. K., LEPICOVSKI, J. and BROWN, W. H. (1986) Some unresolved questions on hot-jet mixing control through artificial excitation. *AIAA Pap.* 86-1956, 10, 10th Aerocoustics Conference, Seattle, WA.
- ALVING, A. E., SMITS, A. J. and WATMUFF, J. H. (1990) Turbulent boundary-layer relaxation from convex curvature, *J. Fluid Mech.* 211, 529–556.
- ANDERS, J. B., WATSON, R. D. (1985) Airfoil large-eddy breakup devices for turbulent drag reduction. *AIAA Pap.* 85-0520.
- APALT, C. J. and WEST, G. S. (1975) The effects of wake splitter plates on bluff-body flow in the range $10^4 < Re < 10^5$, *J. Fluid Mech.* 71, 145–160.
- ARBEL, H. and FLOWKS WILLIAMS, J. E. (1984) Active Cancellation of pure tones in an excited jet. *J. Fluid Mech.* 149, 445–454.
- ARMSTRONG, R. R. (1981) Influence of Mach number on coherent structures relevant to jet noise. *AIAA Pap.* 81-4133, 19 (6), 677–683.
- ARMSTRONG, R. R., MICHALKE, A. and FUCHS, H. V. (1977) Coherent structures in jet turbulence and noise, *AIAA J.* 15 (7), 1011–1017.
- ARNAL, D. (1977) Effect of free-stream turbulence on turbulent boundary layers in incompressible flow. *ESA TT-411*.
- BAKHTIN, S. N., VLASOV, E. V., KARAVOSOV, R. K. and PIMSHTIN, V. G. (1983) The effect of external boundary layer flow on jet-noise characteristics. The acoustics of turbulent flow, Moscow, *Izdatel'stvo. Nauka* 61–66.
- BANDYOPADHYAY, P. R. (1986) Review-mean flow in turbulent boundary layers disturbed to alter skin friction, *J. Fluids Eng.* 108, 127–140.
- BANDYOPADHYAY, P. R. (1989) Viscous drag reduction of a nose body, *AIAA J.* 27, 274–282.
- BARAKHOV, S. P. and KOZLOV, V. V. (1987) Onset and Development of Coherent Structures in Turbulent Shear Flows. *Perspective in Turbulence Studies* (eds. H. U. Meier and P. Bradshaw), Springer, Berlin.
- BAR-SEVER, A. (1989) Separation control on an airfoil by periodic forcing, *AIAA J.* 27, 820–821.
- BARTENWERFER, M. and BECHERT, D. W. (1987) Die viskose Strömung über Oberflächen mit Längsrippen. *Forschungsbericht DFVLR-FB 87-21*.

- BATT, R. G. (1975) Some measurements on the effect of tripping the two-dimensional shear layer, *AIAA J.* 13 (2), 245-247.
- BEARMAN, P. W. (1965) Investigation of the flow behind a two-dimensional model with a blunt trailing edge and fitted with splitter plates, *J. Fluid Mech.* 21, 241-255.
- BEARMAN, P. W. (1978) Turbulence effects on bluff body mean flow. In: *Proc. 3rd US Nat. Conf. on Wind Engineering*, Florida, LV-1.
- BEARMAN, P. W. and MOREL, T. (1983) Effect of free-stream turbulence on the flow around bluff bodies, *Prog. Aerosp. Sci.* 20, 97-123.
- BEARMAN, P. W. and ZDRAVKOVICH, M. M. (1978) Flow around a circular cylinder near a plane boundary, *J. Fluid Mech.* 89, 33-47.
- BECHERT, D. W. (1985) Excitation of instability waves, *Z. Flugwiss. Weltraumforsch.* 9, Heft 6, 356-361.
- BECHERT, D. W. (1988) Excitation of instability waves in free shear layers. Part 1, Theory, *J. Fluid Mech.* 186, 47.
- BECHERT, D. W. (1990) Turbulence control—Invited lecture, *3rd European Turbulence Conf.*, Stockholm.
- BECHERT, D. W. and BARTENWERFER, M. (1989) The viscous flow on surfaces with longitudinal ribs, *J. Fluid Mech.* 206, 105-129.
- BECHERT, D. W. and MICHEL, U. (1975) The control of a thin free shear layer with and without a semi-infinite plate by a pulsating flow field, *ACUSTICA* 33, 287-307.
- BECHERT, D. and PFIZENMAIER, E. (1976) On the amplification of broadband jet noise by a pure tone excitation. *AIAA Pap.* 76-489.
- BECHERT, D. W. and STAHL, B. (1988) Excitation of instability waves in free shear layers. Part 2, Experiments, *J. Fluid Mech.* 186, 63pp.
- BECHERT, D. W., BARTENWERFER, M., HOPPE, G. and REIF, W.-E. (1986) Drag reduction mechanisms derived from shark skin. *ICAS Pap.* 86-1.8.3, London.
- BEELER, G. B. (1986) Turbulent boundary-layer wall pressure fluctuations downstream of a tandem LEBU, *AIAA J.* 24, 689-691.
- BEJAN, A. (1981) On the buckling property of inviscid jets and the origin of turbulence, *Lett. Heat Mass Transfer* 8, 187-194.
- BERG, V.D. B. (1981) Role of laminar separation bubbles in airfoil leading-edge stall, *AIAA J.* 19, 553-556.
- BERGER, E. (1967) Suppression of vortex shedding and turbulence behind oscillating cylinders, *Phys. Fluids Suppl.*, 191.
- BERGER, E. (1989) Paper presented at *ONR Workshop Bluff-Body Near-Wake Instability*, Lehigh Univ., Bethlehem Pa.
- BERGER, E. and SCHUMM, M. (1988) Untersuchungen der Instabilitätsmechanismen im Nachlauf von Zylindern. Contract Rep. No. Be 343/18-1, Techn. Univ., Berlin.
- BERGER, E. and WILLE, R. (1972) Periodic flow phenomena, *Ann. Rev. Fluid Mech.* 4, 313-340.
- BERGER, E., SCHOLZ, D. and SCHUMM, M. (1990) Coherent vortex structures in the wake of a sphere and a circular disk at rest and under forced vibrations, *J. Fluids Structures* 4.
- BERNAL, L. P. (1981) The coherent structure of turbulent mixing layers. I. Similarity of the primary vortex structure II. Secondary streamwise vortex structure. Ph. D. Thesis, Caltech.
- BERNAL, L. and SAROHA, V. (1984) Large amplitude forcing of a high speed two-dimensional jet. JPL Publication 84-91.
- BERTELRUD, A. (1987) Manipulated turbulence structure in flight. In: *Adv. Turbulence. Proc.* (ed. G. Comte-Bellot and J. Matthieu), Springer, Berlin.
- BERTELRUD, A., TRUONG, T. V. and AVELLAN, F. (1982) Drag reduction in turbulent boundary layers using ribbons. *AIAA Pap.* 82-1370.
- BETZ, A. (1961) History of boundary-layer control in Germany. In: *Boundary Layer and flow Control*, Vol. 1, pp. 1-20 (ed. G. Lachmann), Pergamon Press, Oxford.
- BEVILAQUA, P. M. and LYKODIS, P. S. (1978) Turbulence memory in self-preserving wakes, *J. Fluid Mech.* 89, 589-606.
- BHATTACHARJEE, S., SCHEELKE, B. and TROUTT, T. R. (1986) Modification of vortex interactions in a reattaching separated flow, *AIAA J.* 24, 623-629.
- BINDER, G. and FAVRE-MARINET, M. (1981) Some characteristics of pulsating or flapping jets. In: *Unsteady Turbulent Shear Flows. IUTAM Symp. Toulouse*, Springer, Berlin.
- BINDER, G., FAVRE-MARINET, M., KUENY, J. L., CRAYA, A. and LATY, R. (1971) Jets instationnaires. Labor de Mecanique des Fluides, Universite de Grenoble.
- BIRCH, S. F. and EGGERS, M. (1972) A critical review of the experimental data for developed free turbulent shear layers. Free Turbulent Shear Flows, NASA SP-321, pp. 11-40.
- BLACKWELDER, R. F. and KOVASZNY, L. S. G. (1972) Large scale of a turbulent boundary layer during relaminarization, *J. Fluid Mech.* 53, 61-83.
- BLAIR, M. F. (1983) Influence of free-stream turbulence on turbulent boundary layer heat transfer and mean profile development, *Trans ASME J. Heat Transfer* 105, 33-40, 41-47.
- BÖTTCHER, M. (1990) Private communication.
- BORISOV, YU. YA. and GYNKINA, N. M. (1975) Excitation of high-velocity jets by acoustic oscillations, *Akust. zh.* 21 (3), 616-619.
- BOUSSINESQ, J. (1879) Theorie de l'écoulement tourbillant. Mem. Pre. par. div. Sav. XXIII, Paris.
- BRADSHAW, P. (1966) The effect of initial conditions on the development of a free shear layer. *J. Fluid Mech.* 26, 225-236.
- BRADSHAW, P. (1972) Imperial College Aero Rept. 72-10.
- BRADSHAW, P. (1981) Effect of free-stream turbulence on boundary layers. In: *The 1980-81 AFOSR-HTTM Stanford Conf.* Vol. 1, pp. 86-93, Mech. Eng. Dept, Stanford Univ.
- BRADSHAW, P. and CUTLER, A. D. (1987) Three-dimensional flows with imbedded longitudinal vortices. In: *Perspectives in Turbulent Studies*, p. 382, Springer, Berlin.
- BRAZIER-SMITH, P. R. and SCOTT, J. F. (1984) Stability of fluid flow in the presence of a compliant surface, *Wave Motion* 6, 547-60.

- BREDERODE, V. DE and BRADSHAW, P. (1974) Influence of the side walls on the turbulent centre plane boundary layer in a square duct. Imperial College of Science and Technology, I. C. Aero Rept 74-06.
- BREIDENTHAL, R. (1986) The turbulent exponential jet, *Phys. fluids* 29 (8), 2346-2347.
- BREMHORST, K. (1979) Unsteady subsonic turbulent jets. In: *Recent Developments in Theoretical and Experimental Fluid Mechanics*, (eds U. Müller, K. G. Roesner and B. Schmidt), Springer, Berlin.
- BREMHORST, K. and HARCH, W. H. (1979) Near field velocity measurements in a fully pulsed subsonic air jet. In: *Turbulent Shear Flows I* (eds F. Durst, B. E. Launder, F. W. Schmidt and J. H. Whitelaw), Springer, Berlin.
- BREMHORST, K. and HOLLIS, P. G. (1988) Velocity field of a circular, fully pulsed, subsonic air jet, submitted for publication.
- BREMHORST, K. and WATSON, R. D. (1981) Velocity field and entrainment of a pulsed core jet, *J. Fluid Eng., Trans ASME* 103 (4), 605-608.
- BROWAND, F. K. and HO, C.-M. (1983) The mixing layer: an example of quasi two-dimensional turbulence, *J. Mech. Numer. Special: Turbulence Bidimensionnelle*, 99-120.
- BROWAND, F. K. and LATIGO, B. O. (1979) Growth of the two-dimensional mixing layer from a turbulent and non-turbulent boundary layer, *Phys. Fluids* 22, 1011-1019.
- BROWAND, F. K. and WEIDMANN, P. D. (1976) Large scales in the developing mixing layer, *J. Fluid Mech.* 76, Part 1, 127-144.
- BROWN, G. B. (1935) On vortex motion in gaseous jets and the origin of their sensitivity to sound, *Phys. Soc. XLVII* 4, 703-732.
- BROWN, G. L. and ROSHKO, A. (1974) On density effects and large structure in turbulent mixing layers, *J. Fluid Mech.* 64, 4, 775-816.
- BUELL, J. C. and HUERRE, P. (1988) Inflow/outflow boundary conditions and global dynamics of spatial mixing layers. In: *Proc. NASA Ames/Stanford Cent. Turbul. Res. Summer Prog., Rept. CTR-S88*, pp. 19-27.
- BUSHNELL, D. M. (1983) Turbulent drag reduction for external flows. AIAA Pap. 83-0227.
- BUSHNELL, D. M. (1984) Body-turbulence interaction. AIAA Pap. 84-1527.
- BUSHNELL, D. M. (1985) Turbulent drag reduction for external flows. AGARD Rept.-723, 5.1-5.26, Rhode-St-Genese.
- BUSHNELL, D. M. and MCGINLEY, C. B. (1989) Turbulence control in wall flows, *Ann. Rev. Fluid Mech.* 21, 1-21.
- BUSHNELL, D. M., HEFNER, J. N. and ASH, R. L. (1977) Effect of compliant wall motion on turbulent boundary layers. In: *Concepts for Aircraft Drag Reduction*, AGARD/VKI Special course AGARD-R-654.
- CARMICHAEL, B. H. (1981) Low Reynolds number airfoil survey. NASA CR 165803.
- CARPENTER, P. W. (1988) The optimization of complaint surfaces for transition delay. In: *Turbulence Management and Relaminarization*, pp. 305-313 (eds H.-W. Liepmann and R. Narasimha), Springer, Berlin.
- CARPENTER, P. W. and GARRAD, A. D. (1985/1986) The hydrodynamic stability of flows over Kramer-type compliant surfaces Pt-1 and Pt-2. Flow-induced surface instabilities, *J. Fluid Mech.* 155, 464-510; 170, 199-232.
- CARY, A. M., BUSHNELL, D. M. and HEFNER, J. N. (1977) Slot injection for skin friction drag reduction. In: *Concepts for Aircraft Drag Reduction*, AGARD/VKI Course, AGARD-R-654.
- CASTRO, I. P. (1971) Wake characteristics of two-dimensional perforated plates normal to an airstream, *J. Fluid Mech.* 46, 599-609.
- CASTRO, I. P. (1984) Effects of free-stream turbulence on low Reynolds number boundary layers, *Trans ASME I. J. Fluids Eng.* 106, 298-306.
- CASTRO, I. P. (1988) Effects of free-stream turbulence on separated shear layers. Zaric Memorial Meet., Dubrovnik.
- CASTRO, I. P. and HAQUE, A. (1988) The structure of a shear layer bounding a separation region, Pt II, Effects of free-stream turbulence, *J. Fluid Mech.* 192, 577-595.
- CHANDRSUDA, C., MEHTA, R. D., WEIR, A. D. and BRADSHAW, P. (1978) Effect of free-stream-turbulence on structure in turbulent mixing layer, *J. Fluid Mech.* 85, 693-704.
- CHEN, D. and SHIYING, Z. (1989) Control of separation in diffusers using forced unsteadiness. AIAA Pap. 89-1015.
- CHOI, H., KIM, J. and MOIN, P. (1989) Active turbulence control in wall-bounded flows, *Bull. Am. Phys. Soc.* 34, 2270.
- CIMBALA, J. M., NAGIB, H. M. and ROSHKO, A. (1988) Large structures in the far wakes of two-dimensional bluff bodies, *J. Fluid Mech.* 190, 265-298.
- CIMBALA, J. M., NAGIB, H. M. and DESRUELLE, D. (1988) Controlled excitation of instabilities in the far wake of a circular cylinder, submitted for publication.
- COANDA, H. (1934) Procédé et dispositif pour faire dévier une veine fluide pénétrant autre fluide. French Pat. 788, 140.
- COHEN, J. and WYGNANSKI, I. (1987) The evolution of instabilities in the axisymmetric jet. Part 1. The linear growth of disturbances near the nozzle, *J. Fluid Mech.* 176, 191-219.
- COHEN, J. and WYGNANSKI, I. (1987) The evolution of instabilities in the axisymmetric jet. Part 2. The flow resulting from the interaction between two waves, *J. Fluid Mech.* 176, 221-235.
- COLLINS, F. G. (1981) Boundary control on wings using sound and leading edge serrations, *AIAA J.* 19, 129-130.
- COLLINS, F. G. and ZELENIEVITZ, J. (1975) Influence of sound upon separated flow over wings, *AIAA J.* 13, 408-410.
- CORKE, T. C. (1981) A new view on origin, role and manipulation of large scales in turbulent boundary layers. Thesis, Graduate School of Illinois Institute of Technology.
- CORRSIN, S. and UBEROI, M. (1949) Further experiments on flow and heat transfer in a heated turbulent air jet. NACA Rept. 988.
- CRIGHTON, D. G. (1981) Jet noise and the effects of jet forcing. In: *The role of Coherent Structures in Modelling Turbulence and Mixing*, (ed. J. Jimenez), Lecture Notes in Physics, Vol. 136.
- CROW, S. C. and CHAMPAGNE, F. H. (1971) Orderly structure in jet turbulence, *J. Fluid Mech.* 48, 567pp.
- DENGEL, P. and FERNHOLZ, H. H. (1990) An experimental investigation of an incompressible turbulent boundary layer in the vicinity of separation, *J. Fluid Mech.* 212, 615-636.
- DHANAK, M. R. and DE BERNARDINI, B. (1981) The evolution of an elliptic vortex ring, *J. Fluid Mech.* 109, 189-216.
- DIDDEN, N. and HO, C.-M. (1985) Unsteady separation in a boundary layer produced by an impinging jet, *J. Fluid Mech.* 160, 235-256.

- DIMOTAKIS, P. E. and BROWN, G. L. (1976) The mixing layer at high Reynolds number: large-structure dynamics and entrainment, *J. Fluid Mech.* 78 (3), 535-560.
- DIMOTAKIS, P. E. and KOOCHEFAHANI, M. M. (1987) Active feedback interaction with a shear layer. Ann. Prog. Rept, AFOSR-84-0120.
- DIMOTAKIS, P. E., MIAKE-LYE, R. C. and PAPANTONIOU, D. A. (1982) Structures and dynamics of round turbulent jets. GALTIT Rept FM82-01, California Institute of Technology.
- DINKELACKER, A., NITSCHKE-KOWSKY, P. and REIF, W.-E. (1987/88) On the possibility of drag reduction with the help of longitudinal ridges in the walls. In: *Turbulence Management and Relaminarisation, IUTAM Symp.* Bangalore, India 1987, pp. 109-120, Springer, Berlin.
- DI STEFANO, J. J., STUBBERUD, A. R. and WILLIAMS, I. J. (1979) "Schaum's Outline" — *Theory and Problems of Feedback and Control Systems with Applications to the Engineering, Physical and Life Sciences*, McGraw Hill.
- DIJORDJEVIC, V., PAVITHRAN, S. and REDEKOPP, L. G. (1989) Stability properties of subsonic mixing layers. AIAA Pap. 89-1020.
- DOWLING, A. P. (1985) The effect of large-eddy breakup devices on oncoming vorticity, *J. Fluid Mech.* 160, 447-463.
- DRAZIN, P. and REID, H. (1981) *Hydrodynamic Stability*, Cambridge University Press.
- DRIVER, D. M. and SEEGLER, H. L. (1982) Features of a reattaching shear layer subject to an adverse pressure gradient. AIAA Pap. 82-1029.
- DRIVER, D. M. and SEEGLER, H. L. (1985) Features of a reattaching turbulent shear layer in divergent channel flow, *AIAA J.* 23, 163-171.
- DUBUAT, (1779) *Principes d'hydraulique*, Paris.
- DURBONOVICH, G. I., ZEMSKAYA, A. S., REPIK, Y. U. and SOSEDKO, Y. P. (1981) Optimum wire screens for control of turbulence in wind tunnels, *Fluid Mech. Soviet. Res.* 10, 136-147.
- DZIOMBA, B. (1981) Experimentelle Untersuchung zum Einfluß von Anfangs- und Randbedingungen auf die Ausbreitung einer freien zweidimensionalen Scherschicht. Dissertation, Technische Universität Berlin.
- DZIOMBA, B. and FIEDLER, H. E. (1979) Der turbulente Mischvorgang in einer freien Scherschicht bei kontrollierbaren Anfangsbedingungen. DFG-FI 178/18; I. Zwischenbericht.
- DZIOMBA, B. and FIEDLER, H. E. (1985) Effect of initial conditions on two-dimensional free shear layers, *J. Fluid Mech.* 152, 419-442.
- EATON, J. K. and JOHNSTON, J. P. (1981) A review of research on subsonic turbulent flow reattachment, *AIAA J.* 19, 1092-1100.
- EDBERG, M. (1989) LDV measurements of the velocity and temperature field in a disturbed turbulent jet. Rept UL-89:34, Vattenfall Alfvénlaboratoriet.
- EDBERG, M. (1990) LDV measurements of the velocity and temperature field in a disturbed turbulent jet. In: *Third European Turbulence Conf.*, Stockholm, Sweden.
- EICKHOFF, H. (1982) Turbulent hydrocarbon jet flames, *Prog. Energy Combust. Sci.* 8, 159-168.
- EICKHOFF, H. (1982) Instability and coherent structures in jet flames. In: *Recent Contributions to Fluid Mechanics*, (ed. W. Haase), Springer, Berlin: Heidelberg, New York.
- EILERS, R. E., KOPER, C. A., MCLEAN, J. D. and CODER, D. W. (1985) An application of riblets for turbulent skin friction reduction. *Twelfth Symp. Sailing*, Seattle, AIAA.
- ELENA, M. (1984) Suction effects on turbulence statistics in a heated pipe flow, *Phys. Fluids* 27, 861-866.
- ERICSSON, L. E. (1980) Karman vortex shedding and the effect of body motion, *AIAA J.* 18, 18pp.
- ERICSSON, L. E. and KARLSSON, R. I. (1990) Turbulence modification of a circular jet caused by drag-reducing cationic surfactant solutions. In: *Third European Turbulence Conf.*, Stockholm, Sweden.
- EZERSKIĬ, A. B. (1983) Nonlinear resonant interaction of acoustic waves with Tollmien-Schlichting waves. *Akademiia Nauk SSSR, Izvestiia, Mekhanika Zhidkosti i Gaza*, pp. 23-28.
- FAVRE-MARINET, M. and BINDER, G. (1987) Amplification and decay mechanisms of coherent structures in a round jet. In: *6th Symp. on Turbulent Shear Flows*, Toulouse.
- FAVRE-MARINET, M., BINDER, G. and HAK, T. V. (1981) Generation of oscillating jets. *J. Fluid Eng.* 103, 609-614.
- FERNHOLZ, H. H. (1966) Eine grenzschichttheoretische Untersuchung optimaler Unterschalldiffusoren, *Ing. Arch.* 35, 192-201.
- FERNHOLZ, H. H. (1968) Experimentelle Untersuchung einer inkompressiblen turbulenten Grenzschicht mit Wandreibung nahe Null an einem längsangeströmten Kreiszylinder, *Z. Flugwiss.* 16, 402-406.
- FIEDLER, H. E. (1984) The mono-frequency shear layer. In: *Turbulence and Chaotic Phenomena in Fluids*, pp. 411-420 (ed. T. Tatsumi), (IUTAM/KYOTO), Elsevier.
- FIEDLER, H. E. (1988) Coherent structures in turbulent flows, *Prog. Aerosp. Sci.* 25, 231-269.
- FIEDLER, H. E. (1988) Accelerated Mixing Layer. In: *Current Trends in Turbulence Research*, Vol. 112, pp. 100-104 (eds H. Brannover, M. Mond and Y. Unger), AIAA Series.
- FIEDLER, H. E. and HILBERG, D. (1990) Control of turbulent shear flows via stationary boundary conditions. In *NATO Advances Research Workshop: The Global Geometry of Turbulence*, Rota, Spain.
- FIEDLER, H. E. and KORSCHULT, D. (1979) The two-dimensional jet with periodic initial conditions. In: *Proc. 2nd Symp. on Turbulent Shear Flows*, London.
- FIEDLER, H. E. and MENSING, P. (1985) The plane turbulent shear layer with periodic excitation, *J. Fluid Mech.* 150, 281-309.
- FIEDLER, H. E. and THIES, H. J. (1978) Some observations in a large two-dimensional shear layer. *Structure and Mechanisms in Turbulence I*, Lecture Notes in Physics, Vol. 75 (ed. H. Fiedler), Springer, Berlin.
- FIEDLER, H. E., KORSCHULT, D. and MENSING, P. (1978) On transport mechanism and structure of scalar field in a heated plane shear layer. In: *Lecture Notes in Physics*, Vol. 76 (ed. H. Fiedler), Springer, Berlin.
- FIEDLER, H. E., DZIOMBA, B., MENSING, P. and RÖSGEN, T. (1981) Initiation, Evolution and Global Consequences of Coherent Structures in Turbulent Shear Flows. The Role of Coherent Structures in Modelling Turbulence and Mixing. In: *Lecture Notes in Physics*, Vol. 136 (ed. J. Jimenez), Springer, Madrid.

- FIEDLER, H. E., GLEZER, A. and WYGNANSKI, I. (1988) Control of plane mixing layer: Some novel experiments. In: *AIAA Series, Current Trends in Turbulent Research*, Vol. 112, pp. 30-64 (eds H. Brannover, M. Mond, and Y. Unger), AIAA Series.
- FIEDLER, H. E., KIM, J.-H. and KÖPP, N. (1990) The spatially accelerated mixing layer in a tailored pressure gradient, to appear in *Eur. J. Mech./B-Fluids*.
- FIEDLER, H. E., LUMMER, M. and NOTTMAYER, K. (1990) The plane mixing layer between parallel streams of different velocities and different densities. *Prog. Astronaut, AIAA*.
- FLEISCHMANN, S. T. and WALLACE, J. M. (1984) Mean streamwise spacing of organized structures in transitional and developed bounded turbulent flows, *AIAA J.* 22 (6), 766-768.
- FLORA, J. J. and GOLDSCHMIDT, V. M. (1969) *AIAA J.* 7, 2344.
- FOSS, J. F. (1977) The effects of the laminar/turbulent boundary layer state on the development of a plane mixing layer. In *Turbulent Shear Flows*, pp. 11.33-11.42, The Penn State Univ., University Park.
- FREYMUTH, P. (1966) On transition in a separated laminar boundary layer, *J. Fluid Mech.* 25 (4), 683-704.
- FUCHS, H. V., MERCKER, and MICHEL, U. (1979) Mode expansion of coherent structures in the wake of a circular disk, *Turbulent Shear Flows* 2, 282-296.
- FUJI, S., NISHIWAKI, H. and TAKEDA, K. (1981) Suppression of jet noise peak by velocity profile reshaping, *AIAA J.* 19, 872-877.
- FUKUNISHI, Y. (1984) Influence of ordered motions on the structure of outer region of the turbulent boundary layer. In: *Turbulence and Chaotic Phenomena in Fluids*, pp. 371-376 (ed. T. Tatsumi), (IUTAM/KYOTO), Elsevier.
- FULACHIER, L., BENABID, T., ANSELMET, F., ANTONIA, R. A. and KRISHNAMOORTHY, L. V. (1987) Behaviour of coherent structures in a turbulent boundary layer with wall suction. *Advances in Turbulence, Proc.* (ed. G. Comte-Bellot and J. Mathieu), Springer, Berlin.
- GAD-EL-HAK, M. (1984) The response of a two-layer compliant coating to a turbulent boundary layer, *Bull. Am. Phys. Soc.* 29.
- GAD-EL-HAK, M. and BLACKWELDER, R. F. (1985) The discrete vortices from a delta wing, *AIAA J.* 23, 961-962.
- GAD-EL-HAK, M. and BLACKWELDER, R. F. (1987) A drag reduction method for turbulent boundary layers. *AIAA Pap.* 87-0358.
- GAD-EL-HAK, M. and BLACKWELDER, R. F. (1989) Selective suction for controlling bursting events in a boundary layer, *AIAA J.* 27, 308-315.
- GAL, S. L. and SHARMA, S. D. (1987) Pressure distributions behind a rearward facing segmented step, *Exp. Fluids* 5, 154-158.
- GALITSEISKII, B. M. (1979) Heat transfer in turbulent gas flows with high-frequency pressure oscillations, *Soviet Aeron.* 22 (1), 11-15, translated from *Izv. Vyssh. Ucheb. Zaved. Aviat. Tekhn.* 22 (1), 7-23.
- GAMPERT, B., HOMANN, K. and RIEKE, H. B. (1980) The drag reduction in laminar and turbulent boundary layers by prepared surfaces with reduced momentum transfer, *Israel J. Technol.* 18 (6), 287-292.
- GASTER, M. (1962) A note on the relation between temporally-increasing and spatially increasing disturbances in hydrodynamic stability, *J. Fluid Mech.* 14, 222-224.
- GASTER, M. (1966) The structure and behaviour of laminar separation bubbles, *AGARD CP* 4, 819-854.
- GASTER, M. (1985) Growth of instability over compliant surfaces, *Bull. Am. Phys. Soc.* 30, 1708.
- GASTER, M. (1988) Is the dolphin a red herring? In: *Turbulence Management and Relaminarization*, pp. 285-304 (eds H.-W. Liepmann and R. Narasimha), Springer, Berlin.
- GASTER, M., KIT, E. and WYGNANSKI, I. (1985) Large scale structures in a forced mixing layer, *J. Fluid Mech.* 150, 23-39.
- GEDNEY, C. J. (1983) The cancellation of a sound-excited Tollmien-Schlichting wave with plate vibration, *Phys. Fluids* 26, 1158.
- GIGER, M. (1987) Der ebene Freistrahle im flachem Wasser. Dissertation ETH Zürich.
- GILLIS, J. C. and JOHNSTON, J. P. (1983) Turbulent boundary layer flow and structure on a convex wall and its redevelopment on a flat wall, *J. Fluid Mech.* 135, 123-153.
- GLEZER, A. (1981) An experimental study of a turbulent vortex ring. Thesis, California Institute of Technology.
- GLEZER, A. (1990) Private communication.
- GLEZER, A., WYGNANSKI, I. J. and GU, X. (1989) Amplitude modulated excitation of a turbulent mixing layer, submitted to *Phys. Fluids*.
- GOLDSCHMIDT, V. W. and BRADSHAW, P. (1972) Flapping of a plane jet, *Phys. Fluids* 16 (3), 354-355.
- GOLDSCHMIDT, V. W. and KAISER, K. (1971) Interaction of an acoustic field and a turbulent plane jet: mean flow measurements, *Chem. Eng. Prog. Symp. Ser.* 67 (109), 91-98.
- GOLDSTEIN, R. J. (1971) Film cooling. In: *Advances in Heat Transfer*, Vol. 7, pp. 321-379, Academic Press, New York.
- GOODMAN, W. L. (1985) Emmons spot forcing for turbulent drag reduction, *AIAA J.* 23, 155-157.
- GOUGAT, P. (1969) Influence d'un champ acoustique extérieur sur un couche limite turbulente. No d'enregistrement au C.N.R.S.A.O. 3384, Paris.
- GRAY, D. D. and SHELTON, G. F. (1982) Growth of two-dimensional wakes behind solid and porous strips, *AIAA J.* 20, 150-152.
- GUICKING, D. (1988) Active noise and vibration control. *Reference Bibliography*, 3rd edn, Göttingen.
- GURECKI, D. J. (1981) Effect of modification of the trailing edge of a separating wall on the downstream mixing of parallel flowing streams. MS-Thesis, Air Force Institute of Technology, Ohio.
- GUTMARK, E. and HO, C.-M. (1983) On a forced elliptic jet. In: *Proc. 4th Turbulence Shear Flow Conf.*, Karlsruhe, Germany.
- GUTMARK, E. and HO, C.-M. (1983) Preferred modes and the spreading rates of jets, *Phys. Fluids* 26 (10), 2932.
- GUTMARK, E. and HO, C.-M. (1986) Visualization of a forced elliptical jet. *AIAA J.* 24 (4), 684-685.
- GUTMARK, E., WOLFSTEIN, M. and WYGNANSKI, I. (1978) Selective amplification of fluctuations in a turbulent impinging jet, *J. Fluid Mech.* 88, 737pp.

- GUTMARK, E., SCHADOW, K. C., WILSON, K. J. and PARR, D. M. (1986) Small-scale mixing enhancement in acoustically excited jets. AIAA Pap. 86-1885, 10th Aeroacoustics Conf., Seattle, WA.
- GUYON, E. (1988) Self-sustained oscillations in low density jets. Intern. Rept., Dept Aerospace Eng., Univ. South Calif., Los Angeles.
- GYR, A. (ed.) (1990) *IUTAM Symp. on Structure of Turbulence and Drag Reduction*, Springer, Berlin.
- HAERTIG, J. (1981) Une solution analytique du probleme de l'instabilite d'une jet libre rond incompressible. ISR-Bericht R 119/81.
- HÄRTL, A. P. (1989) Optimierung von Diffusoren durch Konturierung der Wände auf der Basis des Grenzschichtkonzepts. Fortsch. Berichte, Reihe 7, Nr 159. VDI-Verlag.
- HANCOCK, P. E. (1980) The effect of free-stream turbulence on turbulent boundary layers. Ph.D. thesis, Imperial College, London.
- HANCOCK, P. E. and BRADSHAW, P. (1983) The effect of free-stream turbulence on turbulent boundary layers, *Trans ASME J. Fluid Eng.* 105, 284-289.
- HANCOCK, P. E. and BRADSHAW, P. (1989) Turbulence structure of a boundary layer beneath a turbulent free stream, *J. Fluid Mech.* 205, 45-76.
- HANNEMANN, K. (1988) Numerische Simulation und stabilitätstheoretische Untersuchung des absolut und konvektiv instabilen Nachlaufs. DFVLR Rept. No. FB 88-09.
- HANNEMANN, K. and OERTEL, H. JR (1989) Numerical simulation of the absolutely and convectively unstable wake, *J. Fluid Mech.* 199, 55-88.
- HASAN, M. A. Z. and HUSSAIN, A. K. M. F. (1982) The self-excited axisymmetric jet, *J. Fluid Mech.* 115, 59-89.
- HAYAKAWA, M. and HUSSAIN, F. (1989) Three-dimensionality of organized structures in a plane turbulent wake, *J. Fluid Mech.* 206, 375-404.
- HEAD, M. R. (1961) Boundary layer control for low drag in U.K. In: *Boundary Layer and Flow Control*, pp. 104-121 (ed. G. Lachmann), Pergamon Press, Oxford.
- HEFNER, J. N. and BUSHNELL, D. M. et al. (1977) Concepts for aircraft drag reduction. AGARD-R-654.
- HEFNER, J. N., ANDERS, J. B. and BUSHNELL, D. M. (1983) Alteration of outer flow structures for turbulent drag reduction. AIAA-Pap. 83-0293, Reno.
- HESKESTAD, G. (1966) Hot-wire measurements in a radial turbulent jet, *J. Appl. Mech.* 1-8.
- HESS, J. L. (1976) On the problem of shaping an axisymmetric body to obtain low drag at large Reynolds number, *J. Ship Res.* 20, 51-60.
- HILBERG, D. and FIEDLER, H. E. (1989) The spanwise confined one-stream mixing layer. In *Adv. Turbulence*, Vol. 2, pp. 443-448 (eds H. H. Fernholz and H. E. Fiedler), Springer, Berlin.
- HILL, W. G. and JENKINS, R. C. (1976) Effect of the initial boundary layer state on turbulent jet mixing, *AIAA J.* 14 (11), 1513-1514.
- HILLIER, R. (1976) Investigation of the mean flow properties in the separated region downstream of a forward facing step. CERL Rep. RD/L/N 242/75.
- HILLIER, R. and CHERRY, N. J. (1981) The effects of free-stream turbulence on separation bubbles, *J. Wind Eng. Ind. Aero.* 8, 49-58.
- HINO, M. and KANEKO, D. (1971) Interaction between an oscillating plate and shedding vortices, *Wind Effects Buildings Struct.*, IV, 31, 1-10.
- HO, C.-M. (1981) Local and global dynamics of free shear layers. In: *Numerical and Physical Aspects of Aerodynamics Flows*, pp. 521-533 (ed. T. Cebeci), Springer, Berlin.
- HO, R. T. and GELHAR, L. W. (1973) Turbulent flow with wavy permeable boundaries, *J. Fluid Mech.* 58, Part 2, 403-414.
- HO, C.-M. and GUTMARK, E. (1982) Visualization of an elliptical jet, *Bull. Am. Phys. Soc.* 27, 1184.
- HO, C.-M. and GUTMARK, E. (1987) Vortex induction and mass entrainment in a small-aspect-ratio elliptic jet, *J. Fluid Mech.* 179, 383-405.
- HO, C.-M. and HUANG, L.-S. (1982) Subharmonics and vortex merging in mixing layers, *J. Fluid Mech.* 119, 443-473.
- HO, C.-M. and HUERRE, P. (1984) Perturbed free shear layers, *Ann. Rev. Fluid Mech.* 16, 365-424.
- HOERNER, S. F. (1965) *Fluid Dynamic Drag*, published by the author, Bricktown, New Jersey.
- HOFFMANN, P. H. and BRADSHAW, P. (1978) Turbulent boundary layers on surfaces of mild longitudinal curvature. Imp. College of Science and Technology, Dept of Aeronaut., IC Aero Rept 78-04.
- HOFFMANN, J. A. and GONZALES, G. (1984) Effects of small scale, high intensity inlet turbulence on flow in a two-dimensional diffuser, *J. Fluids Eng.* 106, 121-124.
- HOFFMANN, P. H., MUCK, K. C. and BRADSHAW, P. (1985) The effect of concave surface curvature on turbulent boundary layer, *J. Fluid Mech.* 161, 371-403.
- HOFFENZIZ, H. (1984) Experimentelle und theoretische Untersuchungen turbulenter Wandgrenzschichten unter Einfluß von Außenturbulenz und Druckgradienten. VDI-Verlag, Reihe Strömungstechnik 7/86.
- HORSTMANN, K. H. and QUAST, A. (1981) Drag reduction using pneumatic turbulators (laminar airfoils). DFVLR-FB-81-33.
- HOUGH, G. R. (Ed.) (1980) Viscous flow drag reduction, *AIAA Prog. Astronaut. Aeronaut.* 72.
- HOWARD, F. G., QUASS, B. F., WEINSTEIN, L. M. and BUSHNELL, D. M. (1981) Longitudinal afterbody grooves and shoulder radiusing for low-speed bluff body drag reduction. ASME 81-WA/FES.
- HOWARD, F. G., GOODMAN, W. L. and WALSH, M. J. (1983) Axisymmetric bluff-body drag reduction using circumferential grooves, presented at the *AIAA Applied Aerodynamics Conf.*
- HOYT, J. W. (1979) Polymer drag reduction—A literature review drag reduction. In: *2nd Int. Conf. on Drag Reduction*, BHRA Fluid Eng. Cranfield, U.K.
- HOYT, J. W., ALTMAN, R. L. and TAYLOR, J. J. (1980) Drag reduction—Jet breakup correlation with kerosene-based additives, *J. Rheology* 24 (5), 685-699.
- HSIAO, F., LIU, C., SHYU, J. and WANG, M. (1989) Control of separated flow by internal acoustic excitation. AIAA Pap. 89-0974.
- HUANG, L. S., MAESTRELLO, L. and BRYANT, T. D. (1987) Separation control over an airfoil of high angle of attack by sound emanating from the surface. AIAA Pap. 87-1261.

- HUERRE, P. and MONKEWITZ, P. A. (1985) Absolute and convective instabilities in free shear layers, *J. Fluid Mech.* **150**, 151–168.
- HUERRE, P. and MONKEWITZ, P. A. (1990) Local and global instabilities in spatially developing flows, *Ann. Rev. Fluid Mech.* **22**, 473–537.
- HULTGREN, L. S. and AGGARWAL, A. K. (1987) A note on absolute instability of the Gaussian wake profile, *Phys. Fluids* **30**, 3383–87.
- HUMMEL, D. (1988) Documentation of separated flows for computational fluid dynamics validation. AGARD CP 437, 2, 15.1–15.24.
- HUSAIN, H. S. and HUSSAIN, A. K. M. F. (1983) Controlled excitation of elliptic jets, *Phys. Fluids* **26** (10), 2763–2766.
- HUSAIN, H. S. and HUSSAIN, F. (1989) Subharmonic resonance in a shear layer. In: *Advances in Turbulence 2* pp. 96–101 (eds H. H. Fernholz, H. E. Fiedler), Springer, Berlin.
- HUSAIN, H. S., BRIDGES, J. E. and HUSSAIN, F. (1987) Turbulence management in free shear flows by control of coherent structures. In: *Int. Symp. Transport Phenomena in Turbulent Flows*, Tokyo.
- HUSAIN, Z. D. and HUSSAIN, A. K. M. F. (1979) Axisymmetric Mixing Layer: Influence of the initial and boundary conditions, *AIAA J.* **17** (1), 48–55.
- HUSSAIN, A. K. M. F. (1986) Coherent structures and turbulence, *J. Fluid Mech.* **173**, 303–356.
- HUSSAIN, A. K. M. F. and CLARK, A. (1977) Upstream influence on the near field of a plane turbulent jet, *Phys. Fluids* **20** (9), 1416–1426.
- HUSSAIN, A. K. M. F. and HUSAIN, H. S. (1988) Passive and active control of jet turbulence, submitted for publication.
- HUSSAIN, A. K. M. F. and HASAN, M. A. Z. (1985) Turbulence suppression in free turbulent shear flows under controlled excitation. II—Jet-noise reduction, *J. Fluid Mech.* **150**, 159–168.
- HUSSAIN, A. K. M. F. and REYNOLDS, W. C. (1970) The mechanics of a perturbation wave in turbulent shear flow. AFOSR Scientific Rept, AFOSR 70-1655TR, Rept FM-6, Thermosciences Division, Dept Mech. Eng., Stanford University.
- HUSSAIN, A. K. M. F. and ZAMAN, K. B. M. Q. (1978) Controlled perturbation of circular jets. In: *Lecture Notes in Physics*, 31 pp. (ed. H. Fiedler), Springer, Berlin.
- HUSSAIN, A. K. M. F. and ZAMAN, K. B. M. Q. (1980) Vortex pairing in a circular jet under controlled excitation. Part 2. Coherent structure dynamics. *J. Fluid Mech.* **101** (3), 493–544.
- HUSSAIN, A. K. M. F. and ZAMAN, K. B. M. Q. (1981) The preferred-mode coherent structure in the near field of an axisymmetric jet with and without excitation. Unsteady turbulent shear flows. In: *Proc. Symp.*, Toulouse, pp. 390–401, Springer, Berlin.
- HUSSAIN, A. K. M. F. and ZEDAN, M. F. (1978) Effects of initial condition on the axisymmetric free shear layer: effects of the initial momentum thickness, *Phys. Fluids* **21** (a), 1100–1111. Effects of initial fluctuation level, *Phys. Fluids* **21** (b), 1475–1481.
- HUSSAIN, A. K. M. F., HUSAIN, H. S., ZAMAN, K. B. M. Q., TSO, J., HAYAKAWA, M., TAKAKI, R. and HASAN, M. A. Z. (1986) Free shear flows: organized structures and effect of excitation. AIAA 24th Aerosp. Sci. Meet., Reno (AIAA-86-0235).
- INGEN, J. L. VAN (1975) On the calculation of laminar separation bubbles in two-dimensional incompressible flow. AGARD CP 168.
- ISOMOTO, K. and HONAMI, S. (1989) The effect of inlet turbulence intensity on the reattachment process over a backward facing step, *J. Fluids Eng.* **111**, 87–92.
- JACKSON, T. L. and GROSCHE, C. E. (1989) Absolute/convective instabilities and the convective Mach number in a compressible mixing layer, submitted for publication.
- JANG, P. S., BENNEY, D. J. and CHEN, Y. M. (1984) Origin of streamwise vortices in turbulent boundary layers, *Bull. Am. Phys. Soc.*, Ser. II, **29** (9), Pap. B88, 1528.
- KATO, S. M., GROENEWEGEN, B. C. and BREIDENTHAL, R. E. (1987) Turbulent mixing in nonsteady jets, *AIAA* **25** (1), 165–168.
- KATZ, Y., NISHRI, B. and WYGNANSKI, I. (1989) The delay of turbulent boundary layer separation by oscillatory active control, *Phys. Fluids A* **1** (2), 179–181.
- KAUL, U. (1988) Do large structures control their own growth in a mixing layer? An assessment, *J. Fluid Mech.* **19**, 427–450.
- KAWALL, J. G. and KEFFER, J. F. (1981) The role of coherent structures in the development of a uniformly strained turbulent wake. *Turbulent Shear Flows 3* (ed. Bradbury, Durst, Launder, Schmidt and Whitelaw), 132–145.
- KEFFER, J. F., KAWALL, J. G., HUNT, J. C. R. and MAXEY, M. R. (1978) The uniform distortion of thermal and velocity mixing layers, *J. Fluid Mech.* **86** (3), 465–490.
- KELLY, R. E. (1967) On the instability of an inviscid shear layer which is periodic in space and time, *J. Fluid Mech.* **27**, 657–689.
- KIBENS, V. (1980) Discrete noise spectrum generated by an acoustically excited jet, *AIAA J.* **18**, 434–441.
- KIBENS, V. (1981) The limits of initial shear layer influence on jet development. AIAA Pap. 81-1969.
- KIBENS, V. (1989) Jet flows and turbulence control. AIAA Pap. 89-105.
- KLEIS, S. J. and FOSS, J. F. (1974) NASA Lewis Research Center, Tech. Rept NGR-23-004-068, Michigan State University, East Lansing.
- KOCH, W. (1985) Local instability characteristics and frequency determination of self-excited wake flows, *J. Sound Vib.* **99**, 53–83.
- KOCH, C. R., POWELL, J. D. and REYNOLDS, W. C. (1989) An experimental investigation of closed loop control of a round jet diffuser, *Bull. Am. Phys. Soc.* **34**, 2317.
- KÖNIG, O. and FIEDLER, H. (1990) The structure of round turbulent jets in counterflow—A flow visualisation study. In: *Third European Turbulence Conf.*, Stockholm.
- KOENIG, K. and ROSHKO, A. (1985) An experimental study of geometrical effects on the drag and flow field of two bluff bodies separated by a gap, *J. Fluid Mech.* **156**, 167–204.
- KOGA, D. J. (1983) Control of separated flow fields using forced unsteadiness. Ph.D. thesis, Illinois Inst. Techn.
- KONDRATIEV, V. I. and RIMSKI-KORSAKOV, A. V. (1971) Investigation of sound influence on a turbulent gaseous jet. In: *Proc. 7th Int. Congr. Acoust.*, Budapest, Vol. 4, No. 12, pp. 473–476.

- KONRAD, J. H. (1976) An experimental investigation of mixing in two-dimensional turbulent shear flows with application to diffusion-limited chemical reactions. Ph.D. thesis, California Institute of Technology.
- KOOCHESFAHANI, M. M. and DIMOTAKIS, P. E. (1987) Effects of a downstream disturbance on the structure of a turbulent plane mixing layer. *AIAA-87-0197*.
- KOOCHESFAHANI, M. M. and FRIELER, C. E. (1987) Inviscid instability characteristics of free shear layer with non-uniform density. *AIAA-87-0047*.
- KORSCHULT, D. (1980) Experimentelle Untersuchung zum Wärme- und Stofftransport im turbulenten ebenen Freistrahle mit periodischer Anregung am Düsenaustritt. Dissertation, Technische Universität Berlin.
- KROTHAPALLI, A., BAGANOFF, D. and KARAMCHETI, K. (1979) Some observations of flow structure in multiple jet mixing. In: *2nd Symp. Turbulent Shear Flows*, Imperial College, London, NASA 2233.
- KROTHAPALLI, A., BAGANOFF, D. and KARAMCHETI, K. (1981) On the mixing of a rectangular jet, *J. Fluid Mech.* 107, 201-220.
- KUMORI, S. and UEDA, H. (1985) The large-scale coherent structure in the intermittent region of the self-preserving round free jet, *J. Fluid Mech.* 152, 337-359.
- KUZNETSOV, V. M. and MUNIN, A. G. (1982) An evaluation of the effectiveness of methods for reducing the noise of jets. *TsAGI, Uchenye Zapiski* 13 (6), 1-7.
- KWADE, M. (1982) Beeinflussung der Turbulenzstruktur in der ebenen Mischungsschicht zweier Ströme durch Polymerzustände, *Rheologica Acta* 21, 120-149.
- KYLE, D. (1988) LIF images of He/N₂ jets. Mech. Eng. Rept No. FM88DK1, Yale Univ., New Haven, Conn.
- KYLE, D. and SREENIVASAN, K. R. (1989) Stability properties of He/air jets. In: *Proc. ASME Fluids Eng. Spring Conf.*, La Jolla, CA.
- LACHMANN, G. V. (ed.) (1961) *Boundary Layer and Flow Control—its Principles and Application*, Vols I and II, Pergamon Press, New York.
- LANDAHL, M. T. and HENNINGSON, D. S. (1985) The effects of drag reduction measures on boundary layer turbulence. *AIAA Pap.* 85-0560.
- LANDAU, L. D. and LIFSHITZ, E. M. (1966) *Lehrbuch der Theoretischen Physik. Band VI—Hydrodynamik*, Akademie, Berlin.
- LASHERAS, J. C. and CHOI, H. (1986) Three-dimensional instability of a plane, free shear layer: an experimental study of the formation and evolution of streamwise vortices, submitted to *J. Fluid Mech.*
- LASHERAS, J. C., CHO, J. S. and MAXWORTHY, T. (1986) On the origin and evolution of streamwise vortical structures in a plane, free shear layer. *J. Fluid Mech.* 172, 231-258.
- LASHERAS, J. C., LECUONA, A. and RODRIGUEZ, P. (1990) Topology of the vorticity field in 3-D coflowing forced jets. In: *The Global Geometry of Turbulence*, Nato Advance Research Workshop, Spain.
- LAUFER, J. and MONKEWITZ, P. A. (1980) On turbulent jet flow in a new perspective. *AIAA Pap.* 80-0962.
- LAUFER, J. and TA-CHUN, Y. (1983) Noise generation by a low-Mach-number jet, *J. Fluid Mech.* 134, 1-31.
- LAWS, E. M. and LIVESEY, J. L. (1978) Flow through screens, *Ann. Rev. Fluid Mech.* 10, 247-266.
- LECONTE, J. (1858) On the influence of musical sounds on the flame of a jet of coal-gas, *Philos. Magazine J. Sci. (Lond., Edinburgh and Dublin)* XV, 235-239.
- LECORDIER, J. C., HAMMA, L. and PARANTHOEN, P. (1988) The control of vortex shedding behind heated circular cylinders at low Reynolds numbers, submitted for publication.
- LEE, A. H., NAGIB, H. M., TAN, ATICHA, J. and WITTWER, D. M. Experiments on identification and control of inflow disturbances in contracting streams. Technical Rept, Illinois Institute of Technology, Chicago (IB067780).
- LEE, M. and REYNOLDS, W. C. (1985) Bifurcating and blooming jets. Rept TF-22, Thermo Sciences Division, Dept of Mech. Eng., Stanford University.
- LEONHARD, A. (1985) Computing three-dimensional incompressible flows with vortex elements, *Ann. Rev. Fluid Mech.* 17, 523-559.
- LEPICOVSKY, J., AHUJA, K. K., SALIKUDDIN, M. and MORRIS, P. J. (1984) Tone excited heated jets. Part 1, Rept LG84ER0032, Lockheed-Georgia Co.
- LEPICOVSKY, J., AHUJA, K. K., BROWN, W. H. and BURRIN, R. H. (1986) Coherent large-scale structures in high Reynolds number supersonic jet of Mach number 1.4. *AIAA Pap.* 86-1941, 9, 10th Aeroacoustics Conf., Seattle, WA.
- LESSEN, M. and PAILLET, F. (1976) Marginal instability of turbulent shearing layers and the break point of a jet, *Phys. Fluids* 19, 943.
- LEVICH, E. and TSINOBER, A. (1983) On the Role of helical structures in three-dimensional turbulent flow, *Phys. Lett.* 93A (6), 293-297.
- LIEBECK, R. H. (1973) A class of airfoils designed for high lift in incompressible flow, *J. Aircraft* 10, 610-617.
- LIEPMANN, H. W., BROWN, G. L. and NOSENCHUCK, D. M. (1982) Control of laminar-instability waves using a new technique, *J. Fluid Mech.* 118, 187-200.
- LIN, J. C. HOWARD, F. G. and SELBY, G. V. (1989) Turbulent flow separation control through passive techniques. *AIAA Pap.* 89-0976.
- LISSAMAN, P. B. S. (1983) Low Reynolds number airfoils, *Ann. Rev. Fluid Mech.* 15.
- LITTLE, B. H. and WHIPKEY, R. R. (1979) Locked vortex afterbodies, *J. Aircraft* 16, 296-302.
- LIU, J. T. C. (1981) Interactions between large-scale coherent structures and fine-grained turbulence in free shear flows. In: *Transition and Turbulence*, pp. 167-213, Academic Press.
- LOEHRKE, R. I. and NAGIB, H. M. (1976) Control of free-stream turbulence by means of honeycombs: a balance between suppression and generation. *Trans. ASME J. Fluid Eng.* 98, 342-353.
- LONG, D. F., KIM, H. and ARNDT, R. E. A. (1984) Controlled suppression or amplification of turbulent jet noise. *AIAA Pap.* 84-0401.
- LOWERY, P. S. and REYNOLDS, W. C. (1986) Numerical simulation of spatially-developing, forced plane mixing layer. Rept TF-26, Dept Mech. Eng., Stanford Univ., Stanford, CA.
- LOWSON, M. (1989) Acoustic forcing of three-dimensional shear layers. *AIAA Pap.* 89-1063.
- LUDWIG, H. (1982) Widerstandsreduzierung bei kraftfahrzeugähnlichen Körpern. *Proc. Vortex Motion*, pp. 68-81 (eds H. Hornung and E. A. Müller), Vieweg and Sohn, Wiesbaden.

- LUMMER, M. (1989) Numerische Untersuchung der inkompressiblen ebenen Scherschicht zwischen Gasen unterschiedlicher Dichte. Dissertation, Technische Universität Berlin.
- LUXTON, R. E. (1972) Flow over surfaces of changing roughness. The University of Sydney, Charles Knolling Res. Lab. Tech. Note F-12.
- LYNN, T. B., GERICH, D. A. and BECHERT, D. W. (1989) LEBU-manipulated flat plate boundary layers: Skin friction and device drag measured directly. In: *IAHR Drag Reduction 89 Conf.*, Davos.
- MAESTRATI, J. (1987) La réduction de traînée pour les avions d'affaires. AAAF Pap. NT-87-23, 3175 pp.
- MAESTRELLO, L., BADAVID, F. F. and NOONAN, K. W. (1988) An application of active surface heating for augmenting lift and reducing drag of an airfoil. NASA-TM-100563.
- MAIR, W. A. (1965) The effect of a rear-mounted disc on the drag of a blunt based body of revolution, *Aeronaut. Quart.* 16, 350-360.
- MAIR, W. A. (1969) Reduction of base drag by boat-tailed afterbodies in lowspeed flow, *Aeronaut. Quart.* XX, 307-320.
- MAIR, W. A. (1978) Drag-reducing techniques for axi-symmetric bluff bodies. *Aerodynamic Drag Mechanisms*, pp. 161-187 (eds G. Sovran *et al.*), Plenum Press, New York.
- MANGALAM, S. M. and PFENNINGER, W. (1984) Wind-tunnel tests on a high performance low-Reynolds number airfoil. AIAA Pap. 84-0628.
- MANKBADI, R. R. (1984) Mixing enhancement and suppression by forced disturbances (in turbulent round jet shear layer growth). AIAA Pap. 84-2340, 14.
- MANKBADI, R. R. (1985) The mechanism of mixing enhancement and suppression in a circular jet under excitation conditions, *Phys. Fluids* 28, 2062-2074.
- MARCHMAN, J. F. (1987) Aerodynamic testing at low Reynolds numbers, *J. Aircraft* 24, 107-114.
- MARCHMAN, J. F., SUMANTRAN, V. and SCHAEFER, C. G. (1987) Acoustic and turbulence influences on stall hysteresis, *AIAA J.* 25, 50-51.
- MARUMO, E., SUZUKI, K. and SATO, T. (1978) A turbulent boundary layer disturbed by a cylinder, *J. Fluid Mech.* 87, 121-141.
- MASK, R. L. (1980) Low drag airfoil design utilizing passive laminar flow and coupled diffusion control, *Prog. Astronaut. Aeronaut.* 72, 212-232 (ed. G. R. Hough).
- MCCORMACK, P. D. and COCHRAN, D. (1966) Periodic vorticity and its effect on jet mixing, *Phys. fluids* 9 (8), 1555-1560.
- MCCROSBY, W. J. (1977) Some current research in unsteady fluid dynamics, *Trans. ASME, J. Fluids Eng.* 99, Ser. I, 1, 8-38.
- MCDONALD, H. and KRESKOWSKY, J. P. (1974) Effect of free stream turbulence on the turbulent boundary layer, *Int. J. Heat Mass Transfer* 17, 705-716.
- McLACHLAN, B. G. (1987) On the effect of leading edge blowing on circulation control airfoil aerodynamics. NASA-CP-2432, pp. 199-208.
- McMICHAEL, J. M., KLEBANOFF, P. S. and MEASE, N. E. (1980) Experiment investigation of drag on a compliant surface. Viscous Flow Drag Reduction, *AIAA Prog. Astronaut. Aeronaut.* 72, 410-438.
- MECHEL, F. and SCHILZ, W. (1964) Untersuchungen zur akustischen Beeinflussung der Strömungsgrenzschicht in Luft, *Acustica* 14 (6).
- MEHTA, R. D. (1984) Turbulent flow through screens. AIAA 84-0538.
- MEHTA, R. D. (1988), Vortex-separated boundary-layer interactions at transonic Mach numbers, *AIAA J.* 26, 15-26.
- MEHTA, R. D. Effekt of velocity ratio on plane mixing layer development: Influence of the splitter plate wake, submitted for publication.
- MEIER, H. U. and ZHOU MING DE (1989) Boundary layer transition controlled by flush mounted electro acoustic generators. In: 2nd Shear Flow Conf., Tempe, AZ. AIAA-89-1005.
- MENSING, P. (1981) Einfluß kontrollierter Störungen auf eine ebene turbulente Scherschicht. Dissertation HFI.
- MICHALKE, A. (1965) On spatially growing disturbance in an inviscid shear layer, *J. Fluid Mech.* 23, 521-544.
- MICHALKE, A. (1970) The instability of free shear layers. A Survey on the State of Art. DLR Mitt. 70-04.
- MICHALKE, A. (1971) Instabilität eines kompressiblen runden Freistrahls unter Berücksichtigung des Einflusses der Strahlungsgrenzschichtdicke, *Z. Flugwiss.* 19, 319-28.
- MICHALKE, A. (1978) On source coherence affecting jet noise. In: *Structure and Mechanisms of Turbulence II*, Lecture Notes in Physics, Vol. 76, pp. 171-180 (ed. H. E. Fiedler), Springer, Berlin.
- MICHALKE, A. (1984) Survey on jet instability theory, *Prog. Aerosp. Sci.* 21, 159-199.
- MICHALKE, A. (1990) On the inviscid instability of wall-bounded velocity profiles close to separation, *Z. Flugwiss. Weltraumforsch.* 14, 24-31.
- MICHALKE, A. and HERMANN, G. (1982) On the inviscid instability of a circular jet with external flow, *J. Fluid Mech.* 114, 343-359.
- MICHALKE, A. and WEHRMANN, O. (1962/64) Akustische Beeinflussung von Freistrahlgrenzschichten. In: *Proc. Intern. Council Aeronaut. Sci., Third Congress*, Stockholm 1962, Washington-London 1964, pp. 773-785.
- MIGAY, V. K. (1962) The efficiency of cross ribbed curvilinear diffusers, *Energomashinostroyeniye* 1, 45-46.
- MIGAY, V. K. (1963) Study of ribbed diffusers. English translation issued as A. R. C. Pap. 25.382, *Teploenergetika* 10.
- MIGAY, V. K. (1967) The effect of initial turbulence on the efficiency of diffusor flows. Foreign Technology Division. Wright Patterson Air Force Base, Ohio, FTD-HT-23-536-67.
- MOLLO-CHRISTENSEN, E. (1967) Jet noise and shear flow instability seen from an experimenter's viewpoint, *J. Appl. Mech.* 1-7.
- MONKEWITZ, P. A. (1988) Local and global resonances in heated jets. In: *Proc. AFOSR Contract Meet. Res. Turb.*, Univ. So. Calif., LA, 1-4.
- MONKEWITZ, P. A. (1988) A note on vortex shedding from axisymmetric bluff bodies, *J. Fluid Mech.* 192, 561-75.
- MONKEWITZ, P. A. (1989) Feedback control of global oscillations in fluid systems. In: *2nd Shear Flow Conf.*, Tempe, AIAA-89-0991.

- MONKEWITZ, P. A. and HUERRE, P. (1982) Influence of the velocity on the spatial instability of mixing layers, *Phys. Fluids* 25 (7), 1137-1143.
- MONKEWITZ, P. A. and SOHN, K. D. (1986) Absolute instability in hot jets and their control. AIAA Pap. 86-1882.
- MONKEWITZ, P. A. and SOHN, K. D. (1988) Absolute instability in hot jets, *AIAA J.* 26, 911-16.
- MONKEWITZ, P. A., HUERRE, P. and CHOMAZ, J. M. (1987) Preferred modes in jets and global instabilities, *Bull. Am. Phys. Soc.* 32, 2051.
- MONKEWITZ, P. A., BECHERT, D. W., BARSIKOW, B. and LEHMANN, B. (1989) Experiments on the absolute instability of heated jets. In: *Advances in Turbulence 2*, pp. 455-460 (eds H.-H. Fernholz and H. E. Fiedler), Springer, Berlin.
- MONKEWITZ, P. A., LEHMANN, B., BARSIKOW, B. and BECHERT, D. W. (1989) The spreading of self excited hot jets by side jets, *Phys. Fluids A* 1, 446-48.
- MONKEWITZ, P. A., BECHERT, D. W., BARSIKOW, B. and LEHMANN, B. (1990) Self-excited oscillations and mixing in a heated round jet, *J. Fluid Mech.* 213, 611-639.
- MOREL, T. and BOHN, M. (1980) Flow over two circular discs in tandem, *Trans ASME J. Fluids Eng.* 102, 104-111.
- MORI, Y., HUIKATA, K. and NOBUHARA, T. (1986) A fundamental study of symmetrical vortex generation behind a cylinder by wake heating or by splitter plate or mesh, *Int. J. Heat Mass Transfer* 29, 1193-1201.
- MORRIS, P. J. (1976) The spatial viscous instability of axisymmetric jets, *J. Fluid Mech.* 77, 511-529.
- MORRIS, P. J. (1983) Viscous instability of compressible axisymmetric jets, *AIAA J.* 21, 481-482.
- MORKOVIN, M. V. and PARANJAPÉ, S. V. (1971) On acoustic excitation of shear layers. *Z. Flugwiss.* 19, 328-335.
- MORKOVIN, M. V., LOEHRKE, R. I. and FEIER, A. A. (1971) On the response of laminar boundary layers to periodic changes in free-stream speed. Project Themis Rept R71-2.
- MUCK, K. C., HOFFMANN, P. H. and BRADSHAW, P. (1985) The effect of convex curvature on turbulent boundary layer, *J. Fluid Mech.* 161, 347-369.
- MUELLER, T. J. (1985) Low Reynolds number vehicles. AGARD AG-288.
- MÜLLER, U. R. (1985) Measurements of mean flow and Reynolds stress dynamics in a relaxing boundary layer. Habilitationsschrift RWTH Aachen.
- MÜLLER, U. R. (1987) The structure of turbulence measured in a relaxing boundary layer. In: *Advances in Turbulence, Proc.* (ed. G. Comte-Bellot and J. Mathieu), Springer, Berlin.
- MUMFORD, J. C. (1982) The structure of the large eddies in fully developed turbulent shear flows. Part 1, the plane jet, *J. Fluid Mech.* 118, 241-268.
- MUMFORD, J. C. (1983) The structure of the large eddies in fully developed turbulent shear flows. Part 2, the plane wake, *J. Fluid Mech.* 137, 447-456.
- NACHTIGALL, W. (1974) *Phantasie der Schöpfung*, Hoffmann und Campe.
- NAGEL, R. T. (1988) Enhanced viscous flow drag reduction using acoustic excitation. NASA CR-182734, pp. 1-114.
- NAGEL, A. L., GEORGE-FALVY, D. and MCLEAN, J. D. (1985) Riblet flight tests on a small airplane. In: *Drag Reduction and Boundary Layer Control Symp.*, Natn Academy of Sci., Washington D.C.
- NAGIB, H. M. and CORKE, T. C. (1984) Wind microclimate around buildings: Characteristics and control, *J. Wind Eng. Indust. Aero.* 16, 1-15.
- NAGIB, H. M. and MARION, A. (1984) On the design of contractions and settling chambers for optimal turbulence manipulation in wind tunnels. AIAA 85-0536.
- NAGIB, H. M., REISENTHAL, P. H. and KOGA, D. J. (1985) On the dynamical scaling of forced unsteady separated flows. AIAA-85-0553.
- NAKAMURA, Y. N. and OZONO, S. (1987) The effects of turbulence on a separated and reattaching flow, *J. Fluid Mech.* 178, 477-490.
- NAKAMURA, Y. and TOMONARI, Y. (1976) The effect of turbulence on the drag of rectangular prisms, *Trans. Jap. Soc. Aerospace Sci.* 19 (44), 81-86.
- NAKAYA, C. (1976) Instability of the near wake behind a circular cylinder, *J. Phys. Soc. Jap.* 41, 1087-88.
- NARASIMHA, R. (1983) The turbulence problem: A survey, *J. Indian Inst. Sci.* 64 (A), 1-59.
- NARASIMHA, R. and SREENIVASAN, K. R. (1979) Relaminarization of fluid flows, *Adv. Appl. Mech.* 19, 221-309.
- NEUBÜRGER, D. and WYGNANSKI, I. (1987) The use of a vibrating ribbon to delay separation on two-dimensional airfoils. In: *Workshop on Unsteady Separated Flow*, Air Force Academy.
- NEUWALD, P. (1990) Anregung der Kelvin-Helmholtz-Instabilität durch einlaufende Tollmien-Schlichting-Wellen. Dissertation Math.-Nat. Fakultät, Universität Göttingen.
- NIEBERLE, R. (1985) Entwicklung einer Methode der Mustererkennung zur Analyse kohärenter Strukturen und ihre Anwendung im turbulenten Freistrah. Dissertation HFI/TUB.
- NISHIOKA, M. and MORKOVIN, M. V. (1986) Boundary-layer receptivity to unsteady pressure gradients: experiments and overview, *J. Fluid Mech.* 171, 219-261.
- NISHIOKA, M., ASAI, M. and YOSHIDA, S. (1989) Control of flow separation by acoustic excitation. AIAA Pap. 89-0973.
- NORUM, T. D. (1982) Screech suppression in supersonic jets. AIAA-Pap. 82-0050.
- NOTO, K., ISHIDA, H. and MATSUMOTO, R. (1985) A breakdown of the Karman vortex street due to the natural convection. In: *Flow Visualization III*, pp. 348-52 (ed. W. J. Yang), Hemisphere, Washington, DC.
- NOTTMAYER, K. (1990) Experimentelle Untersuchung der Ausbildung und Turbulenzstruktur von turbulenten Scherschichten zwischen Gasströmen unterschiedlicher Geschwindigkeit und Dichte. Dissertation Technische Universität, Berlin.
- NYGAARD, K. J. and GLEZER, A. (1989) A spanwise nonuniformly forced plane mixing layer. *Advances in Turbulence 2*, pp. 461-466 (eds H. H. Fernholz and H. E. Fiedler), Springer, Berlin.
- NYGAARD, K. J. and GLEZER, A. (1990) Evolution of streamwise vortices and generation of small-scale motion in a plane mixing layer, submitted to *J. Fluid Mech.*
- v. OHAIN, P. (1944) Die Ausbreitung heißer Gasstrahlen in bewegter Luft. Deutsche Luftfahrtforschung, Untersuchungen und Mitteilungen 8004 und 8007.

- O'MEARA, M. M. and MUELLER, T. J. (1987) Laminar separation bubble characteristics on an airfoil at low Reynolds numbers, *AIAA J.* 25, 1033-1041.
- OSTER, D., WYGNANSKI, I. and FIEDLER, H. (1976) Some preliminary observations on the effect of initial conditions on the structure of the two-dimensional turbulent mixing layer. In: *Turbulence in Internal Flows: Turbomachinery and other engineering applications, Proc. SQID Workshop*, Warrenton, VA.
- OSTER, D., WYGNANSKI, I., DZIOMBA, B. and FIEDLER, H. (1978) On the effect of initial conditions on the two-dimensional turbulent mixing layer. In: *Structure and Mechanisms of Turbulence I, Lecture Notes in Physics*, pp. 48-64 (ed. H. E. Fiedler).
- OSTER, D. and WYGNANSKI, I. (1982) The forced mixing layer between parallel streams, *J. Fluid Mech.* 123, 91-130.
- PAMADI, B. N., PEREIRA, C. and LAXMANA GOWDA, B. H. (1988) Drag reduction by strakes of noncircular cylinders, *AIAA J.* 26, 292-300.
- PAEKH, D. E., LEONARD, A. and REYNOLDS, W. C. (1988) Bifurcating jets at high Reynolds numbers. Stanford Univ. Dept. Mech. Eng., N89-23829, 1-265.
- PASCHEREIT, C. O. and WYGNANSKI, I. (1989) A detailed study of a subharmonic resonance occurring near the nozzle of an axisymmetric jet, *Bull. Phys. Soc.* 34 (10), 2327.
- PASCHEREIT, C. O., SCHÜTTEPPEL, M. and FIEDLER, H. E. (1989) The mixing layer between non-parallel walls. In: *Advances in Turbulence 2* (eds H. H. Fernholz and H. E. Fiedler), Springer, Berlin.
- PASCHEREIT, C. O., OSTER, D., LONG, T. A. and WYGNANSKI, I. (1990) The use of flow visualization in detecting second-order interactions among large coherent structures in an axisymmetric jet. Submitted for publication.
- PAULEY, W. R. and EATON, J. K. (1988) Experimental study of the development of longitudinal vortex pairs embedded in a turbulent boundary layer, *AIAA J.* 26, 816-823.
- PAVITHRAN, S. and REDEKOPP, L. G. (1989) The absolute-convective transition in subsonic mixing layers, *Phys. Fluids*, in press.
- PAYNE, F. M., NG, T. T., NELSON, R. C. and SCHIFF, L. B. (1986) Visualization and flow surveys of the leading edge vortex structures on delta wing planforms. AIAA-86-0330.
- PEAKE, D. J. and OWEN, F. K. (1979) Control of forebody three-dimensional flow separation. NASA TM-78593.
- PEARCY, H. H. (1961) Shock-induced separation and its prevention by design and boundary layer control. In: *Boundary Layer and Flow Control*, Vol. 2, pp. 1166-1344 (ed. G. Lachmann), Pergamon Press, Oxford.
- PETERKA, J. A. and RICHARDSON, P. D. (1969) Effects of sound on separated flows, *J. Fluid Mech.* 37, 265-287.
- PETERS, N. and WILLIAMS, F. A. (1981) Coherent structures in turbulent combustion. In: *The Role of Coherent Structures in Modelling Turbulence and Mixing* (ed. J. Jimenez), Springer, Madrid.
- PETERSON, R. A. (1978) Influence of wave dispersion on vortex pairings in a jet, *J. Fluid Mech.* 89 (3), 469-495.
- PETERSON, R. A. and MADDALON, D. V. (1982) NASA research on viscous drag reduction. Conference Pap., NASA-TM-84518, Seattle.
- PETERSON, R. A. and SAMET, M. M. (1988) On the preferred mode of jet instability, *J. Fluid Mech.* 194, 153-173.
- PFENNINGER, W. (1977) Laminar flow control laminarization. AGARD Rep. 654, 3.1-3.75.
- PFENNINGER, W., VIKEN, J., VEMURU, C. S. and VOLPE, G. (1988) All laminar supercritical LFC airfoil with natural laminar flow in the region of the main wing structure. In: *Turbulence management and Relaminarization* (eds H.-W. Liepmann and R. Narasimha), Springer, Berlin.
- PLASCHKO, P. (1979) Helical instabilities of slowly diverging jets, *J. Fluid Mech.* 92, 209-215.
- PLATZER, M. F., SIMMONS, J. M. and BREMHORST, K. (1978) Entrainment characteristics of unsteady subsonic jets, *AIAA J.* 16 (3), 282-284.
- POWERS, S. G. (1988) Flight tests of external modification used to reduce blunt base drag. AIAA 88-2553-CP.
- PRANDTL, L. (1904) Über Flüssigkeitsbewegung bei sehr kleiner Reibung, *Gesammelte Abhandlungen II*, 575-584.
- PRANDTL, L. (1914) Der Luftwiderstand von Kugeln, *Nachr. Ges. Wiss. Göttingen Math. Phys. Klasse*, 177-190.
- PRANDTL, L. (1935) The mechanics of viscous fluids. In: *Aerodynamic Theory III*, pp. 34-208 (ed. W. F. Durand), Springer, Berlin. (See also SCHLICHTING, H. *Grenzschichttheorie* 1964, 200-202.)
- QUINN, W. R. and MILTZER, J. (1988) Experimental and numerical study of a turbulent free square jet, *Phys. Fluids* 31 (5), 1017-1025.
- QUINN, W. R., POLLARD, A. and MARSTERS, G. F. (1985) Mean velocity and static pressure distributions in a three-dimensional turbulent free jet, *AIAA J.* 23 (6), 971.
- RAGHU, S. (1987) Control of Combustion in acoustically coupled fluid dynamic instabilities. Ph.D. thesis, Yale University.
- RAGHU, S., LEHMANN, B. and MONKEWITZ, P. A. (1990) On the Mechanism of "side-jet" generation in periodically excited axisymmetric jets. ETC 3/Stockholm.
- RAJARATNAM, N. (1976) *Turbulent Jets*, Elsevier, Amsterdam.
- RAMANCHANDRAN, P., SCARONI, A. W., KOOPMANN, G. and YAVUZKURT, S. (1989) Sonic combustion of micronized coal water slurry fuel. In: *14th Int. Conf. on Coal and Slurry Technology*, Clearwater, FL, U.S.A.
- RAMAN, G. (1976) Enhanced mixing of an axisymmetric jet by aerodynamic excitation. NASA-CR-175059, 177.
- RAO, D. M. and JOHNSON, T. D. (1980) Investigation of leading-edge devices for drag reduction of a 60° Delta wing at high angles of attack. AIAA-80-0310 Pap.
- RAO, D. M. and KARIYA, T. T. (1988) Boundary layer submerged vortex generators for separation control—an exploratory study. AIAA 88-3546-CP, 2, 839-846.
- RASHIDNIA, N. and FALCO, R. E. (1986) Changes in the turbulent boundary layer structure associated with net drag reduction by outer layer manipulators. Rept TSL-86-1, Turbulence Structure Laboratory, Dept of Mech. Eng., Michigan State University, East Lansing.
- REBOLLO, M. R. (1972) Analytical and experimental investigation of a turbulent mixing layer of different gases in a pressure gradient. Ph.D. thesis, Caltech.
- REIF, W.-E. (1985) Squamation and ecology of sharks, *Courier Forschungsinstitut Senckenberg* 78, 1-255.
- REISENTHAL, P. (1988) Hybrid instability in an axisymmetric jet with enhanced feedback. Ph.D. thesis, School of Advanced Studies, Illinois Institute of Technology.
- REISENTHAL, P. H., KOGA, D. J. and NAGIB, H. M. (1984) Dynamic scaling of reattachment control using forced unsteadiness, *Bull. Am. Phys. Soc.* 29.

- REISENTHAL, P. H., NAGIB, H. M. and KOGA, D. J. (1985) Control of separated flows using forced unsteadiness. In: *Shear Flow Control Conference*, Boulder, Colorado, AIAA-85-0556.
- REYNOLDS, G. A. and SARIC, W. S. (1982) Experiments on the stability of the flat plate boundary layer with suction. AIAA Pap. 82-1026.
- REYNOLDS, O. (1883) An experimental investigation of the circumstances which determine whether the motion of water shall be direct or sinuous, and of the law of resistance in parallel channels, *Phys. Trans. R. Soc., Lond.* 174, 935-82.
- REYNOLDS, O. and JUVET, P. (1990) Control of organized structures in jets at high Reynolds numbers. In: *The Global Geometry of Turbulence*, Nato Advance Research Workshop, Spain.
- RIEDIGER, S. (1989) The influence of drag reduction additives on the coherent structures in a free shear layer. In: *Advances in Turbulence 2*, Proc. (eds H. H. Fernholz and H. E. Fiedler), Springer, Berlin.
- ROBERTS, F. A. (1985) Effects of periodic disturbance on structure and mixing in turbulent shear layers and wakes. Ph.D. thesis, California Institute of Technology.
- ROCKWELL, D. O. (1971) The macroscopic nature of jet flows subjected to small amplitude periodic disturbances, *Chem. Eng. Prog., Symp. Ser.* 67 (109), 99-107.
- ROCKWELL, D. O. (1972) External excitation of planar jets, *J. Appl. Mech.*, 883-890.
- ROCKWELL, D. O. (1982) Oscillations of impinging shear layers. Invited lecture, Twentieth Aerospace Sciences Meeting AIAA.
- ROCKWELL, D. O. and NAUDASCHER, E. (1979) Self-sustained oscillations of impinging free shear layers, *Ann. Rev. Fluid Mech.* 11, 67-94.
- ROCKWELL, D. O. and SCHACHENMANN, A. (1980) Self-generation of organized waves in an impinging turbulent jet at low Mach number. Dept of Mech. Eng. and Mechanics, Lehigh University, Bethlehem.
- ROCKWELL, D. O. and TODA, K. (1971) Effects of applied acoustic fields on attached jet flows, *J. Basic Eng.* 93, 63-73.
- ROFFMAN, G. L. and TODA, K. (1969) A discussion of the effects of sound on jets and flueic devices, *J. Eng. Industry*, 1161-1167.
- ROOS, F. W. and KEGELMAN, J. T. (1986) Control of coherent structures in reattaching laminar and turbulent shear layers, *AIAA J.* 24, 1956-19.
- ROSHKO, A. (1954) On drag and shedding frequency of two-dimensional bluff bodies. NACA TN-3169.
- ROSHKO, A. and KOENIG, K. (1978) Interaction effects on the drag of bluff bodies in tandem. In: *Aerodynamic Drag Mechanisms*, pp. 253-286 (eds G. Sovran et al.), Plenum Press, New York.
- ROTH, K. W. and LEEHEY, P. (1989) Velocity profile and wall shear stress measurements for a large eddy break-up device. MIT Acoustics + Vibration Lab. Rept 71435-1.
- RUDERICH, R. (1985) Entwicklung des Nachlaufs einer senkrechten Platte längs einer zur Anströmung parallelen Wand. Dissertation TU Berlin D83.
- SAHLIN, A., JOHANSSON, A. V. and ALFREDSSON, P. H. (1988) The possibility of drag reduction by outer layer manipulations in turbulent boundary layers, *Phys. Fluids* 31, 2814-2821.
- SATO, H. and OKADA, O. (1966) The stability and transition of an axisymmetric wake, *J. Fluid Mech.* 26, 2pp.
- SAVAS, Ö and HARITONIDIS, J. H. (1989) The response of a turbulent boundary layer to suction through a spanwise slot, *Bull. Am. Phys. Soc.* 34, 2270.
- SAVILL, A. M. (1987) On the manner in which outer layer disturbances affect turbulent boundary layer skin friction. In: *Advances in Turbulence, Proc.* (ed. G. Comte-Bellot and J. Mathieu), Springer, Berlin.
- SAVILL, A. M. and MUMFORD, J. C. (1988) Manipulation of turbulent boundary layers by outer-layer devices: skin friction and flow visualization results, *J. Fluid Mech.* 191, 389-418.
- SCHADOW, K. C., WILSON, K. J. and GUTMARK, E. (1985) Identification and control of large-scale structures in highly turbulent shear flow. In: *7th Int. Symp. on Air Breathing Eng.*, Beijing, China, pp. 385-392, AIAA, New York.
- SCHADOW, K. C., WILSON, K. J., PARR, D. M. and GUTMARK, E. (1986) Mixing characteristics of a ducted elliptical jet with dump. AIAA Pap. 86-1399.
- SCHADOW, K. C., WILSON, K. J., LEE, M. J. and GUTMARK, E. (1987) Enhancement of mixing in reacting fuel-rich plumes issued from elliptical nozzles, *J. Propulsion Pwr* 3, 145-149.
- SCHADOW, K. C., GUTMARK, E., PARR, D. M. and WILSON, K. J. (1988) Selective control of flow coherence in triangular jets, *Exp. Fluids* 6, 129-135.
- SCHILZ, W. (1965/66) Experimentelle Untersuchung zur akustischen Beeinflussung der Strömungsgrenzschicht in Luft, *Acustica* 16 (4).
- SCHNEIDER, P. E. M. (1979) Geräuschverstärkung und Geräuschverminderung bei beeinflussten Freistrahlen aus kreisförmigen und nichtkreisförmigen Öffnungen unter Berücksichtigung der Ringwirbel-Instabilität. Max-Planck-Institut Göttingen, MPIS-3/1979.
- SCHNEIDER, P. E. M. (1980) Sekundärwirbelbildung bei Ringwirbeln und in Freistrahlen, *Z. Flugwiss. Weltraumforsch.* 5, 307pp.
- SCHOLZ, D. (1985) Kohärente Wirbelstrukturen im Nachlauf einer ruhenden und einer schwingungsregten Kreisscheibe. Dissertation TU-Berlin.
- SCHUBAUER, G. B. and SPANGENBERG, W. G. (1960) Forced mixing in boundary layers, *J. Fluid Mech.* 8, 10-32.
- SCOTT, I. (1980) The effect of free-stream turbulence on the flow behind a rearward-facing step. M.Sc. dissertation, Dept Aeronautics, Imperial College, London.
- SELBY, G. V. (1989) Passive control of three-dimensional separated vortical flow associated with swept rearward facing steps, *J. Fluids Eng.* 111, 99-101.
- SELBY, G. V. (1989) Effect of various vortex generating devices on turbulent separated flow, *Bull. Am. Phys. Soc.* 34, 2342.
- SEYER, F. A. and METZNER, A. B. (1967) Turbulent flow properties of viscoelastic fluids. University of Delaware, Dept of Chem Eng., Tech. Rept.
- SHABAKA, I. M. M. A., MEHTA, R. D. and BRADSHAW, P. (1985) Longitudinal vortices imbedded in turbulent boundary layers. Pt 1. Single vortex, *J. Fluid Mech.* 155, 37-57.

- SHEARIN, J. and JONES, M. (1989) Airfoil profile drag increase due to acoustic excitation. AIAA Pap. 89-1069.
- SIGURDSON, L. W. and ROSHKO, A. (1984) The large scale structure of a turbulent reattaching flow, *Bull. Am. Phys. Soc.* 29.
- SIGURDSON, L. W. and ROSHKO, A. (1988) The structure and control of a turbulent reattaching flow. In: *Turbulence Management and Relaminarization*, pp. 497-514 (eds H.-W. Liepmann and R. Narasimha), Springer, Berlin.
- SMITH, A. M. O. (1977) Stratford's turbulent separation criterion for axially-symmetric flows, *ZAMP* 28, 929-939.
- SMITH, A. M. O., STOKES, T. R. and LEE, R. S. (1981) Optimum tail shapes for bodies of revolution, *J. Hydronaut.* 15, 67-73.
- SMITS, A. J. (1982) Scaling parameters for a time averaged separation bubble, *Trans. ASME J. Fluids. Eng.* 104, 178-184.
- SMITS, A. J. and WOOD, D. H. (1985) The response of a turbulent boundary layer to sudden perturbations, *Ann. Rev. Fluid Mech.* 17, 321-358.
- SPAID, F. W. and KEENER, E. R. (1987) Boundary layer and wake measurements on a swept, circulation-control wing. NASA CP 2432, 239-266.
- SPANGENBERG, W. G., ROWLAND, W. R. and MEASE, N. E. (1967) Measurements in a turbulent boundary layer maintained in a nearly separating condition. In: *Fluid Mechanics of Internal Flow*, pp. 110-151 (ed. G. Sovran), Elsevier, Amsterdam.
- SQUIRE, L. C. (1989) Interactions between wakes and boundary layers, *Prog. Aerosp. Sci.* 26, 261-288.
- SREENIVASAN, K. R. and NARASIMHA, R. (1974) Rapid distortion of shear flows. In: *Aero. Soc. of India Silver Jubilee Tech. Conf.*, Bangalore.
- SREENIVASAN, K. R., RAGHU, S. and KYLE, D. (1989) Absolute instability in variable density round jets, *Exp. Fluids* 7, 309-317.
- STONE, J. P. and MCKINZIE, D. J. (1984) Acoustic excitation—a promising new means of controlling shear layers. Nasa Technical Memorandum 83772.
- STOSIC, N. and HANJALIC, K. (1982) Numerical study of unsteady convective heat transfer in pulsating duct flows. In: *Proc. 7th Int. Conf.*, Munich.
- STRATFORD, B. S. (1959a) The prediction of separation of the turbulent boundary layer, *J. Fluid Mech.* 5, 1-16.
- STRATFORD, B. S. (1959b) An experimental flow with zero skin friction throughout its region of pressure rise, *J. Fluid Mech.* 5, 17-36.
- STRATFORD, B. S. and TUBBS, H. (1965) The maximum pressure rise attainable in subsonic diffusers, *J. R. Aeronaut. Soc.* 69, 275-278.
- STRAWN, R. C. and KLINE, S. J. (1983) A stall margin design method for planar and axisymmetric diffusers, *J. Fluids. Eng.* 105, 28-33.
- STRYKOWSKY, P. J. (1986) The control of absolutely and convectively unstable shear flows. Ph.D. thesis, Yale University, New Haven/U.S.A.
- STRYKOWSKY, P. J. and SREENIVASAN, K. R. (1989) On the formation and suppression of vortex "shedding" at low Reynolds numbers, submitted for publication.
- SUBBARAO, E. R. (1987) An experimental investigation of the effects of Reynolds number on the structure of a co-flowing buoyant jet. Ph.D. thesis, Stanford University.
- SUMER, B. M., JENSEN, B. L. and FREDIS, J. (1987) Turbulence in oscillatory boundary layers. In: *Advances in Turbulences, Proc.* (eds G. Comte-Bellot and J. Mathieu), Springer, Berlin.
- SYMES, C. R. and FINK, L. E. (1978) Effects of external turbulence upon the flow past cylinders. In: *Structure and Mechanisms of Turbulence I*, Lecture Notes in Physics 75 (ed. H. E. Fiedler), Springer, Berlin.
- SZAJNER, A. and TURNER, J. T. (1986) Visualization of an aerodynamically excited free jet. In: *Proc. Int. Conf. Flow Visualization*, Paris.
- SZAJNER, A. and TURNER, J. T. (1987) Coherent structures in a free circular jet surrounded by a pulsed annular jet. In: *6th Symp. on Turbulent Shear Flows*, Toulouse, France.
- TAKAKI, R. (1975) Numerical analysis of distortion of a vortex filament, *J. Phys. Soc. Jap.* 38 (5), 1530-1537.
- TAKEUCHI, M. and OKAMOTO, T. (1983) Effect of side walls of wind-tunnel on turbulent wake behind two-dimensional bluff body. Manuscript.
- TAM, C. K. W. (1974) Discrete tones of isolated airfoils, *J. Acoust. Soc. Am.* 55 (6), 1173-1177.
- TAN-ATICHAT, J., NAGIB, H. M. and LOEHRKE, R. I. (1982) Interaction of free-stream turbulence with screens and grids: a balance between turbulence scales, *J. Fluid Mech.* 114, 501-528.
- TANEDA, S. (1959) Downstream development of wakes behind cylinders, *J. Phys. Soc. Jap.* 14, 843-848.
- TANNER, M. (1975) Reduction of base drag, *Prog. Aerosp. Sci.* 16, 369-389.
- TANNER, M. (1989) Calculation of the rate of spread of two-dimensional turbulent mixing layers, *Z. Flugwiss.* 13 (6), 393-398.
- TARDU, S., BINDER, G. and BLACKWELDER, R. (1987) Response of turbulence to large amplitude oscillations in channel flow. In: *Advances in Turbulence, Proc.* (eds G. Comte-Bellot and J. Mathieu), Springer, Berlin.
- TAVOULARIS, S. and CORRISIN, S. (1981) Preliminary results on the structure of a turbulent shear layer embedded in turbulence. In: *Int. Symp. Appl. Fluid Mechanics and Heat Transfer to Energy and Environment Problems*, Patras, Greece.
- THOMAS, A. S. W. (1984) Aircraft drag reduction technology. AGARD CP-365, 11.1-20.
- THORNTON, B. S., BOTTEN, L. C. and GOSTELOW, J. P. (1986) Proposed control of compressor stall by pressure perturbation and blade design. ICAS-86-3.6.2, pp. 820-826.
- THRING, M. W. and NEWBY, M. P. (1952) *4th Symp. Combust.* 789, Cambridge, MA.
- TOMS, B. A. (1984) *Proc. 1st Int. Cong. Rheol.* 2, pp. 135-41, North-Holland, Amsterdam.
- TOYODA, K. (1990) Manipulation of noncircular jets by controlled excitation. In: *Int. Symp. Eng. Turbulence Modelling Measurements*.
- TRENTACOSTE, N. and SFORZA, P. M. (1967) Further experimental results for three-dimensional free jets, AIAA-J. 5, 885-891.
- TSIOLAKIS, E. P., KRAUSE, E. and MÜLLER, U. R. (1983) Turbulent boundary layer wake interaction. In: *4th Symp. Turbulent Shear Flows*, pp. 5.19-5.24.

- Tso, J. (1983) Coherent structures in a fully-developed turbulent axisymmetric jet. Dissertation, Johns Hopkins University.
- Tso, J., KOVASZNAV, L. S. G. and HUSSAIN, A. K. M. F. (1980) Search for large-scale coherent structures in the nearly self-preserving region of an axisymmetric turbulent jet. *AIAA-80-1355*.
- TYNDALL, J. (1867) On the action of sonorous vibrations on gaseous and liquid jets. *Philos. Magazine J. of Sci.*, Lond., Edinburg, Dublin 33, 375-391.
- UKHANOVA, L. N. and VOITOVICH, L. N. (1984) Certain features characterizing the development of coherent flow structures in the initial region of three-dimensional turbulent jets, *Inzhenerno-Fizicheskii Zhurnal* 47, 537-543.
- VAGT, J. D. (1969) Untersuchung der Turbulenzstruktur runder Freistrahlen. *Forsch. Bericht Scha* 154/1, HFI/TUB.
- VEYNANTE, D., CANDEL, S. M. and MARTIN, J. P. (1986) Influence of the system response on the coherent structures in a confined shear layer. *Phys. Fluids* 29 (12), 3912-3914.
- VOGEL, J. C. and EATON, J. K. (1984) Heat transfer and fluid mechanics measurements in the turbulent reattaching flow behind a backward-facing step. *Thermo. Sci. Div., Dept. Mech. Eng., Stanford University*.
- VLASOV, E. V. (1965) Investigation of turbulence in connection with the determination of the acoustic characteristics of a jet. *Inzhenerno-Fizicheskii Zhurnal* 8 (5), 568-573.
- VLASOV, YE. V. and GINEVSKIY, A. S. (1967) Acoustic effect on aerodynamic characteristics of a turbulent jet. Foreign Technology Division—AN SSSR. *IZV Estiya. Mekhanika Zhidkosti i Gaza*.
- VLASOV, YE. V. and GINEVSKIY, A. S. (1976) The dual nature of acoustic effect on free turbulent jets. *Fluid Mech.—Soviet Res.* 5 (6).
- WALKER, J. D. A. and ABBOT, D. E. (1977) Implications of the structure of the viscous wall layer. In: *Turbulence in Internal Flows*, (ed. S. N. B. Murthy), Hemisphere.
- WALSH, M. J. (1982) Turbulent boundary layer drag reduction using riblets. *AIAA Pap.* 82-0169.
- WALSH, M. J. and ANDERS, J. B. (1985) Riblets optimized for flight application. *Abstr., Drag Reduction and Boundary-Layer Control Symposium*, Nat. Acad. of Sciences, Washington D.C.
- WALSH, M. J. and LINDEMANN, A. M. (1984) Optimization and application of riblets for turbulent drag reduction. *AIAA Pap.* 84-0347.
- WALSH, M., SELLERS, W. and MCGINLEY, C. (1988) Riblet drag reduction at flight conditions. *AIAA Pap.* 88-2554.
- WAY, J. L., NAGIB, H. M. and TAN-ATICHAT, J. (1973) On aeroelastic coupling in free stream turbulence manipulators. In: *AIAA Aero-Acoustics Conf.*, Seattle, Washington.
- WEHRMANN, O. H. (1957) Akustische Steuerung der turbulenten Anfachung im Freistrah. *Jahrbuch d. Wiss. Ges. f. Luftfahrt*. Braunschweig.
- WEHRMANN, O. H. (1967) Self-adjusting feedback loop for mechanical systems to influence flow in transition. *Flight Sciences Laboratory, Boeing Scient. Res. Lab. Document* D1-82-0632, Seattle, Washington.
- WEHRMANN, O. H. (1967) The influence of vibrations on the flow field behind a cylinder. *Flight Sciences Laboratory, Boeing Scientific Research Laboratories Document* D1-82-0619, Seattle, Washington.
- WEIR, A. D. and BRADSHAW, P. (1974) The interaction of two parallel shear layers. *Dept of Aeronaut., Imperial College, London*, AR 74-09.
- WEIR, A. D. and BRADSHAW, P. (1975) Resonance and other oscillations in the initial region of a plane turbulent jet. *Imperial College of Science and Technology, Dept of Aeronaut., I.C. Aero Rept* 75-07.
- WEISBROT, I. and WYGANSKI, I. (1988) On Coherent structures in a highly excited mixing layer, *J. Fluid Mech.* 195, 137-159.
- WELLS, C. S. (ed.) (1969) *Viscous Drag Reduction*, Plenum Press.
- WESKE, J. R. and RANKIN, T. M. (1962) Production of secondary vortices in the field of a primary vortex. *University of Maryland, Inst. for Fluid Dynamics and Appl. Math., T. N. B-244, AFOSR-623*.
- WESTPHAL, R. V. (1983) Experimental study of flow reattachment in a single-sided sudden expansion. *Ph.D. thesis, Mech. Eng. Dept., Stanford Univ.*
- WESTPHAL, R. V. and JOHNSTON, J. P. (1984) Effect of initial conditions on turbulent reattachment downstream of a backward-facing step, *AIAA J.* 22, 1727-1731.
- WESTPHAL, R. V., EATON, J. K. and PAULEY, W. R. (1985) Interaction between a vortex and a turbulent boundary layer in a streamwise pressure gradient. In: *Turbulent Shear Flows*, pp. 266-277 (ed. Durst et al.), Springer, New York.
- WESTPHAL, R. V., PAULEY, W. R. and EATON, J. K. (1987) Interaction between a vortex and a turbulent boundary layer Pt 1. *NASA TM-88361*.
- WIDNALL, S. E. and SULLIVAN, D. B. (1973) On the stability of vortex rings, *Proc. R. Soc. Lond. A* 322, 335-353.
- WIGELAND, R. A., AHMED, M. and NAGIB, H. M. (1977) Management of swirling flows with application to wind tunnel design and V/STOL testing. In: *AIAA/NASA Ames V/STOL Conf.*, Palo Alto, CA.
- WIGELAND, R. A., AHMED, M. and NAGIB, H. M. (1978) Management of swirling flows with application to wind-tunnel design, *AIAA J.* 16, 1125-1131.
- WILKINSON, S. P., ANDERS, J. B., LAZOS, B. S. and BUSHNELL, D. M. (1988) Turbulent drag reduction research at NASA Langley: Progress and Plans, *Int. J. Heat Fluid Flow* 9, 266-277.
- WILLE, R. (1963) Beiträge zur Phänomenologie der Freistrahlen, *Z. Flugwiss.* 11, 222 pp.
- WILLE, R. (1963) Growth of velocity fluctuations leading to turbulence in free shear flow. Technical rept. Hermann-Föttinger Institut für Strömungstechnik, Technische Universität Berlin, U.S. Air Force: AF 61 (052)-412, TR, 30.
- WINTER, K. G. and EAST, L. F. (1982) The design of optimum diffusers for incompressible flow. In: *Recent Contributions to Fluid Mechanics*, pp. 312-320 (ed. W. Haase), Springer, Berlin.
- WLEZIEN, R. W. and KIBENS, V. (1984) Passive control of jets with indeterminate origins. *AIAA Pap.* 84-2299.
- WOOD, C. J. (1964) The effect of base bleed on a periodic wake, *J. R. Aeronaut. Soc.* 68, 477-82.
- WOOD, D. H. and BRADSHAW, P. (1982) A turbulent mixing layer constrained by a solid surface. Part 1. Measurements before reaching the surface, *J. Fluid Mech.* 122, 57-89.
- WOOD, N. J. and ROBERTS, L. (1987) The control of vortical lift on delta wings by tangential leading edge blowing. *AIAA* 87-0158.

- WYGNANSKI, I. (1981) The effects of Reynolds number and pressure gradient on the transitional spot in a laminar boundary layer. The role of coherent structures in modelling turbulence and mixing, pp. 304-332 (ed. J. Jimenez), Springer, Berlin.
- WYGNANSKI, I. and PETERSON, R. A. (1985) Coherent motion in excited free shear flows. *AIAA J.* 25 (2), 201, (1987).
- WYGNANSKI, I. and WEISBROT, I. (1988) On the pairing process in an excited plane turbulent mixing layer, *J. Fluid Mech.* 195, 161-173.
- WYGNANSKI, I., OSTER, D., FIEDLER, H. and DZIOMBA, B. (1979) on the perseverance of quasi-two-dimensional eddy-structure in a turbulent mixing layer, *J. Fluid Mech.* 93 (2), 325-335.
- WYGNANSKI, I., CHAMPAGNE, F. and MARASLI, B. (1986) On the large-scale structures in two-dimensional small-deficit, turbulent wakes, *J. Fluid Mech.* 168, 31-71.
- YAJNIK, K. S. and ACHARYA, M. (1977) Non-equilibrium effects in a turbulent boundary layer due to the destruction of large eddies. In: *Structure and mechanisms of turbulence I*, Lecture Notes in Physics Vol. 75, pp. 249-260 (ed. H. E. Fiedler), Springer, Berlin.
- YANG, X. and ZEBIB, A. (1989) Absolute and convective instability of a cylinder wake, *Phys. Fluids A* 1, 689-696.
- YODA, H. (1981) Effects of dilute polymer additives on the turbulence structure near a wall. M. S. thesis, Michigan State University.
- YOUNG, A. D. (1977) Some special boundary layer problems, *Z. Flugwiss.* 1, 401-414.
- YOUNG, A. D. and RAO, K. N. (1978) Some low speed experimental results on the effects of swirl and velocity distribution on an axisymmetric jet, *Aeronaut. Quart.* 29, 270-284.
- YU, M.-H. and MONKEWITZ, P. A. (1988) Self-excited oscillations in a low-density two-dimensional jet, *Bull. Am. Phys. Soc.* 33, 2246.
- ZABUSKY, N., FELZ, R. and BORATAV, O. (1990) Vortex scattering: Collapse and reconnection of orthogonally offset vortex tubes, *The Global Geometry of Turbulence*, Nato Advance Research Workshop, Spain.
- ZAMAN, K. B. M. Q. and HUSSAIN, A. K. M. F. (1981) Turbulence suppression in free shear flows by controlled excitation, *J. Fluid Mech.* 103, 133-159.
- ZAMAN, K. B. M. Q. and HUSSAIN, A. K. M. F. (1982) The dominant coherent structure of the jet organized by controlled perturbation. Structure of turbulence in heat and mass transfer, *Hemisphere*, 149-166.
- ZAMAN, K. B. M. Q. and MCKENZIE, D. J. (1989) Control of laminar separation over airfoils by acoustic excitation. NASA TM 101379.
- ZAMAN, K. M. B. Q., BAR-SEVER, A. and MANGALAM, S. M. (1987) Effect of acoustic excitation on the flow over a low-Reynolds-number airfoil, *J. Fluid Mech.* 182, 127-148.
- ZDRAVKOVICH, M. M. (1977) Review of flow interference between two circular cylinders in various arrangements, *Trans. ASME J. Fluids Eng.* 99, 618-633.
- ZHOU, M. DE (1988) A preliminary study on the manipulation of turbulent structures. Manuscript.
- ZHOU, M. DE and SQUIRE, L. C. (1985) The interaction of a wake with a turbulent boundary layer, *J. Aeronaut.* 89, 72-81.
- ZIADA, S. and ROCKWELL, D. (1981) Generation of higher harmonics in a self-oscillating mixing layer-wedge system. Rept, Lehigh University.
- ZILBERMAN, M., WYGNANSKI, I. and KAPLAN, R. E. (1977) Transitional boundary layer spot in a fully turbulent environment, *Phys. Fluids* 20, 258-276.



Turbulent Mixing, Stability And Secondary Flow In A Confined Configuration

vorgelegt von
M.Eng. Guiren Wang
aus Xian/China

Vom Fachbereich 10
Verkehrswesen und Angewandte Mechanik
der Technischen Universität Berlin
zur Erlangung des akademischen Grades
Doktor-Ingenieur
genehmigte Dissertation

Promotionsausschuss:

Vorsitzender:	Prof. Dr.-Ing. J. Hourmouziadis
Gutachter:	Prof. A Dillmann
	Prof. H. Eckelmann
	Prof. H. Fiedler

Tag der wissenschaftlichen Aussprache: 14. Januar 1999

Berlin 1999
D 83



**“Great are the works of the Lord,
studied by all who have pleasure
in them”.**

—Psalm 111:2

Turbulent Mixing, Stability and Secondary Flow In A Confined Configuration

Guiren Wang



This work consists of two parts. Part 1 deals with turbulent mixing: its meaning, mechanism, criteria, measurement and control based on stability mechanism (receptivity). First a new model of an ideal relative turbulent mixing process is proposed for turbulent mixing criterion. Then the experiment is conducted in a confined configuration, i.e. confined plane wake and mixing layer in a pipe to realize the ideal relative turbulent mixing process. A high spatial resolution of around $4 (\mu\text{m})^3$ scalar measurement with laser induced fluorescence is achieved to study the mechanism of turbulent mixing. Some new problems with the high spatial resolution measurement are investigated. These include low signal to noise ratio, thermal blooming and photobleaching. The results shows that the turbulent mixing is extraordinarily enhanced under strong forcing of a new receptivity mechanism. Even within one diameter of the pipe downstream of the trailing edge, the large and small scalar structures have already been homogeneously distributed in the whole local cross section. According to the experiment result, a new controlled flow is proposed for turbulence theory study with experiment and direct numerical simulation, where the turbulent statistical properties at high Reynolds number can be realized at low Reynolds number with specific forcing, and thus the resolution is relatively improved.

Part 2 describes some new phenomena: dual receptivity, pairing burst, secondary vortices in the confinement, sudden transition to turbulence and a new symmetric breaking hysteresis phenomenon, discovered through visualization in the confined configuration, especially under strong temporal periodic forcing. It seems that there are two different receptivity mechanisms for the large forcing. One of them corresponds to the traditional instability mechanism in two dimensional shear layer and the other is a new one. The new instability mechanism has a much higher receptivity than the traditional one, especially under high forcing level. The experimental result shows that there is no universal spread rate for the mixing layer and plane wake under forcing. Two types of secondary vortices are found to be dominant and they are related to the new instability mechanism. A sudden transition to turbulence is observed. To achieve the sudden transition, the instability mechanism is very important. Another new phenomenon called symmetric breaking hysteresis is also observed, which becomes weak with increase of Reynolds number. A new phenomenon, named here, pairing burst is also observed. The relation of pairing burst to Reynolds number, velocity ratio λ and forcing is investigated.

The direct applications of this work include: a new anemometer based on the photobleaching with laser induced fluorescence, a new rapid mixing process for mixer and reactor and a new process for heat transfer enhancement.

Turbulente Mischung, Stabilität und sekundäre Strömungen in einer begrenzten Konfiguration

Guiren Wang

Diese Arbeit besteht aus zwei Teilen. Der erste Teil befasst sich mit turbulenter Mischung: ihrer Bedeutung, den Mechanismen, den Kriterien, der Messung und der Kontrolle über Instabilitätsmechanismen (Rezeptivität). Zuerst wird ein neues Modell eines idealen relativen turbulenten Mischungsprozesses entworfen. Dann wird die Untersuchung in einem begrenzten Nachlauf und einer Scherschicht in einem Rohr durchgeführt, um die idealen relativen turbulenten Mischungsprozesses zu erreichen. Eine Laser-Induced-Fluorescence-Messung mit einer räumlichen Auflösung von ca $4 (\mu m)^3$ wurde durchgeführt, um den Mechanismus der turbulenten Mischung zu studieren. Einige neue Probleme wie niedriges Signal-Rausch-Verhältnis, Beeinflussung des thermal bloomings und Photobleaches bei der Messung hoher Auflösung wurden untersucht. Das Ergebnis zeigt, dass unter starker Anregung einer neuen Rezeptivität, die relative turbulente Mischung aussergewöhnlich verstärkt ist, und sogar innerhalb eines Rohrdurchmessers sind die grossen und kleinen Skalarstrukturen schon homogen im ganzen lokalen Querschnitt verteilt. Für die turbulente Grundlagenforschung mit Experiment und direct numerical simulation (DNS) wird eine kontrollierte Strömung vorgeschlagen, wo die statistischen Eigenschaften, die ohne Anregung sonst erst bei grosser Reynolds-Zahl auftreten, unter einer speziellen Anregung, wegen der verbesserten räumlichen Auflösung schon bei kleiner Reynolds-Zahl erreicht werden kann.

Der zweite Teil beschreibt einige neue Phänomene: Dual receptivity, pairing burst, Sekundärwirbel, rascher Umschlag zur Turbulenz und ein neues Symmetrie-Brechung-Hysterese-Phänomen werden in der begrenzten Konfiguration, besonders unter starker Anregung entdeckt. Es scheint, dass zwei unterschiedliche Rezeptivitätsmechanismen für starke Anregung auftauchen. Eine ist der entsprechende traditionelle Instabilitätsmechanismus der 2-D Scherschicht und der andere ist neu. Die neue Instabilität hat eine höhere Rezeptivität als die traditionelle, besonders unter starker Anregung. Nach dem Ergebnis der Untersuchung gibt es keine universelle Ausbreitungsrate für Scherschicht und Nachlauf unter Anregung. Zwei Typen der sekundären Wirbel, welche eine Beziehung zur neuen Instabilität haben, werden als wichtig erachtet. Ein rascher Umschlag zur Turbulenz wird beobachtet. Der neue Instabilitätsmechanismus ist sehr wichtig, um den raschen Umschlag zu erreichen. Ein Symmetrie Brechung Hysterese-Phänomen wird auch hier entdeckt, welches schwach wird, wenn Reynolds-Zahl steigt. Ein neues Phänomen, pairing burst genannt, wird auch beobachtet. Die Beziehung des pairing bursts mit Reynolds-Zahl, Geschwindigkeitsverhältnis λ und Anregung wird untersucht.

Die direkten Anwendungen dieser Arbeit sind: ein neues auf dem Effect des Photobleachs basierendes Anemometer, ein neues Verfahren zur raschen und homogenen Mischung von Flüssigkeiten im kontinuierlichen Durchlaufbetrieb und ein effektiver Wärmetauscher durch begrenzten symmetrischen oder asymmetrischen Nachlauf in der Rohrströmung.

Acknowledgments

First of all, I would like to use this chance to show my deepest sorry that, my advisor, Prof. H. E. Fiedler, left us several months ago. He passed away too early!

This is a long period experimental work lasting more than 7 years. Without the help of many people, it impossible to finish the extremely difficult experiment, since the ultra-high spatial resolution experiment needs a lot of optical, mechanical and electrical work of high demand. I would like to use the chance here to thank all of those, who have helped me during last 7 years.

Foremost, I want to thank Prof. H. E. Fiedler for providing me with a research environment with a lot of personal freedom. He brought me into a world of turbulent mixing for an adventure, where I slipped into an eddy due to its dangerous complexity. After the "turbulent mixing" of different concepts and ideas in the field, I was confused as a result of the stirring, which made things more homogeneous so that no clear direction could be found. After seven years of struggle in the whirls, I finally came out of the chaotic mixing world under his guidance as well as his great patience of waiting of long-term risk and finished the adventurous trip in the turbulent mixing world.

Thank to Prof. H. Eckelmann for introducing me to Prof. Fiedler, his helpful discussions and the acceptance of the second advisor. Thank to Prof. J. Houmoziadis and A. Dillmann for their attendance of the defense and the helpful correction of the dissertation by Prof. Dillmann. Prof. R. S. Brodkey from Ohio has given many helpful discussions on the problems of turbulent mixing. Thank you Bob. Prof. H. Zhou from Tianjing University/China advised me during the whole period when I tried to apply his program for wall boundary instability to free shear layer when he was in Berlin. This excited me for my interest of flow instability. Many discussions with him are very helpful. Prof. J. S. Lou from Tianjing University/China also gave me a lot of help in discussion of problems of instability and during my experiments as he was in Berlin.

Many help comes from DLR. Here especially thank to Dr. B. Lehmann and J. Mante for their general support in providing optical components and Dr. W. Neise's group for their laser and instruments. The discussion with Dr. B. Lehmann for experiment is very appreciated.

The stable experimental table was constructed from Dr. D. Hilberg and it is very much appreciated. Mr. B. Stefes helped me in constructing the experimental setup. The help from workshop in constructing the experimental setup is very much appreciated. Here, especially, thank is to Mr. Barzantny for his 'magic' in constructing of mechanical parts. Electronical help from Dr. R. Eschenhagen is also appreciated.

Thank also to Dr. Yi Ding from Optical Institute for many helpful discussions on optical problems. Ms. Julia Stone has kindly helped me for the English correction. Thank you very much Julia.

Definitely many helps come from the crew of Werk-3. Especially, my colleague. R. Spieweg, has given me a lot of help in using his programs and solving computer problems. Thank you Rene. Dr. O. Koenig corrected my German in writing proposals. S. Berneno gave many helpful discussions.

At last, I want to thank my wife Dr. Hong Jiang for all her supporting during last seven years.

The work is partially supported by Deutsche Forschungsgemeinschaft (DFG).

Contents

I Turbulent mixing: meaning, mechanism, criteria, measurement and control	1
1 Introduction	2
1.1 Turbulent mixing: meaning, mechanism and criteria	2
1.2 High spatial resolution measurement for scalar	2
1.3 Experimental results of turbulent mixing and ideal relative turbulent mixing process	3
1.4 Scalar power spectrum density	4
1.5 Some new phenomena in the confined configuration	4
2 Turbulent mixing: meaning, mechanism and criteria	5
2.1 The meaning of turbulent mixing	5
2.1.1 Terminology	5
2.1.2 Meaning of turbulent mixing	6
2.2 Turbulent mixing criteria	7
2.2.1 Collection of existing turbulent mixing criteria	7
2.2.2 Classification	11
2.2.3 Analysis	11
2.3 Mechanism of mixing in a turbulent flow	12
2.3.1 Scenario of mixing in turbulent flow	12
2.3.2 Three characteristics of turbulent mixing	12
2.3.3 Scale sizes	13
2.3.4 Geometry of small scale	13
2.3.5 Timescales of two processes	13
2.4 Ideal relative turbulent mixing process and state	14
2.5 New criteria for turbulent mixing	16
2.5.1 Mixing rate	17
2.5.2 Mixing state	17
3 Experimental set-up and measurement procedures	19
3.1 Water channel	19
3.2 Forcing methods	20
3.2.1 Loudspeaker	20
3.2.2 Valve	20
3.3 Optics	20
3.3.1 Optics for focusing laser beam	20
3.3.2 Optics for photomultiplier tube (PMT)	21
3.3.3 How to determine the focused diameter	21
3.4 Measurement Processing	22
4 Laser Induced Fluorescence (LIF)	24
4.1 Thermal blooming	24
4.2 Photobleaching	24
4.2.1 A model of the photobleaching effect	24
4.2.2 The principle for measuring bleaching constant τ	25
4.3 Analysis of signal to noise ratio (SNR)	26

4.4	Results	27
4.4.1	Thermal blooming	27
4.4.2	Photobleaching	27
4.4.3	Calibration between fluorescence intensity I_f and concentration C	31
4.4.4	Noise characteristic	31
4.4.5	Noise influence on scalar measurement	33
4.4.6	Methods to increase signal level	33
4.5	Discussion	38
4.5.1	A new anemometer of photobleaching with LIF	38
4.5.2	Some considerations about photobleaching influence	38
4.5.3	Measurement of focused beam diameter d_f	39
4.5.4	Detector and SNR	39
4.5.5	Amplifying signal	39
4.5.6	Fluorescence saturation	40
4.5.7	Attenuation	40
5	Experimental results of turbulent mixing	41
5.1	Wake	41
5.1.1	Visualization	41
5.1.2	Concentration distribution at near field	41
5.1.3	Evolution downstream	44
5.2	Mixing layer	48
5.2.1	Concentration distribution at near field	48
5.2.2	Evolution downstream	49
5.3	Influence of Reynolds number	51
5.4	Influence of initial velocity ratio λ	54
5.5	Influence of forcing frequency	56
5.6	Influence of forcing level	56
5.7	Relative turbulent mixing rate R_r	56
5.8	Power-spectrum-density	57
5.8.1	-5/3 exponent with low Reynolds number	57
5.8.2	Batchelor -1 spectrum beyond -5/3	58
5.8.3	-1 exponent before -5/3	58
6	Discussion	60
6.1	Homogeneous whole local flow fields	60
6.2	Control between l_K and l_B	60
6.3	Comment on ideal relative turbulent mixing process	60
6.4	Mechanism of the turbulent mixing enhancement	61
6.5	Zero crossing point number of gradient G_z	61
6.6	-1 exponent spectrum	61
6.7	A new method for turbulence study	62
7	Conclusion	63
II	New phenomena in a confined configuration	65

8	Introduction	66
8.1	Simultaneous visualization of three light sheets	66
8.2	Dual receptivity	66
8.3	Sudden transition to turbulence	67
8.4	A new symmetry breaking hysteresis phenomenon	67
8.5	Pairing burst	68
9	Experimental set-up	69
9.1	Water channel	69
9.2	Optics	69
10	Results	72
10.1	Dual receptivity	72
10.1.1	Wake	72
10.1.2	Mixing layer	77
10.1.3	Quasi-step flow	77
10.2	Secondary vortices	79
10.2.1	Wake	79
10.2.2	Mixing layer	83
10.2.3	Quasi-step flow	85
10.3	Sudden transition	85
10.3.1	Mixing layer	86
10.3.2	Wake	89
10.4	Symmetry breaking hysteresis phenomenon	89
10.4.1	Phenomenon	89
10.4.2	Relation to concentration distribution	89
10.5	Pairing burst	90
10.5.1	Where does pairing burst happen	90
10.5.2	Velocity ratio λ effect	90
10.5.3	The influence of initial Re_θ	91
10.5.4	Forcing influence	92
10.5.5	Three dimensional pairing burst	94
10.5.6	Re in the confined mixing layer	95
11	Discussion	98
11.1	Dual receptivity	98
11.1.1	Relation to secondary vortices	98
11.1.2	High receptivity	98
11.1.3	Qualitative amplification curves with Re	99
11.1.4	No universal spread rate	99
11.1.5	Small scale and mixing transition	99
11.1.6	Influence of non-linearity and 3-D on amplification	100
11.1.7	Receptivity capacity	101
11.1.8	Mixing receptivity	101
11.1.9	Difference from mechanical stirring	101
11.1.10	Philosophy on control	102
11.2	Secondary vortices	102
11.3	Sudden transition	103
11.4	Symmetry breaking hysteresis	103

11.5	Pairing burst	103
11.5.1	Mechanism of the pairing burst origin	103
11.5.2	Quasi-step flow	103
11.5.3	Control of wall free and wall bounded turbulent flow	104
11.5.4	On turbulent burst	104
12	Conclusion	106
13	Summary	108
14		109
15	Appendix: Some applications	114
A	A new Anemometer based on photobleaching with LIF	114
A.1	Principle	114
A.2	Discussion	114
A.3	Problems	114
B	A new rapid mixing process for mixer and reactor	115
B.1	Status	115
B.2	New mixer	115
B.3	The disadvantage of other mixers	115
B.4	The advantage of new mixer	115
C	A new process for heat transfer enhancement	116
C.1	Status	116
C.2	New heat exchanger	116
C.3	Disadvantages of other heat exchangers	116
C.4	Advantages of the new heat exchanger	116

List of Figures

2.1	A simple sketch of turbulent mixing process.	15
3.1	Experimental schematic.	19
3.2	A simple sketch of low noise current amplifier.	22
4.1	Relation between fluorescence intensity and fluid velocity with different values of P_l at $C = 0.67 * 10^{-6} M$	28
4.2	Fluorescence intensity decay with residence time for different laser power P_l and $C = 10^{-6} M$	28
4.3	Relationship between photobleaching half-life constant $\tau_{1/2}$ and laser power P_l at constant $C = 1.0 * 10^{-6} M$	29
4.4	Relationship between fluorescence intensity and fluid velocity u for different concentrations but constant $P_l = 0.5 W$	30
4.5	Fluorescence intensity decay with residence time for different C and constant laser power $P_l = 0.5 W$	30
4.6	Relationship between photobleaching half-life $\tau_{1/2}$ and C with constant laser power $P_l = 0.5 W$	31
4.7	Calibration between I_f and C with different velocities.	32
4.8	Coefficient k between I_f and C changes with different velocities.	32
4.9	Timetrace of signal.	33
4.10	Relationship between noise RMS of fluorescence intensity and square root of signal level.	34
4.11	Relationship between noise RMS of fluorescence intensity and square root of frequency bandwidth.	34
4.12	Relationship between fluorescence intensity and concentration with different P_l	36
4.13	Relationship between laser power attenuation and concentration with different P_l	36
4.14	Influence of concentration on fluorescence intensity saturation to P_l at $U = 32 cm/s$	37
4.15	Fluid velocity influence on fluorescence intensity saturation to P_l at constant $C = 6.7 * 10^{-7} M$	37
5.1	Visualization for turbulent mixing with and without forcing in a wake of $\bar{U} = 40 cm/s$	41
5.2	Time trace with and without forcing in a wake with $\bar{U} = 40 cm/s$ at $x/D = 0.25$. a: no forcing at $y = -0.5 mm$; b, c and d: with forcing at $2y/D = 0.75, 0$ and -0.75 respectively.	42
5.3	Concentration variance for different y-positions under forcing in a wake with $\bar{U} = 40 cm/s$ at $x/D = 0.25$	43
5.4	pdf under forcing for different y-positions in a wake with $\bar{U} = 40 cm/s$ at $x/D = 0.25$	43
5.5	Power spectrum density for different y-positions under forcing in a wake with $\bar{U} = 40 cm/s$ at $x/D = 0.25$	44
5.6	Timetrace with and without forcing in a wake with $\bar{U} = 40 cm/s$ at different downstream positions. a: $x/D = 0.25$; b: $x/D = 1.6$; c: $x/D = 7.5$; d: $x/D = 25.4$	45
5.7	Concentration variance evolution along x-positions with and without forcing in wakes.	46
5.8	pdf under forcing for different x-positions in a wake with $\bar{U} = 40 cm/s$	46
5.9	Comparison between the pdf results of with and without forcing in a wake with $\bar{U} = 40 cm/s$	47

5.10	Power spectrum density evolution for different x-positions under forcing in a wake with $\bar{U} = 40 \text{ cm/s}$.	47
5.11	Comparison for power spectrum density evolution for different x-positions with and without forcing in a wake with $\bar{U} = 40 \text{ cm/s}$.	48
5.12	Concentration variance for different y-positions under forcing in a wake and different mixing layers at $x/D = 0.25$.	49
5.13	pdf under forcing for different y-positions in a mixing layer with $U_1 = 48 \text{ cm/s}$ and $\lambda = 0.2$ at $x/D = 0.25$.	50
5.14	Power spectrum density for different y-positions under forcing in a mixing layer with $U_1 = 48 \text{ cm/s}$ and $\lambda = 0.2$ at $x/D = 0.25$.	50
5.15	Concentration variance for different x-positions under forcing in different mixing layers with and without forcing.	51
5.16	pdf with forcing for different x-positions in a mixing layer with $U_1 = 48 \text{ cm/s}$ and $\lambda = 0.2$.	51
5.17	Comparison between the results of with and without forcing for pdf in a mixing layer with $U_1 = 48 \text{ cm/s}$ and $\lambda = 0.2$.	52
5.18	psd $E(f)$ without forcing for different x-positions in a mixing layer with $U_1 = 48 \text{ cm/s}$ and $\lambda = 0.2$.	52
5.19	psd $E(f)$ with forcing for different x-positions in a mixing layer with $U_1 = 48 \text{ cm/s}$ and $\lambda = 0.2$.	53
5.20	Comparison between the results of with and without forcing for psd in a mixing layer with $U_1 = 48 \text{ cm/s}$ and $\lambda = 0.2$.	53
5.21	Timetrace of different y-positions with and without forcing in a wake with $\bar{U} = 1 \text{ cm/s}$ at $x/D = 0.25$. a: no forcing; b, c and d: with forcing at $2y/D = 0.75$, 0 and -0.75 respectively.	54
5.22	Concentration variance for different y-positions under forcing in a wake with $\bar{U} = 1 \text{ cm/s}$ at $x/D = 0.25$.	55
5.23	pdf under forcing for different y-positions in a wake with $\bar{U} = 1 \text{ cm/s}$ at $x/D = 0.25$.	55
5.24	Power spectrum density for different y-positions under forcing in a wake with $\bar{U} = 1 \text{ cm/s}$ at $x/D = 0.25$.	56
5.25	Power spectrum density with -5/3 exponent for different Re .	57
5.26	Power spectrum density for different flows with no -1 spectrum exponent beyond -5/3 region.	58
9.1	Experimental schematic.	69
9.2	Simultaneous 3-D visualization of a mixing layer.	71
10.1	Dual receptivity phenomenon from side view of a wake. $\bar{U} = 4 \text{ cm/s}$, $A = 10\%$, a: $f = 0 \text{ Hz}$; b: $f = 1.6 \text{ Hz}$; c: $f = 4.4 \text{ Hz}$; d: $f = 6.0 \text{ Hz}$ and e: $f = 8.5 \text{ Hz}$.	73
10.2	Forcing amplitude influence on receptivity. $\bar{U} = 25 \text{ cm/s}$, a: $f = 0 \text{ Hz}$; b: $f = 6.0 \text{ Hz}$, $A = 1\%$; c: $f = 6.0 \text{ Hz}$, $A = 5\%$; d: $f = 6.0 \text{ Hz}$, $A = 25\%$; e: $f = 6.0 \text{ Hz}$, $A = 35\%$; f: $f = 6.0 \text{ Hz}$, $A = 45\%$; g: $f = 16 \text{ Hz}$, $A = 5\%$; h: $f = 16 \text{ Hz}$, $A = 45\%$; i: $f = 22 \text{ Hz}$, $A = 5\%$.	74
10.3	Relation between threshold forcing amplitude and initial Re .	75
10.4	Relation between maximum receptivity frequency and \bar{U} .	76
10.5	Influence of A with $f = 5.6 \text{ Hz}$ in a mixing layer of $U_1 = 10 \text{ cm/s}$ and $U_2 = 5 \text{ cm/s}$.	78
10.6	Response to forcing in a quasi-step flow. a: no forcing; b: with forcing $f = 6 \text{ Hz}$, $A = 15\%$; c: with forcing $f = 11 \text{ Hz}$, $A = 15\%$.	78

10.7	Side view of separation reduction under forcing in a quasi-step flow with $U_1 = 80$ cm/s.	79
10.8	A sketch of the main secondary vortices. a: Type A Vortices; b: Type B Vortices.	80
10.9	Cross view of types of secondary vortices: a: $\bar{U} = 4$ cm/s, $f = 4.5$ Hz, $A = 15\%$, $x/D = 0.1$; b: $\bar{U} = 1$ cm/s, $f = 5.21$ Hz, $A = 25\%$ $x/D = 1$; c: $\bar{U} = 10$ cm/s, $f = 5.48$ Hz, $A = 7\%$ $x/D = 4$	80
10.10	Cross view to show the origin of the secondary vortices of a wake. $\bar{U} = 10$ cm/s, $f = 5.48$ Hz, $x/D = 1$, $\delta t = 0.04$ s, $A = 7\%$	81
10.11	Evolution of secondary vortices (cross view). $\bar{U} = 4$ cm/s, $f = 4.9$ Hz. $A = 20\%$. a: $x/D = 0.1$; b: $x/D = 1$; c: $x/D = 3$; d: $x/D = 7$	82
10.12	Cross view of the geometry of secondary vortices in a wake. $\bar{U} = 1$ cm/s, $f = 4.62$ Hz, $A = 10\%$. For a, b and c x/D is 1, 4 and 7 respectively.	83
10.13	Secondary vortices under forcing with different A values in a wake.	83
10.14	Secondary vortices with forcing for different A values in a mixing layer at $x/D = 0.2$	85
10.15	Evolution of the secondary vortices in a mixing layer without forcing. $U_1 = 9$ cm/s, $U_2 = 6$ cm/s. For a, b, c and d the x/D are 0.2, 1, 2 and 4 respectively.	86
10.16	Evolution of the secondary vortices in a mixing layer with forcing. $U_1 = 9$ cm/s, $U_2 = 6$ cm/s, f is 5.6 Hz, A is around 6%. For a, b, c and d the x/D are 0.2, 1, 2 and 4 respectively.	86
10.17	Comparison for different receptivity mechanism through secondary vortices.	87
10.18	Sudden transition under strong forcing with f being 6 Hz. $U_1 = 30$ cm/s and $U_2 = 20$ cm/s.	88
10.19	No sudden transition with strong forcing under f being 16 Hz. $U_1 = 30$ cm/s and $U_2 = 20$ cm/s.	88
10.20	Pairing burst is not apparent in a mixing layer where U_1 and U_2 are 12 cm/s and 8 cm/s respectively.	91
10.21	Pairing burst is apparent in a mixing layer where U_1 and U_2 are 16 cm/s and 4 cm/s respectively.	91
10.22	Relationship between λ_c and Re_θ	92
10.23	No pairing burst for small Re_θ in a quasi-step flow.	92
10.24	There is pairing burst in a quasi-step flow.	93
10.25	Pairing burst in a mixing layer with $U_1 = 24$ cm/s, $U_2 = 16$ cm/s. $\lambda = 0.2$ and $\delta t = 0.12$ s.	93
10.26	Pairing burst in a mixing layer with $U_1 = 36$ cm/s, $U_2 = 24$ cm/s, $\lambda = 0.2$ and $\delta t = 0.08$ s.	94
10.27	No forcing with the weak pairing burst.	94
10.28	With pairing burst under forcing.	95
10.29	Pairing burst is weakened through forcing.	95
10.30	Pairing burst is relatively weak when U_1 and U_2 is 17.5 and 1.5 cm/s respectively.	96
10.31	Pairing burst is relatively strong when U_1 and U_2 is 25 and 9 cm/s respectively.	97
11.1	Sketch of qualitative amplification rate with Reynolds number.	100

List of Symbols

a_F	lens focus length
A	relative forcing amplitude $\sqrt{u'^2}/\bar{U}$
A_c	critical relative forcing amplitude for the new receptivity
b_F	lens focus length
f_F	focus length of combined lenses
c	local concentration
\bar{c}^2	local concentration fluctuation intensity
C	local average concentration
\bar{C}	average concentration $\bar{C} = (C_a + C_b)/2$
D	pipe inner diameter
D_m	molecular diffusivity
D_l	is the diameter of the incident light beam
d_f	laser focus diameter
$E(f)$	power spectrum density
f	frequency
f_{1max}	the first maximum receptivity frequency
f_{2max}	the second maximum receptivity frequency
G_z	zero cross point of concentration gradient
h	molecular diffusion length $l_s/4$
I_f	fluorescence intensity
I_{f0}	initial fluorescence intensity for bleaching
I_l	laser intensity
l	length scale corresponding to u'
l_B	Batchelor scale, $l_B = (D_m^2 \nu / \epsilon)^{1/4}$
l_K	Kolmogorov scale, $l_K = (\nu^3 / \epsilon)^{1/4}$
l_l	length of light path in dye medium
l_{OC}	Obukhov Corrsin scale, $l_{OC} = (D_m^3 / \epsilon)^{1/4}$
l_s	small-scalar scale used for the ideal relative turbulent mixing process
L	large scale of scalar
L_i	initial large scalar scale
P_l	laser power
pdf	probability density function of concentration c
psd	power spectrum density
Q_f	fluorescence quantum yield
r_m	mixing rate $r_m = ((L_i - l_s)/L_i)/(T_s/(L_i/U))$
r_{im}	mixing rate of the ideal relative turbulent mixing process $r_{im} = [((L_i - l_s)/L_i)/(t_m/(L_i/U))]_i$
R_r	relative turbulent mixing rate $r_m/r_{im} = t_m/T_s$
Re	Reynolds number based on pipe diameter and average velocity
Sc	Schmidt number

t	time
t_K	the time needed to reduce L_i to l_k
t_m	the time needed to for molecular mixing at scale l_s
T_s	time needed to reach l_s from L_i
u	local fluid velocity
u'	local fluid velocity fluctuation
U_1	initial high average velocity of a mixing layer
U_2	initial low average velocity of a mixing layer
$\overline{u'^2}$	mean square of velocity fluctuation
\bar{U}	average velocity of $(U_1 + U_2)/2$
δt	residence time deviation due to velocity deviation δu
δu	velocity deviation δu in measuring volume
ΔU	initial velocity difference $(U_1 + U_2)$
ΣU	initial velocity sum $(U_1 + U_2)$
V	measuring volume
x	downstream position from trailing edge
y	transverse position
z	spanwise position
α	spatial amplification rate
ϵ	turbulent energy dissipation
λ	initial velocity ratio $(U_1 - U_2)/(U_1 + U_2)$
λ_c	critical initial velocity ratio for pairing burst $(U_1 - U_2)/(U_1 + U_2)$
λ_w	wave length of light
ν	kinematic viscosity
σ	dye absorption cross section
τ	fluorescence decay time constant
$\tau_{1/2}$	half fluorescence decay time constant

Part I

Turbulent mixing: meaning, mechanism, criteria, measurement and control



1 Introduction

This work deals with turbulent mixing: its meaning, criteria, mechanism, measurement and control based on stability mechanism (receptivity) in part 1. In part 2 some new phenomena in the confined configuration are investigated. These include: a new receptivity mechanism, secondary vortices, sudden transition from laminar to turbulence, a new symmetrical breaking hysteresis phenomenon and pairing burst.

1.1 Turbulent mixing: meaning, mechanism and criteria

Turbulent mixing plays an important role not only in many engineering divisions (for example, chemical engineering, combustion, aerospace and so on), but also in nature, i.e. the heat and mass transfer phenomena in the atmosphere and oceans. With the discovery of turbulent coherent structures in a mixing layer and its receptivity to initial disturbance, the active and passive turbulent control, i.e. the control of these large coherent structures, has become very active in the field of turbulence. These structures have an essential influence on molecular mixing of different chemical species in the turbulent flows. The control of the molecular mixing can indirectly be achieved through the control of these structures in turbulent flows.

It seems the molecular mixing of fluids in turbulent flow is very closely related to the concept of turbulent mixing. Therefore there are now more and more works on turbulent mixing and the concept of turbulent mixing is often used in articles. However Ottino [83] wrote "Presently, the study of fluid mixing has very little scientific basis; processes and phenomena are analyzed on a case-by-case basis without any attempt to discover generality.... The analysis of mixing.....share little in common with each other, except possibly the nearly universal recognition among researchers that they are very difficult problems." This is also true for turbulent mixing. Different papers use the same name, i.e. turbulent mixing, but they means quite different things. Until now there is still no universal definition and criteria for turbulent mixing. The definition and criteria vary from case to case. One aim of this work is to give a clear picture of turbulent mixing and establish a broad general criterion of it.

Before a turbulent mixing criterion can be established, it is necessary to understand the role of turbulence for turbulent mixing and the mechanism of turbulent mixing. For this purpose, a model of an ideal relative turbulent mixing process and its corresponding state is proposed. The new criterion is based on this model.

1.2 High spatial resolution measurement for scalar

The new criteria must be proved by experiment. For this aim, an confined symmetrical wake and asymmetric wake (mixing layer) in a pipe is constructed and a high spatial resolution measurement (around $4 (\mu m)^3$) measuring volume of scalar with Laser Induced Fluorescence is developed here.

There are many measurement methods for scalars which are cited in the review of Brodkey [14], but it seems that Laser Induced Fluorescence (LIF) provides the best non-intrusive method for high spatial resolution measurement of concentration in turbulent flow. Until now the best realized spatial resolution, which is really measured, is to our knowledge, in the order of $40 \sim 60 \mu m$ (Miller [73]). This is much larger than the smallest scalar scale in turbulent flows, which is in the order of $0.1 \sim 10 \mu m$. It is, therefore, very difficult to measure the smallest scale directly. The fine focusing of the laser beam in fluid mechanics is not as easy as in micro-optical and electronic technology (as used for example in CDs) since in the former the working distance is much longer.

LIF is widely used in fluid mechanics today since the first work of Owen [84] and later contributions by [62], [25], [73], [109] and others. However, LIF is still a relatively new method and there seems to be only limited effort to study and improve the method of LIF itself. For instance, there are only few papers dealing with its signal to noise ratio (SNR), the possible influence of photobleaching and thermal blooming in this method and its calibration, especially for very high spatial resolution measurement of, say, several micrometers.

At the beginning, it was thought that the fine focusing of the laser beam is the most difficult task for high resolution measurement. However, having achieved very fine focusing of around $4\text{ }\mu\text{m}$, it is found that the signal level is very low due to the small measuring volume. This results in low SNR, especially for the high frequency region where signal amplitude is also small. Furthermore it turned out that the signal can not be simply increased by increasing dye concentration and laser input power due to the fact that attenuation, photobleaching and thermal blooming would contaminate the signal if concentration and laser power are too high. It is expected that this is also a crucial point for high spatial resolution measurement of all measuring techniques based on light scattering.

LIF is often used for concentration measurement (it can also be used for temperature measurement). Its principle is that if the laser intensity at the measuring point is constant, for a given specific dye and a fixed optical construction for the emitting signal to be collected to the light detector, the signal from the detector should depend only on the concentration. Thus when the concentration is constant, the signal of fluorescence intensity should also be unchanged for a given optical system. However, in this work, it was found that even if the concentration is constant, the fluorescence intensity changes with fluid velocity in a certain range. The higher the velocity is, the higher the signal becomes. Thus the measurement could be contaminated. The laser beam focusing diameter is measured to be around $4\text{ }\mu\text{m}$ and the average fluid velocity range is from 4 to 80 cm/s. The reason of the contamination is photobleaching and thermal blooming, which becomes strong when laser is very fine focused. The photobleaching has strong influence on measurement results, not only because of the signal becoming smaller, but also depending on velocity. This is also a crucial point for high resolution measurement of LIF and is investigated in this work.

1.3 Experimental results of turbulent mixing and ideal relative turbulent mixing process

In order to find a more general turbulent mixing criterion, a concept of ideal relative turbulent mixing process is proposed in this work (see later). To study the turbulent mixing mechanism and the ideal relative turbulent mixing process, the high spatial resolution measurement is necessary. The ideal relative turbulent mixing process is traditionally very difficult to be carried out. To achieve the ideal relative turbulent mixing process, some special turbulent mixing control is essential. The control is based on a new receptivity mechanism discovered in this work (see Part 2). The flows in the confined configuration (confined plane wake and mixing layer in a pipe) are strongly forced to realize the ideal relative turbulent mixing process. With the high spatial resolution measurement, the turbulent mixing is measured at the near field with different transverse positions and different downstream positions for the evolution of the mixing in both cases with and without the active strong forcing. The results show that the turbulent mixing is extraordinarily enhanced and ideal relative turbulent mixing process is approximately realized under the new strong forcing mechanism.

1.4 Scalar power spectrum density

There are two fields of research in turbulence study: one is statistics, which concentrates on universal law of small scale structures in turbulent flows, and the other is structure, which searches for large coherent structures in turbulent flows and the ways to control them. These two fields are relatively independent each other. There are few works, to our knowledge, which bring the two together. This work attempts to use the structural method to the study of statistical turbulence.

Power spectrum density is important for both turbulent theory and turbulent mixing [70]. It describes the scale distribution in the flow field. Traditionally, both studies concentrate on small scale structures which are approximately local isotropic when Reynolds number is very high. For turbulent theory, there is Kolmogorov [58] local isotropic turbulent flow where there is a universal $-5/3$ law of power spectrum density for velocity fluctuation (Kolmogorov used structure function in physical space and the result corresponds to $-5/3$ law in power spectrum density). Obukhov [79] and Corrsin [23] applied this theory to scalar fluctuation in turbulent flows, and pointed out that there was also a $-5/3$ power spectrum density for scalar. Batchelor [5] found later that scalar spectrum depended on the Schmidt number Sc . If $Sc \sim 1$, the power spectrum is the similar for both velocity and scalar; but when $Sc \gg 1$, there is also a -1 spectrum in a frequency range higher than $-5/3$ region. All these theories are based on the assumption that Re is high enough. To prove these theories, it necessary to use very high Re , which is very difficult to carry out both experimentally and numerically due to the following factors: the higher Re is, the smaller Kolmogorov scale l_K and so Batchelor scale l_B ; high Re requires high velocity and commands high temporal resolution; small l_K and l_B requires high spatial resolution which is difficult to realize experimentally, especially for l_B . For turbulent theory study, the experiments are usually undertaken without periodic forcing, i.e. no receptivity of flows to external excitation is used for this aim.

In this work, a new method is used to reach a local homogeneous isotropic turbulence. It is based on receptivity theory, especially a new receptivity mechanism, which is, to our knowledge, unknown. The interesting result is that the $-5/3$ spectrum can also be obtained in a very small Re under strong forcing and for a given Re the $-5/3$ spectrum can be obtained much earlier under forcing. When Re is small, the Kolmogorov scale l_K will be large and so is l_B . Then the spatial resolution is relatively higher. For very small Re under strong forcing, the spatial resolution can be high enough to be able to measure l_B . However no -1 exponent is found beyond $-5/3$. Instead, the spectrum exponent is smaller than $-5/3$, i.e. it decays faster than $-5/3$. There is indeed a -1 exponent region, which is, however, in the frequency region lower than $-5/3$ region, and therefore is not the Batchelor spectrum.

1.5 Some new phenomena in the confined configuration

To achieve the ideal relative turbulent mixing process and state, a new turbulent mixing control mechanism is discovered in the light of a new receptivity mechanism in the confined flow configuration. Although, as far as we know, there is no report on such flow, the flow is in fact of great interest for science and engineering. There are some new phenomena in this flow: dual receptivity, secondary vortices, an extraordinary spread rate of the mixing layer, sudden transition from laminar to turbulence, symmetric breaking hysteresis under strong forcing in a wake and paring burst. These phenomena are studied through visualization and form the part 2 of this dissertation.

2 Turbulent mixing: meaning, mechanism and criteria

To control turbulent mixing it is first necessary to know the special aim for mixing, i.e. to define the mixing according to the scale (large scale, meso scale, microscale or molecular scale) and decide: Which scale does the mixing require? To what extent can turbulent mixing fulfill the purpose? How can turbulent mixing be controlled through the control of turbulent flow to fulfill the purpose? To answer these questions quantitatively, it is necessary to know what the corresponding turbulent mixing criteria are? This is the main issue dealt with in part 1. To give a clear answer for turbulent mixing criteria, it is also necessary to know the meaning and mechanism of turbulent mixing.

2.1 The meaning of turbulent mixing

Although there are some rigid mathematical definitions of mixing (for example, Aref [1]), it is very difficult to give a definition of turbulent mixing, since, in reality, there are not even clear definitions of turbulence and mixing. Regarding turbulence definition, Panton [85] wrote: "It is probably not wise to make a rigid definition of a turbulent flow." Brodkey [13] said of mixing: "The term mixing is a loose one, and encompasses nearly as many definitions as there are workers in the field." Therefore the concept of turbulent mixing is widely used with great confusion. For instance, in the field of turbulence study, when looking at the mixing layer, the spread rate of the mixing layer is often used as a criterion of turbulent mixing. In chemical engineering and combustion and some turbulence studies, the concept of turbulent mixing is used to describe the molecular mixing of two different chemicals. In respect of turbulent flows: "On the other hand, the flows we call turbulent do have certain properties in common" [85]. Turbulent mixing also has some general properties, which will be investigated in this work.

The quantities to be mixed in a turbulent flow can be vectors (impulse, vorticity for instance) and scalar (turbulent energy, temperature, concentration and so on). The mixing of two scalar species in a turbulent flow is considered here, due to its practical importance and prerequisite of impulse and turbulent energy mixing for scalar mixing. However, the results here are not just applicable to scalar concentration, but also to temperature and vector (energy and vorticity) and so on. Therefore the Schmidt number (Sc) used here can also be regarded as general Prandtl number including Prandtl and Schmidt numbers.

2.1.1 Terminology

To give a relatively clear meaning of turbulent mixing, some related terminologies with turbulent mixing are first discussed. These include: stirring, dispersion, advection, diffusion, chaotic mixing and mixing.

1. **Stirring:** Stirring signifies the mechanical process whereby fluids are distributed more uniformly within a given domain, i.e., stirring is a process of stretching of material line and surface through vortices in turbulent flows. It results in the change of quantity per volume and the increase of interface per volume, being a pure kinematic aspect depends on fluid parameters. Stirring accelerates molecular mixing through the increase of interface or gradient [11].
2. **Dispersion [12]:** Dispersion normally describes the process by which a quantity disperses in a continually flowing fluid without considering molecular mixing. Only fluctuation movement of velocity (or vorticity) has influence on dispersion, which can decrease Scale of Segregation ($G_s(r)$), but not the Intensity of Segregation ($I_s(r)$).

3. Convection: It is also used to describe the stretching, i.e., mixing process [5] and does not include molecular mixing. Since convection can also be used for the bulk convection of fluids, which is not turbulence property, it is not proposed to use this terminology to describe turbulent mixing.
4. Diffusion: Diffusion means not only the movement because of fluctuation in turbulence but also the molecular mixing within the flow [12]. This can be described by, for instance, the turbulent diffusion term in energy equation of turbulent velocity fluctuation. Particle movement because of turbulent diffusion is similar to Brownian movement [67]. Diffusion also means spreading, and so it has a flux of quantity.
5. Chaotic mixing: In comparison to others, chaotic mixing is relatively a new concept. It means that the initial distance between two fluid particles is exponentially increased [82]. We make reference to it here, since some papers e.g. [91] and [11] questioned whether chaotic mixing plays a role in the mixing layer. If so, it is not clear how the chaotic mixing affects the molecular mixing in the mixing layer.
6. Molecular diffusion or molecular mixing: is an irreversible thermodynamic process, a Brownian movement. It is not the characteristic of turbulence. Turbulent can not change the characteristic of molecular mixing, but provides a favorable condition for the molecular mixing (i.e. increases the interface for the molecular mixing).
7. Mixing: Mixing in turbulence can be regarded as the change of quantity per volume. The scale ranges from large scale to molecular scale. When such a mixing process is conducted, the mixing entropy increases thermodynamically. Mixing means both the action of homogenization and the result of homogenization. The concept of mixing should not be dependent on the scale, i.e. whether it is molecular, micro-, meso- or large scale.
8. Transport: This term is widely used to describe transport phenomena. All the above terminologies belong to transport phenomena. Here it is necessary to mention the difference between transport (which is also closely related to transfer) and mixing. In a steady heat transfer process with fixed temperature difference in a heat exchanger, there is heat transfer (transport), but no mixing (based on spatial homogeneity). However, if mixing occurs, there is also transport.

According to these terminologies, stirring, dispersion and convection mean the same process. We use only stirring here. There are also some other terminologies related to mixing used in chemical engineering, for example, polymer blending, compounding and so on. To simplify our task, these are not considered here. This study will only consider Newton single phase fluids.

2.1.2 Meaning of turbulent mixing

The following must first be made clear:

1. This study not only aims to understand the physical mechanism of turbulent mixing and describe turbulent mixing more generally with turbulent mixing criteria, but also to control the turbulent mixing based on the given turbulent mixing criteria.
2. Turbulent mixing criteria should be not only directly related to flow characteristic, but also fluid property, since on the one hand it is only the flow property that can be controlled directly by the control of flow, not fluid property; and on the other hand, the smallest scalar scale is related to fluid property for a given flow.

3. In determining which process mentioned above is used to describe turbulent mixing criteria, it is necessary to know if a process is just based on fluid flow characteristic or fluid physical properties or both.
4. The turbulent mixing criteria should be a more common property and controllable one.

Mixing means both the action of causing homogeneity and the result of mixing (or stirring), i.e., mixedness. Mixing here means to make the distribution of different quantities more homogeneous spatially, regardless of whether it is molecularly mixed or not, as for example, in chemical reaction engineering, the concept of "ideal mixed reactor". Even if originally, on a large scale, two initially separated fluids (on large scale) are not molecularly mixed in turbulent flow, it can be said that they are mixed on some smaller scales which are still much larger than the molecular scale. It depends on the meaning of scale. The stirring in a turbulent flow can make two fluids more homogeneous if the mixing is indicated as the change of homogeneity from large to small scale (also called as microscale) in a given control volume. As we know if Sc is different, the molecular mixing can be different even though the turbulent flows are the same. If the two streams to be mixed are mutually insoluble, i.e., molecular diffusivity D_m is zero, there will be no molecular mixing, but turbulence really does stir (and therefore mix) them to be more homogeneous from large to small scale. Therefore although turbulent mixing can enhance molecular mixing, the molecular mixing itself is a fluid property, not a characteristic of turbulence, and turbulent mixing would also be dependent on species diffusivity D_m (If D_m is zero, we can not use molecular mixing at all to describe turbulent mixing). So it is necessary to give a clear and more general concept of turbulent mixing which is independent of molecular mixing. The process from large to small scales in turbulent flow is a flow characteristic which is related to stirring and coupled with fluid property.

Therefore the stirring in a turbulent flow is the flow property and describes what turbulent mixing essentially mean here, although a lot of other concepts have also been used to describe turbulent mixing (see later). However, due to the fact that for a long time molecular mixing in turbulence has traditionally been regarded as turbulent mixing, it is preferable to divide turbulent mixing into general turbulent mixing and relative turbulent mixing, in order to distinguish turbulent mixing from molecular mixing in a turbulent flow, which is not the characteristic of turbulence. This helps to describe more clearly what turbulence can do for molecular mixing. The general turbulent mixing includes all mixing processes, i.e. mixing from large scale to small scale (where molecular mixing can be neglected) and molecular mixing (which is the end of general turbulent mixing). The relative turbulent mixing only refers to the process from large scale to smallest scale which turbulence can produce, i.e., the process of stirring independent of molecular mixing. It can be seen that relative turbulent mixing is related to turbulence coupled with fluid property in determining the smallest scalar scale and general turbulent mixing relates not only to turbulence, but also to molecular mixing. General turbulent mixing includes relative turbulent mixing. For convenience, we also refer to general turbulent mixing simply as turbulent mixing.

2.2 Turbulent mixing criteria

2.2.1 Collection of existing turbulent mixing criteria

As mentioned above, the terminology of turbulent mixing is very widely used, so that there are a lot of different parameters used for the description of turbulent mixing. These parameters are actually consciously and unconsciously used as turbulent mixing criteria.

Danckwerts [28] was the first to study the criteria of mixing using statistical methods. He proposed both scale segregation and intensity of segregation to describe the scale of unmixed scalar and the molecular unmixedness of scalar respectively. These only describe the state of mixing, i.e., the degree of mixing, not the mixing rate, i.e., the dynamics. However, the control of turbulent mixing directly concerns the mixing rate. It seems that scale of segregation is only an integral scale, not a microscale. However, the mechanism of turbulent mixing is closely related to small structures.

Of the existing criteria for mixing and turbulent mixing, twenty two are collected and classified in table 1.

Criterion	Advantage	Disadvantage	Condition	Author(s)
1 Visualization with dye and smoke and so on	Easy description of global large structures and scalar mixing	With difficulty for quantitatively high resolution and small scale measurement	For a	Green(1989)
2 Entrainment E and entrainment ratio E_1/E_2	Easy, only large structures information	No detailed information on the large and small structures	For b and e	Fernado (1991)
3 Spreading rate db/dx	Similar to 2	Similar to 2	For b	Cantwell (1981)
4 Contaminant flux $\gamma S_0(U_c \Delta c) * R_e^{\frac{3}{4}(D-7/3)S_c^{0.5(D'-3)}}$, D is fractal dimension with $S_c > 1$	Capable of description of structure	No mixing state information	For b	Sreenivansa et al. (1989)
5 Mixing coefficient D_{mc} and ϵ $\tau = -\epsilon \frac{\partial u}{\partial y}$ $N = -D_{mc} \frac{\partial c}{\partial y}$	Easy to deal with mathematics	Regarding turbulent characteristic as that of fluid and thus neglecting the physical meaning	For c	Schlichting (1979)
6 Vertical diffusivity of heat $K_\theta = 3D \frac{\overline{(\partial T'/\partial y)}}{\partial T'/\partial y}$	Similar to 5	Similar to 5	For e	Oakey (1989)
7 Scalar dissipation rate $2D_j \propto abs \nabla c'(x, t)^2$	Providing information on small structures	Difficult to measure	For a	Landau & Lifshitz (1959) Dowling-(1990)
8 Decay of fluctuation of velocity and scalar (concentration) $du'^2/dt, dc'^2/dt$	Easy to estimate molecular mixing	No information on scale distribution	For a and d	Sirivat & Warhaft (1983)
9 Scale of segregation $g(r) = \frac{c'(x)c'(x+r)}{c'^2}$ $L_s = \int_0^\infty g(r)dr$	Providing with state of large scale due to turbulent mixing	No small scale information	For a	Danckwerts (1953)
10 Intensity of segregation $I_s = \frac{c'^2}{c_0'^2}$	With the information of molecular mixing	No mixing dynamics and incapable using be if molecular diffusion coefficient D is approximately zero	For a	Danckwerts (1953)
11 Unmixedness 1 $1 - (\overline{c_a c_b})/\overline{c_a} \overline{c_b}$	valid for both reaction and non-reaction systems	Similar to 10	For a	Hill (1976)

12 Unmixedness 2 $\frac{\int_{t_1} (c-\bar{c})dt_1 + \int_{t_2} (\bar{c}-c)dt_2}{\int_{t_1} (1-\bar{c})dt_1 + \int_{t_2} (\bar{c})dt_2}$ $t_1 = \text{time when } c > \bar{c}$ $t_2 = \text{time when } c \leq \bar{c}$	The experiment noise is smaller when \bar{c} is near 1 or 0	Similar to 10	For a	Konrad (1977)
13 Mixedness parameters $1 - \frac{N^2}{N_0^2}$ $N_0^2 = -\frac{g}{\rho_0} \frac{d\rho(y)}{dy}$ $N^2 = -\frac{g}{\rho_0} \frac{d\rho_r(y)}{dy}$	Similar to 10	Similar to 10	For e	De Silva & Fernando (1991)
14 PDF (probability density function) of vector (e.g. velocity) and scalar (e.g. temperature)	Related to molecular mixing result and capable of being used for flows with reaction when scalar is passive	No structures information	For a	Toor (1962) Sosinovich (1991) O'brien (1980)
15 Velocity distribution in transverse direction	Easy to measure and model	No turbulent structure information	For c	Vlasov (1965)
16 RTD (residence time distribution)	Able to prove mixing model	Unable to predict mixing	For f	Baldyga & Bourne (1986)
17 Degree of segregation defined by "age of fluid at a point"	Similar to 16	Similar to 16	For f	Baldyga & Bourne (1986)
18 Ratio of diffusion to convection $\frac{\frac{\partial u_i q^2/2}{\partial x_i}}{\frac{\partial u_i q^2/2}{\partial x_i}}$	Providing with more about turbulent structure	Only refers to mixing without molecular mixing	For c	Fiedler et al (1991)
19 Turbulent Peclet number	Good for open systems	No details of structures	For a	Brodkey (1967)
20 Mixing efficiency $\frac{R_f}{1-R_f}$, where R_f is flux Richardson number	Similar to 18	Similar to 18	For e	Peters & Gregg (1989)
21 Striation thickness of mechanical mixing $S = \frac{1}{2}(S_a + S_b)$	Able to describe velocity field	Not for turbulent flow	For g	Ottino (1989)
22 Amount of area between fluid or interfacial area per unit volume	Similar to 21	Similar to 21	Similar to 21	Ottino (1989)

Table 1: Collection of existing mixing and turbulent mixing criteria. a: all flows; b: free turbulent flows; c: shear flows; d: homogeneous flows; e: geophysical stratified flows; f: reactors; g: chaotic advection.

2.2.2 Classification

To analyze the turbulent mixing criteria, it is better to classify them first.

2.2.2.1 Mixing rate (including above collected criteria from 1 to 8) The mixing rate is related to the dynamics of mixing. Some terms in the turbulent kinetic energy equation and transport equation of scalar correlation can be used here to describe the mixing rate. They are:

- a. Diffusion rate (2 ~ 6): This group describes transport property through a flux under a gradient.
- b. Dissipation rate (criterion 7): Dissipation of scalar is used as criterion.
- c. Fluctuation decay rate (criterion 8): Due to turbulent diffusion and dissipation, the fluctuation will be decayed. For homogeneous isotropic turbulent flow, the dissipation rate is equal to the decay rate.

2.2.2.2 Mixing state (including criteria from 9 to 15 and 1) Based on different scales (macro-, micro- and molecular scale) this type of criterion describes the homogeneous distribution of different scalar in a turbulent flow. It includes:

- d. Macromixing state (criteria 1 and 9): This group relates to the mixing state on macroscale in a turbulent flow, but with no details on turbulent and scalar structure.
- e. Molecular mixing state (criteria 10 ~ 15): These describe the mixing result on molecular scale.

2.2.2.3 Ratio of diffusion to convection or molecular mixing For a limited bulk convection time, i.e. fixed volume, the way in which scalar mixing in cross direction compares with bulk convection is also important for mixing control. Such a mixing is related to turbulent mixing because of velocity fluctuation.

f. Ratio of turbulent diffusion to bulk convection (criterion 18): As bulk convection is not a characteristic of turbulence, the influence of turbulence on mixing (due to turbulent diffusion) can be obtained from this criterion.

g. Turbulent Peclet Number Pe (criterion 19): There are as many different types of Pe as Reynolds number (Brodkey [12]). Here we mean the ratio of turbulent diffusion to molecular mixing.

All the above mentioned criteria can be used for a vector and its corresponding scalar.

2.2.3 Analysis

It seems that there is no a general criterion for turbulent mixing and only one criterion is not sufficient. Different criteria are used for different situations. Although visualization is a good method, it is, at present, more qualitative and not quantitative enough. (However Dahm *et al* [26] have successfully used high resolution four-dimensional measurements on fine scale structures. This provides a promising way in the future to combine visualization and quantitative measurement for both whole field and fine structures.)

Measurement just in one point is not sufficient, and neither is only within shear layer. Usually the measurement is conducted only within turbulent flow (for example in the mixing layer). In the study of engineering, the whole flow field is of interest. This criterion should be used on the whole flow field.

Entrainment is a large scale process. Large entrainment is the favorite process for mixing in the whole flow field, but it cannot provide details of small scale structures. Scalar scale under large entrainment at fixed position downstream is not absolutely smaller than that under small entrainment. If molecular mixing is of interest, entrainment is not enough for the turbulent mixing criterion.

Only the mixing rate from the large to small scale i.e., relative turbulent mixing, can be controlled, not molecular mixing itself. The molecular mixing is not directly, but indirectly related to flow characteristic. With the use of molecular mixing it is difficult to predict at what flows conditions, i.e., under which dominating scale is the scalar mixed. Only with some models the molecular mixing may show the flow condition under which molecular mixing is strong. If different Sc are used, the same mixing rate of the relative turbulent mixing will have a different molecular mixing. The turbulent

mixing can be described indirectly by molecular mixing, but not definitely if D_m is zero. The relative turbulent mixing is of fluid flow characteristic and general turbulent mixing both flow and species. So it is necessary to establish a turbulent mixing criterion to describe the relative turbulent mixing on the point of turbulence control. Final result of the relative turbulent mixing establishes a bridge between flow and molecular mixing. The relative turbulent mixing directly related to flow property and can be used to describe the mixing control mechanism more directly. None of the criteria considered above can be used to describe the relative turbulent mixing, i.e., no of them can establish a direct relation between turbulent flow and molecular mixing directly. Here we are concentrating on relative turbulent mixing.

The concept of mixing rate and mixing state are different. The rate is a dynamics process of mixing of two quantities. It expresses how fast a mixing process is. However, mixing state shows at what a degree they have be mixed, i.e., mixedness of mixing results. A larger mixing rate does not mean the unmixedness is small, and vice versa. It depends on the initial conditions. They are only related when the initial condition is the same, i.e., large rate results in large mixedness at the same spatial and temporal point. Therefore both the mixing rate and state should be used for a complete description in some cases.

2.3 Mechanism of mixing in a turbulent flow

The mechanism of turbulent mixing is very complicated. The vector mixing is already very difficult to understand, let alone the scalar mixing in turbulent flow. If a scalar molecular mixing is involved, the size of the smallest scalar scale, Obukhov and Corrsin scale (l_{OC}), Batchelor scale l_B is important for molecular mixing. The smallest scalar size l_B depends on the smallest vector scale, Kolmogorov scale l_K , which, in turn, depends on flow properties. On the one hand the smallest vector scale is a flow characteristic and on the other hand, the smallest scalar scale l_{OC} and l_B is also related to the physical properties of the quantity, e.g. Sc for scalar. Different flow has a different smallest vector scale and under the same flow, different Sc have different smallest scalar scales. Furthermore, the mixing dynamics also depends on the initial condition, e.g. initial scalar scale.

2.3.1 Scenario of mixing in turbulent flow

In chemical engineering, mixing is divided into three stages (Beck and Mueller [6]; Baldyga and Bourne [4] and Villiermaux [108]).

1. Macromixing: Distribution of one fluid through the other and uniformization of average composition without decreasing local concentration variance.
2. Micromixing: which consist of:
 - Large scale to small scale and
 - Molecular mixing at small scale.

In turbulence group, Fiedler [36] observed, that a mixing layer entrains the two streams at first stage just on the large scales, then the large scales break down into small scales, and the scalar (temperature) distribution in the large vortices in transverse direction is almost constant, and there is still no molecular mixing. This is a new observation, which is contrary to the traditional understanding of the gradient transport model for such a flow. Similar result is also observed by Konrad [61], who found that with further downstream (i.e. increase of Re), the molecular mixing increases rapidly in the whole transverse direction, which he named as mixing transition. Such a new concept of mixing transition is thought as a new contribution for mixing mechanism [91] and [10].

2.3.2 Three characteristics of turbulent mixing

Corresponding to the scenario of turbulent mixing, there are three characteristics for turbulent mixing.

1. Macro-dispersion (Entrainment): Macro-dispersion means one quantity disperses into the other on large scale (entrainment from jet and mixing layer can also be regarded as dispersion). Vortex diffusion resulted from large scale fluctuation is the reason for the macroscale dispersion. This process make the fluids in large space homogeneous, i.e. macromixing.
2. Micro-dispersion and more small scales: Micro-dispersion means that in turbulent flows the original two large scalar scales disperse each other on microscale (i.e. small scale). In this process the molecular mixing resulting from molecular diffusion becomes greater and greater, but still does not dominate. Because of the fluctuation of velocity, the material line and surface will be stretched, and the large vortices lose their stability and more and more small scales emerge through relative turbulent mixing. This results in the microscale dispersion. As the results of this process there is a large interface between the two quantities with the initial gradient at the interface between them in the whole field.
3. Large molecular mixing: After (2), if $D_m > 0$, the large interface and gradient will increase the molecular mixing rapidly between the two quantities and result in a transition process for molecular mixing. This is why molecular mixing is stronger in turbulence than in laminar. The molecular mixing (or diffusion) will obliterate the interface and gradient. The process happens in turbulent flows with and without average velocity gradient.

2.3.3 Scale sizes

The largest scale for vector and scalar is the scale of geometry considered. For vector, the smallest scale is the order of Kolmogorov scale $l_K = (\nu^3/\epsilon)^{1/4}$. The smallest scalar scales are Obukhov and Corrsin scale (l_{OC}) and Batchelor scale depending on Sc . These can be divided into three situations:

1. $Sc \ll 1$: The smallest scalar scale is approximately $l_{OC} = (D_m^3/\epsilon)^{1/4}$ ($l_{OC} \gg l_K$).
2. $Sc \sim 1$: The smallest scalar scale is around the scale l_{OC} ($l_{OC} \sim l_K$).
3. $Sc \gg 1$: The smallest scalar scale is about $l_B = (D_m^2\nu/\epsilon)^{1/4}$ ($l_B \ll l_K$).

Scales larger than l_K can be controlled by turbulence control, but scale smaller than Kolmogorov scale are controlled by viscous-convection and viscous-diffusion, not turbulence.

2.3.4 Geometry of small scale

The geometry of small structures is still not quite clear. There are three possibilities: slab, tube and sphere. Townsend [105] showed that the small structure of a vector is sheet-like and line-like in his experiment; Kuo and Corrsin [63] conclude that fine structures are more like to be line-like than sheet-like or sphere-like. Dahm *et al* [26] found in their experiment that the small scalar structure for high Sc is slab. Sphere is better for molecular mixing since the interface is larger than with the other two. It is still unclear if such small scale structures can be controlled.

2.3.5 Timescales of two processes

According to the above mentioned turbulent mixing mechanism, that there are two important processes for turbulent mixing: (1) The initial large scale vortices in turbulent flow become small scales due to their instability creating small scale scalar out of initial large scale scalar. The smallest scalar scale is dependent on Sc . (2) The molecular mixing dominates at the small scale.

2.3.5.1 Large to small scale In Broadwell & Breidenthal model [10], it is estimated according to Kolmogorov cascade theory at high Re , that the time needed for molecular mixing at initial scale L_i is almost infinite compared with the time turbulence takes to reduce large scales L_i to small ones l_s . Initially molecular mixing can be negligible since the interface is too small. With the reduction

of scale, molecular mixing becomes more and more important. Near l_s molecular mixing dominates. The molecular mixing time t_s at l_s is then very small. If small scale l_s is l_k , the time needed to reduce initial large scale to small scale l_k is

$$T_K = k_1 L / \Delta U \quad (2.1)$$

for $Re \gg 1$, where k_1 is a constant.

2.3.5.2 Molecular mixing of small scale According to Broadwell and Breidenthal model, the time needed for molecular mixing at scalar size l_K is approximately [10]

$$t_K \sim \frac{l_K^2}{D_m} \sim \frac{L}{\Delta U} \frac{Sc}{Re^{1/2}} \sim t_K \frac{Sc}{Re^{1/2}} \quad (2.2)$$

In Broadwell and Breidenthal model, the time T_K needed from large to small scale is much larger than t_K , which is needed for molecular mixing of small scale l_K , and t_K given in eqn (2.2) is a upper limit for the time required for the fluids to reach homogeneity for $Sc > 1$ when Re is high enough, i.e. $t_K > t_B$. (here t_B means the time needed for molecular mixing at scale of l_B) The time t_K is negligent compared with T_K .

2.3.5.3 New mechanism for turbulent mixing According to the Broadwell and Breidenthal model, $T_K \gg t_K$. However, the new experimental result (see later in this work) shows us that, under special management, when a flow with a given initial Re number, is specially controlled, e.g. through periodical forcing, the developing length or time the flow takes to reach l_K from L_i , i.e. T_K , can indeed be much reduced compared with its corresponding unforced one, so that T_K could be in the same order of t_K ; Furthermore, the flow properties of statistical structures with a large initial Re , can be obtained in a flow with a small initial Re under specific forcing (see later experiment result in this work).

2.4 Ideal relative turbulent mixing process and state

To give a criterion, it is helpful to propose a "standard process" for comparison. For instance, in thermodynamics, there is a Carnot cycle as an ideal cycle and we can compare a practical process with the ideal cycle to estimate the goodness of the process. A question is if there is an ideal relative turbulent mixing process? If there is, what is an ideal relative turbulent mixing process? What is the relationship between the ideal relative turbulent mixing process and a more general turbulent mixing criterion? These questions are needed to be answered before a new and more general turbulent mixing criterion can be established. Turbulent mixing criteria should involve the turbulence property for a given Schmidt number. Different flow has different small scale structures. The small scale of turbulent flow is the important parameter for molecular mixing. The ideal relative turbulent mixing process should be related to the small scale structure of a turbulent flow.

Let us consider the case of a given initial Re number. Fig. 2.1 shows the turbulent mixing process. The initial two scalar A and B at scale of L_i will be molecularly mixed. Suppose there is a small scale l_s , which is controllable, and under which the molecular mixing will dominate and be finished within time t_m . From the initial scale, they are mixed initially into large scale within time T_1 . Through the large vortices, the large scalar scale breaks down into meso scale in time T_2 . Within time T_3 , the scalar becomes small scale l_s . The time that turbulence takes to decrease L_i into l_s homogeneously in the whole flow field is T_s . The smaller l_s , the smaller t_m . The smallest l_s is fixed for the given Re and Sc . What turbulence can do is to achieve l_s from L_i in time scale of Eq. (2.2) and length scale of

$$l_K = k_a L / Re^{-3/4} \quad (2.3)$$

as l_s is related to the Kolmogorov scale l_K as mentioned above. Where k_a is a constant.

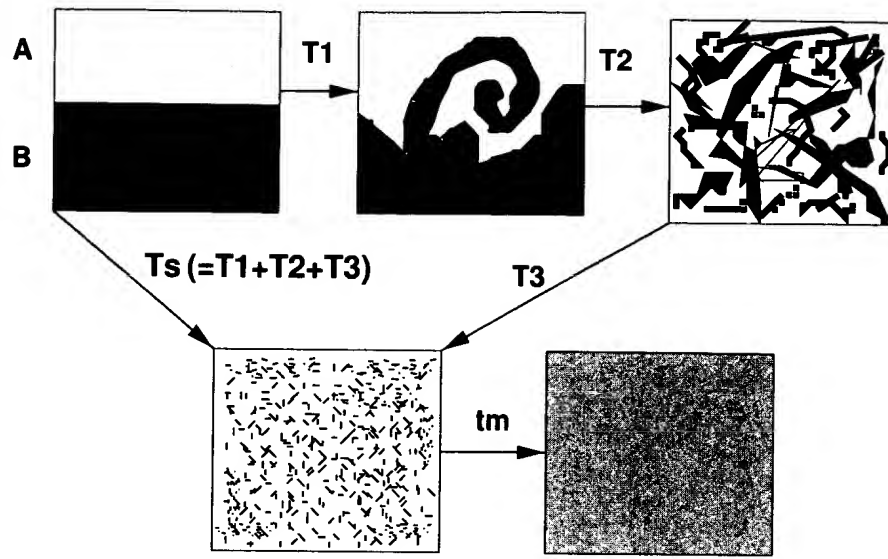


Figure 2.1: A simple sketch of turbulent mixing process.

The relative turbulent mixing (from L_i to l_s) and molecular mixing progress simultaneously. At the initial large scale, the molecular mixing is negligible. With the development of turbulent mixing, molecular mixing becomes more and more important. At small scale l_s , the molecular mixing dominates. The molecular mixing can be approximately described by an one dimensional diffusion equation at small scale of a slab.

$$\frac{\partial c}{\partial t} = D_m \frac{\partial c}{\partial X} \quad (2.4)$$

with initial condition approximately

$$c = c_0, \quad -h < x < +h \quad (2.5)$$

where h is the character length, i.e., here $l_s/4$. Its solution is according to Crank [24]

$$c = \frac{1}{2} c_0 \left(\operatorname{erf} \frac{h-x}{2\sqrt{D_m t}} + \operatorname{erf} \frac{h+x}{2\sqrt{D_m t}} \right) \quad (2.6)$$

where x is the coordinate normal to the interface and erf is the error function. The time for molecular mixing depends on small scale size h and D_m .

As we know from Broadwell and Breidenthal model, traditionally $T_s \gg t_m$. If, however, we could find a bypass process, where turbulent mixing (i.e. from L_i to l_s) in the local whole flow field is so fast, that $T_s \leq t_m$, such a process is called ideal relative turbulent mixing process. This means that, before molecular mixing dominates at scale l_s , the scalar is already on the local whole field distributed homogeneously at scale of l_s through turbulence. In ideal relative turbulent mixing process, turbulence has done its best for mixing within t_m and the whole mixing rate is not controlled by turbulent mixing.

Batchelor [5] pointed out that, turbulent mixing increased the interface and the gradient of the scalar. At the local point far away from the initial interface the gradient is indeed at the beginning zero. However, it is thought here that turbulence globally keeps the initial large gradient from diffusion region at the interface and only increases the interface for the molecular mixing in the initial period. So we have only one parameter, i.e., the interface surface per volume.

l_s depends on Sc and chemical reaction kinetics if there is a reaction. The higher Sc is, the smaller l_s , and thus the more difficult to reach such a ideal process. The higher the chemical reaction kinetics rate is, the smaller t_m , and the larger l_s .

- $Sc \leq 1$: $l_s = l_{OC}$,
- $Sc \gg 1$: $l_s = l_B$.

The range from l_K to l_B is related to strain rate at scale l_K , i.e., viscid-convection region, which may be difficult to control, since the process is stochastic. Generally we have $l_K \geq l_s \geq l_B$ if $Sc \gg 1$.

The flow corresponding to the ideal turbulent mixing state should be approximately isotropic. The result of the ideal relative turbulent mixing process is an ideal relative turbulent mixing state, under which the small scale is homogeneously distributed in space with one another (dissipation intermittency is not considered here for simplification) and the molecular mixing is not finished. The unmixedness is still not small and the power spectrum density corresponding to scale of l_s is not negligible. The statistical property of scalar is almost homogeneously distributed on the surface perpendicular to bulk convection direction at the local position. All these results are more apparent for $Sc \gg 1$ than $Sc \leq 1$. After the ideal relative turbulent mixing state, the above mentioned parameters (i.e. the unmixedness, power spectrum of small wave length) will reduced dramatically.

The ideal relative turbulent mixing process is quite different from Broadwell and Breidenthal model, since in Broadwell and Breidenthal model $T_s \gg t_m$, but in ideal relative turbulent mixing process $T_s \leq t_m$. Therefore the ideal relative turbulent mixing process is a very harsh condition. In practice it is very difficulty to realize such a process. The ideal relative turbulent mixing process shows us the highest rate which turbulence can reach to enhance molecular mixing, and how far away an actual process is from the ideal relative turbulent mixing process and how much potential is left for mixing control through turbulence control.

The ideal relative turbulent mixing process is a relative one, not an absolute one, since the L_i depends on the initial flow condition and l_s depends on Sc . The smaller L_i is, the closer the process is to the ideal relative turbulent mixing process. It is a question of flow management. But once L_i is determined (i.e. geometry), and when initial Re is also fixed, the difference between a practical process and the ideal relative turbulent mixing process is dependent on flow and flow control. t_m could be related to a required time scale, i.e. it is *ad hoc*. For example in the case of a very fast reaction, t_m should be as small as possible to match reaction time scale. However, for middle rate reaction, t_m could be larger.

For a jet and mixing layer, since there is always a new large scale entrainment, multi-lump model is needed to revise the above mentioned ideal relative turbulent mixing process, v.z., the local entrained fluids will mix with their last shear layer fluids composition.

For engineering, the requirement of the *whole* flow field is important concerning the compact, e.g. in aircraft. In such an ideal process, the relative turbulent mixing will have transformed the scalar from large to small scale within t_m .

It should be clear that even though we are concerned with molecular mixing, the turbulent mixing criterion concentrates on flow characteristic. It is not contradicted, due to the fact that the result of ideal relative turbulent mixing process is the condition, where molecular mixing dominates. The molecular mixing can measured through chemical reaction, but the measurement resolution is not the molecular mixing scale. The measurement scale for reaction result is still limited by the spatial resolution of sensor. The concept of the relative turbulent mixing, ideal relative turbulent mixing process and state can be used not only for molecular mixing in dissolvable single phase fluids, but also for indissoluble fluids and multiphase flows.

2.5 New criteria for turbulent mixing

Turbulent mixing criteria should provide some certain quantities (or parameters) for the quantitative description of turbulent mixing. Danckwerts [28] has given four requirements for mixing criterion in practice. Here, a fifth should be added: turbulent mixing criteria should be able to help for the turbulent mixing control.

The new criteria are related to the relative turbulent mixing and ideal relative turbulent mixing process. It is better to use more than just one criterion to describe turbulent mixing because of both,

its physical complexity and its stochastic property. From the reviewed criteria, it is found that there is no criterion to describe the microscale mixing rate and state which provides information on small scale structures distribution as a result of the relative turbulent mixing. The new criteria concentrate on the small scale (or microscale) property.

2.5.1 Mixing rate

Due to the fact that ideal relative turbulent mixing process is related to the initial scale, the spatial and time scale used for mixing rate should be dimensionless and scaled with initial length L_i for physical length scale and large scale convection time L_i/U for time. Then the mixing rate r_m can be described as

$$r_m = ((L_i - l_s)/L_i)/(T_s/(L_i/U)). \quad (2.7)$$

The mixing rate r_{im} of ideal relative turbulent mixing process is

$$r_{im} = [((L_i - l_s)/L_i)/(t_m/(L_i/U))]_i. \quad (2.8)$$

The relative turbulent mixing rate

$$R_r = r_m/r_{im} = t_m/T_s. \quad (2.9)$$

One should be careful in using R_r because l_s is not absolutely the same for different flows. However for a given initial condition, R_r strongly depends on the control of the flow. If $R_r = 1$, turbulence has done its best for molecular mixing through ideal relative turbulent mixing process. The relative mixing rate R_r is relatively a general turbulent mixing criterion and gives a relatively clear limit for turbulent mixing regardless of whether fluids are mutually soluble.

2.5.2 Mixing state

2.5.2.1 Zero crossing point number of gradient (G_z) When the scalar is not molecular mixed for a given scale, there is a zero crossing point of concentration gradient along a spatial direction [44]. At the ideal relative turbulent mixing state, the zero crossing point number G_z gets its maximum value per unit length. If a image measurement has a sufficient high spatial resolution, the number of zero crossing per length G_z in any direction perpendicular to bulk convection direction should have a maximum value at the ideal relative turbulent mixing state. For temporal point measurement with a high enough resolution (both spatial and temporal) and signal to noise ratio, a maximum value of G_z can be obtained by calculating G_z of the concentration time trace gradient per unit time, i.e. G_z of dc/dt . This value should relate to l_s .

2.5.2.2 Power spectrum density (psd) At the beginning, there is no small scale scalar, so the psd has no contribution from high frequency. With the proceeding of turbulent mixing, more and more small scales will emerge and for high enough Re , there will be a -5/3 exponent for psd of concentration (c) because of its corresponding -5/3 exponent of psd of velocity spectrum. If $Sc \gg 1$, there could also be a -1 exponent after -5/3. If there is such a -5/3 or -1 exponent for psd of c , it indicates that the corresponding small scale in physical space is achieved. If there is no such a -5/3 at all during the proceeding of turbulent mixing, the relative turbulent mixing can not be good even though the Re may be small (see result later).

At the ideal relative turbulent mixing state, there could be a frequency, higher than which the power spectrum density reduces its exponent rapidly from either -5/3 or -1. This frequency should correspond to l_s and can also be used to estimate l_s . After the state, the exponent will be smaller than -5/3 around this frequency and pad decrease very fast around this high frequency region.

2.5.2.3 Probability density function (pdf) For a given $Sc > 0$, pdf and intensity of segregation can also be used for easiness. At the ideal relative turbulent mixing state, the pdf of C still has its contribution from unmixed fluid if the spatial resolution is high enough, and after the state, the pdf decreases very fast to almost zero from unmixed fluids. The pdf of \bar{C} increases then very fast.

2.5.2.4 Intensity of segregation Although molecular mixing is not turbulence property, for a given $Sc > 0$, molecular mixing can indirectly exhibit the characteristic of turbulent mixing. At the beginning, the intensity of segregation is zero, but increases very fast as turbulent mixing progresses. Then decreases very fast near the ideal relative turbulent mixing state.

3 Experimental set-up and measurement procedures

In order to achieve a strong mixing (which helps to reach the ideal state), a steady state (which makes the measurement and later analysis easier) and no further large scale entrainment (which makes the model flow simple), a confined plane wake and mixing layer in a pipe is used for this study.

3.1 Water channel

The experimental configuration is shown in Fig. 3.1. Two vessels 300 liter volume, 2.5 m higher than test section supply water and water solution (dye) to the water channel respectively. The water level changes little during 40 s run so that the fluid velocity is almost constant. One vessel is filled with water, and the other with the molecular mixed disodium fluorescein water solution. Rotameters are used to control and measure the velocity of the fluids, which are filled into the settling chamber from the side of the wall respectively. The settling chamber upstream of the nozzle is 400 mm long, and has one honeycomb and two sieves. The Nozzle contraction ratio is 10:1, and 100 mm long. The nozzle is designed in the light of Börger's theory [8]. In the axial-symmetrical center of settling chamber and nozzle there is a splitter plate, which has a uniform thickness of 5 mm in the settling chamber and a sharp trailing edge at the end in the nozzle. A Plexiglas pipe of 42 mm inner diameter, 4 mm thick is connected with the nozzle. The pipe is totally 2.1 m long. At 1 m x-position downstream, there is a cube. In the middle of the cube a mirror is placed for visualization. The cross section of the cube is large enough so that the block of the mirror has no influence on the flow in the test section.

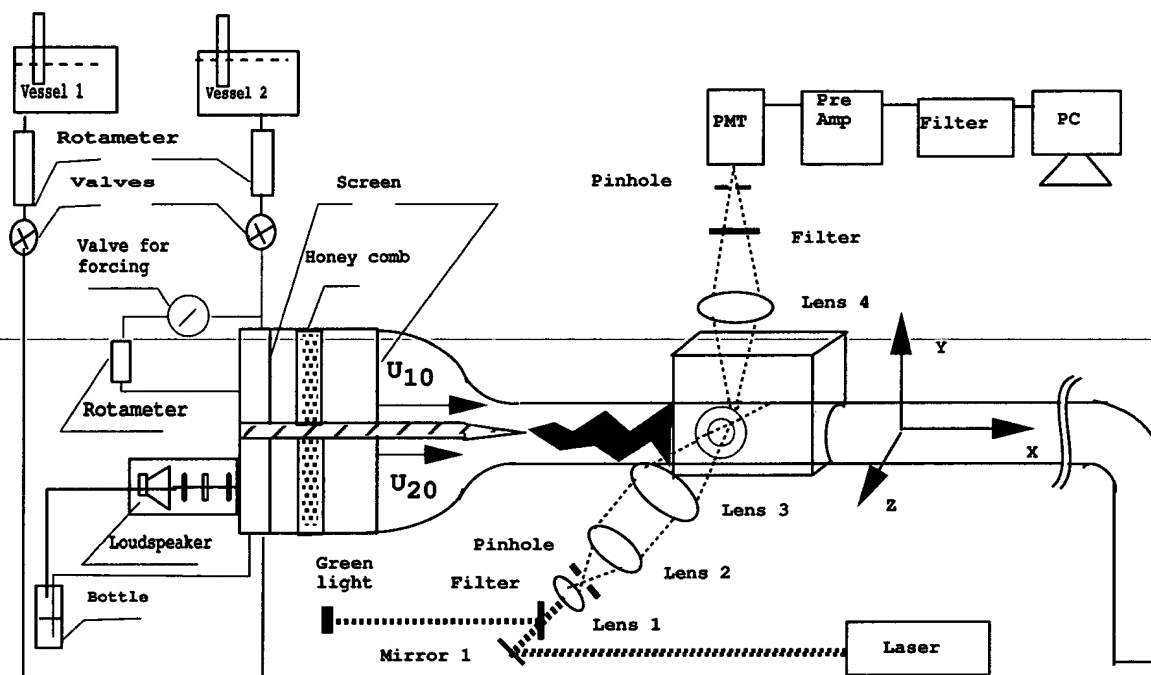


Figure 3.1: Experimental schematic.

At the measuring position there is a rectangular water vessel with a window made of quartz glass (for high optical quality), which is used to prevent refractive distortions from air to the circular Plexiglas pipe and water. Since the optical quality of the thick Plexiglas wall of the pipe is rather poor and its refracting index is not exactly the same as that of the water, there is a window at the measurement point of the pipe which is replaced by a plastic sheet of the kind used for overhead projectors with thickness 0.17 mm. The transparency is sealed by Sikaflex-260. This enables better focusing of the laser beam.

3.2 Forcing methods

Two different methods are used for forcing.

3.2.1 Loudspeaker

Near the input of the settling chamber, there is a loudspeaker in the axial-direction on the low velocity side which is used as the actuator. The speaker excites the flow through the connection with a plastic membrane, which in turn connects directly with water. Due to high pressure of the water, the membrane is under too much pressure, so that it cannot be forced to move by the speaker. For this reason, a sealed flash is used and the speaker is also sealed. There is some water in the flash. The water in the flash is connected with the fluid in the settling chamber through a tube and the air in the flash is connected with the loudspeaker. If the pressure in the settling chamber is increased, the pressure in the flash will rise. This also results in an increase in the pressure on the speaker side of the membrane, so that the membrane can keep in equilibrium and oscillate. A condensator is constructed between the speaker and membrane to measure the amplitude of the membrane. The condensator is connected to a frequency bridge, which is connected to an oscilloscope. The relationship between the amplitude of the speaker and the signal from the frequency bridge can first be calibrated (it is linearly related). Through this construction the amplitude of the speaker can be controlled. The signal generator used for loudspeaker is HP 33120A. The forcing signal is sinusoid. A DFVLR power amplifier is used to amplify the signal for the loudspeaker.

3.2.2 Valve

The loudspeaker cannot be used for higher Reynolds numbers, therefore another forcing method is used. The high speed fluid is first divided into two parts, and each is followed by a rotameter. One of them has a valve, which can be rotated by a motor. The rotation of the valve results in a periodic blocking of the fluid, and thus a periodic velocity. The forcing frequency can be controlled through the speed of the motor and the amplitude through the flow volume of the two streams. The frequency of this method is not as accurate as the first one.

3.3 Optics

In order to understand the mechanism of turbulent mixing and to prove the above mentioned model of ideal relative turbulent mixing process experimentally, it is necessary to measure the scalar distribution at scales as small as possible. The smallest scale of scalar can be very fine, say, of the order of $0.1 \sim 10 \mu m$ in water flows depending on the flow itself and the physical properties of the fluid, i.e. Schmidt number (Sc). If the spatial resolution is not high enough (i.e. the measuring volume is larger than the smallest scalar scales in the flow), some physical details will be lost and this in turn obstructs the understanding of the physical process of turbulent mixing. Laser Induced Fluorescence (LIF) is used for the measurement. The optics should be optimized both for fine focusing and maximum signal collection to the photomultiplier tube (PMT).

3.3.1 Optics for focusing laser beam

In order to get high spatial resolution for fine scalar scale, the laser beam must be extremely fine focused. For this purpose, a complex optical system is constructed. At the output of the laser beam, an optical filter is used to obtain only blue light, since the laser output consists of green and blue light. The green light is directed to an optical fiber for visualization. Behind the optical filter, there is a spatial filter consisting of a lens 1.5/10 and a pinhole of $30 \mu m$. After that a beam expander consisting of the spatial filter and a tele-objective is used. The expanded beam is about 55 mm in diameter. After that, an objective 1.4/150 (Astro-Berlin, No. 26862.) is used to focus the beam in the pipe through the thin plastic windows described above. The focus waist is measured to be about $4 \mu m$.

3.3.2 Optics for photomultiplier tube (PMT)

Perpendicular to the laser beam, an objective 1.4/50 (Nikon) is used to image the focus point onto the photomultiplier tube (PMT). The diameter and numerical aperture of the objective should be large, and the objective should be as close as possible to the focus point, so that more emitted light from the fluorescence can be collected, and thus the signal to noise ratio (SNR) increases. The high modulation transfer function (MTF) of the lens is also needed for the fine focusing measurement. Before the PMT cathode, a pinhole of 10 μm is mounted to ensure that no more than 4 μm of the beam waist will be seen by the photocathode of the PMT when the image distance is 2.75 times larger than the object distance. Such an arrangement can also reduce the deviation of the signal if the focus point is not perfectly imaged into the pinhole during measurement. Thus at the measuring point the spatial resolution is about 4 (μm)³. The pinhole must be as close as possible to the cathode, otherwise because of the small aperture, diffraction behind the pinhole can occur, and some light after the pinhole can be lost. Just before the pinhole, an optical filter 540FD66-50SX from Oriel is used to permit only the light between 500 nm and 600 nm to pass, which is the most of the fluorescence light, and filter out other "noise" light (including possibly UV noise), especially the blue light which is emitted by the particles in the water. The pinhole and filter for the PMT are fixed to the PMT. A three dimensional positioning system is used to adjust PMT until maximum output from PMT is reached. This ensures that the focusing point is best imaged into the pinhole.

3.3.3 How to determine the focused diameter

According to Ready [88] the waist of a focused laser beam can theoretically be calculated by

$$d_f = 2.44 * \lambda_w * F / D_l \quad (3.1)$$

where d_f is the waist diameter of the focused beam; λ_w is the wave length of light; F is the focus length of the lens and D_l is the diameter of the aperture. In reality, however, this theoretical result is scarcely achieved because of imperfect quality of optical parts and optical assemblies, especially for very fine focus diameter, i.e. near the diffraction limit. For instance, it is found that too large a beam diameter is not always good for fine focusing due to the phase difference of imperfect lenses, although theoretically the larger the diameter is the smaller the focused diameter should be. Therefore, for fine focusing, it is necessary to measure the focused diameter in order to determine its real focused diameter. Four methods have been applied here.

1) Thin wire scanning ¹: The wire must be much smaller than the focused diameter. The wire is controlled to move across the focus point of the laser beam at different laser axial positions. When the wire moves inside the laser beam, it reflects light. An optical detector can be used to register the signal. When the wire goes across the focus beam, a Gaussian light intensity distribution is obtained. The width is defined between the points of 16% of maximum beam intensity [33]. With the change of axial positions, a number of such curves can be obtained, from which the narrowest width is determined.

2) diffraction: This is a Fourier optical image. When the wire arrives at the edge of the beam, there will be a dark circular area on a screen which is placed behind the focus point. When the wire reaches the center of the focus point, there are three dark areas on the paper. With the further movement of the wire to the other edge of the beam, there is again only one dark area but on the other side. Before and after the focus point these pictures are symmetric and larger. At the waist, the picture is the smallest.

3) Pinhole: The light power at the focus point is measured with a photodiode first without a Pinhole. Then, a pinhole is placed just at the focus point and the photodiode is fixed just behind the pinhole. When the light power is reduced to about 84%, the pinhole diameter is approximately equal to the focus diameter.

4) Image + microscope: Use a lens to image the focus point in the water channel to some point outside. A microscope is then used to measure the smallest beam diameter.

¹This method is recommended by Dr. Lehmann from DLR.

3.4 Measurement Processing

3.4.0.0.1 Laser: The laser is a Coherent Inova 90 with a power of 5 Watt. The laser light is composed of blue (488 nm) and green (514 nm) light and is adjusted to TEM₀₀ mode. Since the fluorescence emission spectrum is strong at 514 nm, and thus the scattered laser light (514 nm) from the particles in water can cause noise, only the blue color light is used as exciting light and an optical filter is placed at the output of the laser, which only passes the blue light. Fluorescein disodium is used here as dye and its Schmidt number is about 2000 [17].

3.4.0.0.2 Light detector: In this experiment, the maximum input light power is estimated from measurement to be in the order of $10^{-10}W$. To achieve a frequency bandwidth of 100 kHz, which is the order of frequency of very small scales, i.e. in the range of Batchelor spectrum, it is impossible to use a photodiode as the light detector because of the very small level of the signal, and a photomultiplier tube (PMT) is therefore used. To reduce dark noise to a negligible level, a PMT R6060-2 with peltier and heat sink from Hamamatsu is used here under cooled condition.

3.4.0.0.3 Amplifier: The output current from the PMT is very small and must be amplified by a current amplifier to match the analog to digital convert (ADC) input range and get the best resolution. The Re number is in the range of 400 ~ 33000 based on pipe diameter and average velocity. The corresponding frequency of the smallest scale is around 100 kHz. The maximum frequency we can measure from ADC is 125 kHz. To make sure that no extra noise comes from the amplifier, a low noise current transimpedance amplifier with transimpedance (gain) of $2.5 \times 10^6 V/A$ and frequency bandwidth of 280 kHz was constructed by the author. To receive instantaneous signal 100 kHz without 3dB loss of its amplitude, the bandwidth of the amplifier should be about 280 kHz according to our test. The noise current from the amplifier is only about $100 fA/Hz^{1/2}$ (it was measured by FEMTO Messtechnik GmbH). Fig. 3.2 shows the diagram of the amplifier. The amplifier consists of two operational amplifiers in series. The first one is inverse amplified through JFET of LF657 because of its low input noise current and the second one is non-inverse with OP37 because of its low input noise voltage. The feedback resistance is high enough so that the Johnson noise is much smaller than dark noise. The dark noise and Johnson noise from the amplifier and the PMT can be negligible (see later).

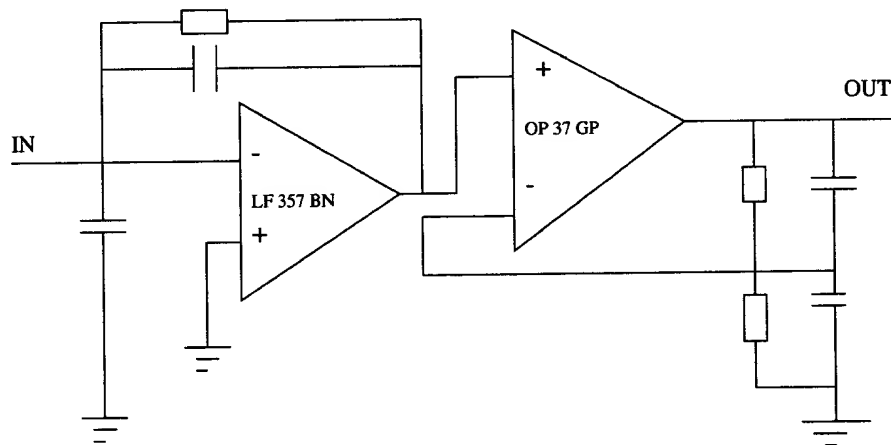


Figure 3.2: A simple sketch of low noise current amplifier.

3.4.0.0.4 Filter: The noise coming from the PMT has a very wide frequency bandwidth, especially for frequencies higher than 100 kHz. The maximum frequency which can be measured in this system is 125 kHz, therefore a low pass analog filter is needed. Low pass analog filter is used for two reasons: eliminating the high frequency noise from the PMT and being anti-alias for the ADC.

To get real time trace signal, it is expected that the filter should have small phase distortion and high attenuation rate (rolloff). For this aim, two 4th-order analog low pass Bessel Filters EWR-3-4-BE-T/S from MessTeam are used in series to obtain a 8th-order filter. The cutoff frequency range is from 10 Hz to 999 kHz. With the low pass filter the signal to noise ratio is considerably improved.

3.4.0.0.5 ADC: The analog to digital converter (ADC) DT2821-G-16SE by Data Translation is used here. It has 12 bits resolution and its maximum sampling rate is 256 kHz. The data are directly saved on a hard drive. The sampling program from Data Translation was changed to enable data storage continuously at 256 kHz rate for more than 40 s. The computer used for sampling is a Pentium 90. The sampling rate was changed with Reynolds number.

HP 3562A Dynamic Signal Analyzer is used due to its low noise characteristics. A multimeter Model 2000 from Keithley is also used to read the signal.

4 Laser Induced Fluorescence (LIF)

4.1 Thermal blooming

According to Beer's law, the laser light will attenuate along the dye medium because of absorption. Energy conservation implies that the absorbed energy will be partially converted to emitted light and partially to heat due to the quantum yield of fluorescence and photobleaching (for instance increasing molecular collisional quenching without radiation). Too high laser intensity I_l can result in more heat absorption and temperature increase at the measuring volume when concentration C is not very small. This can result in the change of fluid density and consequently a refraction gradient there, i.e. thermal blooming [62]. If the fluid flow velocity is too small, thermal blooming could have an influence on experimental result. The effects of thermal blooming are very complicated by more than one fact: the index of the refraction gradient can act as a lens, so that the focus diameter would become larger and thus the spatial resolution become lower; the focus length would also change and become shorter, and thus result in a low signal (For the detailed influence of refraction gradient due to temperature difference on focus length the reader is referred to the work [53]); the high temperature could result in stronger excited molecular collision without light emission and thus also lead to signal reduction. The fluorescence intensity decrease with temperature is given for example in [46] and [109]. With increasing I_l and C , the thermal blooming effect also increases. If the fluid is in motion with high enough velocity, the heat can be advected from the measuring volume and thus the thermal blooming may become negligible. If, however, the velocity is not high enough, the thermal blooming could contaminate the measuring results.

4.2 Photobleaching

The term photobleaching is used to describe the phenomenon that the emission light intensity of a molecule decays with time, due to photodecomposition or collisional quenching etc. If the exciting laser intensity is high enough for LIF, photobleaching occurs.

4.2.1 A model of the photobleaching effect

Although according to [93] photobleaching can contaminate experimental results, no description is given about how photobleaching influences the measurement. (Usually the concern, especially in optics research, is that the emitted light intensity becomes smaller).

The lifetime of fluorescence is very short, about $10^{-8} \sim 10^{-9}$ s. This indicates that fluorescence rise time is fast enough for fluid mechanical application. Since here the dye is continuously pumped, the photobleaching decay time constant τ is larger than the lifetime. However the decay time constant decreases with exciting laser intensity I_l and dye concentration C in water solution. For a given τ , the fluorescence intensity decays with time.

A simple model to describe the influence of photobleaching on measurement results is proposed as follows. First, let us consider the relation between I_f and fluid velocity u . As we know, the decay of fluorescence can be approximately described by an exponential decay law [62]

$$I_f = I_{f0} * e^{-t/\tau} \quad (4.1)$$

Here τ is the decay time constant and t is the decay time. The decay time can be replaced by the dye residence time in the measuring volume, i.e.

$$t = d_f/u \quad (4.2)$$

where u is the fluid velocity and d_f is the laser focus diameter. Then

$$I_f = I_{f0} * e^{-d_f/(u\tau)} \quad (4.3)$$

I_{f0} is the fluorescence intensity approximately at its lifetime. Eqn (4.3) means that, if $d_f/u \ll \tau$, photobleaching can be negligible. The smaller τ is, the stronger photobleaching becomes, and the smaller u is, the larger t is and thus the smaller I_f . If photobleaching is strong, I_f would not only depend on concentration but also on velocity although the laser power keeps constant.

Second let us consider the effect of photobleaching on I_f through the deviation of velocity. Suppose there is a velocity deviation δu and its corresponding δt , From eqn (4.2), we have

$$|\delta t/(\delta u/u)| = d_f/u \quad (4.4)$$

The term $\delta t/(\delta u/u)$ represents the resulting time deviation due to a given relative velocity deviation. We define it as the time to relative velocity deviation ratio. Eqn (4.4) indicates that the time to relative velocity deviation ratio decreases with velocity for a given d_f . If $\delta t \ll \tau$, the deviation of I_f (indicated here as δI_f), resulting from relative velocity deviation due to photobleaching is negligible. However, if $\delta t \sim \tau$, δI_f would become large enough to contaminate the measurement results because of the deviation of u , which is what often happens in turbulent flows and what emerges when velocity effect is investigated. For a given τ , the smaller δt , the less the influence of photobleaching through the deviation of velocity is. From eqn (4.4), it is obvious that for a given $\delta u/u$, higher u results in smaller δt . Therefore, three conclusions can be obtained:

1. Photobleaching influences I_f through the deviation of velocity.
2. For a given δt , i.e. a given flow situation, the lower τ , the stronger the influence of photobleaching on I_f through the deviation of velocity will be.
3. The influence of photobleaching on I_f decreases with increasing u .

In fluid mechanics photobleaching for LIF was cited by [62], but the bleaching decay time constant was 20 s in the experimental condition reported there. This time scale is much larger than the residual time of fluid in the measuring volume for fluid mechanics research, so that photobleaching influence can be negligible. However for high spatial resolution measurement, the situation can be quite different. Since the laser intensity I_l increases very rapidly with the reduction of laser beam diameter, i.e. $I_l \sim 1/d_f^2$, and if the beam is focused to a very small diameter, the I_l will be very high. When I_l is very high and the concentration is not small, photobleaching will be strong and the decay time constant could be of the same order of fluid residence time in the measuring volume as in the situation here.

Shortly after it was found that photobleaching was very important in the measurement [117], we found that Saylor [93] warned that, when the laser was very fine focused (33 μm) in his experiment) with 1 Watt or greater laser power level, one should take measures to prevent contamination of the data due to photobleaching.

4.2.2 The principle for measuring bleaching constant τ

The time constant τ for photobleaching depends on experimental conditions, physical and chemical dye properties, dye concentration, laser intensity and so on.

In [93] the measurement of photobleaching is undertaken with motionless fluid. Actually this is not a correct method. As we know, the thermal blooming could also have influence on the measured I_f if the fluid velocity is sufficient slow. When fluid is at rest, the measured I_f would be smaller because of both thermal blooming and photobleaching. It is difficult to separate them when the fluid is motionless. Therefore the measurement of photobleaching should be undertaken under the prerequisite that the fluid velocity is high enough. If u is not zero but very small so that the thermal blooming has influence on I_f , the measured I_f would be smaller than in the case with only photobleaching effect. If we know laser focus diameter and fluid velocity, we can calculate the residence time of the fluid in the measuring volume (for very small focus, i.e. near the diffraction limit, d_f should be determined through measurement). With many measured I_f for different u , the averaged τ can be estimated

from equation (4.3) through least-square method. If the velocity is higher, the residence time will be shorter and therefore the signal is higher.

This method of measuring photobleaching introduced here is not only useful for fluid mechanics, but also for other cases where the thermal effect has an influence and cooling is not easy to achieve.

4.3 Analysis of signal to noise ratio (SNR)

For the PMT there are three major noise sources in the photocathode. These are dark noise, Johnson noise and shot noise in the signal. Their root mean square values are [18] for

$$I_{drms} = (2ei_d\Delta f)^{1/2}, \quad (4.5)$$

Johnson noise

$$I_{jrms} = (4kT\Delta f/R)^{1/2}, \quad (4.6)$$

shot noise in the signal

$$I_{srms} = (2ei_f\Delta f)^{1/2}. \quad (4.7)$$

Here e is the charge of the electron and Δf is the frequency bandwidth, I_d and I_f denote dark and fluorescence signal current, k is the Boltzmann constant and T the temperature. In practice, the experimental result depends on the SNR. The SNR corresponding to the shot noise in the signal is

$$SNR = (i_f/(2\Delta f))^{1/2}. \quad (4.8)$$

At sufficiently low I_l and C , it is known that fluorescence intensity is linearly proportional to laser intensity and dye concentration as

$$I_f = k_c Q_f I_l C V, \quad (4.9)$$

and

$$V \sim d_f^3. \quad (4.10)$$

Here V is the measuring volume, i.e. the spatial resolution. Q_f represents the fluorescence quantum yield and k_c is a coefficient related with optics for the collection of emitted light to the PMT and dye species. C and I_l represent concentration and laser intensity at the measuring point respectively. I_f decreases very fast with d_f by a 3rd power. The finer the focused diameter is, the smaller the light signal I_f becomes. Miller [73] focused the laser beam to around $40 \sim 60 \mu m$ (this is one of the best measured focused diameter for temporal measurement at present to our knowledge). This means that here the signal is approximately three orders smaller than in [73], keeping other parameters to be the same and only changing the measuring volume. Even though I_l is increased, i.e. $I_l \sim 1/d_f^2$ when the beam is fine-focused, I_f will not increase linearly with I_l , because Eq. (4.9) is only valid when it is far from saturation of absorption, i.e. when the laser intensity is low enough for fixed concentration. If I_l is high, the saturation will emerge and I_f will not increase with I_l . In this experiment, I_l is already in the near saturation region (see later).

From eqn (4.8), it is known that the SNR decreases with the reduction of the signal level and the increase of frequency band. When I_f is small, the SNR will also be small, especially for the high frequency signal corresponding to fine scale structures of scalar in turbulent mixing.

4.4 Results

4.4.1 Thermal blooming

Whether blooming has influence on I_f or not can be tested experimentally, and it is not necessary to do the time-consuming estimation through calculation according to energy conservation principle. The following experiment was done. First let the fluid be still, adjust the PMT with the pinhole and seek for the maximal output from the PMT. When the focus point is best imaged into the pinhole, there will be a maximal output. Then adjust it again to search for the maximal output when fluid is moving at a given velocity, say, 10 cm/s. It is found that the focus length increases. If we arrest the fluid and measure the maximal output again, it is observed that the focus length is again reduced. This is qualitatively identical to the analysis above, because if the fluid is at rest, the refraction gradient is negative and the focus length is short. Higher I_f and C would cause increased heat absorption and so the thermal blooming would become worse. It was tested with above method that in the experimental condition where C is $0.5 \times 10^{-6} M$ and P_l is 0.5 W, the thermal blooming can be negligible when $u > 6 \text{ cm/s}$.

Another possibility of estimating the influence of the thermal blooming is to measure first the decay curve with relatively high velocity, then extrapolate the result to low velocity using an exponential decay curve and compare it with the measured result. If the measured value of I_f is smaller than the estimated one, the thermal blooming has an influence.

4.4.2 Photobleaching

There are only few data published on photobleaching in fluid mechanics in just one situation. It seems that Saylor [93] is the only one, who measured photobleaching in just one situation. Nevertheless, his result is suspect, since it is done with the fluid at rest neglecting the influence of the thermal blooming, which must be assumed to be of strong effect and cannot be neglected for $u = 0$. Here the results of the influence of laser intensity and concentration on photobleaching are measured with the fluid in motion, and the influence of thermal blooming is therefore excluded.

4.4.2.1 Influence of laser intensity

4.4.2.1.1 Relation between I_f and u Fig. 4.1 shows the influence of I_l on the measurement of I_f with the change of fluid velocity at constant $C = 0.67 \times 10^{-6} M$. Normally if I_l and C are constant, I_f should also be constant, yet we find that I_f increases with the fluid velocity in some range of fluid velocity, i.e. for a fixed C and I_l , there is a region of velocity, within which I_f increases with fluid velocity. This confirms our conclusion 1 of the model given above. When the velocity is above this range, I_f changes little with velocity, i.e. I_f saturates with velocity. This is identical to the conclusion 3 of the model given above. The larger I_l is, the wider the range becomes. The velocity influence is not small at all. Therefore I_l should not be too high. According to the above-mentioned analysis and the experimental result of the thermal blooming, we can propose that photobleaching is the main reason for the relation between I_f and u (when u is very low, the thermal blooming would also have influence). If u is high, the residence time is short, and the decay time is shorter than for low velocity, The I_f signal is therefore for high velocity u larger than for low velocities. It is a serious problem for scalar measurement in fluid mechanics, especially for turbulence where the velocity fluctuates, because the measurement results I_f depends not only on C , but also u , and our measurement is based on the assumption that I_f depends only on C .

It must be clear that the photobleaching at low u is also related with thermal blooming, but it is difficult to separate these effects. At low u the decrease of I_f is even stronger.

4.4.2.1.2 Decay of I_f with time The photobleaching curve is measured with the method described above and is shown in Fig. 4.2. This is at constant $C = 1.0 \times 10^{-6} M$ but different I_l , and it is clear that the higher the laser power is, the faster the decay. With $C = 1.0 \times 10^{-6} M$, the decay is

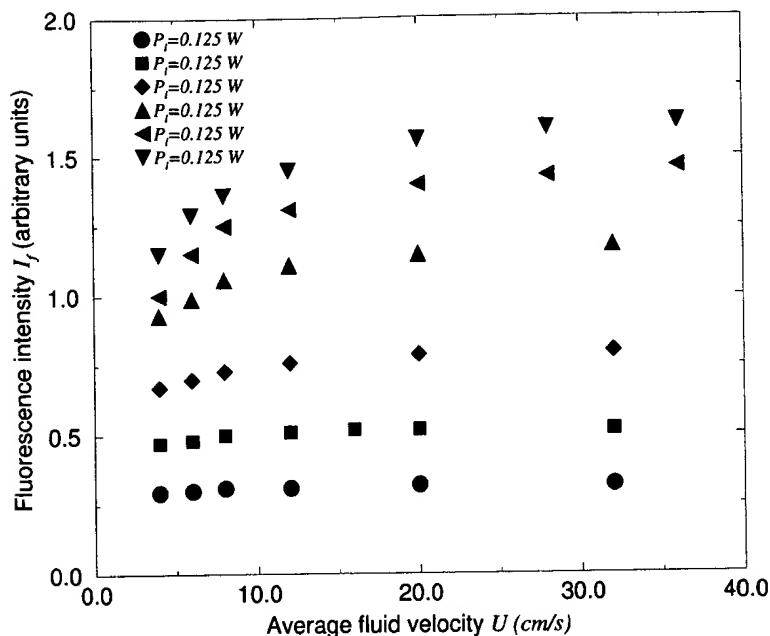


Figure 4.1: Relation between fluorescence intensity and fluid velocity with different values of P_l at $C = 0.67 \cdot 10^{-6} M$.

relatively slow when P_l is 0.04 W in the measured time range and fluorescence intensity decays from 0.014 to 0.1 ms by about 4.5%. When P_l is 1.0 W, however, the decay is fast and from 0.01 to 0.1 ms I_f has already decayed by 31 %. For too small u (here large t), the decay would not only occur because of photobleaching, but also thermal blooming, i.e. it would be faster than in the case with only the influence of photobleaching.

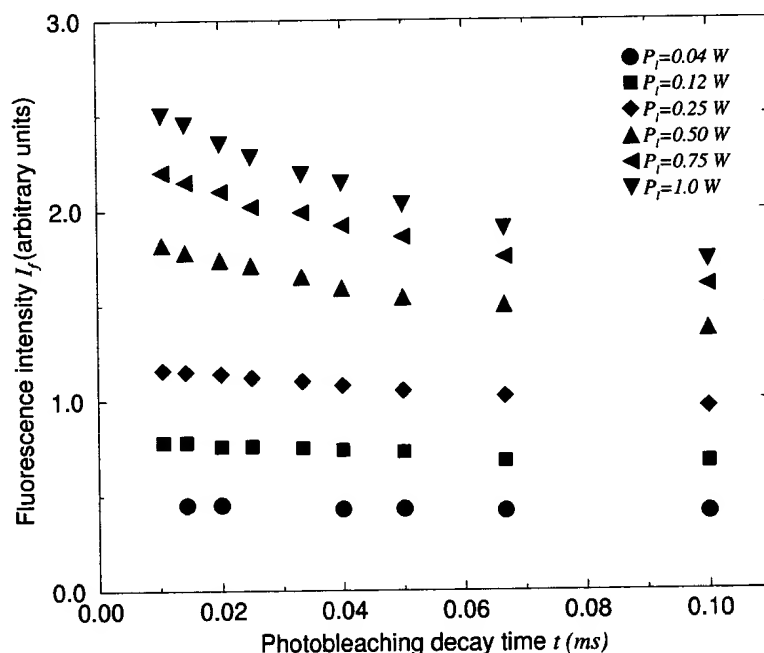


Figure 4.2: Fluorescence intensity decay with residence time for different laser power P_l and $C = 10^{-6} M$.

4.4.2.1.3 Half-life time constant $\tau_{1/2}$ To describe photobleaching decay, it is better to use the half-life decay time constant [93], which can be obtained from the measured results. Fig. 4.3 shows that $\tau_{1/2}$ decreases with the increment of P_l under constant $C = 1.0 \times 10^{-6} M$. This is identical to the conclusion 2 above. The decay behavior is not linear. At lower P_l it decreases faster than at higher P_l . The result indicates that the half-life time constant $\tau_{1/2}$ is much smaller than [62] by almost five orders of magnitude. Even for the smallest P_l of 0.04 W at $C = 1.0 \times 10^{-6} M$, $\tau_{1/2}$ was found to be only about 0.43 ms.

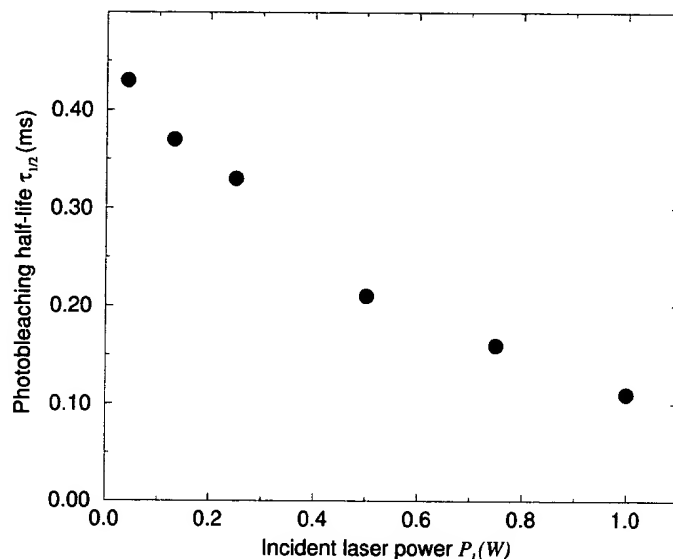


Figure 4.3: Relationship between photobleaching half-life constant $\tau_{1/2}$ and laser power P_l at constant $C = 1.0 \times 10^{-6} M$.

4.4.2.2 Influence of concentration

4.4.2.2.1 Relation between I_f and u The influence of concentration on photobleaching decay is qualitatively similar to that of P_l . Fig. 4.4 indicates the influence of concentration on the measurement. Here the laser power is about 0.5 W. Similarly as for the influence of I_l , there is also a velocity region, within which the I_f increases with velocity. For higher C the stronger photobleaching effect increases. For example, when $C = 1.0 \times 10^{-6} M$, for $u = 4 \text{ cm/s}$ and $u = 32 \text{ cm/s}$, I_f is 1.36 and 1.77 respectively. The relative deviation is 23 %. At $C = 0.17 \times 10^{-6} M$, for $u = 4 \text{ cm/s}$ and $u = 32 \text{ cm/s}$, I_f is instead, 0.25 and 0.28 respectively, and the relative deviation is about 11%. At low u and high C , photobleaching has strong influence, for instance of $u = 4 \text{ cm/s}$ and $C = 1.0 \times 10^{-6} M$ the relative deviation is approximately $2.8\%/u(\text{cm/s})$. When the velocity is beyond this range, I_f changes little with velocity, getting into saturation. For larger C , the range is increased. For $C = 0.17 \times 10^{-6} M$, the upper limit of the range is a velocity of 12 cm/s and for $C = 1.0 \times 10^{-6} M$, it goes up to 32 cm/s approximately. The higher C is, the worse the dependence of I_f on u . Therefore C must not be too high and u must be sufficiently high.

4.4.2.2.2 Decay of I_f with time The influence of C on photobleaching decay is shown in Fig. 4.5. This was at a constant laser power of 0.5 W, but with different concentrations. It shows that for higher concentration, the photobleaching becomes stronger. At $C = 0.17 \times 10^{-6} M$ the decay is relatively weak, but becomes stronger at $C = 1.0 \times 10^{-6} M$.

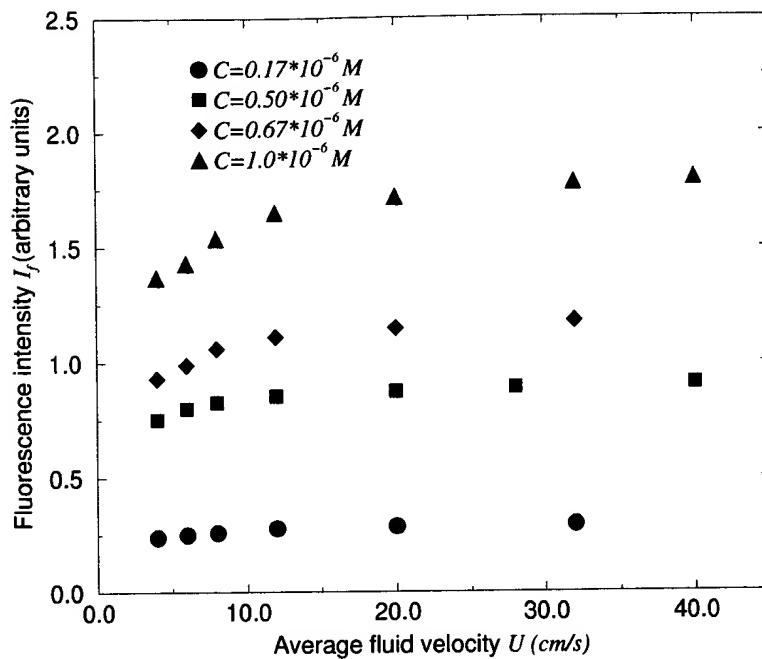


Figure 4.4: Relationship between fluorescence intensity and fluid velocity u for different concentrations but constant $P_l = 0.5 W$.

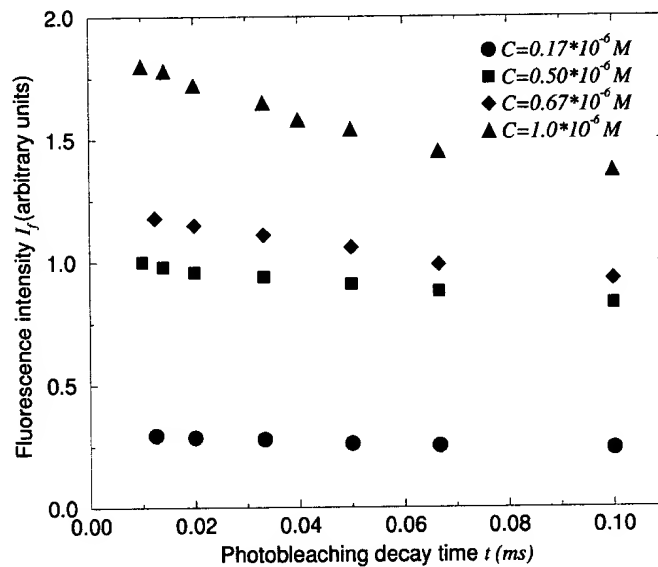


Figure 4.5: Fluorescence intensity decay with residence time for different C and constant laser power $P_l = 0.5 W$.

4.4.2.2.3 Half-life time constant Fig. 4.6 shows the change of $\tau_{1/2}$ with concentration at constant $P_l = 0.5 W$. It is found that $\tau_{1/2}$ decreases with C almost linearly in the measured range of C .

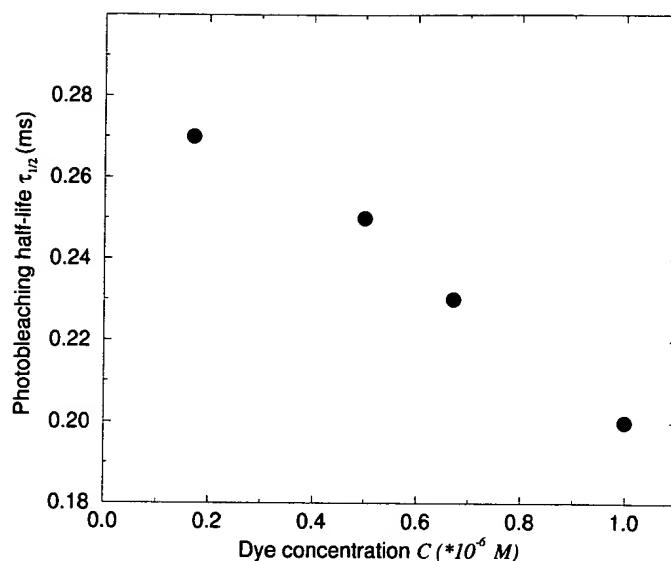


Figure 4.6: Relationship between photobleaching half-life $\tau_{1/2}$ and C with constant laser power $P_l = 0.5 W$.

4.4.3 Calibration between fluorescence intensity I_f and concentration C

For LIF measurement of concentration, it is necessary to calibrate the relation between C and I_f . It is expected that this relation is linear and that the proportionality coefficient is constant when P_l and the measurement volume are fixed and I_f depends only on C . If this were so, the concentration C could be calculated through the measured I_f . However Fig. 4.7 shows the calibration results between C and I_f at different velocities, which shows that even if I_f is linear proportional to C , the coefficient depends on velocity u . This is again due to the thermal blooming and photobleaching.

On the other hand, if u is high enough, the coefficient will asymptotically reach a constant value almost independent of u as shown in Fig. 4.8 with constant $P_l = 0.5 W$ and $P_l = 1.0 W$. To reduce the influence from photobleaching, the measurement should be carried out beyond the range of velocity over which the asymptotical value of the coefficient reaches a constant. At the situation of $P_l = 0.5 W$, the asymptotical coefficient value is reached at about $U = 12 cm/s$. Therefore the measurement should be done with an average velocity higher than 12 cm/s. However for $P_l = 1.0 W$, the asymptotical value is reached at about $U = 25 cm/s$. This means that, if $P_l = 1.0 W$, and the experiment is undertaken at velocity smaller than 25 cm/s, the result would be contaminated.

Fig. 4.7 and Fig. 4.8 tell us that, when I_l or C is large enough, photobleaching and thermal blooming will contaminate the measurement results. The calibration should only be carried out when the fluid is in motion and the fluid velocity beyond a certain threshold to keep the residence time small enough compared with half-life time constant and move the heat away from the measurement volume to omit the influence of photobleaching and thermal blooming. If the calibration is undertaken with fluid at rest, no steady I_f can be obtained until the photobleaching effect becomes negligible and the thermal blooming gets in equilibrium for a long time, under which the result is quite different from the real flowing situation. If the fluid flow velocity is too low, the dye residence time cannot be negligible compared with the decay half-life time constant.

4.4.4 Noise characteristic

The following results indicate that the dominating noise in this experiment is the shot noise in signal.

With Fig. 4.9 the noise can be demonstrated directly. This is a time trace for the period of signal

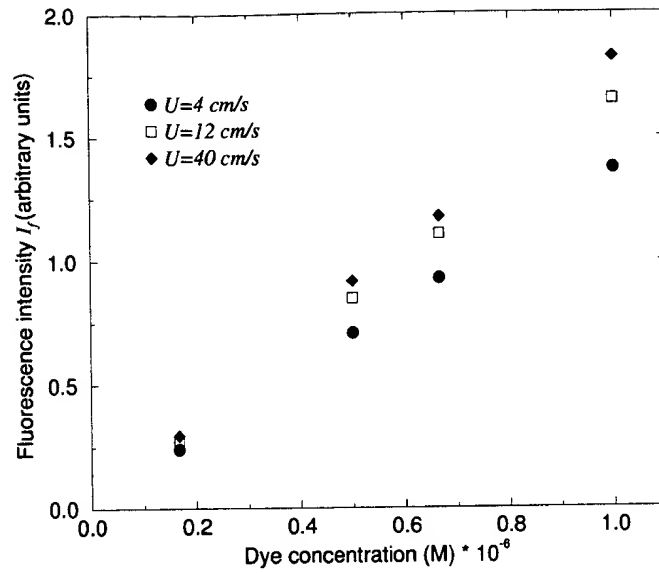


Figure 4.7: Calibration between I_f and C with different velocities.

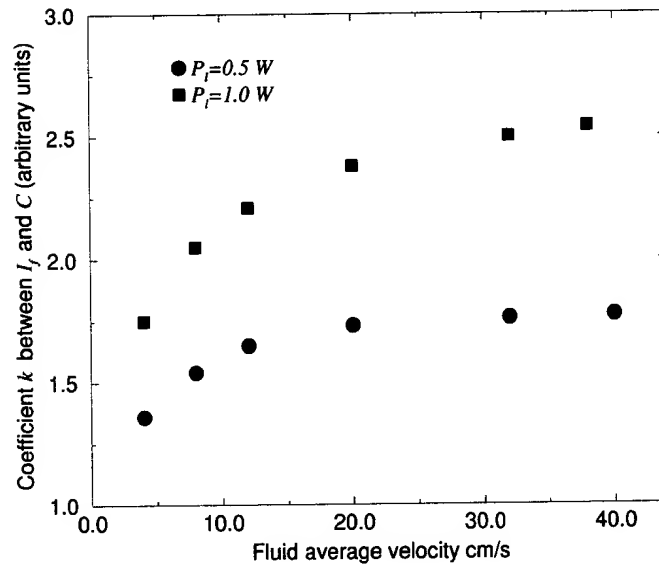


Figure 4.8: Coefficient k between I_f and C changes with different velocities.

from lowest to highest level, i.e. from water to unmixed dye when the dye lump is moving into the measurement volume and replacing the clean water at very low velocity. It can be seen that there is superimposed noise fluctuation on the signal, and the higher the signal level is, the larger the noise becomes. Here it must be emphasized that the fluctuation is noise, because the flow is actually laminar in this measurement. An influence from dye solution inhomogeneity can also be excluded, because the dye solution used is already molecularly mixed.

From Fig. 4.9, it is also obvious that, at the lowest level, there is only water and the fluctuation is very small compared with the one at high signal level. This indicates that the dark noise is very

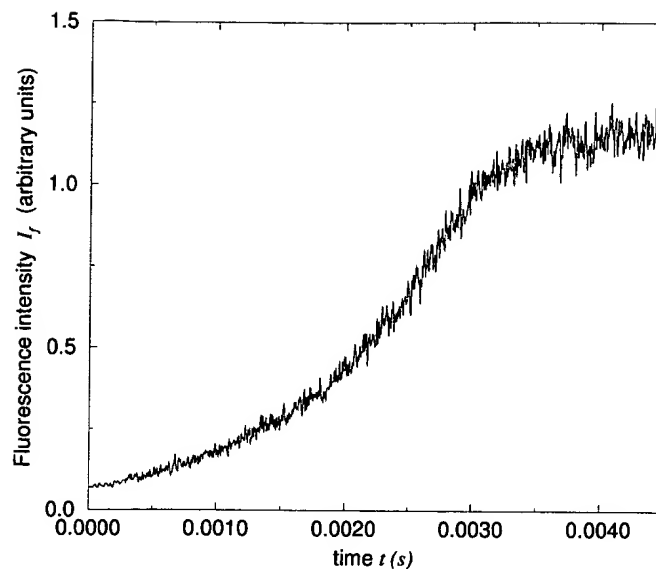


Figure 4.9: Timetrace of signal.

small and can be negligible. It was also tested that there is almost no difference between the SNR with and without cooling. The temperature difference between the cases with and without cooling is $15\text{ }^{\circ}\text{C}$. This implies that the Johnson noise is also negligible. The current amplifier has a very low noise with a noise current of only about $1.2 \times 10^{-13}\text{ A/Hz}^{1/2}$. This causes less than 0.1% of the noise and can therefore be neglected. It was also measured that the maximum laser power fluctuation is below 2%. When the measurement is done near saturation, such a fluctuation effect can be negligible. All this indicates that the noise is primarily from shot noise in the signal.

The following noise characteristics further imply that the dominant noise is from the shot noise in signal from the PMT. Fig. 4.10 shows the relation of the root mean square of the noise (RMS) to the square root of the signal level. It is obtained by measuring the signal fluctuation at different dye concentration levels (molecularly mixed solution) within the linear region. It is found that the root mean square noise is linearly proportional to the square root of signal amplitude. Fig. 4.11 shows that the noise is also proportional to the square root of frequency bandwidth. This was measured at constant concentration level by changing the low pass cut-off frequency of the filter. This corresponds to eqn (4.7). It can be concluded from the experimental results that the shot noise in signal is the main source of noise, that limits the resolution of the measurement. This is due to the lower quantum efficiency of the PMT.

4.4.5 Noise influence on scalar measurement

When the SNR is too low, some physical details will be lost. The details of influence of the noise on the measurement result is referred to next section. The influences, for instance, on probability density function and power spectrum density of concentration are shown in Fig. 5.9 and Fig. 5.25 respectively.

4.4.6 Methods to increase signal level

Only the shot noise in the signal needs to be reduced since the dark and Johnson noise are negligible. Unfortunately it is very difficult to reduce the shot noise in the signal due to the fact that it originates from the signal itself, i.e. it is the characteristic of the PMT. Although the noise increases with signal

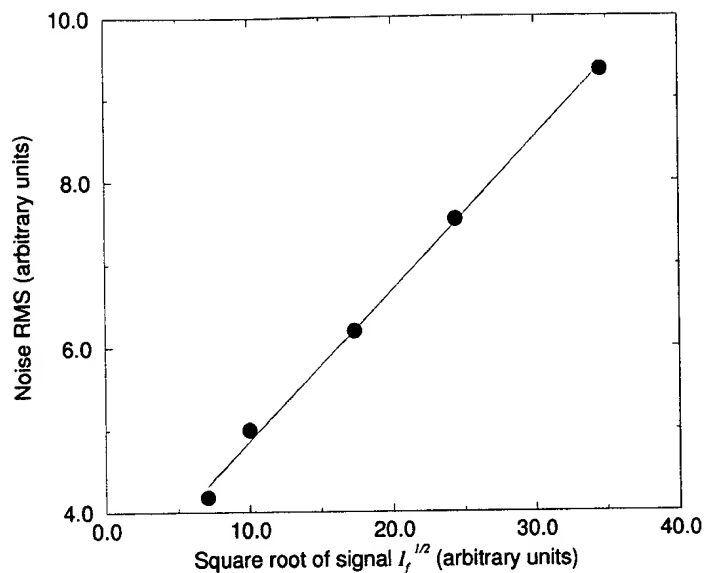


Figure 4.10: Relationship between noise RMS of fluorescence intensity and square root of signal level.

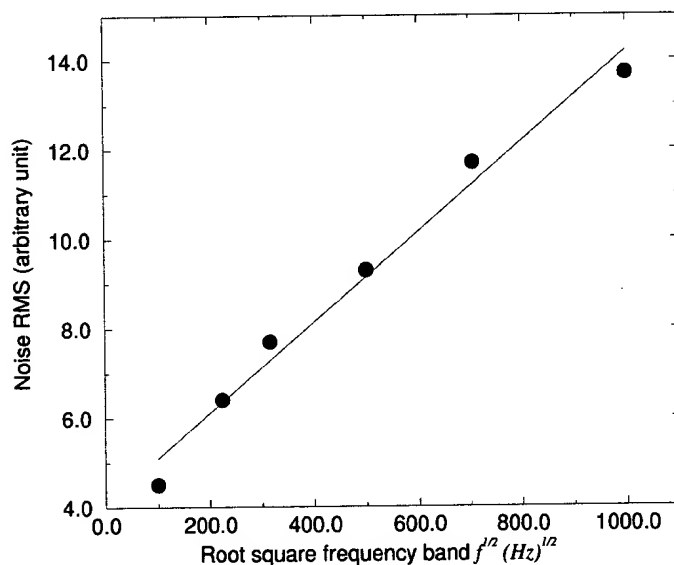


Figure 4.11: Relationship between noise RMS of fluorescence intensity and square root of frequency bandwidth.

level as indicated in eqn (4.7), eqn (4.8) shows that the SNR increases with signal level. Therefore, in order to improve the SNR the only thing which can be done is to increase the source signal level. From eqn (4.9) it can be seen that the signal can be increased with increasing Q_f , I_l , C and V respectively. However, V can not be increased when high spatial resolution is asked for. Q_f depends on the physical and chemical properties of the specific dye and is not considered here. The following shows that neither I_l nor C can be increased without limitation. The most important limitation, due to bleaching, is

shown in [115].

4.4.6.1 Increasing concentration C Increasing C would result in some problems, e.g. laser intensity attenuation, nonlinear response, photobleaching and thermal blooming.

4.4.6.1.1 Nonlinear Response As described by Guilbault [46], I_f and C have a linear relation at small concentration, but for higher C a nonlinear relationship emerges until fluorescence saturates against concentration, i.e. I_f increases little with the increment of C . Further increase of C will even result in a reduction of I_f , which is mainly due to the absorption of the laser light according to Beer's law [98], v.z.

$$I_f = I_{f0} e^{-C\sigma l_l}. \quad (4.11)$$

Here I_{f0} is the incident laser intensity; σ represents the dye absorption cross section and l_l is the length of light path. It is usually expected, that the measuring range lays in the linear range. If the linear range is large, it is possible to get high signal using high C . Guilbault [46] commented that in order to keep linear relationship between I_f and C , the decay of I_l in the liquid up to the point of measurement should be less than 5%.

The linear range depends on the specific dye used, i.e. its molecular absorption cross section, the path length of laser and laser intensity distribution in the fluorescence solution. It can be expected that the larger σ and l_l , the smaller the linear range is.

To increase the linear range when the path length of laser is very long for large flow field, the distribution of laser intensity in the medium can be designed according to the Q-switch theory used in solid-state laser for tuning laser power [57]. The Q-switch theory tells us that when the pumping light intensity is high enough, the dye will be saturated and the attenuation of the pumping light becomes small. If the laser beam has a small cross section propagating in the medium with a high intensity at the near saturation condition, the decay of the laser will be smaller and thus result in a larger linear range.

The linear range of I_f and C increases with laser intensity I_l as shown in Fig. 4.12. At $P_l = 0.075$ W the linear range is about 1×10^{-6} M. By increasing P_l to 0.25 W and 0.875 W, the linear range is increased to about 2×10^{-6} M and 3×10^{-6} M respectively. Unfortunately, the restriction of concentration due to the non-linear response is not the dominant factor for high spatial resolution measurement, since the photobleaching restricts the maximum of C to much smaller value than, for instance, 3×10^{-6} M when P_l is 0.875 W.

4.4.6.1.2 Attenuation of laser beam power The absorption effect would become too strong for high C . In such a case at the measurement point the fluctuation of I_l is large corresponding to the integral change of C along the incident path of laser light in a turbulent mixing flow, due to the high absorption. The color moves randomly, and so does I_l . This can result in noise in the measurement, especially in turbulent flows. This effect can be decreased if I_l is high and reaches saturation and C is small. The attenuation found in this experiment is shown in Fig. 4.13, where the decay distance of the laser beam is approximately 40 mm. This is measured at fluid velocity of 8 cm/s. It is clear that the higher P_l , the smaller the relative attenuation will be. The consideration of attenuation of laser beam power requires small C .

4.4.6.2 Increasing laser power P_l As stated earlier, when I_l is not high I_f increases linearly with P_l , but for I_l very high the emitted light intensity of the dye does not increase linearly with increasing laser intensity, because of fluorescence absorption saturation. If it is not at saturation condition, increasing P_l can enlarge source signal level.

The experimental results demonstrate that the linear range is increased with increase of concentration C . The influence of C on the relationship between I_f and P_l is shown in Fig. 4.14, where the saturation for $C = 1.7 \times 10^{-7}$ M appears at about $P_l = 0.5$ W, but for $C = 1 \times 10^{-6}$ M at about 1 W

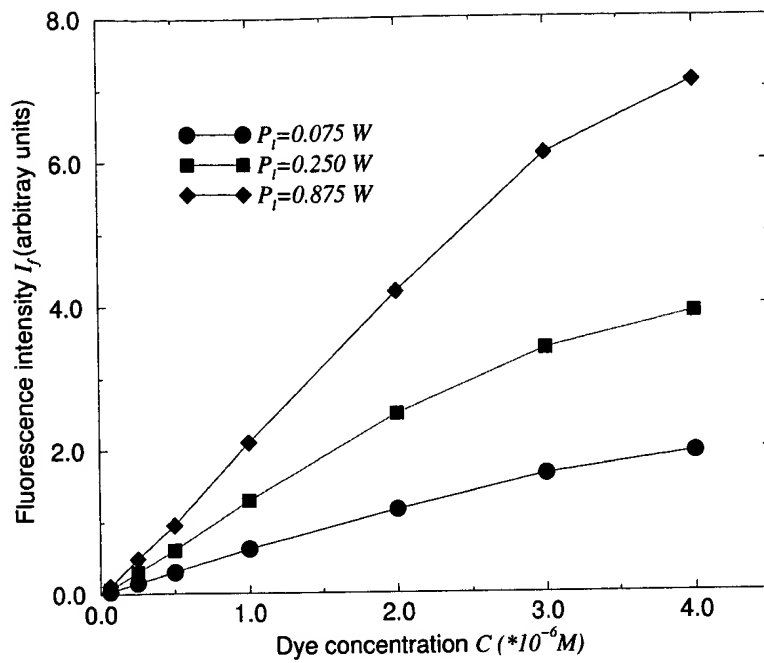


Figure 4.12: Relationship between fluorescence intensity and concentration with different P_l .

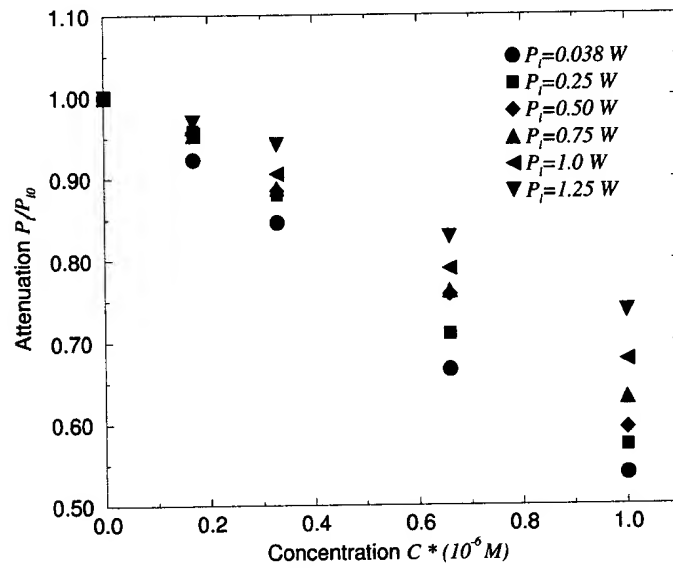


Figure 4.13: Relationship between laser power attenuation and concentration with different P_l .

saturation is still not reached. The fluid velocity is 32 cm/s. In the investigated power range of the laser, there is almost no linear relationship between I_f and P_l and the saturation is only asymptotically achieved with increasing P_l . However, as stated earlier, C can not be very high. For this reason the possibility of increasing the signal through an increase of P_l at constant C is limited.

It is also observed that the linear range increases with fluid velocity and the result is shown in Fig. 4.15. Here the concentration is constant, $C = 6.7 \times 10^{-7} M$. At $U = 4$ cm/s, the saturation is around $P_l = 0.7$ W, but at $U = 32$ cm/s, the saturation point is about $P_l = 1.0$ W. Fig. 4.15 also implies that when the velocity is high enough, the linear range will increase little with velocity. For

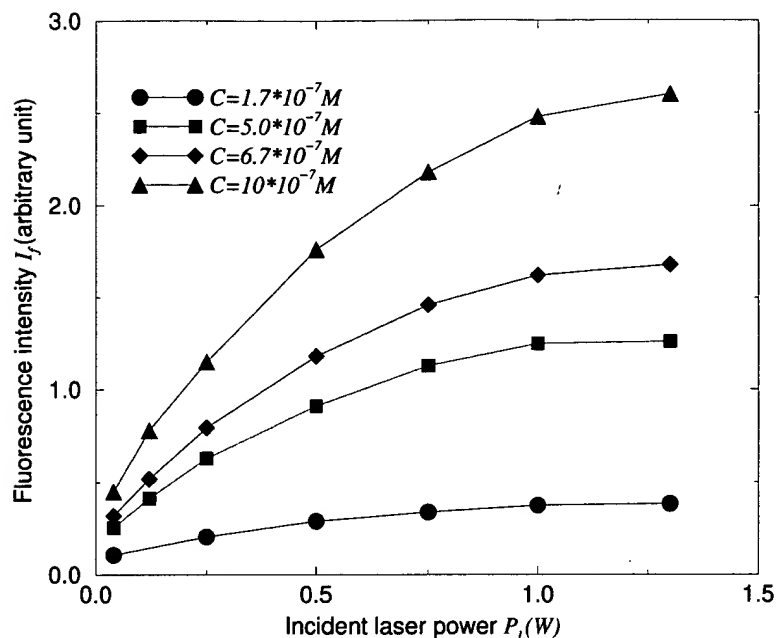


Figure 4.14: Influence of concentration on fluorescence intensity saturation to P_l at $U = 32 \text{ cm/s}$.

example, the linear range is almost the same for $U = 20 \text{ cm/s}$ and $U = 32 \text{ cm/s}$. It is also needed to note that the signal difference for low laser power is smaller than that for higher laser power. All these phenomena are caused by photobleaching and thermal blooming. The higher I_l , the stronger the influence from photobleaching and thermal blooming. The influence of photobleaching and thermal blooming is as if fluorescence were approaching saturation.

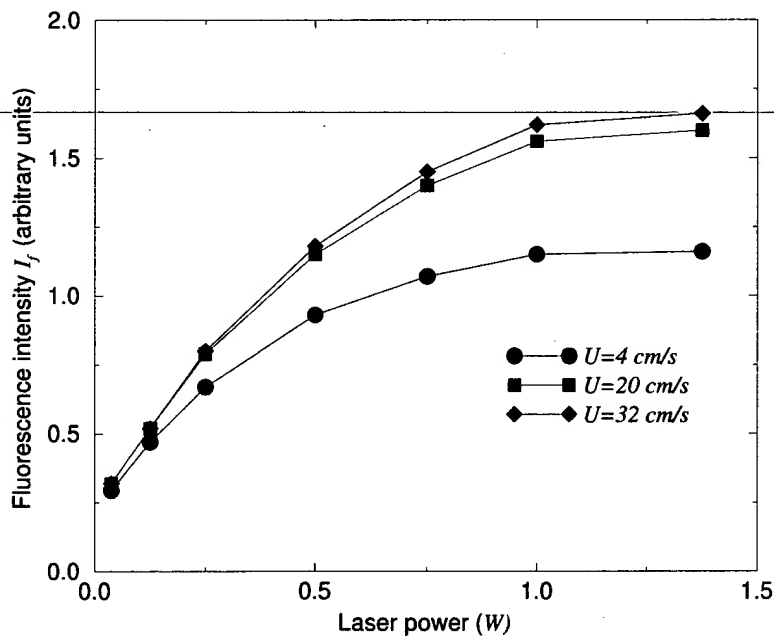


Figure 4.15: Fluid velocity influence on fluorescence intensity saturation to P_l at constant $C = 6.7 \times 10^{-7} M$.

There are two causes which can result in the laser intensity fluctuation at the measurement point. One is that laser power itself fluctuates and the other one is due to the fact that the integral con-

centration fluctuates along the laser path as mentioned above which, in turn, results in the change of laser attenuation. It is tested that the ratio of laser intensity fluctuation to average laser intensity level decreases with increasing laser power. Its maximum is less than 2% and can be negligible. As shown in Fig. 4.13, the above mentioned attenuation effect would also become smaller if P_l is high and reaches attenuation, because the limited change of I_l has little influence on the fluorescence intensity when it is near the saturation state and in the saturation region I_f does not change with P_l .

All these arguments suggest that the larger P_l is, the higher SNR becomes due to the increase of I_f . However the following reasons restrict P_l from being too high. First, at high laser power the laser beam has bad mode for fine focusing, i.e. if the power is too high it is difficult to get TEM₀₀ mode of laser beam which is the best mode for fine focusing. Second, and most important, when I_l is too high, the thermal blooming and photobleaching will become serious. Combined with the bleaching result, it is found that photobleaching limits the laser power P_l .

4.5 Discussion

According to the above-mentioned analysis and experimental results, the following should be considered in practice for fluid mechanics.

4.5.1 A new anemometer of photobleaching with LIF

The photobleaching model and measured results here can be used as a new kind anemometer: photobleaching anemometer with LIF [41]. Some simple description is referred in the appendix of this work.

4.5.2 Some considerations about photobleaching influence

1. To our knowledge, only in the work of Prasad and Sreenivasan [86] the focused laser beam is as low as $5.5 \mu m$, but no details are given about that how this value is obtained. The dye used is the same one as in the present investigation. The laser power used is 7 W and the concentration is of the order of a few parts per million (as described), which should be higher than 1×10^{-6} , and fluid velocity could be about 15 cm/s. However, unfortunately, no comparison could be made because in [86] nothing is said about the possible photobleaching and thermal blooming influences.
2. The fact that photobleaching reduces signal alone has already had negative effects on LIF experiments. What is even worse is that in fluid mechanics the fluid velocity is not constant, and especially in turbulent flows, it is an unknown parameter for scalar (concentration or temperature) measurement. This is a different influence of photobleaching on fluid mechanics compared with laser research.
3. The fluid residence time t also depends on d_f . If C and I_l are high enough and d_f is not small, photobleaching can also have an influence.
4. If LIF is used for temperature measurements, photobleaching and thermal blooming could even have stronger effects, because they can also cause a change of temperature at the measuring point.
5. Pulse recovery against photobleaching is proposed by [93], but it is difficult to be used for high resolution measurement of turbulent mixing due to the high frequency signal there.
6. Arcoumanis *et al* [3] have investigated the stability of different dyes which is actually related with the photobleaching discussed here. Their result is that no satisfactory stability of solutions of fluorescein could be found and its use should be abandoned in favor of Rhodamine B. Some work is needed to find a more suitable new dye.

7. Based on this work, it is recommended to use P_l and C as small as possible to prevent from thermal blooming and photobleaching. However if P_l and C are too low, the signal I_f will be too weak and this will result in low signal to noise ratio.

4.5.3 Measurement of focused beam diameter d_f

In [86] it was reported that the laser beam was focused to $5.5 \mu m$, but no description was given about how this value of the diameter was obtained. To our experience, it is needed to measure the focused diameter in order to determine such a fine focused beam diameter because the theoretical formula describes only an ideal situation and in practice, due to the imperfection of optical parts and assembly, the actual focused diameter is larger than the theoretically calculated one, especially near the diffraction limit. Miller [73] used a knife to measure the focused diameter, but that could be difficult to use for very fine focusing. Komori *et al* [60] used power spectrum to estimate d_f . They found a broadening in their power spectrum and assumed its frequency to correspond to the spatial resolution. This is not accurate, because one can also get a high frequency spectrum even if there is no such a corresponding structure in the real physical space. This is the statistical feature of a random signal in a stochastic process. This could be shown in our experiment, where the power spectrum is visible at high frequency, but no corresponding time trace could be distinguished.

4.5.4 Detector and SNR

Although it was reported in [62] (where a photodiode is used as light detector) that the shot noise in signal was negligible, it dominates in our experiment. In the paper of Dowling *et al* [31], it is concluded that a photodiode should be used instead of PMT in order to reach high SNR. The criterion for choosing a photodiode is that the input signal is higher than 50 pA. Dowling *et al* [31] also mentioned that in their experiment, where Rayleigh scattering was used, the focused diameter was about 0.2 mm and the frequency bandwidth was 100 kHz, the signal was so high that photodiode could be sufficient. Supposing the photodiode responsivity is 0.2 A/W (this is the normal order of magnitude in the spectrum range of interest for a photodiode), the input light power for 50 pA is in the order of $2.5 \times 10^{-10} W$. However, in the work of Durst and Sender [32], for input power less than $10^{-9} W$ and a frequency bandwidth of $10^5 Hz$, the SNR of PMT is clearly better than that of photodiode-and-avalanche-diode. In our experiment the signal is in the order of $10^{-12} \sim 10^{-10} W$ and the frequency bandwidth is 100 kHz. The results indicate that SNR of PMT is higher than that from a photodiode even in the frequency bandwidth of $10^{-4} kHz$. With the up-to-date commercial silicon photodiode, the signal must be amplified by about $10^{10} V/A$, or more than $10^8 V/A$ with an avalanche photodiode. It is difficult to get such a high transimpedance low noise current amplifier with a frequency bandwidth of about 300 kHz and is limited by bandwidth and noise. The reason is that the signal is simply too small for high resolution measurement.

In [18], it is shown that if the photocathode current is higher than $10^{-15} A$ and the signal frequency bandwidth is higher than 1 kHz, the SNR is limited by shot noise in signal, and therefore cooling has no influence to improve SNR. This is identical with the present results. The signal level is relatively too weak for photodiode. If the frequency bandwidth is small (less than 1 kHz), the SNR of PMT can be much improved, and photodiode may also be used. However in turbulent flow the frequency bandwidth is higher. Therefore it is expected to improve the method of LIF to get high signal level so that photodiode can be used to improve SNR, because the quantum yield of photodiode is about five times higher than that of a PMT. For example, in [3] it is recommended to use Rhodamine B as a fluorescent dye.

4.5.5 Amplifying signal

The signal from the PMT is a current signal, which needs to be converted to voltage to match the ADC. The signal is also too weak and has to be amplified to the ADC input range to get maximum resolution. There are two possibilities to amplify the signal: increasing supply voltage for the PMT

and increasing amplification of the amplifier. In this experimental conditions the result shows that it is better to use relative small amplification from the PMT and as much as possible amplification (transimpedance) from current amplifier (until the limitation of frequency band) to improve SNR.

Another experiment is also conducted, using high amplification of PMT with a load resistance (its magnitude is limited by rise time) and a low noise voltage amplifier (also constructed by the author). It is found that, to reach a 100 kHz frequency bandwidth, the SNR result of this method is not so good as the one used above, i.e. transimpedance amplifier.

4.5.6 Fluorescence saturation

In [73] the fluorescence is already near saturation, where the focused beam diameter is about $40 \sim 60 \mu m$ with 1 W laser power and the concentration C is $1 * 10^{-6} M$ with the same dye as here. Here in the range of $P_l = 0 \sim 0.2 W$, however, the fluorescence is still not in saturation as indicated in Fig. 4.14. The laser intensity at the measuring point I_l here is much higher than that of Miller (about ten times if P_l is 0.1 W here). The reason could be that in [73] the measurement was undertaken when the fluid was in rest. As shown in Fig. 4.15, the saturation point of laser power decreases with the reduction of velocity. So even the calibration between I_f and P_l should also be undergone when the fluid is in motion and beyond a threshold.

4.5.7 Attenuation

The attenuation of laser power shown in Fig. 4.13 is strong compared with others. For instance, in Miller's experiment, the attenuation across the entire jet width was determined from the measurement to be about 1%. In the present experiment, instead, at concentration of $0.5 * 10^{-6}$ and $P_l = 0.5 W$ the attenuation across the pipe is about 12%. It can be expected that this is also related to photobleaching and thermal blooming and fluorescence saturation. If the fluid is at rest, it is easier for the dye to be bleached and it is closer to the saturation range and so the attenuation is small. However, if the dye is in motion, the fluorescence intensity is higher and more laser power is absorbed and thus the attenuation is stronger. Therefore it is expected that the attenuation increases with velocity until a threshold similarly to the phenomenon in Fig. 4.15 and the attenuation measurement should also be undertaken when the fluid is in motion and beyond a threshold velocity.

5 Experimental results of turbulent mixing

The concept of the ideal relative turbulent mixing process and state is very harsh. The following experimental results are introduced to prove them. The mixing under special forcing is extraordinarily fast [118].

5.1 Wake

We will study a wake of $\bar{U} = 40 \text{ cm/s}$, where the forcing frequency is around 6 Hz and amplitude $\sqrt{u'^2}/\bar{U}$ is about 45%.

5.1.1 Visualization

The details on visualization is covered in Part 2 of this work. Under strong forcing of maximum receptivity, the visualized pictures of the mixing results are almost similar (i.e. no visible large structures). Fig. 5.1 shows two situations of with and without forcing of a wake with $\bar{U} = 40 \text{ cm/s}$. Without forcing, there are only large structures in the wake and the fluids are almost unmixed within the view of the picture. However, there is almost no visible large structure right after the splitter plate in the whole cross section and the fluids are mixed at least on the resolution of eyes. The mixing is on the large scale (even on microscale) dramatically enhanced.

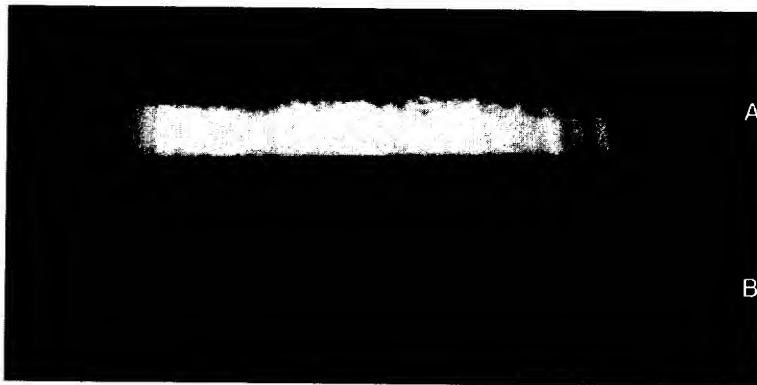


Figure 5.1: Visualization for turbulent mixing with and without forcing in a wake of $\bar{U} = 40 \text{ cm/s}$.

5.1.2 Concentration distribution at near field

5.1.2.1 Timetrace In Fig. 5.2 the timetrace for $\bar{U} = 40 \text{ cm/s}$ is shown at different y -positions of $x/D = 0.25$ with and without forcing. Fig. 5.2a is measured at around $y = -0.5 \text{ mm}$ from the axis of the pipe. It is very difficult to measure the plane wake exactly in the middle of $y = 0$ at such a short downstream distance, because the middle of the wake can change its position within $4 \mu\text{m}$ easily with some change of initial conditions, which are impossible to be excluded. Here the flow is still laminar and the fluids do not mix at all even on large scales. However with forcing, the timetrace is dramatically changed. Even at $2y/D = 0.75$ and -0.75 , the fluids have already partially mixed, at least on the large scale, i.e. the above mentioned relative turbulent mixing. The timetraces show that the fluid is more homogeneous under forcing not only in the middle region of the wake, but also in the whole cross section, i.e. the spread of the wake is almost 180° . In the pure water side, it can be seen in Fig. 5.2b that the dye is entrained into the water side by large coherent structures, and mixed in it; but there are still water lumps which have not mixed. This occurs almost symmetrically in the dye side in Fig. 5.2d. In the middle of the wake, the mixing result is better and relatively symmetrical for water and dye fluids as indicated in Fig. 5.2c.

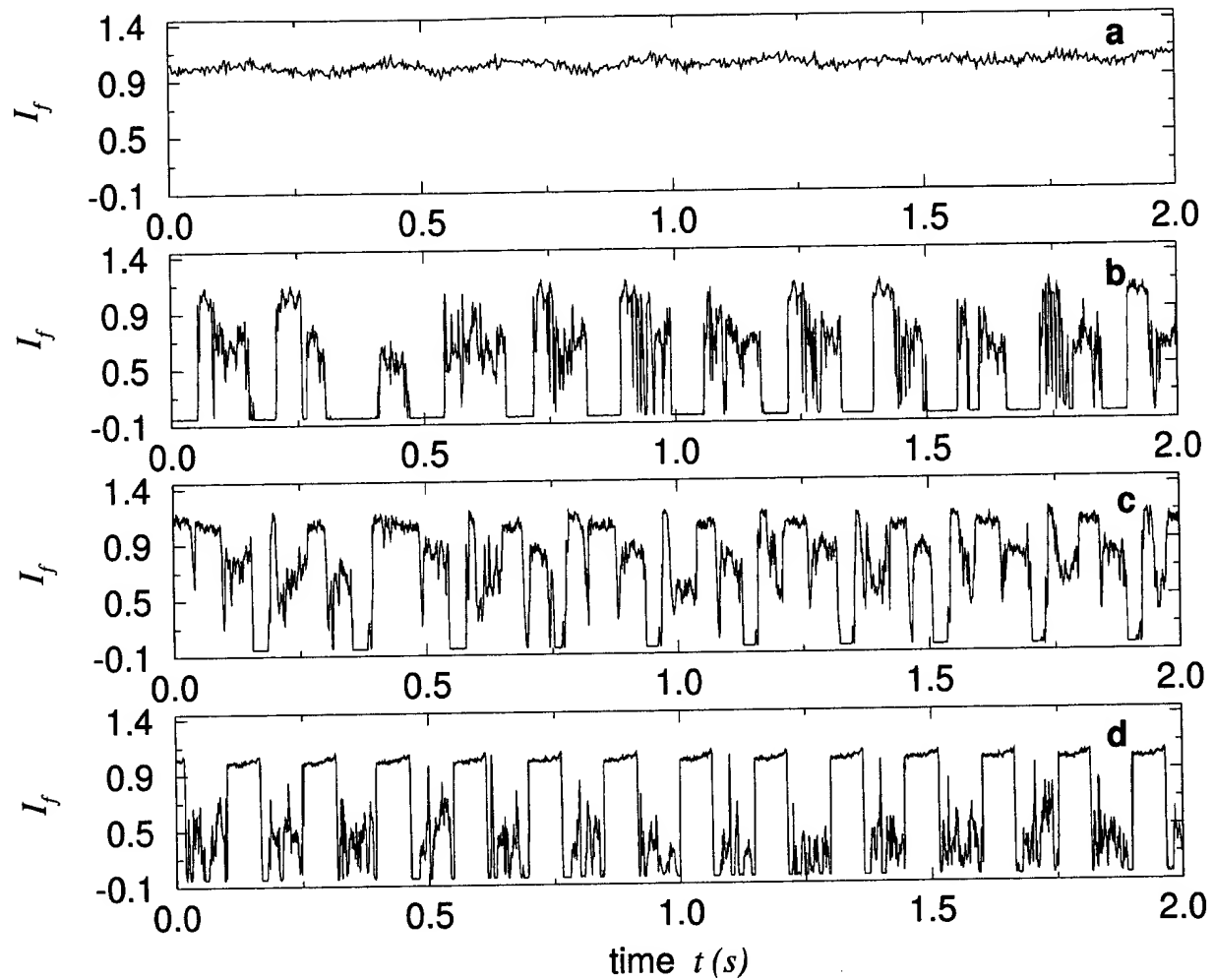


Figure 5.2: Time trace with and without forcing in a wake with $\bar{U} = 40 \text{ cm/s}$ at $x/D = 0.25$. a: no forcing at $y = -0.5 \text{ mm}$; b, c and d: with forcing at $2y/D = 0.75, 0$ and -0.75 respectively.

5.1.2.2 variance The variance of concentration fluctuation is shown in Fig. 5.3 for wake $\bar{U} = 40 \text{ cm/s}$. It is found that in y-direction, the variance is almost the same. Without forcing the variance is actually zero for the whole cross section due to the fact that there is no mixing either for the relative turbulent mixing or for molecular mixing. This indicates that under forcing the fluids have, at least on the large scale, mixed in this local cross section. However, there is little molecular mixing here.

5.1.2.3 probability density function (pdf) The pdf of concentration for wake of $\bar{U} = 40 \text{ cm/s}$ at $x/D = 0.25$ is shown in Fig. 5.4 and it is found that in y-direction the pdf is qualitatively the same and the pdf at the average concentration is already larger than zero. This means either some fluids are already molecularly mixed or the scalar scale is smaller than the spatial resolution. The molecular mixing at scale of $4 \mu\text{m}$ is relatively fast and the time needed is estimated to be less than 0.1 s . Therefore in many cases, the fluids are approximately considered to be molecularly mixed when the measurement shows that they are mixed at the given resolution. Here the pdf for the unmixed high concentration side is wider than its corresponding water side. This is because the shot noise in the signal mentioned above. The high pdf value in the water and dye side implies that the molecular mixing is very poor here.

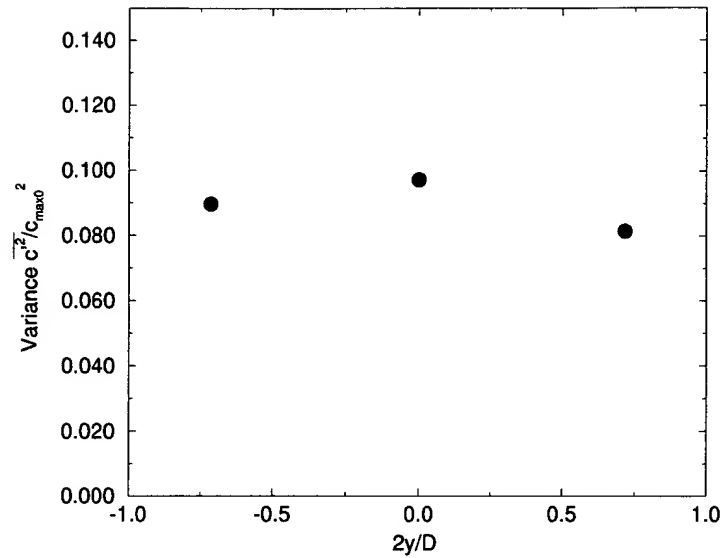


Figure 5.3: Concentration variance for different y-positions under forcing in a wake with $\bar{U} = 40 \text{ cm/s}$ at $x/D = 0.25$.

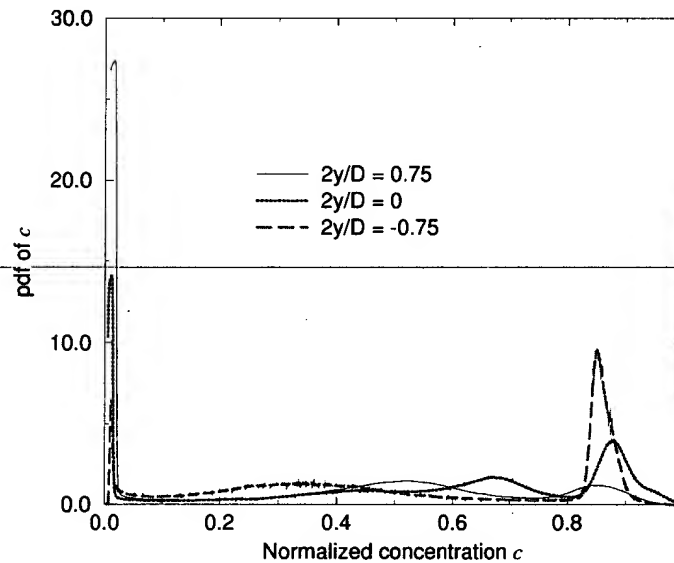


Figure 5.4: pdf under forcing for different y-positions in a wake with $\bar{U} = 40 \text{ cm/s}$ at $x/D = 0.25$.

5.1.2.4 power spectrum density (psd) In Fig. 5.5 the power spectrum density is shown for wake of $\bar{U} = 40 \text{ cm/s}$ at $x/D = 0.25$ and different y-positions. The power spectrum densities for different y-positions are almost the same qualitatively. The sampling frequency is 50 kHz. Fig. 5.5 shows that after around 200 Hz, the psd decreases faster with f in an exponent of about -2.8. This indicates that physical space scale corresponding to 200 Hz dominates in the flow field. Around 3 ~ 5 kHz, psd is almost constant showing that the noise begins dominating the signal. It is difficult to

compare with the unforced one due to the fact that, for the unforced wake, the psd is the same as that of noise.

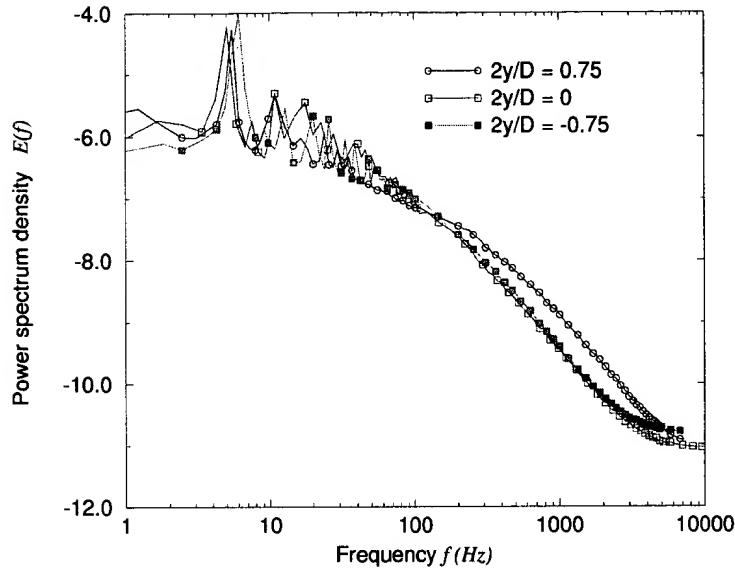


Figure 5.5: Power spectrum density for different y -positions under forcing in a wake with $\bar{U} = 40 \text{ cm/s}$ at $x/D = 0.25$.

5.1.3 Evolution downstream

Fig. 5.6 shows the evolution of timetrace with and without forcing at different x -positions. As in Fig. 5.2 the unforced timetrace in Fig. 5.6a is at approximately $y = -0.5 \text{ mm}$ and $x/D = 0.25$. The forcing condition is the same as above mentioned. For the unforced one, the fluids are completely separated, but they have already partially mixed at least for the relative turbulent mixing in the forced case. In Fig. 5.6b where $x/D = 1.6$, the wake has already spread out for the unforced one and its measured result shows that the fluids are clearly unmixed, and the signal is quasi periodic and fluctuates from water to dye. However, the average concentration for the forced one is almost achieved. Fig. 5.6c shows that for the unforced one at $x/D = 7.5$, most of the fluids are still completely separated, but there are more small scales than that at $x/D = 1.6$. However, the fluids are almost mixed on the scale of measurement resolution for the forced one. The fluids are partially mixed in Fig. 5.6d for the unforced one where $x/D = 25.4$ and there are much more small scales than that at $x/D = 7.5$. For the excited one, the fluids seems already completely mixed.

Fig. 5.7 displays the evolution of fluctuation intensity. It can be seen that the difference between forced and unforced is dramatic especially for small x -positions. At $x/D = 7.5$, for the forced one, the fluctuation intensity is almost zero, i.e. $\bar{c}^2/c_{max}^2 = 2.99 \times 10^{-3}$, but for the unforced one, $\bar{c}^2/c_{max}^2 = 1.46 \times 10^{-1}$. At $x/D = 25.4$, \bar{c}^2/c_{max}^2 is 2.73×10^{-4} and 7.07×10^{-2} respectively for the forced and unforced wakes. According to pdf (see later), the fluids can be considered mixed molecularly at $x/D = 25.4$. The time needed for molecular mixing in the forced wake x/\bar{U} is smaller than 2.6 s. It is impossible to compare the mixing time, because for the unforced wake, the fluids are still not mixed at the last x -position. In a mixing process, the variance changes from zero at the beginning to a maximum value by large scale mixing without molecular mixing, and then decays to zero again by molecular mixing or dissipation. The decay time constant τ_d should be quite different between the forced and unforced wake.

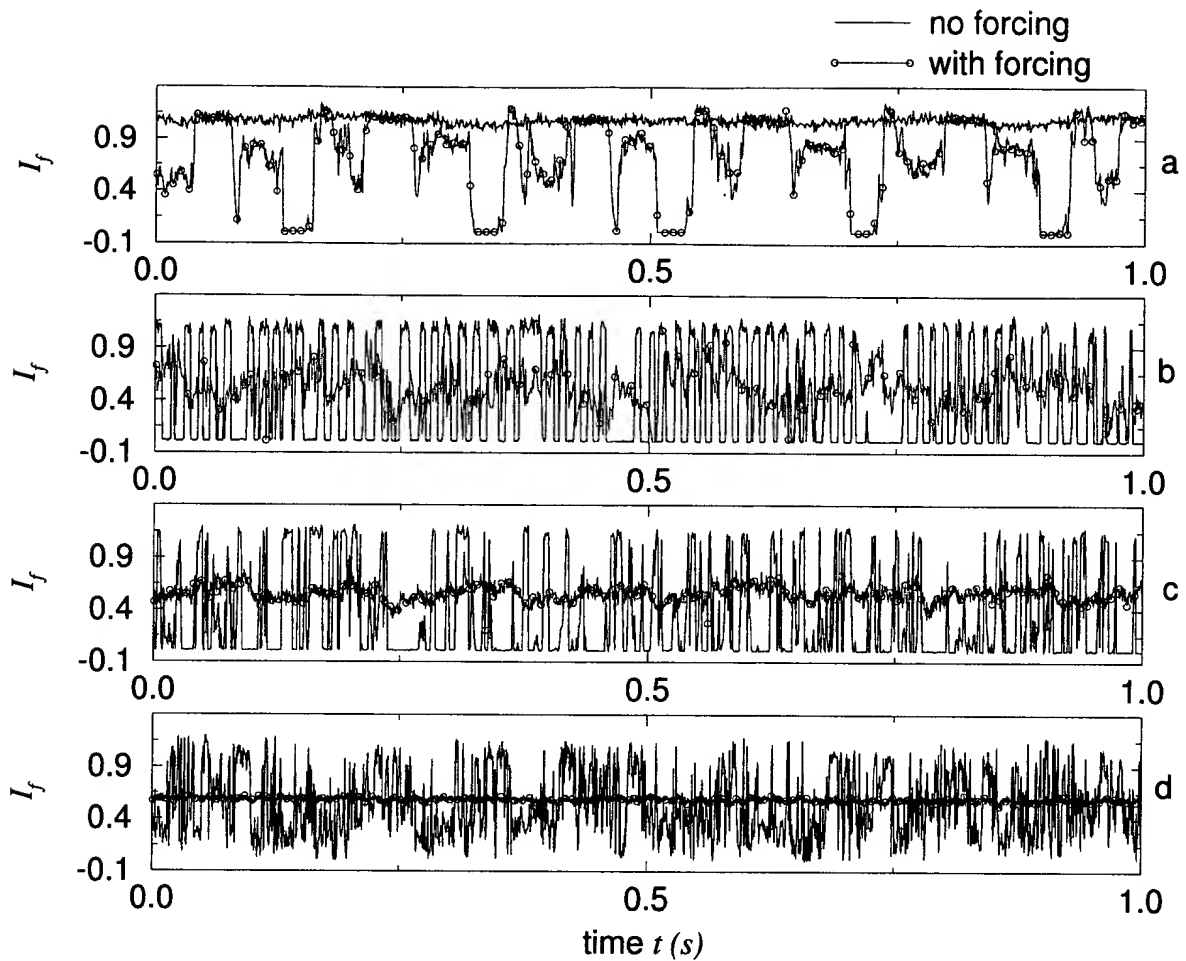


Figure 5.6: Timetrace with and without forcing in a wake with $\bar{U} = 40 \text{ cm/s}$ at different downstream positions. a: $x/D = 0.25$; b: $x/D = 1.6$; c: $x/D = 7.5$; d: $x/D = 25.4$.

Fig. 5.8 shows the pdf of c under forcing. At $x/D = 0.25$, the pdf at its average c has already a maximum value. The pdf has its higher peaks at c corresponding to water and dye, indicating the fluids are not molecularly mixed. The c is not only condensed at the pure unmixed fluid, but also has widely non-zero contribution of concentration between the unmixed fluids. At $x/D = 0.71$, the distribution of pdf is similar to that of $x/D = 0.25$, but higher at the average point of c . The pdf distribution at $x/D = 1.6$ is concentrated at the average point of c and does not peak in the high c side and its distribution is nearly symmetric. From $x/D = 4.4$, no peak for the c corresponding to unmixed water can be distinguished. At $x/D = 25.4$, the pdf does not concentrate to the point of the average c , i.e. approximately a Delta function, but has a nearly Gaussian distribution around it. This is also due to the shot noise in the signal.

The comparison of pdf for the forced and unforced wakes is shown in Fig. 5.9 at three x -positions. At $x/D = 1.6$ and 7.5 , the pdf distributes only on the pure water and dye for without forcing, but for the forcing cases, the pdf already has a peak at the average c . At $x/D = 25.4$ for the unforced one, the peak of pure dye concentration disappears, but there still exists a peak for pure water c . This indicates the pure dye c is smoothed by shot noise. The concentration c is widely distributed and no peak at the average c can be obtained. For the forced one, the mixing is already finished according to its pdf distribution.

In Fig. 5.10 the evolution of psd $E(f)$ with forcing is displayed. It can be seen that there is already -1 and -5/3 exponent at $x/D = 1.6$. There is no -1 exponent at $x/D = 0.25$ and 0.71 . At $x/D = 1.6$, the -1 spectrum is obvious in the range of $10 \sim 500 \text{ Hz}$. At $x/D = 3.0, 4.4$ and 7.5 , the -1 spectrum

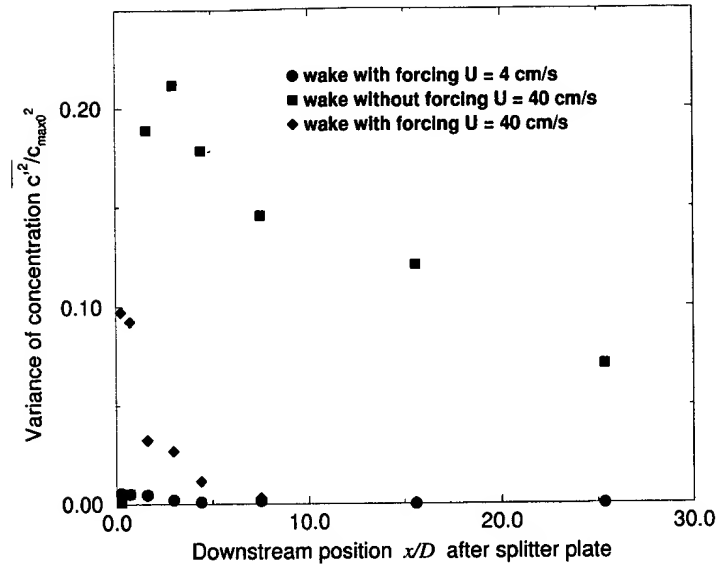


Figure 5.7: Concentration variance evolution along x-positions with and without forcing in wakes.

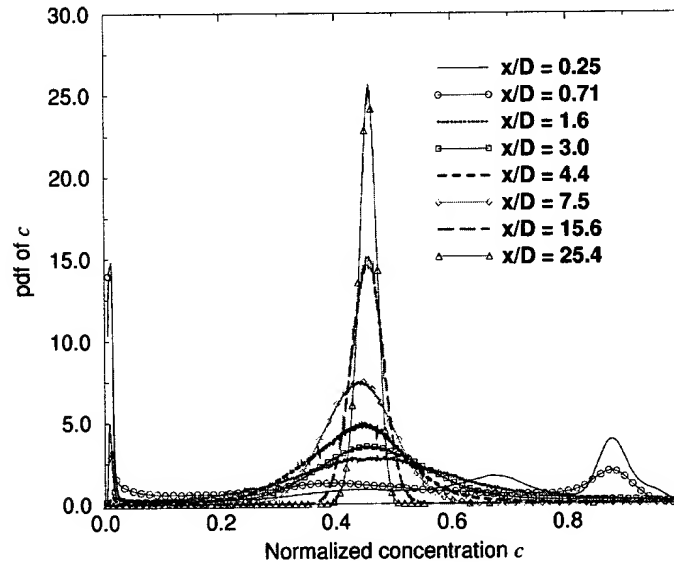


Figure 5.8: pdf under forcing for different x-positions in a wake with $\bar{U} = 40 \text{ cm/s}$.

ranges are $10 \sim 900 \text{ Hz}$, $10 \sim 1000$ and $10 \sim 1000$ respectively. At $x/D = 15.6$, the -1 exponent is between $1 \sim 6000 \text{ Hz}$. The -1 spectrum range increases downstream (from $x/D = 1.6 \sim 15.6$) until molecular mixing is finished according to pdf result (at $x/D = 25.4$). The spectrum decays along x-direction keeping the -1 exponent before molecular mixing ends.

The -5/3 range increases at first until some point (at $x/D = 7.5$, where pdf result shows that, the molecular mixing is still not finished), then decreases with the x-position until it disappears (after $x/D = 15.6$). At $x/D = 0.25$, there is approximately a -5/3 exponent in the frequency range of 10

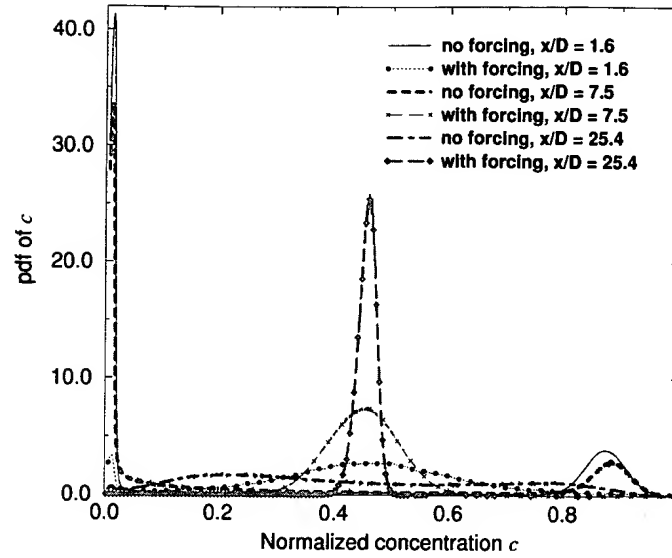


Figure 5.9: Comparison between the pdf results of with and without forcing in a wake with $\bar{U} = 40 \text{ cm/s}$.

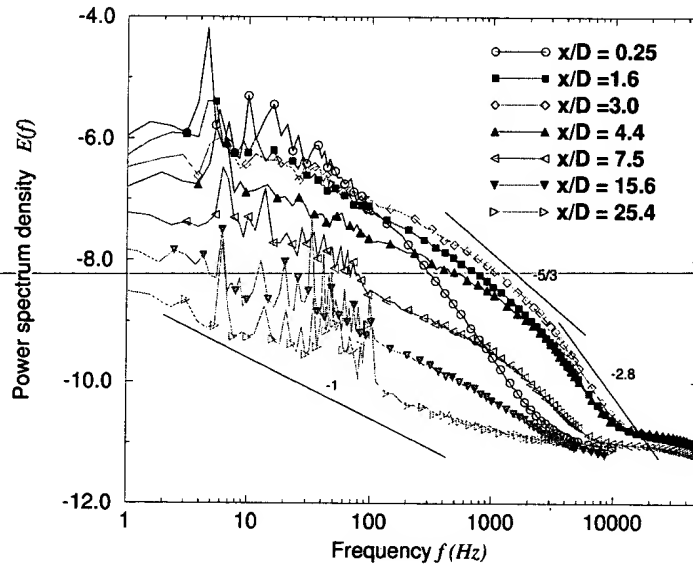


Figure 5.10: Power spectrum density evolution for different x-positions under forcing in a wake with $\bar{U} = 40 \text{ cm/s}$.

$\sim 100 \text{ Hz}$. After around 100 Hz , the spectrum decreases quickly through an exponent of about -2.8 until about 3 kHz where noise begins to dominate. At $x/D = 1.6, 3.0$ and 4.4 , the $-5/3$ is around the range of $300 \sim 2000 \text{ Hz}$, $500 \sim 3000$ and $600 \sim 2000 \text{ Hz}$ respectively followed by a -2.8 exponent. At $x/D = 7.5$, the $-5/3$ is in the range of $700 \sim 8000 \text{ Hz}$. After 8000 Hz , the noise dominates and no signal can be distinguished. If dissipation intermittency is not concerned for simplification, the $-5/3$ exponent spectrum indicates that there are its corresponding eddies with space filling in the physical

space which originates from the larger scale instability.

Fig. 5.11 gives the comparison of $E(f)$ between with and without forcing. It is obvious that the spectrum with forcing at $x/D = 1.6$ is similar to that without forcing at $x/D = 25.4$, but the power of the former is smaller than that of the latter and identical to Fig. 5.7. Both spectrum has a similar large -1 exponent range. This indicates that the small structures, which are created once the scalar has traveled far enough downstream from the trailing edge, i.e. when Re is large enough, can be achieved much earlier with strong forcing. However, after the -1 exponent, the decay exponent for unforced is steeper (about -3.5) than for the forced one (-2.8).

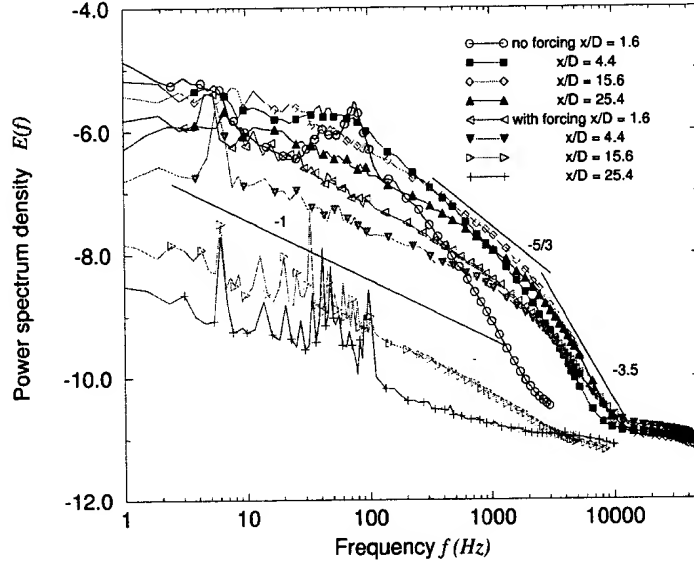


Figure 5.11: Comparison for power spectrum density evolution for different x -positions with and without forcing in a wake with $\bar{U} = 40 \text{ cm/s}$.

At $x/D = 4.4$ there is a $-5/3$ exponent in the range of around $80 \sim 400 \text{ Hz}$ for the unforced situation, but this does not correspond to the Kolmogorov spectrum, since it is the exponent evolution from value smaller than $-5/3$ to -1 asymptotically along the x -position, compared with the spectrum of $x/D = 1.6$ and 15.6 .

It should also be noted, that some comparisons introduced above are conducted in the center of the wake, and that the difference at the near wall region for the forced and unforced wakes can be expected to be even more apparent than the center one according to the results of different y -positions at $x/D = 0.25$.

5.2 Mixing layer

The above mentioned rapid mixing process in a wake can also be obtained in a mixing layer. The results for a mixing layer of $U_1 = 48 \text{ cm/s}$ and $U_2 = 32 \text{ cm/s}$ is shown as follows.

5.2.1 Concentration distribution at near field

The variance of concentration of the mixing layer at $x/D = 0.25$ for different y -positions is shown in Fig. 5.12. Unlike the wake result, the variance distribution is not homogeneous in the mixing layer cross section and the variance is higher in the low velocity side ($2y/D = -0.75$). This indicates that the flow characteristic in the high velocity side is different from that of the low one. The mixing in the high velocity side is stronger than that in the low velocity side. This result is related to a

new phenomenon called symmetric breaking hysteresis which will be discussed in Part 2 of this work. Although the variance is not homogeneous in the local y -positions at $x/D = 0.25$, the mixing is very much enhanced under strong forcing.

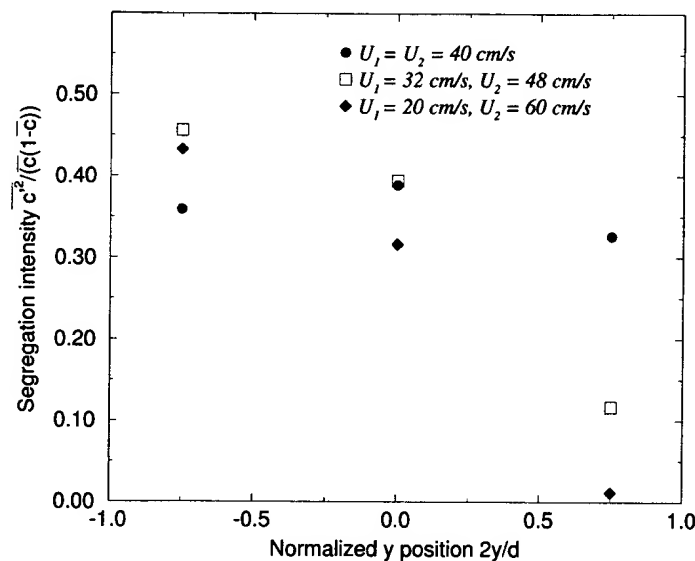


Figure 5.12: Concentration variance for different y -positions under forcing in a wake and different mixing layers at $x/D = 0.25$.

Fig. 5.13 presents the pdf result. The pdf is qualitatively similar for the three different y -positions and there are three peaks for pdf. Two of them are for pure dye and water respectively and one for the average concentration point \bar{C} . However, in the high velocity side (water side), the pdf value of concentration corresponding to pure water is much higher than the other two peaks due to two reasons: the pure water has high volume rate and low shot noise in the signal.

The psd $E(f)$ of the mixing layer is given in Fig. 5.14. The spectrums are also qualitatively similar except that at $2y/D = 0.75$, the spectrum is a little lower than the other two in the frequency range of 20 ~ 200 Hz. All the spectrums have a -5/3 exponent in the frequency range of around 10 ~ 200 Hz followed by a -2.8 exponent until about 3000 Hz, indicating that there are small structures and their contribution to psd is not small in the whole local cross section even at the near field ($x/D = 0.25$).

5.2.2 Evolution downstream

The evolution of concentration variance is shown in Fig. 5.15. Like the case of wake, with forcing the variance decays very fast and is almost zero at $x/D = 7.5$.

For the forced one, Fig. 5.16 shows its pdf evolution. At $x/D = 0.25$, there is already an apparent peak at the average \bar{C} and at $x/D = 25.4$, pdf has a narrow Gaussian distribution around its average \bar{C} . This indicates that the fluids have already mixed between $x/D = 15.6$ and 25.4. The comparison between forced and unforced pdf is shown in Fig. 5.17. For the unforced situation, even at $x/D = 15.6$, emerges no apparent peak at the average c and a peak for pure water is still discernible. The huge difference of pdf between the forced and unforced flow is obvious.

The psd of the unforced mixing layer can be seen in Fig. 5.18. The spectrum evolution is similar to that of the unforced wake in Fig. 5.11. No -5/3 exponent can be observed even at the last x -position of $X/D = 25.4$. There are mainly two exponents, i.e. -1 and -3.5. The psd of the forced mixing layer can be seen in Fig. 5.19. Qualitatively the evolution in psd in the forced flow is similar to that of the forced wake shown in Fig. 5.10. Between $x/D = 1.6 \sim 4.4$, there are mainly -1 and -2.8 exponents. At

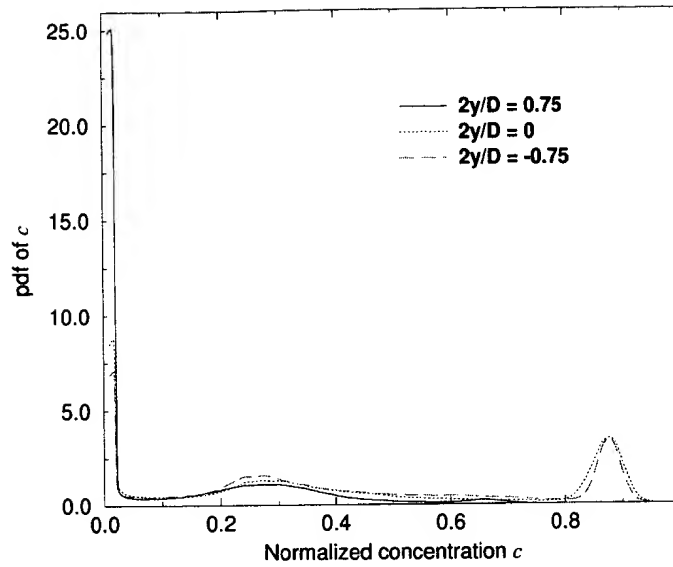


Figure 5.13: pdf under forcing for different y -positions in a mixing layer with $U_1 = 48 \text{ cm/s}$ and $\lambda = 0.2$ at $x/D = 0.25$.

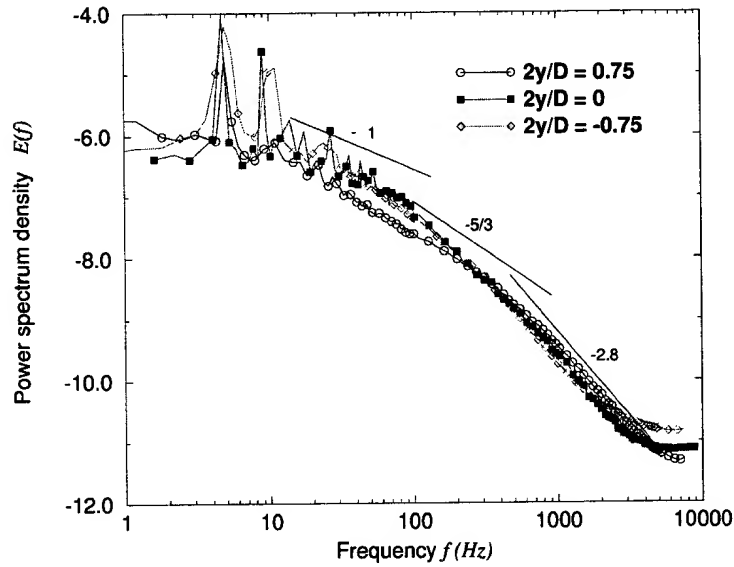


Figure 5.14: Power spectrum density for different y -positions under forcing in a mixing layer with $U_1 = 48 \text{ cm/s}$ and $\lambda = 0.2$ at $x/D = 0.25$.

$x/D = 7.5$, there is clearly a $-5/3$ spectrum in the range of $500 \sim 7000 \text{ Hz}$. The comparison between the forced and unforced psd is given in Fig. 5.20. Combined with the result of variance evolution, the turbulent mixing difference is very large between the forced and unforced mixing layer.

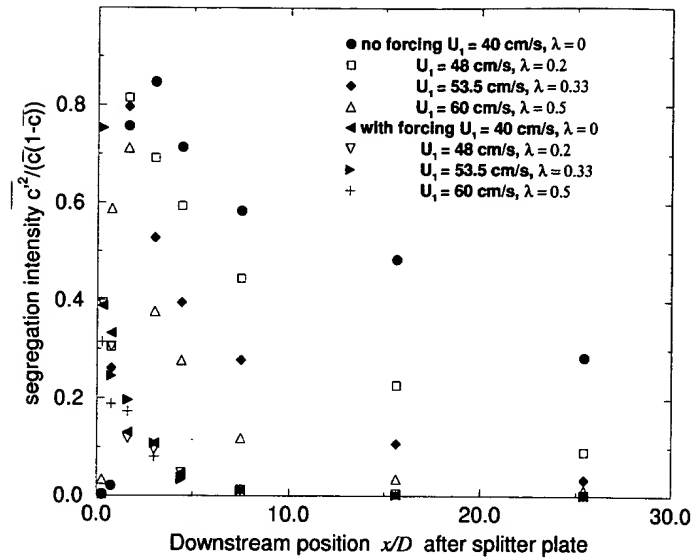


Figure 5.15: Concentration variance for different x -positions under forcing in different mixing layers with and without forcing.

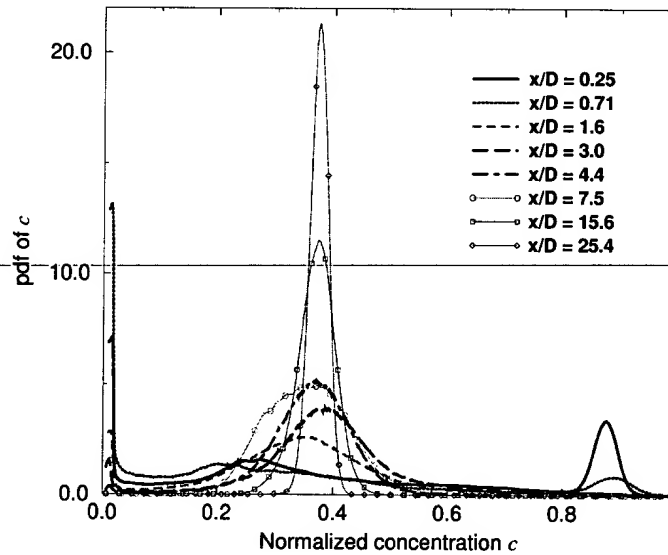


Figure 5.16: pdf with forcing for different x -positions in a mixing layer with $U_1 = 48 \text{ cm/s}$ and $\lambda = 0.2$.

5.3 Influence of Reynolds number

The rapid relative turbulent mixing happens not only for the relative moderate Reynolds number, it is especially apparent for low Reynolds number. For a wake of $\bar{U} = 1 \text{ cm/s}$ without forcing, the corresponding Re based on pipe diameter is about 400, 40 times smaller than the wake shown above. (It should be cleared that the Reynolds number based on pipe diameter is not the best choice, since the physical process could be more closely related to the initial momentum thickness of the wake. The

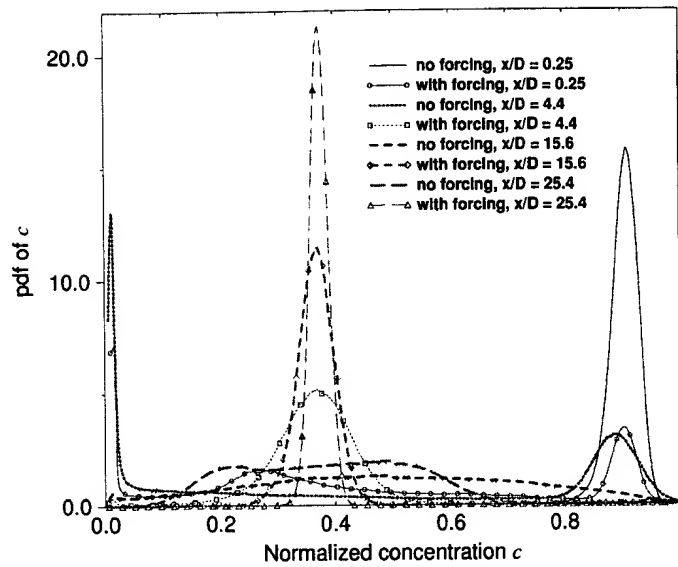


Figure 5.17: Comparison between the results of with and without forcing for pdf in a mixing layer with $U_1 = 48 \text{ cm/s}$ and $\lambda = 0.2$.

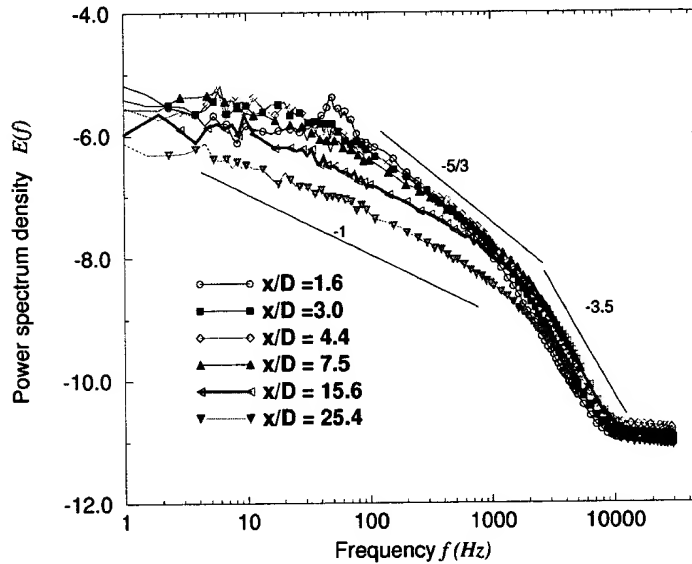


Figure 5.18: psd $E(f)$ without forcing for different x -positions in a mixing layer with $U_1 = 48 \text{ cm/s}$ and $\lambda = 0.2$.

pipe diameter is used here just for simplicity.) There is almost no mixing in the whole pipe (2 m) according to the visualization. The input contraction has influence on the critical Reynolds number Re_c [27] from laminar to turbulence and the favorable input condition used here makes Re_c larger than 2100. The flow is laminar within 2 m of the pipe because of the low Re although there is a wake in the input of the pipe. For the laminar flow, it needs at least 150 D for the fluids to be mixed molecularly.

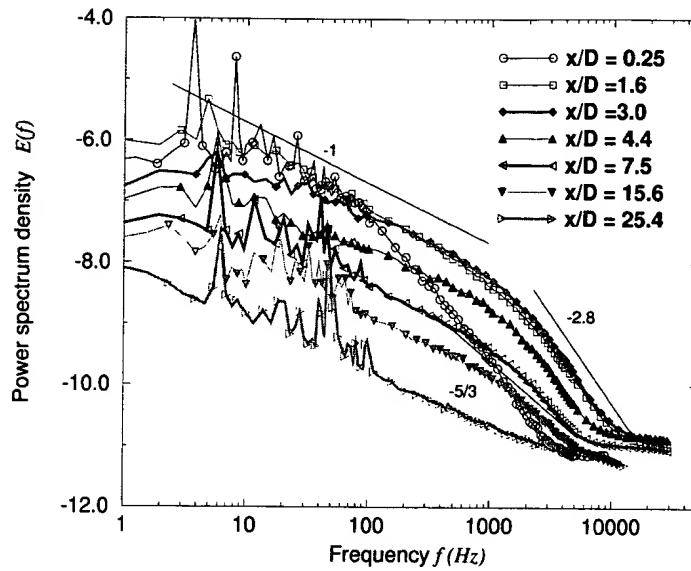


Figure 5.19: psd $E(f)$ with forcing for different x -positions in a mixing layer with $U_1 = 48 \text{ cm/s}$ and $\lambda = 0.2$.

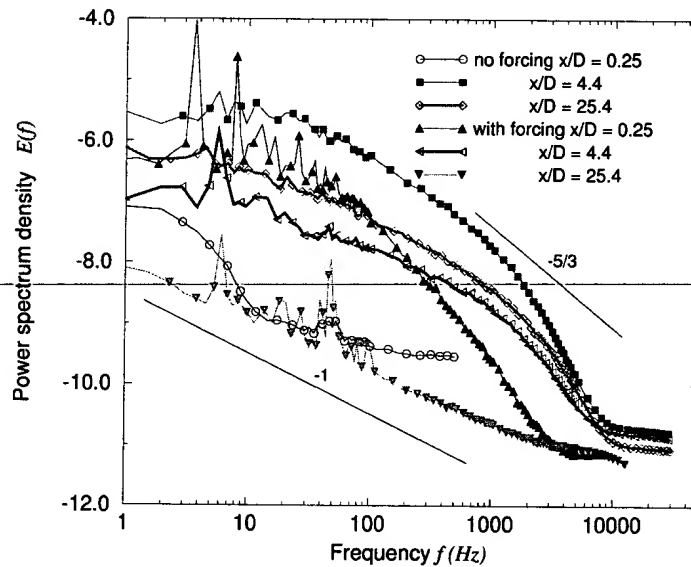


Figure 5.20: Comparison between the results of with and without forcing for psd in a mixing layer with $U_1 = 48 \text{ cm/s}$ and $\lambda = 0.2$.

However, with strong forcing, the fluid has almost already mixed (at least for the relative turbulent mixing) at $x/D = 0.25$ according to the timetrace and pdf results. The timetrace, variance, pdf and $E(f)$ for different y -positions for the wake of the low Reynolds number with strong forcing of amplitude about 100% is shown in Fig. 5.21, Fig. 5.22, Fig. 5.23 and Fig. 5.24 respectively. For such a wake with low Re in a pipe under strong forcing at $x/D = 0.25$, there is already the inertial subrange spectrum with a $-5/3$ exponent. It should be noted that all results are asymmetric in y -direction for the wake of

low Reynolds number. The asymmetric result in y-direction is due to a symmetric breaking hysteresis and will be explained in part 2.

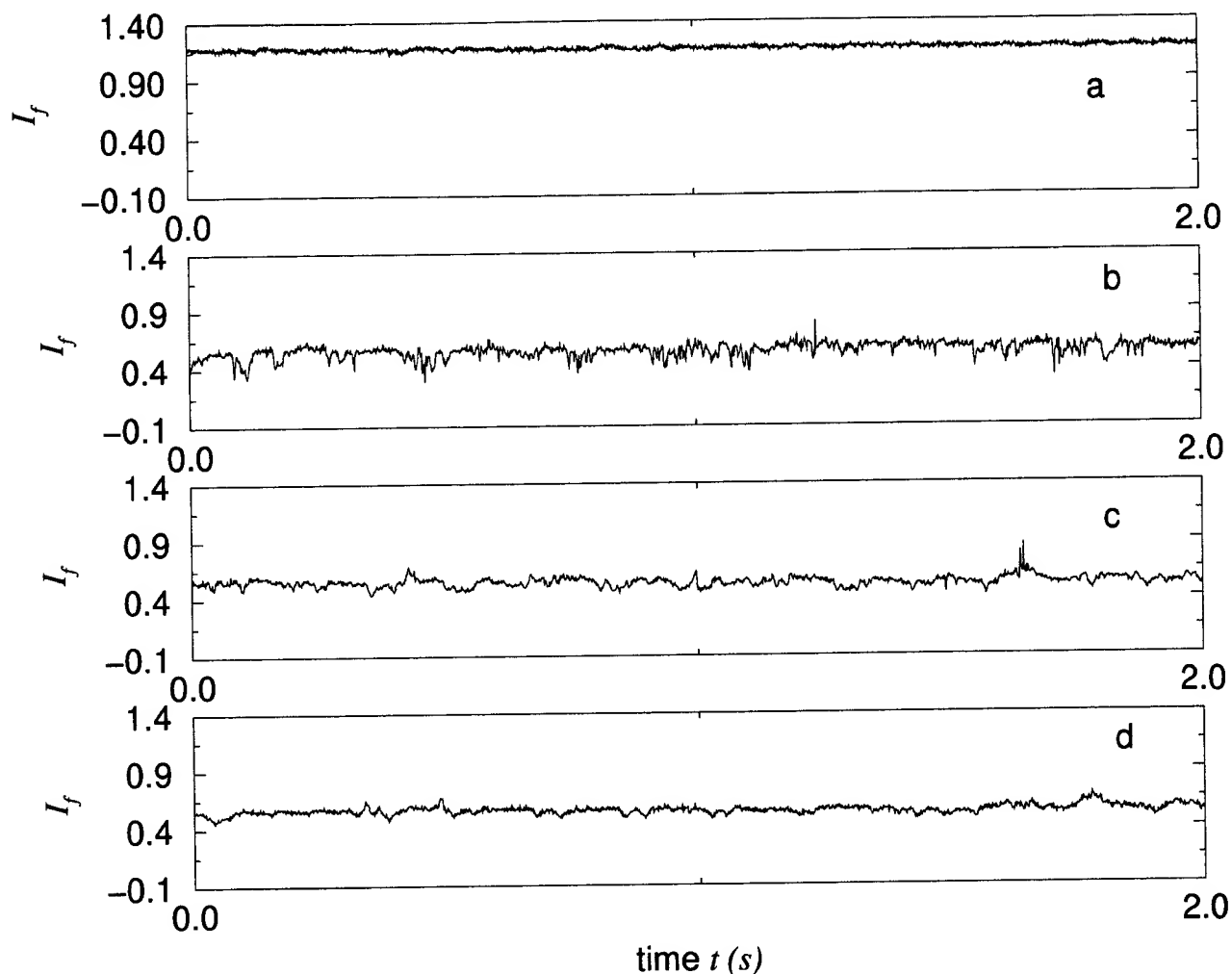


Figure 5.21: Timetrace of different y-positions with and without forcing in a wake with $\bar{U} = 1$ cm/s at $x/D = 0.25$. a: no forcing; b, c and d: with forcing at $2y/D = 0.75, 0$ and -0.75 respectively.

5.4 Influence of initial velocity ratio λ

The initial velocity parameter for mixing layer is $(\lambda = U_1 - U_2)/(U_1 + U_2)$. The influence of λ on mixing with and without forcing can, for instance, be seen in Fig. 5.12 and Fig. 5.15 through the variance. Here the Reynolds numbers based on the average velocity and pipe diameter are the same, but λ is different. U_1 are 40, 48, 53.5 and 60 cm/s and U_2 40, 32, 26.5 and 20 respectively. $\bar{U} = (U_1 + U_2)/2$ is 40 cm/s for all cases and λ are 0, 0.2, 0.33 and 0.5 respectively. The forcing frequency is around 6 Hz for all cases and the forcing levels for $U_1 = 40, 48, 53.5$ and 60 cm/s are 45, 52, 59 and 40 percent respectively. The forcing frequency is almost the same around 6 Hz. It can be seen in Fig. 5.12 that the asymmetry in y-direction increases with λ and in the higher velocity side, the mixing is stronger than that of the low velocity side.

According to the results of variance evolution in Fig. 5.15, for the unforced one, the higher λ is, the better the mixing is. However, for the strong forced one, the difference is not so evident as that

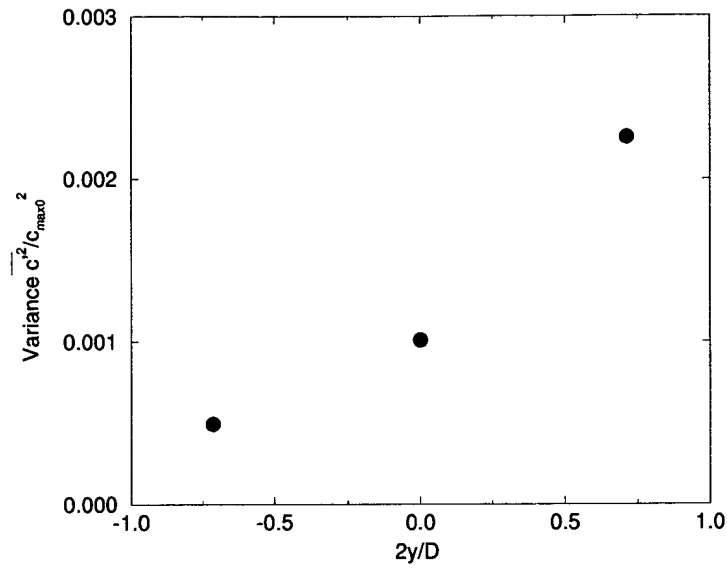


Figure 5.22: Concentration variance for different y-positions under forcing in a wake with $\bar{U} = 1 \text{ cm/s}$ at $x/D = 0.25$.

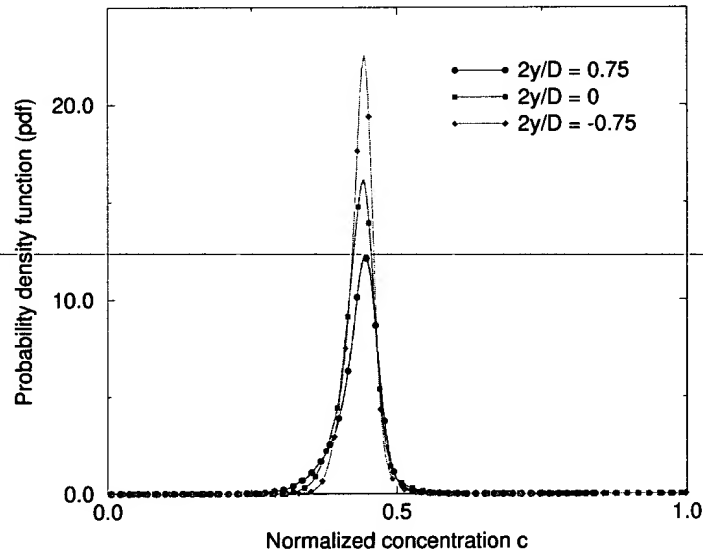


Figure 5.23: pdf under forcing for different y-positions in a wake with $\bar{U} = 1 \text{ cm/s}$ at $x/D = 0.25$.

of unforced one, i.e. the forcing is so strong that the λ influence is not important. This result also indicates that the forcing is more efficient for wake than mixing layer.

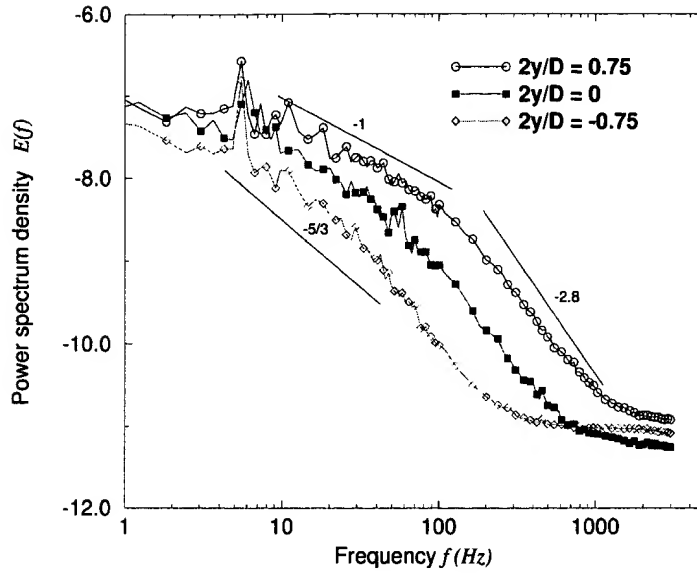


Figure 5.24: Power spectrum density for different y -positions under forcing in a wake with $\bar{U} = 1 \text{ cm/s}$ at $x/D = 0.25$.

5.5 Influence of forcing frequency

Here it is only necessary to mention that in the light of receptivity theory, there is only one frequency, under which the forcing has a maximum mixing enhancement if the forcing level is small. When the forcing level is large enough, however, the influence of the non-linear effect comes into play and the effect of forcing frequency on mixing is complicated and will be discussed in part 2. Here it is only necessary to mention that the above mentioned forcing frequencies are all undertaken around 6 Hz.

5.6 Influence of forcing level

Here it is only necessary to state that at a given forcing frequency, the higher the forcing level, the stronger the mixing, if there is the receptivity in a flow. However the effect of the forcing level on mixing depends on the receptivity mechanism and forcing frequency; the influence of the forcing level on mixing efficiency is also complicated and all this will be discussed in part 2.

5.7 Relative turbulent mixing rate R_r

According to the results of timetrace, variance, pdf and psd distribution shown above, the ideal relative turbulent mixing process and state mentioned earlier are approximately realized. Let us consider the examples of wake with $\bar{U} = 1 \text{ cm/s}$ and $\bar{U} = 40 \text{ cm/s}$. Compared to the unforced situation, the fluids in the forcing situation of $\bar{U} = 40 \text{ cm/s}$, are first quickly mixed on large scales and a small partial fine scale at $x/D = 0.25$ in the whole local cross section with little molecular mixing and then quickly become to small scales filling the space with partial molecular mixing until the position of x/D is in the range of from 4.4 to 7.5. In this region the small scale will have more and more contribution for psd and the large one less and less relatively. The process from the beginning of the wake to this region is approximately the ideal relative turbulent mixing process and the state in this region is the ideal relative turbulent mixing state. After the ideal relative turbulent mixing state, molecular mixing proceeds very fast because of the small scale structures until molecular scale is homogeneous for x/D being from 15.6 to 25.4.

It is difficult to estimate the physical size of small scale and its distribution in the flow. From spectrum, we can only know the eddy distribution. Unfortunately, the exact relation between the eddy and physical space scale is not clear. Therefore the estimation used here is just an approximation to express a picture for the physical process of ideal relative turbulent mixing process. For the sake of simplification, we consider the situation that l_s is l_K .

For low Re , in the wake of $\bar{U} = 1 \text{ cm/s}$ at $x/D = 0.25$, the end of $-5/3$ exponent spectrum f_K is around 120 Hz. Its corresponding $l_K \approx \bar{U}/f \approx 83 \text{ } \mu\text{m}$. According to eqn (2.6), it can be estimated, that the time t_m needed for initial dye of concentration $c \approx 1$ to decay to 0.5 is $\sqrt{D_m t_m}/h^2 \approx 1.2$, i.e., $t_m \approx 0.95 \text{ s}$. The time $T_s \approx x/\bar{U} \approx 1 \text{ s}$. Therefore $R_r \approx t_m/T_s \approx 0.95$. For the wake $\bar{U} = 40 \text{ cm/s}$ at $x/D = 7.5$, the end of $-5/3$ exponent spectrum f_K is around 6000 Hz. Its corresponding l_K is $67 \text{ } \mu\text{m}$. t_m is about 0.8 s. The time T_s is also around 0.8 s. Therefore R_r is about 1. Thus the ideal relative turbulent mixing process is approximately realized in these experiments under the given conditions.

5.8 Power spectrum density

5.8.1 $-5/3$ exponent with low Reynolds number

Fig. 5.25 represents the result that even at low Reynolds number (i.e. here a laminar flow without forcing), under strong forcing there can be a $-5/3$ exponent of concentration psd, which usually should be obtained at high Reynolds number. Three flows are considered here. One is a wake with low Re about 420 based on pipe diameter and average velocity $\bar{U} = 1 \text{ cm/s}$; another is a mixing layer with Re about 3150 based on the pipe diameter and the average velocity $\bar{U} = (U_1 + U_2)/2 = 7.5 \text{ cm/s}$; the other is a mixing layer with Re about 33500 based on the pipe diameter and the average velocity $\bar{U} = 80 \text{ cm/s}$. Both mixing layer have the same $\lambda = 0.5$.

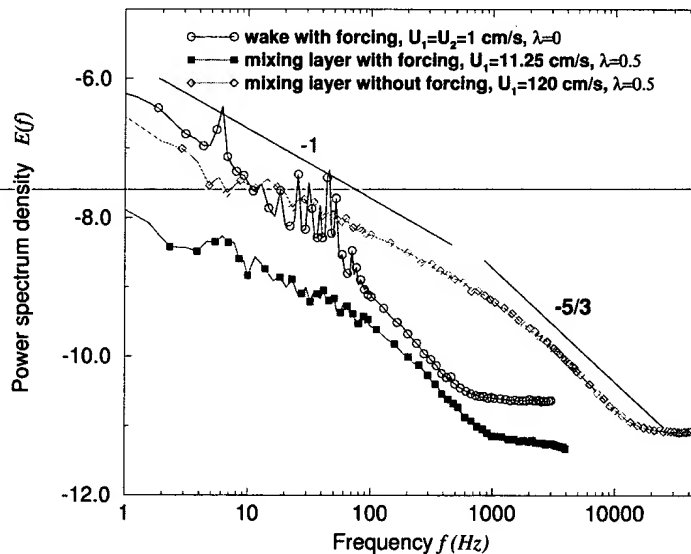


Figure 5.25: Power spectrum density with $-5/3$ exponent for different Re .

The forcing level for the wake and the low Reynolds number mixing layer is around 100%, and 75% respectively; the forcing frequency is around 6 Hz. For the large Reynolds number mixing layer no forcing is supplied. The downstream x -positions for the measurement are different: The x/D for wake, small and large Reynolds number mixing layer are 1.6, 4.4 and 25.4 respectively. It can be seen that all the three flows have a $-5/3$ exponent. The fluctuation of psd for the wake in the region of $20 \sim 70$ Hz is from the noise, which is resulted in as the water surface in the water vessel oscillates slightly

due to the strong forcing. This is because of the extremely high spatial resolution. Unfortunately it is impossible to tell at which frequency the $-5/3$ ends and what spectrums exist after $-5/3$ exponent, because before the end of $-5/3$ spectrum, the shot noise in the signal has already been higher than signal.

For a given Re the psd form at a long distance downstream position without forcing can also be obtained much earlier with forcing. This can be seen in Fig. 5.11, where the psd form of the wake at $x/D = 25.4$ without forcing is similar to that at $x/D = 1.6$ with forcing.

5.8.2 Batchelor -1 spectrum beyond $-5/3$

No -1 region beyond $-5/3$ exponent for psd can be obtained. For high Re , although the spatial resolution is high enough to measure at least partial region of Batchelor spectrum, no -1 region can be obtained as in the case of Fig. 5.25. The main factor making the measurement for Batchelor spectrum region impossible is the shot noise which begins dominating and is even higher than the signal before the end of $-5/3$ region. This makes it impossible to see if there is a -1 exponent region after $-5/3$ region. However, for forced low Reynolds number, the signal frequency-band is narrow, so that the SNR is relatively improved; the smallest scale is larger for low Re so that the spatial resolution will be relatively higher. Fig. 5.26 shows the forced wakes with low Re . The wake with $\bar{U} = 1 \text{ cm/s}$ at $x/D = 0.25$, displays a $-5/3$ exponent in the region of about $10 \sim 120 \text{ Hz}$ followed by an approximately -2.8 exponent region clearly instead of -1 . The wake with $\bar{U} = 4 \text{ cm/s}$ at $x/D = 3$ has a $-5/3$ exponent in the region of about $90 \sim 360 \text{ Hz}$ and after $-5/3$ region there is also no -1 , but instead, somewhat -2.8 exponent. For these two wakes, the experiment spatial resolution is in the same order as Batchelor scale, i.e. at least sufficient to measure partial -1 exponent spectrum if there is.

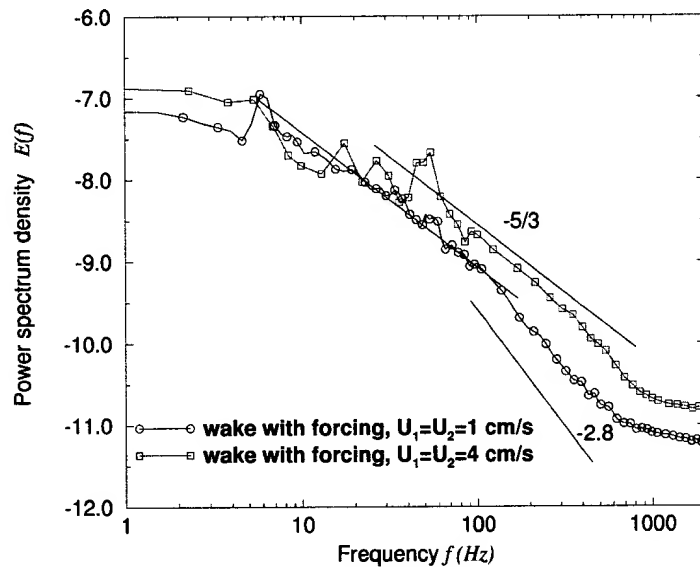


Figure 5.26: Power spectrum density for different flows with no -1 spectrum exponent beyond $-5/3$ region.

5.8.3 -1 exponent before $-5/3$

All the results of psd, with and without forcing, demonstrate that the psd changes asymptotically to -1 exponent from large to small scale, for instance, as clearly shown in Fig. 5.25 and Fig. 5.11. This indicates that the -1 exponent is more universal than $-5/3$ and others at least in the experimental

conditions used here. The -1 exponent spectrum establishes first in the low frequency range, i.e. large scalar structures, then moves asymptotically from low to high frequency. The psd decays downstream, but keeps in -1 exponent until the fluids are molecularly mixed or mixed in the measuring resolution.

6 Discussion

6.1 Homogeneous whole local flow fields

There are two important requirements for the ideal relative turbulent mixing process: the whole local homogeneous cross section and $T_s \leq t_m$. The whole local homogeneous cross section means that at each local position downstream from the initial mixing state, the whole cross section perpendicular to the streamwise direction is homogeneous. This is corresponding to the cases of free and wall boundary turbulent flows (including flow in pipe and static mixer). For stirred tank, the whole local homogeneous cross section means the whole tank. The whole local homogeneous cross section is very difficult to be realized for normal flows and is therefore a strong restriction. This actually also implies a relative turbulent mixing criterion. The whole local homogeneous cross section at short downstream distance indicates that the ratio of mixing in the transverse direction to the bulk convection is extremely high. The above given comparisons in the center of wake and mixing layer in y-direction have shown the dramatic difference of mixing with and without forcing. The difference is actually even more obvious in the near wall region. This is especially shown in the comparisons of position of $x/D = 0.25$. It indicates that the forcing has higher efficiency for mixing in the whole flow field rather than just the center of the wakes and that the extent of homogeneity of the whole flow field is also an important criterion for the ideal relative turbulent mixing process. It should also be mentioned that although the measurement is only undertaken in a two dimensional surface, it can be extrapolated that the mixing in three dimensions is also in the same order, since the most difficult region for mixing is in the near wall region of initial x-position, i.e. here $2y/D = 0.75$ and -0.75 with $x/D = 0.25$, and if the fluids in these region is mixed, the fluids downstream should be also mixed.

6.2 Control between l_K and l_B

It could be expected that, in order to control in the region of l_k and l_B , i.e. prompt the process for l_k to become l_B , the energy must be inputted in the corresponding frequency region and there should be no influence on scalar structure in these high frequency region if the input energy is inputted in the large scale region, i.e., low frequency region. From Fig. 5.11 at $x/D = 4.4$, the comparison shows that the smallest scale with forcing is much smaller than that without forcing. The difference is here about an order. This indicates that the region from l_k to l_B can, at least, be controlled *indirectly*. Here indirectly means that the l_k of the forced one is smaller than that of unforced one, i.e. with the reduction of small scale l_k through the control of low frequencies corresponding to large scale. The corresponding *directly* means that the forcing is undertaken at high frequencies corresponding to the region from l_k to l_B .

6.3 Comment on ideal relative turbulent mixing process

The traditional turbulent mixing criteria (for example, segregation intensity, pdf and variance decay rate) are useful to describe mixing goodness and rate, but the new concept of ideal relative turbulent mixing process help us to search for an optimized mixing control.

The proposed ideal relative turbulent mixing process is, for controlling the flow, a useful model, which can, in turn, be used for the mixing and reaction estimation, since the range of scale and concentration variation is largely reduced. Thus, the flow can be regarded as that, the small scale scalar fills the physical spacing and distributed homogeneously at nearly initial concentration. When the ideal relative turbulent mixing state is achieved, the mixing can be estimated at the scale of, for example, l_k (by eqn (2.6)) with approximately initial concentration. This is only a simplified model, since ideal relative turbulent mixing process and molecular mixing occur at the same time, even when l_K is not reached yet. However, the model is mainly aimed at evaluating different mixing controls, and the higher R_r is, the more accurate the model is.

For a given initial Reynolds number, the criterion R_r can be used to compare different control

results and the higher R_r , the higher the mixing rate. However, for different Reynolds number, R_r should be applied with care. This is due to that the higher Re , the smaller l_k is. The smaller l_k , the smaller the time t_m . This can be shown by the relation

$$l_K \sim LRe^{-3/4} \quad (6.1)$$

$$t_m \sim l_K^2/D_m \sim L^2/D_m Re^{3/2} \sim S_c \nu^{1/2} L^{1/2}/U^{3/2} \quad (6.2)$$

$$T_s \sim x_i/U \quad (6.3)$$

here x_i represents the downstream position, where the ideal relative turbulent mixing state is achieved. That is to say, with the increase of Re (through velocity) for a fixed large scale, t_m reduces faster than T_s . In order to achieve $R_r \geq 1$, x_i must be smaller for higher velocity, i.e. turbulence has less time to achieve the ideal relative turbulent mixing state. However at a given Re , R_r can tell us how far away a relative turbulent mixing process is from its corresponding ideal relative turbulent mixing process and how much potential is left for control to enhance turbulent mixing.

6.4 Mechanism of the turbulent mixing enhancement

The above mentioned rapid transition from an initial large to a small scale for mixing enhancement indicates a strong nonlinear process and an optimized energy transfer from large to small scale. It is based on a new receptivity mechanism and will be investigated in the part 2.

6.5 Zero crossing point number of gradient G_z

Even though G_z is proposed as a criterion for turbulent mixing, unfortunately, due to the high shot noise, it is difficult to get good experiment result with low noise. As the noise is too high, it is difficult to have a correct G_z . Therefore no result for G_z is shown here. However, if the SNR is improved, G_z would be a useful parameter. It may help us to understand the relation between eddies in frequency domain and the structures in physical space.

6.6 -1 exponent spectrum

There are two theories which result in -1 exponent spectrum. One is Batchelor spectrum for scalar [5] and the other is Tchen's -1 theory [48] for near wall region in boundary flow where the vorticity due to velocity gradient is relative high. Fig. 5.25 shows that there is a -1 exponent spectrum in the frequency range lower than that of -5/3 exponent. In Fig. 5.26, there is no -1 exponent spectrum in the frequency range higher than that of -5/3 exponent. The Re used here is low. Batchelor said that, "the form of psd beyond the viscous cut-off wave-number do not require the Reynolds number of the turbulence to be so large that an inertial subrange exists. Whatever the Reynolds number of the turbulence, the distortion of sufficiently small material elements of fluid will be a pure straining motion". However, if the -1 exponent spectrum is in the lower frequency range than that of -5/3 exponent, it is difficult to believe that in this region the flow is a pure straining process. It is, therefore difficult to regard the -1 exponent range as the Batchelor spectrum, even if the Reynolds number is low, as it is in the frequency range below that of -5/3 exponent, i.e. where turbulent stirring is relative strong. That if the -1 spectrum is related to Tchen's -1 spectrum is unclear.

The -1 exponent spectrum before -5/3 has probably another reason. The large Sc renders the turbulent mixing mechanism different from that of small Sc . For large Sc , the diffusivity of scalar is much smaller than its counterpart of vorticity. For velocity fluctuation,

$$u' \sim (\epsilon l)^{1/3} \quad (6.4)$$

where u' corresponds to the length scale l . This means turbulent velocity fluctuation increases with scale. However, in the initial stage from large to small scalar scale in turbulent mixing process,

the scale is so large that the molecular diffusion can be negligible when $Sc \gg 1$. This indicates that the dependence of concentration fluctuation on scale is not so strong as its velocity counterpart shown in eqn (6.4). On the other hand, with the further deduce of the scale, the behavior of velocity and scalar would be the same and have a common $-5/3$ exponent where molecular mixing has a little influence.

6.7 A new method for turbulence study

The $-5/3$ exponent spectrum is a necessary condition for local isotropic turbulent flow. A necessary condition for the universality of the scalar field is that the velocity field must be universal [103]. The classical turbulent theory seeks a universal law of turbulence which is based on local isotropic turbulent flow and the necessary condition for the local isotropic turbulent flow is that turbulent Reynolds number must be high enough. This, in turn, means that Re must be high enough. In the traditional flows, grid, jet, wake, boundary layer and pipe flows and so on, which are used for turbulence study, the energy transfer from large to small scale is not optimally controlled, thus to achieve a given turbulent Reynolds number, the Reynolds number must be very high so that a given amount energy from average motion could be transferred to turbulent movement. However, using receptivity mechanism, the energy from average motion and extra input could be received by turbulent motion more efficiently, so that a given turbulent Reynolds number could be carried out at relatively low Re if the receptivity is strong.

According to the experiment result here, e.g. Fig. 5.25 which indicates that the high Reynolds number properties can be achieved with low Re under forcing, it is possible to study high Reynolds number phenomena, which is sometimes difficult to investigate experimentally and numerically, through low Reynolds number with special forcing. Numerically if Re is small, the l_k will be increased, and it will be easier and cheaper to use direct numerical simulation (DNS) for simulation of turbulence due to the fact that DNS has difficulty with high Re where Kolmogorov scale l_k is very small. Experimentally, the relative signal to noise ratio, spatial and temporal resolution will be higher and the experiment will also be much easier if Re is lower. Thus, with the use of special receptivity mechanism (methodology used by structure group), the forced flow provides a new opportunity for the the study of statistics of turbulence.

7 Conclusion

Experimental Method

1. A high spatial resolution of around $4 (\mu m)^3$ scalar measurement of LIF is achieved. The laser intensity at the measuring volume is so high that thermal blooming and photobleaching could become serious and contaminate experimental results.
2. Investigation on the influence of photobleaching and thermal blooming on LIF is conducted and a model describing the influence of photobleaching through the velocity deviation is proposed and is supported by experimental results.
3. The effect of laser power and concentration on photobleaching is measured through the relationship between fluorescence intensity and flow velocity, decay curve and half-life time constant.
4. Scalar measurements should be conducted only when the velocity is high enough, i.e. there is a lower limit for the velocity.
5. Calibration and photobleaching measurements should also only be done when the fluid is in motion and the fluid velocity is beyond a threshold value.
6. A new method to measure photobleaching is proposed.
7. A new velocimetry based on the photobleaching of LIF is invented.
8. For high spatial resolution measurement of LIF, the measuring volume is very small and so is the signal level. This results in low signal to noise ratio, especially in the high frequency region. The dominating noise is the shot noise in the signal.
9. A corresponding low noise current amplifier is constructed.
10. Laser beam power and dye concentration cannot be increased without limitation to improve signal to noise ratio because of photobleaching.
11. The measurement of attenuation of laser beam and saturation of dye absorption should also be undertaken when the fluid is in motion.

Turbulent Mixing

1. Around 20 existing turbulent mixing criteria are collected and reviewed.
2. A new model for an ideal relative turbulent mixing process and state is proposed for the turbulent mixing criteria.
3. The model is based on both turbulent flow and scalar physical properties and related to turbulent mixing control.
4. The ideal relative turbulent mixing process and state is approximately realized in experiments.
5. Even for low Reynolds number, the ideal relative turbulent mixing process and state can be realized.
6. Through management and control, the pipe flow can also obtain the same fast mixing properties as a mixing tank.
7. The relative turbulent mixing is drastically enhanced under strong forcing. Even within a quarter pipe diameter downstream of the trailing edge, the large and small scale have already been homogeneously distributed in the whole local cross section.

8. Without forcing, the higher velocity ratio λ is, the stronger the relative turbulent mixing. However under strong forcing, the influence of velocity ratio λ is relatively small.

Turbulence theory

1. A new controlled flow is proposed for turbulence theory study, where the turbulence statistical properties at high Reynolds number can be realized at low Reynolds number with specific forcing, e.g. $-5/3$ exponent of power spectrum density can be obtained for a laminar flow with strong forcing due to a new strong receptivity mechanism.
2. For low Reynolds number, the spatial resolution is the same order as the Batchelor scale, However no Batchelor -1 exponent spectrum is found in the frequency range higher than that of $-5/3$ exponent spectrum, instead, there is an approximately -2.8 exponent spectrum.
3. There is indeed a -1 exponent spectrum from large to small scale and its range increases with downstream distance. However the -1 spectrum is in the frequency region lower than that of the $-5/3$ spectrum. It is not the Batchelor spectrum. The power spectrum density decays in a downstream direction keeping -1 exponent until molecular mixing is finished.

Part II

New phenomena in a confined configuration

8 Introduction

On the one hand mixing layers are basic fluid modules for free turbulence and turbulent mixing, and so is a pipe flow for wall bounded configurations. Reynolds used pipe flow to do his famous experiment of transition from laminar to turbulence. Brown and Roshko found coherent structure in a mixing layer. On the other hand, mixing (i.e. transport) properties are the central point for turbulence study. Taylor studied the diffusion property and established some important concepts, e.g. turbulent diffusion coefficient and so on for turbulence; Prandtl proposed the mixing-length model according to the transport characteristics.

However, a combination of these two flows, i.e. a mixing layer (including wake) at the intake of a pipe flow has, to the author's knowledge, never been investigated in details for both turbulence and turbulent mixing. Usually such flows are not considered of general interest for fundamental research, since additional complications of the wall influence are introduced which may obscure the study of turbulence mechanisms. In all realistic cases there is, however, always a wall influence present, albeit often only to a negligible extent, and it may not be unwelcome under all circumstances.

The confined mixing layer in a pipe is not simply a superposition of a mixing layer and pipe flow, and visualization discloses a variety of phenomena which cannot be explained by the simple superposition. This is particularly true for the case of periodic forcing where one observes singular critical (mixing) phenomena, which are unknown in the "ordinary" mixing layer and are also not found in a simple pipe flow. Those phenomena are interesting both for the fundamental researcher and for the engineer and may even provide new insights for those making basic studies on the origin of turbulence in an open flow.

Since we could find no reports on this flow, the first step in studying this flow is visualization. In this work, some new phenomena of a confined mixing layer (including wake and quasi-step flow) in a pipe are shown, both the vortices and their effects on turbulent mixing under the influence of an actuator through visualization.

8.1 Simultaneous visualization of three light sheets

Flow visualization is always a powerful experimental method for the study of fluid mechanics. Especially for complex flows, we sometimes need to have a simultaneous view of three light sheets of flows in order to understand better the 3-D large structures in the flow. Laser-Induced-fluorescence (LIF) can provide us with a powerful method for this aim. Usually the visualization of the three light sheets includes a side view of spanwise structures, a plan view of spanwise and streamwise structures and a cross view of streamwise structures, for example, in a mixing layer. To the author's knowledge, while there are some works that can visualize the side and plan view simultaneously (e.g. Konrad [61]), no work has been found that can visualize the three light sheets, i. e. side, plan and cross view simultaneously. One main reason for this is that the three light sheets have different image distances, especially the cross view, which has a much longer image distance than the other two. In this work, a method, which can solve this problem, is realized.

8.2 Dual receptivity

As pointed out in part 1, Fig. 5.1 shows the extraordinary spread rate of the wake for mixing. Such a fast spread, to the author's knowledge, has never been obtained. This is based on a new receptivity mechanism. Receptivity is a fundamental concept for the study of turbulence and turbulence control. It is widely used to describe how a flow responds to an external disturbance and how the external disturbance develops in a shear flow. When a free shear flow has receptivity to an external disturbance, its corresponding instability theory indicates that, as the disturbance is periodic and its amplitude is small, there is one frequency (or Strouhal number St), under which the disturbance reaches its maximum development. If the disturbance is large, there can be a subharmonic or superharmonic components of the fundamental frequency due to non-linear effect, at which the disturbance reaches

its maximum level. These frequencies are commensurable. This is the fundamental knowledge of turbulence control.

Here a new concept "dual receptivity" is introduced. What does dual receptivity mean? The dual receptivity is, defined as follows: There are two frequencies, under which the initial disturbances reach their maximum development, if the disturbances are periodic; these two frequencies must be incommensurable. Such a phenomenon, to the author's knowledge, has not been reported, especially for free turbulent flow and boundary turbulent flows control. However, in a confined configuration, i.e. here a symmetrical plane wake (wake) and asymmetrical plane wake (mixing layer) in a pipe (or in the other word, there is a plane wake or mixing layer at the inlet of the pipe), the dual receptivity is observed. One type of the dual receptivity is the well-known spanwise Karman or Kelvin-Helmholtz instability mechanism and the other is unknown.

The dual receptivity tells us there is a new instability mechanism. This new one is quite different from the traditional one and its receptivity is much stronger than the traditional one, especially in the near field of the wakes. One of its applications is mixing enhancement as described in part 1.

8.3 Sudden transition to turbulence

The scenario of transition to turbulence is an important topic for turbulence study. Landau [65] proposed a scenario for the transition from laminar to turbulence. It is based on the idea that a system becomes turbulent through a succession of instabilities, where each instability creates a new degree of freedom (through an indeterminate phase) of a time-periodic nature with the frequencies successively higher and incommensurate (not harmonics). Since the resulting motion is given by the superposition of these modes, it is quasi-periodic. Later Ruelle and Takens [92] suggested that this idea was in some sense too linear. In fact, nonlinear interactions among a small number of modes generically yield chaotic behavior characterized by a decay of correlations that more appropriately describe a turbulent regime. Experiments also tell us, that only a small number of modes need to be forced to produce turbulence. However, the number of modes participating in the transition is, as of now, an open question to be answered experimentally [34].

One interesting transition is a sudden transition from laminar to turbulence, during which, the flow loses its stability at once with no bifurcation taking place at all [95][19]. A sudden transition would reveal the mechanism of transition in the most direct way as pointed out by Schutz-Grunow [95]. This may be similar to a snap-through transition in a plane parallel shear flow [55].

Usually in a mixing layer and plane wake there is always a transition process to turbulence beyond the splitter plate when the flow in the trailing edge is laminar. The transition in a mixing layer could be related to double periodic or Feigenbaum bifurcation [52].

However, the visualization here shows that under some conditions, e.g. periodic temporal forcing, a sudden transition from laminar to turbulence can happen through some bypass in a confined configuration, i.e. plane mixing layer and wake in a pipe, even without any apparent mode, i.e. the production of successive subharmonics, which emerge as a possible route to turbulence. This phenomenon is also discussed here.

8.4 A new symmetry breaking hysteresis phenomenon

Symmetry breaking and hysteresis are often interesting for physicists (see, e.g. [96]), because it could be related to some instability mechanism. So is the symmetry. In this work, a new symmetry breaking hysteresis is observed under strong forcing for a plane wake, as mentioned in part 1 for the scalar measurement of a small Reynolds number plane wake. This new symmetry breaking hysteresis may be related to some bifurcation mechanism and will be described here.

8.5 Pairing burst

Vortex pairing is an important phenomenon for mixing layer development and the turbulent mixing mechanism proposed by Winant and Browand [120]. The burst phenomenon is an essential property in the boundary layer and pipe flow as proposed by Kline et al. [56] and Corino and Brodkey [22]. Pairing is important for mixing as is burst for drag reduction, heat and mass transfer. Here a new phenomenon known as "pairing burst" is introduced. It means that when pairing happens near the wall, it will result in a burst, i.e., large scale ejection from the wall. The word "burst" here is used to describe such a large vortex ejection.

In a confined mixing layer in a pipe, the mixing layer behavior, is similar to that in a normal 2-D mixing layer, also has pairing under some conditions and the central line of the mixing layer is biased to the low velocity side with or without an initial temporal periodical forcing. With the increase of velocity ratio λ , the mixing layer not only spread faster but also has a steep bias to the low velocity side, and the pairing can sometimes happen near the wall in a sweep way. The major point of interest is that if the pairing appears steeply near the wall, the amalgamated large vortex will eject quickly from near wall region to the center of the pipe just as with a burst, and therefore we call this phenomena as "pairing burst". On the one hand, pairing burst is an interesting phenomenon fundamentally. On the other hand, the mixing layer spread rate will be much increased at the streamwise position where pairing burst happens. Thus pairing burst not only increases mixing, but can also enhance heat and mass transfer from the wall to fluid.

In this work, the phenomenon of pairing burst, the influence of Re , λ and initial temporal forcing on pairing burst are investigated. The wall has a relatively strong influence on the flow. It may help us to better understand the free turbulent flow, (for example, the mixing layer) and wall boundary turbulent flow, the relation and interaction between them. Even if there are a lot of works on turbulent burst, it is still an issue in turbulent boundary flow according to the review of Robinson [90]. For instance, its dynamic mechanism is still unclear, and so is the interaction between inner and outer flow. If we take pairing burst as a model for turbulent burst, it may help us to understand the dynamic process.

9 Experimental set-up

9.1 Water channel

It is almost the same as that used in part 1, except that the water vessel against the refracting distortion is removed.

9.2 Optics

The optics used here is quite different from that used in part 1 and is shown in Fig. 9.1. LIF is applied here for the flow visualization. The peak absorption and emission spectrum of sodium is blue (488 nm) and green (530 nm) respectively, and the reflecting laser light from glass is strong. In order to get clear pictures without reflecting light, the exciting light of the laser should be different from the emitting light in the wave length. For this aim only blue light is expected to be the exciting light. Using an etalon we can get only blue color (488nm) light. A narrow band light filter 500 ~ 600 nm and yellow color filter before a CCD camera are used to filter away the reflecting light. The filter is the same as used in part 1.

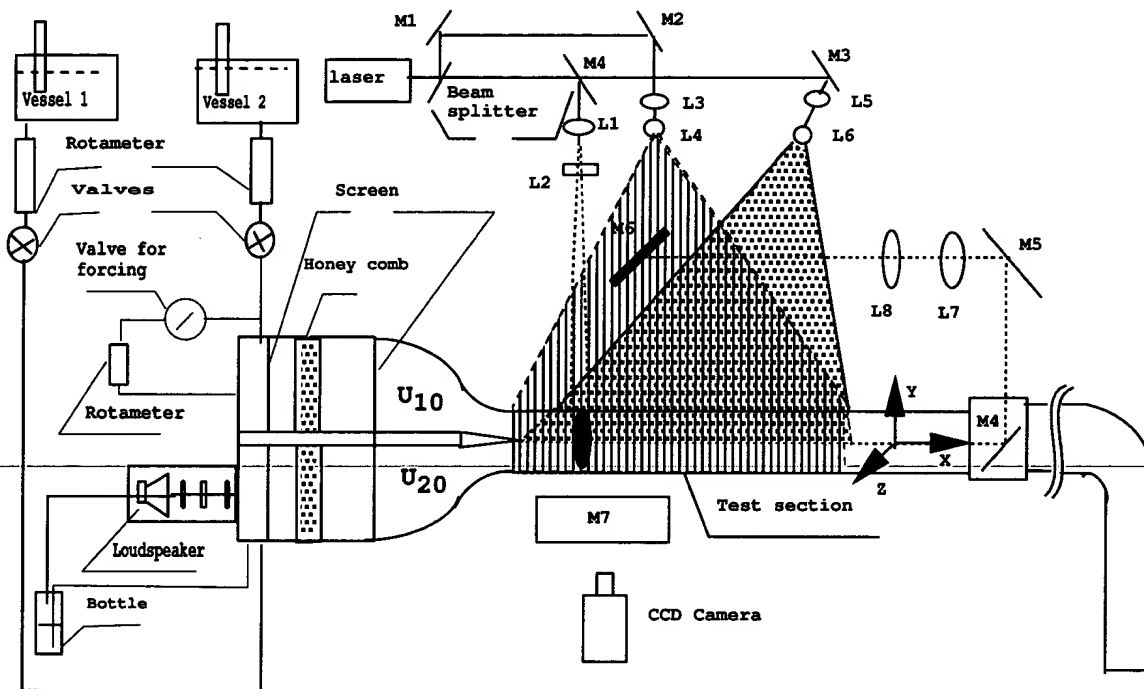


Figure 9.1: Experimental schematic.

In order to understand this complex flow, it is helpful to see the three light sheets (x-, y- and z-direction) of the flow field simultaneously. The three light sheets, i.e. x-, y- and z-sheet represent cross, plan and side view respectively. For this purpose, the light coming from the laser is first led through a beam splitter with 40 percent reflection. The reflected light passes through the mirrors M1 and M2, lens L3 and cylinder lens L4 for the z-sheet. The 60 percent light again goes through a second beam splitter M4 with 30 percent reflection. The 30 percent light passing through the lens L1 and cylinder lens L2, is used for the x-sheet, which has a smaller sheet view compared with the other two, and the other beam goes through the mirror M3, lens L5 and cylinder lens L6 for the y-sheet. Thus the light intensity difference of the three light sheets is sufficiently small.

If the laser light sheets are too thick, it is very difficult to see the visualized pictures from the sheets because the projections of the light on them from the other two light sheets are too strong.

Therefore the three light sheets must be as thin as possible. There are different methods to produce thin light sheets. Due to the fact that the optical is already very complex for the three light sheets, the optics for thinning light sheets should be as simple as possible. For this purpose, some long focus length lenses are used on every light sheet, and placed before the cylinder lenses that are used for light sheets. The focus lengths of the lenses L1, L3 and L5 are 0.8, 1 and 1 m respectively. The distances of these lenses from the pipe axis are the focus lengths, so that the light sheets can be sufficiently thin. The long focus lenses are chosen to make sure that a sufficient length of the viewed thin sheet field can be obtained.

If the laser intensity of one sheet is too strong, the images from the other two sheets will not be clear. For this reason, the laser power should not be too high (but must be high enough). The optimized laser power should be found through some probe tests.

The image of the three light sheets of the flow field is diagnosed with a monitor and received by a Sony CCD camera and Beta recorder. The CCD camera can only see the z-sheet directly. To place the three light sheets on the monitor simultaneously, some mirrors are used for the other two sheets. A mirror M7 is placed under the pipe for the y-sheet at 45°. The difficulty is the x-sheet. It is impossible to see the x-sheet clearly by placing a mirror simply near the x-sheet at an angle, because the pipe wall is round. For that reason, a mirror M4 at 45° to the x-direction is placed in the center of an Plexiglas cube, which is positioned 1 m downstream from the trailing edge (to make sure that there should be no influence on the near field of the test section). Over the cube there is a mirror M5 at 45° to the x-direction. Over the mirror M7 and pipe, there is a mirror M6 at 45° to the z-direction, which finally reflects the image of the x-sheet to the camera. In this case, the image distance of x-sheet is much larger than the other two. Now the difficulty emerges. To see the three light sheets clearly and simultaneously, the image distances for the three light sheets should be almost the same. The difference of the image distance between z- and y-sheet is relatively small, therefore the two sheet can clearly been viewed simultaneously. However, since the light passing length of the x-sheet image, i.e. the image distance of the x-sheet is much longer than the other two, the x-sheet image is too small and unclear.

It was initially thought that, if the image distances for all the three light sheets were very long, the difference of image distances among them would be relatively small. For this reason, the camera is placed quite far from the test section, but the pictures are too small and unclear. It is also impossible to overcome this problem, by simply reducing the iris of the camera. One possible method is to reduce the image distance of the x-sheet, which is shown as follows.

Let us consider the combination of lens a and b when they are placed in tandem. In the viewpoint of the principle of geometric optics, there is the relation

$$1/a_F + 1/b_F = 1/f_F \quad f_F < a \text{ and } f_F < b. \quad (9.1)$$

where a_F and b_F are the focus lengths of both lenses a and b respectively and f_F is the focus length of the combined lenses. If a_F and b_F are positive, f_F is then always smaller than both a_F and b_F . As some lenses are added between the x-sheet and camera, the image distance of the x-sheet will be decreased. Based on this principle, both lens L7 (f1000/50) and lens L8 (f600/70) are placed between mirrors M5 and M6. The positions of these two lenses are adjusted to receive a clear and sufficiently large size picture of the x-sheet. These two lenses should also have large enough diameters, so that the picture is not blocked. Given the complicated optics and small size for the x-sheet, it is also important that the mirrors used for x-sheet are surface mirrors. All the mirrors used, except the mirror M7, are surface mirrors. Now the image distance of the x-sheet is almost the same as the other two, and thus the three light sheets are clearly and simultaneously shown on the monitor.

Fig. 9.2 shows a sample of the simultaneously visualized pictures of the three light sheets in a confined mixing layer, where U_1 and U_2 are 7.5 and 3.0 cm/s respectively. The top, middle and bottom pictures are cross, side and plan views respectively. The fluids flow from left to right. The large primary vortices in the side view and the secondary vortices in the cross and plan view are clearly displayed. The visualization of the three light sheets shows clearly the 3-D large structures and their topology, especially through the video.

Therefore, the main problem for the simultaneous visualization of three light sheets is the different image distances. It can be overcome by using extra lenses in the viewpoint of geometry optics. Thus this work presents a successful method to visualize simultaneously three light sheets perpendicular to each other for complex flows [111]. The method may also be used for reconstruction of 3-D large structures through the scanning of the x-sheet. The details of these structures will be investigated next. In this work, for all pictures, where the 3-D visualization is simultaneously shown, the top, middle and bottom pictures are cross, side and plan views respectively.

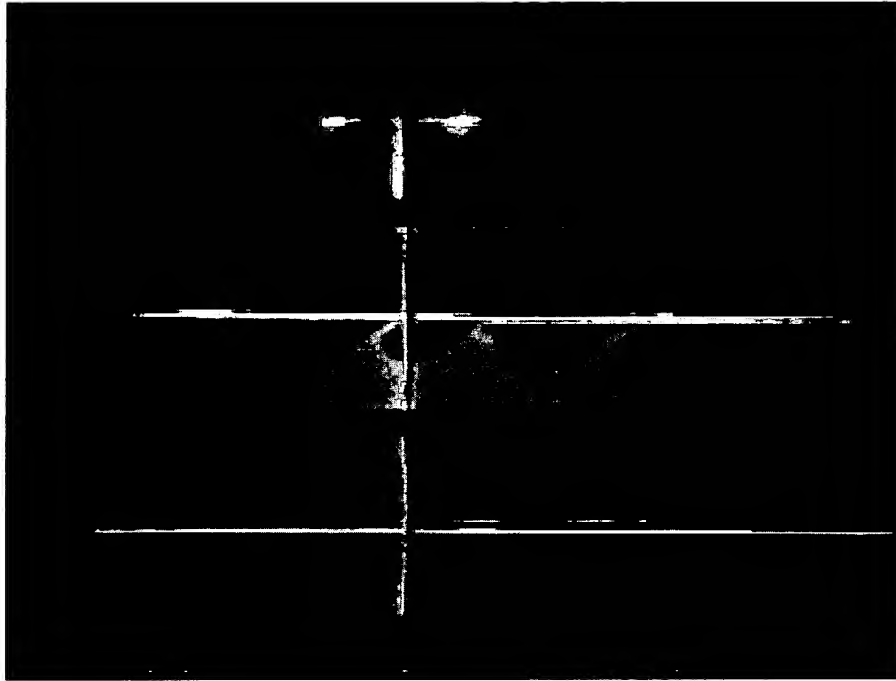


Figure 9.2: Simultaneous 3-D visualization of a mixing layer.

10 Results

10.1 Dual receptivity

10.1.1 Wake

The initial momentum thickness is often used for the scaling in shear flows. Here, its value in the mixing layer originating at the trailing edge can be approximately estimated through 2-D spatial mode of linear instability theory, since the flow is approximately two dimensional just after the splitter plate without forcing, and the forcing result can be described by linear theory although it is a non-linear process (Ho & Huang [49]). The program (which was originated for boundary flow instability using Orr-Sommerfeld equation) was offered by Prof. H. Zhou and was changed for a three dimensional plane mixing layer by the author under Zhou's advice when he was in Berlin. Firstly the dimensionless frequency, i.e. Strouhal number, is theoretically calculated, at which the spatial amplification rate of a disturbance $-\alpha_i$ decreases to zero. Secondly, the forcing frequency is experimentally increased until no receptivity can be found anymore. Then the momentum thickness θ can be obtained. Once a momentum thickness is obtained for a given velocity, the momentum thickness of the other velocity can be estimated through the relationship between velocity and laminar boundary momentum thickness, due to the fact that the flow is laminar on the splitter plate.

The visualized scalar structures size and their corresponding shear layer thickness are approximately used as the criterion of receptivity even though the instability theory is usually described as the disturbance of velocity. The argument is that, at the beginning of the wakes, the larger the coherent composition of the velocity, the wider its corresponding vortex in the shear layer of the wakes, which can be recognized by scalar large structures at least in the near field. In this work, there is no attempt to provide the fundamental data for the receptivity study quantitatively, instead the work introduces a new phenomenon of receptivity and its possible mechanism qualitatively.

Temporal periodic forcings of the flows with a certain of frequencies and amplitudes are introduced. The relative average velocity-perturbation amplitude of forcing (henceforth called forcing amplitude or level) resulting from the membrane corresponds to

$$A = \sqrt{\bar{u}'^2}/\bar{U}(\%) = 2a_M f(A_M/A_N)/(1.414\bar{U}). \quad (10.1)$$

where the ratio of membrane to nozzle area $A_M/A_N = 2$ in this experiment. f is forcing frequency and a_M is the maximum displacement of the membrane.

The estimated initial Reynolds number based on initial momentum thickness is

$$Re_\theta = \sum \theta_{1,2} \bar{U} / \nu, \quad (10.2)$$

where $\sum \theta_{1,2}$ is the sum of the momentum thickness of the upper and the lower boundary layer at the trailing edge.

The visualization is undertaken in the near field of the wakes. The fluids flow from left to right. The trailing edge of the splitter is within the view of the pictures.

10.1.1.1 Phenomenon and forcing frequency f effect Fig. 10.1 shows the responses of a wake to the forcing from loudspeaker in side view through the axis of the pipe. The forcing amplitude $A = \sqrt{\bar{u}'^2}/\bar{U}$ is about 10% and average velocity \bar{U} is 4 cm/s. Fig. 10.1a is the flow with no forcing. In Fig. 10.1b the flow is forced at frequency $f = 1.6$ Hz. It can be seen that, the disturbance is, relatively, strongly amplified and there are only large coherent structures. When f is increased to 4.4 Hz in Fig. 10.1c, it is observed that the growth rate of the disturbance is much reduced compared with Fig. 10.1b even though it is increased at the beginning. Traditionally, it indicates that, frequency of 1.6 Hz corresponds the maximum amplification, and with the further increase of frequency, the amplification will decrease. However, what is interesting is that, at $f = 6.0$ Hz, the disturbance is again increased as shown in Fig. 10.1d, and there are more small scale vortices and scalar structures

in comparison to the other situations. This indicates that, the disturbance at $f = 6.0$ Hz amplifies faster than all other frequencies. If f is further incremented, the amplifying rate will decreased as shown in Fig. 10.1e until there is no receptivity anymore.

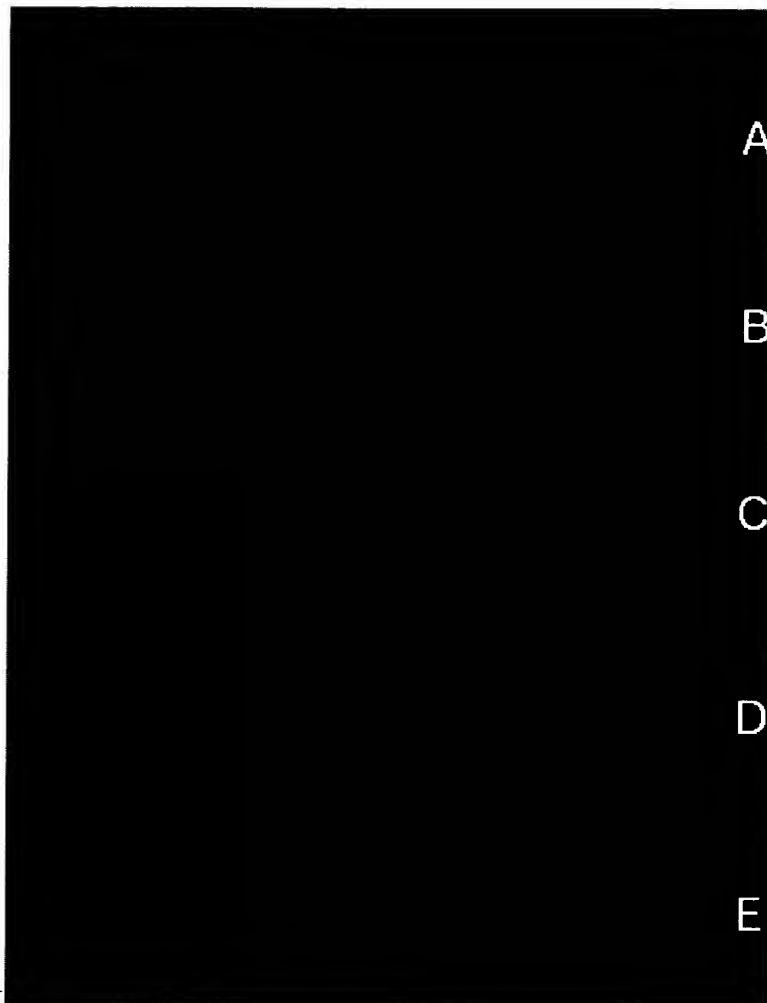


Figure 10.1: Dual receptivity phenomenon from side view of a wake. $\bar{U} = 4$ cm/s, $A = 10\%$, a: $f = 0$ Hz; b: $f = 1.6$ Hz; c: $f = 4.4$ Hz; d: $f = 6.0$ Hz and e: $f = 8.5$ Hz.

From the linear instability theory, we know that, for plane wake there should only be one frequency at which the amplification reaches its maximum. However, in this experiment, it is obviously that there are two frequencies, at which the amplification reaches its maximum. At the beginning it was thought that one frequency was the subharmonic of the other, because the forcing was very strong, and non-linear may dominate even at the beginning of the wake. However, combined with experiments at some other Re number conditions, it is found that they are incommensurable, i.e. the frequency of the first maximum receptivity f_{1max} does not depend on the frequency of the second maximal receptivity f_{2max} (see later). That is to say, the first one is not the subharmonic of the second one and the second one is not the superharmonic of the first one. At the frequency of two times f_{2max} , i.e. its superharmonic frequency, the receptivity is relatively very small. It seems that there are two different receptivity mechanisms in the confined plane wake in the pipe under strong forcing. The first one (1.6 Hz) corresponds to the traditional receptivity mechanism and the second one (6 Hz) is unknown.

10.1.1.2 Amplitude effect The influence of the forcing amplitude $A = \sqrt{u'^2}/\bar{U}$ depends on the forcing frequency. Fig. 10.2 (side view) displays the influence of A under different values of f . Again, at around $f = 6$ Hz (the new receptivity mechanism), A has the strongest influence on the evolution

of the wake in the near field. In Fig. 10.2a, no forcing is supplied. From Fig. 10.2b to Fig. 10.2f, the flow is forced at 6 Hz with different A values of 1%, 5%, 25%, 35% and 45% respectively. On the one hand, it is found that, the receptivity at 6 Hz is very high, and has not yet reached a saturation when A is around 30%. On the other hand, the influence of the amplitude on the spread rate of the wake becomes smaller with the increase of A , e.g. the amplification difference of the disturbances between Fig. 10.2e and Fig. 10.2f is not so high compared with other values of A . However at $f = 16$ Hz, the receptivity has already reached its saturation when A is about 5%, as shown in Fig. 10.2g and Fig. 10.2h, where A is about 5% and 45%. Observation indicates that the maximum receptivity frequency corresponding to the traditional one seems to be around 16 Hz for this flow. For $f = 22$ Hz in Fig. 10.2i, A has almost no effect on the spread rate of the wake even though A is 5% compared with Fig. 10.2a, i.e. no receptivity.

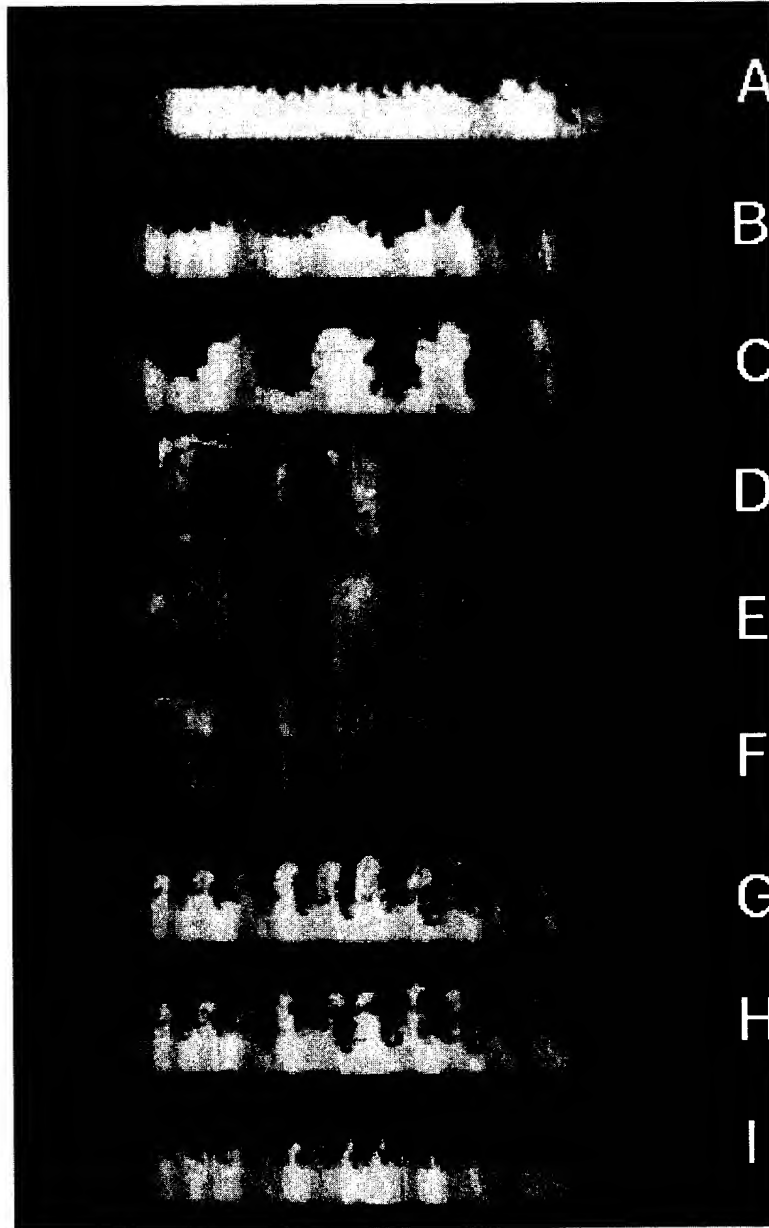


Figure 10.2: Forcing amplitude influence on receptivity. $\bar{U} = 25$ cm/s, a: $f = 0$ Hz; b: $f = 6.0$ Hz, $A = 1\%$; c: $f = 6.0$ Hz, $A = 5\%$; d: $f = 6.0$ Hz, $A = 25\%$; e: $f = 6.0$ Hz, $A = 35\%$; f: $f = 6.0$ Hz, $A = 45\%$; g: $f = 16$ Hz, $A = 5\%$; h: $f = 16$ Hz, $A = 45\%$; i: $f = 22$ Hz, $A = 5\%$.

For very small A , e.g. 0.5%, only one receptivity mechanism (here 16 Hz) can be observed. With

other results (see below), it can be recognized that this corresponds the traditional 2-D plane wake receptivity mechanism. It is also found that in the confined wake, this receptivity has similar response to the amplitude effect as the traditional 2-D wake, i.e. the receptivity has its saturation to strong forcing amplitude as shown above in Fig. 10.2g and Fig. 10.2h for $f = 16$ Hz.

Fig. 10.2 indicates that the amplitude influence strongly depends on the receptivity mechanism and forcing frequency. At some frequencies (here about 6 Hz), where there is a receptivity, the receptivity decreases with A , but it is still larger than zero. Therefore the larger A is, the larger the Karman vortex street. In other frequency regions where there is no receptivity, the amplitude has almost no influence on receptivity. The influence of A can be quite different for different receptivity mechanisms.

Even if the forcing amplitude is very high, at which the first (traditional) receptivity reaches saturation, the second one still has a relatively large receptivity. Generally, the second (new) receptivity is much stronger than the first one if the forcing amplitude is high enough. This can be distinguished by Fig. 10.2. The second one is related to the secondary vortices, i.e. Type A Vortices in this flow (see later).

The second receptivity strongly depends on the forcing amplitude and can take place only when the forcing amplitude reaches a threshold value. This indicates that, the secondary receptivity corresponds to a nonlinearly unstable mechanism. At relatively small forcing amplitude, the first receptivity can be seen, but the second one can not. Fig. 10.3 shows the result of the relation of the threshold with Reynolds number Re . It can be seen that, the higher initial Re numbers, the lower the threshold amplitude is. The result indicates the influence of wall on the flow through the viscosity, i.e. the wall can confine the development of a disturbance under some conditions.

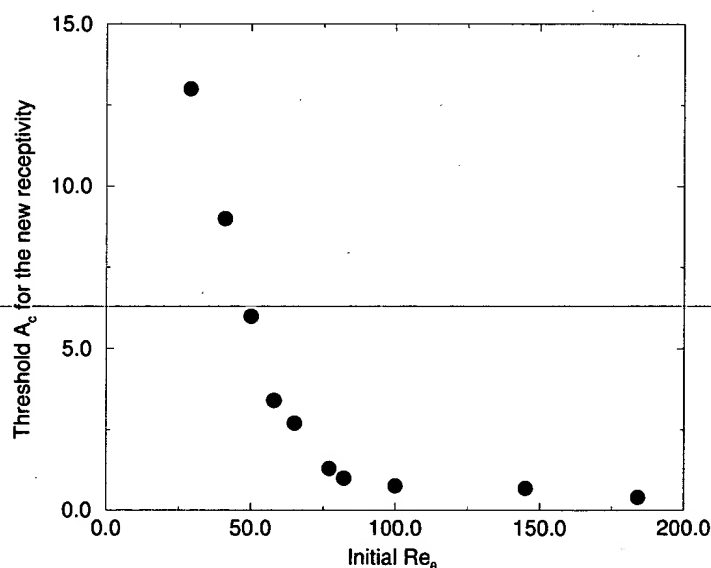


Figure 10.3: Relation between threshold forcing amplitude and initial Re .

In a traditional 2-D-plane wake, even a small disturbance can be amplified. There are few investigations into the large forcing amplitude on free turbulent flows, except some papers, e.g. [81] [119] and [37]. Fiedler and Mensing [37] found that in plane mixing layer, the receptivity had a saturation to large forcing amplitude, i.e. in their experiment, when the forcing was as high as 6.5%, there was almost no influence of the forcing level on the flow anymore.

For small Reynolds number ($Re_\theta < 10$) and frequency in the range of $0.5 \sim 5$ Hz investigated (not shown here), the visualization results indicate that the saturate amplitude, over which the influence of A reaches saturation, is larger than the traditional one, e.g. the saturation is not achieved when A is already 10%. When the forcing amplitude is sufficient high, e.g. at 50%, the spread rate of

the Karman vortex street can be similar to that of Fig. 10.2e, i.e. much higher than the one of a traditional plane wake. But for higher Re_θ , no such a high receptivity can be observed.

10.1.1.3 Re effect The Re is increased through the increase of velocity. Similar to the normal 2-D plane wake, the frequency of the first maximal receptivity f_{1max} is increased with the increment of \bar{U} . For a given flow, according to the instability theory, the corresponding Strouhal number St_{max} is a constant for the maximum amplification rate, i.e. maximum receptivity.

$$St_{1max} = f_{1max} \sum \theta_{1,2} / \bar{U}. \quad (10.3)$$

Near the trailing edge the flow is laminar, so

$$\sum \theta_{1,2} \sim 1/\bar{U}^{1/2}. \quad (10.4)$$

For a constant St

$$f_{1max} \sim \bar{U}^{3/2}. \quad (10.5)$$

The experiment result Fig. 10.4 shows that the first receptivity f_{1max} is qualitatively increased with \bar{U} . The observation also shows that the f_{2max} , corresponding to the second receptivity, is almost independent of \bar{U} . It is approximately a constant in the range of 5.2 ~ 7 Hz in the experiment range of \bar{U} (1 ~ 40 cm/s) for the wake. The result is also shown in Fig. 10.4. For mixing layer with $U_1 = 80$ cm/s and $U_2 = 40$ cm/s, f_{2max} is also around 6 Hz.

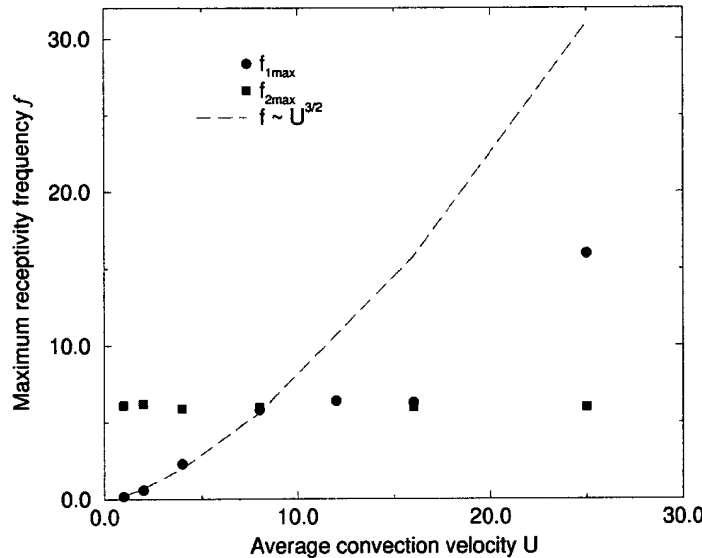


Figure 10.4: Relation between maximum receptivity frequency and \bar{U} .

Due to the above mentioned two reasons, the difference between the two maximal receptivity frequencies decreased first with the increment of \bar{U} . When \bar{U} is in the range of 7 ~ 15 cm/s, no apparent double receptivity can be recognized, because they overlap each other. As U increases further, the difference increases again.

10.1.2 Mixing layer

The dual receptivity phenomenon mentioned above in the wake can also be obtained in the mixing layer and quasi-step flow. The influence of forcing frequency f , amplitude A and Re on the receptivity in a mixing layer is similar to that in a wake and therefore will not be displayed here. The details will be given later in a corresponding publication. Here only the unusual receptivity phenomena about the center line bias of the mixing layer, counter-rotating primary vortex and λ effect responding to the strong forcing will be discussed.

10.1.2.1 Unusual phenomena Fig. 10.5 (side view) shows the influence of A under a frequency of 5.6 Hz for a mixing layer of $U_1 = 10$ cm/s and $U_2 = 5$ cm/s. The dynamical result of forcing is very interesting. As we know, the center line of a traditional mixing layer biases to the lower velocity side beyond the trailing edge. This is also true in Fig. 10.5a and Fig. 10.5b. In Fig. 10.5a there is no forcing and in Fig. 10.5b the flow is forced and A is about 1%. The vortices are Kelvin-Helmholtz vortices. However, in Fig. 10.5c where A is about 5%, even though the center line of the mixing layer still biases to the low velocity side, the vortices at the beginning are almost not the pure Kelvin-Helmholtz vortices. This is in a critical point. That means there are two kinds vortices, and both vortices are counter-rotating similar to the Karman Vortex in a wake. One is very clearly visible and the other is still not. However in Fig. 10.5d where A is around 8%, the two kinds vortices are very clearly visible, and unusually the center line of the mixing layer does not bias to the low velocity side anymore. The visualized mixing layer is almost symmetrical to the trailing edge now. From this point, the primary spanwise vortex in the mixing layer is no longer a Kelvin-Helmholtz vortex with the increase of A , but a new kind counter-rotating vortex. When A is increased further to 18%, the center line of the mixing layer begins to bias to the high velocity side as shown in Fig. 10.5e and the counter-rotating vortex becomes more clear. When A is around 32%, Fig. 10.5f shows that, only the first counter-rotating vortex beyond the trailing edge is distinguished, and no large structure can be seen after $x/D = 2$. Finally, when A is about 52% as in Fig. 10.5g the disturbance is so strong that the flow has already become turbulence just downstream of the trailing edge due to the high receptivity, and no large structure can be seen just beyond the trailing edge because of the rapid relative turbulent mixing. The corresponding spread rate of the mixing layer seems to be about 180° for this situation. If the forcing is outside this narrow frequency-band, the receptivity will be very small or there may be no any receptivity at all even though the forcing amplitude is very high.

No report has indicated that the center line of a mixing layer could bias to the high velocity side and there could be two counter-rotating vortices in a mixing layer. Its mechanism is still not clear. It is found that, the secondary vortices in this flow could play an important role for these two unusual phenomena (see later). Annular effect [94] may be the reason for the two counter-rotating vortices phenomenon.

Very strong forcing results (not shown here) also show the influence of velocity ratio λ effect under the new receptivity. Without forcing or with small forcing, the spread rate of mixing layer is increased with λ . However, for strong forcing, the λ has little influence, and the spread rate of the wake ($\lambda = 0$) can even be a little higher than that of a mixing layer. This indicate that the wake is more sensitive to the strong forcing of the new receptivity.

10.1.3 Quasi-step flow

As in mixing layer, the phenomena found in the wake can also be observed in the quasi-step flow when the low velocity in the mixing layer is zero. Here the term "quasi-step flow" is used since the back-facing surface is not solid, but fluid. This is different from the traditional 2-D mixing layer, where the flow is a jet when the low velocity is zero. Fig. 10.6 (side view) shows the result with and without forcing in a quasi-step flow with $U = 50$ cm/s ($\bar{U} = 25$ cm/s). It is found that compared with the unforced one in Fig. 10.6a, the forced one at $f = 6$ Hz and $A = 15\%$ has an apparent receptivity as shown in Fig. 10.6b, while the forced one at $f = 11$ Hz, and $A = 15\%$. has a small receptivity as shown in Fig. 10.6c. It seems that the traditional receptivity is at f of around 11 Hz.

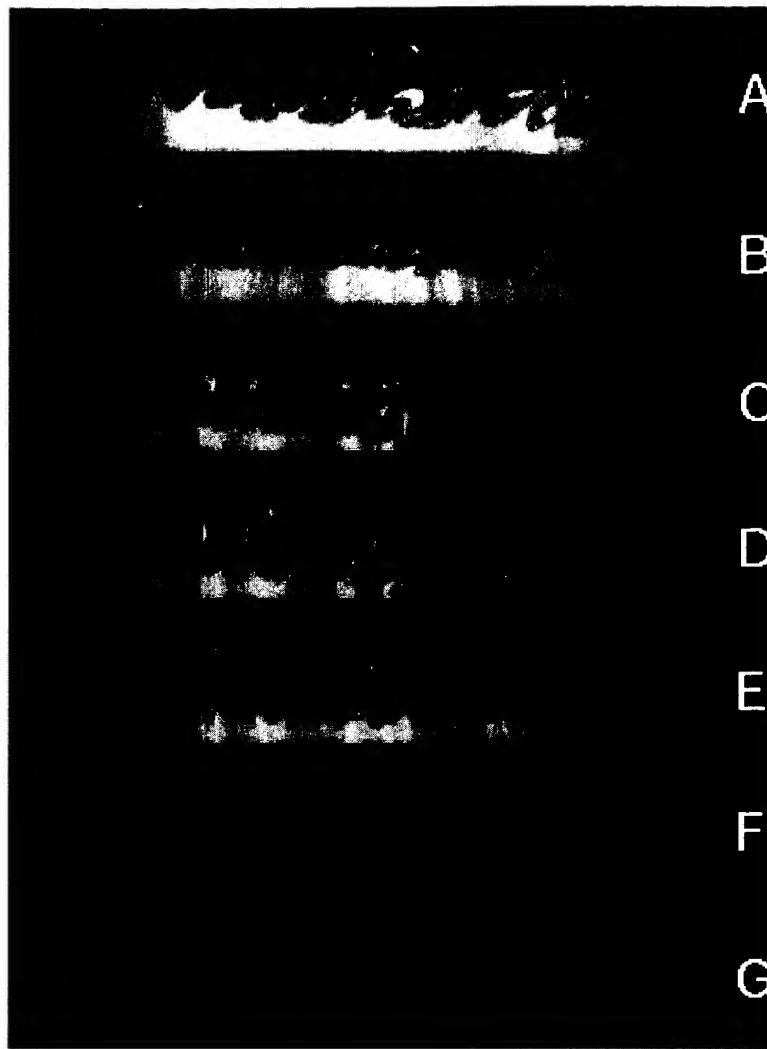


Figure 10.5: Influence of A with $f = 5.6$ Hz in a mixing layer of $U_1 = 10$ cm/s and $U_2 = 5$ cm/s.



Figure 10.6: Response to forcing in a quasi-step flow. a: no forcing; b: with forcing $f = 6$ Hz, $A = 15\%$; c: with forcing $f = 11$ Hz, $A = 15\%$.

The phenomenon of center line bias of the mixing layer described above can also be observed in

the quasi-step flow. With strong forcing the separation region of the quasi-step flow can be much reduced due to the large spread angle just beyond the trailing edge. A example is shown in Fig. 10.7. The velocity U_1 is 80 cm/s. Fig. 10.7a is the case without forcing and Fig. 10.7b with forcing at forcing amplitude 45% and frequency of 6 Hz. In Fig. 10.7a the bright region is the separation region, while in Fig. 10.7b the bright separation region disappears. This provides us with a new possibility to control the flow separation and the details of separation reduction will be given in a paper later.

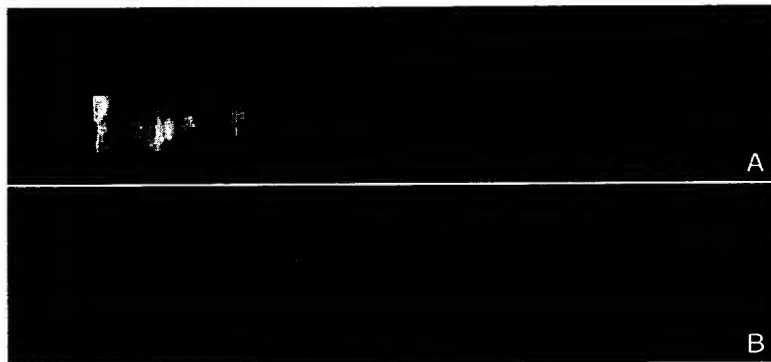


Figure 10.7: Side view of separation reduction under forcing in a quasi-step flow with $U_1 = 80$ cm/s.

10.2 Secondary vortices

In order to understand the mechanism of the dual receptivity, especially the new one, it is necessary to investigate the secondary vortices in the confined configuration. It should be clear first that in some cross view pictures, there is one sharp dark area, for instance in Fig. 10.10, or there are two sharp dark areas, for instance in Fig. 10.13f. This is due to the fact that the pipe wall can act as a lens and result in these dark areas.

To make the secondary vortices more distinguished, forcing are used to excite them. The phenomenon of the secondary vortices could also be observed when the flow is without forcing.

10.2.1 Wake

We concentrate here on the wake, as most of its result is similar to that of mixing layer and quasi-step flow. Only the difference between the wake and mixing layer will be given when mixing layer is considered.

10.2.1.1 Type There are actually many different secondary vortices in this flow, but the important ones are four symmetric vortices (even if it seems that there are, sometimes, only two vortices), i.e. two different type secondary vortices. Fig. 10.8 is a sketch of these vortices. The first two move toward the axis of the pipe in the spanwise (z -) direction and are named here as Type A Vortices; the other two move away from the axis of the pipe in the vertical (y -) direction and are named here as Type B Vortices. It is in some cases difficult to distinguish these two different kinds of vortices from one another through visualization. Some actual pictures can be seen in Fig. 10.9. The vortices in Fig. 10.9a are the Type A Vortices. The Type B Vortices are clearly seen in Fig. 10.9b and Fig. 10.9c.

Apart from these two main type vortices, there are also some different superharmonic secondary vortices that are, for example, demonstrated in Fig. 10.9b and Fig. 10.9c. In 10.9b, $\bar{U} = 1$ cm/s, $f = 5.21$ Hz, and $x/D = 1$. and in Fig. 10.9c where $\bar{U} = 10$ cm/s and $f = 5.48$ Hz, $x/D = 4$. The vortices in 10.9b are so symmetric that they are very similar to the Tai-Chi symbol, a natural Tai-Chi symbol! With increase of the Re number and evolution downstream, the structures of the superharmonic secondary vortices become more complex. This can be seen in Fig. 10.9c.

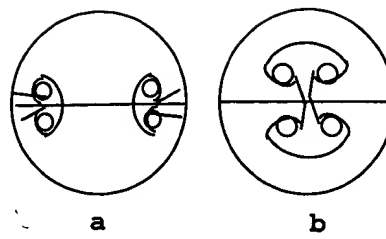


Figure 10.8: A sketch of the main secondary vortices. a: Type A Vortices; b: Type B Vortices.

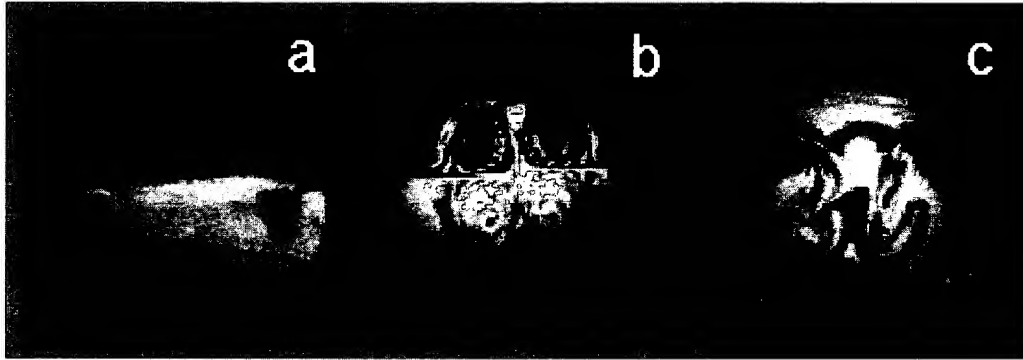


Figure 10.9: Cross view of types of secondary vortices: a: $\bar{U} = 4$ cm/s, $f = 4.5$ Hz, $A = 15\%$, $x/D = 0.1$; b: $\bar{U} = 1$ cm/s, $f = 5.21$ Hz, $A = 25\%$ $x/D = 1$; c: $\bar{U} = 10$ cm/s, $f = 5.48$ Hz, $A = 7\%$ $x/D = 4$.

10.2.1.2 Origin The disturbance from the forcing results in an impulse just at the trailing edge in vertical direction. This impulse will enhance the corner streamwise vorticity between the nozzle side wall and splitter plate due to the confinement. The streamwise vorticity would result in two secondary counter-rotating vortex pairs, i.e. Type A Vortices, just at the beginning of the wake (it may also induce the Type B Vortices directly but weaker than Type A Vortices). The Type A Vortices develop very fast at the initial stage depending on the forcing level. They could even meet at the axis of the pipe just at $x/D = 0.2$ (see Fig. 10.13). The disturbance also enhance the induction and development of the primary spanwise vortices, i.e. Karman vortex street (their axis is in spanwise direction) downstream of the trailing edge. The Type A Vortices and Karman vortex street, in turn, induce and strengthen the two Type B Vortices. They are all approximately symmetric in the vertical and spanwise direction and positively give impulse back to strengthen each other. Without forcing or with small forcing levels for small Re , Type A Vortices are weak. For such a case the Type B Vortices are mainly induced by spanwise vortex later.

Fig. 10.10 shows a time series of pictures at the same x -position for different time with an equal time difference δt of 0.04 s. The cross view shows the origin of the secondary vortices of a wake at $x/D = 1$, where $\bar{U} = 10$ cm/s, $f = 5.48$ Hz, $A = 7\%$. The impulse which is introduced by the forcing, can be distinguished in Fig. 10.10a. Such an impulse forces fluids in motion up and down in a vertical direction. Due the confinement of the wall, the forced fluids will turn to the sides in a counter-rotating direction symmetrically. When the fluids leave the splitter plate, it is easier for them to form the Type A Vortices, because Type A Vortices are much smaller at beginning than the Type B Vortices. This can be observed in Fig. 10.10a and Fig. 10.10b. Once two Type A Vortices are induced, they will, in turn, favor the induction of the two Type B Vortices which can be clearly seen in Fig. 10.10c and 10.10d. The development of both kinds of secondary vortices will also enhance the amplification of primary spanwise vortices. Due to the periodic forcing, this process also proceeds periodically and can be seen from Fig. 10.10a to Fig. 10.10f where a period is finished. This process emerges at once

when the fluids leave the trailing edge, which can be seen in 10.9a, where $x/D = 0.1$.

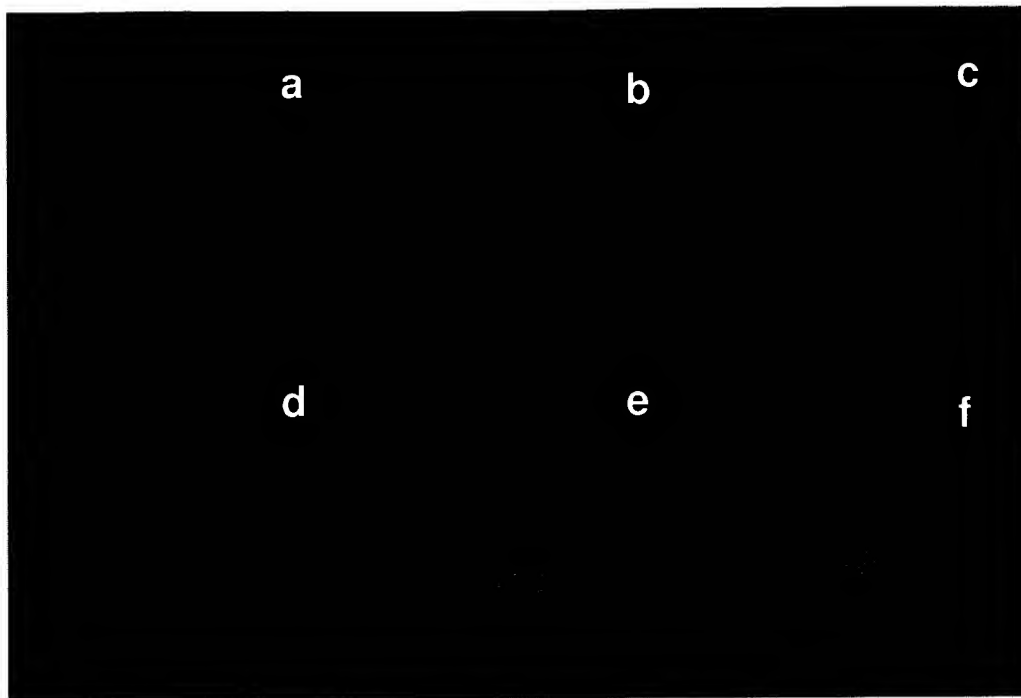


Figure 10.10: Cross view to show the origin of the secondary vortices of a wake. $\bar{U} = 10$ cm/s, $f = 5.48$ Hz, $x/D = 1$, $\delta t = 0.04$ s, $A = 7\%$.

10.2.1.3 Evolution Knowing the type and origin of the secondary vortices, we can better understand the evolution of the vortices. The Type A Vortices first develop very fast towards the axis of the pipe until they reach an equilibrium. During this developing process, the Type B Vortices are amplified in the vertical direction for two reasons: one is due to the development of the Type A Vortices, which give an impulse to the Type B Vortices; the other is due to the evolution of the primary spanwise vortex. As we know from instability theory, if the flow has the receptivity, the disturbance will amplify downstream and result in spanwise vortices. The amplification of spanwise structure will strengthen the Type B Vortices directly, which, in turn, enhance the development of the Type A Vortices due to the confinement of the wall.

Such an evolution is shown in Fig. 10.11, where $\bar{U} = 4$ cm/s, $f = 4.9$ Hz. A is around 20% at four different streamwise positions. In Fig. 10.11a, the Type A Vortices can be seen at the very beginning of the wake $x/D = 0.1$. These Type A Vortices amplify very fast at the beginning of the wake until they reach an equilibrium. They have already reached their equilibrium position, i.e. the axis of pipe even at $x/D = 1$ as shown in Fig. 10.11b. During this period, the Type B Vortices also develop their size. With the development of the Type A Vortices (which move towards the axis of the pipe) and the evolution of the primary vortex, the Type B Vortices are amplified in the vertical direction and the flow becomes three dimensional. This is shown in Fig. 10.11b. With further evolution downstream, only the Type B Vortices amplify. The Type A Vortices do not, because they have already reached the equilibrium. The amplification of the primary vortices, which directly induces the Type B Vortices later, takes a relatively long time. For these reasons, only the Type B Vortices are distinguished later in Fig. 10.11c, which indicates that the Type B Vortices have achieved their equilibrium state near $x/D = 3$. With further downstream, the no essential change could be observed as shown in Fig. 10.11d. It seems that this flow provides with a favorable condition for heat transfer enhancement.

A model for the Type A Vortices has been proposed by Roberts [89], which suggests that the velocity defect in the side wall is the reason for the origin of the Type A Vortices. However, this model

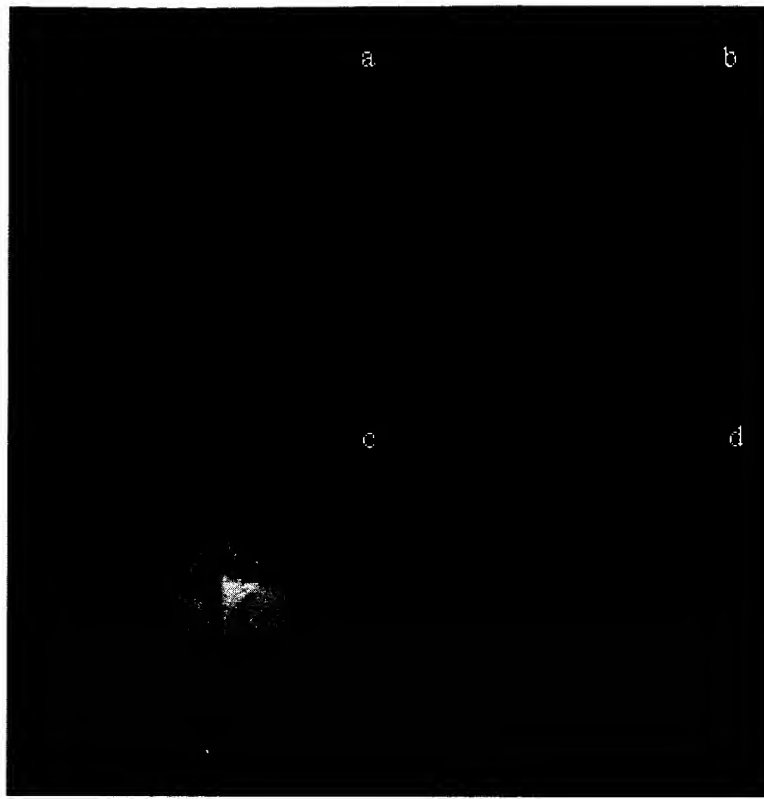


Figure 10.11: Evolution of secondary vortices (cross view). $\bar{U} = 4$ cm/s, $f = 4.9$ Hz. $A = 20\%$. a: $x/D = 0.1$; b: $x/D = 1$; c: $x/D = 3$; d: $x/D = 7$.

can not explain some results in this experiment (see discussion).

10.2.1.4 Characteristics

10.2.1.4.1 Symmetry The geometry of the dominate secondary vortices are approximately mirror symmetrical through the axis of vertical and horizontal planes. They can be seen in Fig. 10.9 and Fig. 10.12.

10.2.1.4.2 Geometry Usually the Type B Vortices are longer than the Type A Vortices at the beginning of the wake if the force level is not very strong. This is visible in Fig. 10.10b and Fig. 10.10c. With the evolution downstream, the sizes of the Type A Vortices and Type B Vortices are approximately at the same order. This can be seen in Fig. 10.11b. At small forcing or small Reynolds number, the Type A Vortices are amplified weakly, so the Type B Vortices are longer than the Type A Vortices in the investigated region, i.e. x/D is not larger than 7. This is shown in Fig. 10.12, where $\bar{U} = 1$ cm/s, $f = 4.62$ Hz, $A = 10\%$. However, for strong forcing under the maximum receptivity frequency of the new receptivity mechanism, the Type A Vortices can reach the axis of the pipe at once after the trailing edge. This can be seen in Fig. 10.13f.

10.2.1.5 Response to the forcing The dynamics of the secondary vortices, i.e. Type A Vortices and Type B Vortices is strongly related to the second receptivity mechanism under strong forcing. Fig. 10.13 shows the results at $x/D = 0.2$ for $\bar{U} = 7.5$ cm/s with $f = 5.6$ Hz for different A values. Fig. 10.13a represents the unforced one and there are already the Type A Vortices but no the Type B Vortices. In Fig. 10.13b and Fig. 10.13c, the flow is forced with A around 1% and 2% respectively. There is no apparent change for either the Type A Vortices or Type B Vortices. As A

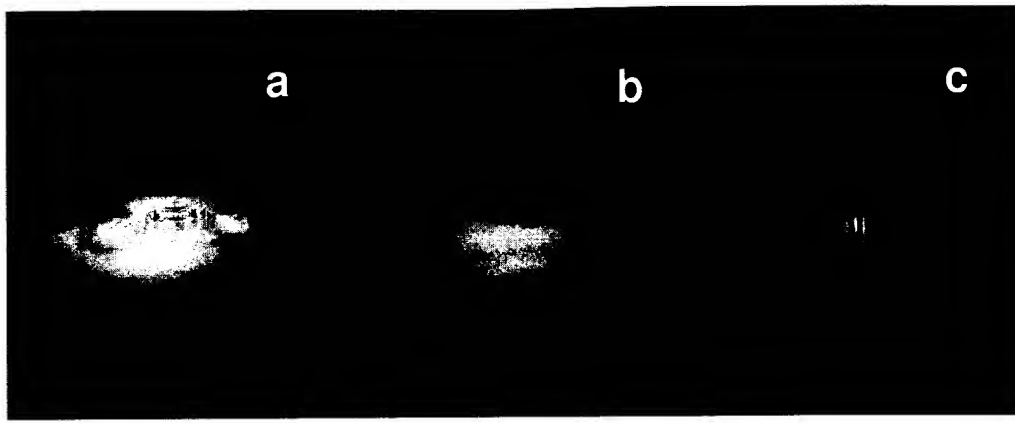


Figure 10.12: Cross view of the geometry of secondary vortices in a wake. $\bar{U} = 1 \text{ cm/s}$, $f = 4.62 \text{ Hz}$, $A = 10\%$. For a, b and c x/D is 1, 4 and 7 respectively.

is increased to around 7% as shown in Fig. 10.13d, the Type A Vortices are apparently amplified, both in size and propagating length, but there are still no the Type B Vortices here. However, in Fig. 10.13e, where A is around 30%, the Type A Vortices are greatly amplified, again in both size and propagating length because of the strong forcing. Due to the strong forcing and the development of the Type A Vortices, the Type B Vortices can now be observed too. Finally when A is about 60% in Fig. 10.13f, the forcing is so strong that the Type A Vortices have already reached the axis of the pipe and the Type B Vortices reach the wall of the pipe; the flow is so strongly disturbed that no clear Type A Vortices and Type B Vortices can be distinguished.

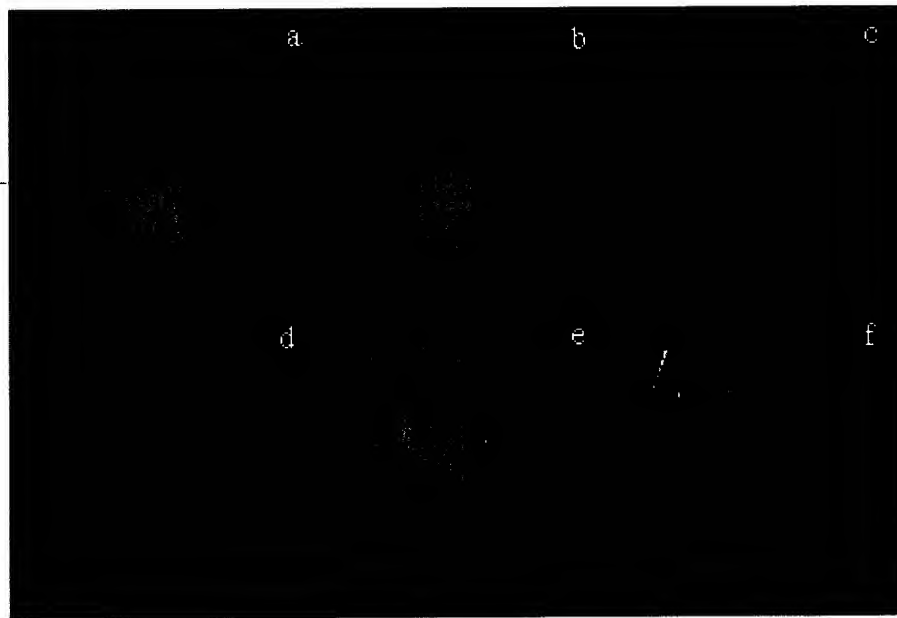


Figure 10.13: Secondary vortices under forcing with different A values in a wake.

10.2.2 Mixing layer

The above mentioned results for secondary vortices in a wake can also be obtained in a mixing layer. Here only the results showing the difference between the mixing layer to the wake will be discussed.

As mentioned for dual receptivity, the mixing layer displays the unusual bias and two counter-rotating vortices under strong forcing. These phenomena are related to the secondary vortices, which are shown below.

Fig. 10.14 displays the responses of the Type A Vortices and Type B Vortices to the forcing in a mixing layer, where U_1 and U_2 are 10 and 5 cm/s respectively under $f = 5.6$ Hz at $x/D = 0.2$ for different A . The flows here are under the same conditions as in Fig. 10.5. The unforced situation is shown in Fig. 10.14a. The Type A Vortices here are different from that of the wake, and so are the Type B Vortices. The Type A Vortices are not symmetric to the horizontal plane passing through the pipe axis, but are symmetric to the vertical one. The vortices of high velocity side are much smaller than that of low velocity side, so only the vortices of high velocity side are clearly seen, and the vortices of high velocity side are almost invisible. The fluid of the low velocity side moves to the high velocity side along the pipe wall and this show again a new secondary vortex. Fig. 10.14b shows the case with forcing A of about 1%. No essential difference for Type A Vortices can be observed between Fig. 10.14a and Fig. 10.14b. However, in Fig. 10.14c, where A is about 6%, the Type A Vortices are apparently amplified, and are again similar to their corresponding ones in the wake, i.e. the vortices of the counter-rotating vortex pairs from the high and low velocity side in each corner of the trailing edge, have nearly the same size. It is interesting that this situation corresponds to the case where the other kind counter-rotating vortex pairs in the side view of Fig. 10.5c begins to appear. This means that these two kinds counter-rotating vortices would occur under almost the same conditions and they could also be correlated to each other. The reason is that, the wake effect will play a dominating role for a mixing layer when the forcing is sufficiently strong. There are also the Type B Vortices here which are approximately two times wider than the Type A Vortices.

When the forcing A is increased to 8% as shown in Fig. 10.14d, the Type A Vortices do not propagate to the axis of the pipe, but at an angle to the high velocity side. Under the same conditions, the center line of the mixing layer in Fig. 10.5d begins not to bias to the low velocity side. This would be reason why the center line of the mixing layer does not bias to the low velocity side under strong forcing. In Fig. 10.14e, A is about 18%, the angle is increased and the mixing layer is biased to the high velocity side. The size of the Type A Vortices is larger than that in Fig. 10.14d. With further increase of A to around 32%, the Type A Vortices and Type B Vortices are further increased as shown in Fig. 10.14f and the difference between the size of these two vortices becomes smaller. Until A is around 52%, the forcing is so strong, that the Type A Vortices and Type B Vortices are rapidly amplified. The flow is strongly disturbed and becomes turbulence without any visible transitional process and thus no large structures of the Type A Vortices and Type B Vortices can be observed.

The evolution of the secondary vortices without and with forcing in the mixing layer, where U_1 and U_2 are 9 and 6 cm/s respectively, is shown in Fig. 10.15 and Fig. 10.16. In Fig. 10.15a and Fig. 10.15b, where x/D are 0.2 and 1 respectively, the Type A Vortices can be observed. Interesting is that the Type A Vortices are also counter-rotating vortex pairs in the mixing layer, although the vortex size in the high velocity side is much smaller than that in low one. During the evolution process, the high velocity fluid moves to the low velocity side in the center region of the pipe, while the low velocity side fluid moves to the high velocity side along the wall. Thus the Type A Vortices are also convected to the high velocity side as shown in Fig. 10.15c. and Fig. 10.15d where x/D are 2 and 4 respectively. The Type A Vortices keep their form during their evolution in the investigated range of x/D . For the forced one, f is 5.6 Hz and A is about 6%, the Type A Vortices are similar to those in a wake as shown in Fig. 10.16a ($x/D = 0.2$) and Fig. 10.16b ($x/D = 1$). Further downstream, the Type A Vortices develop very fast and almost reach to the axis of the pipe, which can be seen in Fig. 10.16c and Fig. 10.16d. A comparison of Fig. 10.15 and Fig. 10.16 indicates that the Type A Vortices are dramatically enhanced and amplified under forcing.

Another important phenomenon is that the Type A Vortices amplify very fast with strong forcing only under a special receptivity mechanism, i.e. the new receptivity mechanism, when Re is not small. Under traditional receptivity, the amplification of Type A Vortices is not so rapid. This can be observed in Fig. 10.17, where $U_1 = 30$ cm/s, $U_2 = 20$ cm/s. In Fig. 10.17a ($x/D = 0.2$), Fig. 10.17b ($x/D = 1$) and Fig. 10.17c ($x/D = 2$), the forcing is under the new receptivity mechanism, i.e. f is

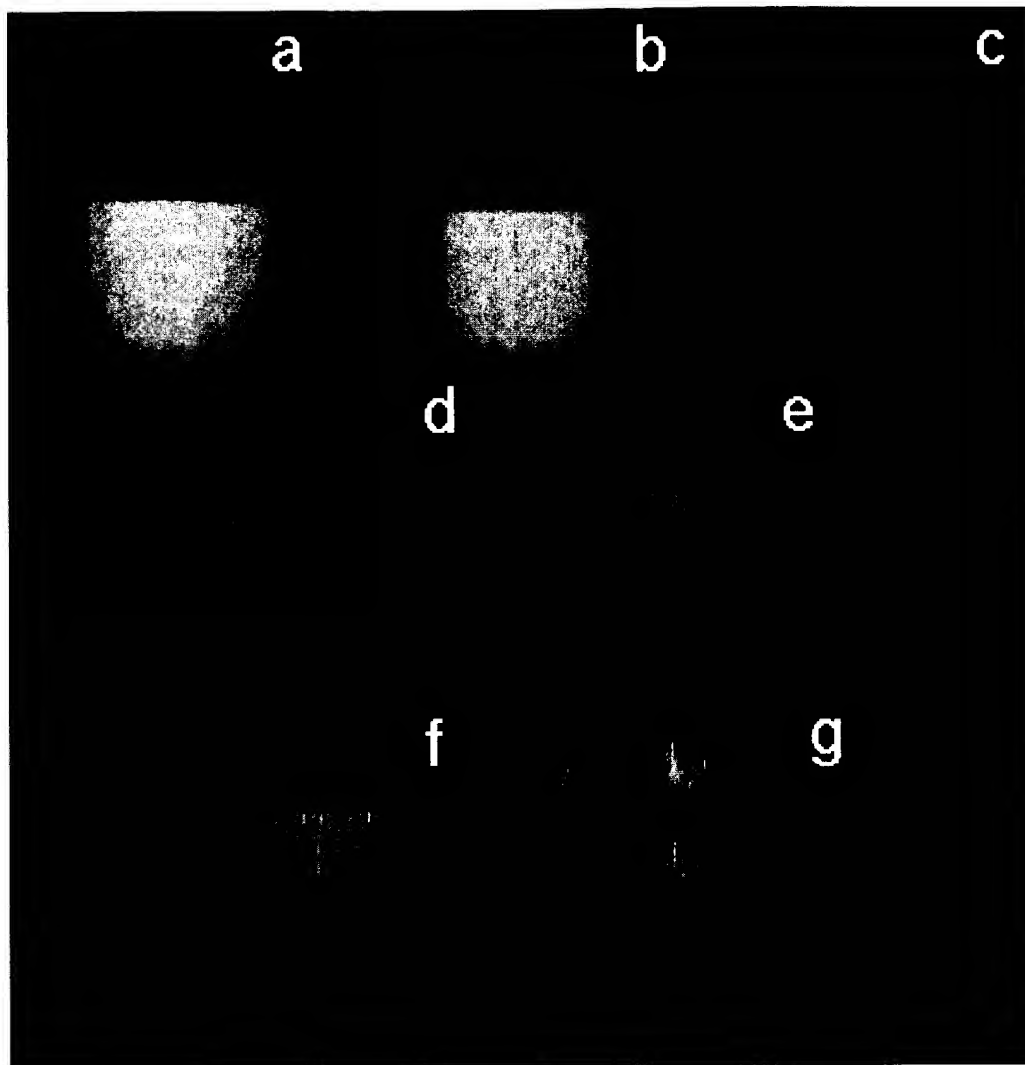


Figure 10.14: Secondary vortices with forcing for different A values in a mixing layer at $x/D = 0.2$.

6 Hz, while Fig. 10.17d ($x/D = 0.2$), Fig. 10.17e ($x/D = 1$) and Fig. 10.17f ($x/D = 2$) represent the forcing result under the traditional receptivity mechanism, i.e. f is 16 Hz. In the initial x-position, Fig. 10.17a and Fig. 10.17d show little difference. However, with the evolution, in Fig. 10.17e and Fig. 10.17f, the Type A Vortices propagate and amplify little, while in Fig. 10.17b and Fig. 10.17c, the Type A Vortices propagate and amplify much faster. Both have the same A value around 8%. The result indicates that under the traditional receptivity mechanism, the Type A Vortices develop much more slowly than under the new receptivity mechanism.

10.2.3 Quasi-step flow

The results of the secondary vortices in the quasi-step flow are qualitatively similar to that of the mixing layer. Details will be given later in a corresponding publication.

10.3 Sudden transition

It is found that the forcing, which leads to the sudden transition, depends on the receptivity mechanism, forcing frequency and forcing amplitude.

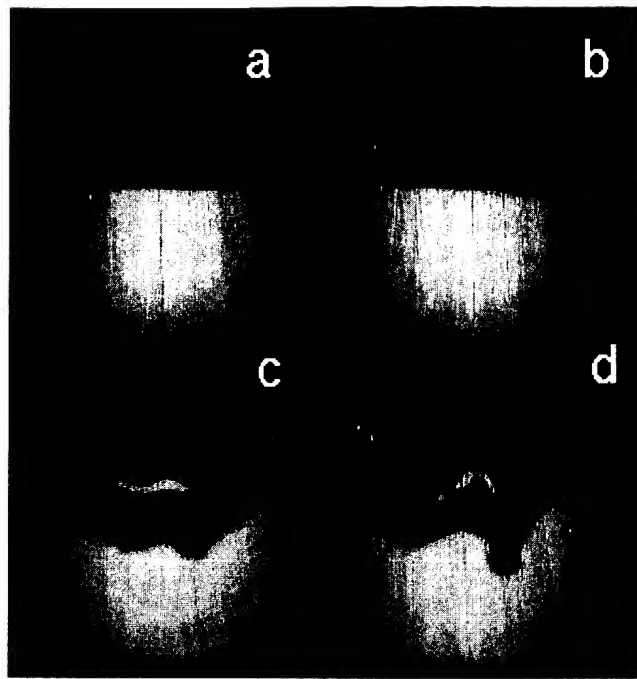


Figure 10.15: Evolution of the secondary vortices in a mixing layer without forcing. $U_1 = 9$ cm/s, $U_2 = 6$ cm/s. For a, b, c and d the x/D are 0.2, 1, 2 and 4 respectively.

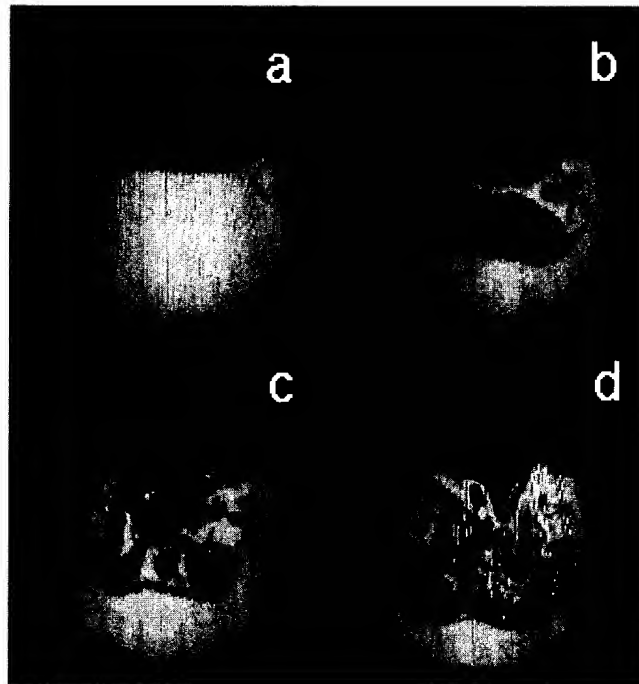


Figure 10.16: Evolution of the secondary vortices in a mixing layer with forcing. $U_1 = 9$ cm/s, $U_2 = 6$ cm/s, f is 5.6 Hz, A is around 6% . For a, b, c and d the x/D are 0.2, 1, 2 and 4 respectively.

10.3.1 Mixing layer

Fig. 10.18 and Fig. 10.19 show the forcing results for two different forcing frequencies under different forcing amplitudes. The frequency f in Fig. 10.18 and Fig. 10.19 is 6 and 16 Hz respectively. For

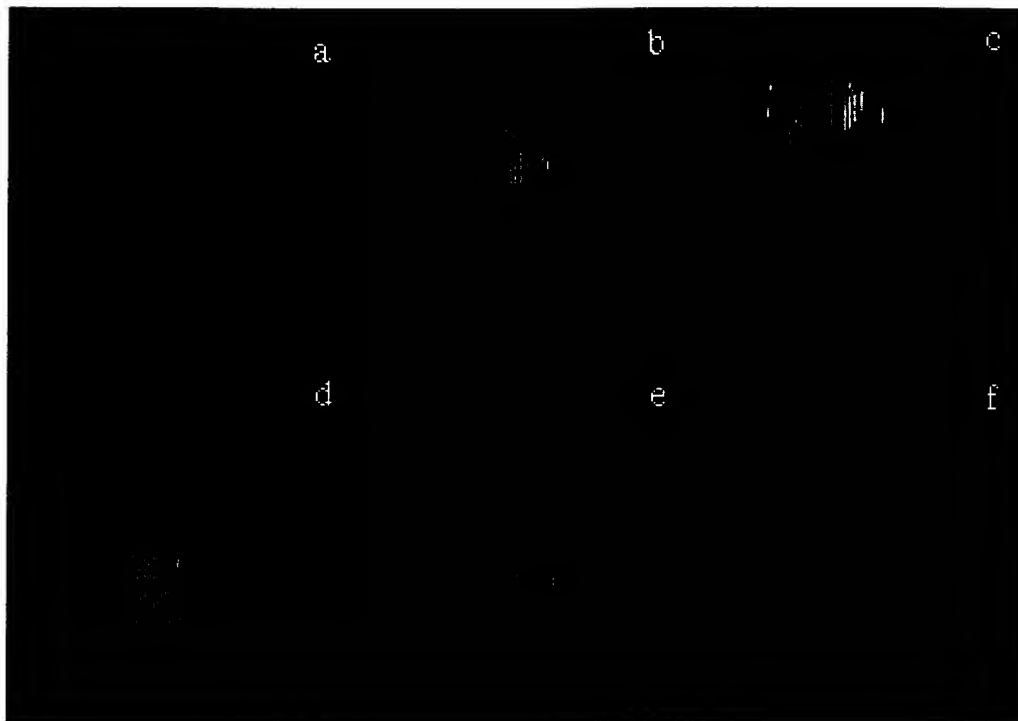


Figure 10.17: Comparison for different receptivity mechanism through secondary vortices.

the both cases, $U_1 = 30$ cm/s and $U_2 = 20$ cm/s. The visualization results show that under these two frequencies, the flow receives its maximum receptivity. However, the flow transition results are quite different for these two f values even though the forcing A values are the same under some conditions. There is no forcing in Fig. 10.19a and the flow at the beginning of the mixing layer is laminar. The forcing A from Fig. 10.19b to Fig. 10.19e is around 1%, 16%, 45% and 55% respectively. In Fig. 10.19, no sudden transition can be obtained even if A in Fig. 10.19e is about 55%. However, in Fig. 10.18 the transition result is quite different. Fig. 10.18a is the same flow as Fig. 10.19a, i.e. without forcing. From Fig. 10.18b to Fig. 10.18d, the value of A is increased to around 1%, 7%, 16% respectively. The flow seems to transit to turbulence earlier downstream as the value of A increases, but is still laminar at the beginning of the mixing layer, while in Fig. 10.18e where A is about 45%, it becomes turbulence immediately downstream from the trailing edge, i.e. the transition from laminar to turbulence takes place suddenly. Such a sudden transition becomes even stronger in Fig. 10.18f with the value of A about 55%. Here no bifurcation leading to turbulence can be observed.

The results of Fig. 10.19 and Fig. 10.18 indicate that the sudden transition to turbulence is related to the receptivity mechanism of forcing, i.e. the instability mechanism. Even though the flow is unstable to the external disturbance under traditional receptivity mechanism, it can not result in the sudden transition as in the case of Fig. 10.19, where the forcing level A is very high. However, if the flow has a strong receptivity, its instability mechanism to an external disturbance can result in the sudden transition under strong forcing as shown in Fig. 10.18.

In the side view of Fig. 10.5, the sudden transition produces a similar result to the transition in Fig. 10.18 here. Considering together Fig. 10.5 and its corresponding cross view of Fig. 10.14, one can suggest that the new kind primary counter-rotating vortex, the secondary vortices (Type A Vortices and Type B Vortices) and the interaction among these three kinds vortices are the reason for the sudden transition. The interaction strongly depends on the forcing mechanism, i.e. f and the forcing level A . The forcing level A must, for a given frequency, be sufficient high to cause the interaction, which, in turn, causes the sudden transition.

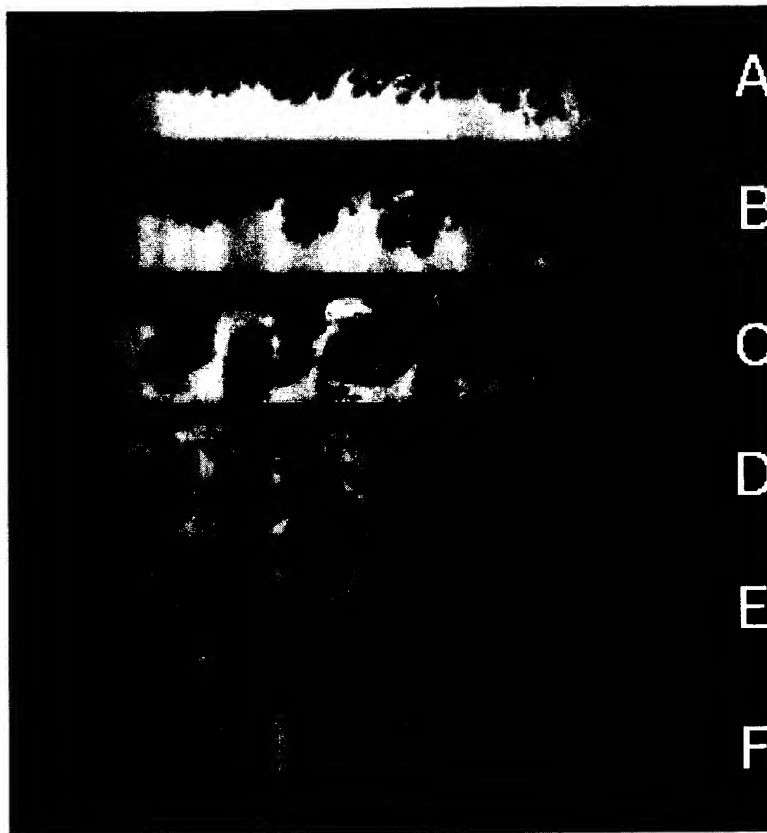


Figure 10.18: Sudden transition under strong forcing with f being 6 Hz. $U_1 = 30$ cm/s and $U_2 = 20$ cm/s.

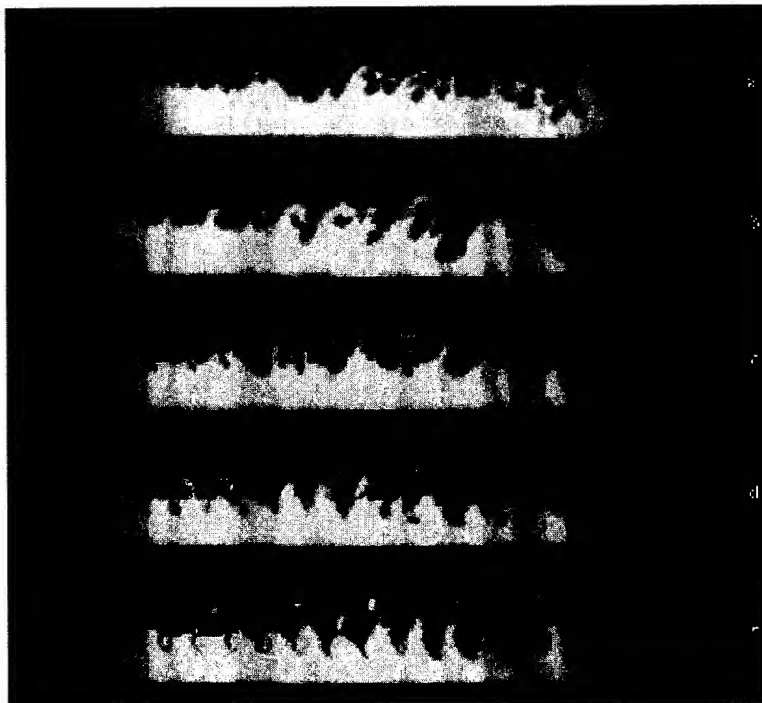


Figure 10.19: No sudden transition with strong forcing under f being 16 Hz. $U_1 = 30$ cm/s and $U_2 = 20$ cm/s.

10.3.2 Wake

The above mentioned sudden transition in a mixing layer can also be observed in a plane wake, as the dual receptivity can be obtained in both mixing layer and wake. The results can be seen in Fig. 10.2 and will not be discussed here.

The visualization results also indicate that with the increase of the initial Reynolds number, the forcing level needed to cause the sudden transition decreases with the Reynolds number. The velocity ratio λ has a weak effect on sudden transition.

10.4 Symmetry breaking hysteresis phenomenon

10.4.1 Phenomenon

In Fig. 10.1 where A is around 10%, the wake is normal and is symmetric to the splitter plate. In Fig. 10.5a and Fig. 10.14a of a mixing layer, where no forcing is supplied, the flow biases to the low velocity side as usual, while in Fig. 10.5e and Fig. 10.14e, the mixing layer biases to the high velocity side where the forcing amplitude is very high and around 18%. All these results indicate that for the strong forcing, the wake is symmetric, while the mixing layer has an asymmetric shear layer and biases to the high velocity side. However, here there is another very interesting phenomenon.

The visualization shows following results for a wake with $\bar{U} = 4$ cm/s under strong forcing with f being 6 Hz. At small forcing levels, the visualized wake is symmetric with a clear Karman vortex street. With the continuous increase in A , the Karman vortex street becomes larger in the near field keeping its symmetry. However, when the value of A is high enough at around 50%, i.e. achieves the sudden transition to turbulence, it is found that the wake suddenly becomes asymmetric and the highly churned up side of the wake biases to one side of the splitter plate (to which side it biases is a random process, and let us consider, for example, U_1 side here). At this state, the flow in the biased side is much more strongly disturbed than that in the other side (U_2 side). As we have known, for a mixing layer, the shear layer will bias to the high velocity side when the forcing is strong enough. Now we can postulate that it would be possible that the velocity U_1 of the biased side could be higher than U_2 of the other side even if the difference is very small due to the experimental error. Therefore the U_2 should, now, be increased very slowly in order to realize a symmetric wake. When the U_2 is increased to, for example, 4.5 cm/s, i.e. U_2 is apparently larger than U_1 , it is found that the bias of the wake does not change. Only when U_2 is increased to around 5 cm/s, will the highly churned up side of the wake suddenly bias to U_2 side and no symmetric wake can be obtained. Now if we decrease U_2 to 4 cm/s, the bias is still in the U_2 side. Only when U_2 is decreased to around 2.8 cm/s, will the bias again change to the U_1 side suddenly. Many trials have been done to keep the difference of $(U_1 - U_2)$ as small as possible, but they fail to obtain a symmetric wake when the sudden transition to turbulence was achieved. This phenomenon is called a symmetry breaking hysteresis phenomenon here.

It is difficult to show such a bias phenomenon using a static picture. Therefore no picture is shown here for the hysteresis phenomenon. However, it can be shown by using a video or quantitative vector or scalar measurements.

10.4.2 Relation to concentration distribution

Now it is the time to recall the results of the quantitative concentration measurements in part 1. If the wake is symmetric, the turbulent statistical results of concentration measurement should also be symmetric to the splitter plate in the y-direction. However, as mentioned earlier, when the forcing is strong enough to achieve the sudden transition, the highly churned up wake will demonstrate a random bias to one side of the splitter plate. Under this bias condition, the fluids on the biased side are more strongly stirred and move faster than on the other side. The ideal relative turbulent mixing process mentioned in part 1 is actually related to the sudden transition process described above, i.e. the sudden transition is a necessary condition for the ideal relative turbulent mixing process to be realized. This is why Fig. 5.21, Fig. 5.22, Fig. 5.23 and Fig. 5.24 show that the mixing results are

different and asymmetric in the y-direction, i.e. they are not symmetric to the splitter plate in the transverse direction, due to the symmetry breaking hysteresis phenomenon.

It is also observed that such a symmetry breaking hysteresis weakens as the Reynolds number increases. This can be proved by the comparison of Fig. 5.22 and Fig. 5.3, whose \bar{U} is 1 cm/s and 40 cm/s respectively. The asymmetric of concentration variance in Fig. 5.22 is stronger than in Fig. 5.3.

The symmetry breaking hysteresis phenomenon here indicates that the symmetric wake is a quasi-stable state under very strong forcing. This hysteresis is clearly related to the new receptivity mechanism mentioned above. Under other forcing frequencies, no such symmetry breaking hysteresis could be observed.

10.5 Pairing burst

The pairing burst is influenced by some parameters: the velocity ratio λ , the initial Reynolds number, temporal periodic forcing and so on, which are described as follows.

10.5.1 Where does pairing burst happen

It is found that the pairing burst is not apparent if the pairing happens relatively far away from the wall. Only when the pairing happens near the wall, the pairing burst will appear. Fig. 10.20 shows the case where $U_1 = 12$ cm/s, $U_2 = 8$ cm/s. The four pictures are in a time series with time difference between each one $\delta t = 0.28$ s. We are concerned with the arrows showing the vortices. In Fig. 10.20a, we can see the two vortices, which are pairing. Fig. 10.20b shows the moment just before pairing is completed. In Fig. 10.20c they have already paired. From Fig. 10.20d, it can be seen that the shear layer of the amalgamated vortex is still linearly spreading in the y-direction, i.e. no apparently ejection of the amalgamated vortex happens. This means that, there is pairing but no apparent burst. Fig. 10.20 is the critical situation between the situation of with and without the pairing burst. In Fig. 10.21, however, where λ is increased, $U_1 = 16$ cm/s, $U_2 = 4$ cm/s, δt is 0.08 s, we can see a different phenomenon. Fig. 10.21a shows that two vortices are pairing at a nearer wall region and in a more sweep-like way compared with Fig. 10.20. At this point the vortices have began to eject. In Fig. 10.21b, the two vortices are just paired, and at the same time, the amalgamated vortex ejects apparently from near wall region to the center of pipe in a burst-like way. Here we can see that the spread rate of the mixing layer is greatly increased. Fig. 10.21c is the continuation of the process in Fig. 10.21b. Fig. 10.21d shows the end of this process where the mixing is increased. The process from Fig. 10.21a to Fig. 10.21c is called "pairing burst". The difference in the pairing burst point of view between Fig. 10.20 and Fig. 10.21 is obvious.

10.5.2 Velocity ratio λ effect

The observation show here that for a given initial Reynolds number $Re_\theta = \sum \theta_{1,2} \bar{U} / \nu$, λ must be larger than a critical value λ_c , so that the pairing burst can happen. The larger λ is, the stronger pairing burst. The word "strong" here is just a qualitative description and means that it happens more frequently (for the same \bar{U}), and the vortex ejects to a greater distance from the wall. The above mentioned Fig. 10.20 and Fig. 10.21 are two situations with the same $\Sigma U = 20$ cm/s, but different λ . The λ of Fig. 10.20 and Fig. 10.21 are 0.2 and 0.6 respectively. From the above mentioned findings, it is clear that Fig. 10.21 has much stronger pairing burst than Fig. 10.20. Further observation finds that, with the increase of Re_θ , the λ_c will decrease, from which pairing burst can emerge. Fig. 10.22 shows the relationship between λ_c and Re_θ . It is revealed that, at low Re_θ , λ_c decrease with Re_θ very fast. However, with relatively high Re_θ , λ_c decrease slowly with the increase of Re_θ .

It can also be said, that at a given λ , there is a critical Re_θ , over which pairing burst can occur. If the Re_θ is small, pairing burst is still very weak, even if λ is very large. This is showed in Fig. 10.23, where λ is 1 and U_1 is 8 cm/s with $\delta t = 0.16$ s. This is a quasi-step flow, where U_2 is zero. However, if Re_θ is large enough, there is pairing burst in the quasi-step flow as shown in Fig. 10.24 where U_1 is

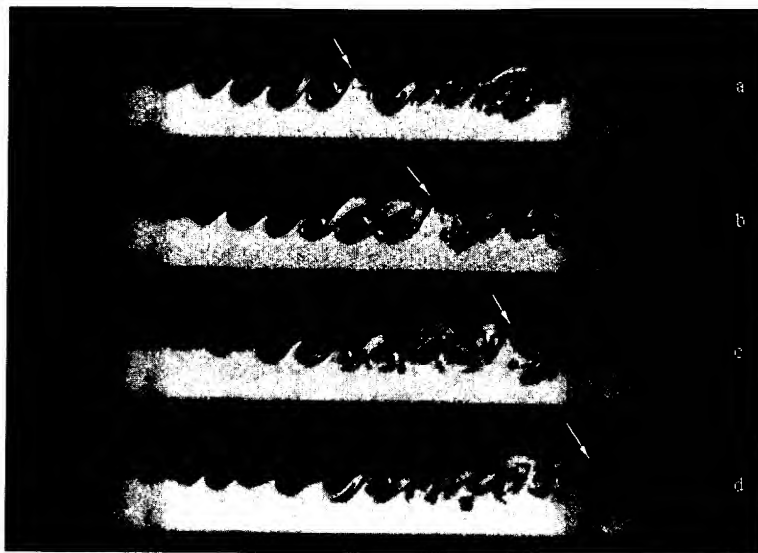


Figure 10.20: Pairing burst is not apparent in a mixing layer where U_1 and U_2 are 12 cm/s and 8 cm/s respectively.

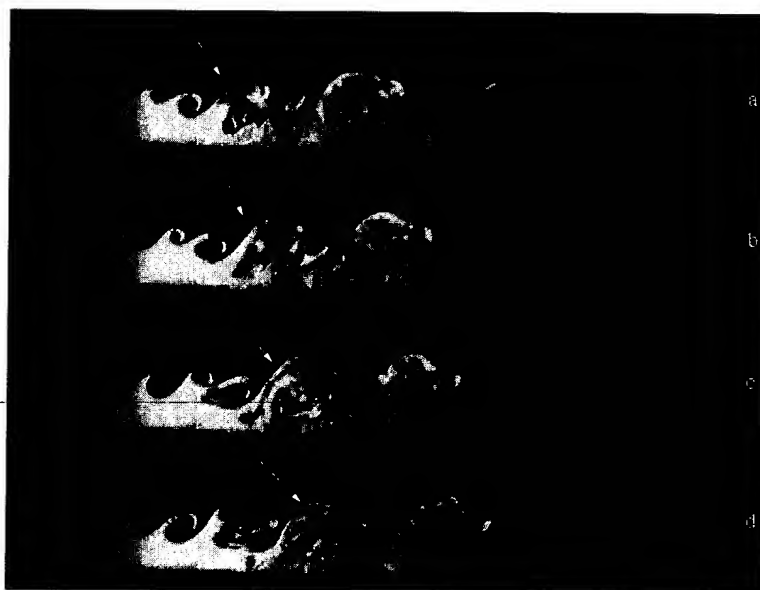


Figure 10.21: Pairing burst is apparent in a mixing layer where U_1 and U_2 are 16 cm/s and 4 cm/s respectively.

12 cm/s with $\delta t = 0.12$ s. That means there is also pairing burst in a quasi-step flow. The higher Re is, the stronger pairing burst is.

10.5.3 The influence of initial Re_θ

The pairing burst will be strengthened as Re_θ is increased. Fig. 10.25 and Fig. 10.26 show the situations with the same λ , but different initial Re_θ . In Fig. 10.25, $U_1 = 24$ cm/s, $U_2 = 16$ cm/s. $\lambda = 0.2$, $\delta t = 0.12$ s, and in Fig. 10.26, $U_1 = 36$ cm/s, $U_2 = 24$ cm/s, $\lambda = 0.2$, $\delta t = 0.08$ s. The difference is apparent compared to the pairing burst process in Fig. 10.25 and Fig. 10.26, the pairing burst in Fig. 10.26 is stronger than in Fig. 10.25.

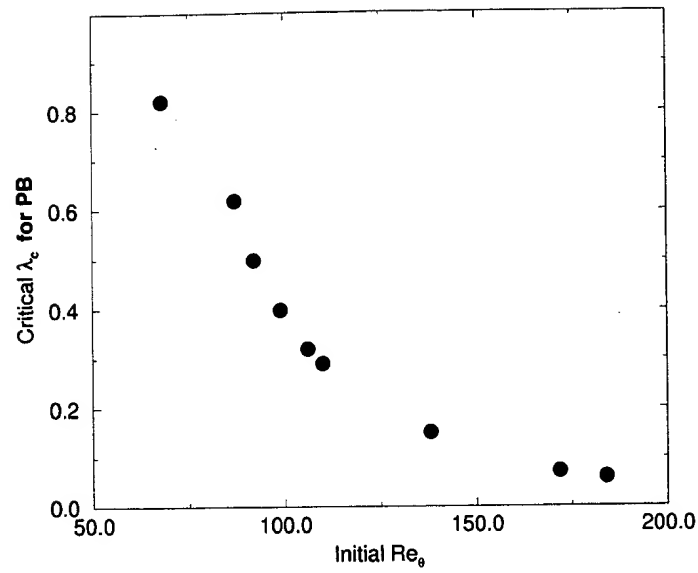


Figure 10.22: Relationship between λ_c and Re_θ .



Figure 10.23: No pairing burst for small Re_θ in a quasi-step flow.

10.5.4 Forcing influence

Temporal periodic forcing can under some conditions influence the pairing burst, i.e. either enhance or weaken the pairing burst. Fig. 10.27 shows the case without forcing where $U_1 = 15$ cm/s, $U_2 =$

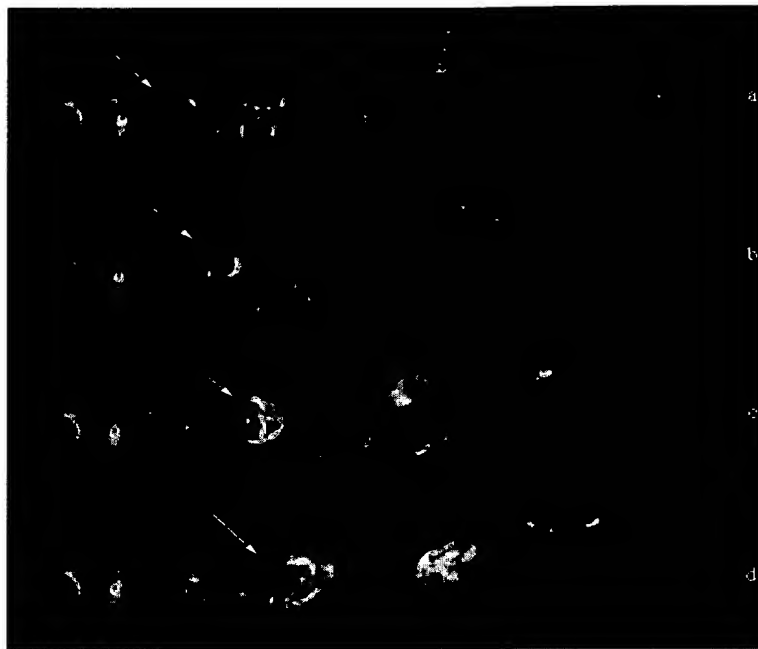


Figure 10.24: There is pairing burst in a quasi-step flow.

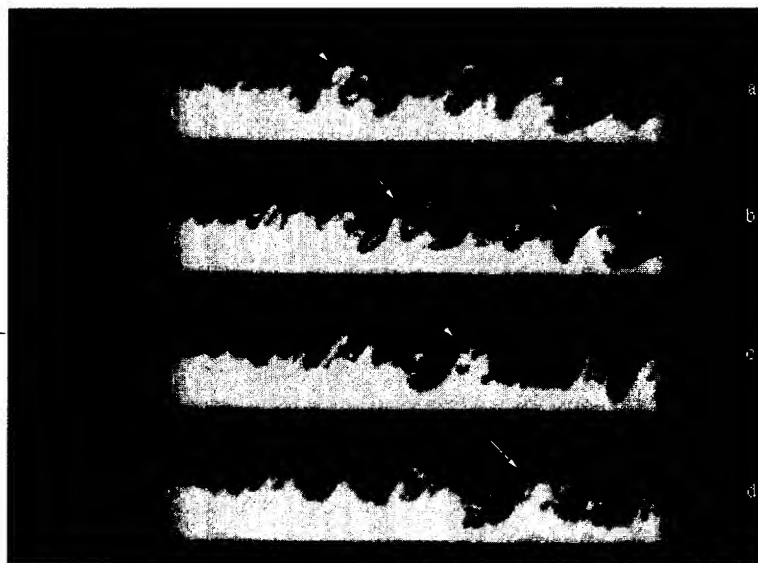


Figure 10.25: Pairing burst in a mixing layer with $U_1 = 24$ cm/s, $U_2 = 16$ cm/s. $\lambda = 0.2$ and $\delta t = 0.12$ s.

3 cm/s, δt is 0.16 s, while Fig. 10.28 shows the enhancement case with forcing for the same flow as shown in Fig. 10.28 and its δt is 0.12 s, f is 3.2 Hz and A is around 5%. Both are three sheets, i.e. 3-D views. From the side views (middle one) of Fig. 10.27, the pairing is clearly visible, but the ejection is relatively weak, while Fig. 10.28 clearly displays a forced-vortices pairing burst. The amalgamated vortex ejection is obviously enhanced and occurs earlier under this forcing condition than unforced one. That means forcing not only strengthens the pairing burst, but also makes it happen earlier.

Fig. 10.29, on the other hand, presents a result of weakening the pairing burst. Here $U_1 = 16$ cm/s, $U_2 = 4$ cm/s, δt is 0.16 s, $f = 5$ Hz and A is around 2%. Its unforced case is shown in Fig. 10.21 where there is an apparent pairing burst. However, the turbulent mixing under forcing is apparently

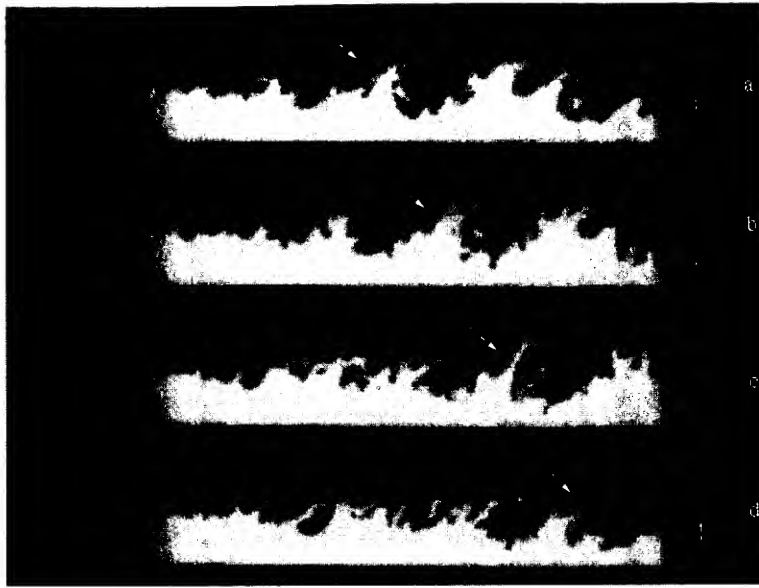


Figure 10.26: Pairing burst in a mixing layer with $U_1 = 36$ cm/s, $U_2 = 24$ cm/s, $\lambda = 0.2$ and $\delta t = 0.08$ s.

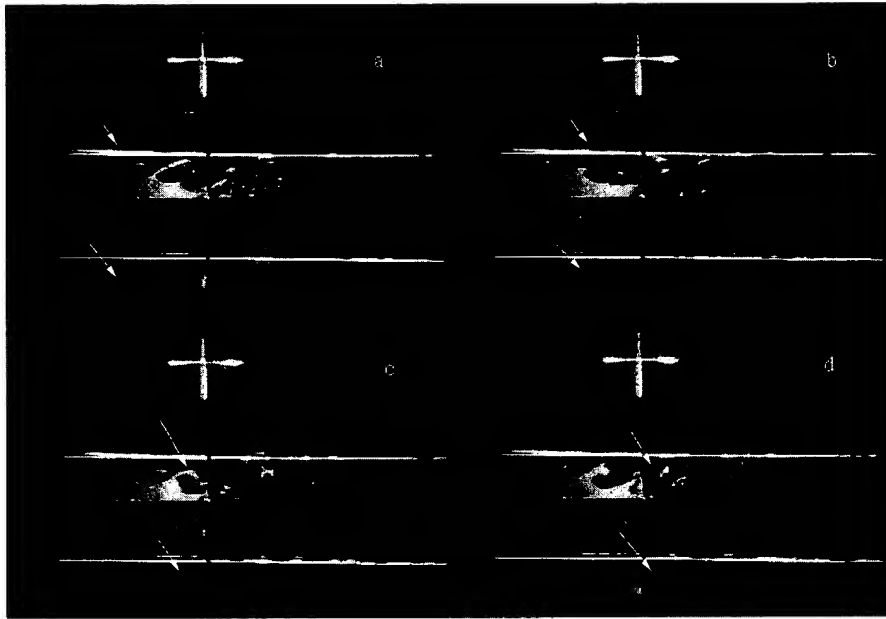


Figure 10.27: No forcing with the weak pairing burst.

enhanced in comparison between Fig. 10.21 and Fig. 10.29. This indicates that, although the pairing burst can enhance turbulent mixing, the turbulent mixing can be even stronger without pairing burst than with pairing burst in some case.

10.5.5 Three dimensional pairing burst

Since this is a 3-D mixing layer, the pairing burst happens three dimensionally. This means, it can also be distinguished in the plan view. The pairing burst in plan views are also shown in Fig. 10.27 and Fig. 10.28. The plan view in Fig. 10.27a shows the two vortices which are going to pair. Its corresponding three dimensional vortices are also visible in the side view. In Fig. 10.27b the two

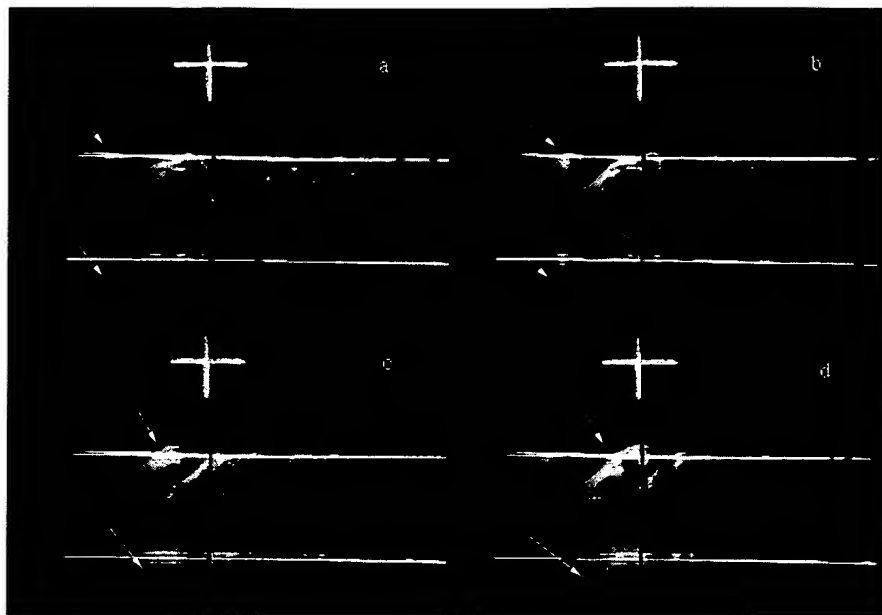


Figure 10.28: With pairing burst under forcing.



Figure 10.29: Pairing burst is weakened through forcing.

vortices in plan view have already paired, and the pairing burst can also be distinguished. The corresponding two vortices in side view have, however, still not paired. The pairing burst in the side view happens in Fig. 10.27c and continues until Fig. 10.27d. The pairing burst in plan view also continues until Fig. 10.27d, where they are coincident with their corresponding parts of the spanwise view in almost the same streamwise position. This process means that the pairing burst in plan view appears earlier than the corresponding pairing burst in the spanwise view, due to the fact that they are more close to the wall than the corresponding pairing burst in the spanwise view. However they are on topology the same vortices, therefore they end such a kinematic process at almost the same streamwise position. The similar phenomenon can more clearly been seen in Fig. 10.28, where the flow is under strong forcing. There is, a little difference. The pairing bursts from both the side and plan view emerge at almost the same x-position under strong forcing. The result indicates that the forcing strengthens the whole 3-D pairing burst.

10.5.6 *Re* in the confined mixing layer

An important question is: what is the Reynolds number for the pairing burst in this 3-D mixing layer, i.e. what is the characteristic length and velocity? For a traditional 2-D mixing layer, the initial

momentum thickness is usually used as the characteristic length and ΔU is used as the characteristic velocity since it is the potential of the shear layer. However, in the confined mixing layer, it is found that the average \bar{U} could be the characteristic velocity for the pairing burst in the investigated Reynolds number range. This can be explained in Fig. 10.30 and Fig. 10.31. In Fig. 10.30, $U_1 = 17.5$ cm/s, $U_2 = 1.5$ cm/s, $\lambda = 0.84$, $\delta t = 0.2$ s, and in Fig. 10.31, $U_1 = 25$ cm/s, $U_2 = 9$ cm/s, $\lambda = 0.47$, $\delta t = 0.16$ s. As far as λ is concerned, the pairing burst in Fig. 10.30 should be stronger than that in Fig. 10.31, but actually the pairing burst is stronger in Fig. 10.31 than in Fig. 10.30. If ΔU is used as the characteristic velocity, the initial Re of Fig. 10.31 is smaller than that of Fig. 10.30, since the ΔU is the same for the two cases and the initial momentum is higher in Fig. 10.30 than in Fig. 10.31. If ΣU is used as the characteristic velocity, however, the initial Re in Fig. 10.31 is larger than that in Fig. 10.30. Therefore the ΣU should be used as the characteristic velocity, at least when Re is within the range of this experiment.

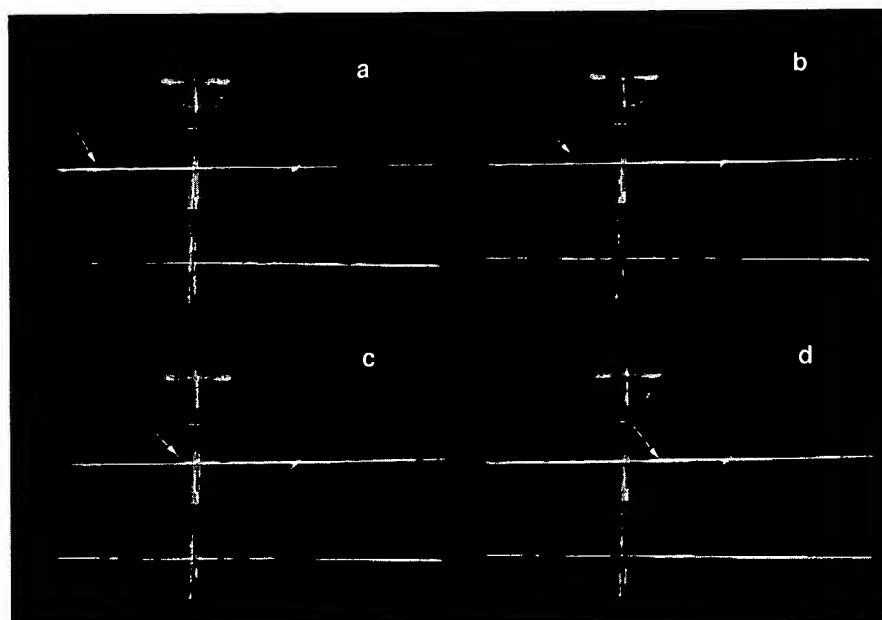


Figure 10.30: Pairing burst is relatively weak when U_1 and U_2 is 17.5 and 1.5 cm/s respectively.

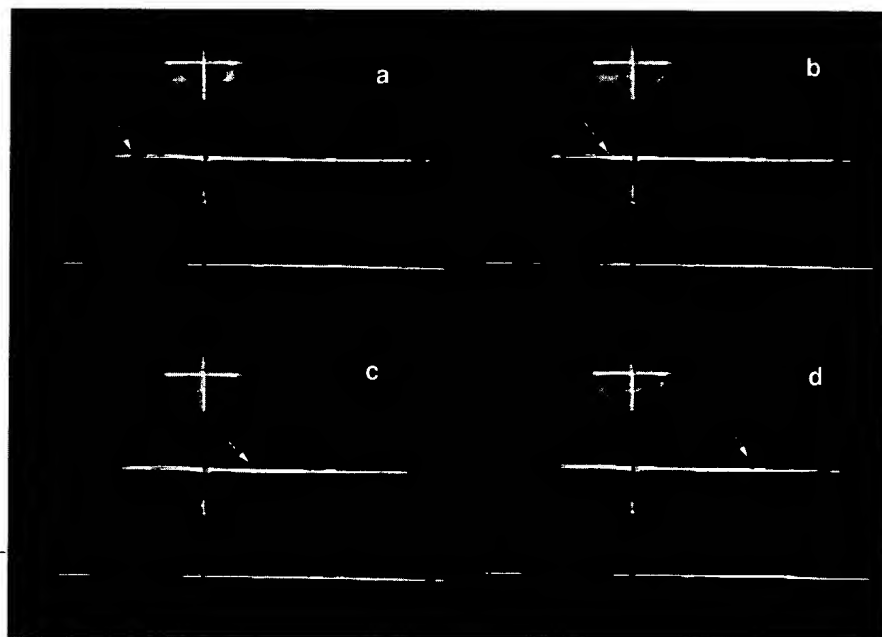


Figure 10.31: Pairing burst is relatively strong when U_1 and U_2 is 25 and 9 cm/s respectively.

11 Discussion

11.1 Dual receptivity

11.1.1 Relation to secondary vortices

Now we can discuss the mechanism of the receptivity in the confined wakes. As mentioned above, the first one corresponds to the traditional 2-D plane wakes and will not be discussed here.

The visualization results indicate that the new receptivity is related to the secondary vortices, i.e. Type A Vortices and Type B Vortices. Firstly, to get fast amplification of type A vortices and the new (second) receptivity, the forcing level should be high enough as shown in Fig. 10.13, Fig. 10.16 and Fig. 10.3. Secondly, the large forcing can enhance the development of the Type A Vortices and Type B Vortices because of the wall confinement. These two kinds vortices impulse each other, and enhance the amplification of primary vortices. Due to the fast development and strong amplification of the Type A Vortices in the initial period shown in Fig. 10.17, the second receptivity is much stronger than the traditional (first) one. Consequently this 3-D wakes have much stronger receptivity than its corresponding 2-D ones. This is the reason for the rapid mixing enhancement and the fundamental of the realization of the ideal relative turbulent mixing process investigated in part 1. Thirdly, the reason of why the value of f_{2max} is constant, appears to be related to the secondary vortices too. If the Type A Vortices are the initial vortices which cause the large second receptivity, the Strouhal number St should be related with the convection velocity in the direction, where the Type A Vortices amplify. However, since there is no convection velocity in the spanwise direction, i.e., the convection velocity has a zero decomposition in this direction, f_{2max} is not scaled with U . That why f_{2max} is around 6 Hz is still open, it may depend on the geometry, the size of the channel, and the inlet initial conditions. Interesting is that in the work of Mackinnon & Koochesfahani [69] they also use 6 Hz where the geometry is different from here.

It seems that the 6 Hz is not the resonance frequency of the water channel. Two experiment results can be used to prove it. First, the actuator forces at 6 Hz with the fluid at rest, and no vibration of the water channel can be observed. Second, when the flow with the velocity in the experimental range is forced in the frequency range of $37 \sim 40$ Hz, the water channel begins to vibrate with some acoustic noise. This means the system resonance frequency of the water channel would be in the range of about $37 \sim 40$ Hz.

Although the wall has strong influence in this flow, it is also distinguishable from Tollmien-Schlichting wave mechanism, which is often the main reason for boundary turbulent flow receptivity. It should be mentioned here that the confined plane wake is a 3-D flow and more complicated than its corresponding 2-D wake.

Finally, it is needed to mention that no matter if the mechanism of the new receptivity is clear or not, one thing is already clear: the large receptivity and thereby the resulted in extraordinary rapid mixing is very attractive for mixing enhancement of mixers, reactors and combustion in industry. One of the related application topic is referred to Wang [112].

11.1.2 High receptivity

The papers of Liu & Merkin [68], Alper & Liu [2] and Gatski & Liu [43] using energy integral methods indicate that, a large energy transfer from the mean flow to the fine-scale motion as the large-scale disturbance reaches a maximum. For the strongest forcing of the new receptivity mechanism, the small-scale is achieved extraordinarily fast as e.g. shown in Fig. 5.20 and Fig. 10.5. This indicates that large-scale disturbance could reach a maximum value in a very short downstream distance from the trailing edge, and thus, a very high receptivity in the confined configuration.

11.1.3 Qualitative amplification curves with Re

From Michalke's work [71], it is known that inviscid instability can be applied to the free shear layer. The theoretical prediction of disturbance amplification indicates that there is only one Strouhal number St , at which the flow has maximum spatial amplification rate. This St is a constant and independent of Re for a given flow. In other word, if the dimensional frequency is used instead of St , the traditional instability theory will show that the frequency, which corresponds to maximum amplification rate, is scaled with the average convection velocity \bar{U} . Wygnanski et al [121] showed that the inviscid linear instability could also be used in a plane wake. However, in this confined plane wakes, it is found that, except the traditionally one, there is also another St corresponding to the maximum amplification rate of the second (new) receptivity, which is related to the Re or \bar{U} (Re is increased through the increase of \bar{U}). Its corresponding dimensional frequency f is a constant. In this viewpoint, the result here extends the scope of classical theory. Fig. 11.1 gives a diagram to qualitatively describe the extended result of this instability mechanism, at least to show the influence of the wall on the instability. Fig. 11.1a uses dimensional frequency and Fig. 11.1b dimensionless St .

The large disturbance used here for the new receptivity may cause the flow to be a unsteady one and therefore the new receptivity could be related to the instability mechanism of a unsteady flow, which may has a high receptivity, as first suggested by Zhou [122].

11.1.4 No universal spread rate

Many different results shown here are different from that of the traditional 2-D free shear layer. This indicates that the wall effect on the flow is very strong, especially under forcing. Usually it is thought that, the 2-D spanwise structures are the main reason for the entrainment (and thereby the spread rate of the shear layer), e.g. [16]. Winant & Browand [120] thought that, the pairing is important for the growth of the shear layer. However, Some others, e.g. [47] [37] pointed out that the pairing process was not the only mode of growth of the shear layer, and that most entrainment is achieved during the normal life of the large spanwise vortex structures, but not during the pairing. Lasheras et al. [66] found that, the streamwise vortices also contribute to a substantial part of the entrainment, i.e. the spread rate.

The visualization results shown in this work indicate that without forcing, the pairing has more contribution to the spread rate, and its effect on the spread could increase with velocity ratio. However, with strong forcing, the pairing plays no role for the spread, but both the primary spanwise and the secondary vortices during their normal life, and the effect of secondary vortices on the spread rate increase with the forcing level.

Due to the published common and limited range of the spread rate in mixing layers, Browand and Ho [15] proposed a universal spread rate for mixing layers, which also includes forced flow situations. Dimotakis [30] remarked that there was a rather large spread of values in the spread rate of mixing layer, and it was even not clear whether the inequality bounds represented the actual limiting values. Normally, in a 2-D mixing layer, the spread angle at the beginning is no larger than 30° when forcing is applied, and the half-velocity isotach is moved slightly to the lower velocity side. In this investigation, it is found that for some different forcing amplitudes and frequencies, this isotach can not only keep symmetric to the trailing edge (i.e. not bias to the low velocity side), but also even bias to the higher velocity side, where the spread angles exceed 30° by far and even can reach to 180° (the limitation). Therefore it seems that there is no universal spread regime. This strong deviation from known cases might be related to wall effects, secondary vortices, and in particular to the new receptivity mechanism.

11.1.5 Small scale and mixing transition

When the mixing layers are initially laminar, they become eventually turbulent in a process know as the small-scale transition. For scalar mixing, Konrad (1976) proposed a concept called "mixing transition", which takes place at downstream position, where the molecular "mixedness" of scalar increases sharply [61] [9] [62]. It is speculated that, from the results of, e.g. Jimenez et al. [54] and

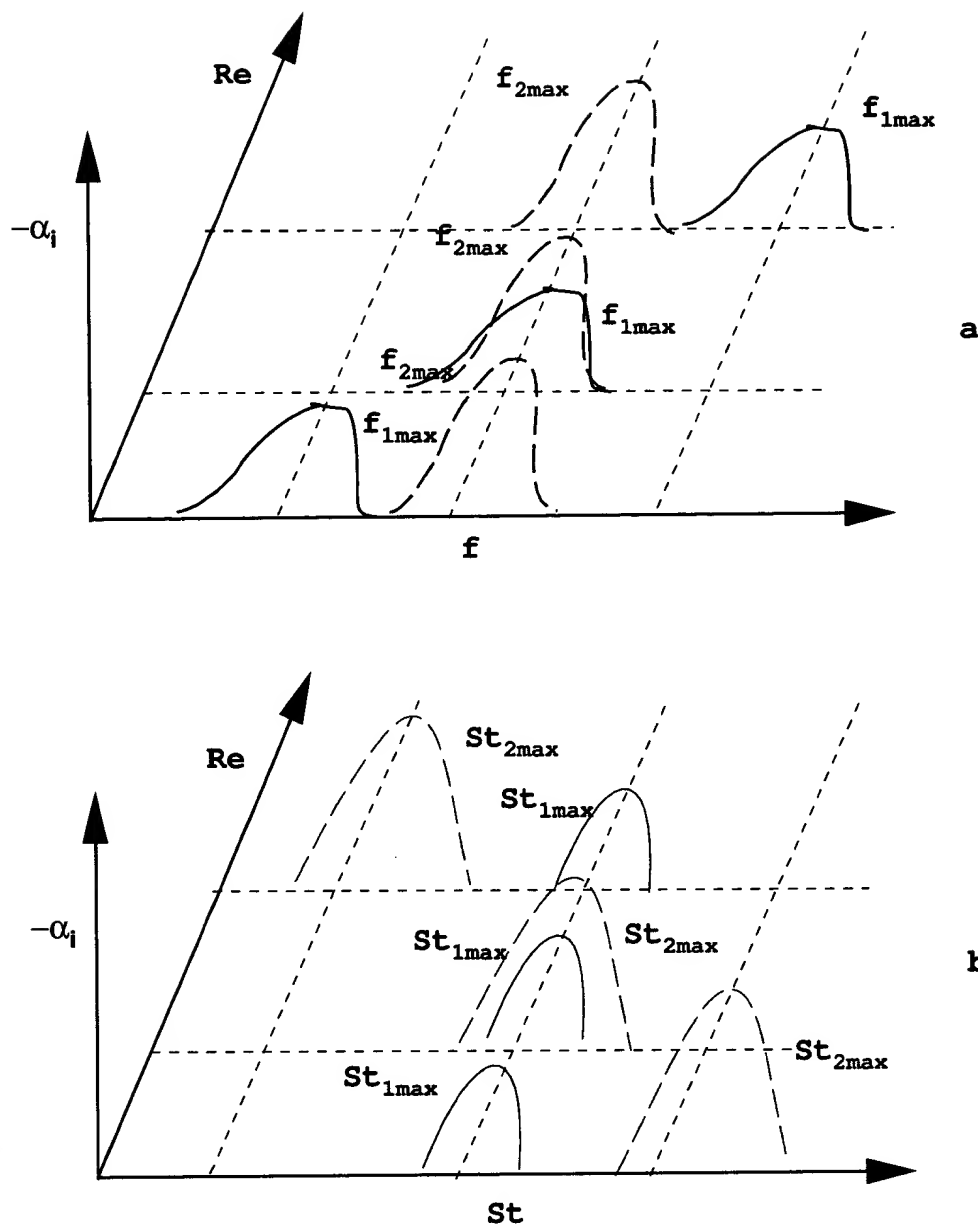


Figure 11.1: Sketch of qualitative amplification rate with Reynolds number.

[51], the large strain rates that result from the coalescence of the orderly structures are responsible for the generation of small-scale eddies [50] and [91].

However, under the strong forcing of the new receptivity mechanism, no spanwise rolls and coalescence in the shear layers for the entrainment and small-scale transition can be observed as shown in Fig. 10.5d-g. This is because under strong forcing, the secondary develops very fast, and the momentum transfer between the two streams are very high, the strain rate will not be very high. This is again a fact that shows the different mechanism of the new receptivity from the traditional one.

11.1.6 Influence of non-linearity and 3-D on amplification

Squire theorem [101] tells us that, the 3-D flow has a smaller amplification than its corresponding 2-D flow. Wall usually makes a flow more stable, since near the wall the viscosity has more influence to decay the disturbance than in a wall-free shear flow. In the shear layer, the disturbance amplifies

first to a certain range, where the non-linearity will dominate, and this non-linearity often hinders the amplification of the disturbance. Based on these viewpoints, the receptivity in the confined wakes ought to be smaller than its corresponding 2-D wakes. However, the experiment results of this work, in contrast, tell us that, the receptivity in a confined plane wakes in a pipe is stronger than in the 2-D wakes. This implies that the wall has two effects. On the one hand, it makes the flow more stable in response to the external disturbance; on the other hand, the confinement of the wall facilitates the Type A Vortices and Type B Vortices, which, in turn, increase the receptivity of the flow.

11.1.7 Receptivity capacity

Traditionally the receptivity can be described through the amplification rate in a spatial or temporal mode. The larger the amplification rate is, the stronger the receptivity is. The concept was first used for transition from laminar to turbulence in aerodynamics. However in some processes concerning the control of mixing, noise, and combustion instability, such a criterion is sometimes not sufficient to describe the processes. For example, the coherent velocity component \tilde{u} is an important quantity. If the value of coherent velocity component \tilde{u} is large in the initial stage, the relative turbulent mixing will be stronger. The fluids will then be more homogeneous for mixing in combustion and reaction flow in a reactor (especially for the whole flow field), and the combustion will be more stable and the noise can be smaller. When the initial \tilde{u} is small, \tilde{u} will not be large in a limited developing space even if the spatial amplification rate $-\alpha_i$ is large. If the flow can accept large external disturbance, that means, \tilde{u} is large even at the beginning of the shear layer, and if $-\alpha_i$ is also large, a much larger \tilde{u} can be obtained even in a limited initial developing distance. In such a case, a new criterion should be used for receptivity. It can be the product of disturbance \tilde{u} and amplification rate $-\alpha_i$, i.e. $-\alpha_i\tilde{u}$, for instance, in a spatial mode. We can first call it "*receptivity capacity*". According to the experimental results, it can be seen, the above mentioned new receptivity has a larger receptivity capacity than the traditional one. The higher the forcing amplitude, the larger the receptivity capacity of the new receptivity mechanism as compared to the traditional one.

11.1.8 Mixing receptivity

Receptivity concept is used for the amplification of velocity disturbance as mentioned above. On the one-hand, the visualization results in the very near-field presented here at least qualitatively show a new receptivity mechanism and its receptivity (or receptivity capacity) is much stronger than the traditional one, especially for the high forcing amplitude. On the other hand, the visualization in this part and quantitative scalar measurement in part 1 have already quantitatively shown the response of scalar mixing to the initial external forcing. A corresponding concept of "*mixing receptivity*" is therefore proposed to describe this phenomenon, i.e. the receptivity of a flow to an external forcing for the mixing enhancement. The parameters used to describe the mixing receptivity for vector can be the amplification rate and receptivity capacity, since they are related to momentum, energy and vorticity mixing. The parameters used to describe the mixing receptivity for scalar can be those used in part 1, e.g. the relative mixing rate, the variance, pdf and psd of scalar. It describes how a flow accept the external disturbance to change its mixing property. The result in Fig. 10.2, shows that the mixing receptivity for the new receptivity mechanism is much stronger than the traditional one. This provides us with a new way of controlling the turbulent mixing to achieve the ideal relative turbulent mixing process and state proposed in part 1. Therefore the concept of the ideal relative turbulent mixing process and state propose a goal for turbulent mixing control and the mixing receptivity mechanism here provides a way to achieve the aim, and thus a new system for the mixing study and mixing control is established.

11.1.9 Difference from mechanical stirring

It is worth mentioning that the second receptivity here is not simply just a result of a large disturbance or mechanical stirring, and therefore is not of interest of studying receptivity. It is a phenomenon of

receptivity, since only when the disturbance is in the narrow frequency band, there is the receptivity. If the disturbance is not in the narrow band, there is no receptivity at all even though the disturbance can be larger at a high frequency. This is the important difference between the confined configuration here and the agitated tank used in chemical engineering, where the higher the rotation of the turbine impeller is, the stronger the mixing is.

11.1.10 Philosophy on control

Traditionally the philosophy of control is that a small disturbance produces a large effect like Tai-Chi-Chuan principle: use only 0.2 kg to move 500 kg. In fluid mechanics, a small initial disturbance is introduced to the flow to expect a large effect, e.g. mixing augmentation. It is fine if this is possible and sufficient for the practical requirement. Unfortunately the coherent velocity component \tilde{u} due to disturbance amplification with a small initial disturbance is, in many cases, not large enough, for instance, for mixing dominating processes, since rapid mixing process needs first large \tilde{u} to achieve macromixing and then to develop from large to small scale as discussed above. For mixing dominating processes, a new concept of ideal relative turbulent mixing process has been proposed in part 1, which can be used for turbulent mixing criteria. For such a process, the traditional idea that a small disturbance causing a large effect fails. The rapid mixing in the whole local position needs large receptivity capacity as mentioned above. For this reason, the philosophy for turbulence control is: when a small disturbance is sufficient for a practical aim, it is preferable to use the small disturbance; however, a large disturbance can be used to produce a larger effect if the effect of a small disturbance is limited.

11.2 Secondary vortices

The The origin of the secondary vortices in free shear layer have been studied by some works, e.g. [21] [89] [66] and [76]. The visualization results shown here indicate that, there may be more than one instability mechanism for the secondary structures. The sources of initial spanwise disturbances could be from the corner or inhomogeneity on the splitter plate. That which has dominate influence could depend on the confinement (wall influence), forcing level and method.

In Roberts [89] work, a model for the secondary vortices, which are the Type A Vortices here, is proposed to describe the side wall effects for mixing enhancement. However, there is some difference between the model of Roberts and the results here. First, the origin of the Type A Vortices could not be necessarily the same. In Roberts' model, the Type A Vortices are originated from the velocity defect in the side wall boundary layers; The model here emphasizes that under strong forcing, there is an impulse in the vertical direction, which strengthens the counter-rotating of the fluids along the wall. This rotation results in high vorticity of streamwise direction, which in turn, produces the induction of the Type A Vortices due to their instability mechanism, when the fluids leave the trailing edge. This process strengthens the amplification of the Type A Vortices. The Type A Vortices then strengthen the Type B Vortices, and the Type B Vortices give a positive feedback to the Type A Vortices again and this process repeats until the Type A Vortices reach their final equilibrium state.

Secondly, the equilibrium state of the Type A Vortices is strongly dependent on the forcing mechanism and forcing level. If the forcing is strong enough, the Type A Vortices can reach the axis of the pipe in the wake or meet each other in the high velocity side in the mixing layer. Similar result for a wake is also obtained by Mackinnon & Koochesfahani [69]. In the Roberts model, the Type A Vortices reach an equilibrium state and the distance between the two pairs of the Type A Vortices is twice the distance from either pair to the side wall from which they originate.

Thirdly, for a mixing layer under strong forcing, the Type A Vortices not only amplify strongly, but also have two counter-rotating vortex pairs, i.e. vorticity of two sign exists as in a wake. However, in Roberts model, there is only one sign vorticity for the mixing layer.

11.3 Sudden transition

The phenomenon observed in this visualization might also be used as an experiment for the study of deterministic chaos. Firstly, with the change of control frequency we observe a variety of critical vortex motions, e.g. as shown in Fig. 10.1. These are closely related to coherent structures and their formation. On the one hand, through the control of the vortex motion, we can better understand the turbulent coherent structures and their scenario; on the other hand, vortex dynamics can be better described by dynamic chaos theory. Secondly, similar to a forced spherical pendulum - where Tritton [106] used forcing frequency as a system control parameter, the control frequency could possibly also be used here as the system control parameter to study the vortex dynamics for the confined configuration in a pipe.

11.4 Symmetry breaking hysteresis

The symmetry breaking hysteresis could be related to some bifurcation mechanisms and be used for chaos study. On the one hand, under a given forcing f and A for the new instability mechanism, the very small difference of $(U_1 - U_2)$ (which could be a random parameter) could be regarded as a system control parameter, and its value determines the bias direction for the sudden transition. It provides an example of an open system. On the other hand, either A or f could be regarded as a system parameter like the Reynolds number to describe this instability phenomenon.

11.5 Pairing burst

11.5.1 Mechanism of the pairing burst origin

The pairing vortices are forced by the steep impulse of upstream vortices. This can be clearly seen in Fig. 10.28. This force steeply pushes the pairing vortices along the bias direction of the mixing layer, so that the pairing vortices have an impulse force against the fluid near the wall. This force is not parallel to the surface of the wall. The fluid near the wall will force the pairing vortices in the way of Newton's third law. The summed force results in the pairing burst. Due to the fact that the pairing burst is related to the large coherent structures, such a pairing burst is also quasi-period.

It should be clear that vortices pairing is neither a necessary nor sufficient condition for the large vortex ejection (burst). Under certain conditions, vortices pairing can enhance the ejection. However, without pairing, if a vortex convects at a certain angle to the wall or with a sufficiently high Reynolds number, there can also be vortex ejection, but not pairing burst. This can also be observed in this experiment.

11.5.2 Quasi-step flow

Step flow is widely studied and many works are concentrated on its large structures. Through the visualization, it is found that the large vortex ejection due to the pairing burst is a characteristic of this flow. There is a little difference between the present step flow and the normal step flow. Here the backward surface is not a solid, but water. Therefore it is called quasi-step flow. However, in the work of Kuo [64], it is found that there is little difference between these two kind step flows. To the author's knowledge, there is no report on the pairing burst in step flow, for example, in the flow of a pipe with a sudden expansion.

It is not known, if there is such an ejection caused by upstream vortices pairing in a normal 2-D step flow. Due to the fact that there is a mixing layer in a normal 2-D step flow and the pairing also happens there steeply to the wall, it is postulated that the pairing burst investigated here could also emerge in a normal 2-D step flow. However, the wall influence could enhance the pairing burst in the confined quasi-step flow.

11.5.3 Control of wall free and wall bounded turbulent flow

Burst is one of the most important phenomena in the turbulent boundary flow. Its control, on the one hand helps us to understand its mechanism, and on the other hand, has application for engineering, for example, drag reduction and heat transfer enhancement. There are many different methods to control turbulent boundary flow [38]. Here we use the Tai Chi idea, i.e. a system view, to propose another idea for controlling the turbulent boundary flow: the near wall region flow can be controlled through the control of the flow far away from the wall. Pairing is a property of free turbulence. Through this experiment we can see that the wall flow can also be strongly influenced if the out-layer is a mixing layer.

Free turbulence is often used for turbulent mixing. For the study of free turbulent flow, the wall effect is usually omitted, as on the one hand it can cause greater complexity for a fundamental study, and on the other hand, due to the existence of the wall, the viscosity effect will be large, which could decrease relative turbulent mixing. However in the confined mixing layer, because of the pairing burst, the influence of wall can also sometimes increase mixing as shown in this work.

The quantitative measurement of turbulent mixing before, during and after the pairing burst will be given in a later corresponding publication.

11.5.4 On turbulent burst

Turbulent burst is related to the mechanism of turbulent energy production and transport in the turbulent boundary flow. Although there are a lot of models for it, some disagreements still exist [90]. It is intended to use the visualization result of the pairing burst in the confined mixing layer to discuss some problem connected to the burst, even though the burst is usually measured through some conditional sampling, because the conditional sampling is more accurate than visualization. From the visualization of the pairing burst in a confined mixing layer, we can clearly see the large coherent structure in the turbulent boundary flow. Reckoning the pairing burst as a model flow for turbulent burst in the turbulent boundary flow, we may understand the turbulent burst better.

One point of interest is that the critical velocity parameter λ_c decreases with the increase of Reynolds number Re . If Re is sufficient high, the λ_c may decrease to almost zero corresponding to a plane wake. As shown in Fig. 10.22, when Re_θ is 184, λ_c is only 0.06. This is approximately a plane wake, which in turn, due to the sharp trailing edge, is approximately a boundary flow with some initial disturbance that can result in the pairing burst if the Re is high enough.

11.5.4.1 Dynamics of burst The kinematic combinations and dynamic relationship of the local tilted shear layer and the vortices in turbulent boundary flow does not have unique formation mechanisms [90]. The dynamics, i.e. the origin of burst could be related to the model flow of the pairing burst as mentioned above. There may be two kinds of sweeps for burst process. The first one is the upstream sweep of ejection, which is the reason of the pairing burst and usually ignored. The second one is the downstream sweep of ejection, which is often mentioned. According to this visualization result, it seems that the upstream sweep is more related to the dynamics of the first burst, and the downstream sweep to the kinematics of burst. The reason is that if there is no upstream sweep, the pairing burst will not appear. This can be seen in Fig. 10.20, where no apparent sweep can be seen, and hence no pairing burst appears. The first burst in a turbulent boundary flow, where the Re is high enough, could be created by some unknown initial disturbance, which is related to the upstream sweep. This first burst could result in the shear layer, which then results in the second burst. The second one will result in the third one and so on. Even if there is no pairing, if some disturbance results in a steep impulse, there can still be large vortex ejection as mentioned above.

Offen and Kline [80] proposed a shear layer model for the burst. Here, however, it is another shear layer model, which is related to the pairing burst and is the reason for the first burst.

11.5.4.2 Interaction between inner and outer flow The dynamical relationships between the inner region of intense turbulent production and the larger scale, less active outer layer are poorly

understood [90]. The model proposed above to explain the dynamics of burst could also be related to Reynolds scaling in the turbulent boundary flow. Assume that the pairing burst is an interaction process between inner and outer flows. For a small Re , large λ is needed for a pairing burst to occur. Large λ is more related the free shear layer, which is an out region flow. This means for a small Re , the out-region dominates. However for a large Re , the inner-shear flow has sufficient energy to initiate the burst, and the out region function is therefore relatively weak, i.e. for low Re , the inner region dominates.

In the confined mixing layer, the horseshoe and hairpin vortex is also apparent. This can be seen in the plan view of the figures in this work, as for example, shown in the plan view of Fig. 10.28.

12 Conclusion

In part 2, the following works are conducted.

Experimental Method

A simultaneous visualization method of three light sheets is successfully realized for a complex flow study.

Dual receptivity

1. A new receptivity mechanism is discovered. It seems that there are two different receptivity mechanisms for the large forcing in the confined configuration in a pipe. One of them corresponds to the traditional 2-D instability mechanism and the other is a new one.
2. The new instability mechanism has a much stronger receptivity than the traditional one, especially for the high forcing level. In reality it has a higher receptivity capacity as is suggested here.
3. The maximum receptivity frequency for the new instability mechanism is almost a constant of around 6 Hz and is independent of the convection velocity. This indicates that the Strouhal number of the maximum receptivity for the new one is not constant.
4. The confinement has two opposing influences on disturbance amplification. On the one hand, the existence of the wall amplifies the effect of viscosity, which makes the flow more stable; on the other hand, the wall can strengthen the secondary vortices, and this three dimensionality, in turn causes the flow to be more unstable.
5. For the new instability mechanism, the mixing layer exhibits an unusual phenomenon, i.e. its center line does not bias to the low velocity side, but to the high velocity side under strong forcing.
6. There are counter-rotating vortex pairs for the primary structure in a mixing layer under strong forcing, which are also unusual to the normal mixing layer, where there is only one sign of the Kelvin-Helmholtz vortex.
7. There is no universal spread rate for the mixing layer and plane wake under forcing. The maximum spread rate can be as high as 180° .
8. For strong forcing the back-flow in the quasi-step flow can be much reduced.
9. According to the results here, a concept of mixing receptivity is proposed for the control of mixing.

Secondary vortices

1. The two types of secondary vortex are the dominant vortices, i.e. Type A Vortices and Type B Vortices named here, even if there are also some other secondary vortices.
2. The Type A Vortices originate from the corner between the splitter plate and the pipe wall, while the Type B Vortices originate due to the primary vortex and the Type A Vortices.
3. The new instability mechanism is related to the secondary vortices, i.e. the Type A Vortices and Type B Vortices named here, especially Type A Vortices, which amplify very fast in the initial stage.
4. The sudden transition is also related to the Type A Vortices and Type B Vortices.

5. The unusual bias of the mixing layer and the counter-rotating vortex pairs of the primary structure are related to the Type A Vortices, which develop to the high velocity side under strong forcing.

Sudden transition

1. A sudden transition from laminar to turbulence is observed in the confined configuration (i.e. wake, mixing layer and quasi-step flow), which could be used, as a new example, for the scenario from laminar to turbulence in an open system.
2. The new instability mechanism is very important to achieve the sudden transition. Under the traditional instability mechanism, it is impossible to realize the sudden transition due to the saturation.

Symmetry breaking hysteresis

1. A new phenomenon called as symmetry breaking hysteresis is observed in the confined configuration, which may also be used for chaos study in an open system.
2. The symmetry breaking hysteresis results in an asymmetric statistical distribution of concentration and velocity.
3. The symmetry breaking hysteresis phenomenon becomes weakened as Reynolds number Re_θ increases.

Pairing burst

1. A new phenomenon named here as pairing burst is discovered in a confined mixing layer and quasi-step flow in a pipe.
2. At a given initial Reynolds number Re_θ , there is a critical velocity ratio λ_c , over which the pairing burst can happen. The higher the Reynolds number Re_θ , the lower the critical velocity ratio λ_c . The critical velocity ratio λ_c seems to be asymptotically zero as initial Reynolds number Re_θ is very high.
3. The higher the velocity ratio, the stronger the pairing burst.
4. With the increase of initial Reynolds number Re_θ , the pairing burst can be enhanced.
5. Pairing burst can be controlled through a temporal periodic forcing, i.e. the pairing burst can either be enhanced or reduced by control.
6. The pairing burst phenomenon provides us with a new method to control boundary turbulent flow by a outer flow acting as a shear layer.

Some applications

The work here has some applications shown in the appendix.

1. A new Anemometer based on photobleaching with LIF
2. A new rapid mixing process for mixer and reactor
3. A new process for heat transfer enhancement.

13 Summary

The turbulent mixing criteria and the ideal relative turbulent mixing process determine the aims for turbulent mixing control. The new receptivity mechanism (including mixing receptivity) provides us with the basis to achieve the requirements. The experimental methods discussed here help us to study turbulent mixing both on large scale (visualization of three light sheets of a complex flow) and fine structure (high spatial resolution measurement). Thus, combining with computational fluid dynamics, a new system could be established for the study of turbulent mixing.

References

- [1] Aref, H., 1991. Stochastic particle motion in laminar flows, *Phys. Fluids A*, **3**, 1009-1016.
- [2] Alper, A., Liu, J. T. C. 1978. On the interactions between large-scale structure and fine grained turbulence in a free shear flow. II. The development of spatial interactions in the mean. *Proc. R. Soc. London Ser. A* **359**, 497-523.
- [3] Arcoumanis, G, McGuirk, J. J., Palma, J. M. 1990. On the use of fluorescent dye for concentration measurements in water flows. *Exp. Fluids*, **10**, 177-80.
- [4] Baldyga, J. and Bourne, J.R. 1986. Principles of micromixing, *Encyclopedia of Fluid Mech.*, **1**, 147-201, ed. Cheremisinoff, N.P..
- [5] Batchelor, G. K. 1959. Small-scale variation of convected quantities like temperature in turbulent fluid. Part 1. General discussion and the case of small conductivity. *J. Fluid Mech.* **5**, 113-133.
- [6] Beck, J. Jr., Miller, R. S. 1959. *Chem. Eng. Progr. Symposium Ser. No. 25*, **55**, 23.
- [7] Bernal, L. P., Roshko, A. 1986. Streamwise vortex structure in plane mixing layers. *J. Fluid Mech.* **170**, 499-525.
- [8] Börger, G. 1975. Optimierung von Windkanaldüsen für den Unterschallbereich. *Z. Flugwiss.* **23**, 45-50.
- [9] Breidenthal, R. E. 1981. Structure in turbulent mixing layers and wakes using a chemical reaction. *J. Fluid Mech.* **109**, 1-24.
- [10] Broadwell, J. E., Breidenthal, R. E. 1982. A simple model of mixing and chemical reaction in a turbulent shear layer. *J. Fluid Mech.* **125**, 397-410.
- [11] Broadwell, J. E., Mungal, M. G., 1991. Large-scale structures and molecular mixing. *Phys. Fluids* **3**, 1193-1206.
- [12] Brodkey, R. S. 1967. *The phenomena of fluid motions*. Addison-Wesley Publishing Company, Inc. Reading, Mass.
- [13] Brodkey, R. S. 1968. Turbulent motion, mixing, and kinetics. *Prof. dev. lec.* **1**, no.2. West Virginia university-Kanawha Valley Graduate Center.
- [14] Brodkey, R. S. 1978. Turbulent motion, mixing, and kinetics. *Proceedings of the 60th birthday conf. for V. G. Levich*.
- [15] Browand, F. K., Ho, C.-M. 1987. Forced, unbounded shear flows. *Int. conf. on Phy. of Chaos and Sys. far from equil.* ed. Duong-Van, M.
- [16] Brown, G. L., Roshko, A. 1974. On density effects and large structure in turbulent mixing layers. *J. Fluid Mech.* **64**, 775-816.
- [17] Buch, K. A., Dahm, W. J. A. 1991. Fine scale structure of conserved scalar mixing in turbulent shear flow: $Sc \gg 1$, $Sc \approx 1$ and implications for reacting flows. Report No. 026779-5. The Univ. Michigan.
- [18] Burle 1980. *Photomultiplier Handbook*. Burle Industries Inc.
- [19] Busse, F. H. 1983. An example of direct bifurcation into a turbulent state. *Nonlinear Dynamics and Turbulence*. ed. Barenblatt, *et al.* 101-138, Pitman.
- [20] Cantwell, B. J. 1981. Organized motion in turbulent flows. *Annu. Rev. Fluid Mech.* **13**, 457-515.
- [21] Corcos, G. M., Lin, S. J. 1984. The mixing layer: deterministic models of a turbulent flow. Part 2. The origin of the three-dimensional motion. *J. Fluid Mech.* **139**, 67-95.
- [22] Corino, E. R., Brodkey, R. S. 1969. A visual investigation of the wall region in turbulent flow. *J. Fluid Mech.* **37**, 1-30.
- [23] Corrsin, S. 1951. On the Spectrum of isotropic temperature fluctuations in an isotropic turbulence. *J. Appl. Phys.* **22**, 469-473.
- [24] Crank, J. 1979. *The mathematics of diffusion*. Oxford Science Publication.
- [25] Dahm, W. J. A. 1985. Experiments on entrainment, mixing and chemical reactions in turbulent jets at large Schmidt number. Ph. D. thesis, Caltech.

- [26] Dahm, W. J. A., Southerland, K. B., Buch, K. A. 1991. Direct, high resolution, four-dimensional measurements on fine scale structure of $Sc \gg 1$ molecular mixing in turbulent flows. *Phys. Fluids* **3**, 1115-1127.
- [27] Dai, G. C., Wang, G. R., Fan, Z. H. 1989. Transition from laminar to turbulent flow in artificially roughened pipes. *J. East China Inst. Chem. Techn.* **15**.
- [28] Danckwerts, P.V. 1952. The definition and measurement of some characteristics of mixtures. *Appl. Sci. Res.* **v3**.
- [29] De Silva, I. P. D., Fernando, H. J. S 1991. Some aspects of mixing in stratified turbulent patch. *J. Fluid Mech.* **240**, 601-25.
- [30] Dimotakis, P. E. 1991. Turbulent free shear layer mixing and combustion. In "High-speed flight propulsion systems", ed. Murthy, B., Curran, E. T., *Progress in Astronautics and Aeronautics*, **137**.
- [31] Dowling, D. R., Lang, D. B., Dimotakis, P. E. 1989. An improved Laser-Rayleigh scattering photodetection system. *Exp. in Fluids* **7**, 435-40.
- [32] Durst, F., Sender, J. 1990. Photodetectors for Laser-Doppler measurements. *Exp. in Fluids* **9**, 13-16.
- [33] Eckbreth, A. C., 1988. *Laser Diagnostics for Combustion Temperature and Species*, Energy and engineering science series, vol. 7, Abacus Press.
- [34] Feigenbaum, M. J. 1983. Universal behavior in nonlinear systems. *Nonlinear Dynamics and Turbulence*. ed. Barenblatt, et al. 101-138, Pitman.
- [35] Fernando, H. J. S, 1991. Turbulent mixing in stratified fluids, *Annu. Rev. Fluid Mech.* **23**, 455-93.
- [36] Fiedler, H. E, 1974. On turbulence structure and mixing mechanism in free turbulent shear flows. *Turbulent mixing in non-reactive and reactive flows*, ed. S. N. B. Murthy.
- [37] Fiedler, H. E., Mensing, P. 1985. The plane turbulent shear layer with periodic excitation, *J. Fluid Mech.* **150**, 281-309.
- [38] Fiedler, H. E., Fernholz, H. H. 1990. On management and control of turbulent shear flows, *Prog. Aerospace Sci.* **27**, 305-387.
- [39] Fiedler, H.E., Kim, J. H. & Köpp, N. 1991. The spatially accelerated mixing layer in a tailored pressure gradient *Eur. J. Mech. B/Fluids*, **10**, 349-76.
- [40] Fiedler, H. E., Wang, G. R. 1998a. Ein neues Verfahren zur raschen und homogenen Mischung von Flüssigkeiten im kontinuierlichen Durchlaufbetrieb. Deutsches Patent. No. 19816354.1.
- [41] Fiedler, H. E., Wang, G. R. 1998b. Anemometer basierend auf dem Effect des Photobleachens. Deutsches Patent. No. 19838344.4.
- [42] Fiedler, H. E., Wang, G. R. 1998c. Effektiver Wärmetauscher durch begrenzten symmetrischen oder asymmetrischen Nachlauf in der Rohrströmung. Deutsches Patent. No. 19850190.0.
- [43] Gatski, T. B., Liu, J. T. C. 1980. On the interactions between large-scale structure and fine grained turbulence in a free shear flow. III. A numerical solution. *Philos. Trans. R. Soc. London*, **293**, 473-509.
- [44] Gibson, C. H. 1968. Fine structure of scalar fields mixed by turbulence. I. Zero-gradient points and minimal gradient surfaces. *Phys. Fluids*, **11**, 2305-2315.
- [45] Green, H. G., Desselberger, M., 1989. Turbulent mixing in nonlinear vortex flow. 5th international symposium on flow visualization. Prague.
- [46] Guilbault, G.,G. 1973. *Practical fluorescence, Theory, methods, and techniques*. Marcel Dekker, INC.
- [47] Hernan, M. A., Jimenez, J. 1982. Computer analysis of a high speed film of the plane turbulent mixing layer. *J. Fluid Mech.* **119**, 323-345.
- [48] Hinze, J. O. 1975. *Turbulence*. McGraw-Hill Inc.
- [49] Ho, C.-M., Huang, L.-S. 1982. Subharmonics and vortex merging in mixing layer, *J. Fluid Mech.* **119**, 443-473.
- [50] Ho, C.-M., Huerre, P. 1984. Perturbed free shear layers, *Ann. Rev. Fluid Mech.* **16**, 365-423.

- [51] Huang, L.-S., Ho, C.-M. 1990. Small-scale transition in a plane mixing layer, *J. Fluid Mech.* **210**, 475-500.
- [52] Huang, Y. Y. 1994. Introduction to chaos theory. Turbulence (in Chinese). ed. Shi, X. G. Tianjing Univ. Press.
- [53] Jackson, W. B. *et al* 1981. Photothermal deflection spectroscopy and detection. *Appl. Opt.* **20**, 1333-44.
- [54] Jimenez, J., Martinez-Val, R., Rebollo, M. 1979. On the origin and evolution of three dimensional effects in the mixing layer. Inter. Rep. DA-ERO 79-G-079, Univ. Politec. Madrid.
- [55] Joseph, D. D. 1976. *Stability of Fluid Motions 1*. Springer-Verlag.
- [56] Kline, S. J., Reynolds, W. C., Schraub, F. A., Runstadler, P. W. *et al*. 1967. The structure of turbulent boundary layers. *J. Fluid Mech.* **30**, 741-73.
- [57] Koechner, W. 1976. *Solid-state laser engineering*, Springer-Verlag.
- [58] Kolmogorov, A. N. 1941. *C. R. Acad. Sci. USSR* **30**, 299-303.
- [59] Komori, S., Hunt, J. C. R., Kanzaki, T., Murakami, Y. 1991. The effects of turbulent mixing on the correlation between two species and on concentration fluctuations in non-premixed reacting flows. *J. Fluid Mech.* **228**, 629-659.
- [60] Komori, S., Nagata, K., Kanzaki, T., Murakami, Y., 1993. Measurements of mass flux in a turbulent liquid flow with a chemical reaction. *AIChE J.* **39**, 1611-1620.
- [61] Konrad, J.H. 1976. An experimental investigation of mixing in two- dimensional turbulent shear flows with application to diffusion limited chemical reactions. Ph. D. Thesis, Caltech.
- [62] Koochesfahani, M. M., 1984. Experiments on turbulent mixing and chemical reactions in a liquid mixing layer. Ph. D. thesis, Caltech..
- [63] Kuo, A. Y., Corrsin, S. 1972. Experiments on the geometry of the fine-structure regions in fully turbulent fluid. *J. Fluid Mech.* **56**, 447-79.
- [64] Kuo, C. C. 1995. Diplomarbeit. TU Berlin.
- [65] Landau, L , Lifschitz, L. 1959. *Fluid Mechanics*. Pergamon Oxford.
- [66] Lasheras, J. C., Cho, J. S., Maxworthy, T. 1986. On the origin and evolution of streamwise vortical structures in a plane, free shear layer. *J. Fluid Mech.* **172**, 231-258.
- [67] Lin, C. C., Deid, W. H. 1963. Turbulent flow, Theoretical aspects. *Encyclopedia of physics. Fluid dynamics 2*. ed Flüge.
- [68] Liu, J. T. C., Merikine, L. 1976. On the interactions between large-scale structure and fine grained turbulence in a free shear flow. I. The development of temporal interactions in the mean. *Proc. R. Soc. London Ser. A* **352**, 213-47.
- [69] Mackinnon, C. G., Koochesfahani, M. M. 1997. Flow structure and mixing in a low Reynolds number forced wake inside a confined channel. *Phys. Fluids* **10**, 3099-3101.
- [70] McComb, W. D. 1990. *The physics of fluid turbulence*. Oxford science publications.
- [71] Michalke, A. 1965. On spatially growing disturbance in an inviscid shear layer, *J. Fluid Mech.* **23**, 521-544.
- [72] Michalke, A. 1971. Instabilitaet eines kompressible runden Freistrahls unter Beruecksichtigung des Einflusses der Strahlgrenzschichtdicke, *Z. Flugwiss.* **19**, 319-28.
- [73] Miller, P. L. 1991. Mixing in high Schmidt number turbulent jets. Ph. D Thesis, Caltech. Pasadena, CA.
- [74] Musschenga, E. E., 1992. Transfer processes in turbulent pipe flow: The random surface renewal approach. Ph. D thesis. University of Amsterdam.
- [75] Nye, J. O., Brodkey, R. S., 1967. The scalar spectrum in the viscous-convective subrange. *J. Fluid Mech.* **29**, part 1, 151-163.
- [76] Nygaard, K. J., Glezer, A. 1991. Evolution of streamwise vortices and generation of small-scale motion in a plane mixing layer. *J. Fluid Mech.* **231**, 257-301.
- [77] Oakey, Neil S. 1989. Estimates of mixing inferred from temperature and velocity micro-structure. 239-47.
- [78] O'Brien, E.E. 1980. Turbulent reactional flows. *Topics in Applied Physics.* **44**, 185- 218.
- [79] Obukhoff, A. M. 1949. *Izv. Akad. Nauk, SSSR, Geogr. i Geofiz.*, **13**, 58.

- [80] Offen, G. R., Kline, S. J. 1974. Combined dye-streak and hydrogen-bubble visual observations of a turbulent boundary layer. *J. Fluid Mech.* **70** 209-28.
- [81] Oster, D., Wygnanski, I. 1982. The forced mixing layer between parallel streams, *J. Fluid Mech.* **123**, 91-130.
- [82] Ottino, J.M. 1990. Mixing, chaotic advection, and turbulence, *Annu. Rev. Fluid Mech.* **22**, 207-53.
- [83] Ottino, J. M. 1989. *The kinematics of mixing: Stretching, Chaos and Transport*. Cambridge Univ. Press.
- [84] Owen, F. K., 1976. Simultaneous laser measurements of instantaneous velocity and concentration in turbulent mixing flows. AGARD-CP193, Paper no. 27.
- [85] Panton, R. L. 1984. *Incompressible flow*. John Wiley & Sons Inc.
- [86] Prasad, R. R., Sreenivasan, K. R. 1990. The measurement and interpretation of fractal dimensions of the scalar interface in turbulent flows. *Phys. Fluids, A* **2**, 792-807.
- [87] Peters, H., Gregg, M. C. 1989. Some dynamical and statistical properties of equatorial turbulence. 185-200.
- [88] Ready, J. F., 1978. *Industrial application of laser*. Academic press.
- [89] Roberts, F. A. 1985. Effects of periodic disturbance on structure and mixing in turbulent shear layers and wakes. Ph. D. thesis, Caltech.
- [90] Robison, S. K. 1991. Coherent motions in the turbulent boundary layer. *Annu. Rev. Fluid Mech.* **23** 601-39.
- [91] Roshko, A. 1991. *The mixing transition in free shear flows. The global geometry of turbulence*. ed. Jimenez, J. Plenum Press. 1991.
- [92] Ruelle, D., Takens, F. 1971. On the nature of turbulence. *Comm. Math. Phys.* **20**, 167.
- [93] Saylor, J. R. 1995. Photobleaching of disodium fluorescein in water. *Exp. Fluids* **18**. 445-447.
- [94] Schlichting, H. 1979. *Boundary-layer theory*. McGraw-Hill, New York.
- [95] Schultz-Grunow, F. 1980. Sudden transition to turbulence. *Laminar-Turbulent Transition*. Springer, 388-95.
- [96] Shtern, V., Hussain, F. 1999. Collapse, symmetry breaking, and hysteresis in swirling flows. *Annu. Rev. Fluid Mech.* **31**, 537-566.
- [97] Sirivat, A. and Warhaft, Z. 1983. The mixing of passive helium and temperature fluctuations in grid turbulence, *J. Fluid Mech.* **120**, 475-504.
- [98] Snavely, B. B. 1973. Continuous-wave dye lasers. in *Dye lasers*. ed. Schöfer, F. P., Springer-Verlag.
- [99] Smith, J. M. 1990. Industrial needs for mixing research. *Trans. IChemE*, **68**, 3-6.
- [100] Sosinovich, V. A., 1991. Allowance for many length scales in the description of turbulent mixing. Kline, S. and Afgan, N.H., edit., *Near-wall turbulence*, Hemisphere Publ.
- [101] Squire, H. H. 1933. On the stability of three-dimensional disturbance of viscous flow between parallel walls. *Proc. R. Soc. London Ser. A* **142**, 621-628.
- [102] Sreenivasan, K. R., Ramshankar, R., Meneveau, C. 1989. Mixing, entrainment and fractal dimensions of surfaces in turbulent flows. *Proc. R. Soc. Lond.* **A421**, 79-107,
- [103] Sreenivasan, K. R. 1991. On local isotropy of passive scalars in turbulent shear flows. *Proc. R. Soc. Lond.* **A434**, 165-182,
- [104] Tennekes, H., Lumley, J. L. 1972. *A first course in turbulence*. MIT Press.
- [105] Townsend, A. A. 1951. On the fine-scale structure of turbulence. *Proc. Roy. Soc. Lond.* **A208**, 534-42.
- [106] Tritton, D. J. 1986. Ordered and chaotic motion of a forced spherical pendulum. *Eur. J. Phys.* **7**, 162.
- [107] Vlasov, Ye. V., Ginevskiy, A. S. 1967. Acoustic effect on aerodynamic characteristics of a turbulent jet. Foreign Technology Division, FTD-MT-24-232-68.
- [108] Villermaux, J. 1986. Micromixing phenomena in stirred reactors. *Encyclopedia of Fluid Mech.* **2**, 707-771, ed. Cheremisinoff, N.P..

- [109] Walker, D. A. 1987. A fluorescence technique for measurement of concentration in mixing liquids. *J. Phys. E: Sci. Instrum.* **20**, 217-224.
- [110] Wang, G. R. 1996. Turbulente Stroemung in einer Begrenzten Scherschicht im einen Rohr. Institutsbericht, 1995-1996, Hermann-Foettinger-Institut.
- [111] Wang, G. R. 1999a. Simultaneous visualization of three light sheets. Submitted to *Exp. Fluids*.
- [112] Wang, G. R. 1999b. A new mixing process for mixer, reactor and combustion. Submitted to *Chem. Eng. Sci.*
- [113] Wang, G. R., Fiedler, H. E. 1996. The paring burst - a new phenomenon. *Bulletin of Am. Phys Soc.* Oct. **41**
- [114] Wang, G. R., Fiedler, H. E. 1998. On turbulent mixing criterion. AIChE 1998 Annual Meeting, Miami, USA.
- [115] Wang, G. R., Fiedler, H. E. 1999a. On High spatial resolution scalar measurement with LIF. Part 1: Photobleaching and Thermal Blooming. *Accepted to Exp. Fluids*.
- [116] Wang, G. R., Fiedler, H. E. 1999b. On High spatial resolution measurement of concentration with LIF. Part 2: The Noise Characteristic *Accepted to Exp. Fluids*.
- [117] Wang, G. R., Stefes, B. 1995. Experimentelle Untersuchung über Mischungsmechanismen und -kriterien. Institutsbericht 1993-1994, Hermann-Föttinger-Institut, Technische Universität Berlin.
- [118] Wang, G. R., Spieweg, R., Fiedler, H. 1998. Turbulent mixing in a confined plane wake in a pipe. *Bulletin of Am. Phys Soc.* Oct. **43**.
- [119] Weisbrot, I., Wygnanski, I. 1988. On coherent structures in a highly excited mixing layer. *J. Fluid Mech.* **195**, 137-159.
- [120] Winant and Browand 1974. Vortex pairing: mechanism of turbulent mixing layer growth at moderate Reynolds number. *J. Fluid Mech.* **63**, 237-55.
- [121] Wygnanski, I., Champagne, F., Marasli, B. 1986. On the large-scale structure in two-dimensional small-deficit turbulent wake. *J. Fluid Mech.* **168**, 31-71.
- [122] Zhou, H. 1997. Private communication.

15 Appendix: Some applications

This work is a fundamental one, however, it has some applications. Its corresponding applications are referred to the patents [40], [41] and [42]. Here it is a brief introduction to these three patents.

A A new Anemometer based on photobleaching with LIF

On the one hand, photobleaching is generally an unwelcome phenomenon, contaminating the LIF measurement of scalar (concentration and temperature). On the other hand it can be used for measuring fluid velocity. To the author's knowledge, there is no publication in which photobleaching is used for the measurement of fluid velocity. Here a new method of measuring fluid velocity based on photobleaching is introduced.

A.1 Principle

The principle of the method is outlined in the section of part 1 dealing with a model of photobleaching effect. The lifetime of fluorescence is very short, about the order of $10^{-9} \sim 10^{-8}$ s. This means that if the laser dye molecules being pumped by a laser stayed in the measuring volume longer than 10^{-9} s, photobleaching would occur, and the light intensity of fluorescence would then decay with time exponentially. The longer it stays, the lower the fluorescence intensity is. This indicates that fluorescence rise time is fast enough for fluid velocity measurement in fluid mechanics. Because the dye is continuously pumped, the lifetime of fluorescence is not the photobleaching time constant used here. The photobleaching decay time constant τ used here is larger than the lifetime. The decay time constant for photobleaching depends on the experiment conditions, dye, concentration, laser intensity, exciting light wave length and so on as shown in eqn (4.3). Fig. 4.1 and Fig. 4.4 in part 1 can be regarded as a calibration curve between I_f and u .

A.2 Discussion

This method has many advantages compared with hot-wire, Laser Doppler Anemometer (LDA) and Particle Image Velocimetry (PIV).

1) Like LDA, it is a non-intrusive method. 2) It can have a very high spatial resolution and may be useful for the velocity measurement in very small scale devices (for example in Microelectromechanical systems (MEMS) and very fine blood vessels in medicine). The measuring spatial resolution is about $4 (\mu m)^3$ in our experiment with a working distance of about 150 mm. It can be smaller depending on the diffraction limit of the laser beam focusing. 3) The same measuring system can be used to measure both scalar and velocity and their correlation. 4) There is no problem with particle seeding and tracing velocity as in LDA. 5) This method may be useful for velocity measurement in the region very near to the wall where LDA has difficulties. 6) It could measure very small velocity for medicine and biotechnology. 7) With its principle the new technique could be used not only for point but also for field measurement as PIV. 8) The operation and procedure could be simpler and easier than LDA.

A.3 Problems

This is a new method and some works are needed to develop this method to measure vector. Its success could provide the possibility of measuring vorticity of a scale smaller than the Kolmogorov scale.

1) Velocity range: In this paper, the velocity range measurable is relatively small. But if spatial resolution is not crucial, the focus diameter can be larger and it can be expected that the measuring range will increase with the increment of focus diameter if laser intensity remains unchanged. 2) Laser

dye: The laser dye disodium fluorescein used here may not be the best for measuring velocity using the photobleaching method, because it does not bleach very fast. In order to improve the method, another dye is needed, which bleaches very strongly. 3) One dimension: This experiment, which is only the first step, can only measure one dimensional velocity because it is based on the residence time and is independent of direction. More works are needed to improve this method.

B A new rapid mixing process for mixer and reactor

B.1 Status

Mixer is always important for industry and technology. For example, direct losses in USA chemical processing industries, due to the problems of mixing, are estimated at \$10Bn per year (Smith, 1990). Mixing layer, jet, wake, mixing tank and motionless mixers (including static mixers) are all widely used in engineering. These mixers are either only through mechanical force (mixing tank and static mixer) or through fluid dynamic mechanism (mixing layer, jet and wake). The former uses much energy and the latter can not achieve the rapid mixing in a short space and time.

B.2 New mixer

The results shown in Fig. 10.5 of part 2 provide us with a new process for mixing enhancement in industry. A new mixer is proposed. This mixer is based on a new mixing receptivity mechanism and can result in extraordinarily rapid mixing keeping energy costs lower. The process and principle of mixing is explained in part 2 of this work.

B.3 The disadvantage of other mixers

With mechanical forcing, the agitated mixers use too much energy in order to achieve better mixing, since the process of energy transportation from large to small scale is not optimized. The product quality could be affected due to the approximately exponent residence time distribution and some died region. Cells can be destroyed by too strong shear stress near blade surface in biotechnology. Mixing through jet, mixing layer, wake, motionless and static mixer could be too slow, especially for low Reynolds number. All these flows have a large range of different structures (scales), which make the modeling of the mixing and reactor design more complicated, and so is the scale-up and scale-down.

B.4 The advantage of new mixer

In this new mixing process and mixer, the new knowledge of flow control is effectively used, both passive and active methods. Due to the very high receptivity of the new instability mechanism, the input energy is first optimally transfered to large scales and then to small scales, so that the achieved mixing enhancement is clearly much higher than other mixers, especially for low Reynolds number. Since it is similar to a pipe flow, the mixer would approximately have a residence time distribution of a plug flow and there is no back mixing (flow) and died region. The mixing chamber is fully used. Since no blade is used, the problem with cell breaking can be moderated. The process is a continuous operation and easier to control mixing and temperature distribution. Due to the the possibility of the control of the small structures, and the fact that the scale of scalar is more homogeneous distributed, the reactor modeling can be more easier and accurate. When used for reactor with multi-pipes, the new mixing process could bypass the classical problem of scale-up. All these factors make the installation of the new mixer and its construction much easier and simpler.

C A new process for heat transfer enhancement

The heat exchanger is always important. One of the criterion for a good heat exchanger is that it has high efficiency, i.e. high heat transfer coefficient and lower friction coefficient. In order to achieve this aim many heat exchangers are designed for heat transfer augmentation.

C.1 Status

Today heat transfer enhancement methods can be classified as: 1) The heat exchanger surface are extended; 2) The heat exchanger surfaces are designed as roughened ones; 3) The flows in the heat exchanger are swirl flows; 4) Wall Jet. All these are not ideal because of the fluid flow properties. The augmentation is either low or consumes a lot of energy.

C.2 New heat exchanger

It is well-known that, the most resistance for heat transfer is in the near wall region (especially viscous sublayer). According to the random surface renewal model of transfer process in a turbulent boundary flow [74], we know that if the fluid from the near wall region can be replaced by the turbulent core, the heat transfer would be enhanced. From Fig. 10.11d, we know that, the wake flow here is an useful one to replace the near wall region fluid by the center one for heat transfer enhancement. Since it is large coherent motion, the energy loss is relatively small. The new heat exchanger is based on this flow configuration, i.e. based on modern fluid dynamics knowledge and control of coherent structure. The construction of the heat exchanger is a confined symmetrical and asymmetrical wakes in a tube with or without forcing.

C.3 Disadvantages of other heat exchangers

The heat transfer rate is low if the geometry is simple, especially for low Reynolds number. If heat transfer is high, the geometry is then complex, e.g. snake tube. Over a longer period time, efficiency of heat transfer can be reduced for roughened surface.

C.4 Advantages of the new heat exchanger

The geometry is simple. The efficiency of the heat exchanger is high, i.e. low energy cost and high heat exchange. The efficiency could also be high even for a low Reynolds number.

On large structures and turbulent mixing in confined mixing layers under active control

G. R. Wang

Hermann-Föttinger-Institut für Strömungsmechanik

Technische Universität Berlin, Germany

Present address: 1547 Mississauga Valley Blvd, Suite 1503

Mississauga, Ontario, Canada L5A 3X8

Email: sophie96@idirect.com

A confined plane mixing layer in a pipe (i.e. the inlet of the pipe is a mixing layer) is experimentally investigated through visualization of laser induced fluorescence. Compared with conventional two-dimensional mixing layers, the confinement due to the side-wall causes not only quantitative change (e.g. spreading rate of the mixing layer), but also important new phenomena. It is observed that many well-known classical results in a traditional two-dimensional mixing layer may not be applicable to the confined configuration, especially under strong temporal periodic forcing. There seems to be two different instability (receptivity) mechanisms for the external forcing. One corresponds to the traditional Kelvin-Helmholtz instability and the other is a new instability, in which, the mixing layer exhibits some unusual phenomena. The primary vortex can become an asymmetric counter-rotating pair (contradicted to the one sign of the Kelvin-Helmholtz vortices) with forcing. The central line (isotach line) does not bias to the low speed side, but to the high speed side under strong forcing of the new instability. The traditional saturation phenomenon under strong forcing is not observed for the new instability. Compared with the conventional Kelvin-Helmholtz instability, the new instability has a very high receptivity, which can yield a quasi 180° spreading rate of the mixing layer. As a result, an extraordinarily dramatic mixing is realized immediately downstream of the trailing edge under strong periodic forcing. The inherent frequency corresponding to the new instability is almost a constant independent of mean flow velocity. The new instability could be related to the streamwise vortices, which result from interaction of the primary vorticity and the vorticity originated from the streamwise corner flow between the splitter plate and side-wall immediately downstream of the trailing edge of the splitter plate. These streamwise vortices are very sensitive to initial periodic forcing of the new instability and amplify very fast. The results here indicate that the confined mixing layer is a very interesting flow for both science and engineering.

1 Introduction

With the discovery of large coherent structures in turbulent flows the active and passive turbulent control, i.e. the control of these large coherent structures, has become very active in the fields of turbulence and aerodynamics. This is due to the fact that these large structures play an important role for the flow property, and they are very sensitive to initial external disturbance. These structures can be therefore controlled with initial disturbance.

Flow control based on receptivity has many different applications, such as fluids mixing enhancement, the flow separation, drag, and acoustic noise reduction, e.g. Ho & Huerre (1984), Fiedler & Fernholtz (1990) and Gad-el-Hak, Pollard & Bonnet (1998). For mixing control, the large structures in mixing layers have an essential influence on molecular mixing of different chemical species in turbulent flows. The control of the molecular mixing can indirectly be achieved through the control of these structures.

Mixing layers are important in many applications, e.g. combustion and chemical lasers, where the mixing enhancement of two fluids can be very helpful and even imperative, especially for the reduction of chemical emission concerning the environmental protection. The control of mixing layer can be used to augment mixing, to reduce acoustic noise and to improve combustion instability.

The spreading rate of a mixing layer is an important parameter used to describe mixing in a mixing layer (Cantwell 1981). Brown & Roshko (1974) pointed out that the large spanwise coherent structures played an important role for the entrainment and spreading rate of the mixing layer. Winant & Browand (1974) demonstrated that successive vortex mergings were the primary processes governing the streamwise spreading of the mixing layer. These structures and hence the spreading rate could be influenced through the initial periodic forcing, as investigated by Oster *et al.* (1978), Oster & Wygnanski (1982), Ho & Huang (1982), Fiedler & Mensing (1985) and many others. One important common conclusion from these works is that the spreading rate can be enhanced through the active control.

Fiedler *et al.* (1981) observed the same excitation behavior for all frequencies used. The forcing causes the strongest spread on the low speed side. Fiedler & Mensing (1985) also found that the flow was not frequency selective. The response of the mixing layer to forcing is frequency-dependent only inasmuch as the downstream position of saturation is inversely proportional to the forcing frequency. Ho & Huang (1982) found that the forcing frequency had the most pronounced effect on the mixing layer. In the initial region, the instability frequency of the forced mixing layer was not necessarily the same as forcing frequency. The initial response frequency is seen to correspond to that particular harmonic of the forcing frequency that is nearest to but smaller than nature frequency. Simultaneous merging as many as two, three or four vortices can be promoted through subharmonic forcing of the most-amplified frequency.

Ho & Huang (1982) also found out that both collective interaction and vertex merging could increase the spreading rate. The collective interaction, which was first identified by Ho & Nosseir (1981) (see also Aref & Siggia 1980), can be achieved under sufficient high forcing level with forcing frequency much smaller than most-amplified frequency of the mixing layer. If forcing amplitude is high enough closing to saturation, the large vortex is formed directly. The vortex merging can appear earlier with increase of the forcing frequency (also see Fiedler *et al.* 1981).

Fiedler & Mensing (1985) observed the saturation when the forcing amplitude was sufficient high, i.e. the intensity of the maximum periodic transverse velocity constituents and saturation Strouhal number became constant and independent of forcing amplitude when it was higher than 6.5%. They obtained the same mean spread for strong and weak forcing, i.e. twice the neutral value and independent of forcing amplitude. Weisbrot & Wygnanski (1988) also investigated strong forcing, but no distinguished difference in the spreading rate could be found from that of Fiedler *et al.* (1981) and Oster & Wygnanski (1982).

Fiedler *et al.* (1981) and Oster & Wygnanski (1982) observed three regions for the development of the mixing layer. In region I, the initial spreading rate of the forced mixing layer exceeds the linear growth in the natural one. In region II, the spreading rate slows or stops and may even become negative under extreme condition of large forcing level. Vortices decay downstream and loose coherence before merging. The mixing layer resonates with the imposed oscillation in this region. In region III, the mixing layer spreading rate assumes the unforced characteristics.

The velocity ratio is an important parameter for the spreading rate in the mixing layer (Monkewitz & Huerre 1982), e.g. the spreading rate is scaled with velocity ratio (e.g. Brown & Roshko 1974).

On account of above mentioned observations, Browand & Ho (1987) proposed a universal spreading rate of

mixing layers for different initial conditions with and without forcing. Dimotakis (1991), however, suspected if a universal spreading rate existed.

Another well-known phenomenon is that in addition to the primary two-dimensional vortex structure, the mixing layers also contain a well-organized array of streamwise vortices that superimposed onto the spanwise eddies, as first observed by Miksad (1972), and later by Konrad (1976), Breidenthal (1981) and Bernal & Roshko (1986).

For the origin of the streamwise vortices, Breidenthal (1981) noted a wiggle disturbance in the outer edge of the primary vortices, from which the longitudinal streaks originated due to 'the global strain field of the flow'. Bernal & Roshko (1986) regarded the appearance of streamwise vortices uninfluenced by upstream conditions, indicating that far enough downstream of the splitter plate, the streamwise vortices (or rib like structure (Hussain 1986)) might result from an instability of the primary vortices. Using a linear instability analysis of a family of coherent Stuart vortices to stimulate the array of spanwise eddies, Pierrehumbert & Widnall (1982) suggested that the streamwise vortices could result from a translative instability of these vortical arrays.

Jimenez (1983) suggested that the streamwise vortices tended to lock onto small geometric details (e.g. imperfections in the splitter plate, orientation of screens, etc) in the experimental apparatus. In the numerical simulation from Lin & Corcos (1984), an initial weak spanwise-periodic variation of streamwise vorticity was unstable in the braids between two consecutive spanwise vortices with uniform strain field, and could evolve into concentrated streamwise round vortices. Lasheras, Cho & Maxworthy (1986) found experimentally that under the effect of strain field created by spanwise vortices, small localized upstream disturbance spread laterally by strong self-induction resulting in the sideways formation of counter-rotation pairs of streamwise vortices; The streamwise structures were always observed to generate in the braids between the spanwise vortices and to propagate into their cores; The origin of streamwise vortices could be changed by the control of spanwise vorticity distribution in spanwise upstream the splitter plate and could be considerably moved upstream by the mounting of small vortex-generating elements on the splitter plate. Having a spanwise-periodic forcing, Nygaard & Glezer (1991) observed the streamwise vortices downstream of the trailing edge, but upstream of the first rollup of the spanwise vortices, presumably due to cross-stream shear and the wave-like motion of the vorticity-containing layer between the two streams. Following the rollup, the streamwise vortices resided in the braid region between the consecutive primary vortices.

Although spanwise vorticity non-uniformities within the braid region lead to the formation of streamwise vortices, experimental (e.g. Breidenthal 1981, Bernal & Roshko 1986, Browand & Troutt 1980, 1985) and numerical evidence (Ashurst & Meiburg 1988) suggested that the same disturbance caused little or no distortion of the primary vortices. However, Nygaard & Glezer (1991) observed that when the wavelength of spanwise forcing was larger than that of primary vortices, the primary vortices developed spanwise undulations. This experimental result indicated that spanwise forcing wavelength had a profound effect on the primary vortices.

Corcos & Lin (1984) found numerically that the growth rate of three-dimensional linear instability remained relatively constant during the rollup phase. However, vortex merging considerably delayed the linear development of the streamwise vortices. Metcalfe *et al.* (1987) observed that pairing might inhibit the three-dimensional instability, while suppression of pairing might drive the three-dimensional mode to turbulent-like states.

Lasheras *et al.* (1986) showed that a significant portion of the overall entrainment might take place due to the streamwise vortices. However, Lasheras & Choi (1988) did not observe a range of maximum amplification for the relatively long wavelength of spanwise perturbations, and suggested that the three-dimensional instability had a long bandwidth for which the amplitudes grew at a comparable rate.

The interesting topic about small scale and mixing transition in mixing layer was reviewed by Roshko (1991). The streamwise vortices were already quite strongly developed upstream of the mixing transition (see also Moser & Rogers 1991). Huang & Ho (1990) suggested that the small scale transition occurred only after the first pairing of primary vortices. Using spanwise-uniform harmonic excitation, the primary vortices pairing was inhibited in the experiment of Nygaard & Glezer (1991), but they also obtained the small-scale transition. They found that as a result of interaction with the streamwise vortices, the primary vortices developed spanwise-periodic concentration of small-scale motion having a spanwise wavelength of approximately half that of the streamwise vortices within their cores. The breakdown of the cores were believed to be a precursor to mixing transition because further downstream, corresponding distributions of small-scale motion had less spanwise coherence.

The global feedback mechanism of long-range coupling effect between the trailing edge and the dominant flow events was described in Ho & Huerre (1984). Here the vortex merging event along with the stream was assumed to be linked to the trailing edge via a feedback loop, consisting of downstream-propagating subharmonic

instability wave and an upstream-propagating acoustic wave.

Fiedler & Thies (1978) found out that organ-pipe (quasi excitation) had similar influence as forcing. Its corresponding frequency did not scale with mean flow velocity. However, no anomalous result was reported for it.

The forementioned are obtained from the conventional two-dimensional mixing layers, which are assumed to be free from the side-wall effect. The investigations of confined mixing layers, i.e. side-wall could have influence on the dynamics of the mixing layer, are limited. Usually such flows are not considered of general interest for fundamental research, since additional complications of the side-wall influence are introduced, which may obscure the study of turbulence mechanisms. In all realistic cases, however, the side-wall influence is always present, albeit often only to a negligible extent, and it may not be unwelcome under all circumstances. Although Veynante, Candel & Martin (1986), Koochesfahani & Mackinnon (1991) investigated confined situation, no anomalous phenomena were observed compared with the above mentioned knowledge. Although Wood & Bradshaw (1982) concerned the effect of side-wall, no active forcing was applied to investigate the side-wall effect on the instability behavior.

However, recently Wang (1999) found several interesting new phenomena (dual receptivity and dramatic mixing, sudden transition from laminar to turbulence, symmetrical breaking hysteresis, and pairing burst, and so on) in confined mixing layers in a pipe, i.e. the inlet of the pipe is a mixing layer. The side-wall effect not only adds some extra complex and quantitative variation, but also results in some interesting new phenomena, which to the author's knowledge, have never been reported, especially an extraordinary dramatic fluids mixing under the active control of a new instability (Wang & Fiedler 1998). Most above mentioned results in the traditional two-dimensional mixing layers will not be applicable anymore, especially in the cases of strong forcing under the new receptivity mechanism.

The confined mixing layer in a pipe is not simply a superposition of a mixing layer and pipe flow, but a complex three-dimensional flow. Visualization discloses a variety of phenomena, which cannot be explained by the simple superposition. This is particularly true for the cases of periodic forcing. These new phenomena are unknown in the 'ordinary' mixing layers and are not found in a simple pipe flow either. However, they are interesting for both the fundamental researcher and engineer and may even provide new insights for those making basic studies on the origin of turbulence in an open flow.

In the present work, the confined mixing layer in a pipe is experimentally studied through visualization to present some new phenomena, especially under strong forcing under the new receptivity mechanism. Section 2 describes the confined configuration of the facility. In Section 3 the experimental results are presented. Some discussion is given in section 4, and the summary and conclusion is presented finally in section 5.

2 Experimental set-up

The experimental configuration is shown in figure 1. Two vessels of 300 liter at 2.5 m higher than test section supply water and water solution (laser dye) to the water channel respectively. The water level changes little during 30 s run so that the fluid velocity is almost constant. One vessel is filled with water, and the other with aqueous disodium fluorescein solution. Rotameters (which are calibrated with a water vessel) are used to control and measure the velocity of the fluids, which are filled into a settling chamber from the side of the wall respectively. The settling chamber upstream of a nozzle is 400 mm long, and has one honeycomb and two screens. The Nozzle has a contraction ratio of 10:1, and is 100 mm long. The nozzle is designed in the light of theory of (Börger 1975). In the axial-symmetrical center of settling chamber and nozzle there is a splitter plate, which has a uniform thickness of 5 mm in the settling chamber and a sharp trailing edge at the end in the nozzle. A plexiglass pipe of 42 mm inner diameter, 4 mm thick is connected with the nozzle. The pipe is totally 2.1 m long. At 1 m x-position downstream of the trailing edge, there is a cube, in the middle of which a mirror is placed for visualization. The cross section of the cube is large enough so that the block of the mirror has no influence on the flow in the test section.

The mixing layer is forced by active control, for which two different methods are used. The first one involves a loudspeaker. Near the input of the settling chamber, there is a loudspeaker in the axial-direction on the low speed side which is used as the actuator. The speaker excites the flow through the connection with a plastic membrane, which in turn connects directly with water stream. Due to high pressure of the water, the membrane is under too much tension, so that it cannot be forced to move by the speaker. For this reason, a sealed bottle is used and the speaker is also sealed. The bottle is half-filled with water, which is connected with the fluid in

the settling chamber through a tube. The air in the bottle is connected with the loudspeaker. If the pressure in the settling chamber is increased, the pressure in the bottle will also rise. This results in an pressure increase on the speaker side of the membrane, so that the membrane can keep in equilibrium position and oscillate.

A condensator is constructed between the speaker and membrane to measure the amplitude of the membrane displacement. The condensator is connected to a frequency bridge, which is connected to an oscilloscope. The relationship between the amplitude of the speaker and the signal from the frequency bridge has been calibrated before use (it is linearly related). Through this construction the forcing amplitude A_f of the speaker can be controlled. The signal generator used for loudspeaker is HP 33120A. The forcing signal is sinusoid. A DFVLR power amplifier is used to amplify the signal for the loudspeaker.

Since the loudspeaker cannot be used for flow of higher Reynolds numbers, another forcing method uses rotating valve for the active forcing. The high speed fluid is first divided into two parts, and each is followed by a rotameter. One of the stream passes a valve, which can be rotated by a motor. The rotation of the valve results in a periodic blocking of the flow, and thus a periodic velocity. The forcing frequency f_f can be controlled through the speed of the motor and A_f through the flow volume of the two streams. No apparent difference of the mixing layer dynamics can be observed for the two forcing methods.

Laser induced fluorescence is applied here for the flow visualization. The laser is a Coherent Inova 90 with a power of 5 Watt. Disodium fluorescein is used as laser dye. The optics used here is also shown in figure 1. The peaks of absorption and emission spectrum of the fluorescein are blue (488 nm) and green (530 nm) respectively. The reflecting laser light from glass is strong. In order to get clear pictures with minimum reflecting light, the excitation light of the laser should be different from the emitting one in the wave length. Using an etalon we can get only blue color (488nm) light. A narrow band light filter 500 ~ 600 nm and yellow color filter before a Sony CCD camera (which is applied to take the video picture) are used to filter away the reflecting light. Cylinder lens are used to achieve two-dimensional light sheets to visual side, plane and cross views of the mixing layer.

The most-probable frequency (close to the theoretical most-amplified frequency, Ho & Huang 1982) is measured through an extremely high spatial resolution scalar point measurement of laser induced fluorescence in the shear layer. The detail measurement process is given in Wang & Fiedler (2000). Because the measuring point is before the first rollup of primary vortex, it should approximately represent the initial unstable wave frequency. HP 3562A Dynamic Signal Analyzer is used for the measurement of the signal power spectrum.

The initial momentum thickness is often used for the scaling in shear flows (Ho & Huerre 1984). Here, its value in the mixing layer originating at the trailing edge can be approximately estimated through two-dimensional spatial mode of linear instability theory, since the flow is approximately two-dimensional immediately downstream of the trailing edge without forcing. With no forcing, the Strouhal number $St_{n1} = \theta_0 \bar{U} / f_{01}$ corresponding to the most-amplified frequency f_{01} of Kelvin-Helmholtz instability is a constant, i.e. nearly 0.032 (Ho & Huerre 1984), where θ_0 denotes the sum of the initial momentum thickness θ of the mixing layer, $\bar{U} = (U_1 + U_2)/2$ represents the mean flow velocity, U_1 and U_2 are the initial average velocity of the two streams respectively in the mixing layers.

The visualized scalar structure sizes and their corresponding shear layer thickness δ_v and spreading rate $d\delta_v/dx$ are used as the criteria of receptivity in the near field even though the instability theory is usually described as the disturbance of velocity. The argument is that, at the beginning of the mixing layer, the larger the coherent composition of the velocity, the wider its corresponding vortex in the shear layer, which can be recognized by scalar large structures at least in the near field. In this work, there is no attempt to provide the detailed accurate fundamental data for the receptivity study quantitatively, instead, to introduce a new phenomenon of receptivity and its possible mechanism qualitatively.

The active control introduces temporal periodic forcings of the flows with a certain of frequencies and amplitudes. The relative average velocity-perturbation amplitude of forcing (henceforth, called forcing amplitude) resulting from the membrane corresponds to:

$$A_f = \sqrt{\bar{u}^2} / \bar{U} (\%) = 2a_M f_f (A_M / A_N) / (1.414 \bar{U}). \quad (1)$$

where the ratio of membrane to nozzle area $A_M / A_N = 2$ in this experiment. \bar{u} is the initial disturbance of streamwise velocity component. f_f denotes forcing frequency and a_M represents the maximum displacement of the membrane. The estimated initial Reynolds number based on initial momentum thickness is $Re_{\theta_0} = \theta_0 \bar{U} / \nu$.

The visualization is undertaken in the near field of the mixing layers. The fluids flow from left to right for the side views. The laser sheet for the side views passes through the axis of the pipe. The trailing edge of the splitter plate is within the view of the pictures.

3 Results

3.1 Forcing frequency effect and a new instability mechanism

Figure 2 (side view) shows the influence of forcing frequency f_f with constant forcing amplitude A_f . The speed of the two streams is $U_1 = 9 \text{ cm/s}$ and $U_2 = 6 \text{ cm/s}$ respectively, f_f changes in the range of 2.4 - 9 Hz and A_f is a constant of about 6.5%, i.e. strong forcing. Figure 2a is the case with no forcing. The f_{01} of Kelvin-Helmholtz vortices is estimated to be 7.2 Hz (see also figure 10) according to the scalar measurement and visualization result. No apparent difference can be observed between the confined mixing layer and conventional two-dimensional mixing layer. Figure 2b denotes the case of $f_f = 2.4 \text{ Hz}$. Since this is in the second subharmonics region, i.e. in mode III according to Ho & Huang (1982), the tripling of vortices can be observed in the initial stage. The shear layer spreads very fast as the three vortices are merging. After the merging, the shear layer is in the frequency lock region and does not spread. In figure 2c the mixing layer is forced at $f_f = 4.4 \text{ Hz}$. Because this is between the f_{01} and its first subharmonic, i.e. in mode I, no vortex merging is found in the initial stage. The frequency lock region follows the first rollup. Compared with the unforced one, $d\delta_v/dx$ immediately downstream of the trailing edge is much increased. Figure 2d is also in the mode I as the case of figure 2c, but with higher f_f of 6 Hz and more close to f_{01} . According to Ho & Huang (1982), the development of the mixing layer in figure 2d should be similar to that in figure 2c, except that the primary vortex size in figure 2d should be smaller than that in figure 2c. However, surprisingly there is no frequency lock region, i.e. region two from Oster & Wygnanski (1982), and the shear layer linearly spreads until the low speed edge of the shear layer reaches the wall. During this spreading process, no subharmonic component can be observed. The average shear layer $d\delta_v/dx$ is much higher than that of figure 2c. There are small scale structures already at about $x/\theta_0 = 191$ ($x/D = 1.5$, where x represent downstream position from the trailing edge and D the inner pipe diameter.) Figure 2e is forced at 7.2 Hz. The dynamics of mixing layer in figure 2e is similar to that of figure 2d. However, the vortex size and its corresponding $d\delta_v/dx$ in figure 2e are smaller than those in figure 2d, but larger than those in figure 2c in the near field. In figure 2f where f_f is 9 Hz, as expected, there is only slightly decrease of $d\delta_v/dx$ compared with the unforced one in the initial stage and the receptivity becomes very small. The results from figure 2a, b, c and f are similar to those from Ho & Huang (1982) and Oster & Wygnanski (1982).

The most interesting thing is the comparison among figure 2c, d and e. As we know from Ho & Huang (1982) that in the mode I, the vortical sizes following trailing edge decrease with the increase of forcing frequency. For this reason, the vortices in figure 2e should be smaller than those in figure 2d, which in turn, should be smaller than those in figure 2c. However, the visualization result shows that the vortex size in the figure 2d is surprisingly larger than that in figure 2c in transverse direction after $x/\theta_0 = 63$ ($x/d = 0.5$). The frequency lock region in figure 2c disappears in figure 2d. With further increase of f_f as shown in figure 2e and figure 2f, the vortical sizes become again smaller compared with that in figure 2d. Many tests show that, barring the possibility of an experimental error, the forcing at 6 Hz has higher receptivity than at other ones. Therefore $f_f = 6 \text{ Hz}$ is actually the maximum receptivity frequency. Further experimental results (see later) confirm that forcing around 6 Hz corresponds to a new instability mechanism. It is also noted that the $d\delta_v/dx$ at $f_f = 7.2 \text{ Hz}$ in figure 2e is higher than that at 4.4 Hz in figure 2c and the development of the mixing layer in figure 2d is similar to that in figure 2e. This is because of that at $f_f = 7.2 \text{ Hz}$, the receptivity mechanism is partially influenced by the new instability mechanism, i.e. the most-amplified frequencies of Kelvin-Helmholtz instability and the inherent frequency corresponding to the new instability mechanism are overlapped in figure 2e. In this work the new receptivity mechanism is mainly investigated.

Compared with figure 2b where there is vortex merging, figure 2d, exhibits no vortex merging, but $d\delta_v/dx$ is higher in figure 2d than in figure 2b following $x/D = 2$, and there are even more small-scale structures in figure 2d than in figure 2b. This indicates that the mixing can even be stronger with no vortex merging than with vortex merging (according to the comparison of figure 2b and figure 2d). From this viewpoint, the manipulating of vortex merging is not the only way to enhance mixing efficiently.

Another interesting thing is the vortex merging in figure 2b. Usually the merging bias to the low speed side of the mixing layer, but here the merging seems bias to high speed side. This is related to a phenomenon called 'pairing burst' in Wang & Fiedler (1996).

In the work of Fiedler *et al.* (1981) the flow exhibited the same forcing behavior for all frequencies applied. Fiedler & Mensing (1985) also described that the flow was not frequency selective and the response of the shear layer to forcing was frequency-dependent only inasmuch as the downstream position of saturation was inversely

proportional to the forcing frequency. Figure 2 here displays clearly the different mixing layer behavior between $f_f = 6$ Hz and other values. This reveals a more complicated situation for our understanding of mixing layer in confined configuration and provides us with more possibility to control it.

3.2 Streamwise vortices

In order to understand the flow and the mechanism of the new receptivity in the confined configuration, it is necessary to investigate its streamwise structures. Experimental results show that the above mentioned new receptivity phenomenon and other new phenomena to be discussed later in this work are closely related to the streamwise vortices.

It should be mentioned first that in some cross view pictures, there are two sharp dark areas, for instance in figure 4d, where the laser sheet goes through top to bottom of the pipe. This is due to the fact that the pipe wall can act as a lens and results in these dark areas.

3.2.1. Type and origin. There are many different kinds of streamwise vortices in the confined configuration except the traditional ones. Only the important ones are introduced here. Different streamwise vortices have different origins.

The interaction of the vorticity originated from the four corner flows between the splitter plate and side-wall, and the spanwise vorticity in the mixing layer results in several counter-rotating vortex pairs, which are the most important streamwise vortices in the confined configuration and are called here Type A Vortices. The four corner flows are their main sources. These vortices can be enhanced through periodic forcing and figure 3a gives an example of the forced Type A Vortices at $x/D = 1$, where the U_1 and U_2 are 3 and 1 cm/s respectively, $f_f = 6$ Hz and A_f is about 3.5%.

Due to the momentum transfer from high to low speed in a mixing layer, the mixing layer bias to the low speed side. In the confined mixing layer, this will cause the high speed fluid moving in the center region to the low speed side and the low speed fluid to the high speed side along the wall because of continuity. Thus, a secondary flow is produced. Without forcing, this yields the Type A Vortices to develop to the high speed side along the pipe wall as shown in figure 4a.

As A_f is sufficient high under the new receptivity, the interaction of the Type A Vortices and spanwise vortices can result in two counter-rotating vortex pairs, called Type B Vortices here as shown in figure 3b at $x/D = 4$, where U_1 and U_2 is 9 and 6 cm/s, f_f is 2.6 Hz and A_f is about 8%. These vortices originate from around the axis of the pipe and develop to the wall. The counter-rotating vortex pair at high speed side is smaller than that at low speed side due to the positive impulse from each other between the above-mentioned secondary flow and the Type A Vortices at low speeds side.

The above mentioned secondary flow, which is induced by the bias of mixing layer, can be enhanced with increase of velocity ratio $\lambda = (U_1 - U_2)/(U_1 + U_2)$ and periodic forcing. During the development of the mixing layer, the secondary flow and the vorticity of the low speed side vortices of Type A Vortices strengthen each other and their interaction evolve a counter-rotating streamwise vortex pair, called Type C Vortices here. Figure 3c shows an example of Type C Vortices, which result from the further development of the flow in figure 3a at $x/D = 4$. The positive impulse from each other between the secondary flow and the low speed side vortices of Type A Vortices also makes the low speed side vortices of Type A Vortices larger in low speed side than in high speed side.

With sufficiently high λ and x/D , the low speed side fluid moves along the side-wall to high speed side from opposite directions and meets at the top of the pipe wall. Then it flows to low speed side again and results in a vortex pair called Type D Vortices as shown in figure 3d at $x/D = 7$, where U_1 and U_2 are 4 and 1 cm/s respectively, $f_f = 6$ Hz and A_f is about 5%. This process can also enhance mixing, especially when λ and \bar{U} are sufficiently high.

Although their different origins, Type A Vortices and Type B Vortices have the same Topology on the high and low speed sides respectively. The topology of Type C Vortices is also the same as that of the Type D Vortices and the Type A Vortices of the low speed side. All above mentioned streamwise vortices have different origins from those investigated in traditional two-dimensional mixing layers. They are quasi mirror symmetric to the vertical surface through the pipe axis.

3.2.2. Evolution. The evolutions of the Type A Vortices in a unforced and forced mixing layer, are shown in figure 4 and figure 5 respectively, where U_1 and U_2 are 9 and 6 cm/s. In figure 4a and b, where x/D are 0.2 and 1 respectively, the Type A Vortices can be observed. During the evolution process downstream, it can

be clearly seen in the cross view that the high speed fluid moves to the low speed side in the center region of the pipe, while the low speed side fluid moves to the high speed side along the wall. Thus the Type A Vortices also move to the high speed side as shown in figure 4c and d, where x/D are 2 and 4 respectively, since Type A Vortices are originated in the near wall regions. The Type A Vortices keep their form during the evolution in the investigated range of x/D . Without forcing, the vortices of the low speed side within the Type A Vortices are larger than the ones of the high speed side and the difference between the sizes depends on velocity ratio λ . The higher λ , the larger the difference. They are the same size only when $\lambda = 0$. This could be related to the above mentioned secondary flow, which can enhance the vorticity of the vortices of the low speed side. The size of Type A Vortices is the same order of the size of primary vortices in the transverse direction. The spanwise wave length in figure 4c seems to be the same order of the size of Type A Vortices.

In figure 4a, except the Type A Vortices, no spanwise wave can be found. The interface between high and low speed stream is a straight line. In figure 4b, the straight line begin to be distorted. The rollup of primary vortex can be observed in Fig 4c (see also figure 2a). Here we can see the initially spanwise developed undulation, which could develop into streamwise vortex similar to traditional one in two-dimensional mixing layers. Its further development is shown in figure 4d, where the spanwise undulation in figure 4c is distorted by the secondary flow.

The dynamics of Type A Vortices strongly depends on the forcing, e.g. f_f and A_f . When the flow is forced under the new instability mechanism, the evolution of the Type A Vortices is enhanced as shown in figure 5, where f_f is 5.6 Hz and A_f is about 6%. Compared with the unforced ones, the size of Type A Vortices of the high and low speed side in the forced flow is almost the same as shown in figure 5a ($x/D = 0.2$) and figure 5b ($x/D = 1$). They become similar to those in a wake with $\lambda = 0$. This indicates that under forcing, the initial wake of the mixing layer plays an important part in the mixing layer development in the confined configuration. Further downstream, the Type A Vortices develop very fast and almost reach to the axis of the pipe in the spanwise direction. This can be seen in figure 5c and figure 5d. Here the amplification of Type A Vortices and the fluids mixing is strongly enhanced under forcing compared with the unforced case.

While the interface between the high and low speed stream has no apparent undulation in the spanwise direction in figure 5a, it is not as straight as the corresponding unforced one. In figure 5b the undulation already becomes clear compared with the unforced one. With further evolution and interaction between Type A Vortices and primary structure downstream, the undulation has developed into the streamwise vortices, which are similar to those of two-dimensional mixing layers as displayed in figure 5c and figure 5d. Though the forcing is not periodic in spanwise direction, it indeed accelerates and enhances the evolution of streamwise structures, implying that the Type A Vortices have influence on the development of streamwise vortices at least in the confined configuration. The positive impulse feedback between Type A Vortices and Type C Vortices is also distinguished in figure 5c and figure 5d.

Another important phenomenon is that Type A Vortices amplify very fast with strong forcing only under the new receptivity mechanism. Under traditional receptivity, the amplification of Type A Vortices is not so rapid, and thus nor is that of the spanwise vortices. This can be observed in figure 6, where $U_1 = 30$ cm/s, $U_2 = 20$ cm/s. Figure 6a, b and c are the cross views of the figure 9c at $x/D = 0.2, 1$ and 2 respectively and the forcing is under the new receptivity mechanism, i.e. f_f is 6 Hz. Figure 6d ($x/D = 0.2$), figure 6e ($x/D = 1$) and figure 6f ($x/D = 2$) represent the forcing result of cross views of figure 9g under the traditional receptivity mechanism, i.e. f_f is 16 Hz (in mode II, because f_{01} is about 43 Hz). In the initial x-position, figure 6a and d have already shown some difference for Type A Vortices. With the evolution, in figure 6e and f, the Type A Vortices propagate and amplify little, while in figure 6b and c, the Type A Vortices propagate and amplify much faster. Both have the same A_f value around 7%. The result indicates that under the traditional receptivity mechanism, Type A Vortices develop more slowly than under the new receptivity mechanism. As Type A Vortices amplify very fast, so do the spanwise vortices (see also figure 9).

3.3 Forcing amplitude A_f influence

The dramatic effect of forcing amplitude A_f is shown here. Figure 7 (side view) shows the influence of A_f under a constant $f_f = 5.6$ Hz (i.e. the new receptivity mechanism) for a mixing layer of $U_1 = 10$ cm/s and $U_2 = 5$ cm/s. f_{01} is estimated to be about 7 Hz, and the forcing is in the mode I on account of Ho & Huang (1982), i.e. f_f is between f_{01} and its first subharmonic. The response of the mixing layer to A_f under the new receptivity mechanism is very interesting. As we know, the central line of a traditional mixing layer biases to the low speed side beyond the trailing edge and this is also true in figure 7a and figure 7b. In figure 7a there is no

forcing and in figure 7b the flow is forced and A_f is about 1.5%. The vortices are induced by Kelvin-Helmholtz instability. In figure 7b there are the three regions of non-linear spreading observed by Fiedler *et al.* (1981) and Oster & Wygnanski (1982). In region I (corresponding $0 < x/\theta_0 < 67$, or $0 < x/D < 0.5$), the initial $d\delta_v/dx$ of the forced mixing layer exceeds the linear growth of the unforced one. In region II ($67 < x/\theta_0 < 406$, or $0.5 < x/D < 3$), $d\delta_v/dx$ slows or stops and vortices decay downstream. In the region III ($x/\theta_0 > 406$, or $x/D > 3$), $d\delta_v/dx$ assumes the unforced characteristics. However, in figure 7c where A_f is about 5%, even though the center line of the mixing layer still biases to the low speed side, the vortices following the trailing edge are almost no more the pure Kelvin-Helmholtz vortices. This is at a critical point, where the primary vortex becomes asymmetric counter-rotating vortex pair similar to (but is not the same as) the vortices of Karman Vortex street in a wake of $\lambda = 0$. The right side vortex is very clearly visible and the left side is still not. At about $x/D = 1$, the mixing layer does not spread in the high speed side, but only in the low speed side linearly until the wall at about $x/D = 3$. This could be related to the interaction of positive impulse feed-back between the Type A Vortices of low speed side and Type C Vortices. At about $x/D = 1.5$, there are already small scale structures.

In figure 7d where A_f is around 8%, the asymmetric counter-rotating vortex pair is very clearly visible, and anomalously the center line of the mixing layer does not bias to the low speed side anymore. Compared with figure 7c, the edge of the mixing layer moves to the high speed side keeping the low speed side almost unchanged and $d\delta_v/dx$ increases too. The downstream position, where small scale structures appear, is also unchanged. The three regions during the development in figure 7b disappear. The visualized mixing layer is almost symmetrical to the trailing edge now like a wake, but the topology of the vortices is clearly different from that of the Karman vortex street. As we know, for strong forcing, the instantaneous view of the mixing layer usually shows a non-linear spreading of the shear layer in the near field as in figure 7b. However, figure 7d shows an approximately linear symmetric spreading even this is an instantaneous view under strong forcing. The well-known vortex rollup of Kelvin-Helmholtz instability disappears. From this point, with the further increase of A_f the primary spanwise vortices in the mixing layer are no longer the Kelvin-Helmholtz vortices, but new asymmetric counter-rotating vortex pair.

When A_f is increased further to 18%, the central line of the mixing layer surprisingly begins to bias to the high speed side as displayed in figure 7e and the counter-rotating vortex pair becomes more clear. Compared with figure 7d, here the mixing layer spreads to high speed side rapidly at the initial stage until the wall and the high speed side is strongly stirred and mixed, but the low speed side has almost no spreading at all and fluid keeps unmixed until $x/D \approx 4.2$. The mixing is greatly increased in the high speed side, but decreased in the low speed side compared with figure 7d. It is also interesting to note that in the intermediate region between mixed high speed side and unmixed low speed side, the streaks of color are stretched first toward to downstream direction within $x/D = 1$, then toward to high speed side within $x/D \approx 1 \sim 1.2$, and then towards to upstream within $x/D \approx 1.2 \sim 3$. The initial phase angle of the forcing cycle is nearly the same between the two pictures of figure 7b and e. Within $x/D \approx 3$, the streak number is 13 in figure 7e and 8 in figure 7b. Since the forcing frequency is the same, the initial wave length should also be approximately the same for the two cases. This could indicate that the average convection velocity between the mixed high speed side and the unmixed low speed side is decelerated within $x/D \approx 3$. Downstream of $x/D \approx 3$, the color streaks from low speed side are again stretched toward downstream direction.

When A_f is around 32%, figure 7f shows that, only the first counter-rotating vortex pair beyond the trailing edge is distinguished. No large structure can be seen after $x/D \approx 1.5$ due to the dramatic mixing. The low speed streaks mentioned in figure 7e is suppressed within $x/D \approx 1$. Compared with figure 7e, the mixing layer spreads again to the low speed side. It is worthy to mention that the large vortex immediately downstream of the trailing edge here is not due to 'collective interaction', since the forcing frequency is in the mode I, where no many vortex merging can be observed. The large vortex is actually an asymmetric counter-rotating vortex pair here.

Finally, when A_f is about 52% the disturbance is so strong due to the high receptivity that the flow has already become turbulence with small scale structures filling the whole flow in the cross section immediately downstream of the trailing edge as shown in figure 7g. The corresponding $d\delta_v/dx$ seems to achieve its climactic mixing state, i.e. about 180° for this situation, indicating again that the enhancement of vortex merging is not the only way to enhance mixing. No large structure can be observed immediately downstream of the trailing edge because of the dramatic turbulent mixing. The scalar in the whole flow field of test section becomes homogeneous for each downstream position. An quantitative measurement of extremely high spatial resolution

of about $4 (\mu\text{m})^3$ with laser induced fluorescence (Wang 1999) also shows that the concentration distribution along transverse direction is approximately homogeneous for a given downstream position near the trailing edge. This corresponds actually to the culminate state that turbulence control can do to enhance mixing. Figure 7 indicates that the confined mixing layer has an extremely high receptivity when it is forced at 5.6 Hz, (i.e. the new receptivity mechanism). The corresponding cross view of figure 7 is shown in figure 8.

The above mentioned phenomena of unusual bias, asymmetric counter-rotating vortex pair and dramatic mixing under strong forcing would be related to the streamwise vortices, which are shown below. Figure 8 displays the cross view of the corresponding streamwise vortices of the flows shown in figure 7 at $x/D = 0.2$. The unforced situation is shown in figure 8a. The Type A Vortices are not symmetric to the horizontal plane passing through the pipe axis, but are symmetric to the vertical one. The vortices of high speed side are smaller than that of low speed side. The fluid of the low speed side moves to the high speed side along the pipe wall. Figure 8b shows the case with forcing A_f of about 1.5%. No essential difference for Type A Vortices can be observed between figure 8a and figure 8b except that the interface between high and low speed is more distorted near Type A Vortices in figure 8b. However, in figure 8c, where A_f is about 5%, the Type A Vortices are apparently amplified, and begin to be similar to their corresponding ones in the wake with $\lambda = 0$, i.e. the vortices of the counter-rotating vortex pairs from the high and low speed side have nearly the same size. It is interesting that this situation corresponds to the case where the primary counter-rotating vortex pairs in the side view of figure 7c begin to emerge. This means that the primary and secondary counter-rotating vortices would occur under almost the same conditions and they could also be correlated to each other. The reason is that, there is an initial wake in the mixing layer (Ho & Huang 1982), whose effect could play a dominating role when the forcing is sufficiently strong.

When A_f is increased to 8% as shown in figure 8d, the Type A Vortices do not propagate to the axis of the pipe as the case of wake of $\lambda = 0$, but at an angle to the high speed side. Under the same condition, the central line of the mixing layer in figure 7d begins not to bias to the low speed side. This would be reason why the central line of the mixing layer does not bias to the low speed side under strong forcing.

In figure 8e, A_f is about 18%, the angle is increased and the mixing layer is biased to the high speed side. The size of Type A Vortices is larger than that in figure 8d. With further increase of A_f to around 32%, Type A Vortices are further increased, as shown in figure 8f, and there is almost no difference between the size of the Type A Vortices of the low and high speed side. Until A_f is around 52%, the disturbance is so strong, that Type A Vortices are rapidly amplified and broken down. The flow becomes turbulence without any visible transitional process and thus no distinguish large structures of Type A Vortices can be observed.

Figure 8 also indicates that the Type A Vortices and the spanwise structures positively give impulse back to strengthen each other. Since traditional Kelvin-Helmholtz instability has no such a fast spread, Type A Vortices should be the reason of the dramatic spread of the mixing layer under the new instability mechanism. The results also show that the Type A Vortices are very sensitive to the strong forcing of the new instability with no apparent saturation before the state of figure 8g is achieved.

The effect of A_f on the spanwise structures strongly depends on the instability mechanism similar to the cases of figure 6. A_f influence is much smaller for the traditional Kelvin-Helmholtz instability mechanism than for the new instability mechanism. This is shown in figure 9, which displays the effects of A_f for two different f_f , i.e. different receptivity mechanism in a mixing layer with $U_1 = 30$ cm/s and $U_2 = 20$ cm/s respectively. f_f are 6 Hz and 16 Hz respectively. The f_{01} for Kelvin-Helmholtz instability is estimated to be 43 Hz (see also figure 10). Hence the forcing at 6 Hz corresponds to the above mentioned new instability and 16 Hz to the mode II of Kelvin-Helmholtz instability.

There is no forcing in figure 9a and f_f is 6 Hz from figure 9b to figure 9f. In figure 9b, where A_f is around 1.5%, the collective interaction is clearly visible, since f_f is much lower than f_{01} . A_f is about 7% in figure 9c. It is the critical point where the collective interaction is almost not visible and the response frequency f_r of the mixing layer no longer obeys the rule of the mode diagram observed by Ho & Huang (1982), but equals to f_f . The $d\delta_v/dx$ increases very fast downstream in the initial stage as A_f increases. The corresponding fast developing of Type A Vortices in figure 9c is shown in figure 6a, b and c. In figure 9d, where A_f is so high (about 16%) that the asymmetric counter-rotation vortex pair forms directly downstream of the trailing edge and no collective interaction can be seen. The saturation of A_f is still not emerged. In figure 9e, where A_f is about 40%, $d\delta_v/dx$ is further increased. In this case, the first counter-rotating vortex pair is already broken down due to the strong disturbance, but the leg of the first counter-rotating vortex pair is still distinguished immediately downstream of the trailing edge. The spreading angle is slightly smaller than 180° . When A_f is

increased to about 50%, figure 9f shows that the spreading angle become approximately 180° . This implies that A_f does not saturate even at the value of 40%.

However, the influence of A_f on the dynamics of the mixing layer shows quite different result with $f_f = 16$ Hz, which is displayed from figure 9g to figure 9j. The forcing A_f from figure 9g to figure 9j are around 7%, 16%, 40% and 50% respectively. In figure 9g, where A_f is around 7%, the forced flow is similar to that of a forced traditional two-dimensional mixing layer. Compared with figure 9a, the forced $d\delta_v/dx$ in the near field in figure 9g nearly doubles that of the unforced one. However, compared with figure 9c, $d\delta_v/dx$ in figure 9g is apparently smaller. Figure 6d, e and f show the corresponding relatively slow developing of Type A Vortices. This confirms that the amplification of spanwise structures is closely related to their corresponding Type A Vortices. As A_f is increased to 16%, there is only a small change of $d\delta_v/dx$ within $x/D = 2$ due to the very high A_f which makes initial wake distinguished in figure 9h. Since the amplification of the initial wake is very small, it disappears further downstream because of the mixing layer. Therefore in this case the initial wake has no strong influence on the dynamics of the mixing layer. Comparing figure 9g and figure 9h, we find no distinguishing difference between their $d\delta_v/dx$ values, considering the development of the mixing layer further downstream. The result indicates that A_f is already saturated at about 7%. With further increase of A_f to 40% and 50% respectively in figure 9i and 9j, no apparent increase in $d\delta_v/dx$ can be obtained due to the well-known saturation effect. All $d\delta_v/dx$ with $f_f = 16$ Hz is smaller than that of figure 9b where f_f is 6 Hz. In general, the results from figure 9g to figure 9j are similar to that of the traditional forced mixing layer, e.g., that of Fiedler & Mensing (1985).

The large different responses to A_f under the different f_f in figure 9 indicate that the effect of A_f on the dynamics of the mixing layer is related to the receptivity mechanism of forcing. Even though the flow is unstable to the external disturbance under traditional receptivity mechanism, the effect of A_f is limited, and so is the increase of $d\delta_v/dx$, since for high A_f , saturation makes the flow nearly independent of A_f . However, for the new receptivity mechanism, A_f has strong influence although it is already very high. No apparent saturation can be observed until the flow achieves almost 180° of spreading rate with small structure filling the space immediately downstream of the trailing edge.

The investigations of large A_f influence on free turbulent flows are relatively too few, especially for mixing layer. Oster & Wygnanski (1982) showed a saturation trend of forcing amplitude influence and also suggested that at larger A_f the mixing layer resonated with the imposed oscillation in the region II. Fiedler and Mensing (1985) studied the influence of A_f and found that in a plane mixing layer, the effect of A_f reached saturation when it was as high as 6.5%. In the mean, the forced flow always experienced stronger spread than the natural one. It was approximately twice the neutral value and independent of A_f . However, figure 7 indicates that there is no such saturation and $d\delta_v/dx$ strongly depends on A_f for the forcing around 6-Hz. $d\delta_v/dx$ under strong forcing is far larger than twice of the neutral one. If the forcing is higher than this narrow frequency-band (e.g. higher than 10 Hz in figure 7), the receptivity will be very small or there may be no receptivity at all even though the A_f is very high. Hence, although Ho & Huang (1982) proposed that the forcing frequency had the most pronounced effect on the mixing layer, the results here indicate that A_f also has strong influence on the confined mixing layer, but only for the new receptivity mechanism.

Corcos & Lin (1984) found numerically that the growth rate of three-dimensional linear instability remained relatively constant during the rollup phase, but vortex mergings considerably delayed the linear development of the streamwise vortices. Metcalfe *et al.* (1987) observed that pairing might inhibit the three-dimensional instability, while suppression of pairing may drive the three-dimensional mode to turbulent-like states. These seem to be identical to the result shown in figure 5, where there is no vortex merging for the spanwise structures since the forcing is in mode I, and the growth rate of the streamwise vortices is very high under forcing. However, as shown in figure 9b and c, although there is vortex merging for the spanwise structures, the streamwise vortices still continuously grow very fast under forcing of the new instability mechanism. This indicates that the development of streamwise structure depends not only on the merging of the spanwise structures, but also the instability mechanism of the streamwise structures, at least in the confined configuration.

When the mixing layers are initially laminar, they become eventually turbulent in a process know as the small-scale transition. For scalar mixing, Konrad (1976) proposed a concept called 'mixing transition', which took place at downstream position, where the molecular 'mixedness' of scalar increased dramatically following the small scale transition (Konrad 1976; Breidenthal 1981; Koochesfahani 1984). Roshko (1991) suggested that the small scale transition was found to begin after the vortex merging and unlimited increase of the initial Re_{θ_0} would eventually move the small scale transition to the separation point. The Re_θ for the transition in water channel is $750 < Re_\theta < 1700$ (Jimenez, Martinez-Val & Rebollo 1979, Breidenthal 1981 and Ho & Huerre

1984). However, figure 7g shows that the small scale transition takes place immediately downstream of the trailing edge without the vortex merging and the corresponding Re_{θ_0} is not unlimited. Under the forcing of the new instability, the transition can also occur at Re_{θ} much smaller than the above mentioned range. The rapid mixing similar to figure 7g can also be obtained at Reynolds number $Re_D = D\bar{U}/\nu = 400$ based on pipe diameter D , where A_f is about 100% and f_f is 6 Hz (Wang 1999). For this case Re_{θ} should be smaller than 400 because the initial θ_0 is smaller than D . These results indicate that the mechanism of the transition to small scale here could be different from the traditional one.

3.4 Influence of initial Reynolds number

In the present work, the Re_{θ_0} is increased through the increase of stream velocity, i.e. $Re_{\theta_0} \sim \theta_0 \bar{U} \sim \bar{U}^{1/2}$, since the flow at the trailing edge for all Re_{θ_0} investigated is laminar (this is also certified through visualization) due to the settling chamber and contraction in the nozzle. For a given mixing layer, the Strouhal number St_{n1} corresponding to f_{01} of the Kelvin-Helmholtz instability, is a constant (Ho & Huerre 1984), i.e.

$$St_{n1} = f_{01}\theta_0/\bar{U} = \text{constant}. \quad (2)$$

The momentum thickness θ_1 and θ_2 of the boundary layers on the splitter plate scale with $U_1^{-1/2}$ and $U_2^{-1/2}$ respectively when Re_{θ_0} is not very high. Thus, the initial θ_0 of the mixing layer is approximately proportional to $\bar{U}^{-1/2}$, i.e.

$$\theta_0 = (\theta_1 + \theta_2) \sim 1/\bar{U}^{-1/2}. \quad (3)$$

For a constant St_{n1}

$$f_{01} \sim \bar{U}^{3/2}. \quad (4)$$

i.e. for a traditional two-dimensional mixing layer, there is only one f_{01} , which increases with $\bar{U}^{3/2}$.

However, figure 10 shows that for each given \bar{U} , the scalar power spectrum has two peaks: one of which approximately increases with $\bar{U}^{3/2}$ and the other approximately a constant. The two frequencies corresponding to the peaks are incommensurable, i.e. the low frequency is not the subharmonics of the higher one. The measurement is undergone at $x/D = 0.7$ without forcing. For the three cases in figure 10, \bar{U} are 7.5, 25 and 50 cm/s respectively with a constant $\lambda = 0.2$. For $\bar{U} = 7.5$ cm/s, we have mentioned in figure 2 that the frequency corresponding to the new instability and f_{01} are 6 and 7.2 Hz respectively, but here the two peaks are a little smaller than 6 and 7.2 Hz respectively. This is because the measurement is not at $x/D = 0$, and the measured frequencies decrease with the increase of x . With the increase of \bar{U} , the relative difference between the measured frequency at measuring point and the vortex passage frequency at the beginning of the mixing layer decreases. The quasi 6 Hz of the primary structure can also be seen in figure 9, where figure 9a (no forcing) and figure 9b (forced at 6 Hz) have approximately the same phase angle of the structure as indicated by the vertical line. The quasi-periodic large structure in figure 9b corresponds to the forced structure of 6 Hz.

Figure 10 indicates that there are two most-probable frequencies: one corresponds to f_{01} of the traditional Kelvin-Helmholtz instability, and the other to f_{02} of the new instability. Their relations to \bar{U} are displayed in figure 11, where f_{01} approximately increases with $\bar{U}^{3/2}$, but f_{02} is approximately a constant within a narrow frequency band of 5 - 7 Hz. Since Ho & Huang (1982) suggested that f_{01} scaled with the boundary layer of the high speed, λ used for figure 11 was a constant of 0.33 to ensure that equation (4) be as accurate as possible.

Figure 11 is actually not limited only to $\lambda = 0.33$. It is also true for other values of λ and \bar{U} . The \bar{U} used in this work is in the range of 1 - 80 cm/s and λ in 0 - 1. f_{02} is almost a constant and independent of \bar{U} and λ within this range. The possible highest U_1 and U_2 , which can be provided in the experimental apparatus are 120 cm/s and 40 cm/s respectively. Its corresponding f_{02} is also about 6 Hz. It is just under the forcing of this frequency band that the flow has a receptivity much higher than that of the traditional two-dimensional mixing layers. This again shows that narrow band of 6 Hz corresponding to a new instability mechanism.

Another interesting thing is that the confined mixing layer has a higher receptivity at relatively low Re_{θ_0} , especially when A_f is high. This is demonstrated in figure 12, where the flow velocity is the same as figure 2, i.e. $U_1 = 9$ cm/s, $U_2 = 6$ cm/s, but with a constant $f_f = 3.2$ Hz and different A_f , i.e. in the mode II. λ is the same as figure 9, where f_f is 16 Hz and also in mode II, but higher Re_{θ_0} . The A_f are 7%, 16%, and 50% for figure 12a, b and c respectively. The corresponding unforced case is shown in figure 2a. It is found that

the forced flows have much wider spreadings compared with figure 9g, h, and j even though they are in the same mode II and have the same A_f . Accordingly, the flow in the confined configuration is easier to control at lower Re_{θ_0} than at higher Re_{θ_0} in the view point of the receptivity. The forcing is not saturated in figure 12b and $d\delta_v/dx$ of the mixing layer in figure 12c is much higher than that of its corresponding two-dimensional mixing layer. Therefore, the confined mixing layer at low Re_{θ_0} with f_{01} close to or smaller than f_{02} has higher receptivity than its corresponding traditional two-dimensional mixing layer when f_f is smaller than f_{02} .

The side views show that when A_f is not very high (e.g. less than 16%), the mixing layer is dominated by the Kelvin-Helmholtz instability. The primary vortices in figure 12c show, however, some similar topology to those in figure 7d and figure 9d (i.e. asymmetric counter-rotating vortex pair). This could indicate that the new receptivity has partially influenced the confined mixing layer under strong forcing (e.g. here when A_f is about 50%). It also needs to be mentioned that if the flow is also forced at 5.6 Hz with the same forcing level, the result is similar to that of figure 7 and hence is not shown here. This indicates that although the f_f (smaller than f_{02}) has higher receptivity at relatively low Re_{θ_0} than at high Re_{θ_0} in mode II, its receptivity is lower than that of $f_f = f_{02}$.

The critical forcing amplitude A_{fc1} required to change $d\delta_v/dx$ of the unforced mixing layer for the new receptivity is found to decrease with increase of $Re_D = D\bar{U}/\nu$ as shown in figure 13. The fact that the A_{fc1} decreases with Re_D could indicate that the viscosity might have a influence through wall on the confined mixing layer when Re_D is sufficiently low.

3.5 Velocity ratio λ

For the unforced and weakly forced mixing layer, $d\delta_v/dx$ increases with λ as shown in figure 14a and b. In figure 14a, U_1 and λ are 48 cm/s and 0.2 respectively. In figure 14b U_1 and λ are 60 cm/s and 0.5 respectively. There is no forcing for these two cases and their initial Re_{θ_0} are nearly the same. Obviously $d\delta_v/dx$ in figure 14b is higher than that in figure 14a. This is identical to what Monkewitz and Huerre (1982) pointed out, i.e. the higher the λ , the larger $d\delta_v/dx$. However, for the strong forcing, the difference of the shear layer spread becomes smaller as displayed in figure 14c (the forced case of figure 14a) and figure 14d (the forced case of figure 14b). The forcing f_f and A_f are the same for both cases, and are 6 Hz and about 20% respectively.

As we have seen from figure 7c and d that when A_f is sufficient high, there will be asymmetric counter-rotating vortex pairs for the primary structures and they are no longer pure Kelvin-Helmholtz vortices. Here is the starting point where the strongly forced mixing layer in the confined configuration is qualitatively different from the traditional forced two-dimensional mixing layer. Measurement displays that the higher the λ , the higher the needed A_f to produce the counter-rotating vortex pair. This critical A_f is denoted by A_{fc2} . The result is shown in figure 15, where \bar{U} is 7.5 cm/s. It is also found that λ has no apparent influence on f_{02} , i.e. f_{02} is almost independent of λ .

4 Discussion

4.1 Some comments on the experimental results

As we know, in the initial stage, the mixing layer has a wake (Ho & Huang 1982). Usually due to the sharp trailing edge and the Kelvin-Helmholtz instability, such a wake is not visible through visualization. However, under strong forcing, the initial vorticity disturbance of primary vortex is very high and the rollup of vortex occurs near the trailing edge. As a result, the wake effect will be strong and become distinguished. In wake flows, there are counter-rotating vortices. This could be the reason that when the forcing amplitude is sufficiently high, the counter-rotating primary vortices emerge. However, such counter-rotating primary vortices should not be the only reason of the high receptivity. Since in a plane wake with $\lambda = 0$, if the flow is not forced under the new instability mechanism, no such a dramatic mixing can be obtained (Wang 2000b).

Fiedler *et al.* (1981) reported that forcing causes the strongest spreading on the low speed side of a mixing layer. No report has shown that the central line of a mixing layer could bias to the high speed side and there could be an asymmetric counter-rotating vortex pair in a mixing layer as shown in figure 7. The above mentioned initial wake in the mixing layer would be one reason for the unusual bias, but not the only one, since it is difficult to explain the bias to the high speed side. Although the bias of the Type A Vortices and the spanwise structure is related to each other as shown in figure 7 and figure 8, it is not clear which is the cause.

Ho & Nosseir (1981) observed a phenomenon called 'collective interaction', under which the shear layer displayed an extremely large spreading rate. To achieve the collective interaction, the required A_f should be very high and the f_f much lower than the f_{01} . Ho & Huang (1982) further pointed out that if A_f was extremely high and close to the saturation level, the mixing layer could form a large vortex directly. Although figure 7e and f display a large vortex immediately downstream of the trailing edge, the collective interaction should not be the reason for such a large spreading shear layer here at 5.6 Hz. This is due to the fact that the f_f (5.6 Hz) here is in the mode I and only 0.78 times smaller than f_{01} , i.e., it is not very low frequency. Although f_f (= 6 Hz) is much smaller than f_{01} in figure 9b and the collective interaction occurs therein, the formed large counter-rotating vortex pair in figure 9d are not similar to the vortices induced only by Kelvin-Helmholtz instability. Furthermore, the A_f is still not saturated in figure 9d. Hence the collective interaction observed in figure 9 is only a coincidence with the new instability mechanism. The response of the mixing layers to A_f in figure 7 with f_f = 5.6 Hz and figure 9 with f_f = 6 Hz are similar although their λ and Re_{θ_0} are different. The difference of values of f_f for the two cases is relatively small and the f_f corresponding to the maximum receptivity can approximately be regarded as a constant. The extremely fast spreading of the mixing layers in these two cases indicates that they correspond to the same new instability mechanism, which are related to Type A Vortices. This can also be seen by referring to figures 9 and 6, which can explain why the forcing of 6 Hz has a much higher $d\delta_v/dx$ than the traditional two-dimensional mixing layer does in figure 9.

Similar result to figure 12 can also be obtained for other mixing layers, where Re_{θ_0} is smaller than that in figure 2. Since f_{01} is close to f_{02} in figure 2, it could imply that when f_{01} is close to or smaller than f_{02} , the new receptivity could partially contribute to the development of the mixing layer for f_f smaller than f_{02} , even though it is not within the narrow band of f_{02} . The reason for the large receptivity of the low Re_{θ_0} could probably be due to the fact that low Re_{θ_0} has f_{01} close to or smaller than f_{02} . At low Re_{θ_0} , whose f_{01} is close or lower than f_{02} , the two instabilities could influence the mixing layer for f_f lower than f_{02} in the confined mixing layer under strong forcing. Thus the corresponding receptivity may also be relatively high. This could be the reason why the receptivity in figure 12 is higher than that in figure 9 with f_f = 16 Hz, although both cases are in the same mode II. This could probably explain the unsolved phenomenon observed by Roberts (1985), where the side-wall effect can increase mixing which decreases with the increase in \bar{U} . Actually the new receptivity is related to the so-called side-wall effect. According to the result mentioned above, the lower the \bar{U} , the stronger the new instability influence under forcing, and thus the stronger the side-wall effect.

According to the published common and limited range of the spreading rate in mixing layers, Browand and Ho (1987) proposed a universal spreading rate for mixing layers, which also includes forced flow situations. Dimotakis (1991) remarked that there was a rather large spread of values in the spreading rate of the mixing layer, and that it was even not clear whether the inequality bounds represented the actual limiting values. Normally, in a two-dimensional mixing layer, the spreading angle at the beginning is no larger than 30° when forcing is applied, and the half-velocity isotach is moved slightly to the lower velocity side. However, figure 11 and 12 indicates that the Kelvin-Helmholtz instability and the new one could simultaneously influence the mixing layer under forcing. For the forcing of the new receptivity, (e.g. refer to figure 7), the isotach can not only keep symmetrically to the trailing edge (i.e. not bias to the low speed side), but also bias to the high speed side, where the spreading angles exceed 30° and even reach to 180° (the limitation). Since the side-wall and corner always exist (except axisymmetric mixing layer), the new instability could more or less always have influence on the mixing layer dynamics. Hence, it seems that there is no a universal spreading regime and the strong deviation from known cases might be related to the side-wall effect, streamwise vortices, and in particular to the new instability mechanism.

The small influence of velocity ratio under strong forcing of the new instability would be related to the streamwise vortices and initial wake. As we know that Type A Vortices develop very fast with high A_f of the new instability, this indicates that the streamwise Type A Vortices and the initial wake of the mixing layer play an important part for the mixing layer under the strong forcing of the new receptivity and the effect of λ becomes smaller and negligible. Again this implies that the instability of Type A Vortices is the main reason for the rapid spread of the mixing layer under strong forcing of the new instability. With the increase of the velocity ratio, the initial disturbance amplifies faster and the bias of the mixing layer to low speed side could become stronger. Thus it could need more energy to change the trend of the mixing layer development. This would be the reason why the forcing amplitude required to introduce the asymmetric counter-rotating pair of the spanwise structures increases with the velocity ratio.

Since Type A Vortices evolve earlier than the spanwise undulation, which could be the origin of the stream-

wise vortices in a traditional two-dimensional mixing layer, it is not clear according to the figure 4, whether Type A Vortices have effect on the origin of the undulation and hence, the origin of streamwise vortices in the two-dimensional mixing layer. Actually the side-wall and corner always exist in the non-axisymmetric two-dimensional mixing layer, the Type A Vortices should always have more or less influence on the mixing layer. It is also not clear to what extent they do so. There may be more than one possibility for the origin of the streamwise vortices in a traditional two-dimensional mixing layer. The actual result could depend on the competition of the strength of each mode for a given situation.

It should also be pointed out that, traditionally the spreading rate or the width of the free shear layer are often used for mixing criterion (e.g. Cantwell 1981). This is actually not always plausible. The mixing criterion depends actually on the mixing requirement. If molecular mixing enhancement is the goal of mixing control, the shear layer width alone is not enough. This can be seen in figure 2b and figure 2d. It is apparent that the shear layer width in figure 2b is higher than that of figure 2d in the initial stage. However, the amount of small scales in figure 2d is much higher than that in figure 2b, and so is the molecular mixing. Hence the chemical product in figure 2d should also be higher than that in figure 2b. Thus, although $d\delta_v/dx$ is higher in figure 2b than in figure 2d, the molecular mixing should be more in figure 2d than in figure 2b. Details about mixing criteria are discussed in Wang (1999).

4.2 Some comments on the new instability and receptivity

We have seen that there are two peaks in the scalar power spectrum, f_{02} is independent of \bar{U} , forcing around 6 Hz demonstrates some unusual phenomena (spanwise asymmetric counter-rotating pairs, unusual bias and dramatic spread of the mixing layer). These suggest that forcing around the narrow frequency band of 6 Hz corresponds to a new instability mechanism, which is different from the Kelvin-Helmholtz instability. Figure 7 and 8 shows that the primary and streamwise Type A Vortices have approximately the same size in the transverse direction immediately downstream of the mixing layer. Figure 6 and 9 shows that when spanwise vortices develop fast, so do the Type A Vortices, and both develop fast when forcing frequency is about 6 Hz with sufficiently high forcing amplitude. All these indicate that the new instability is related to the streamwise vortices Type A Vortices.

It could be useful to consider a simplified model for Type A Vortices. In the confined configuration, the streamwise corner flow along the junction of the trailing edge and pipe wall, and its interaction with the primary vorticity immediately downstream of the trailing edge determine the topology of Type A Vortices. The streamwise corner flow along the junction of two plates is subject to inviscid instability due to the inflectional nature of the streamwise velocity profile (e.g. Dhanak 1993, Balachandar & Malik 1995). The corner flow is characterized by its secondary flow, which depends on whether the boundary flow is laminar or turbulent. For the laminar corner flow, the secondary flow is outwards from the corner along the plane of symmetry and inwards towards the corner close to the walls (e.g. Zamir & Young 1971) as shown in figure 16a. The secondary flow in a turbulent corner flow is opposite to that of the laminar corner flow (e.g. Gessener & Jones 1965) as shown in figure 16b.

The vorticity of the corner flow leaving the trailing edge will interact with the vorticity of the primary flow in a complex manner. The produced structures depend on the trailing edge geometry, flow state (i.e., laminar or turbulent flow in the corner), with or without forcing, the type of flow (wake with $\lambda = 0$ or mixing layer) and so on. The sharp trailing edge is used here. With no forcing, the corner flow could be laminar in the present experimental range of Reynolds number, since the favorable pressure gradient can stabilize the corner flow (Zamir & Young 1979). If the primary flow is wake ($\lambda = 0$), the boundary vorticity on both side of the trailing edge is the same value with different direction. There will be two streamwise counter-rotating vortex pairs as shown in figure 17a due to the interaction of the corner vorticity and the primary vorticity (Wang 2000b). However, if the primary flow is a mixing layer, there will be only one streamwise counter-rotating vortex pair at each side of the wall as shown in figure 17b, resulting mainly from the high speed side. This could be because of that the boundary vorticity of the high speed side of the trailing edge is higher than that of the low speed side and the low vorticity will be drawn into the high one.

Under periodic forcing with sufficiently high forcing amplitude, the impulse in the transverse direction at the trailing edge is high, since the transverse velocity component is high due to the receptivity at the trailing edge. For a wake with $\lambda = 0$, this impulse will in turn, due to the confinement, positively give the impulse (and thus enhance) only to the vortices which have the same sign with the impulse, although there is originally a counter-rotating pair of vorticity along each corner. Therefore, only one counter-rotating vortex pair of Type A

vortices are yielded as shown in figure 18a at each side of the wall. For the mixing layer, except the impulse, the forcing enhances its initial wake, which is so strong that the Type A vortices in the mixing layer become similar to that in a wake with $\lambda = 0$, as shown in figure 18b. This indicates that there is some difference in Type A Vortices with and without forcing in the mixing layer. The Type A vortices shown in figure 18 is applied to both laminar and turbulent corner flow for sufficiently high forcing amplitude. The same topology of Type A Vortices in wake ($\lambda = 0$) and mixing layer under strong forcing indicate that, the transverse impulse and initial wake of the mixing layer play important role in the evolvement of Type A Vortices. Hence, the model proposed here is different from that of Roberts (1985), which is apparently unable to explain the complex situations (Wang 2000b).

Figure 8 also implies that the forcing introduces an impulse in transverse direction, which in turn, can enhance the development of the Type A Vortices because of the confinement. The development of Type A Vortices favors the amplification of the spanwise structure and hence these two kinds of vortices impulse each other positively. Since no such a rapid spread in the mixing layer can be obtained for the Kelvin-Helmholtz instability, Type A Vortices are supposed to be the corresponding reason. Due to the fast development and strong amplification of Type A Vortices in the initial period shown in figure 6, the new instability has a much stronger receptivity than the traditional one. Consequently, these three-dimensional mixing layers in the confined configuration have a much higher receptivity than its corresponding two-dimensional ones.

Receptivity describes how an initial external disturbance is converted into a vortical instability wave. The very sensitive response of Type A Vortices to forcing implies that Type A Vortices corresponds to some instability mechanism. The input energy from external forcing is converted into spanwise vortices and Type A Vortices, and hence there are two receptivity mechanisms in the confined configuration. We call this phenomenon 'dual receptivity' here to distinguish it from the traditional one, since usually the mixing layer is understood to have only one receptivity mechanism, i.e. the Kelvin-Helmholtz instability although there is also secondary instability.

The concept of dual receptivity could extend our scope about the instability in the mixing layer although Kelvin-Helmholtz instability is more fundamental and has more applications. It is well-known, e.g. from Michalke (1965) and Ho & Huerre (1984), that the mixing layer is subject to inviscid instability. The corresponding Strouhal number St_{n1} of the most-amplified frequency is a constant for sufficient high Reynolds number and should be independent of Reynolds number. In other words, the dimensional frequency is used instead of St_{n1} , the most-amplified frequency at the beginning of the mixing layer scales with mean flow velocity $\bar{U}^{3/2}$. However, in the confined mixing layer, as we know, except for the traditional one there is another new most-amplified frequency f_{02} , which is approximately a constant and independent of mean flow velocity as shown in figure 11. Its corresponding Strouhal number St_{n2} decreases with mean flow velocity \bar{U} , and hence with initial Reynolds number Re_{θ_0} (which is increased through \bar{U}) if the boundary flows on the trailing edge are laminar. Since the corner is always presented in a mixing layer (except some cases, e.g. axisymmetric mixing layer) and the side-wall effect has actually more or less influence on the dynamics of mixing layer, the new instability should also have influence on the mixing layer dynamics. In this viewpoint, the result here extends the scope of classical theory. Figure 19, where α_i represents the spatial amplification rate, gives a sketch to describe qualitatively the extended result of possible existing instability mechanisms in mixing layers. This can at least show the influence of the side-wall on the instability behaviors in mixing layers and provide some new scope of receptivity for mixing layer control. Figure 19a uses dimensional frequency and figure 19b dimensionless Strouhal number St .

It seems at first that the narrow band of f_{02} is similar to the frequency of organ-pipe (quasi excitation) observed by Fiedler & Thies (1978). However, no such a large receptivity was observed in that work. It is not clear if the constant f_{02} of 6 Hz is the resonance frequency of the water channel or not. If it is the resonance frequency, there should always be vibration of the water channel no matter if the fluid is at rest or in motion. An experiment was conducted to test it. The actuator forces at 6 Hz with the fluid at rest, and no vibration of the water channel can be observed. This could indicate that 6 Hz is not the system resonance frequency of the water channel. Although the side-wall has strong influence in the confined configuration, it is also distinguishable from Tollmien-Schlichting wave (which is often the main reason for wall-boundary flow receptivity and could also be established on the splitter plate and side-wall), since frequency corresponding to the Tollmien-Schlichting wave is also related to the mean flow velocity. The feedback mechanism in Ho & Huerre (1984) seems not to be related to the new instability, since no primary vortex merging can be observed under strong forcing of the narrow forcing frequency band as shown in figure 7. So the feedback mechanism could not be the reason for the

Author(s)	Channel size (cm ²)	U_1 (cm/s)	U_2 (cm/s)	f_{01} (Hz)
Ho & Huang (1982)	10*10	9.5	5	5.06
Mackinnon & Koochesfahani (1997)	4*8	9.3	9.3	6
Nygaard & Glezer (1991)	10*22; 22*22	30	10	6

Table 1: References for the most-probable frequencies in water channels.

new instability. Zhou (2000) suggested that the periodic flow might be related to three dimensional property of the experimental setup. The large receptivity of the new instability might also be related to the annular effect (Schlichting 1979) due to the high forcing amplitude. It should be mentioned here that the confined mixing layer is a three-dimensional flow and more complicated than its corresponding two-dimensional one.

The reason why the value of f_{02} is a constant and in the narrow band of 5-7 Hz is still open. Here a rather tentative conjecture is proposed. Obviously the new receptivity converses the initial disturbance at least partially into the unstable Type A Vortices. We could suppose Type A Vortices as the initial disturbance wave, which is responsible for the new instability. If we could see the corner vorticity as the initial inhomogeneous in the spanwise direction on the splitter plate, their corresponding wave number should be a constant for a given geometry of the channel (here pipe diameter). The interaction of the vorticity of Type A Vortices with primary vorticity could induce new waves in spanwise direction, e.g. as shown in figure 4c until some equilibrium state. Type A Vortices always exist and are independent of the streamwise mean flow velocity. Since there is no mean flow velocity in the spanwise direction, f_{02} could therefore be a constant and is independent of streamwise mean flow velocity. Unfortunately no other geometry is investigated. Interestingly in some other publications with water channels, the most-probable frequencies are also within the narrow frequency band of 6 Hz shown in the following table 1 for several examples.

According to figure 10, both the Kelvin-Helmholtz instability and the new instability could have influence on the mixing layer dynamics simultaneously. Figure 7 shows that if the forcing amplitude is not high, the new instability has little effect and the mixing layer development in the confined configuration is similar to that in the conventional two-dimensional mixing layers. This could imply that if the difference between f_{01} and f_{02} is not very large, the measurement of f_{01} , e.g. based on velocity spectrum could have the possibility to be influenced by f_{02} . It is not clear to what degree the new instability could affect the measurement of f_{01} , especially when the difference between the two frequencies is not large. The f_{01} is 5.06 Hz in Ho & Huang (1982) with $U_1 = 9.5$ and $U_2 = 5$ cm/s respectively. This result is nearly identical to the present result of $f_{01} = 7.2$ Hz with $U_1 = 9$ and $U_2 = 6$ cm/s respectively. However, in the experiment of Nygaard & Glezer (1991), the mean flow velocity is relatively high, i.e. $U_1 = 30$ and $U_2 = 10$ cm/s respectively, but f_{01} is also 6 Hz. Although the initial momentum thickness can also influence the most-amplified frequency, the above argument should not be neglected. In the work of Mackinnon & Koochesfahani (1997), where $U_1 = U_2 = 9$ cm/s and f_{01} is approximately 6 Hz, $f_f = 6$ Hz is used to force the wake and the influence of Type A Vortices for the mixing enhancement is obvious. However, in Wang (2000b), if the f_{01} is much larger than f_{02} , the forcing influence at f_f close to f_{01} is limited. Therefore the new instability could have partially influenced the result in Mackinnon & Koochesfahani (1997).

Finally, it is necessary to mention that even if the mechanism of the new receptivity is not clear, one thing is already clear: the large receptivity and thereby the corresponding extraordinary dramatic mixing is very attractive to and would provide new opportunity for mixing enhancement of mixers, reactors and combustion in industry. For instance, the corresponding mixing process also has the most of the advantages of those micromixers, which are now poised to generate big waves in chemical and pharmaceutical industry. The related application topic is referred to Wang (2000a).

4.3 Some comments on side-wall effect and flow control

Squire theorem (1933) tells us that, the three-dimensional flow has a smaller amplification than its corresponding two-dimensional flow. Wall usually could make a flow more stable, since near the wall the viscosity

has more influence to decay the disturbance than a wall-free shear flow (although in a wall boundary laminar flow, viscosity can also result in instability.) Based on these viewpoints, the confined mixing layer ought to have smaller receptivity than its corresponding two-dimensional mixing layer. However, the experimental results of this work tell us in contrast that the receptivity is stronger in a confined plane mixing layer than in the two-dimensional mixing layer due to the Type A Vortices. This implies that the wall has two effects: On the one hand, it makes the flow more stable in response to the external disturbance; on the other hand, the confinement of the wall facilitates the streamwise vortices which, in turn, increase the receptivity of the flow.

Most of our present understanding of receptivity is limited to small disturbance amplitude. When the coherent transverse velocity component \tilde{v} of the vortical instability wave is sufficiently large, saturation will occur in a conventional two-dimensional mixing layer. Its corresponding spatial amplification rate $-\alpha_i$ is then very small and thus the value of \tilde{v} is limited. However, in some processes concerning the control of fluids mixing, acoustic noise control, and reactor (i.e. in combustion) instability, both large \tilde{v} and $-\alpha_i$ could be desirable. If the value of coherent velocity component \tilde{v} is large in the initial stage, the turbulent mixing will be stronger. The fluids will then be more homogeneous for mixing in combustion and reaction flow in a reactor (especially for the whole flow field), and the combustion could be more stable and the noise can be smaller. When its initial value is small, \tilde{v} will not be large in a limited developing space even if the spatial amplification rate $-\alpha_i$ is large. If the flow can accept large external disturbance, that means, \tilde{v} is large even at the beginning of the shear layer, and if $-\alpha_i$ is also large, a much larger \tilde{v} can be obtained even in a limited initial developing distance. In such a case, a new criterion is suggested here for receptivity. It can be the product of disturbance and amplification rate, i.e. $-\alpha_i \tilde{v}$, for instance, in a spatial mode. We call it 'receptivity capacity' here. According to the experimental results, e.g. figure 7, it can be conjectured that, the above mentioned new instability has a larger receptivity capacity in the immediate vicinity of the trailing edge than the traditional one does, especially for the very high forcing amplitude.

Although very high forcing amplitude is needed for the extraordinarily fast mixing, it is worth mentioning that the new receptivity here is not simply just a result of a large disturbance or mechanical stirring, and therefore not of interest of studying receptivity. It is a phenomenon of receptivity, since only when the disturbance is in the narrow frequency band, there is the large receptivity. If the disturbance is not in the narrow band, there can be no receptivity at all even though the disturbance can be larger at too high a forcing frequency. This is the important difference between the confined mixing layer and the agitated tank used in chemical industrial, where the higher the rotation rate of the turbine impeller, the stronger the mixing.

Traditionally the philosophy of control is that a small disturbance produces a large effect like Tai-Chi-Chuan principle: use only 0.2 kg to move 500 kg. In fluid mechanics, a small initial disturbance is introduced to the flow to expect a large effect, e.g. mixing augmentation in free shear flows. It is fine and should be the first candidate for use if this is possible and sufficient for the practical requirement. Unfortunately the coherent velocity component \tilde{v} due to the amplification of a small initial disturbance is, in many cases, not large enough, for instance, for mixing dominating processes with fast chemical reaction, since rapid mixing process needs first large \tilde{v} to achieve macromixing and then to develop from large to small scale to provide favorable condition for molecular mixing. As figure 9 indicated, the traditional mixing enhancement under active control is limited. The rapid mixing in the whole local position needs large receptivity capacity as mentioned above. For this reason, the philosophy for turbulence control could be: when a small disturbance is sufficient for a practical aim, it is preferable to use it; however, a large disturbance can be considered for use to produce a larger effect if the effect of a small disturbance is limited and not enough.

5 Summary and conclusion

It seems that the confined mixing layer in a pipe is a very interesting flow, where there are two different receptivity mechanisms. One of them corresponds to the traditional two-dimensional Kelvin-Helmholtz instability and the other to a new instability, in which the mixing layer exhibits several unusual phenomena. The central line of the mixing layer does not bias to the low speed side, but to the high speed side under strong forcing of the new instability. The primary structures in the mixing layer become asymmetric counter-rotating vortex pairs under strong forcing, which are also anomalous to the 'normal' mixing layer, where the Kelvin-Helmholtz vortices have only one sign. The new instability has a much higher receptivity than the traditional one, which is limited by the well-known saturation phenomenon of the high forcing amplitude. It seems that there is no universal spreading rate for the mixing layer under forcing at least for the confined configuration. The maximum spreading rate

can be as high as 180° . The inherent frequency of the new instability mechanism is within a narrow band of approximately 5-7 Hz and is independent of the mean flow velocity. Hence, the corresponding Strouhal number is not a constant and decreases with initial Reynolds number. Since there may be no primary vortex merging at all for the forcing of the new instability, the vortex merging is not necessarily the main reason for the enhanced entrainment and mixing in the confined configuration. When the most-amplified frequency of Kelvin-Helmholtz instability is close to or smaller than its inherent narrow frequency band, the new instability will have partial influence on the mixing layer development. In these cases, the forcing frequency is not much higher than the most-amplified frequency of Kelvin-Helmholtz instability and is not necessarily within the inherent frequency band of the new instability.

The streamwise vortices play an important role for the mixing layers in the confined configuration. There are many different types of streamwise vortices and among them Type A Vortices are the most important ones for the mixing layer dynamics, especially under strong forcing, since they are related to the new receptivity mechanism. The Type A Vortices, which are counter-rotating vortex pairs, originate from the interaction of the vorticity stemmed from the corner flow between the splitter plate and the pipe wall, and the vorticity of the spanwise structure of the mixing layer immediately downstream of the trailing edge. They amplify very fast in the initial stage, resulting in the dramatic spread of the primary structures under forcing of the new instability. This could also be the reason that the effect of velocity ratio becomes neglected when the forcing amplitude is high under the forcing of the new receptivity, where the initial wake of the mixing layer becomes important.

The work here not only shows the influence of side-wall, but also displays how the side-wall affects the mixing layer under forcing through the streamwise vortices. However, the mechanism of the new instability and the extent of side-wall effect is still not clear, and the velocity field has not been measured. Further investigations are needed.

The author would like to express the appreciation to his advisor, Professor H. E. Fiedler for support and guidance of this study. Professor H. Zhou from Tianjing University/China initially inspired and advised the author to study the instability theoretically in 1993 when he was in Berlin. The discussion with him is very helpful. During experiments of this work, Professor J. S. Luo from Tianjing University/China gave the author a lot of help both in doing the experiment and discussion of the problems, when he was in Berlin in 1995. The discussions with Professors H. Eckelmann, A. Michalke, P. Huerre, M. D. Zhou, J. T. C. Liu, and J. Jemenez are also very much appreciated. Finally, the author wishes to thank Professor H. Zhou for his careful reading and comments regarding an earlier version of the manuscript.

References

- AREF, H. & SIGGIA, E. D. 1980 Vortex dynamics of the two-dimensional turbulent shear layer. *J. Fluid Mech.* **100**, 705-737.
- ASHURST, W. T. & MEIBURG, E. 1988 Three-dimensional shear layers via vortex dynamics. *J. Fluid Mech.* **189**, 87-116.
- BALACHANDAR, S. & MALIK, M. R. 1995 Inviscid instability of streamwise corner flow. *J. Fluid Mech.* **282**, 187-201.
- BERNAL, L. P. & ROSHKO, A. 1986 Streamwise vortex structure in plane mixing layers. *J. Fluid Mech.* **170**, 499-525.
- BÖRGER, G. 1975 Optimierung von Windkanaldüsen für den Unterschallbereich. *Z. Flugwiss.* **23**, 45-50.
- BREIDENTHAL, R. E. 1981 Structure in turbulent mixing layers and wakes using a chemical reaction. *J. Fluid Mech.* **109**, 1-24.
- BROWAND, F. K. & HO, C. M. 1987 Forced, unbounded shear flows. In *Int. conf. on phy. of chaos and sys. far from equil.* ed. Duong-Van, M.
- BROWAND, F. K. & TROUTT, T. R. 1980 A note on spanwise structure in the two-dimensional mixing layer. *J. Fluid Mech.* **97**, 771-781.
- BROWAND, F. K. & TROUTT, T. R. 1985 The turbulent mixing layer: geometry of larger vortices. *J. Fluid Mech.* **158**, 489-509.
- BROWN, G. L. & ROSHKO, A. 1974 On density effects and large structure in turbulent mixing layers. *J. Fluid Mech.* **64**, 775-816.
- CANTWELL, B. J. 1981 Organized motion in turbulent flows. *Annu. Rev. Fluid Mech.* **13**, 457-515.
- CORCOS, G. M. & LIN, S. J. 1984 The mixing layer: deterministic models of a turbulent flow. Part 2. The origin of the three-dimensional motion. *J. Fluid Mech.* **139**, 67-95.
- DHANAK, D. R. 1993 On the instability of flow in a streamwise corner. *Proc. R. Soc. Lond. A* **441**, 201.
- DIMOTAKIS, P. E. 1991 Turbulent free shear layer mixing and combustion. In *High-speed flight propulsion systems*, ed. B. Murthy & E. T. Curran, Progress in Astronautics and Aeronautics, **137**.

- FIEDLER, H. E. & THIES, H. J. 1978 Some observations in a large two-dimensional shear layer. In *Structure and mechanisms of turbulence I*. ed. H. Fiedler, Lecture Notes in Physics, **75**, 108-117, Springer-Verlag, Berlin.
- FIEDLER, H. E., DZIOMBA, B., MENSING, P. & RÖSGEN, T. 1981 Initiation, evolution and global consequences of coherent structures in turbulent shear flows. In *The Role of Coherent Structures in Modelling Turbulence and Mixing*. Lecture Notes in Physics, ed. J. Jimenez.
- FIEDLER, H. E. & MENSING, P. 1985 The plane turbulent shear layer with periodic excitation, *J. Fluid Mech.* **150**, 281-309.
- FIEDLER, H. E. & FERNHOLZ, H. H. 1990 On management and control of turbulent shear flows. *Prog. Aerospace Sci.* **27**, 305-387.
- GAD-EL-HAK, M., POLLARD, A. & BONNET, J.-P. (EDITORS) 1998 Flow Control: Fundamentals and Practices, Springer-Verlag, Berlin.
- GESSENER, F. B. & JONES, J. B. 1965 On some aspects of fully-developed turbulent flow in rectangular channels. *J. Fluid Mech.* **23**, Part 4.
- HO, C. M. & NOSSEIR, N. S. 1981 dynamics of an impinging jet. Part 1. The feedback phenomenon. *J. Fluid Mech.* **105**, 119-142.
- HO, C.-M. & HUANG, L.-S. 1982 Subharmonics and vortex merging in mixing layer, *J. Fluid Mech.* **119**, 443-473.
- HO, C.-M. & HUERRE, P. 1984 Perturbed free shear layers, *Ann. Rev. Fluid Mech.* **16**, 365-423.
- HUANG, L. S. & HO, C. M. 1990 Small-scale transition in a plane mixing layer, *J. Fluid Mech.* **210**, 475-500.
- HUSSAIN, A. K. M. F. 1986 Coherent structures and turbulence. *J. Fluid Mech.* **173**, 306-356.
- JIMENEZ, J. 1983 A spanwise structure in the plane shear layer. *J. Fluid Mech.* **132**, 319-336.
- JIMENEZ, J., MARTINEZ-VAL, R. & REBOLLO, M. 1979 On the origin and evolution of three dimensional effects in the mixing layer. Inter. Rep. DA-ERO 79-G-079, Univ. Politec. Madrid.
- KONRAD, J.H. 1976 An experimental investigation of mixing in two-dimensional turbulent shear flows with application to diffusion limited chemical reactions. Ph. D. Thesis, Caltech.
- KOOCHESFAHANI, M. M. 1984 Experiments on turbulent mixing and chemical reactions in a liquid mixing layer. Ph. D. thesis, Caltech..
- KOOCHESFAHANI, M. M. & MACKINNON, C. G. 1991 Influence of forcing on the composition of mixed fluid in a two-stream shear layer. *Phys. Fluids A*, **3**, 1135-1142.
- LASHERAS, J. C., CHO, J. S. & MAXWORTHY, T. 1986 On the origin and evolution of streamwise vortical structures in a plane, free shear layer. *J. Fluid Mech.* **172**, 231-258.
- LASHERAS, J. C. & CHOI, H. 1988 Three-dimensional instability of a plane free shear layer. An experimental study of formation and evolution of streamwise vortices. *J. Fluid Mech.* **189**, 53-86.
- LIN, S. J. & CORCOS, G. M. 1984 The mixing layer: deterministic models of a turbulent flow. Part 3. The effect of plane strain on the dynamics of streamwise vortices. *J. Fluid Mech.* **141**, 139-178.
- MACKINNON, C. G. & KOOCHESFAHANI, M. M. 1997 Flow structure and mixing in a low Reynolds number forced wake inside a confined channel. *Phys. Fluids*, **9**, 3099-3101.
- METCALFE, R. W., ORSZAG, S. A., BRACHET, M. E., MENON, S. & RILEY, J. J. 1987 Secondary instability of a temporally growing mixing layer. *J. Fluid Mech.* **184**, 207-243.
- MICHALKE, A. 1965 On spatially growing disturbance in an inviscid shear layer. *J. Fluid Mech.* **23**, 521-544.
- MIKSAD, R. W. 1972 Experiments on the nonlinear stages of free-shear-layer transition. *J. Fluid Mech.* **56**, 695-719.
- MONKEWITZ, P. A. & HUERRE, P. 1982 The influence of velocity ratio on the spatial instability of mixing layers. *Phys. Fluids*, **25**, 1137-1143.
- MOSER, R. D. & ROGERS, M. M. 1991 Mixing transition and the cascade to small scales in a plane mixing layer. *Phys. Fluids A*, **3**, 1128-1134.
- NYGAARD, K. J. & GLEZER, A. 1991 Evolution of streamwise vortices and generation of small-scale motion in a plane mixing layer. *J. Fluid Mech.* **231**, 257-301.
- OSTER, D. & WYGNANSKI, I. 1982 The forced mixing layer between parallel streams, *J. Fluid Mech.* **123**, 91-130.
- OSTER, D., WYGNANSKI, I., DZIOMBA, B. & FIEDLER, H. 1978 The effects of initial conditions on the two-dimensional mixing layer. In *Structure and mechanisms of turbulence I*. ed. H. Fiedler, Lecture Notes in Physics, **75**, 48, Springer-Verlag, Berlin.
- PIERREHUMBERT, R. T. & WIDNALL, S. E. 1982 The two- and three-dimensional instability of a spatially periodic shear layer. *J. Fluid Mech.* **114**, 59-82.
- ROBERTS, F. A. 1985 Effects of periodic disturbance on structure and mixing in turbulent shear layers and wakes. Ph. D. thesis, Caltech.
- ROSHKO, A. 1991 The mixing transition in free shear flows. In *The global geometry of turbulence*. ed. Jimenez, J. Plenum Press. 1991.
- SCHLICHTING, H. 1979 Boundary-layer theory. McGraw-Hill, New York.
- SQUIRE, H. H. 1933 On the stability of three-dimensional disturbance of viscous flow between parallel walls. *Proc. R. Soc. London Ser. A*, **142**, 621-628.
- VEYNANTE, D., CANDEL, S. M. & MARTIN, J. 1986 Influence of the system response on the coherent structures in a confined shear layer. *Phys. Fluids*, **29**, 3912-3914.

- WANG, G. R. 1999 Turbulent mixing, stability and secondary flow in a confined configuration. Dissertation, TU Berlin, Germany. Also Wissenschaftliche Schriftenreihe Strömungstechnik, Bd. 8. ISBN 3-89574-376-3, Verlag Dr. Köster, 2000.
- WANG, G. R. 2000a A new mixing process for mixer, reactor and combustion. Submitted to *Chem. Eng. Sci.*
- WANG, G. R. 2000b Strongly forced large structures and turbulent mixing in a confined plane wake. In preparation.
- WANG, G. R. & FIEDLER, H. E. 1996. The pairing burst - a new phenomenon. *Bulletin of Am. Phys Soc. Oct.* **41**
- WANG, G. R. & FIEDLER, H. E. 1998 A new receptivity mechanism in a confined configuration. *Bulletin of Am. Phys Soc. Oct.* **43**.
- WANG, G. R. & FIEDLER, H. E. 2000 On high spatial resolution scalar measurement with LIF. Part 2: The noise characteristic. Accepted to *Exp. Fluids*.
- WEISBROT, I. & WYGNANSKI, I. 1988 On coherent structures in a highly excited mixing layer. *J. Fluid Mech.* **195**, 137-159.
- WINANT, C. D. & BROWAND, F. K. 1974 Vortex pairing: mechanism of turbulent mixing layer growth at moderate Reynolds number. *J. Fluid Mech.* **63**, 237-55.
- WOOD, D. H. & BRADSHAW, P. 1982 A turbulent mixing layer constrained by a solid surface. Part 1. Measurement before reaching the surface. *J. Fluid Mech.* **122**,
- ZAMIR, M. & YOUNG, A. D. 1970 Experimental investigation of the boundary layer in a streamwise corner. *Aeronaut. Q.* **21**, 313-338.
- ZAMIR, M. & YOUNG, A. D. 1979 Pressure gradient and leading edge effects on the corner boundary layer. *Aeronaut. Q.* **30**, 471-484.
- ZHOU, H. 2000. Private communication.

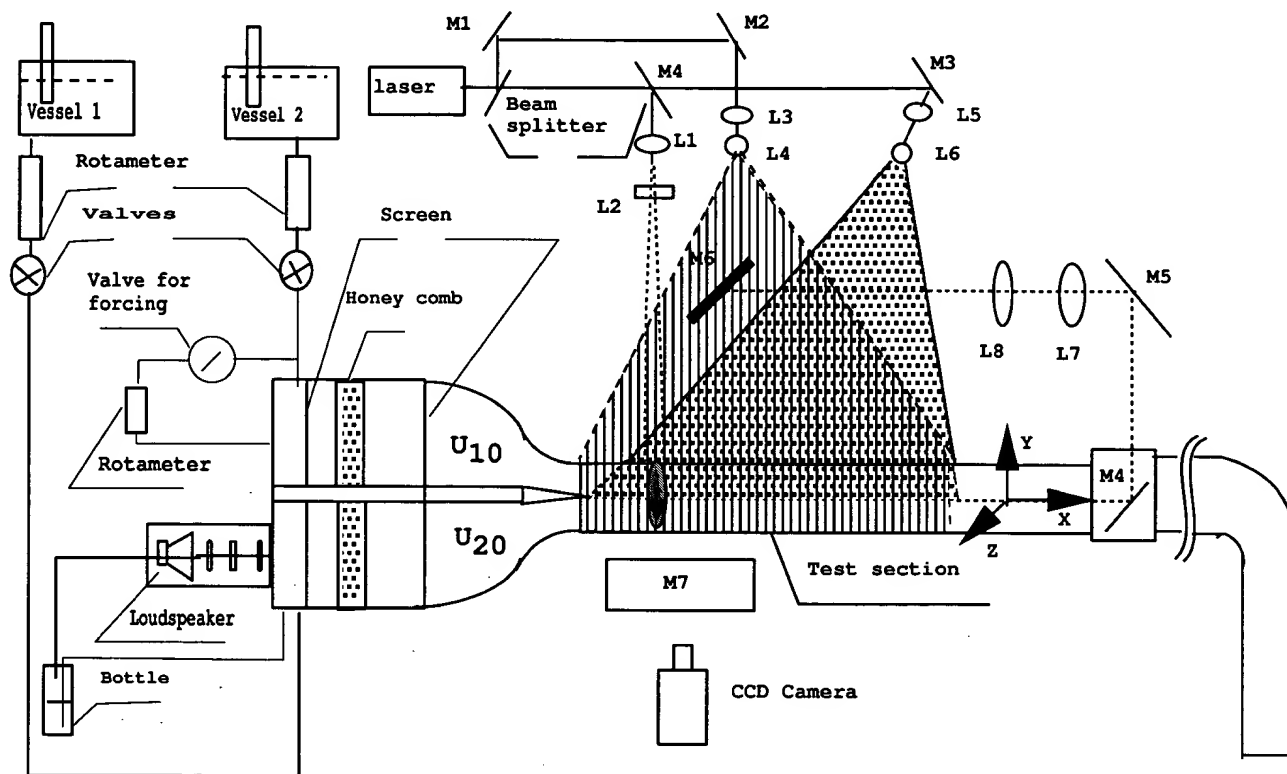


Figure 1: Experimental schematic.

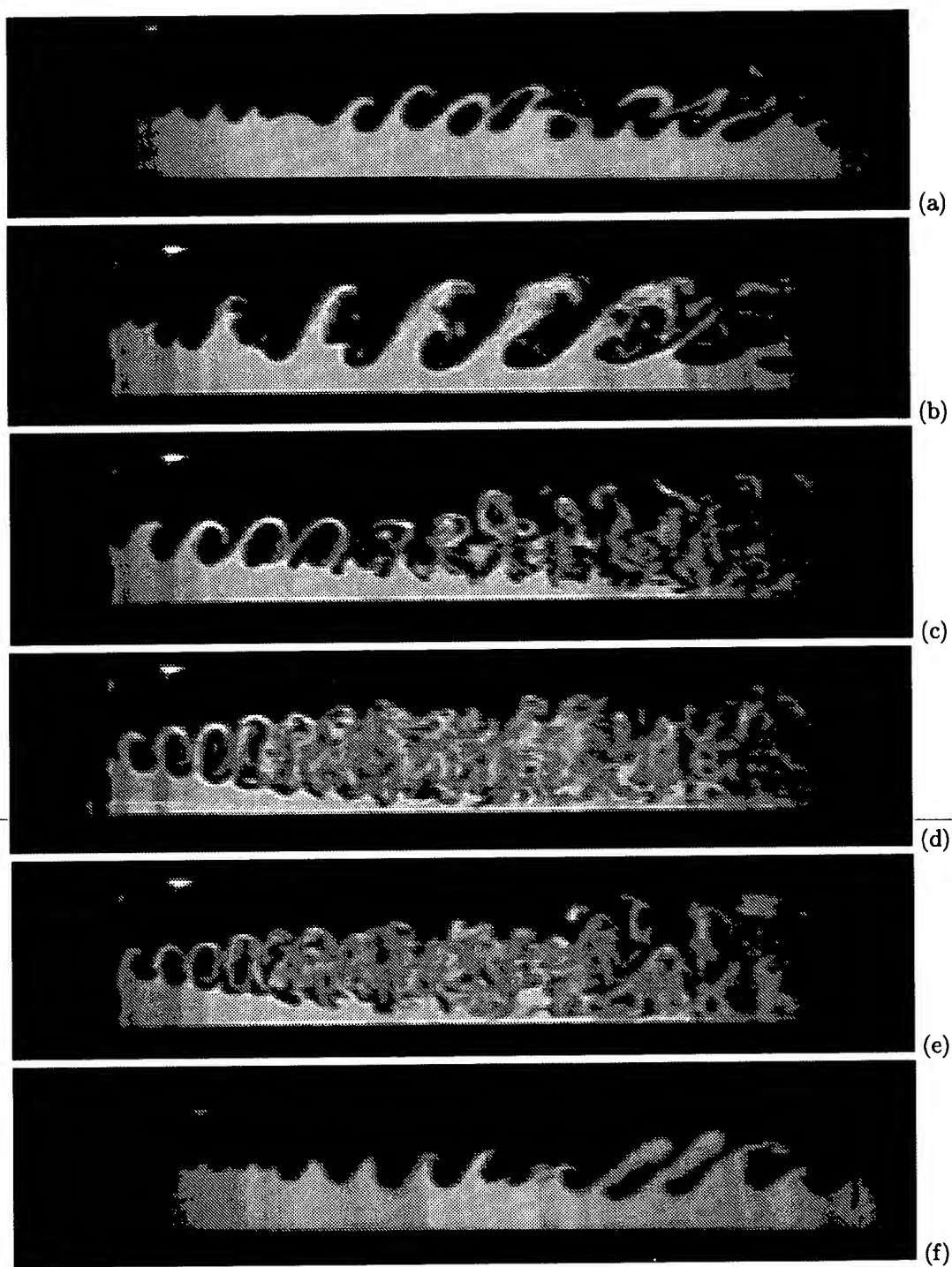


Figure 2: Influence of f_f for a mixing layer with $U_1 = 9$ cm/s and $U_2 = 6$ cm/s under a constant A_f of about 6.5%.
(a) $f_f = 0$ Hz (unforced case); (b) 2.4 Hz; (c) 4.4 Hz; (d) 6.0 Hz; (e) 7.2 Hz; (f) 9.0 Hz.

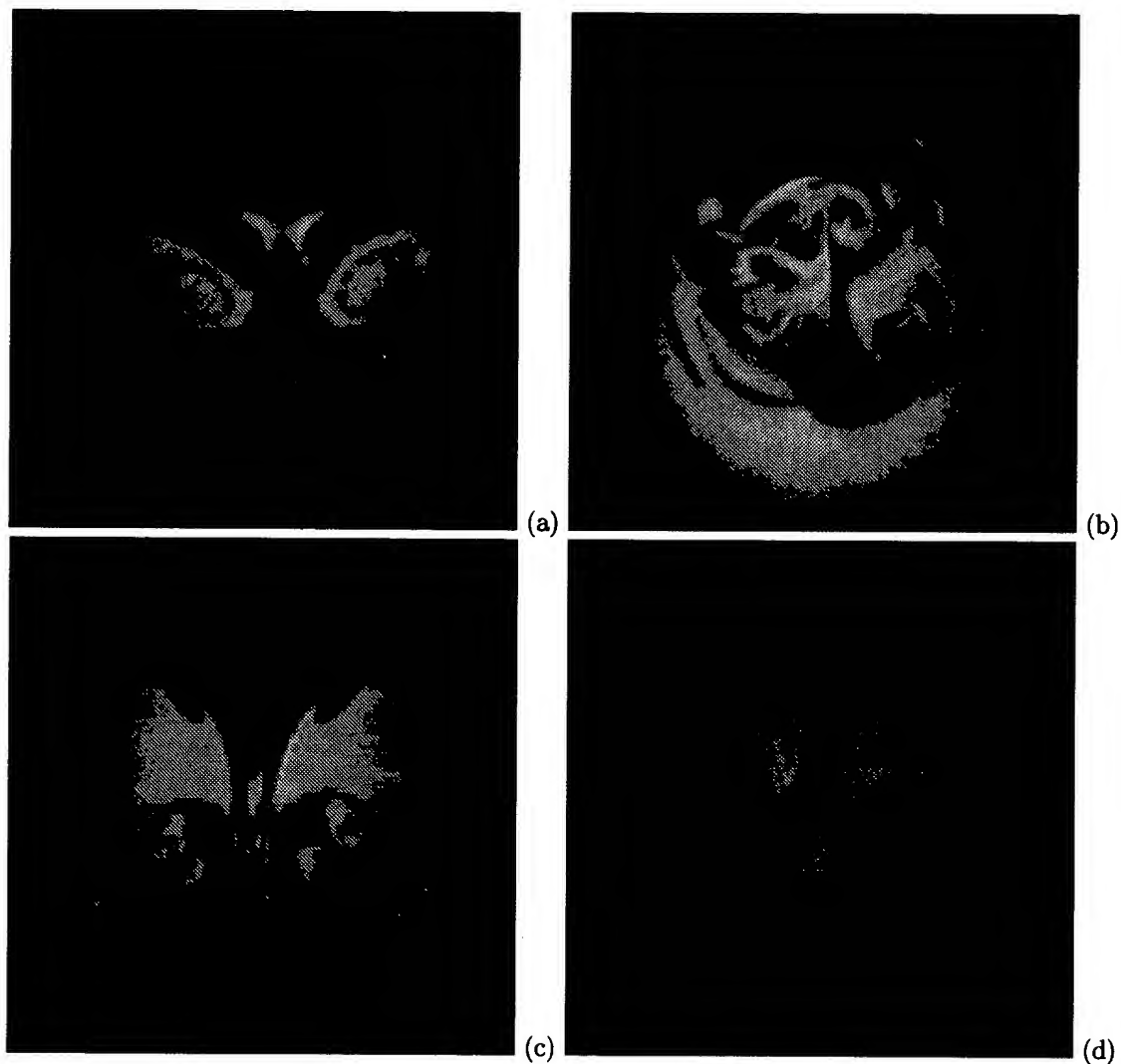


Figure 3: Four types of the streamwise vortices. (a) Forced Type A Vortices: $U_1 = 3$ cm/s, $U_2 = 1$ cm/s, $f_f = 6$ Hz, A_f is about 3.5% at $x/D = 1$; (b) Forced Type B Vortices: $U_1 = 9$ cm/s, $U_2 = 6$ cm/s, $f_f = 2.6$ Hz, A_f is about 8% at $x/D = 4$; (c) Forced Type C Vortices: $U_1 = 3$ cm/s, $U_2 = 1$ cm/s, $f_f = 6$ Hz, A_f is about 3.5% at $x/D = 4$; (d) Forced Type D Vortices: $U_1 = 4$ cm/s, $U_2 = 1$ cm/s, $f_f = 6$ Hz, A_f is about 5% at $x/D = 7$.

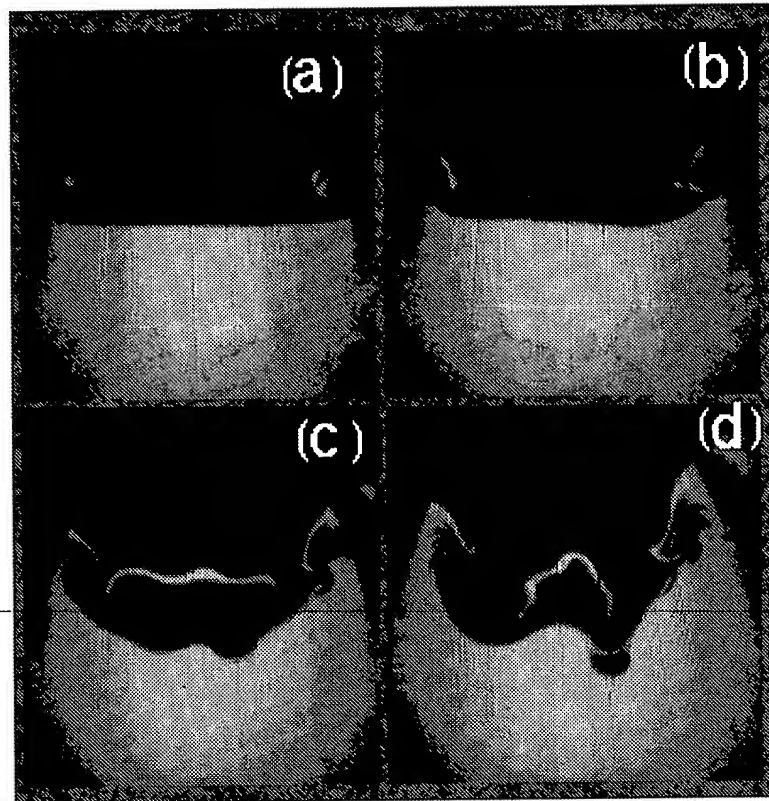


Figure 4: Evolution of the streamwise Type A Vortices along streamwise positions in a mixing layer without forcing. $U_1 = 9$ cm/s, $U_2 = 6$ cm/s. (a) $x/D = 0.2$; (b) 1; (c) 2; (d) 4.

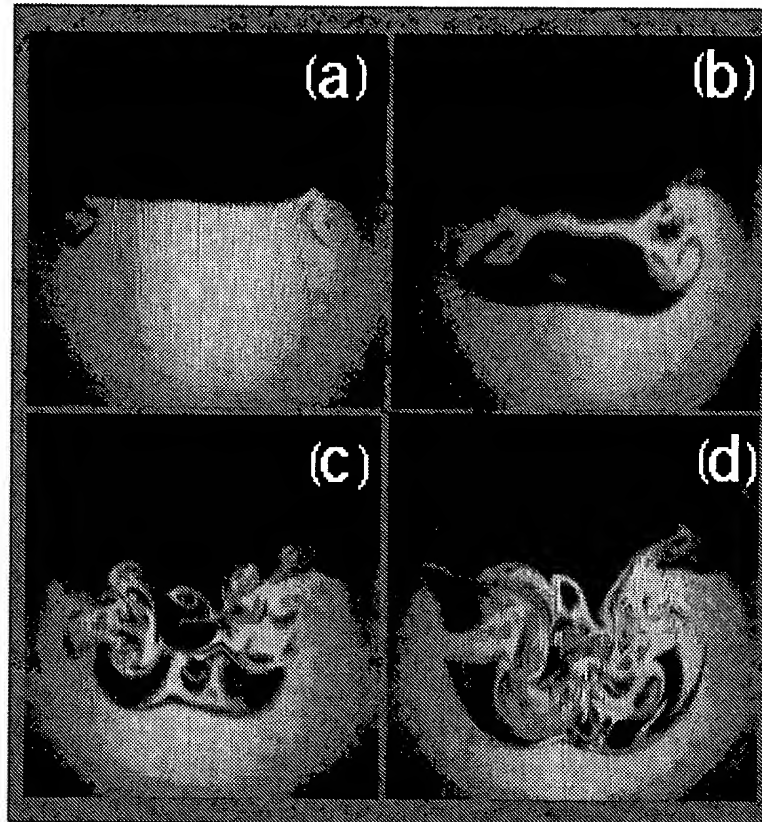


Figure 5: Evolution of the streamwise Type A Vortices in a mixing layer with forcing. $U_1 = 9$ cm/s, $U_2 = 6$ cm/s, $f = 5.6$ Hz, A_f is around 6%. (a) $x/D = 0.2$; (b) 1; (c) 2; (d) 4.

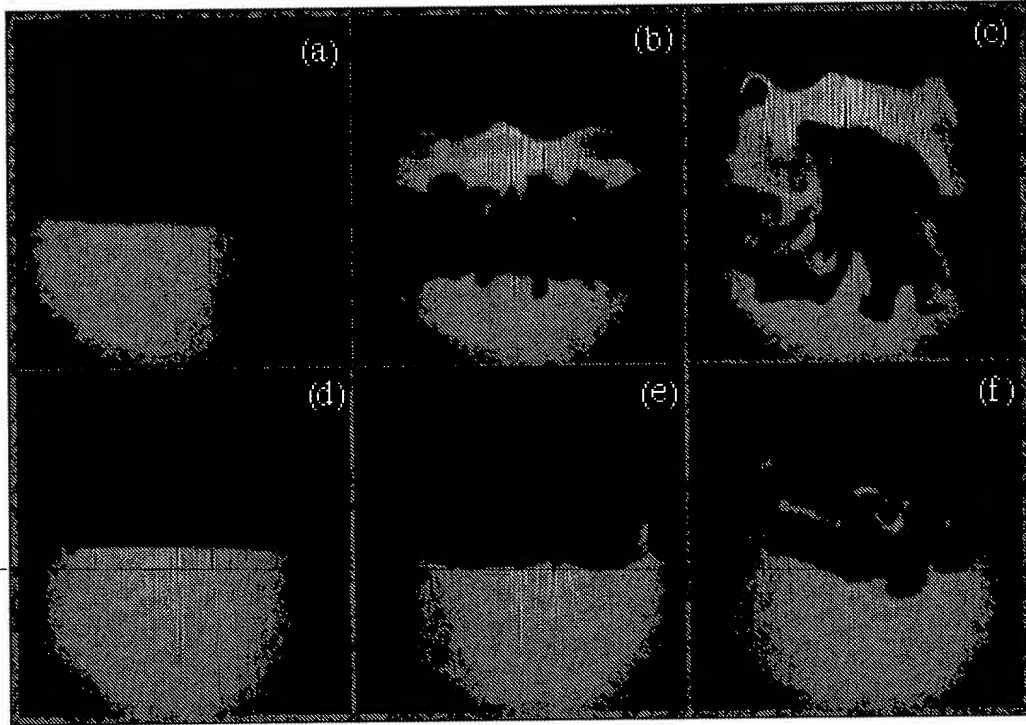


Figure 6: Comparison for different receptivity mechanism through streamwise vortices with $U_1 = 30$ cm/s, $U_2 = 20$ cm/s and $A_f = 7\%$. $f_f = 6$ Hz for (a) $x/D = 0.2$; (b) 1; (c) 2. $f_f = 16$ Hz for (d) $x/D = 0.2$; (e) 1; (f) 2.

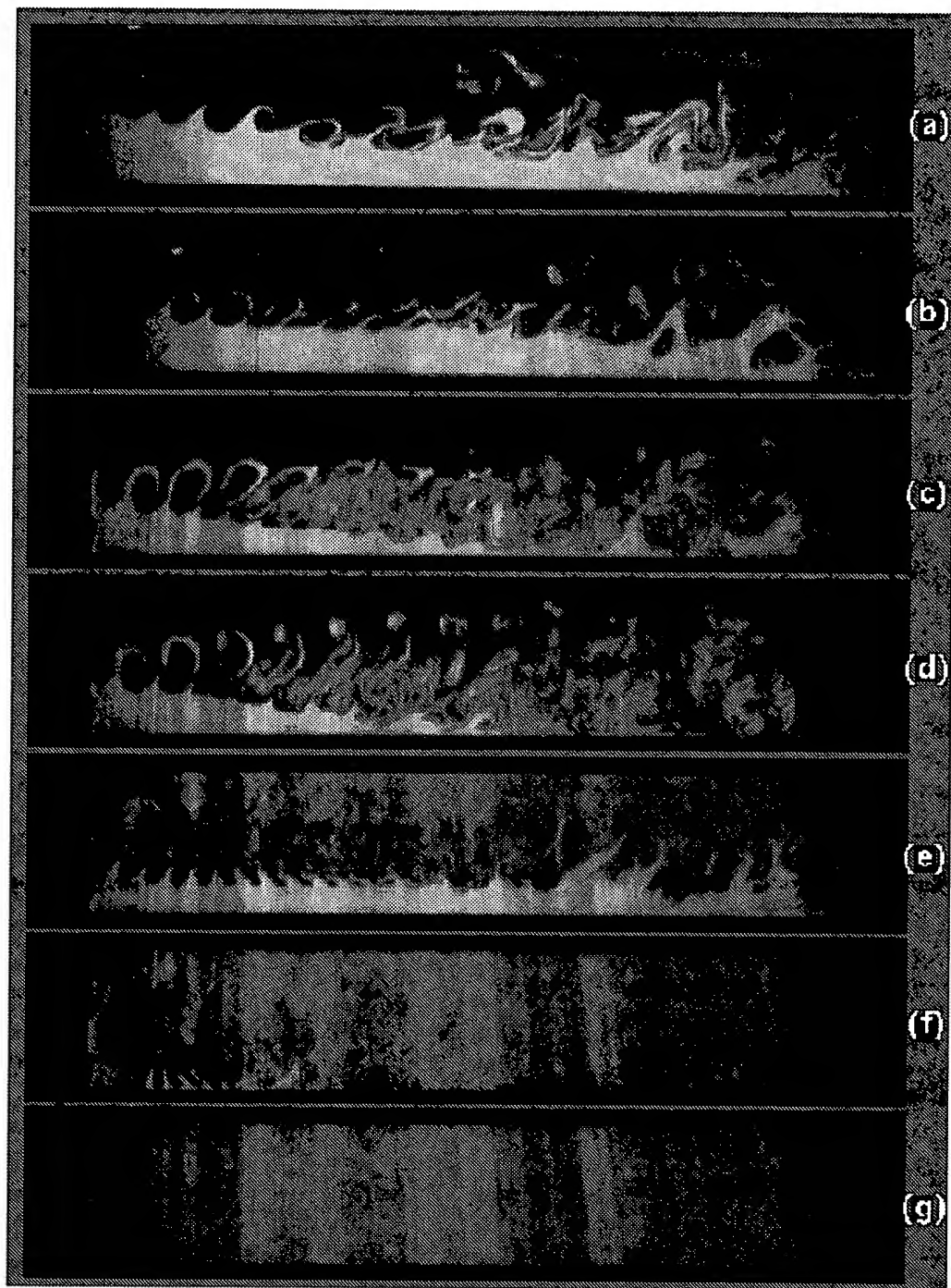


Figure 7: Influence of A_f under $f_f = 5.6$ Hz for a mixing layer of $U_1 = 10$ cm/s and $U_2 = 5$ cm/s. (a) $A_f = 0$ (unforced case); (b) 1.5%; (c) 5%; (d) 8%; (e) 18%; (f) 32%. (g) 52%.

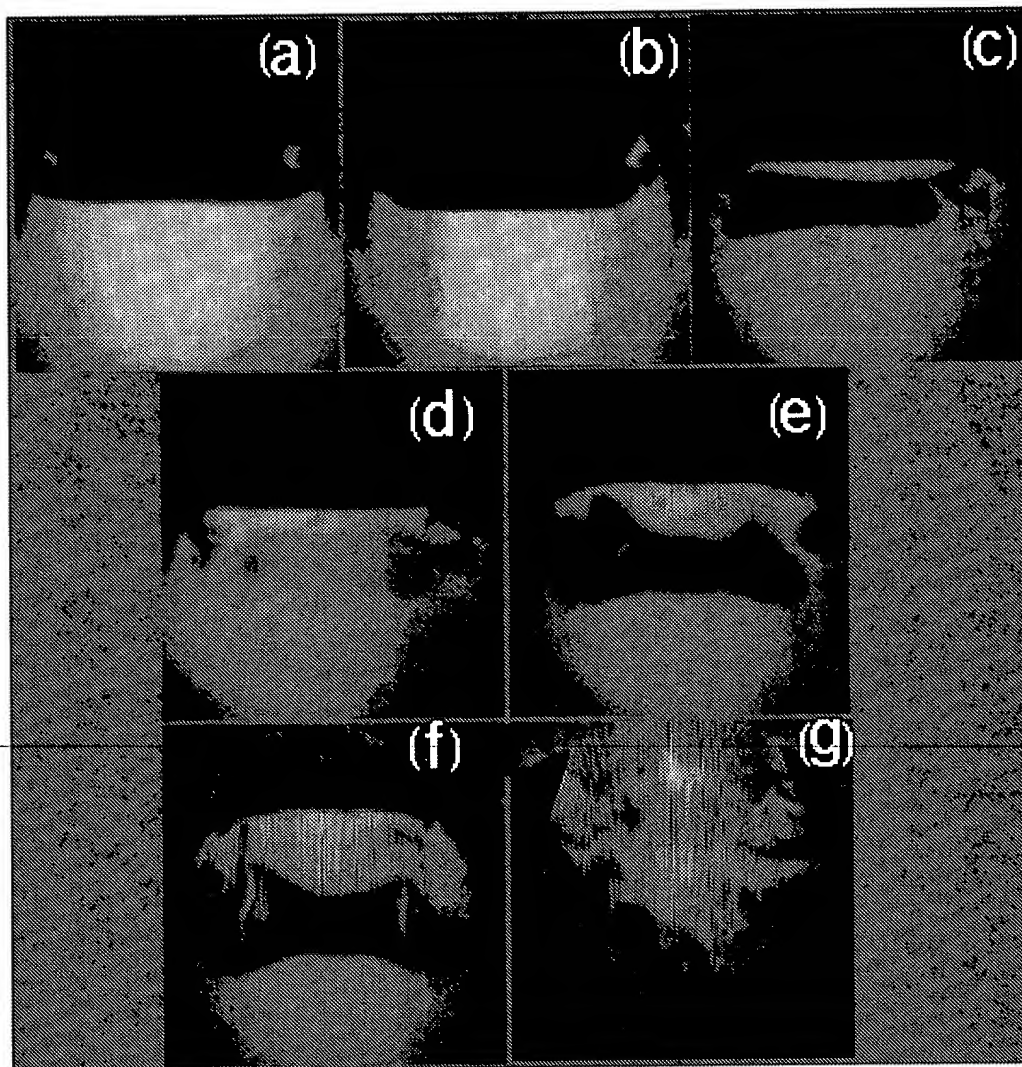


Figure 8: Streamwise vortices at $x/D = 0.2$ with forcing for different A_f in a mixing layer of $U_1 = 10$ cm/s, $U_2 = 5$ cm/s at $f_f = 5.6$ Hz. (a) $A_f = 0$ (unforced case); (b) 1.5%; (c) 5%; (d) 8%; (e) 18%; (f) 32%. (g) 52%.

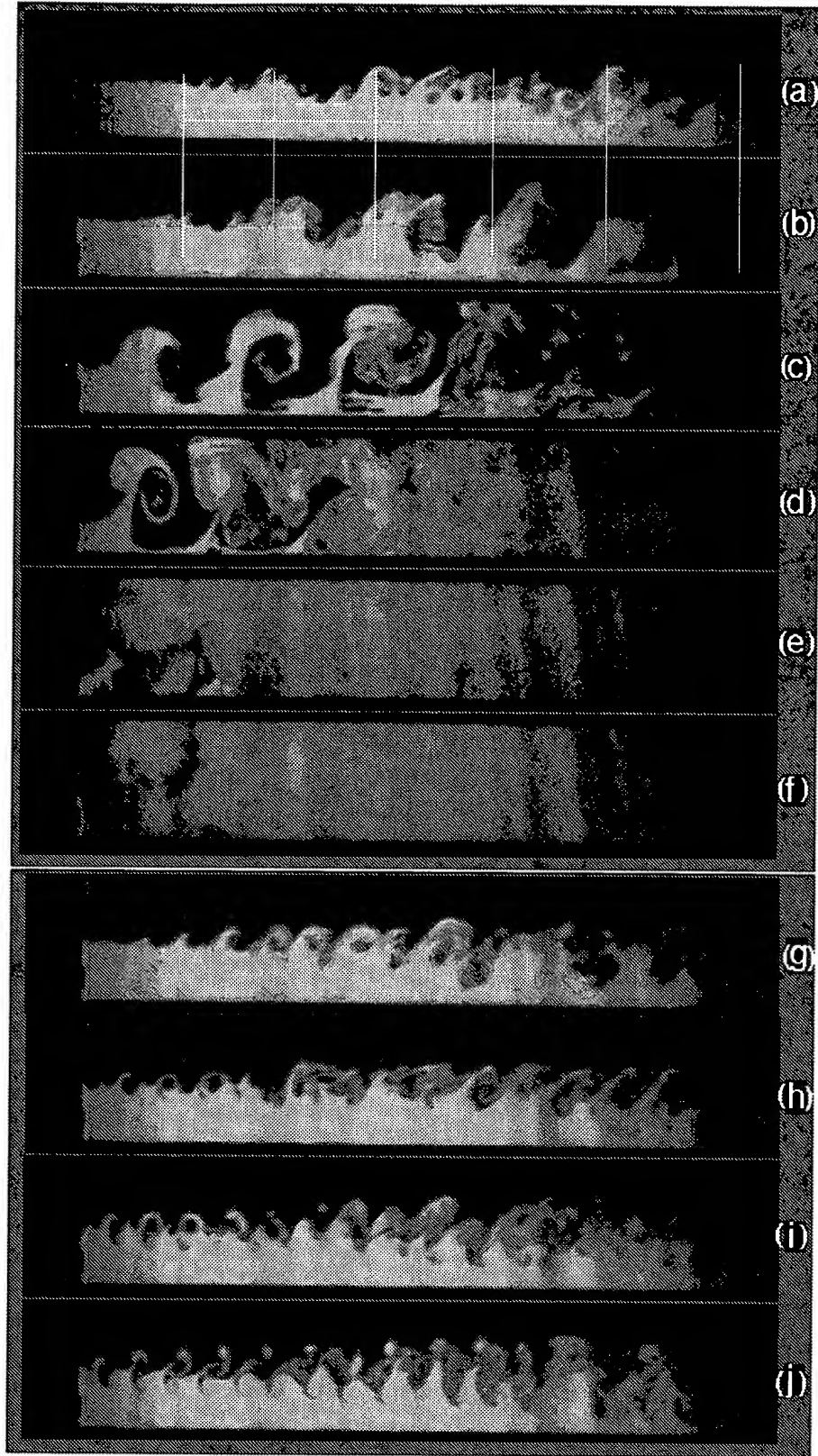


Figure 9: Comparison of the influence of different forcing mechanisms on a mixing layer with $U_1 = 30$ cm/s and $U_2 = 20$ cm/s. $f_f = 6$ Hz (new instability): (a) $A_f = 0$ (unforced case); (b) 1.5%; (c) 7.0%; (d) 16%; (e) 40%; (f) 50%. $f_f = 16$ Hz (mode II of conventional Kelvin-Helmholtz instability): (g) A_f 7.0%; (h) 16%; (i) 40%; (j) 50%.

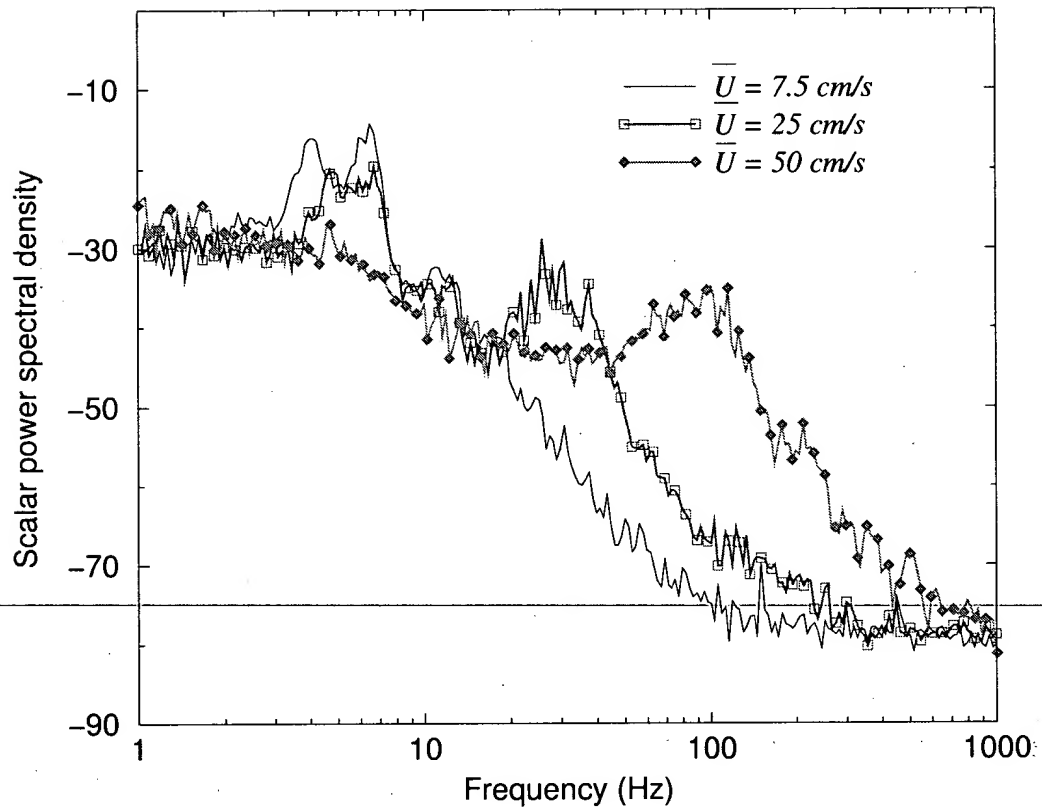


Figure 10: Scalar power spectrum in unforced mixing layers with various \bar{U} for a constant $\lambda = 0.2$.

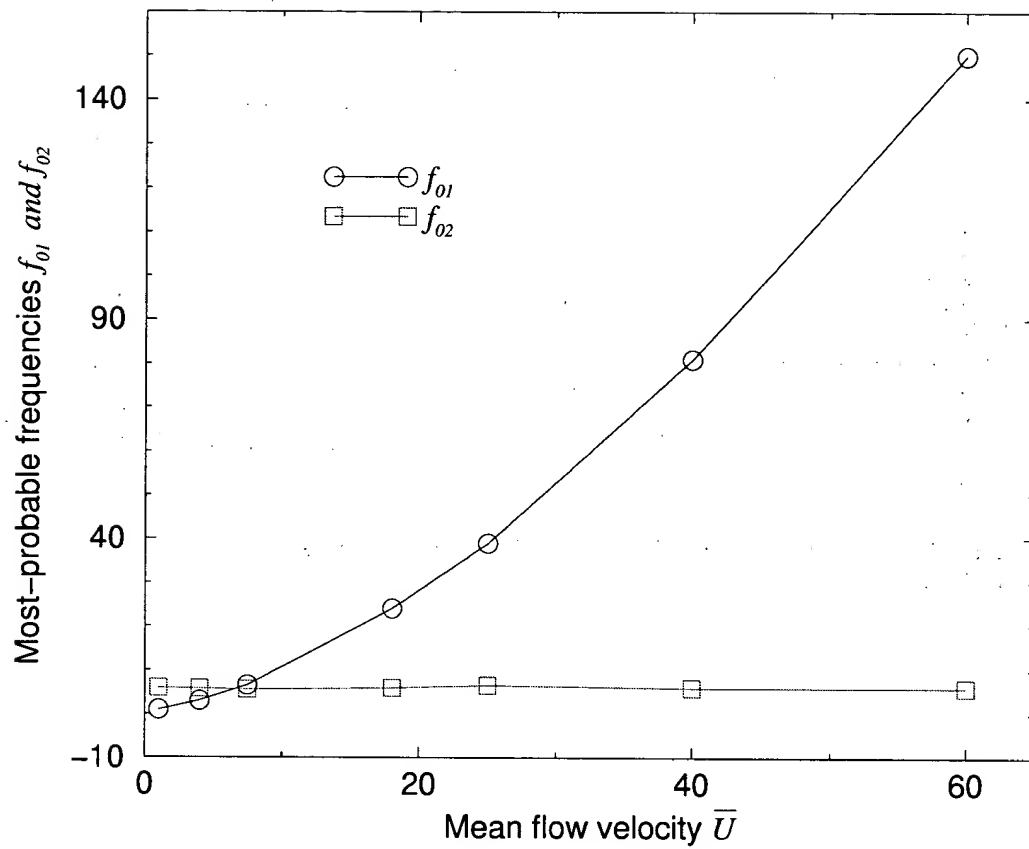


Figure 11: Relationship of f_{01} , f_{02} to \bar{U} for a constant $\lambda = 0.33$.

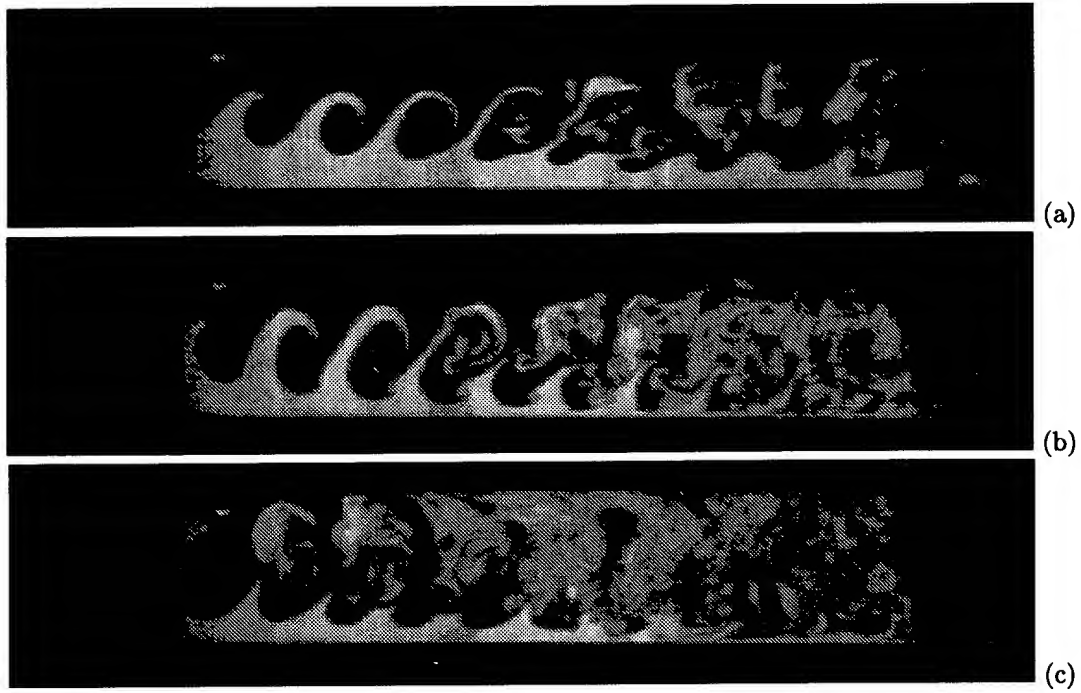


Figure 12: Forcing at lower Re_{θ_0} where $f_f = 3.2$ Hz, $U_1 = 9$ cm/s and $U_2 = 6$ cm/s with different A_f . (a) $A_f = 7\%$; (b) 16% ; (c) 52% .

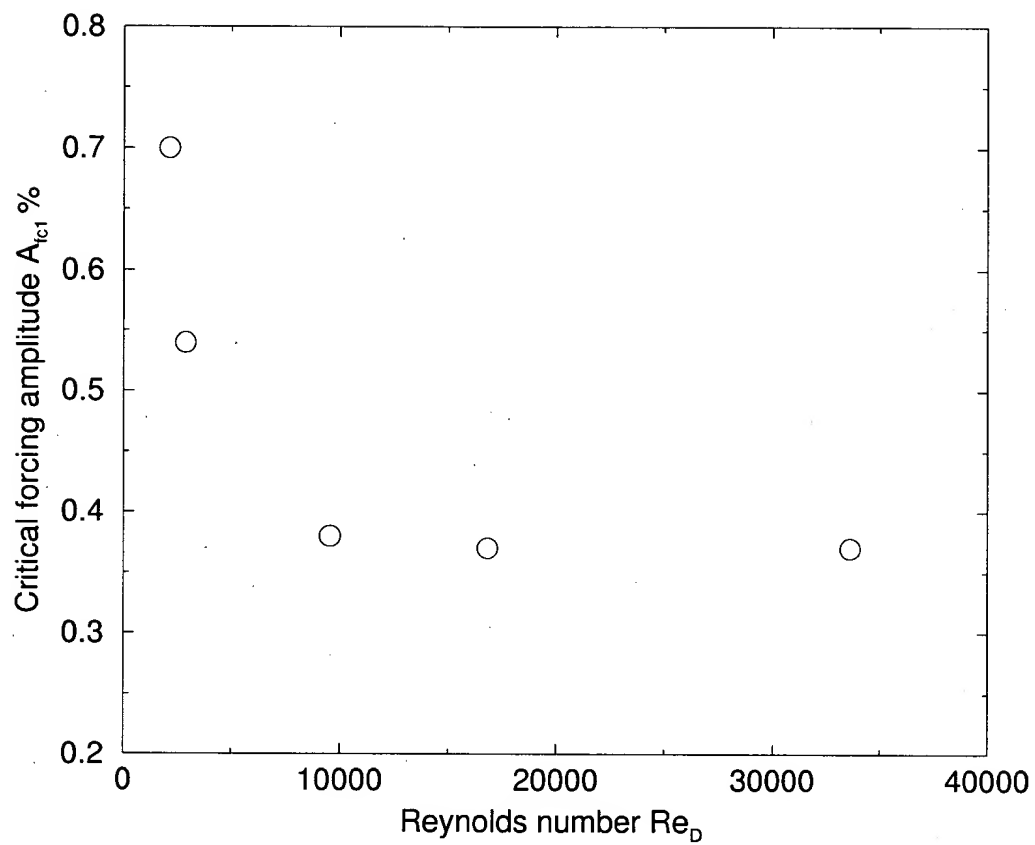


Figure 13: Critical forcing amplitude A_f needed to change the spreading rate of the mixing layer at $f_f = 6$ Hz and $\lambda = 0.5$.

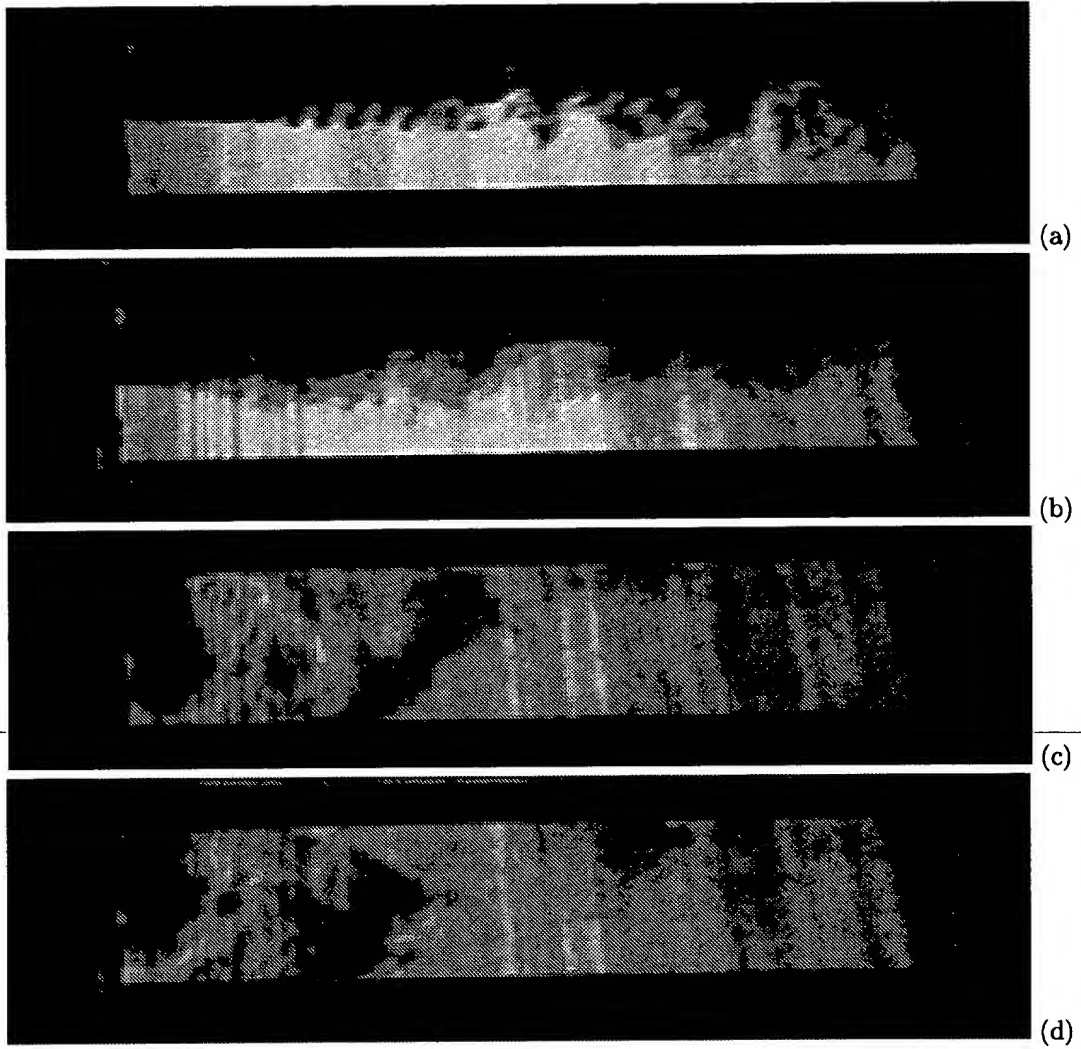


Figure 14: Comparison of λ influence with and without forcing. (a) $U_1 = 48$ cm/s, $\lambda = 0.2$, $A_f = 0$; (b) $U_1 = 60$ cm/s, $\lambda = 0.5$, $A_f = 0$; (c) $U_1 = 48$ cm/s, $\lambda = 0.2$, $A_f = 20\%$; (d) $U_1 = 60$ cm/s, $\lambda = 0.5$, $A_f = 20\%$.

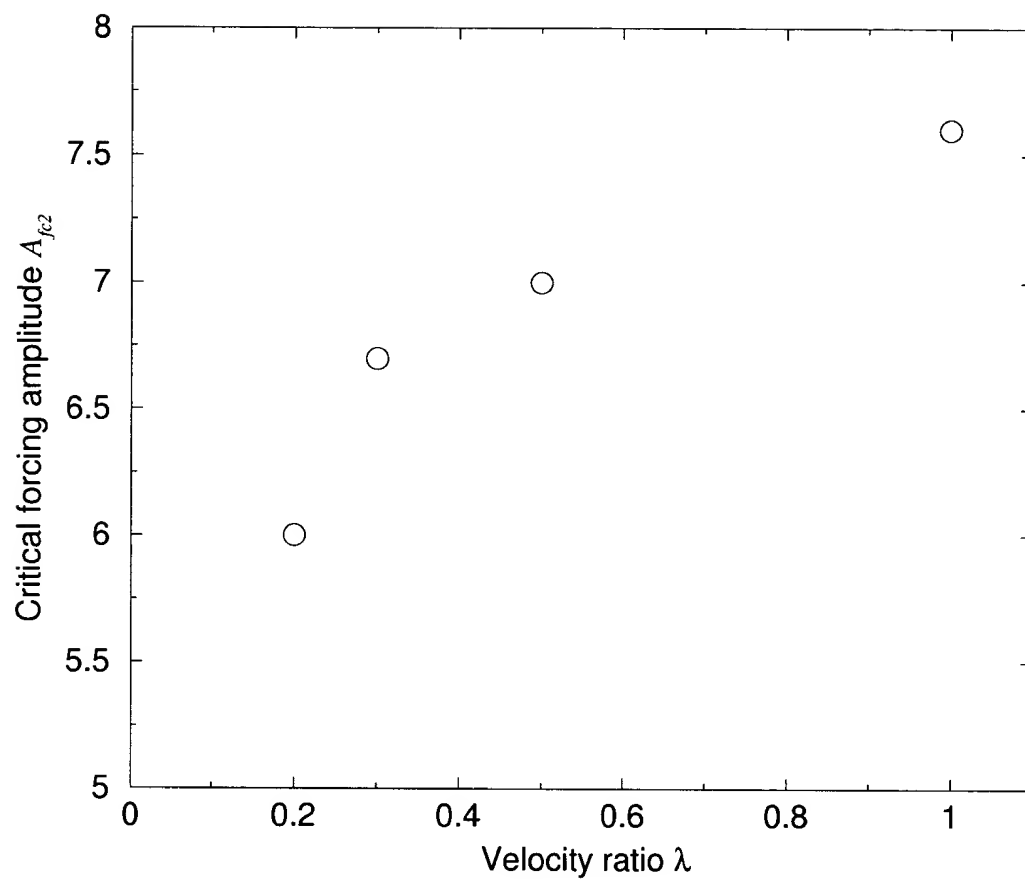


Figure 15: Critical forcing amplitude A_{fc2} required to cause asymmetric counter-rotating vortex pair increases with λ for $Re_D = 3150$.

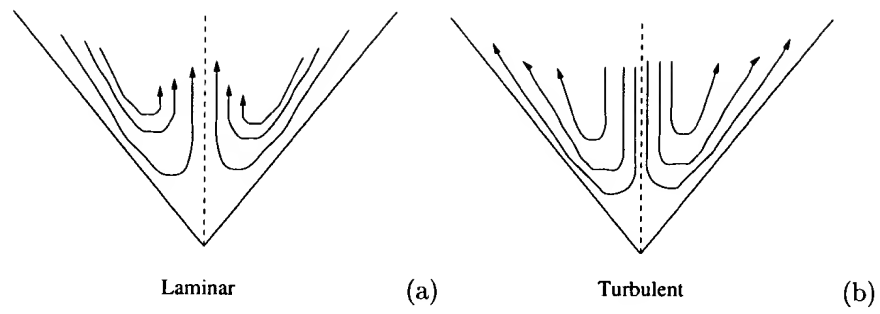


Figure 16: Model of the secondary flow along the streamwise corner.

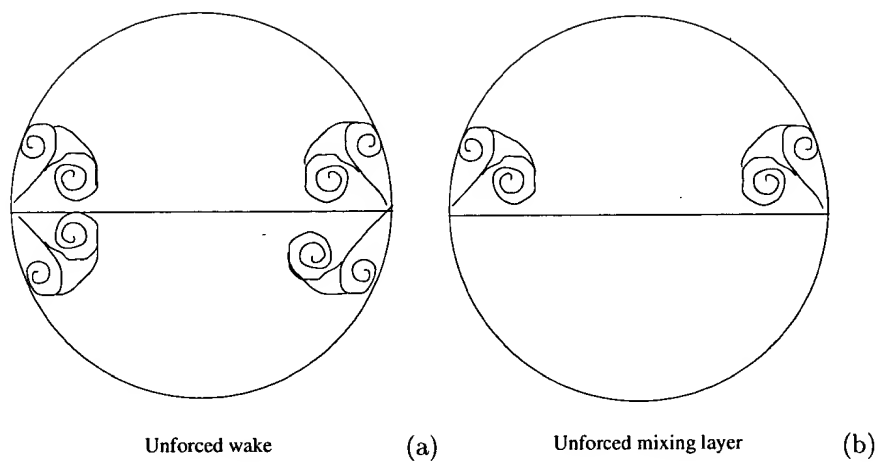


Figure 17: Model of the streamwise Type A vortices of the unforced flows downstream of the trailing edge.

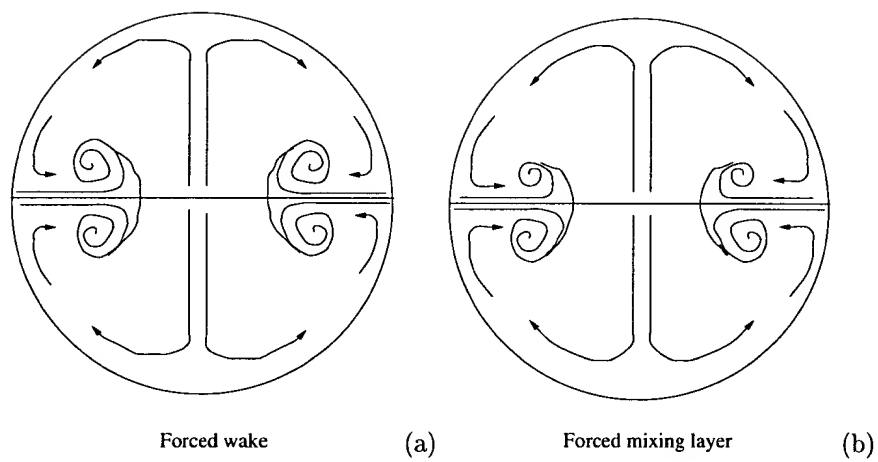


Figure 18: Model of the streamwise Type A vortices of the forced flows downstream of the trailing edge.

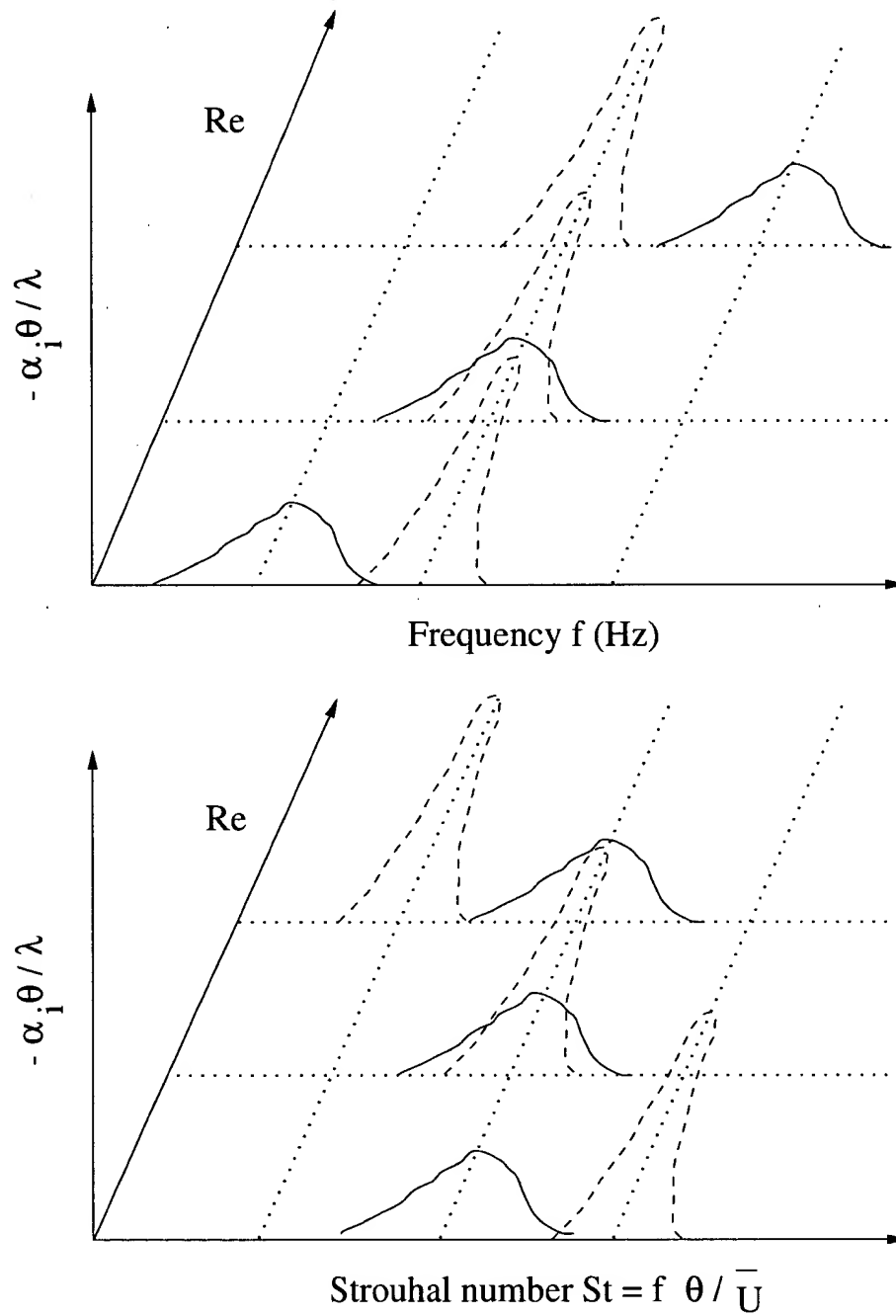


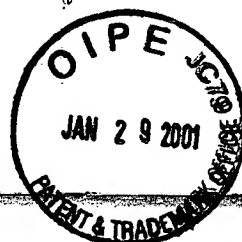
Figure 19: Sketch of qualitative amplification curves with Reynolds number Re . The solid curve represents Kelvin-Helmholtz instability and the dotted curve denotes the new instability.

List of Figures

1	Experimental schematic.	22
2	Influence of f_f for a mixing layer with $U_1 = 9$ cm/s and $U_2 = 6$ cm/s under a constant A_f of about 6.5%.	23
3	Four types of the streamwise vortices.	24
4	Evolution of the streamwise Type A Vortices along streamwise positions in a mixing layer without forcing.	25
5	Evolution of the streamwise Type A Vortices in a mixing layer with forcing.	26
6	Comparison for different receptivity mechanism through streamwise vortices.	27
7	Influence of A_f under $f_f = 5.6$ Hz for a mixing layer of $U_1 = 10$ cm/s and $U_2 = 5$ cm/s.	28
8	Streamwise vortices at $x/D = 0.2$ with forcing for different A_f in a mixing layer.	29
9	Comparison of the influence of different forcing mechanisms on a mixing layer with $U_1 = 30$ cm/s and $U_2 = 20$ cm/s.	30
10	Scalar power spectrum in unforced mixing layers with various \bar{U} for a constant $\lambda = 0.2$	31
11	Relationship of f_{01} , f_{02} to \bar{U} for a constant $\lambda = 0.33$	32
12	Forcing at lower Re_{θ_0} where $f_f = 3.2$ Hz, $U_1 = 9$ cm/s and $U_2 = 6$ cm/s with different A_f	33
13	Critical forcing amplitude A_f needed to change the spreading rate of the mixing layer at $f_f = 6$ Hz and $\lambda = 0.5$	34
14	Comparison of λ influence with and without forcing.	35
15	Critical forcing amplitude A_{fc2} required to cause asymmetric counter-rotating vortex pair increases with λ for $Re_D = 3150$	36
16	Model of the secondary flow along the streamwise corner.	37
17	Model of the streamwise Type A vortices of the unforced flows downstream of the trailing edge.	38
18	Model of the streamwise Type A vortices of the forced flows downstream of the trailing edge.	39
19	Sketch of qualitative amplification curves with Reynolds number Re	40

REFERENCES

- ADAMSON, T. C. 1960 *Phys. Fluids* **3**, 706.
 BIRKAN, M. & KASSOY, D. R. 1983 *Combust. Sci. Tech.* **33**, 125.
 BOWEN, J. R. 1967 *Phys. Fluids* **10**, 290.
 BRADLEY, J. N. 1962 *Shock Waves in Chemistry and Physics*. Methuen.
 BUCKMASTER, J. D. & LUDFORD, G. S. S. 1982 *Theory of Laminar Flames*. Cambridge University Press.
 BUSH, W. B. & FENDELL, F. E. 1970 *Combust. Sci. Tech.* **1**, 421.
 BUSH, W. B. & FENDELL, F. E. 1971 *Combust. Sci. Tech.* **2**, 271.
 CARRIER, G. F., FENDELL, F. E. & BUSH, W. B. 1978 *Combust. Sci. Tech.* **18**, 33.
 CLARKE, J. F. 1983a *Combust. Flame* **50**, 125.
 CLARKE, J. F. 1983b *J. Fluid Mech.* **136**, 139.
 CLARKE, J. F. & MCINTOSH, A. C. 1980 *Proc. R. Soc. Lond. A* **372**, 367.
 COUTANT, R. & FRIEDRICH, K. O. 1948 *Supersonic Flow and Shock Waves*. Interscience.
 CURTISS, C. F., HIRSCHFELDER, J. O. & BARNETT, M. P. 1959 *J. Chem. Phys.* **30**, 470.
 DUFF, R. E. 1978 *J. Chem. Phys.* **28**, 1193.
 ERPENBECK, J. J. 1962a *Phys. Fluids* **5**, 604.
 ERPENBECK, J. J. 1962b *Phys. Fluids* **5**, 1181.
 ERPENBECK, J. J. 1963 *In Proc. 9th Symp. (Intl) on Combustion*, p. 442. The Combustion Institute.
 ERPENBECK, J. J. 1964 *Phys. Fluids* **7**, 684.
 ERPENBECK, J. J. 1967 *Phys. Fluids* **10**, 274.
 ERPENBECK, J. J. 1970 *Phys. Fluids* **13**, 2007.
 FICKETT, W. & DAVIS, W. C. 1979 *Detonation*. University of California Press.
 HIRSCHFELDER, J. O. & CURTISS, C. F. 1949 *J. Chem. Phys.* **17**, 1076.
 HIRSCHFELDER, J. O. & CURTISS, C. F. 1958 *J. Chem. Phys.* **28**, 1130.
 JOHNSON, W. E. 1963 *Arch. Rat. Mech. Anal.* **13**, 46.
 KAPILA, A. K., MATROWSKY, B. J. & VAN HARTEN, A. 1983 *SIAM J. Appl. Maths* **43**, 491.
 KÁRMÁN, T. VON & MILLÁN, G. 1953 *In Anniversary Volume on Applied Mechanics Dedicated to C. B. Biot*, p. 58. Haarlem, N. V. de Technische Uitgeverij H. Stan.
 KASSOY, D. R. 1975 *Q. J. Mech. Appl. Maths* **28**, 63.
 KASSOY, D. R. 1977 *Q. J. Mech. Appl. Maths* **30**, 71.
 KOUMOUTSOS, N. G. & KOVITZ, A. A. 1963 *Phys. Fluids* **6**, 1007.
 LANDAU, L. D. & LIFSHITZ, E. M. 1959 *Fluid Mechanics*. Pergamon.
 LINDER, R., CURTISS, C. F. & HIRSCHFELDER, J. O. 1958 *J. Chem. Phys.* **28**, 1147.
 LU, G. C. & LUDFORD, G. S. S. 1982 *SIAM J. Appl. Maths* **42**, 625.
 NICHOLLS, J. A. 1963 *In Proc. 9th Symp. (Intl) on Combustion*, p. 488. The Combustion Institute.
 SEMENOV, N. N. 1928 *Z. Phys.* **48**, 571.
 SHAPIRO, A. 1964 *The Dynamics and Thermodynamics of Compressible Fluids Flow*, vol. 1. Ronald.
 STEWART, D. S. & LUDFORD, G. S. S. 1983 *J. Mec.* **3**, 463.
 TAVER, C. M. 1982 *Combust. Flame* **46**, 111.
 WILLIAMS, F. A. 1965 *Combustion Theory*. Addison Wesley.
 WOOD, W. W. 1961 *Phys. Fluids* **4**, 46.
 WOOD, W. W. & SALISBURY, Z. W. 1960 *Phys. Fluids* **3**, 549.



The plane turbulent shear layer with periodic excitation

By H. E. FIEDLER AND P. MENSING†

Herman-Föttinger-Institut für Thermo- und Fluidodynamik, Technische Universität Berlin

(Received 10 December 1982 and in revised form 17 May 1984)

The influence of periodic excitation on a plane turbulent one-stream shear layer with turbulent separation was investigated. For the qualitative study flow visualization was employed. Quantitative data were obtained with hot-wire anemometry and spectrum analysis. It was found that sinusoidal perturbations with frequencies of order $f_0 \leq u_0/100\delta_0$ (depending on excitation strength), introduced at the trailing edge are always amplified. Maximum amplification factors are observed for the lowest perturbation levels. The frequency and amplitude of excitation determine the downstream location of the amplification maximum in the flow. At sufficient amplitude two-dimensional vortices are formed which subsequently decay without pairing. The development of the periodic r.m.s. values along x follows a universal curve for all frequencies and amplitudes when properly normalized.

At high excitation amplitudes the flow development depends strongly on the geometrical conditions of the excitation arrangement at the trailing edge. Thus regular vortex pairing as well as suppression of pairing can be achieved.

The excited shear layer has considerably stronger, yet nonlinear, spread than the neutral. The region of vortex formation, irrespective of whether it includes pairing or not, is associated with a step-like increase in width, while after the position of maximum vortex energy, i.e. in the region of decay, the spread is reduced to values below the neutral. There the overall lateral fluctuation energy is increased, while the longitudinal may be decreased as compared with the neutral flow.

1. Introduction

Periodically excited free shear flows tend to roll up into discrete vortices whose shape and strength depend on the type of flow considered, its boundary conditions and the excitation amplitude. This phenomenon, first reported in the nineteenth century, is generally associated with laminar flow. Michalke (1971) showed that inviscid stability theory appears to be applicable also to turbulent flow. The concept of coherent structures, which emerged at about the same time, is essentially based on the inherent large-scale instability of the turbulent flow and the subsequent formation of discrete modules, the coherent structures, whose initiation and strength is, however, not yet fully assessed, even for such simple cases as the neutral shear layer.

In order to quantify the influence of defined periodic perturbations on a plane shear layer and at the same time obtain information about formation and characteristics of coherent structures under defined circumstances, the following investigation was undertaken. The results reported herein are largely based on the dissertation of the second author (Mensing 1981).

† Present address: Amt für Umweltschutz, Hamburg.

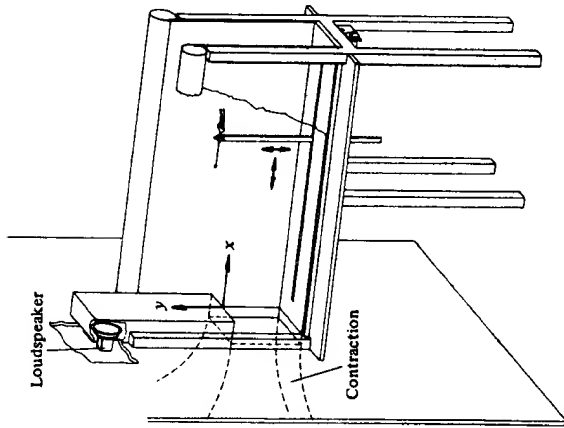


FIGURE 1. Test section and coordinate system.

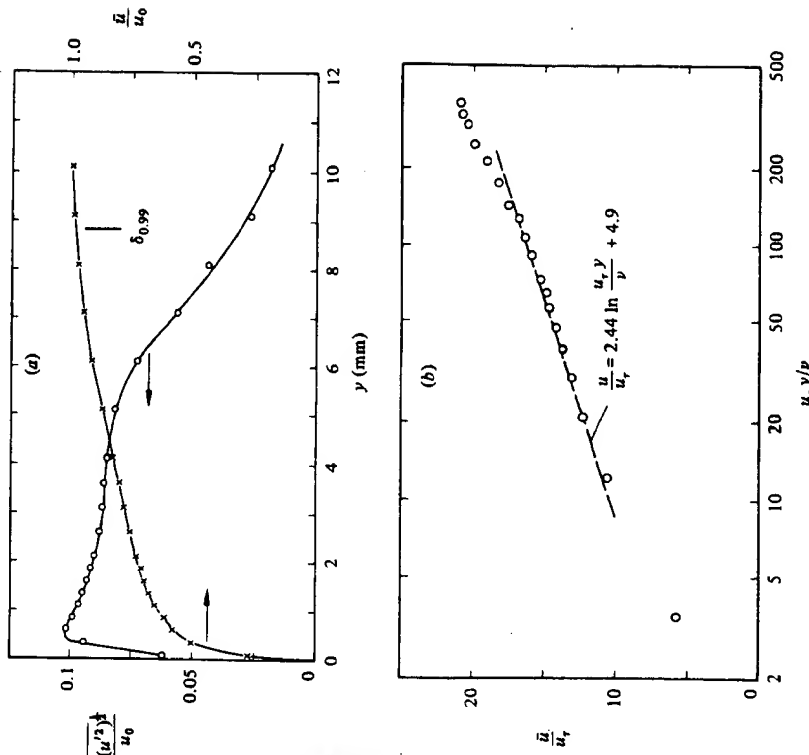
2. Experiments

2.1. General arrangement and initial conditions

This investigation was first started in a blowing facility. It was, however, found that the shear layer then investigated was to some extent disturbed by periodicities apparently caused by the blower as well as by the settling tube, acting as an organ pipe. This was surprising, since these perturbations were too weak to appear in the spectrum of the free-stream turbulence in the nozzle exit.

A new facility was then designed where a contraction with a cross-section of 300×300 mm at the exit is placed between two rooms, which are kept at different pressure levels. Upstream of the nozzle a basket-like foam-rubber screen is placed around the intake. The test section mounted at the nozzle exit has a length of 1260 mm. It is fitted with glass walls and rounded corners at the open upper side to ensure smooth entrainment flow. The turbulence level in the nozzle is $< 0.15\%$, with no single frequency in the spectrum discernible. Figure 1 shows the complete arrangement and the coordinate system used.

The separating boundary layer at the trailing edge was tripped 100 mm upstream of the trailing edge by a strip of coarse sandpaper of 40 mm width. Chosen according to Smith & Clutter (1957), it causes fast transition with no prevailing periodic constituent in the fluctuation spectrum. The boundary-layer profile at the trailing edge is shown in figures 2 (a, b). It corresponds essentially to a boundary-layer profile with slight adverse pressure gradient, having a momentum thickness of $\theta_0 = 1.14$ mm and a form parameter of $H = 1.46$ (see also Hussain & Zedan 1978a, b). According to Bradshaw's (1966) criterion, most of the flow in the test section may not be considered fully self-preserving. Newer evidence suggests, however, a shorter length for the structural development of the flow, so that approximately the second half of

FIGURE 2. (a) Mean-velocity and u' distributions of separating turbulent boundary layer. (b) Logarithmic plot of separating boundary layer.

the shear layer will essentially be self-preserving. For the excited flow this limit is, however, of little relevance. There the thickness of the separating boundary layer is primarily important in providing an upper bound for the excitation frequencies (see §3.2.3).

All measurements reported were done with DFVLR hot-wire equipment. Spectra were obtained with a Hewlett-Packard 3582A analyser.

2.2. Experimental conditions

In discussing free-shear-layer flow we refer to three conditions: neutral flow, disturbed flow and excited flow. A neutral condition is assumed when in no position in the flow are isolated spectral peaks found. Disturbed flow denotes the case where no periodic constituent is observed in the free-stream turbulence in the beginning of the test section, yet isolated spectral peaks of constant, i.e. x -independent, frequency develop downstream (facility forcing). Finally, excited flow describes the situation where periodic disturbances of defined frequency and amplitude are imposed on the

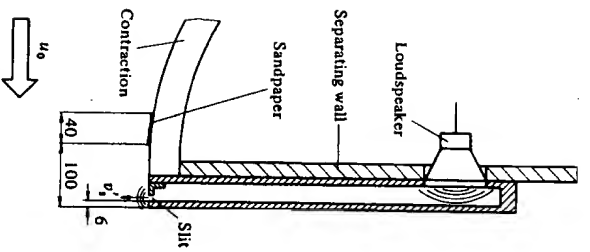


Figure 3. Loudspeaker arrangement at trailing edge (see also figures 8 and 9).

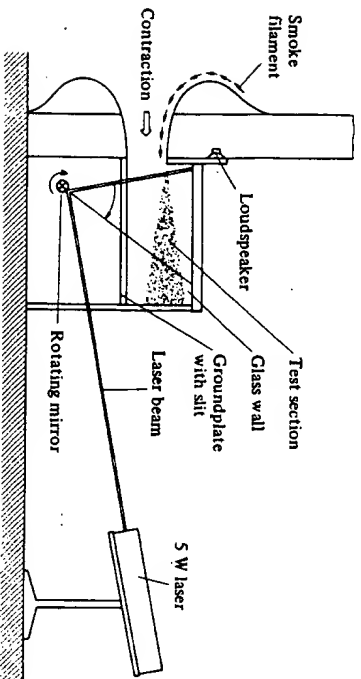


Figure 4. Flow-visualization arrangement.

flow, in particular at the trailing edge. Regarding the flow behaviour, there is only a quantitative distinction between the latter two conditions. The basic requirement for an investigation of excited flow must, however, be the neutral condition, since otherwise mixed conditions in phase or frequency may occur. In the present test arrangement, standing waves in the test room were observed at certain blower speeds, causing a flow disturbance. Perfectly neutral flow was found only for $u_0 = 11$ m/s. All measurements were carried out at this velocity. It corresponds to a Reynolds number $Re_x = xu_0/\nu = x \times 7.3 \times 10^3$ (x in cm).

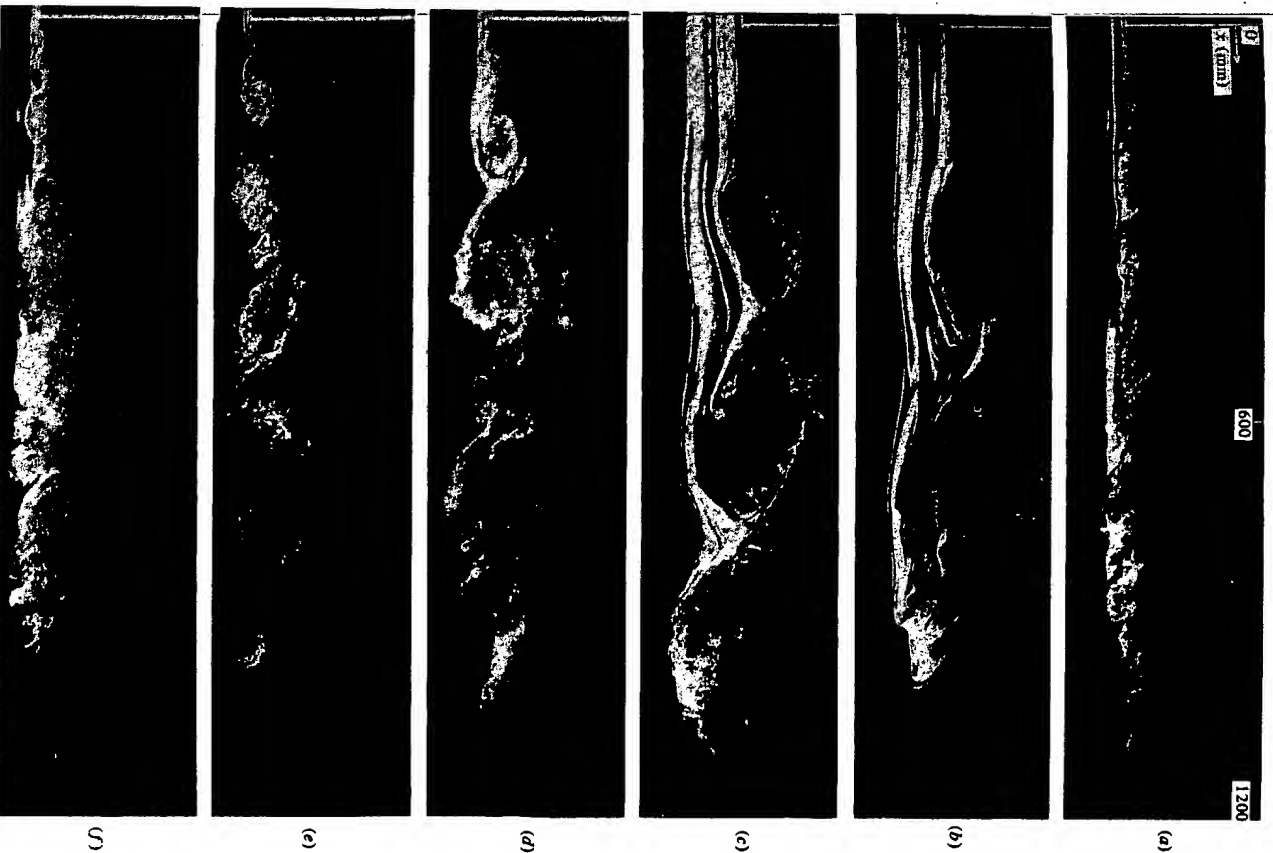
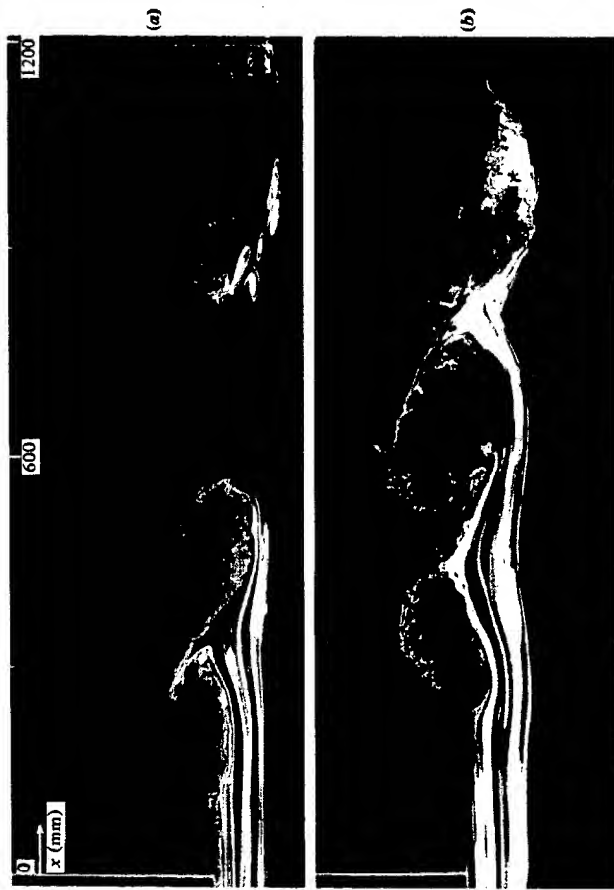


Figure 5. Vortex development for various excitation frequencies and $(u_{p0})'/u_0 = 0.0065$: (a) 0 Hz (neutral case); (b) 20 Hz; (c) 30 Hz; (d) 40 Hz; (e) 50 Hz; (f) 60 Hz; (g) 110 Hz.

FIGURE 6. Vortex formation and entrainment ($U_0 = 30$ Hz).

2.3. Flow excitation

Of the many possible ways to introduce defined periodic perturbations into the flow, some of which were discussed by Korschelt (1980), excitation by loudspeaker was chosen, the arrangement of which is sketched in figure 3. The particle velocity v_g in the slit, caused by the pumping action of the speaker, modulates the separating boundary layer. This technique is probably the most simple one, allowing easily for a large and repeatable range of amplitude and frequency, while being perfectly two-dimensional. For studies of the flow immediately downstream of the trailing edge it must, however, be considered with caution, since in addition to deflecting the boundary layer it also introduces a pulsating mass flow.

2.4. Visualization

The method employed in this study, described in detail by Mensing & Fiedler (1980), utilizes a focused laser beam of 5 W, which is scanned through the test section by a rotating mirror. For a typical time $\Delta t = 0.01$ s for the laser beam to sweep the test section of length L , a beam width of, say, 3 mm and a flow velocity of 11 m/s, an individual smoke particle travels approximately 0.3 mm during its illuminated time. The camera, whose shutter speed may be $\frac{1}{30}$ s, is triggered by a photocell. In this way sharp pictures of the flow structure down to its smallest elements are obtained. The overall flow image, however, appears compressed or expanded, depending on the sweep direction, by some 5%. Figure 4 shows the arrangement.

Flow photographs were taken in a neutral shear layer, a weakly excited flow and a flow with strong excitation. They are shown on figures 5–10. Before discussing the

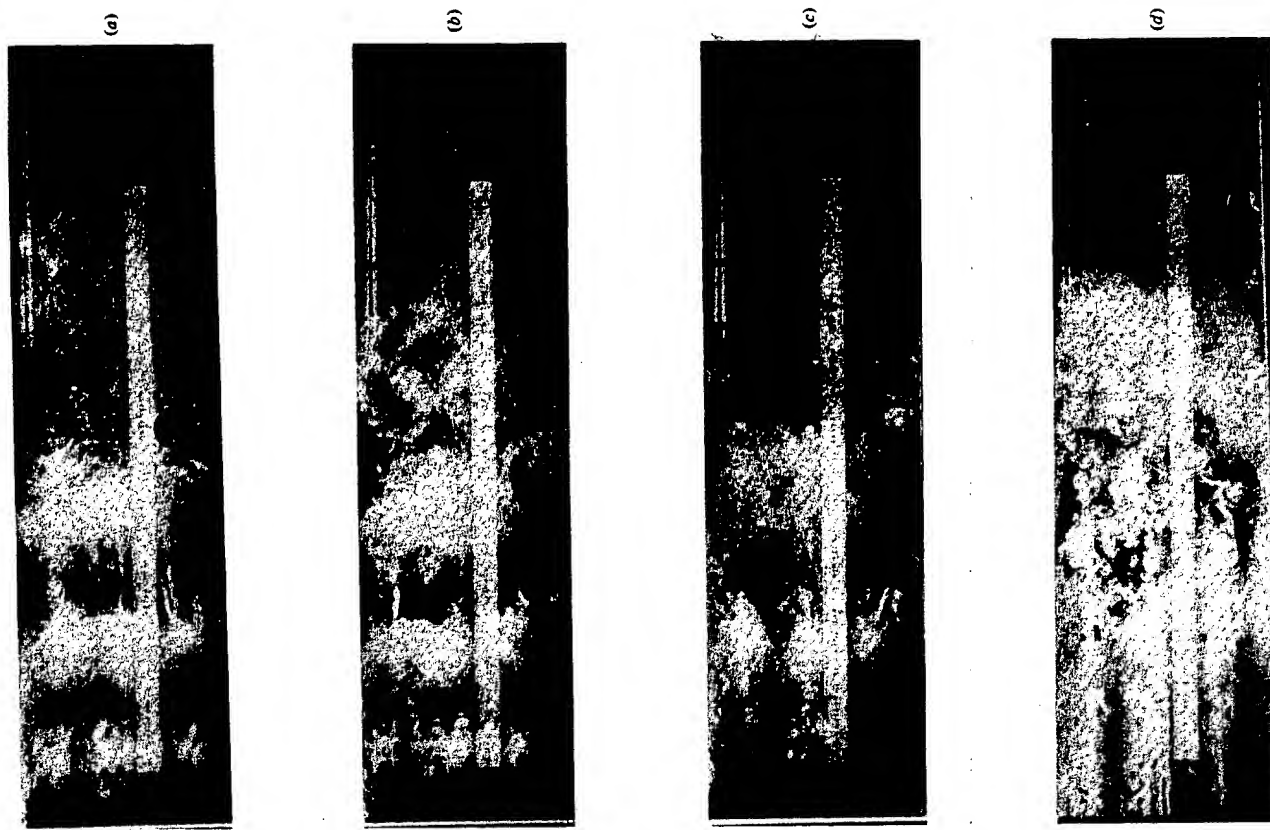


FIGURE 7. Two-dimensionality of excited structures: (a) 30 Hz; (b) 30 Hz; (c) 20 Hz; (d) 15 Hz.

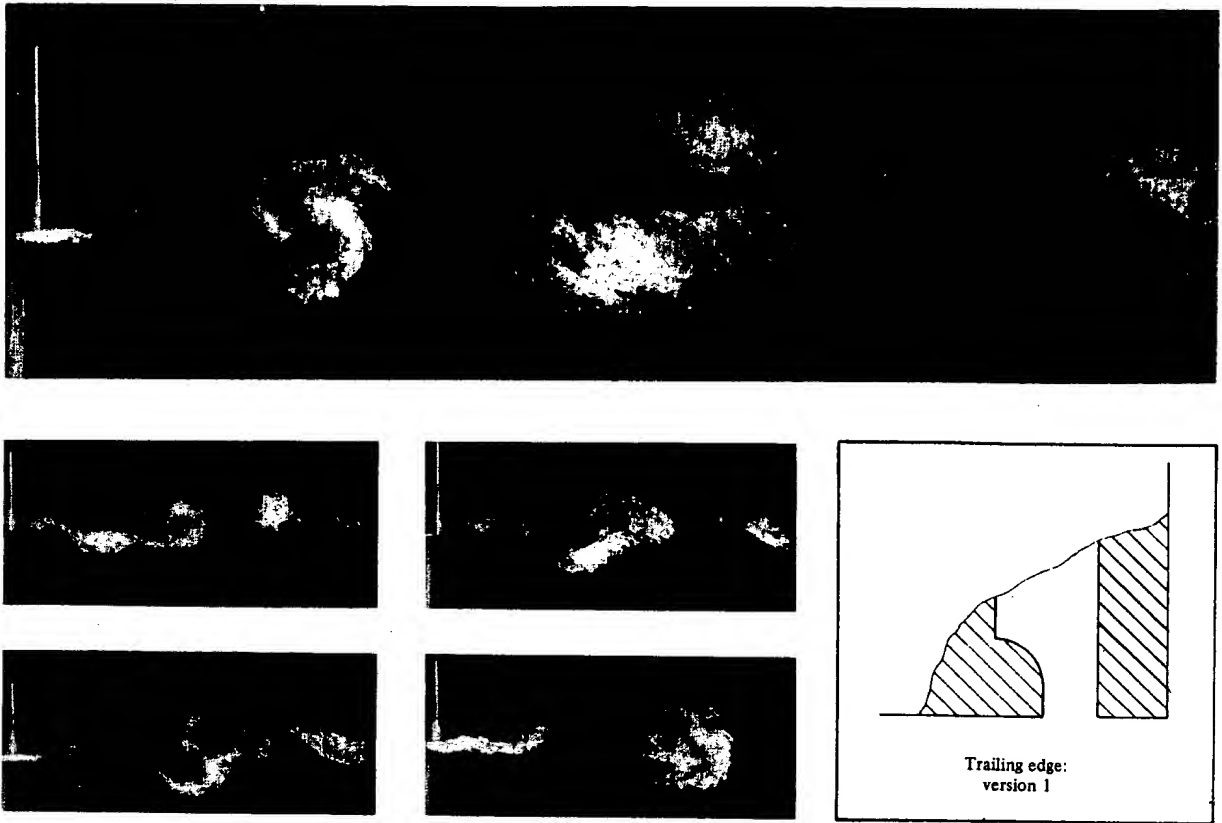


FIGURE 8. Overall flow development with pairing and enlarged sequences of flow near trailing edge with preceding pairing: strong excitation with disturbed separation conditions.

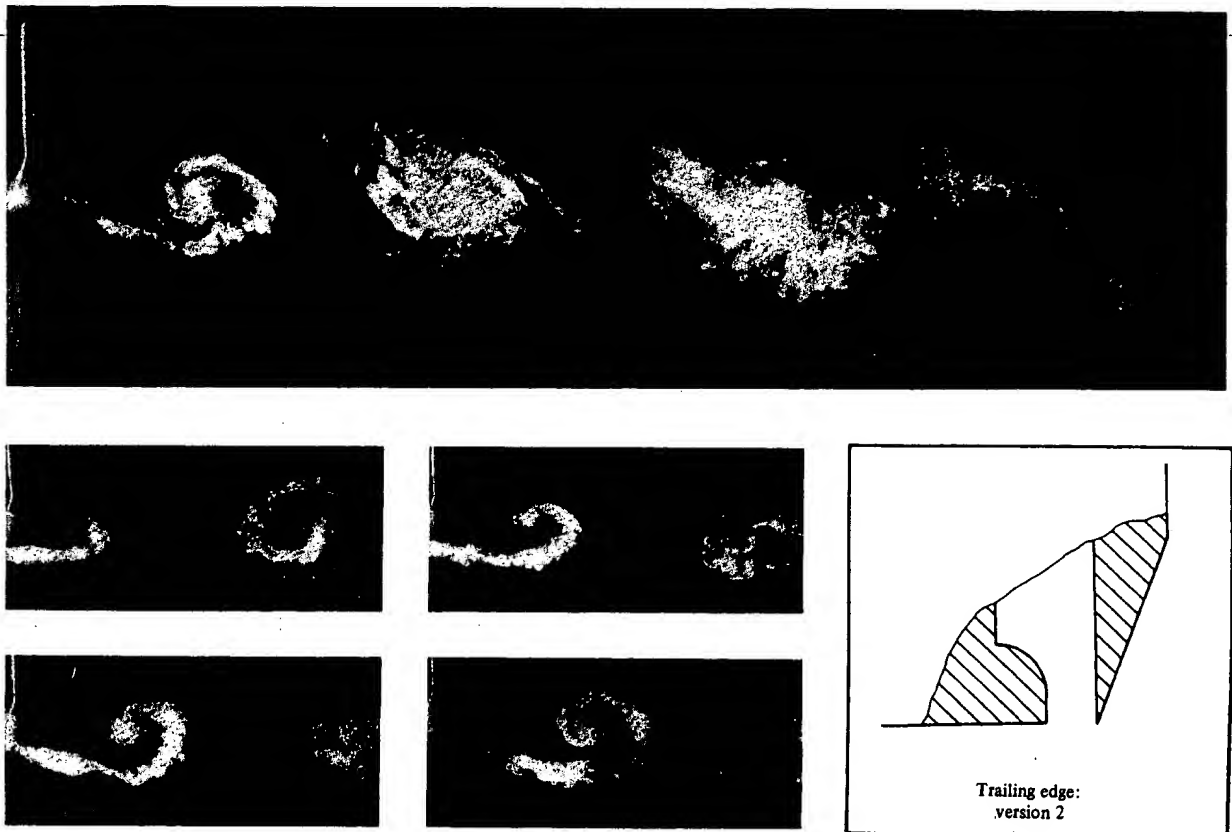


FIGURE 9. Overall flow development without pairing and enlarged sequences of flow near trailing edge: strong excitation with clean separation condition.



FIGURE 10. Flow development at strong excitation and clean separation showing sudden diffusion and vortex breakup.

flow development together with the supporting measurements in detail we may obtain a qualitative picture of the excited flow. Obviously the excitation leads to the formation of strong discrete vortices following a region where the imposed vertical excursions are amplified and cause the shear layer to undulate. The vortices in their final state appear to be stable only for a short time. In due course they lose coherence and are either predominantly torn at weak excitation or may undergo a pairing process at strong excitation (see also Fiedler *et al.* 1981). The artificially triggered structures are approximately two-dimensional, spanning the width of the test section (figure 7).

The smoke may be introduced into the flow through the loudspeaker slit (figures 8–10). This method, however, has the disadvantage of strong dilution of the smoke by the entrained fluid, which renders photography in the downstream region difficult. For a number of photographs we have therefore introduced the smoke far upstream of the trailing edge at the beginning of the contraction, so that the smoke trail is carried in the potential fluid, feeding the turbulent regime by entrainment along x (figures 5–7).

3. Results: structural (periodic) quantities

3.1. Neutral flow

Figure 5(a) juxtaposes this case against the excited cases. Clearly the neutral flow has a smaller spread angle and the structures do not appear to be clearly defined. They are rather lumpy and irregular and show little resemblance to the ones observed, for example, by Brown & Roshko (1974). This difference may be attributable to the different visualization techniques used. According to Wei, Niu & Ma (1982); however, those structures should not appear for $Re^* = \delta_0 u_c / \nu > 34$ (in our case $Re^* = 350$). This criterion is, however, not conclusive, since it was obtained for a low- Re case. Structures of the kind observed may still be quite coherent and two-dimensional, as was observed by Browand & Troutt (1980).

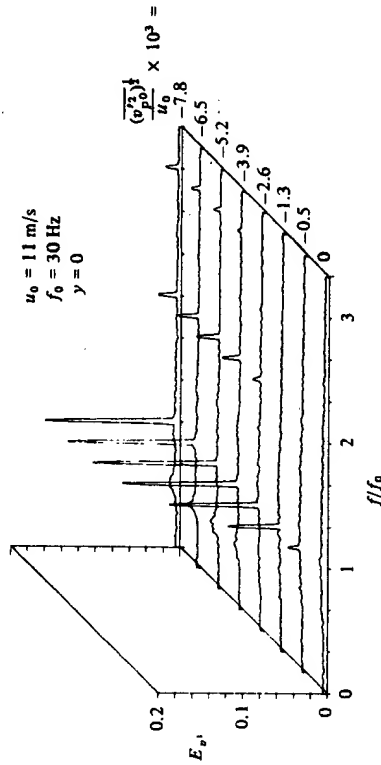


FIGURE 11. v' spectra for different excitation amplitudes at $S_x = 1$.

3.2. Excited flow

3.2.1. Choice of frequency

Most measurements presented were obtained at excitation frequency $f_0 = 30$ Hz. Since the turbulent shear layer is a self-similar flow (except in the dissipation range) with no distinguished lengthscale and with a characteristic frequency $f_c \sim u_0/(x - x_0)$, the reaction of the flow to periodic excitation of a certain amplitude must be independent to the frequency when plotted versus a normalized abscissa (Strouhal number)

$$S_x = (x - x_0^*) f_0 / u_0,$$

where f_0 is the excitation frequency and x_0^* a virtual origin, which is not the same as in the neutral case, but independent of frequency at a given amplitude. Thus the flow is not frequency-selective and for each frequency the degree of randomization of the driving wave at the position of maximum amplification is the same. This proposition is clearly proven by a number of measurements at different frequencies and in particular by the identity of the normalized amplification curve for different frequencies as shown in figure 15.

3.2.2. Amplification at different initial amplitudes

The amplification of a periodic perturbation along the flow was studied by spectral analysis of the v' signal along the x -axis, and for some cases in the whole flow field. The lateral fluctuation was considered to be of particular interest, since the initial perturbation was lateral and it is mainly this fluctuation that reflects the strength of the large vortices in the flow centre. A typical example for the spectra E_v as obtained for different excitation amplitudes at $S_x = 1$ (where approximately maximum amplification is achieved) is shown in figure 11.

For a direct assessment of the periodic constituent the turbulent signal is decomposed into a stochastic and a periodic part:

$$v' = v'_s + v'_p, \quad \text{and thus} \quad \overline{v'^2} = \overline{v_s'^2} + \overline{v_p'^2}.$$

Local periodic intensity is then obtained by subtraction of the stochastic background energy from the peak energy of the spectrum. In the following only the periodic signal content is considered.

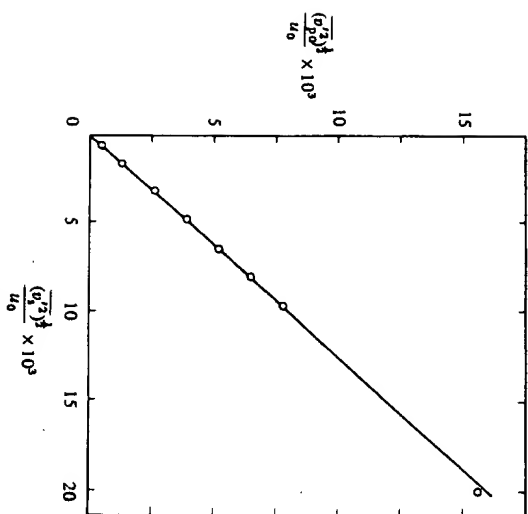


FIGURE 12. Excitation amplitude versus particle velocity in loudspeaker slit at zero flow velocity.

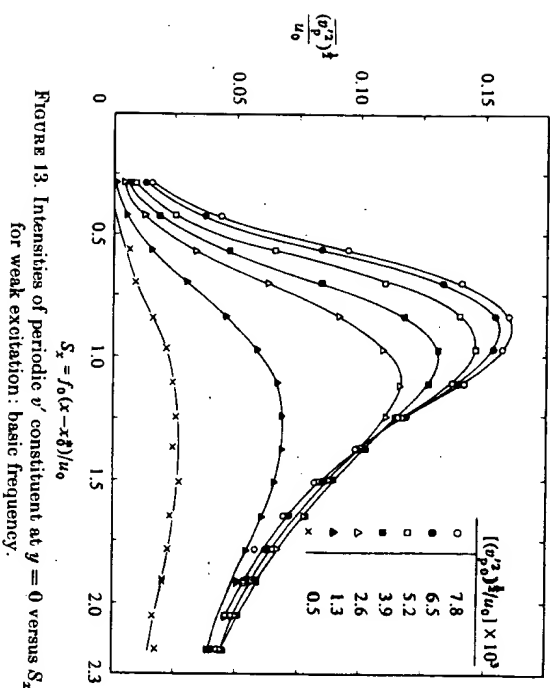


FIGURE 13. Intensities of periodic v' constituent at $y = 0$ versus S_z for weak excitation: basic frequency.

The initial excitation strength $(v_{p0})'$ was determined by cross-correlation of the speaker input with the hot-wire signal in the boundary layer at $x = 0$ and the y -position of maximum correlation, since these fluctuations – at least for weak excitation – appear to be fully embedded in the random turbulence of the separating boundary layer.

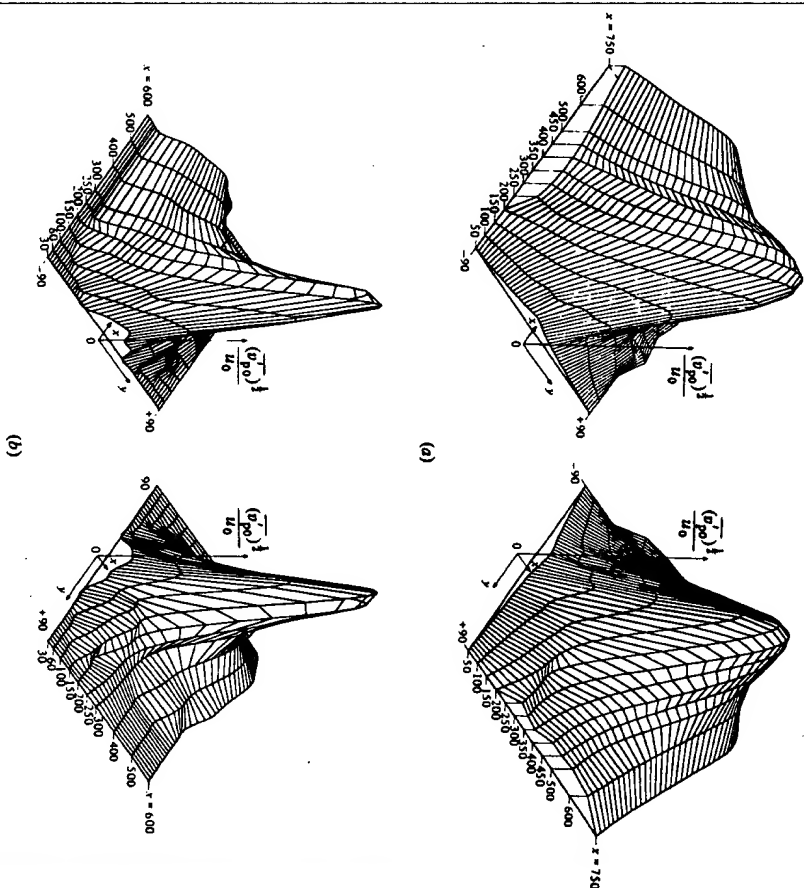


FIGURE 14. (a) Spatial distribution of periodic v' constituent at $f_0 = 30$ Hz. (b) Spatial distribution of periodic v' constituent at $f_0 = 50$ Hz.

The symbol $(\)'$ is used in the following for r.m.s. values and the averaged shear stress.

Although the values thus obtained appear to be most appropriate for scaling, since they truly represent the initial excitation amplitude at working condition, the particle velocity in the slit of the loudspeaker system was also measured for $f_0 = 30$ Hz at corresponding speaker voltages but with the flow turned off. The comparison is presented in figure 12. Obviously there is perfect correlation between the two parameters at 'weak' excitation, with the 'true' initial amplitude being 20% smaller than the amplitude of the particle velocity.

Weak excitation. The main part of the investigation was concerned with the weakly excited flow, i.e. $(v_{p0})'/u_0 \leq 0.0078$. For this situation figure 13 shows the development of the periodic signal intensity at $y = 0$ versus S_z for various excitation amplitudes. Since, in spite of the unequal spreading of the shear layer on the two sides, the locations of the maxima of the lateral $(v_p)'$ distributions are essentially at $y = 0$ (see also figures 14(a, b) and 31), the distributions in figure 13 give the longitudinal development of the maximum value of $(v_p)'$. At $S_z = 1$ (depending on excitation

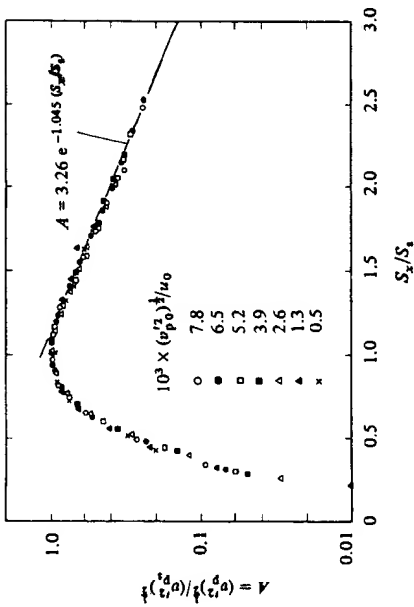


FIGURE 15. Universal excitation curve of periodic v' constituent at $y = 0$ for various excitation amplitudes (and various frequencies).

strength) the curves reach a maximum which corresponds to the position of strongest development of the vortices. The distance from the trailing edge to the location of the maximum is denoted by x_s , and we define a saturation Strouhal number

$$S_s = (x_s - x_0^*)f_0/u_0.$$

Figures 14(a,b) show spatial distributions of the spectral peak envelopes for two frequencies, demonstrating perfect similarity.

Closer inspection of figure 7 discloses a similarity of the amplification curves for the various excitation levels. Indeed, by proper normalization the curves can be made to collapse on to a single one with remarkably little scatter. Figure 15 gives the universal amplification curve, which is independent of amplitude and frequency. It may be approximated by

$$A = \frac{(v')'}{(v')_{\max}} = 20 \left(\frac{S_z}{S_s} \right)^4 \exp \left(-3 \frac{S_z}{S_s} \right),$$

where

$$\frac{S_z}{S_s} = \frac{f}{f_0} \bigg|_{x=\text{const}} = \frac{x}{x_s} \bigg|_{f=\text{const}}$$

Considering only the decaying part of the curve, we may write

$$A = 3.26 \exp \left(-1.045 \frac{S_z}{S_s} \right).$$

This gives an idea of the longevity of a disturbance. We find that only at $S_z/S_s = 3.3$ has the periodic intensity constituent decayed to 10% of its maximum value.

From determination of x_s for different frequencies f_0 and constant amplitudes the actual virtual origin x_0^* is obtained (figure 16). The maxima in figure 13 increase with increasing excitation amplitude, while the amplification factor

$$k = (v_{ps})'/(v_{p0})'$$

versus excitation intensity, as plotted in figure 17, decreases. It is largest for $(v_{p0})' \rightarrow 0$, where $k \approx 53$. This is of some interest, as it explains why the extremely weak

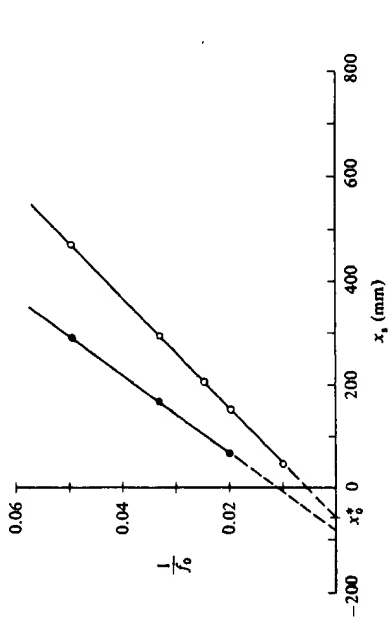


FIGURE 16. Saturation length versus excitation frequency; evaluation of x_0^* : \circ , $(v_{p0})'/u_0 = 0.0065$; \bullet , 0.065.

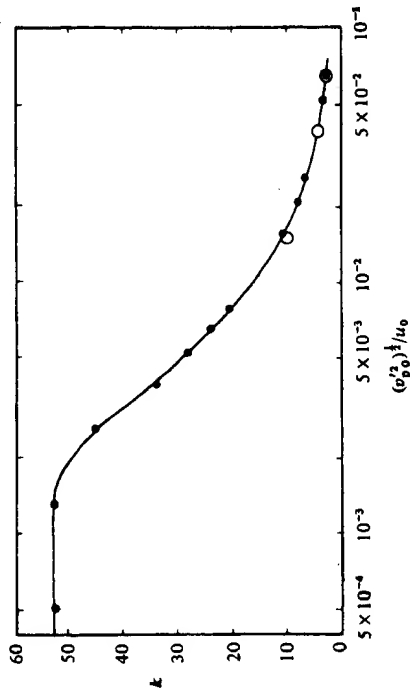


FIGURE 17. Amplification factor versus excitation amplitude.

disturbances, as, for example, from blower periodicity or organ-pipe resonance, may have a remarkable effect on the flow development.

Strong excitation. In this situation it seemed to be of interest to investigate the possibility of an asymptotic value for the maximum periodic energy in the shear layer at high excitation. Figure 18 shows some amplification curves for excitation amplitudes of up to $(v_{p0})'/u_0 = 0.065$. We observe a comparatively weak further growth of the maximum accompanied by its further shift upstream. In the decay range the curves deviate considerably from those at small amplitudes.

Smoke photographs of the flow at strongest excitation show a sequence of pairings, leading to formation of the vortices of basic (f_0) and of subharmonic ($\frac{1}{2}f_0$) frequency (figure 8). Formation of the primary vortices of frequency $2f_0$ is apparently caused by the particular excitation arrangement used. At strong excitation the flow separates upstream of the trailing edge during a 'pumping' cycle. At reattachment then a starting vortex is formed, which moves with retarded speed. It is quickly

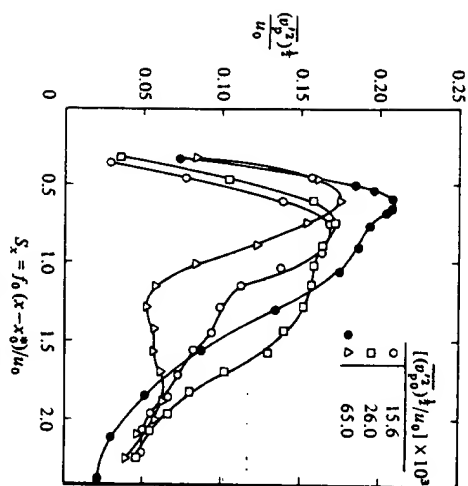


FIGURE 18. Intensities of periodic v' constituent at $y = 0$ versus S_x for strong excitation: basic frequency.

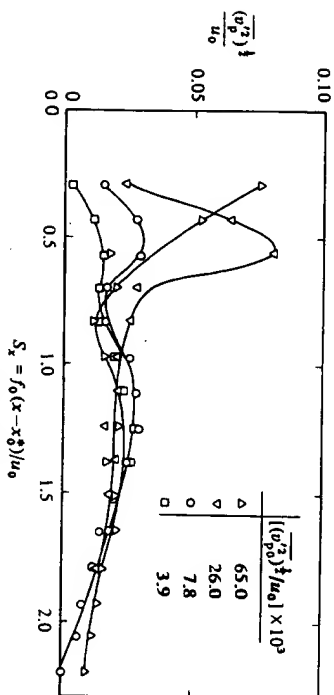


FIGURE 19. Intensities of periodic v' constituent at $y = 0$ versus S_x : 1st harmonic.

overturned by the following 'triggered' vortex and in due course amalgamated, thus forming the basic vortex. This first pairing occurs only at strong excitation amplitudes. It is significant for the further development of the flow, as it is responsible for the subsequent pairing of vortices of basic frequency, which is not observed at weak excitation. By sharpening the coverplate of the loudspeaker box at the trailing edge, pairing can be completely suppressed for all excitation amplitudes studied. In this situation then the basic vortices at strong excitation are strongly stabilized. They exist over a region of more than twice their diameter downstream, followed by a rather sudden disintegration (figure 10).

The two different situations are demonstrated by the flow pictures on figures 8 and 9. The flow at the 'clean' separation condition appears to be only quantitatively different from the weakly excited case. The 'disturbed' separation, on the other hand, has a different quality. It provides a possibility for studying stabilized vortex pairing. In the following discussion primarily the latter case is referred to. Only a few measurements obtained with clean separation are included in some of the figures.

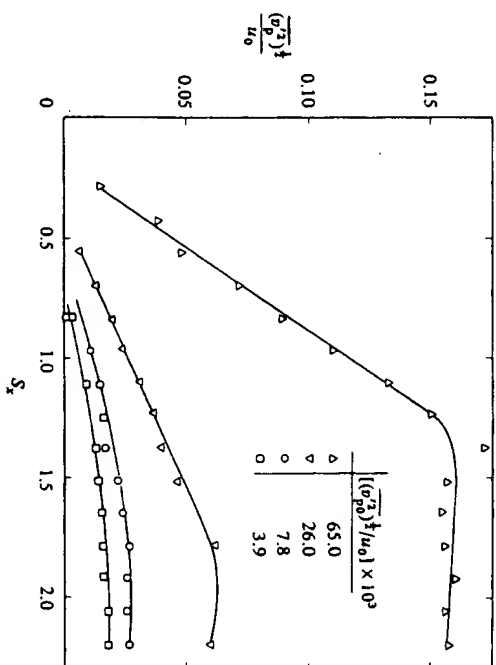


FIGURE 20. Intensities of periodic v' constituent at $y = 0$ versus S_x : subharmonic.

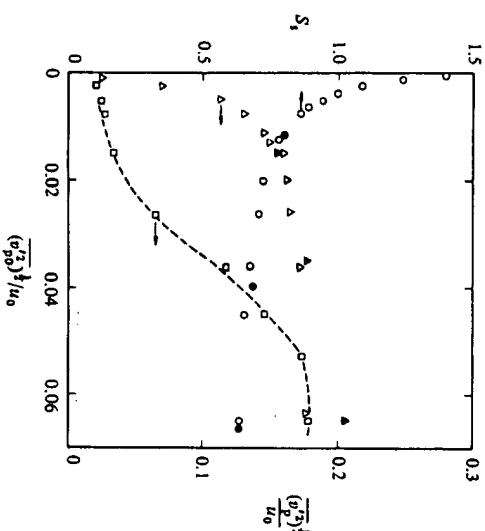


FIGURE 21. Intensities of maximum periodic v' constituents at x_0 and saturation Strouhal number S_b versus excitation amplitude: \circ , Δ , basic frequency; \square , subharmonic frequency (both at disturbed excitation condition), filled symbols, clean condition.

The intensity distribution of the first harmonic ($2f_0$) and of the subharmonic ($\frac{1}{2}f_0$) are presented in figures 19 and 20 respectively. For weak excitation their levels remain approximately one order of magnitude below the intensity of the basic frequency. For higher excitation amplitudes at the disturbed condition the subharmonic intensities in particular increase considerably, reaching maxima equal to those of the basic frequency, thus initiating and indicating the pairing process, which indeed is only observed in those cases where the intensity of the subharmonic locally exceeds

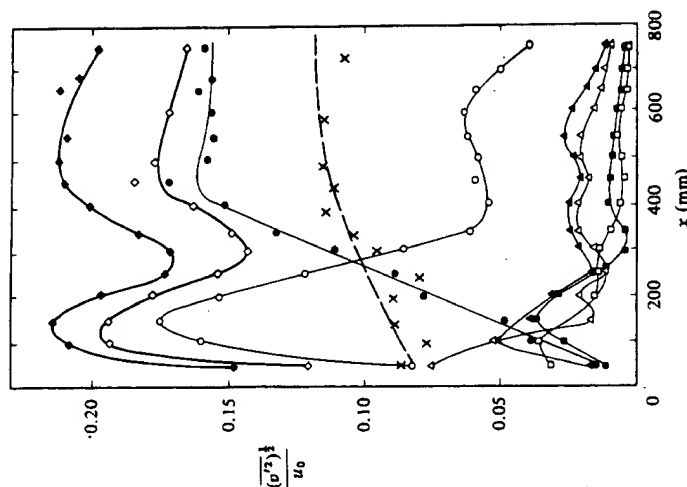


FIGURE 22. Periodic constituents of v' fluctuations at $y = 0$ for $f_0 = 30$ Hz and $(v_{p0})'/u_0 = 0.065$ versus x : \bullet , 15 Hz; \circ , 30 Hz; \blacktriangledown , 45 Hz; \triangledown , 60 Hz; \blacksquare , 75 Hz; \square , 90 Hz; \diamond , overall intensity $(v')/u_0$ (measured); \diamond , total intensity of periodic constituents; \times , intensity of non-periodic fluctuations $(v')/u_0 - (v_{p0})'/u_0$; —, neutral distribution (measured).

that of the basic (see also Ho & Huang 1982). At the clean excitation condition, where pairing is not observed, the intensity of the subharmonic always remains an order of magnitude below that of the basic.

In figure 21 magnitudes and locations of the maxima of periodic intensities are plotted versus relative excitation amplitude. Included are some data for strong excitation with clean excitation condition, which corroborate the observation that for weak excitation the condition at the trailing edge is of no consequence for the flow development (i.e. if flow separation remains fixed to the trailing edge).

For high excitation these curves appear to approach the asymptotic values $S_s \rightarrow 0.6$ and $(v_p)'/u_0 \rightarrow 0.2$.

For the case of strongest excitation $(v_{p0})'/u_0 = 0.065$ the overall intensity of v' is plotted together with the intensity distributions of all periodic constituents found in the spectra for $y = 0$ versus x in figure 22. The maximum at basic frequency indicates the formation of the basic vortices (first pairing). The maximum of the subharmonic at about the downstream distance marks the formation of vortices with frequency $\frac{1}{2}f_0$ (second pairing - see also Ho & Huang 1982). This interpretation is supported by the smoke photographs on figure 8. Subtraction of the periodic energy from the overall v' energy yields the random constituent. It is somewhat surprising that the distribution thus obtained - with all due reservation for its accuracy - is

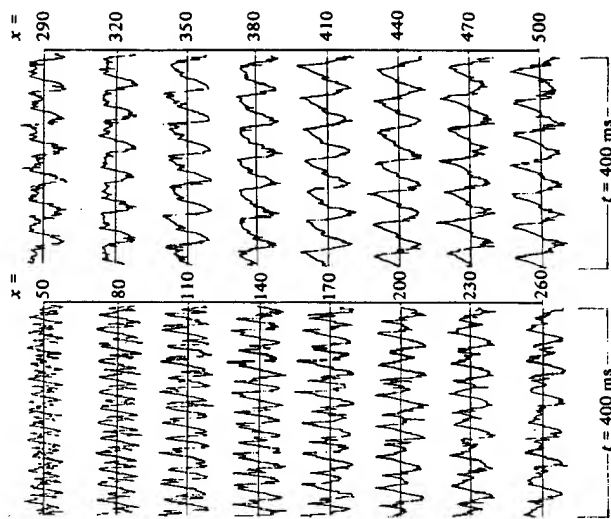


FIGURE 23. v' signal at different stations along x ; $y = 0$, $f_0 = 30$ Hz, $(v_{p0})'/u_0 = 0.065$.

very close to the intensity distribution of the neutral flow, which seems to indicate that the random part of the turbulence remains essentially unaffected by the excitation. This appears to be in contradiction to other findings, but no explanation can be given at this point. Indeed it must be expected that in general the fine-grained turbulence is strongly influenced by the large-scale motions where turbulent laminae are distorted by being rolled up in a large vortex structure.

The regularity of the flow at strong excitation is demonstrated by the signal traces at $y = 0$ and various x -positions and at $x = 150$ (basic saturation length) across the flow, as shown in figures 23 and 24.

The stages described are easily identified and - as in the smoke photographs - considerably stronger determinism is observed on the high-velocity side. According to expectation, the behaviour of the flow shows close resemblance to the laminar shear layer under similar conditions, as, for example, investigated by Freymuth (1966) and by Miksad (1972).

3.2.3. Limitations

Provided the loudspeaker system will produce a pure sine wave at all desired frequencies, an upper frequency limit is introduced by the finite thickness of the separating boundary layer at trailing edge. Thus in the present experiments the amplification curve for 100 Hz no longer follows the similarity distribution in figure 25. Figure 16 shows that for this frequency saturation is reached already close to the trailing edge, where the characteristics of the separated boundary layer are still dominant. For $f_0 > 180$ Hz, x_s becomes negative. This frequency then would no longer experience amplification.

A lower limit for the excitation frequency is given by the size of the test section.

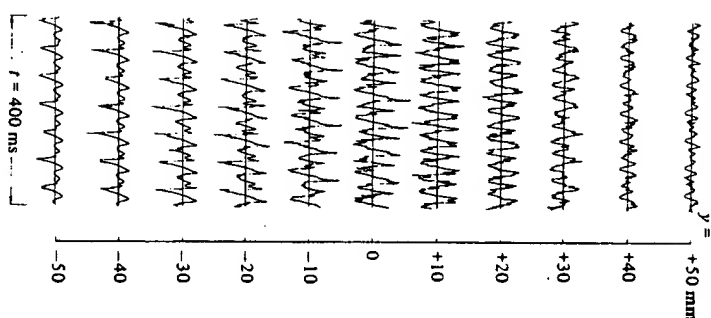


FIGURE 24. v' signal at various y -positions; $x = 150$ mm, $f_0 = 30$ Hz, $(v'_{p0})'/u_0 = 0.065$.

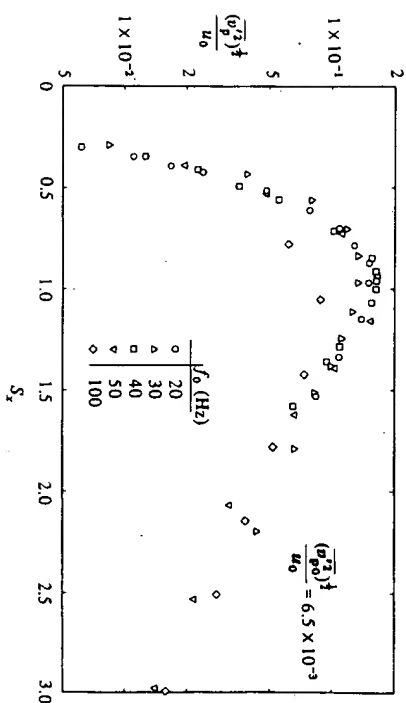


FIGURE 25. Frequency dependence of amplification.

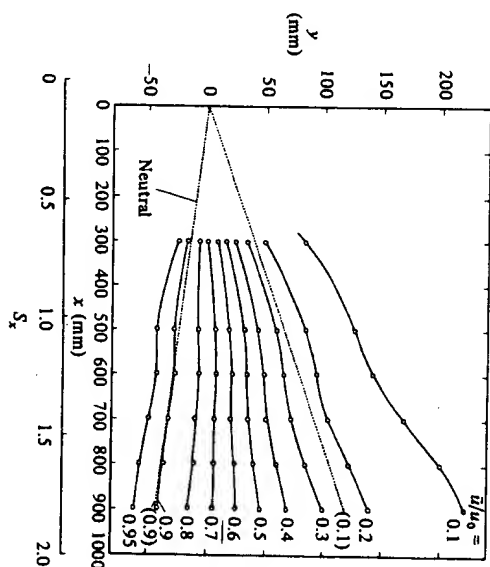


FIGURE 26. Mean-velocity isoachs for $(v'_{p0})'/u_0 = 0.0065$ (weak excitation).

Not only might the interesting phenomena already be outside of the test section at very low frequencies (their downstream location being inversely proportional to f_0), but the proximity of the sidewalls may affect the flow by three-dimensional effects, while the bottom wall will increasingly influence the stability behaviour of the flow (modified boundary conditions) with increasing distance from the trailing edge, i.e. for decreasing frequencies (see also Wood & Bradshaw 1982).

4. Results: mean flow and turbulence characteristics

4.1. Mean-flow development and entrainment

The consequence of excitation on the mean quantities of turbulent shear layers has been described previously (e.g. Fiedler *et al.* 1981; Oster & Wignanski 1982; Ho & Huang 1982). While the mean-velocity profiles, apart from being widened, essentially retain their shape except for very strong excitation (Wignanski, Oster & Fiedler 1979), the excitation effect becomes visible in the isoach plots. Figures 26 and 27 juxtapose isoach distributions for weak excitation $(v'_{p0})'/u_0 = 0.0065$ and strong excitation $(v'_{p0})'/u_0 = 0.065$, where the isoachs for $u/u_0 = 0.1$ and 0.95 of the neutral flow are included for comparison. In contrast with the well-known behaviour at weak (i.e. 'clean') excitation, we observe at strong excitation two regions of steep growth, the first one at $S_x \approx 0.25$, indicating the formation of vortices at basic frequency (first pairing), the second at $S_x \approx 1$, indicating the formation of vortices at subharmonic (second pairing). The subsequent maxima of width are at the positions of maximum vortex strength. This course of events is also partly seen in the smoke photographs on figure 8. The strong influence of the vortices on the spread is particularly obvious from the emergence of slightly negative local growth rates, where the overall production is negative (see Takaki & Fiedler 1980).

Obviously the step-like increase of spread is always a consequence of vortex formation irrespective of whether pairing takes place or not. In these and the

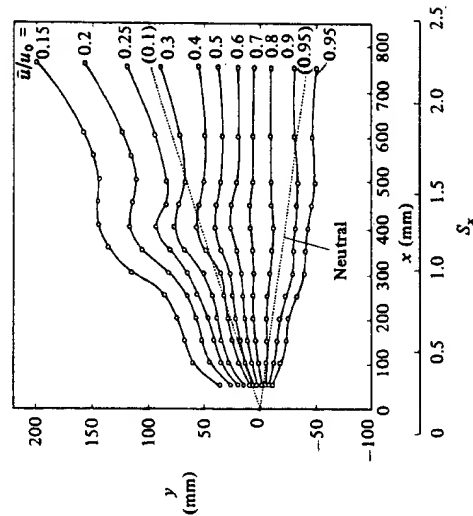


FIGURE 27. Mean-velocity isotachs for $(v_{\theta 0})'/u_0 = 0.065$ (disturbed strong excitation).

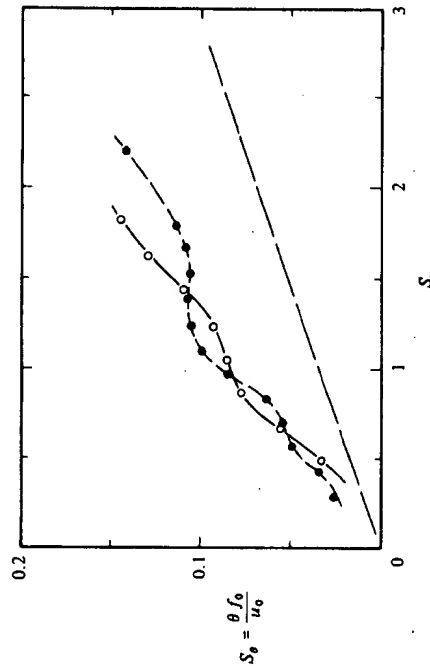


FIGURE 28. Shear-layer spread: O, weak excitation; ●, strong excitation; ----, neutral flow.

following diagrams the lateral coordinate y is retained, since similarity coordinates do not apply.

The spread rate for the two cases is shown in figure 28. Surprisingly the mean spread rate is approximately the same for both cases, being about twice that of the neutral flow.

The spread of the shear layer is accompanied by entrainment of potential fluid from both sides. The mechanism of entrainment becomes particularly clear in the excited flow, where the potential fluid is rolled in on the leesides of the vortices. This is seen in the photographs on figure 6.

Figure 6(a) shows entrainment fluid as a dark region behind the second vortex.

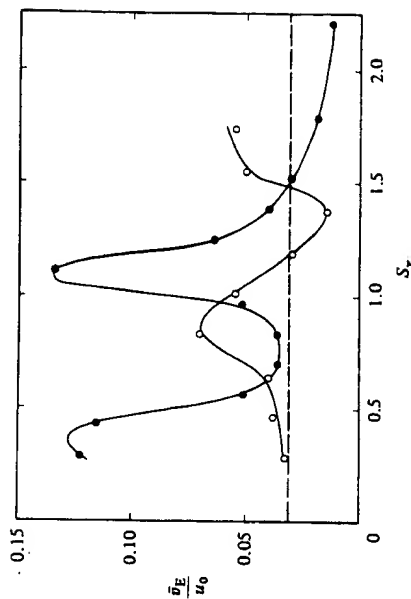


FIGURE 29. Entrainment velocities versus downstream position S_x for weak (O) and strong (●) excitation; ----, neutral flow.

It reaches far into the shear layer and is incorporated only on the other side. In figure 6(b) the entrainment flow is marked by smoke. Again we see the entrained fluid as a connected filament reaching far into the vortex. Thus the fully developed vortex appears to be quasi-laminated, and diffusion becomes a dominating factor only in the decay region (see also figure 10). At the same time small vortices appear on the periphery of the vortex. They may originate from the instability of the spooled-up laminae, which in fact are stabilized to some extent by their curvature.

On the zero-velocity side the entrainment flow is sucked into the turbulent regime from the ambient. We therefore measure a velocity towards the flow. On the high-velocity side the entrainment mechanism is somewhat different: there is no entrainment velocity in the potential flow, but the turbulent regime incorporates potential fluid by 'eating' into it. The flow rate entrained on the high-velocity side is approximately 2 times larger than on the zero-velocity side for the neutral shear layer. This ratio then becomes a function of x in the excited case, depending on the vortex development. Figure 29 shows entrainment velocities on the zero-velocity side versus S_x as obtained by integration of the mean-velocity profiles. The maxima are associated with the positions of strongest growth rates, demonstrating that pairing is not essential for entrainment. (Integration was performed only down to $u/u_0 = 0.1$, since at the outer edge of the flow measurements become increasingly uncertain).

4.2. Turbulence quantities

Longitudinal and transverse overall fluctuation-intensity distributions were measured for weak and strong excitation at various positions downstream. The weak excitation case was measured with $f_0 = 20$ Hz, the strong excitation case with $f_0 = 30$ Hz. The results may be directly compared by conversion of the respective x -position by the similarity relation

$$x_{f_0} = (x_{f_0}^* - x_0^*) f_{0s} / f_{01} + x_0^*.$$

This has been verified by a number of test measurements at various frequencies, some of which are presented in figure 25.

Figures 30 and 31 give the $\langle u' \rangle$ and $\langle v' \rangle$ distributions for weak excitation at various x -positions. Distributions for the neutral flow measured at the farthest downstream

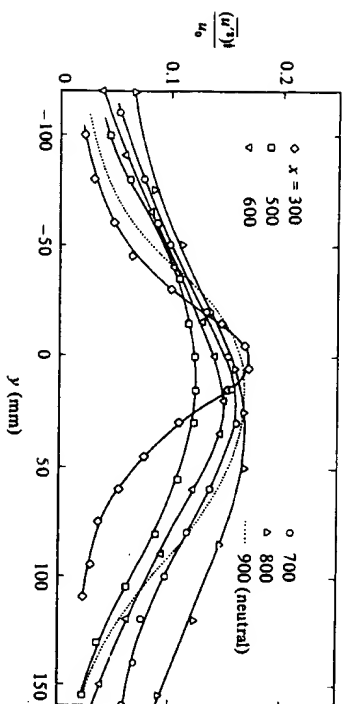


FIGURE 30. u' overall intensity profiles in weakly excited flow ($(v_{90})'/u_0 = 0.0065$) at different x -positions.

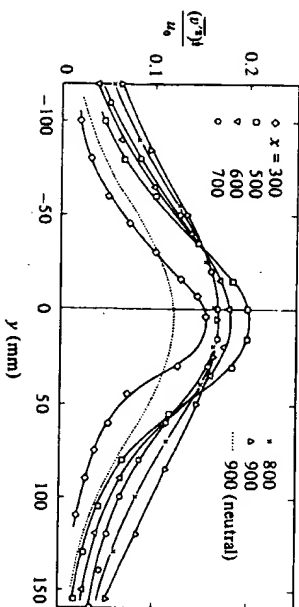


FIGURE 31. v' overall intensities in weakly excited flow.

position are included for comparison. Figures 32 and 33 show the corresponding distributions for the strongly excited case (disturbed condition).

While for weak excitation the distributions themselves, apart from being wider, retain their shape, resembling skewed Gaussian distributions with shifted maximum positions, we find a more complicated pattern at strong excitation. There particularly at the positions $x = 50$ mm and $x = 300$ mm the v' distribution appears to have two maxima, while at the same position the u' distributions are well behaved, their maxima exceeding the natural value. From smoke photographs these locations are identified by considerable vertical displacements preceding the pairing process. A situation where vortices appear in a staggered fashion, is likely to produce a strong u' maximum at the centerline and a double maximum of the v' fluctuations at approximately the vertical positions of the vortex cores. This is in contrast with a single row of vortices, which, when existing over a sufficient fetch as in a two-stream layer, will produce a strong v' maximum on the centreline and a double maximum of (u') at approximately the outer periphery of the vortices (see e.g. Oster & Wygnanski 1982).

Shear-stress distributions were measured only for the weakly excited case. They are shown in figure 34. The values for small x exceed the neutral curve in the region of vortex formation and are well below the latter for $x > x_g$ (decay region with

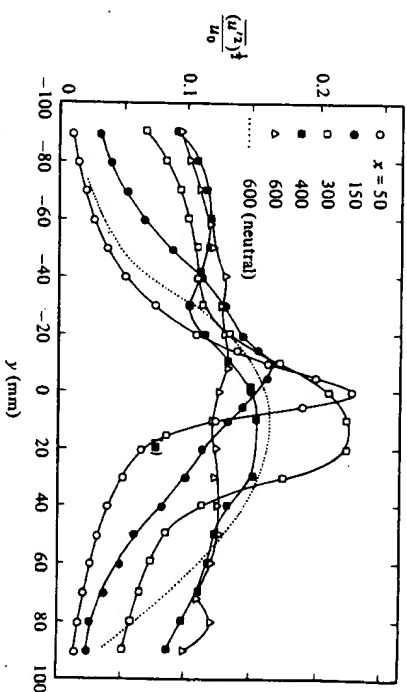


FIGURE 32. u' overall intensities at strong excitation ($(v_{90})'/u_0 = 0.065$).

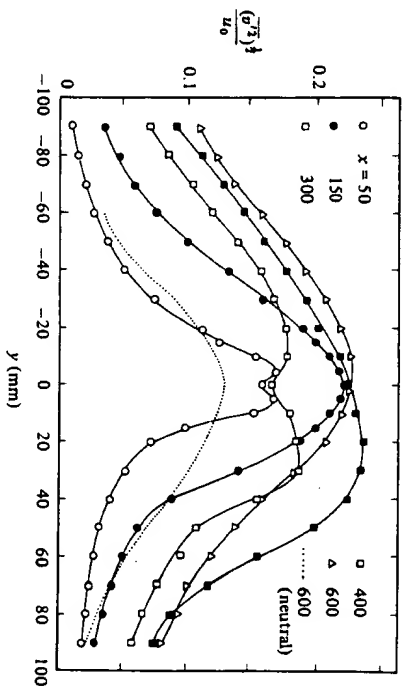


FIGURE 33. v' overall intensities at strong excitation.

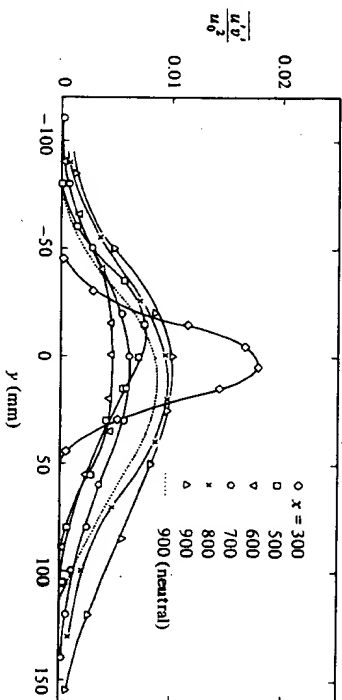


FIGURE 34. Turbulent shear stress at weak excitation.

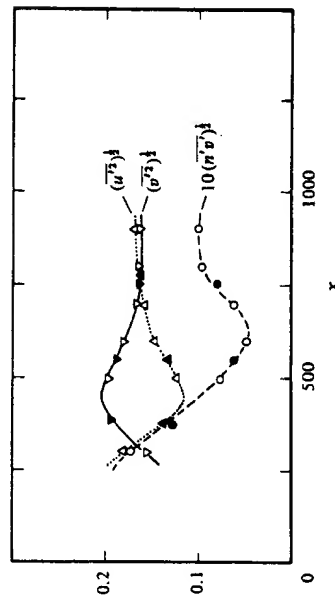


FIGURE 35. Longitudinal development of $(u')^2/(v_p')^2$ and $(uv')^2/(v_p')^2$ at $y = 0$: open symbols, $f_0 = 20$ Hz; full symbols, $f_0 = 30$ Hz, converted to 20 Hz (weak excitation).

negative $(uv')^2$. From the measurements of Wygnanski *et al.* (1979) we know that for strong excitation even negative values of $(uv')^2$ are found.

For better understanding, the axial development of the maximum values of the turbulence intensities and the shear stress as obtained from the previous figures (weak excitation) are presented in figure 35. These curves also include measurements at 30 Hz, where the conversion relation was applied, thus serving as additional proof for the general similarity. One particular aspect deserves mention: while it seems obvious that the turbulent intensity is increased in the excited flow by approximately its periodic constituent – as is indeed observed for the v' component – the reduced u' intensity at certain flow positions is more difficult to understand. A possible explanation may be as follows. A considerable part of the low-frequency random u' fluctuation energy in the neutral flow is caused by large-scale motions (coherent structures) with considerable vertical jitter. In the excited flow these motions are stabilized – most strongly at x_s – and their vertical displacements minimized. The consequence may then be the suppression of the low-frequency u' fluctuations in the central region, as is particularly pronounced in the two-stream layer (Oster & Wygnanski 1982). Clearly this effect is different from the suppression observed for excitation frequencies an order of magnitude higher than those used in the present work by Zaman & Hussain (1981). In their case the excitation acted on the laminar/turbulent transition of an initially laminar shear layer, influencing the turbulence structure a long way downstream.

Another interesting point is the vertical dislocation of the intensity and shear-stress maxima. There we find considerable strong shifts in the (u') and the (uv') distributions, while the (v') maxima essentially remain at $y = 0$.

The shear-stress correlation is generally found to be around 0.45 for stochastic turbulence and monotonic profiles. On the axis of the neutral shear layer a value of 0.43 was indeed determined. In the presence of periodic vortices this value undergoes strong variations, reaching a maximum of 0.70 ahead of x_s , where it goes through the neutral value to a minimum at some position downstream and then back to 0.43. This may be explained by superposition of the deterministic and the stochastic constituents.

5. Summary and discussion

The neutral-plane shear layer is unstable for periodic perturbations introduced at the trailing edge. The perturbation wave is amplified along x , forming two-dimensional vortices of elliptical cross-section. The ratio of the major axes of the cross-sections of the fully developed vortex is approximately 1.8, which is in good agreement with theoretical values of Saffman (1980) and Jimenez (1980). The rate of amplification of the perturbation is highest at the onset of vortex formation (stability curve). It is zero at the saturation point x_s . At stations further downstream the amplification rate is negative (decay). The phenomenon is (ideal test conditions provided) frequency-dependent only inasmuch as the downstream position of saturation x_s is inversely proportional to the perturbation frequency. The total rate of amplification depends on the strength of excitation. It reaches a maximum of around 53 for $(v_p')^2 \rightarrow 0$. At saturation point the periodic energy constituent approaches a saturation value for strong forcing, which is of the order of 70% of the total lateral fluctuation energy.

It was observed that the sequence of periodic events in the flow is sensitive to the separation condition at the trailing edge. When forcing is applied such that the separation remains at all times fixed to the trailing edge only vortices of basic frequency are formed. After the saturation point the periodic energy decays exponentially, while the vortices themselves lose coherence without pairing. The decay of periodicity is rather weak, and return to the neutral state may be expected only at a great distance.

When, on the other hand, at strong forcing the separation point is no longer fixed to the trailing edge but moves periodically upstream, a stable condition of repeated pairing may set in.

Diffusion by small-scale random motion inside the vortices during their formation appears to be comparatively weak. It becomes a major factor only in the decay region. Formation of vortices – be it with or without pairing – is always accompanied by strong increase of spread and thus of entrainment. After saturation the spread rate is strongly decreased and may even become negative. In the mean, however, excited flows always experience considerably stronger spread than the natural. It is approximately twice the neutral value and surprisingly independent of forcing amplitude. At saturation point the longitudinal fluctuation level goes through a minimum, while the lateral fluctuations reach their highest values. The turbulent shear stress has a maximum at vortex formation (maximum amplification) and a minimum at the beginning of decay.

A number of observations may be related to the natural shear layer.

The life cycle of a triggered structure (see Fiedler *et al.* 1981) exhibits essentially two phases.

(1) *Excitation of vortex.* The vortex is backward-leaning. It receives energy from the mean flow, which shows increased growth rate, increased entrainment and high values of (uv') . At the point of maximum energy the structure is deformed such that the vortex becomes forward-leaning.

(2) *Decay of vortex.* The vortex is forward-leaning. Energy is returned to the mean flow. The mean spread, entrainment and turbulent shear stress are reduced and below the average natural values. Subharmonics leading to pairing are often suppressed to such an extent that the vortex will decay before pairing may set in.

In the natural case, on the other hand, pairing is observed as a common feature of structural development. Onset of pairing and the subsequent development of the

	Natural (Herran & Jimenez 1982)	Excited (Mensing 1981)
Vortex geometry a/b	1.84	1.8
Wavelength $\lambda/\lambda_0(x-x_0)^{\dagger}$	0.578	0.56
Convection velocity $u_c/(u_1+u_2)^{\dagger}$	0.49	0.5
$\dagger \lambda_0 = (u_1 - u_2)/(u_1 + u_2)$; here $u_1 = u_0$, $u_2 = 0$.		

TABLE 1

amalgamated structure show, however, the same course of events as the single structure during its amplification phase and thus have the same effects on the mean flow, e.g. increase of spread, shear stress and entrainment.

It therefore appears of little relevance whether a vortex in its amplification phase is formed by a rolled-up vortical layer or of two vortices via their amalgamation. Only the geometrical situation is important for its influence on the flow and this is characterized by a 'forward-leaning position' (Takaki & Fiedler 1980).

Comparison of the present findings with the high-speed film analysis of a natural shear layer by Herran & Jimenez (1982) shows good agreement in some comparable parameters as shown in table 1.

We have found the envelope spectrum of the coherent (periodic) constituent to be universal in amplitude and frequency (figure 15). It may thus be thought of as a probability density distribution for large-scale structures versus frequency at any position on the axis of a neutral layer, i.e. the spectral part of the coherent structures in the natural shear-layer spectrum. Comparison with the neutral spectrum provides us with a crude estimate of the coherent energy content of the natural flow. The approximately 20% thus obtained is in good agreement with the value proposed by Browand & Ho (1983).

Hussain (1983) obtained peak r.m.s. values in the average coherent structure of the natural one-stream shear layer of order 3% of the freestream velocity. We find comparable energy conditions for the lowest excitation amplitude which fits perfectly into the general spectrum curve (figure 15). This supports the above reasoning. Hussain's result should, however, not be misinterpreted: The strongest structures reduced at a certain position are only those at the apex of their life cycle, i.e. at their energetic maximum. They must therefore be expected to be of small, possibly insignificant, energy content as compared with the overall turbulence, while on the other hand the total fraction of coherent turbulent energy at the point of observation over all frequencies may well be of the order of 20%.

This investigation was substantially supported by Deutsche Forschungsgemeinschaft.

REFERENCES

- BRADSHAW, P. 1966 The effect of initial conditions on the development of a free shear layer. *J. Fluid Mech.* **26**, 225-236.
- BROWAND, F. K. & HO, C.-M. 1983 The mixing layer: an example of quasi two-dimensional turbulence. *J. Mec. Numéro Spécial: Turbulence & dimensionnelle*, pp. 99-120.
- BROWAND, F. K. & TROUTT, T. 1980 A note on spanwise structure in the two-dimensional mixing layer. *J. Fluid Mech.* **97**, 771.
- BROWN, G. & ROSHKO, A. 1974 On density effects and large structure in turbulent mixing layers. *J. Fluid Mech.* **64**, 775-816.
- FIEDLER, H., DZOMBKA, B., MENSING, P. & RÖSEN, T. 1981 Initiation, evolution and global consequences of coherent structures in turbulent shear flows. In *The Role of Coherent Structures in Modelling Turbulence and Mixing* (ed. J. Jimenez). Lecture Notes in Physics, vol. 136, pp. 219-251. Springer.
- FRIEDMUTH, P. 1966 On transition in a separated laminar boundary layer. *J. Fluid Mech.* **25**, 683-704.
- HO, C.-M. & HUANG, L.-S. 1982 Subharmonics and vortex merging in mixing layers. *J. Fluid Mech.* **119**, 443-473.
- HUSSAIN, A. K. M. F. 1983 Coherent structures - reality and myth. *Phys. Fluids* **26**, 2816-2850.
- HUSSAIN, A. K. M. F. & ZEDAN, M. F. 1978a Effects of the initial condition on the axisymmetric free shear layer: effects of the initial momentum thickness. *Phys. Fluids* **21**, 1100-1111.
- HUSSAIN, A. K. M. F. & ZEDAN, M. F. 1978b Effects of the initial condition on the axisymmetric free shear layer: Effects on initial fluctuation level. *Phys. Fluids* **21**, 1475-1481.
- HERRAN, M. A. & JIMENEZ, J. 1982 Computer analysis of a high-speed film of the plane turbulent mixing layer. *J. Fluid Mech.* **119**, 323-345.
- JIMENEZ, J. 1980 On the visual growth of a turbulent mixing layer. *J. Fluid Mech.* **96**, 447-460.
- KORSCHNIGT, D. 1980 Experimentelle Untersuchung zum Wärme- und Stofftransport in turbulenten ebenen Freistrahlen mit periodischer Anregung am Düsenaustritt. Dissertation Hermann-Föttinger-Institut, TU Berlin.
- MENSING, P. 1981 Einfluß kontrollierter Störungen auf eine ebene turbulente Scherschicht. Dissertation Hermann-Föttinger-Institut, TU Berlin.
- MENSING, P. & FIEDLER, H. 1980 Eine Methode zur Sichtbarmachung von hochturbulenten Luftströmungen mit großen Reynoldszahlen. *Z. Flugwiss. Weltraumforsch.* **4**, 366-369.
- MONAGHE, A. 1971 Instabilität eines kompressiblen runden Freistrahls unter Berücksichtigung des Einflusses der Strahlungsschichtdicke. *Z. Flugwiss. Weltraumforsch.* **19**, 319.
- MUSKAD, R. W. 1972 Experiments on the nonlinear stages of free-shear-layer transition. *J. Fluid Mech.* **56**, 695-719.
- MUSKAD, R. W. 1973 Experiments on nonlinear interactions in the transition of a free shear layer. *J. Fluid Mech.* **59**, 1-21.
- OSTER, D. & WYGANSKI, I. 1982 The forced mixing layer between parallel streams. *J. Fluid Mech.* **123**, 91-130.
- SARFMAN, P. G. 1980 Coherent structures in turbulent flow. In *The Role of Coherent Structures in Modelling Turbulence and Mixing* (ed. J. Jimenez). Lecture Notes in Physics, vol. 136, pp. 1-9. Springer.
- SMITH, A. M. O. & CLUTTER, D. W. 1957 The smallest height of roughness capable of affecting boundary layer transitions in low-speed flow. *Douglas Aircraft Co. Inc. Rep.* ES 26803.
- TAKAKI, R. & FIEDLER, H. 1980 A phenomenological model of the organized vortex in the two-dimensional mixing layer. *IUTAM Symp. Tugosolava*.
- WEI, Z.-L., NIU, Z.-N. & MA, W.-J. 1982 The disturbances affect Brown-Roshko structures in plane mixing layer. In *Structure of Complex Turbulent Shear Flow, IUTAM Symposium Marseille* (ed. R. Dumas & L. Fulcher), pp. 137-145.
- WOOD, D.-H. & BRADSHAW, P. 1982 A turbulent mixing layer constrained by a solid surface. Part 1. Measurements before reaching the surface. *J. Fluid Mech.* **122**, pp. 57-89.
- WYGANSKI, I., OSTER, D. & FIEDLER, H. 1979 A forced, plane, turbulent mixing layer: a challenge for the predictor. In *Proc. 2nd Symp. on Turbulent Shear Flows, London*.
- ZAMAN, K. B. M. Q. & HUSSAIN, A. K. M. F. 1981 Turbulence suppression in free shear flows. *J. Fluid Mech.* **103**, 133-150.



PERTURBED FREE SHEAR LAYERS

Chih-Ming Ho and Patrick Huerre

Department of Aerospace Engineering, University of Southern California,
Los Angeles, California 90089-1454

言天下之至動而不可亂也 周易 繫辭¹

*Denique si semper motus connectitur omnis,
et vetere exortitur semper novus ordine certo,
nec declinando faciunt primordia motus
principium quoddam quod fuit foedera rumpat,
ex infinito ne causam causa sequatur,
libera per terras unde haec animalibus existat ...?*

Lucretius, *De Rerum Natura*²

1. INTRODUCTION

This review is about free shear layers of the kind that are formed by the merging of two streams initially separated by a thin surface: the flow is sketched in Figure 1. Intensive mixing occurs in the velocity-gradient region between the two free streams, and such layers are often referred to as

¹ Speaking of the most restless phenomenon in the universe,
one should not be distracted by its randomness

I Ching

² Once more, if movement always is to other movement linked
And if the new comes ever from the old,

As in determinist argument;

If atoms in their swerve do not fresh start

To break the bonds of Fate;

If cause may follow cause from infinite time,

Whence comes free will for living things on earth?

Lucretius, *Of the Nature of Things*

0066-4189/84/0115-0365\$02.00

mixing layers. This simple flow configuration is a generic model arising in numerous natural phenomena and in artificial devices, such as combustors and gas lasers. From a practical point of view, one often seeks to manipulate the downstream evolution of shear flows to enhance the efficiency of certain industrial processes. In the present paper, the mixing layer is viewed more fundamentally as the prototype flow of a wider class of inviscidly unstable free shear flows that also includes jets and wakes. For the most part, we focus our attention on homogeneous, incompressible, two-dimensional mixing layers. However, some of the peculiar processes exhibited by two-dimensional or axisymmetric jets are briefly alluded to. Other related topics, such as aerodynamic-noise generation or the interaction between shear layers and downstream solid boundaries, are discussed in recent review articles by Goldstein (1984) and Rockwell (1983).

Two approaches are currently used to study turbulent shear flows. In the more classical theories, turbulence is viewed as an essentially random process, which can only be adequately described *statistically*. The flow field is then decomposed into a mean and a fluctuating part. The main difficulty resides in the derivation of a closed system of governing equations for the mean and fluctuating flows. For recent discussions of statistical theories of turbulence, the reader is referred to Monin & Yaglom (1971, 1975) and Lumley (1978, 1981), among others.

Another approach consists in viewing *quasi-deterministic* vortex structures as the main building blocks of turbulent mixing layers. Cortsin (1943) and Townsend (1947) were the first to notice that the interface separating turbulent and nonturbulent fluid is sharp and corrugated, and three decades later Kovaszny (1970) related this interface to the presence of large-scale vortex structures in boundary layers. Crow & Champagne (1971) discovered that the shear layer of a jet can support orderly vortical structures and operates as a finely tuned amplifier of upstream disturbances. Brown & Roshko (1974) subsequently confirmed that large-scale

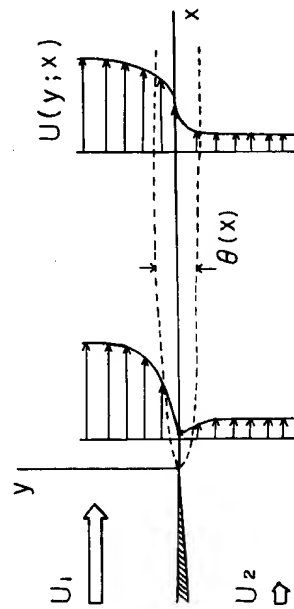


Figure 1 Sketch of spatially developing mixing layer.

coherent structures are indeed intrinsic features of turbulent mixing layers at high Reynolds numbers. Furthermore, sequential mergings of vortices provide the primary mechanism for the spreading of the layer in the downstream direction, as underscored by the experiments of Winant & Browand (1974). These observations have had a major impact on our understanding of turbulence in free shear flows, as discussed, for instance, in the reviews of Roshko (1976), Cantwell (1981), and Laufer (1975, 1983). In the present survey, we unequivocally adopt the coherent-structure point of view. Strong reservations on the part of some researchers [in particular P. Bradshaw and his co-workers (Chandrsuda et al. 1978)] do exist, however, regarding the indefinite persistence of two-dimensional orderly structures at very high Reynolds numbers.

Among the many experimental and theoretical studies of coherent structures, one may distinguish two main modes of approach. A first school would lean toward a description in terms of the evolution of the vorticity field in physical space. The structures are then considered as vortices of a certain characteristic size that undergo different types of nonlinear interactions. General accounts of vorticity dynamics can be found in Saffman & Baker (1979), Zabusky (1981), and Aref (1983). One of the main advantages of this viewpoint is that the results can be compared, using some caution, with flow-visualization studies conducted in the laboratory. The application of vortex methods to direct two-dimensional numerical simulations does yield a realistic fully nonlinear modeling of the roll-up of the shear layer and of vortex mergings. The extraction of detailed information regarding the intrinsic scales of the motion tends, however, to be somewhat more involved. On the experimental side, it should be mentioned that the vorticity field cannot presently be measured satisfactorily with available instruments, and various approximation schemes have to be used.

Other workers have chosen instead to rely on classical hydrodynamic stability theory: the unsteady mixing layer is then conceptualized as a superposition of interacting instability waves that propagate and amplify in the downstream direction. The flow is therefore examined in Fourier space rather than in physical space, and large-scale vortices are themselves composed of several instability waves of different frequency. As a result, measured data in frequency space cannot easily be related to the evolution of the orderly structures, unless a technique such as flow visualization is used to make this crucial connection. As we shall see, linear stability analysis has been shown to describe very satisfactorily the initial development of the mixing layer preceding the establishment of fully rolled-up vortices. There are also strong indications that its use in conjunction with an appropriate phenomenological model can also help to determine the

main length scales of the flow much farther downstream. In contrast with the vortex approach, it is impossible to use stability analyses to model strongly nonlinear phenomena. Some of the observed wave interactions may only be weakly nonlinear, and analytical techniques can be developed to handle such effects. Truly nonlinear processes, however, have to be simulated numerically. General surveys on the stability of mixing layers have been written by Michalke (1972), Liu (1981), Huerre (1984), and Morkovin (1984).

Each individual vortical structure occurring in naturally excited shear layers is known to be subjected to spatial jitter as it travels along the stream. As a result, a large number of probes have to be used at any instant to obtain a detailed knowledge of the flow field. The application of low-level forcing to free shear layers was initially meant to overcome this problem. An excitation provided a clear phase reference and thereby alleviated the need for many simultaneous measurements. The low-level forcing disturbance was thought to have no particular effects on the dynamics of the flow, other than a decrease in broadband noise. It has only recently been realized that the evolution of mixing layers is highly susceptible to very low-amplitude disturbances. Thus, artificially generated perturbations can be used advantageously not only to deepen our basic understanding of shear-layer dynamics, but also to alter significantly the downstream development of the flow.

Naturally or artificially excited shear layers are necessarily perturbed flows. Without prejudice to other interpretations, our tendency has been therefore to emphasize hydrodynamic instability-wave concepts. This article is subdivided into four main sections. The basic mechanisms governing the development of mixing layers are reviewed in Section 2. In Sections 3 and 4, we assess our current knowledge of the effects of operational parameters and artificial forcing on the characteristics of the flow. Finally, Section 5 is devoted to speculations regarding global effects and the feedback mechanism.

2. DYNAMICAL PROCESSES IN FREE SHEAR LAYERS

Within the conceptual framework of stability theory, two laminar streams of velocity U_1 and U_2 ($U_1 > U_2$) are assumed to give rise, by viscous diffusion, to a weakly diverging steady basic flow $U(y; x)$, as shown in Figure 1. The variables x , y , z , and t respectively denote the streamwise, cross-stream, and spanwise coordinate, and time. The momentum thickness $\theta(x)$ initially increases as the square root of x . The flow can conveniently be characterized by two nondimensional parameters R and

Re_0 . The velocity ratio $R = \Delta U/(2U)$ measures the relative magnitude of the total shear $\Delta U = U_1 - U_2$, as compared with the average velocity $\bar{U} = (U_1 + U_2)/2$. When $R = 0$, the flow reduces to a wake. When $R = 1$, only one stream is present, as in the initial mixing region of a jet. The Reynolds number $Re_0 = \bar{U}\theta_0/\nu$, based on the initial momentum thickness θ_0 and kinematic viscosity ν , accounts for viscous effects.

2.1 Linear Instability Regime

The development of mixing layers downstream of a splitter plate is initially dominated by a linear instability mechanism. For general reviews of the hydrodynamic stability of parallel flows, the reader is referred to Lin (1955), Drazin & Howard (1966), Betchov & Criminale (1967) and Drazin & Reid (1981).

The basic vorticity distribution, which possesses a maximum, is inviscidly unstable to small perturbations via the Kelvin-Helmholtz instability mechanism. Thus, two-dimensional waves grow exponentially with downstream distance and are observed to roll up into vortices. If the basic flow $U(y)$ is taken to be strictly parallel and disturbances are infinitesimal, the perturbation stream function can be cast into the form

$$\psi(x, y, t) = \phi(y) \exp \{i(\alpha x - \omega t)\} + c.c., \quad (1)$$

where $\omega = 2\pi f$ is the angular frequency, α is the wave number, and c.c. denotes the complex conjugate.

In the inviscid limit $Re \equiv \infty$, the eigenfunction $\phi(y)$ is obtained by solving the linear Rayleigh equation. Most calculations have been conducted for the hyperbolic-tangent velocity profile $U(y; R) = \bar{U}[1 + R \tanh(y/2\theta)]$. Michalke (1964, 1965a,b) has determined numerically the stability characteristics of both temporal (ω complex, α real) and spatial (ω real, α complex) waves in the limit $R = 1$. More recently, Monkewitz & Huerre (1982) have studied the theoretical dependence of spatially growing waves on R for both the hyperbolic-tangent profile and the Blasius shear layer calculated by Lock (1951). The equivalent problem for axisymmetric jets has been investigated by Michalke & Hermann (1982). The nondimensional spatial growth rate ($-\alpha_i\theta$) and phase velocity $c_p/\bar{U} = \omega/(\alpha\bar{U})$ are found to vary with Strouhal number $St_n = f\theta/\bar{U}$ in the fashion displayed in Figure 2. The Strouhal number $St_n = 0.032$ of the most amplified wave corresponds to the natural frequency f_n of the mixing layer: it changes by only 5% between $R = 0$ and $R = 1$. The maximum amplification rate ($-\alpha_i\theta_{max}$) increases approximately linearly with R , and the associated phase velocity is equal to the average velocity \bar{U} of the two streams. In the limit of small shear $R \ll 1$, the spatial growth rate ($-\alpha_i$) and its temporal counterpart ω_i are related via the transformation ($-\alpha_i)/R \sim \omega_i/\bar{U}$, sug-

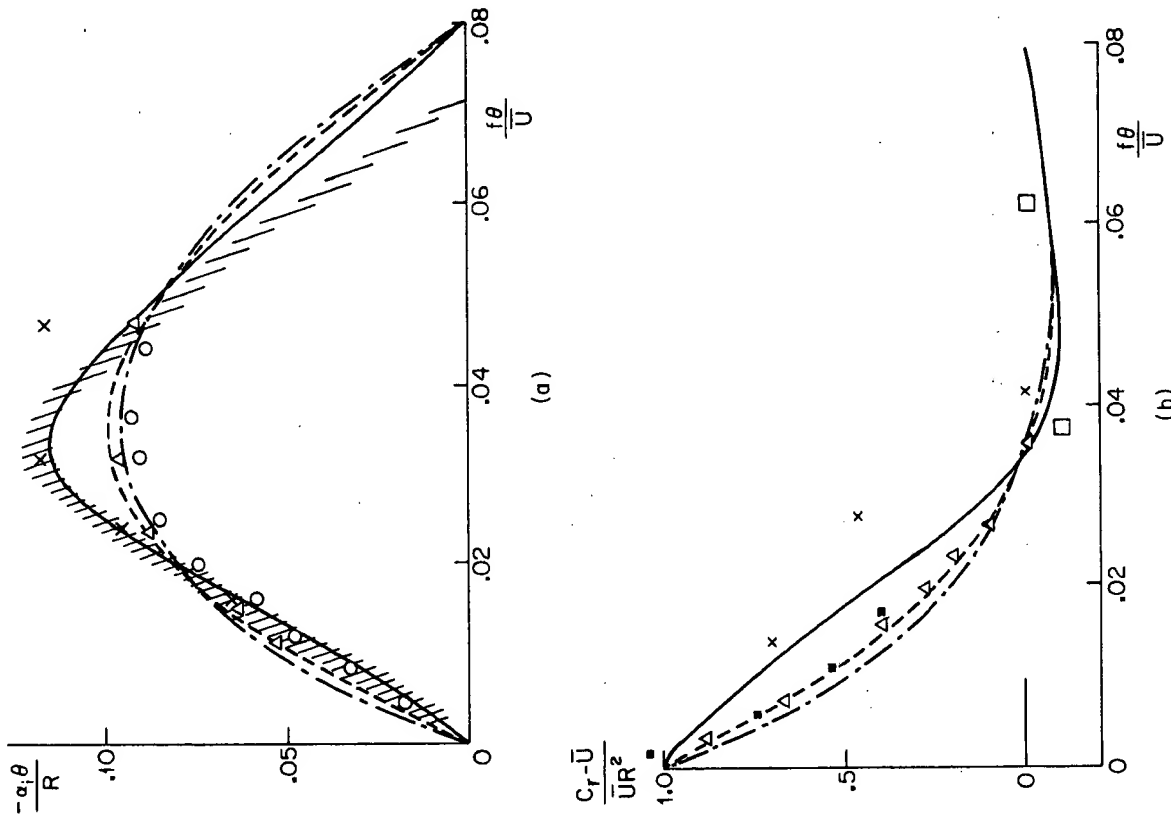


Figure 2 Variations of (a) normalized amplification rate and (b) normalized phase velocity with Strouhal number $f\theta/U$. Linear stability theory (from Monkewitz & Huerre 1982): — $R = 1$; --- $R = 0.5$; - - - $R \ll 1$. Experiments: \square $R = 1$ (Sato 1960); \circ $R = 1$ (Freyruth 1966); \times $R = 0.72$ (Miksad 1972); $\backslash \backslash \backslash$ $R = 1$ (Fiedler et al. 1981); \triangle $R = 0.31$ (Ho & Huang 1982); \blacksquare $R = 1$ (Drukba 1981).

gested by Gaster (1962). As a consequence, the $R \ll 1$ curve in Figure 2a simply represents the variations of the temporal amplification rate ω_i with wave number. We also note (Figure 2b) that, in contrast with temporal waves, spatial waves are *dispersive* below St_n and nondispersive above.

Experimental investigations of the initial instability region (Sato 1956, 1959, Browand 1966, Freyruth 1966, Miksad 1972, Mattingly & Chang 1974, Ho & Huang 1982) have been aimed at testing these predictions. In unforced mixing layers, the peak of the power spectrum immediately downstream of the trailing edge is found to occur at the calculated natural frequency f_n given by $St_0 = f_n \theta_0 / U = 0.032$. In most cases, however, the flow is forced (see Section 4.1) at a specific frequency f_f within the linearly unstable range. As an example, Figure 3 summarizes the response of a

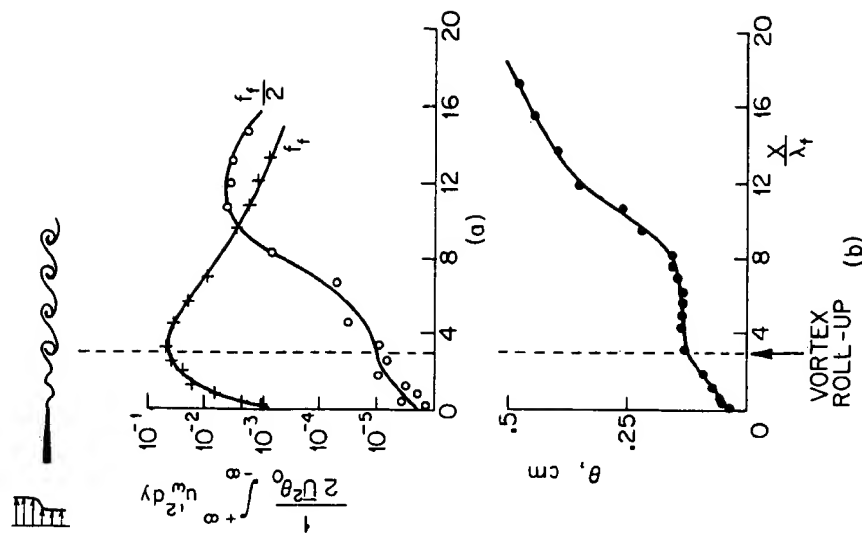


Figure 3 Evolution of (a) spectral components and (b) momentum thickness θ with downstream distance (from Ho & Huang 1982) $\frac{1}{2}f_n < f_f \leq f_n$; $R = 0.31$. u_0 is the narrow-band velocity fluctuation centered at $\omega = 2\pi f$. $\lambda_T = \lambda_T$.

mixing layer to an excitation f_θ close to f_n : the variations of the momentum thickness $\theta(x)$ and of the main frequency components are represented along the streamwise direction. Throughout Section 2, our discussion is restricted to the case $f_\theta = f_n$, which serves as an illustration. Measurements made at a given downstream station compare very favorably with the spatial stability properties of the local parallel velocity profile at the forcing Strouhal number $St_\theta = f\theta(x)/\bar{U}$. The studies of Michalke (1965a,b) and Freymuth (1966), in particular, have clearly demonstrated that only a spatial analysis could account for the observed cross-stream distributions of fluctuating velocity. The use of temporal theory to describe forced instability waves in mixing layers with $0 < R < 1$ is therefore not valid, as confirmed theoretically by Huerre & Monkewitz (1983). To conclude this brief account of the linear stability of parallel shear layers, we note that three-dimensional spatial instability waves have smaller spatial growth rates than their two-dimensional counterparts (Michalke 1969), a feature in agreement with the predominantly two-dimensional character of the instability-wave evolution (see Section 2.4).

It should be recognized, however, that the basic flow is really not parallel, its thickness θ increasing with downstream distance. Furthermore, the velocity profile $U(y; x)$ is wakelike immediately downstream of the plate trailing edge and gradually relaxes to a shear-layer distribution. Thus, to comply with the parallel-flow and small-disturbance assumptions, comparisons between measurements and calculations should be made one instability wavelength downstream of the trailing edge (see Section 4.2) and before any significant nonlinear interactions have occurred. The choice of a station satisfying both these criteria is, in practice, a subjective matter, but it directly influences the predicted value of f_n as given by $f_n(x)/\bar{U} = 0.032$.

To overcome this ambiguity, spatial linear instability theory has been extended to slowly diverging flows of small spreading rate $d\theta/dx = O(\mu)$, with $\mu \ll 1$ (Crighton & Gaster 1976, Plaschko 1979, Gaster et al. 1983). For instance, the parallel hyperbolic-tangent profile can be generalized to the self-similar family $U(y; X) = \bar{U}[1 + R \tanh\{y/2\theta(X)\}]$, where $X \equiv \mu x$ is a slow space scale characterizing the basic flow variations along x . The perturbation stream function then takes the form

$$\psi(x, y, t) \sim A(X)\phi(y; X) \exp\left\{i\left(\int_0^x \alpha(\mu\xi) d\xi - \omega t\right)\right\} + \text{c.c.} \quad (2)$$

The complex amplitude function $A(X)$, which accounts for nonparallel effects, satisfies a linear-evolution equation of the form $dA/dX + p(X)A = 0$, where $p(X)$ is obtained from the detailed calculations. The local stability properties $\alpha(X)\theta(X)$ and $\phi(y; X)/\theta(X)$ are still given by the parallel-flow

results of Figure 2 applied at the Strouhal number $St(X) = f\theta(X)/\bar{U}$. According to this theory, the total amplification rate becomes

$$\frac{1}{|\psi|} \frac{\partial |\psi|}{\partial x} = -\alpha_\ell(X) + \mu \left\{ \frac{1}{A(X)} \frac{d|A(X)|}{dX} + \frac{1}{|\phi(y; X)|} \frac{\partial |\phi(y; X)|}{\partial X} \right\}. \quad (3)$$

It depends not only on the downstream location X but also on the cross-stream coordinate y . One can also show that different flow quantities (pressure, velocity) are characterized by different amplification rates. A qualitative understanding of this approach can be achieved by neglecting temporarily the $O(\mu)$ correction terms of (3) and by reasoning from Figure 2a. For a given value of the frequency f , the local Strouhal number $St(X)$ increases with increasing thickness $\theta(X)$ downstream. As a result, the local amplification rate $-\alpha_\ell(X)$ ultimately decreases to zero at the location $St(X) = 0.079$, where the wave is locally neutral. Thus, unlike parallel flows, slowly diverging flows yield a maximum wave amplitude that occurs at the locally neutral downstream station. This is an approximate reasoning, which ignores the contributions of $O(\mu)$ in Equation (3). Surprisingly enough, this procedure has not yet been applied to the amplitude development in the initial instability region. It has, however, been used to model the evolution of large-scale structures in turbulent mixing layers (Section 2.4) and jets (Section 2.8).

2.2 Nonlinear Instability Regime

Beyond the region of exponential growth, Kelvin-Helmholtz instability waves evolve into a periodic array of compact spanwise vortices moving at the average velocity \bar{U} with a wavelength $\lambda_n = \bar{U}/f_n$. A striking illustration of this phenomenon is provided by the flow-visualization pictures of Roberts et al. (1982) shown in Figure 4. The recirculating regions, which contain most of the vorticity, are usually referred to as *Kelvin cat's eyes*. They are connected to each other via thin vorticity layers or *braids*. The main features of the roll-up process and the ensuing "climax state" have been confirmed by many two-dimensional numerical simulations of temporally evolving shear layers (Amsden & Harlow 1964, Christiansen 1973, Acton 1976, Patnaik et al. 1976, Aref & Siggia 1980, Riley & Metcalfe 1980, Corcos & Sherman 1983). Experimental observations indicate that the roll-up process is predominantly two-dimensional and is completed at the downstream station where the fundamental component at frequency f_n reaches its maximum amplitude (Figure 3a). It is accompanied by the generation of a subharmonic component $f_n/2$, which in the case of Figure 3 is three orders of magnitude below the fundamental. Thus, the linear stability theory of slowly diverging flows outlined in Section 2.1 may only approximately describe the equilibration of the fundamental f_n .

These experimental results do suggest, however, that a *weakly nonlinear* self-interaction approach neglecting the subharmonic $f_n/2$ might be appropriate to model the saturation mechanism of f_n . For general reviews of nonlinear stability theory in fluids, the reader may consult, among others, Stuart (1971), Stewartson (1974), and Maslowe (1981). The specific case of free shear layers is discussed in detail by Huerre (1984). The method takes into account the distortion of the basic flow as well as the generation of higher harmonics, but it relies on two strong assumptions: wave amplitudes are small, and amplification rates remain low during the entire wave development. Additionally, most investigations are restricted to an effectively parallel basic flow. Applications of this formulation to homogeneous free shear layers at large Reynolds number have been limited to nearly monochromatic waves in the vicinity of the neutral mode in Figure 2. The perturbation stream function is again written in terms of a complex amplitude $A(X, T)$ as

$$\psi(x, y, t) \sim \varepsilon A(X, T) \phi_1(y) \exp \left\{ \frac{i}{2\theta} (x - Ut) \right\} + \text{c.c.}, \quad (4)$$

where the subscript 1 denotes the neutral mode. The slow space and time scales X and T are suitably related to the small-amplitude parameter ε , and the nonlinear partial differential equation satisfied by $A(X, T)$ is obtained by making use of singular perturbation methods. The nature of the finite-amplitude motion is very sensitive to the structure of the critical layer, where the phase speed of the wave nearly matches the basic flow velocity. The role of the critical layer in shear flows has been reviewed by Stuart (1971), Stewartson (1981), and Huerre & Redekopp (1983). From a physical standpoint, this region contains the Kelvin cat's eyes of Figure 4. The balance between nonlinear effects and viscous dissipation in the layer can be characterized by a critical-layer Reynolds number $Re_{CL} \equiv Re \varepsilon^{3/2}$, based on its thickness $\varepsilon^{1/2}$ and a typical perturbation velocity ε . Within the classical theory (Lin 1955), $Re_{CL} \ll 1$, and the critical layer is viscous dominated. Benney & Bergeron (1969) and Davis (1969) were the first to investigate the structure of nonlinear critical layers for singular neutral modes in the limit $Re_{CL} = \infty$. These ideas have subsequently been extended by Haberman (1972) to arbitrary values of Re_{CL} , for which viscous and nonlinear phenomena coexist in the layer. The application of these concepts to marginally unstable waves of the form (4) leads to the following results: when $Re_{CL} \ll 1$, i.e. at low-amplitude levels, $A(X, T)$ satisfies a Stuart-Landau equation

$$\frac{dA}{dT} = \sigma A + b|A|^2 A, \quad (5)$$

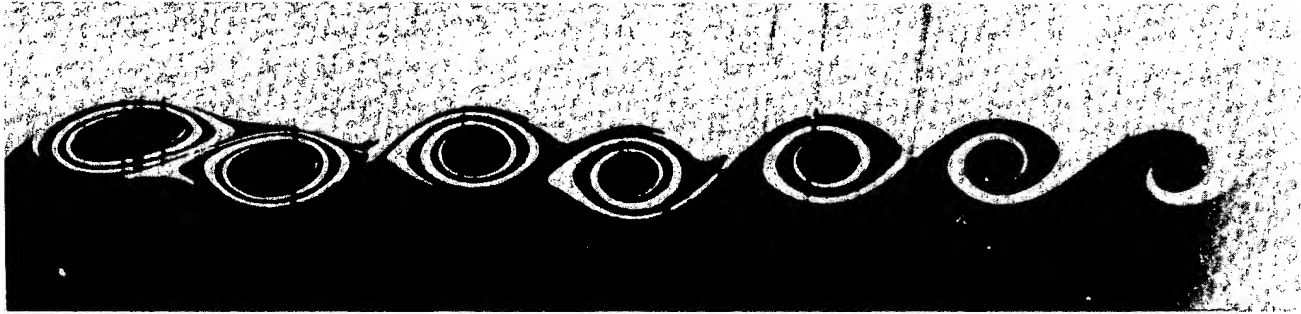


Figure 4 Roll-up of spanwise vortices (from Roberts et al. 1982). $f_1 = f_0$; $R < 1$.

where σ and b are complex constants. The cubic nonlinear term is destabilizing with $\text{Re } b > 0$ (Huerre 1980), a result that corrects the earlier study of Schade (1964). When $\text{Re } c \gg 1$, i.e. for large fluctuations levels, $A(X, T)$ satisfies an equation admitting finite-amplitude oscillatory solutions (Benney & Maslowe 1975). Finally, at finite values of $\text{Re } c$, spatial waves experience decreasing growth rates as they amplify, ultimately giving rise to algebraically growing waves at large distances (Huerre & Scott 1980). When viscous effects are important throughout the flow, namely, $\text{Re} = O(1)$, critical-layer considerations do not apply, and the amplitude A satisfies a Stuart-Landau equation (5) with a stabilizing ($\text{Re } b < 0$) cubic nonlinear term (Maslowe 1977a). The experimentally determined values of $\text{Re } c$, associated with the evolution of the fundamental do encompass these different regimes, as noted by Miksad (1972). But there is presently no theory available that would link them in a specific manner during the course of the amplitude development. Furthermore, all the above analytical studies unfortunately fail to describe the behavior of the Strouhal number St_α of the most amplified wave, which is well below the neutral Strouhal number. This conceptual difficulty can be partially remedied if one adds a stabilizing mechanism, such as a density gradient [see Stewartson (1981) for detailed references] or nearly solid boundaries (Huerre 1983). All linearly unstable waves then fall within reach of the weakly nonlinear formalism.

The introduction of such extraneous agents might well reproduce the main qualitative features of finite-amplitude waves in constant-density free shear layers. It is, however, doubtful that they will lead to quantitative predictions of the saturation level reached by the natural frequency f_n .

The emergence of a subharmonic component at half the frequency of the fundamental constitutes one of the most striking features in mixing-layer dynamics, as underscored by the experiments of Sato (1959), Wille (1963), Browand (1966), Freymuth (1966), Miksad (1972), and Ho & Huang (1982). When the forcing frequency f_f is sufficiently close to f_n , as in Figure 3, the subharmonic first reaches a plateau at the station where the fundamental equilibrates. This is followed further downstream by a sharp increase in the subharmonic amplification rate. The excitation of a large subharmonic disturbance can be accounted for by appealing to a *secondary subharmonic resonance* mechanism that arises when the fundamental f_n has reached its equilibrium level. In the simplest formulation (Lamb 1932), the row of vortex structures with wavelength λ_n is modeled by an array of point vortices. A straightforward linear analysis conducted in the comoving frame indicates that this configuration is most unstable to a disturbance of wavelength $2\lambda_n$. For a more satisfactory representation of the fundamental, we exploit the results of the qualitative reasoning outlined in Section 2.1: the natural component in its equilibrated state can be reasonably well

approximated by a neutral mode. Following Kelly (1967) and the recent discussion of Monkewitz (1982), one then examines the linear temporal instability of the *periodic* flow

$$U(y) + \epsilon \left\{ A \phi_1(y) \exp \left[\frac{i}{2\theta} (x - \bar{U}t) - i\beta \right] + c.c. \right\} \quad (5a)$$

to a subharmonic wave of the form

$$\psi(x, y, t) \sim \epsilon B(T) \phi_{1/2}(y) \exp \left[\frac{i}{4\theta} (x - \bar{U}t) + \omega_{1/2} t \right] + c.c. \quad (5b)$$

In the above relations, $\omega_{1/2}$ and $\phi_{1/2}(y)$ are, respectively, the subharmonic temporal amplification rate and eigenfunction, β is the phase difference between the two waves, and $T = \epsilon t$ is a slow time scale. Note that the subharmonic component (5b), close to the most amplified wave at $\alpha\theta = 0.22$, is the only wave that can reproduce itself via quadratic interactions with the periodic component: this subharmonic resonance mechanism requires that both waves have approximately the same phase speed \bar{U} . The amplitude function $B(T)$ is found to satisfy the equation

$$\frac{dB}{dT} = c \exp(-i\beta) A B^*, \quad (6a)$$

where c is a constant and B^* denotes the complex conjugate of B . The initial total subharmonic growth rate $\omega_{1/2} + \{d(\ln |B|)/dT\}$ is proportional to the periodic amplitude A and varies continuously from a maximum when both waves are in phase ($\beta = 0$) to a minimum when they are out of phase ($\beta = \pi$). These results are in qualitative agreement with numerical simulations (Patnaik et al. 1976, Riley & Metcalfe 1980) and with experimental observations (Zhang et al. 1983). To allow more detailed comparisons with experiments, future theoretical studies could be aimed at extending Kelly's analysis to a spatially developing subharmonic. Spatial waves are dispersive (Figure 2b) and, as emphasized by Petersen (1978), subharmonic resonance can only occur downstream of the station given by $f_n \theta(x)/2\bar{U} = St_n$, where both waves become approximately nondispersive. According to experiments (Figure 3a) the subharmonic growth rate does increase significantly around that same downstream location, as long as the flow is not forced at the subharmonic frequency itself. In more elaborate analyses of subharmonic resonance arising, for example, in stratified shear layers (Kelly 1968, Maslowe 1977b, Weissman 1979), the subharmonic B , governed by the amplitude equation (6a), is allowed to react back nonlinearly on the fundamental A through a second coupled equation

$$\frac{dA}{dT} = g B^2 \exp(i\beta). \quad (6b)$$

Applications of this approach to homogeneous free shear layers have been hampered by the fact that the linear growth rate $\omega_{11/2}$ cannot be regarded as small.

The periodic row of Kelvin cat's eyes (Figure 4) can be more satisfactorily modeled by the exact solution of the two-dimensional Euler equations discovered by Stuart (1967). In the present notation, the associated stream function is

$$\psi(x, y, t) = \frac{\bar{U}a}{4\pi} \left[y + 2R \ln \left\{ \cosh \left(\frac{2\pi y}{a} \right) - \rho \cos \left(\frac{2\pi}{a} (x - \bar{U}t) \right) \right\} \right], \quad (7)$$

where a is the distance between consecutive vortices and ρ is a vorticity concentration parameter: in the limit $\rho \rightarrow 1$, the row of point vortices is recovered, while an expansion of (7) for small ρ reduces to the periodically perturbed parallel tanh shear layer (5a). Browand & Weidman (1976) have compared their observations of fully rolled-up vortices with Stuart's solution (7) and found that the value $\rho = 0.25$ did provide a good overall fit of the measured vorticity distribution. A linear stability analysis recently conducted by Pierrehumbert & Widnall (1982) reveals that the periodic flow (7) is also most unstable to a disturbance of wavelength $2a$: the subharmonic temporal growth rate increases by approximately 20% as the basic vorticity field (7) changes from a parallel tanh shear layer ($\rho = 0$) to point vortices ($\rho = 1$).

2.3 Vortex-Interaction Mechanisms

It is now well established that the selective growth of the subharmonic component leads farther downstream to the *pairing* of neighboring vortices, as shown in the flow-visualization pictures of Figure 5. This remarkable interaction was first identified experimentally by Wille (1963) and subsequently documented by Freymuth (1966). But Winant & Browand (1974) were the first to demonstrate that successive mergings of vortices were indeed the primary process governing the streamwise growth of the mixing layer. Thus, the vorticity initially contained in the basic velocity profile is being constantly redistributed into larger and larger vortices, their wavelength and strength being doubled after each interaction. Equivalently, the passage frequency is halved after each coalescence (Kibens 1980), and the spectrum exhibits a shift toward lower frequencies with increasing distance from the trailing edge. Furthermore, the pairing location, defined by the cross-stream alignment of the two vortices, occurs at the downstream station where the subharmonic reaches a maximum (Ho & Huang 1982). In a jet with $R = 1$, amplification rates are high and this location is close to the station where the subharmonic first becomes nondispersive (Petersen 1978). Under controlled conditions (see Section 4.4

for a more detailed discussion), the first few pairings are accompanied by an approximate doubling in momentum thickness θ , the variations of θ between mergings being negligible. This feature is more readily observed in Figure 19b than in Figure 3b. But in both instances merging interactions eventually occur randomly along the downstream direction and give rise to a linear spreading rate. Beyond the initial roll-up phase, vortex interactions therefore govern in large part the rate of entrainment of surrounding fluid. However, this point of view remains the subject of debate: for instance, the recent digital image analysis of a flow-visualization film performed by Hernan & Jimenez (1982) indicates that most of the entrainment takes place during the growth stage of the large eddies and not during pairing. Finally, we emphasize that interactions between vortices are not necessarily limited to pairings, but may also involve three or more vortices as is further discussed in Section 4.4.

A quasi-analytical description of the vortex-merging mechanism is presently unavailable, and some of the future research effort could be directed at analyzing vortex amalgamations in terms of the spatial weakly nonlinear theories discussed in Section 2.2. However, as pointed out by Huerre (1980), there exist conceptual difficulties in retaining the small growth-rate assumption when the underlying medium is slowly diverging. Alternatively, one may abandon the weakly nonlinear formalism altogether and choose instead to use the *energy integral approach* of Stuart (1958). This has been the path taken by Liu and his coworkers. For instance, in a recent application of the method, Nikitopoulos (1982) and Nikitopoulos & Liu (1982) have considered the spatial nonlinear interaction of a fundamental

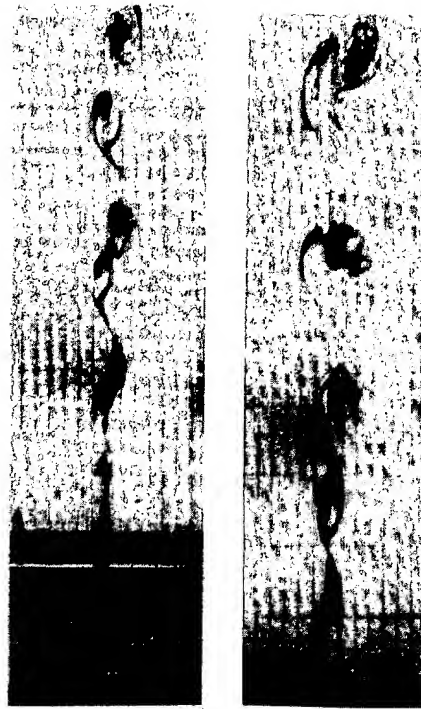


Figure 5 Vortex pairing (from Winant & Browand 1974) in an unforced mixing layer. $R = 0.48$.

wave of frequency f_n

$$\psi_A(x, y, t) = A(x)\phi_A\left(\frac{y}{\theta(x)}\right) \exp(-i\omega_n t - i\beta) + c.c., \quad (8a)$$

and its subharmonic

$$\psi_B(x, y, t) = B(x)\phi_B\left(\frac{y}{\theta(x)}\right) \exp\left\{-i\frac{\omega_n}{2}t\right\} + c.c., \quad (8b)$$

with a phase difference β between the two waves. The energy method usually requires "shape assumptions" to be made. In the present case the

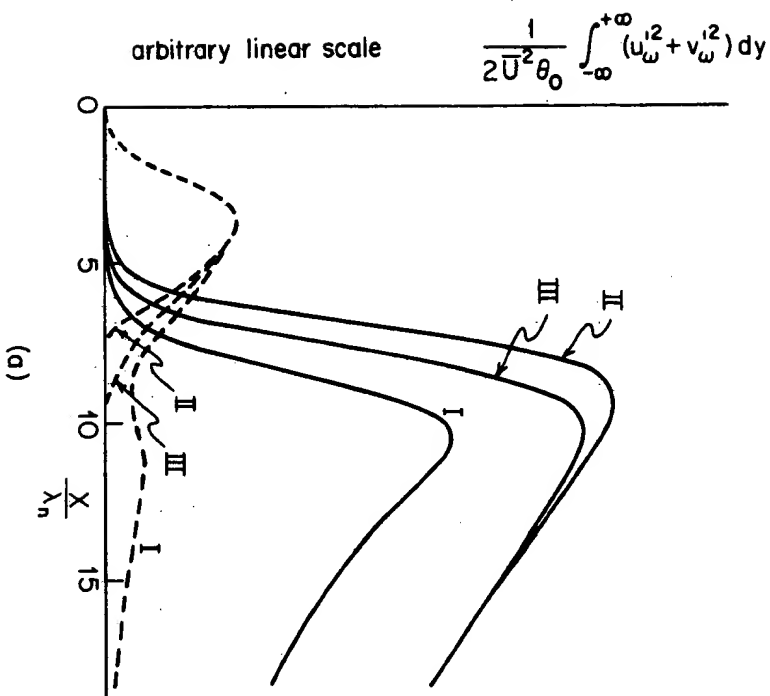
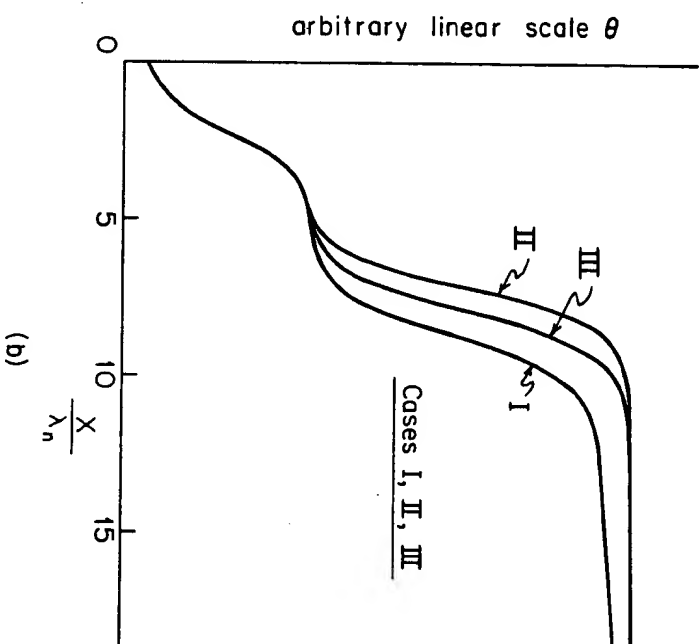
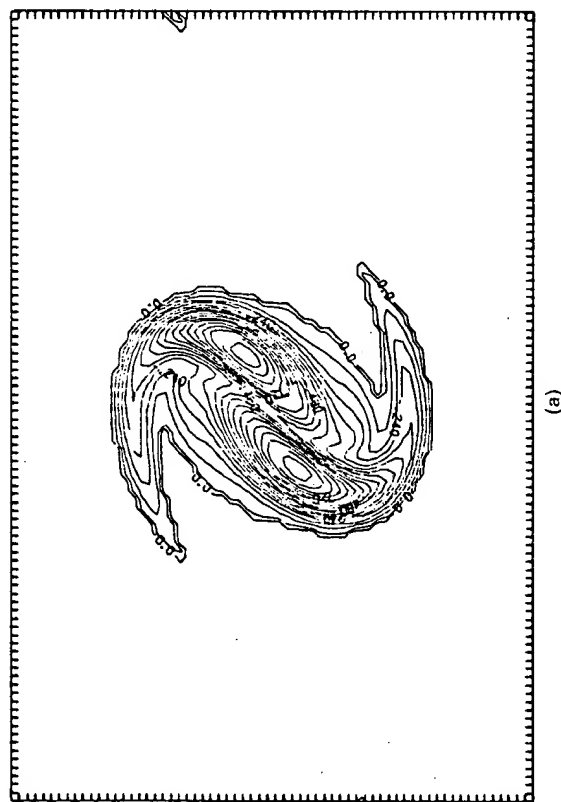


Figure 6 Evolution of (a) spectral components f_n (---) and $f_n/2$ (—) and (b) momentum thickness and downstream distance. Energy integral formulation of Nikitiopoulos (1982). At $x = 0$, the ratio of the initial amplitudes of $f_n/2$ and f_n is 2.6×10^{-2} . The initial phase difference between the two waves is (I) $\beta = \pi$, (II) $\beta = 0$. In case (III), the two waves are decoupled. $R = 0.31$.

mean flow is taken to be self-similar of the form $U(y, x) = U[1 + R \tanh\{y/2\theta(x)\}]$, and the cross-stream distribution functions $\phi_A(y/\theta)$ and $\phi_B(y/\theta)$ are assumed to be given by linear parallel stability theory applied to the mean-flow profile at the station x . The nonlinear evolution equations describing the development of the local thickness $\theta(x)$ and of the amplitudes $|A(x)|$ and $|B(x)|$ are then determined from the time-averaged integral kinetic-energy equations for the mean flow and the two wave components. Typical results are shown in Figure 6 for $\beta = 0$, $\beta = \pi$, and the decoupled case. As expected from Kelly's analysis, the larger the phase difference β , the smaller the subharmonic peak. It is also worth noting that artificially decoupling both waves by neglecting the interaction terms does not considerably alter the development of each wave. This feature may be viewed as indirect evidence that the interaction is indeed only weakly nonlinear. Furthermore, the evolution of the momentum thickness $\theta(x)$, as well as the streamwise location of the wave-amplitude maxima, is in qualitative agreement with the measurements of Figure 19. We note, however, that the energy-integral formulation cannot presently account for nonlinear variations in the phase of the two waves.



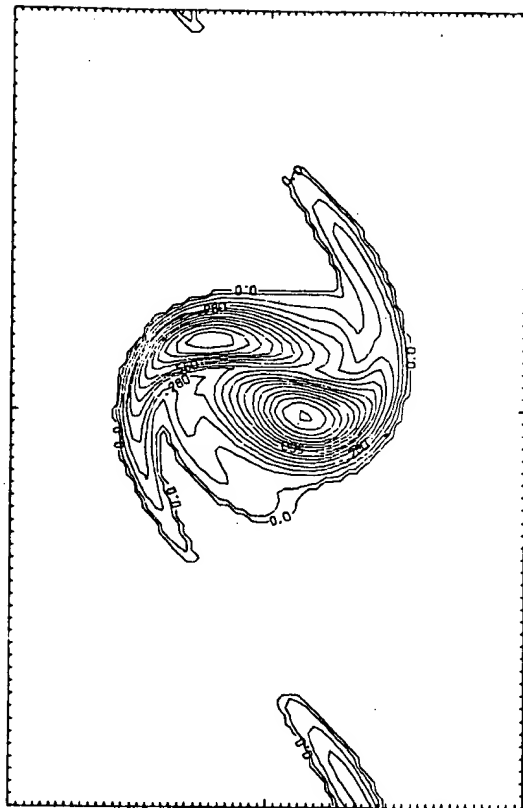
Direct computations of the vortex-pairing interaction in mixing layers have been conducted by Patnaik et al. (1976), Acton (1976), Ashurst (1979), Delcourt & Brown (1979), Riley & Metcalfe (1980), and Corcos & Sherman (1983). In all cases except Ashurst (1979), the flow is assumed to be spatially periodic and evolves in time: in qualitative agreement with the subharmonic resonance mechanism, the smaller the initial phase difference between the fundamental and subharmonic, the faster the coalescence of the two vortices. A pairing interaction is illustrated in Figure 7 for three values of the phase difference. In the limiting case where the two components are in antiphase ($\beta = \pi$), vortex pairing is actually suppressed and replaced by a *shredding interaction* (Patnaik et al. 1976), in which the cores of the fundamental are destroyed in the straining field of the subharmonic. A large strain rate is generated during the pairing interaction ($\beta = 0$), but the two vortices still maintain their identity for relatively large times and are unaffected by viscous diffusion even when $\Delta U/\nu$ is as low as 50 (Corcos & Sherman 1983). Note that flow-visualization techniques based on the detection of streak lines may well obscure the persistence of two distinct structures after pairing, as stressed by Williams & Hama (1980). The onset of small scales (Section 2.6) may also smear the identity of each vortex. The amalgamation mechanism can also be displayed numerically by appli-



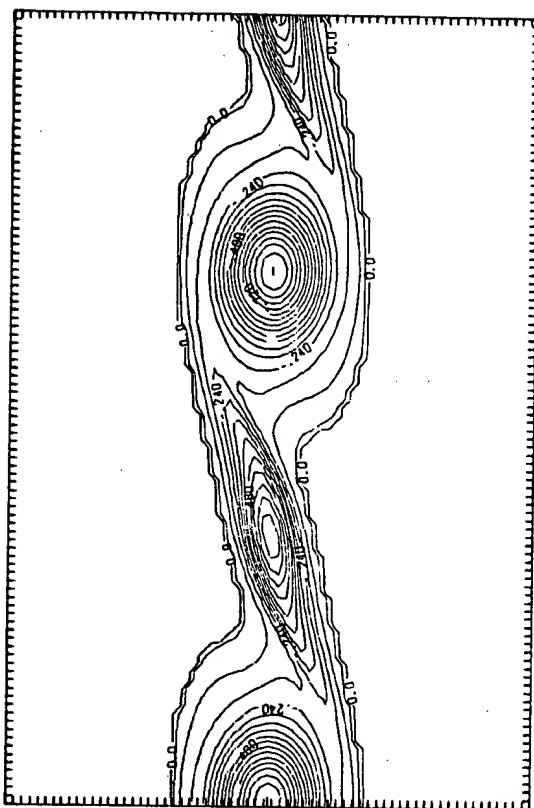
(a)

Figure 7 Interaction between f_a and $f_d/2$ in a temporally developing mixing layer, using numerical simulation of Riley & Metcalfe (1980). The initial phase difference is (a) $\beta = 0$, (b) $\beta = \pi/2$, and (c) $\beta = \pi$.

cation of suitable perturbations to two isolated corotating vortices of uniform vorticity (Overman & Zabusky 1982). The structures, which are solutions of the two-dimensional Euler equations, are observed to merge into a single rotating elliptical vortex with filamentary arms.



(b)



(c)

A different dynamical process, referred to as *tearing*, has been suggested by Moore & Saffman (1975) to explain the growth of mixing layers. The tearing mechanism has recently been linked by Pierrehumbert & Widnall (1981) to the energetic properties of a steady arrangement of streamwise periodic vortex structures with uniform vorticity, simultaneously discovered by Saffman & Szefto (1981). The basis for the tearing process relies on the fact that the ratio between the average vortex radius and the streamwise spacing is found to possess a maximum. Thus, as the vortex radius increases by "turbulent entrainment" of irrotational fluid, this ratio soon reaches its maximum allowable value. Any additional entrainment must then be accommodated by a corresponding increase in spacing through breakup of a vortex by the strain of its neighbors. Tearing, as noted by Corcos & Sherman (1983), implicitly assumes that the dynamical states of the flow are restricted to a particular set of steady configurations. It also presumes that the subharmonic instability has been somehow inhibited. None of these conditions are borne out by numerical simulations. Tearing is in fact rarely observed in experimental situations (Hernan & Jimenez 1982).

In the absence of satisfactory nonlinear theories, one presently relies on approximate analyses to describe the evolution of mixing layers and to establish the main scaling relationships. For instance, in the phenomenological model suggested by Ho (1981), the time-averaged momentum thickness $\theta(x)$ is assumed to increase by vortex pairings only, these events taking place at fixed downstream stations. By invoking experimental results such as those of Figure 19b, one considers $\theta(x)$ to be constant between pairings and to double instantaneously at pairing locations. Except for these obviously *nonlinear* effects, the unsteady response of the shear layer is supposed to be completely governed by linear stability theory. This means that between two consecutive pairings, say $j-1$ and j , the subharmonic of frequency $f_n/2^j$ is assumed to grow by a constant factor G at the maximum amplification rate pertaining to the thickness θ_{j-1} . At the j th pairing station, the thickness θ_{j-1} experiences a step increase to $\theta_j = 2\theta_{j-1}$ and the subharmonic reaches a maximum amplitude, its Strouhal number $f_j\theta_j/U$ becoming locally neutral. At that same location, a new $(j+1)$ th subharmonic is selectively amplified by its predecessor through the resonance mechanism discussed in Section 2.2. A new cycle is thereby initiated, in which the sudden change in momentum thickness has made the original subharmonic neutrally stable while the new subharmonic becomes the locally most amplified wave. From this drastically simplified model of mixing-layer dynamics, one can easily deduce that the streamwise spacing between pairings doubles along the flow. Furthermore, the spreading rate is

found to be

$$\frac{d\theta}{dx} = \frac{(-\alpha_1\theta)_{\max}}{\ln G} \approx 0.12 \frac{R}{\ln G}, \quad (9)$$

where use has been made of the approximate linear dependence of the maximum amplification rate on the velocity ratio R (see Section 2.1). It is worth emphasizing that changes in the mean flow induced by Reynolds stresses have to be *postulated* or *determined from experiments*. Important *nonlinear* effects, such as changes in subharmonic growth rates caused by resonance with the fundamental [Equations (6a) and (6b)] have also been deliberately ignored. It is nonetheless comforting to notice that linear stability theory does provide approximate scaling laws for what is essentially a nonlinear dynamical process: measured spreading rates as well as merging distances are found to be in good agreement with the model. For an alternate evolution model in terms of a row of point vortices, one may consult Jimenez (1980).

Instead of relying on a purely *deterministic* approach, as in the preceding analyses, one can seek to develop *statistical* models in which the turbulent mixing layer is assumed to be in statistical equilibrium. Such formulations, which might very well reproduce the average characteristics of the mixing layer after several pairing generations, have been suggested by Takaki & Kovasznyai (1978), Tam & Chen (1979), Aref & Siggia (1980), and Bernal (1981).

2.4 Large-Scale Structures

It should be made clear that interacting spanwise vortices are observed not only in the early laminar stages of the flow evolution but also farther downstream in the turbulent region, where they coexist with a fine-scale motion. For instance, large-scale structures can clearly be identified in the plan- and side-view shadowgraph pictures of Konrad (1976) shown in Figure 8. These features persist up to values of Re at least as high as 107 (Dimotakis & Brown 1976), well into the self-preserving region of classical theory. By making use of conditional-sampling techniques, it is possible, as shown by Browand & Weidman (1976) at lower Reynolds numbers, to extract from the turbulent flow ensemble-averaged states characterizing different phases of the coherent-structure evolution. From the results, one may infer that the large-scale vortices undergo sequential mergings in the same manner as their low-Reynolds-number counterparts. But pairing locations (in unforced shear layers) are now randomly distributed along the stream and give rise to a linear spreading rate.

The persistence of an organized quasi-two-dimensional motion in high-

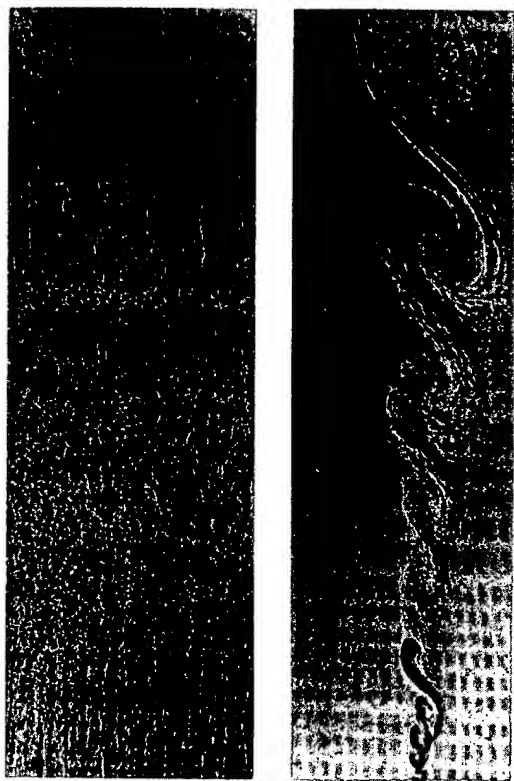


Figure 8 Coherent structures at high Reynolds number. Plan- and side-view shadowgraph pictures from Konrad (1976). $R = 0.45$.

Reynolds-number mixing layers has been the subject of some debate. Chandrsuda et al. (1978), in particular, have argued that a significant level of free-stream turbulence or the tripping of the boundary layers on the splitter plate will lead to the disappearance of the two-dimensional structures. The resulting flow field will then be three-dimensional, as in the classical description of turbulence. Two separate issues need to be examined: the persistence of large-scale structures on the one hand, and their quasi-two-dimensional character on the other. Regarding the first point, Wygnanski et al. (1979) have demonstrated experimentally that, even in the presence of strong random perturbations, primary large-scale vortices re-emerge from the three-dimensional background sufficiently far downstream (see also Browand & Ho 1983). These observations have been confirmed by the three-dimensional numerical simulations of Riley & Metcalfe (1980). Regarding the second point, we note that, according to Browand & Troutt (1980), the spanwise correlations asymptotically scale with the local thickness $\theta(x)$ in the limit of large x . By taking 20% average velocity correlation contours as a measure of eddy size, these authors find that the structures extend approximately $2\theta(x)$ along the stream and only $6\theta(x)$ along the span at $R = 0.8$. Nonetheless, instantaneously most structures span the entire apparatus, the low value of the averaged lateral scale resulting from the presence of spanwise deformations in the rolls.

Finally, we note that the simulations of Riley & Metcalfe (1980) do not reveal a strong lateral coherence: the large-scale structures are only approximately two-dimensional. The two- or three-dimensional character of the structures seems to subjectively depend on the eyes of the beholder!

From the above experimental observations, it is increasingly clear that the evolution of vortical structures in both laminar and turbulent shear layers is governed by essentially the same dynamical processes. It is therefore appealing to apply to turbulent shear layers the same hydrodynamic stability concepts that had originally been developed to describe the roll-up of laminar shear layers. Within this framework, the large-scale structures are then viewed as instability waves propagating on the pseudolaminar flow defined by the time-averaged velocity field. We stress that such a formalism is meaningful only if there exists a large disparity of length scales between the coherent structures and the fine-grained motion (see Figure 8), a requirement that is almost always satisfied in practical high-Reynolds-number flows. As shown by Fiedler et al. (1981), the quasi-parallel inviscid linear approximation (see Figure 2a) satisfactorily predicts the local amplification rate of large-scale structures generated by low-frequency forcing. The more refined slowly diverging flow analysis conducted by Gaster et al. (1983) has been very successful in reproducing the entire development of the wave amplitude. Even more remarkably, the measured cross-stream distribution of fluctuating velocity close to the maximum-amplitude location is adequately described by quasi-parallel linear theory. An example of comparison between theory and experiment is displayed in Figure 9. Natural extensions of these analyses to the description of pairing events have already been discussed. There remains to be considered, however, an aspect peculiar to turbulent mixing layers, namely the interaction between the large-scale coherent motion and the fine-scale turbulence. A recent review by Liu (1981) discusses this topic in the context of the energy-integral method outlined in Section 2.3. The large-scale structure is then modeled by the monochromatic instability wave (8a), and a suitable shape assumption is made regarding the nature of the fine-grained turbulence. To isolate the three components of the flow, namely, the mean flow, the large-scale flow, and the fine scales, the usual time average is supplemented by a conditional average as suggested by Hussain & Reynolds (1970). Amplitude equations for the three components are then derived from the respective integrated energy equations. Temporally evolving and spatially evolving mixing layers have been examined respectively by Liu & Merkin (1976) and Alper & Liu (1978). In more recent developments of the method (Gatski & Liu 1980), the combined motion of the mean and large-scale structure field is computed exactly from the time-

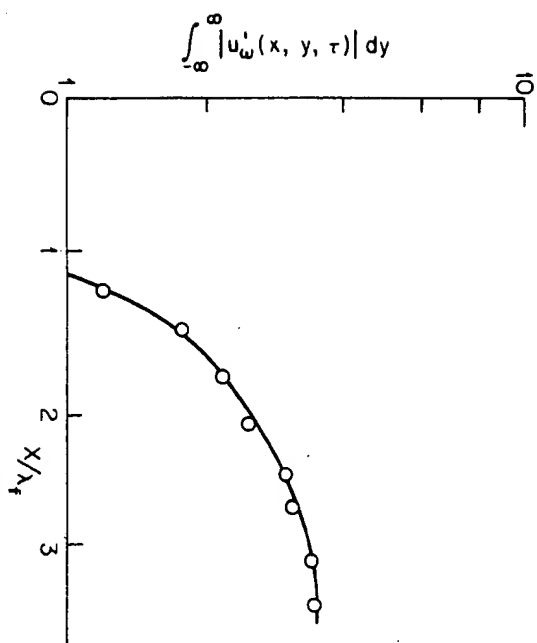


Figure 9 Evolution of forced component with downstream distance in a turbulent mixing layer (from Gaster et al. 1983). $f_1 \ll f_n$; $R = 0.43$. \circ experimental data; — slowly diverging theory.

averaged Navier-Stokes equations. In all instances, a high level of fine-scale motion is found to gradually suppress the large-scale structure and to slightly enhance the spreading rate, as intuitively expected from eddy-viscosity concepts. We emphasize that such a result does not signify the total demise of large scales at high turbulence levels: the thicker mixing layer can still support a most unstable Kelvin-Helmholtz wave of lower frequency, so that a new structure will necessarily be generated.

2.5 Three-Dimensional Structures

The occurrence of significant three-dimensional effects was first discovered by Miksad (1972). For a general overview of these phenomena, the reader is referred to Roshko (1981). The plan-view shadowgraph pictures of Figure 8 taken by Konrad (1976) clearly reveal the existence of periodically distributed streamwise streaks. The dye streaks are generated by secondary counterrotating streamwise vortices superposed on the primary rolls. The average spanwise spacing of the secondary structures increases with downstream distance and remains of the same order of magnitude as the local thickness. More importantly, the spanwise wavelength appears to be rather insensitive to irregularities in the boundary layers on the splitter plate: it is the result of a genuine internal instability. The frame-by-frame movie observations of Bernal (1981) have provided us with a detailed

knowledge of the morphology of the secondary motion, as shown in Figure 10. But it is not yet clear whether this system of mature sinuous vortices represents the finite-amplitude stage of the "wiggle" detected around the first pairing location by Breidenthal (1981).

Ironically, the earliest theoretical analysis of streamwise structures was conducted by Benney & Lin (1960) and Benney (1961) in a mixing layer at a time when experimental evidence of the existence of such structures was available only in boundary layers. The approach, which is by now familiar to the reader (Section 2.2), consists in studying the weakly nonlinear interactions between a two-dimensional wave of wave number α and a three-dimensional wave of *identical* streamwise wave number α and of spanwise wave number γ . A mean (x -independent) spanwise distortion of the basic $\tanh y$ profile is then nonlinearly generated, which takes the form of two horizontal layers of counterrotating streamwise vortices. Each layer is located on either side of the inflection point of the basic flow. If A and B denote the respective amplitudes of the two-dimensional and three-dimensional components, the spanwise wave number associated with the counterrotating eddies varies from γ to 2γ as the ratio $|B|/|A|$ increases from zero to infinity. It is unclear whether such a configuration can be detected experimentally. We note, however, that according to Stuart (1962) A and B are coupled via evolution equations of the form

$$\frac{dA}{dT} = a_A A + b_A |A|^2 A + c_A |B|^2 A + d_A A^* B^2, \quad (10a)$$

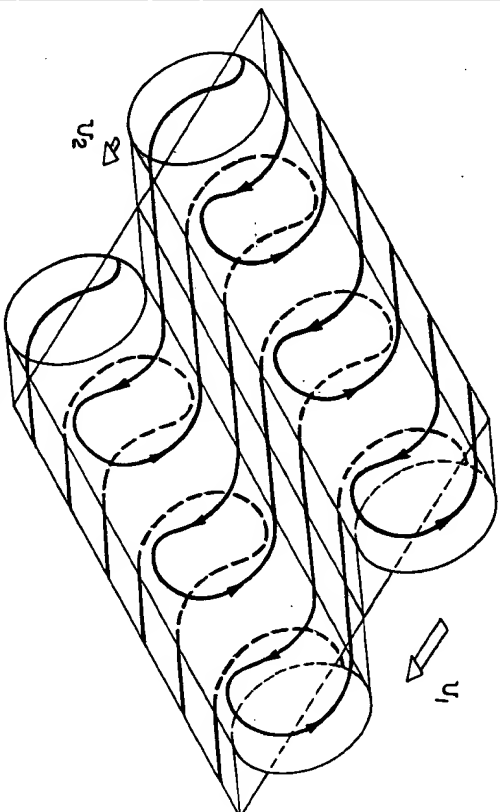


Figure 10 Morphology of secondary streamwise vortices (Bernal 1981).

$$\frac{dB}{dT} = \sigma_B B + b_B |A|^2 B + c_B |B|^2 B + d_B B^* A^2, \quad (10b)$$

when T is a suitably defined slow time scale. The complete streamwise structure is therefore determined by the superposition of the steady mean spanwise distortion and the finite-amplitude three-dimensional wave of amplitude $B(T)$. No detailed calculations of the constants arising in (10a) and (10b) have been performed for mixing-layer profiles, and it is presently not possible to say whether $B(T)$ reaches a steady equilibrium value or remains periodic for different phase relations between the two waves.

Another interaction model initially proposed by Craik (1971, 1980) in the context of boundary-layer transition is likely to be relevant to mixing layers. The formulation is essentially a three-dimensional generalization of the subharmonic evolution model described in Section 2.2. In contrast with the Benney-Lin model, the spanwise wave number is selected so that the three wave number pairs $(\alpha, 0)$, $(\alpha/2, \gamma)$ and $(\alpha/2, -\gamma)$ form a *resonant triad*, and the amplitudes $A(T)$ and $B(T)$ satisfy equations of the form (6a) and (6b). Note that the quadratic interaction terms present in those evolution equations are potentially more influential than the cubic interactions of the Benney-Lin model. The formalism of Craik has recently been shown to describe the development of Tollmien-Schlichting waves in a Blasius boundary-layer (Thomas & Saric 1981). Although the amplification rates of Kelvin-Helmholtz waves are much higher than those of Tollmien-Schlichting waves, these weakly nonlinear models could profitably be adapted to mixing layers.

Alternatively, following Pierrehumbert & Widnall (1982), the two-dimensional flow can be assumed to have equilibrated to a state described by an array of Stuart vortices (7) of wavelength a . The streamwise structures then arise through a secondary three-dimensional instability of this primary finite-amplitude flow. Two principal modes of instability can be distinguished. In the *translative mode*, the periodic base flow is linearly perturbed by a three-dimensional wave of streamwise wavelength a and spanwise wave number γ . The temporal growth rate σ varies with γ , as shown in Figure 11a. The primary spanwise vortex tubes are found to be deformed periodically along the span in the same way as in Figure 10. For a value of the concentration parameter $\rho = 0.25$, the growth rate reaches a maximum when the spanwise spacing is two thirds of the Kelvin-Helmholtz streamwise wavelength, a value in good agreement with the experimental observations of Bernal (1981). Furthermore, the growth-rate curve is relatively flat around its maximum. In the *helical-pairing mode*, the streamwise wavelength of the three-dimensional perturbations is increased to $2a$, and the growth rate is given by Figure 11b. When $\gamma = 0$, the

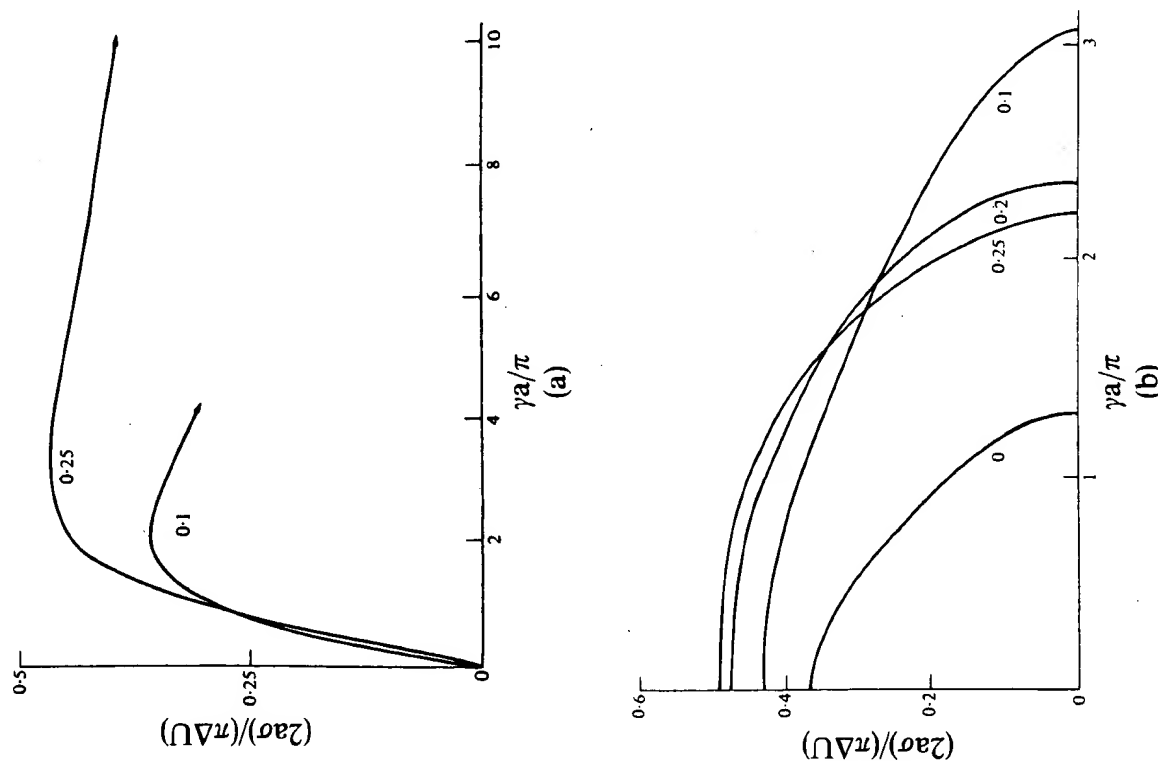


Figure 11 Scaled temporal growth rate $(2\sigma\sigma)/(\pi\Delta U)$ of (a) the translative instability and (b) the helical-pairing instability against nondimensional spanwise wave number $(\gamma a)/\pi$ (from Pierrehumbert & Widnall 1982). Each curve refers to a specific value of the concentration parameter ρ .

characteristics of the two-dimensional subharmonic instability are re-covered (Section 2.2). When $\gamma \neq 0$, pairings occur locally along the span, thereby resulting in the phase dislocations observed by Browand & Trout (1980). As noted by Pierrehumbert & Widnall (1982), the existence of a cutoff at a finite value of $\gamma\theta$ implies that helical pairing cannot completely destroy the two-dimensional structures: a given γ is necessarily stabilized further downstream as $\gamma\theta$ ultimately crosses the cutoff value. We emphasize that these two instabilities are not intrinsically different from the preceding nonlinear interaction models. In the limit $\rho \rightarrow 0$, Stuart vortices take the form of a periodically perturbed $\tanh \gamma$ mixing layer, and the translativ and helical-pairing instabilities reduce respectively to the Benney-Lin instability and the Craik resonant-triad instability.

The generation of three-dimensionality, as exemplified by Breidenthal's wiggle, can also be understood in terms of the fully nonlinear dynamics of vortex filaments. In a private communication, Browand has recently conjectured that *solitary waves* might be generated by the sidewall boundary layers and subsequently propagate in the form of helical twists along the axis of the spanwise structures. In the same spirit, Aref & Flinchem (1983) have examined numerically the evolution of solitary waves on a single vortex filament embedded in a $\tanh \gamma$ mixing layer. Under the combined effects of induction and of interaction with the continuous shear, solitary waves propagate along the vortex tube. Simultaneously, these initially localized entities are found to radiate families of waves. The resulting spanwise deformation of the tube is almost periodic and bears a striking qualitative similarity with the wiggle observed by Breidenthal (1981).

Three-dimensional numerical simulations have been performed by Couet (1979), Riley & Metcalfe (1980), Cain et al. (1981), and Brachet & Orszag (1983). The calculations are, by necessity, still relatively coarse but display the same qualitative features as laboratory experiments. Since current schemes are restricted to temporal mixing layers that are streamwise and spanwise periodic, the effects of the velocity ratio cannot be properly handled. In an interesting extension of classical linear stability theory, Corcos & Lin (1983) have examined in particular the three-dimensional linear stability of the time-developing spanwise vorticity distribution. The growth rate of the translativ instability is found to remain relatively constant during the roll-up phase. However, pairing of the spanwise rolls creates within the cores strong centers of energy transfer from the three-dimensional flow back to the two-dimensional motion. Thus, vortex mergings considerably delay the linear development of streamwise vortices. Furthermore, the Reynolds stresses induced by the three-dimensional disturbances have a negligible effect on the development of the two-dimensional dynamics. This result confirms the suggestion of Corcos (1979)

regarding the secondary nature of the streamwise structures when compared with the primary two-dimensional motion. The *fully nonlinear* calculations of Brachet & Orszag (1983) display essentially the same features, but the three-dimensional motion keeps increasing in magnitude. No steady or time-periodic regime is reached, a feature requiring further study.

Other aspects of the three-dimensional secondary flow can also be investigated by relying on approximate dynamical models. For instance, in the analysis of Lin (1981) and Lin & Corcos (1983), the streamwise vorticity is assumed to be preferentially generated in the braids by the strain field of two neighboring spanwise structures. All streamwise gradients are neglected. Thus, the finite-amplitude instability of vortex layers in the presence of a simple strain is obtained numerically from the two-dimensional equations of motion in the cross-stream y - z plane. It is found that, for a large class of spanwise-periodic initial conditions, such layers are pathologically unstable and collapse into discrete round vortices with a radius of the order of the Taylor microscale $\theta/Re^{1/2}$. A typical stage in the evolution of the counterrotating structures is shown in Figure 12. Calculated "dye patterns" in the y - z plane display a characteristic mushroom shape that is very similar to the cross-stream cuts visualized experimentally by Bernal (1981).

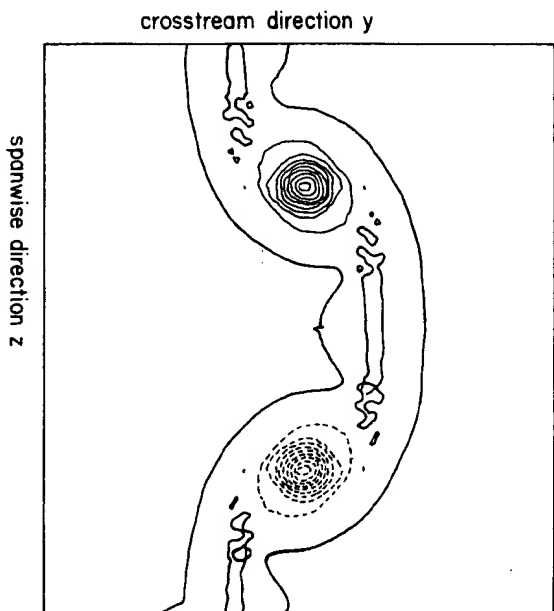


Figure 12 Calculated isovorticity contours of streamwise structures in a y - z plane cut through the braids (from Lin 1981). — positive vorticity; --- negative vorticity.

2.6 Small-Scale Transition

Initially laminar mixing layers eventually become turbulent in a process known as the small-scale transition. The shadowgraph pictures of Figure 8 suggest that the onset of small-scale eddies takes place within the cores of the large structures and is fairly localized along the stream.

Various criteria have been introduced to characterize quantitatively the location of the small-scale transition. Sato (1956, 1960), who initially investigated this question, chose as a measure the departure of the amplitude evolution from its initial exponential growth. Bradshaw (1966) selected instead the location where the peak turbulence level or peak Reynolds stress reaches a maximum. In chemically reacting flows, one can alternatively consider the "mixing transition" taking place at the streamwise station where the "mixedness" P/δ sharply increases (Konrad 1976, Breidenthal 1981). In this context, P/δ measures the amount of product formed in a shear layer initially carrying two distinct chemicals. Finally, the magnitude of the roll-off exponent in the velocity spectrum provides a convenient indicator of the small-scale onset in inert mixing layers (Jimenez et al. 1979, Huang & Ho 1983). The flow is considered to be turbulent when the exponent reaches the value $-5/3$. A clearly identifiable inertial subrange is then established, which extends over approximately one decade of frequency. These different transition criteria are compared in Figure 13. The discrete points all pertain to data taken in air, whereas the dashed curve represents a suitable average of mixedness measurements in liquids. Note that in terms of the normalized coordinate Rx/λ_n , the first three pairings take place on the average at 4, 8, and 16 units, respectively. The transition process is found to span a few λ_n 's. As observed by Bradshaw (1966), the peak turbulence level reaches a maximum at the first merging location and relaxes to its asymptotic value at the second merging location, precisely where the roll-off exponent becomes equal to $-5/3$. By changing the free-stream velocities U_1 and U_2 , Huang & Ho (1983) have deliberately varied the locations of pairing events and checked that transition in air occurs consistently during the second merging interaction at the normalized distance $Rx/\lambda_n = 8$. Furthermore, the data of Jimenez et al. (1979) follow the same scaling. We therefore speculate that the large strain rates that result from the coalescence of the orderly structures are responsible for the generation of small-scale eddies.

As expected on intuitive grounds, the local Reynolds number $Re = U\theta/\nu$ should be sufficiently large for the flow to sustain a fine-scale motion. Konrad (1976) initially suggested a value of the transition Reynolds number of the order of 5×10^3 . On the basis of a wider set of data taken in air, it appears, however, that the onset of small scales does not occur at a precise

value of Re , but rather in a range $3 \times 10^3 < Re < 5 \times 10^3$. For unknown reasons, typical transition Reynolds numbers in liquids are found to be much lower and fall in the range $750 < Re < 1700$ (Jimenez et al. 1979, Breidenthal 1981). Note also from Figure 13 that in liquids the fine-scale motion is established farther downstream around $Rx/\lambda_n = 12$. It should be emphasized that such a discrepancy between the case of liquids and gases cannot be attributed to differences in chemistry or to the choice of transition criterion: the normalized transition locations of liquid flow are found to be the same when determined by the mixedness method or the roll-off exponent method.

Theoretical analyses of the actual transition process are scarce. Energy-integral methods (Liu & Merkle 1976, Alper & Liu 1978, Gatski & Liu 1980) indicate a large energy transfer from the mean flow to the fine-scale motion as the large-scale disturbance reaches a maximum. However, these analyses are restricted to a single monochromatic large-scale instability wave. Lin & Corcos (1983) have proposed, instead, to relate the "mixing" transition to the dynamics of the three-dimensional structures in the braid region. Large increases in the mixed volume of a passive scalar are obtained

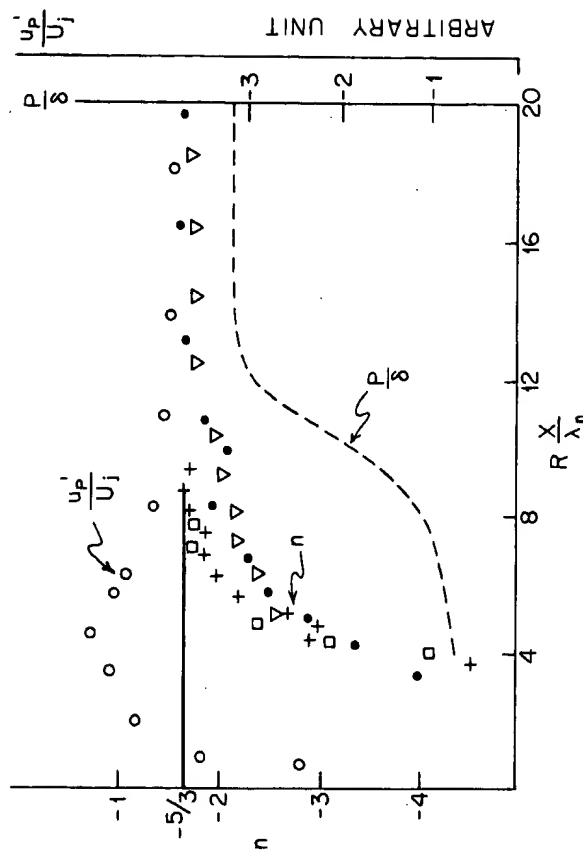


Figure 13 Experimental measures of small-scale transition as a function of streamwise distance U_1/U_2 : Peak turbulence level; \circ $R = 1$ (Bradshaw 1966); n : slope of the inertial subrange; \bullet $R = 1$ (Jimenez et al. 1979); \square $R = 0.45$; $+$ $R = 0.69$; ∇ $R = 1$ (Huang & Ho 1983). P/δ : "Mixedness" ratio; --- $0.14 < R < 0.45$ (Breidenthal 1981).

from the calculations, as streamwise vorticity layers collapse into round vortices, but the resulting scaling predictions are, according to the authors, inconclusive. We stress that no theoretical information is currently available regarding the expected contribution of pairing interactions to the small-scale transition. For a phenomenological model of the mixing process beyond the onset of small-scales, the reader is referred to Broadwell & Breidenthal (1982).

2.7 Preferred Mode in Jets

A fundamental difference between a jet and a mixing layer is the existence of a second length scale that is the diameter D of the axisymmetric nozzle or the height H of the two-dimensional nozzle. In both kinds of jets, a potential flow of velocity U_j issuing from the exit plane comes to an end about $5D$ (or $3H$) downstream, and axisymmetric (or two-dimensional) orderly structures can clearly be identified in the shear layer surrounding the potential core. As in the simple mixing layer, the large-scale vortices experience successive amalgamations that eventually lead to small-scale transition. Beyond the tip of the potential core, these vortical features are more difficult to identify, and their morphology is still unknown (Tso et al. 1981).

The forcing experiments of Crow & Champagne (1971) have indicated that the response of a circular jet to a monochromatic excitation, measured as the gain or ratio of the peak amplitude to initial amplitude of the wave along the jet axis, reaches a maximum for a Strouhal number $f_p D/U_j \approx 0.3$. The passage frequency of the vortical structures at the end of the potential core is given by f_p and the corresponding fluctuating flow field is commonly referred to as the *preferred mode* or *jet-column mode*. It should be distinguished from the *shear-layer mode* of higher frequency f_n associated with the most amplified wave of the initial velocity profile. In qualitative agreement with observations, the slowly diverging linear stability analysis of Crighton & Gaster (1976) does single out a mode with a maximum gain in pressure amplitude at a Strouhal number of $f_p D/U_j \approx 0.4$. Note that this theory is implicitly nonlinear, since the measured mean-velocity profiles used in the calculations already include the effects of Reynolds stresses.

The preferred Strouhal number in circular jets is found to vary between 0.25 and 0.5 in different experiments. This scatter may be due to data-processing techniques (Petersen 1978) or to the nature of the residual noise present in individual facilities (Gutmark & Ho 1983). Recent experimental data, taken under very clean conditions and presumably less affected by background noise, have shed some light on this question. According to the results of Kibens (1981) displayed in Figure 14, the preferred Strouhal number $f_p D/U_j$ is approximately proportional at low jet velocities, i.e. low

$D/(2\theta_0)$, to the Strouhal number $f_n \theta/U$ of the shear-layer mode. For higher flow rates, however, $f_p D/U_j$ remains constant and equal to 0.44, the change of scaling behavior occurring at $D/2\theta_0 = 120$. Similar conclusions have been reached by Drubka (1981) in the range $115 < D/(2\theta_0) < 175$. Ho & Hsiao (1983) have further confirmed the validity of Kibens' result in the case of plane jets, provided that the nozzle radius $D/2$ is replaced by the height of the slit H . Thus, below a critical value of the ratio $D/(2\theta_0)$, or H/θ_0 , the vortex passage frequency f_p at the end of the potential core scales with the initial shear-layer momentum thickness θ_0 . It is simply a fraction of f_n as dictated by the sequence of amalgamations taking place in the mixing layer (see Figure 23). Above the critical value of the length scale ratio, f_p scales with the characteristic size of the nozzle, although the initial passage frequency f_n still decreases to f_p via the same number of vortex mergings. There is presently no satisfactory explanation of this Strouhal-number locking. Ho & Hsiao (1983) have conjectured that the critical value is linked to the appearance of the small-scale transition in the mixing layer. The

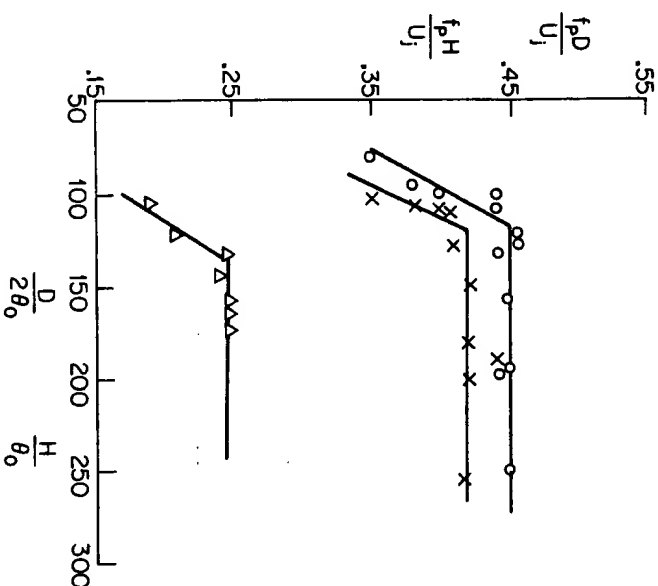


Figure 14 Strouhal number of preferred mode in jets versus characteristic length scale ratio. Axisymmetric jets: \circ Kibens (1981); \times Drubka (1981). Two-dimensional jets: \triangle Ho & Hsiao (1983).

corresponding increase in turbulent diffusion would then lead to a less concentrated vorticity distribution in the primary structures. According to the results of Pierrehumbert & Widnall (1982) shown in Figure 11*b*, this could in turn reduce the growth rate of the pairing instability and keep the number of mergings constant.

2.8 Symmetry-Breaking Modes in Jets

Experiments in circular geometries with low background noise indicate that the coherent vortex rings generated close to the nozzle exit are initially axisymmetric, but that the energy content of helical disturbances increases significantly farther downstream (Browand & Laufer 1975; Drubka 1981). As a support for these observations, the spatial parallel-flow calculations of Michalke (1971) have shown that the axisymmetric mode is indeed slightly more unstable than any of the spinning modes, as long as the basic velocity distribution possesses a potential core. In contrast, the "fully-developed" bell-shape profiles prevailing downstream of the potential core can only support helical instability waves (Batchelor & Gill 1962). Furthermore, according to linear slowly diverging flow theory extended to spinning modes (Plaschko 1979), the axisymmetric mode suffers a larger total gain than helical modes at the higher Strouhal numbers that dominate the flow near the nozzle lip. At lower Strouhal numbers, i.e. near the end of the potential core, the situation is reversed, and the first helical mode achieves the largest maximum amplitude (see also Mattingly & Chang 1974). We also note that the disintegration of the originally axisymmetric structures can also be attractively explained by the azimuthal instabilities taking place on mature vortex rings (Widnall et al. 1974).

It is generally observed (Fuchs & Michel 1977; Drubka 1981; Cohen et al. 1983) that helical components appear closer to the nozzle exit at higher jet velocities. We can only speculate that changes in the characteristics of the background noise or possibly a stronger feedback from the downstream flow are responsible for this peculiar phenomenon.

Finally, the development of the sinuous mode and varicose mode in two-dimensional jets is found to exhibit features that are similar to the evolution of axisymmetric and helical modes in circular jets, as observed by Sato (1960) and Cervantes de Gortari & Goldschmidt (1981).

3. INFLUENCE OF OPERATIONAL PARAMETERS

In this section, we specifically examine how the operational parameters, namely, the velocity ratio, the Reynolds number, and the initial turbulent or laminar state of the boundary layer, may influence the dynamics of free shear layers.

3.1 Velocity Ratio

A mixing layer is characterized by two distinct velocity scales: the velocity difference ΔU provides a measure of the growth rate of the orderly structures, and the average velocity \bar{U} is approximately equal to their convection velocity. For mixing layers that evolve *in time* from some initial state, such as those usually studied in direct numerical simulations, the convection velocity can be rigorously scaled out by a Galilean transformation. A similar relationship is not available for forced shear layers that develop *spatially* in response to excitations applied at the trailing edge, i.e. at a *fixed* streamwise location. Thus, the velocity ratio enters the dynamics in a nontrivial manner. Only in the limit of small R can the temporal and spatial versions of the flow be related by a Galilean transformation. As noted in Section 2.1, the effect of R is particularly apparent in the linear stability characteristics of mixing layers (Monkewitz & Huerre 1982) and jets (Michalke & Hermann 1982).

An approximate scaling law governing the variations of mixing-layer spreading rate $d\theta/dx$ with velocity ratio R is easily obtained from the following heuristic argument (Brown & Roshko 1974). In a time Δt , a spanwise vortical structure travels a distance $x = \bar{U}\Delta t$, and its cross-stream length scale, proportional to ΔU , increases by an amount $\Delta U\Delta t$. The spreading rate $d\theta/dx$ is therefore linearly related to the velocity ratio $R = \Delta U/(2\bar{U})$, as already obtained from the phenomenological model of Ho (1981) outlined in Section 2.3. The experimental data plotted in Figure 15 do follow this approximate scaling law. To leading order, the velocity ratio R is seen to act on the dynamics of the spanwise rolls as a simple stretching parameter. The lower R , the more extended the flow development. Accordingly, whenever it is meaningful, the streamwise coordinate in the figures has been rescaled in the form Rx/λ . Finally, we note that very little is known regarding the dependence of the geometry of the streamwise vortices on R . However, as discussed in Section 2.6, the downstream location for the onset of small scales is proportional to $1/R$.

3.2 Reynolds Number

Although the evolution of the orderly structures is essentially inviscid, viscous effects play an important role both in determining the laminar or turbulent state of the splitter-plate boundary layers and in the transition to small scales in the mixing layer.

For sufficiently low free-stream velocities, the boundary layers at the trailing edge are laminar, their momentum thickness varying as $U_1^{-1/2}$ and $U_2^{-1/2}$, respectively. Thus, on account of viscous diffusion, the initial thickness θ_0 is roughly proportional to $\bar{U}^{-1/2}$ for reasonably large values of

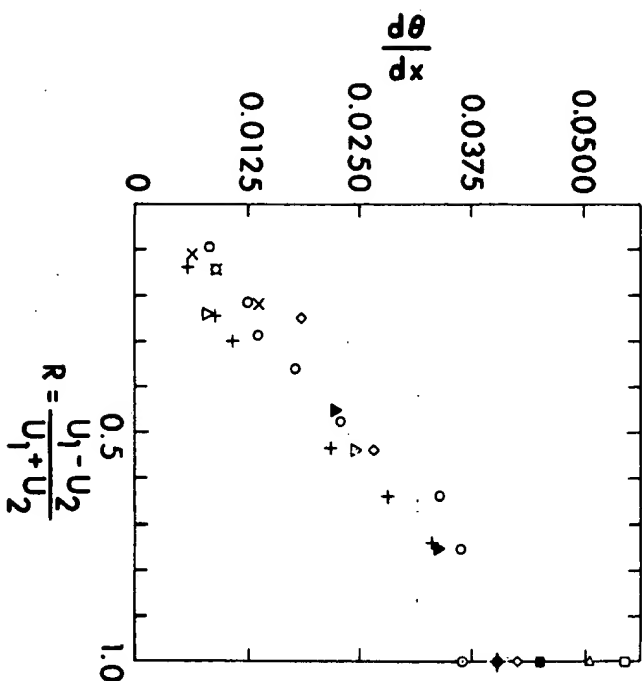


Figure 15 Dependence of mixing-layer spreading rate $d\theta/dx$ on velocity ratio R (from Brown & Rosliko 1974); ● Liepmann & Laufer (1947); ○ Reichardt (1942); ○ Miles & Shih (1968); ◇ Mills (1968); × Pui (1969); □ Wygnanski & Fiedler (1970); + Spencer & Jones (1971); ▽ Sunyach (1971); △ Yule (1972); ■ Patel (1973); ▲ Brown & Rosliko (1974).

R , and the natural frequency f_n given by $f_n \theta_0 / U = 0.032$, scales with $\bar{U}^{3/2}$. Correspondingly, the initial Reynolds number $Re_0 = \bar{U} \theta_0 / \nu$ varies as $\bar{U}^{1/2}$. As the average velocity \bar{U} exceeds a critical value, the boundary layers become turbulent and lead to a turbulent mixing layer immediately downstream of the trailing edge (Section 3.3). It is known that flat-plate boundary layers in a zero pressure gradient undergo transition at a Reynolds number of the order of 10^5 (Tani 1969), but the precise value depends on many factors, such as the level of free-stream turbulence, the design of the contraction leading to the test section, etc. Furthermore, relatively few experimental data are available for the case of natural (untipped) transition in the presence of a pressure gradient. According to Browand (1983, private communication), the boundary layer at the trailing edge of the splitter plate also reaches transition around $Re_0 \approx 10^5$. Above this value, the initial shear layer becomes turbulent and, for presently unexplained reasons, the most amplified Strouhal number St_n changes from a value of 0.032 for a laminar flow to 0.044–0.048 (Hussain & Zaman 1981, Drubka 1981).

Linear stability calculations based on the Orr-Sommerfeld equation (Betchov & Szewczyk 1963, Morris 1976) have indicated that shear layers are not completely stabilized by viscous dissipation, even at low values of Re . Indeed, calculated amplification rates are very much insensitive to variations in Reynolds number, provided $Re > 50$. In most experiments, the initial Reynolds number Re_0 is equal to 100 or more, and vortex roll-up as well as merging interactions are found not to be directly affected by viscosity, provided the boundary layers are laminar. By the same token, increasing the Reynolds number by two orders of magnitude does not significantly alter the downstream variation of the momentum thickness (Browand & Ho 1983).

In contrast, the organized three-dimensional secondary motion and the small-scale transition do involve significant Reynolds-number effects (Sections 2.5, 2.6). The average spacing between streamwise vortices scales with the local thickness $\theta(x)$, as dictated by inviscid stability considerations but, according to the model proposed by Lin & Corcos (1983), the vortex radius should be of the order of the Taylor microscale $\theta/Re^{1/2}$. No detailed measurements have yet been undertaken, which would confirm the latter prediction. Small-scale transition is also dependent on local Reynolds number: $Re(x)$ needs to be of the order of 3×10^3 (Huang & Ho 1983) or more to sustain a well-established inertial subrange; otherwise, viscous dissipation will not permit the establishment of fine-scale motion.

3.3 Laminar-Turbulent Boundary Layer

The downstream development of shear layers is known to be very sensitive to the laminar or turbulent state of the boundary layers on the splitter plate (Bradshaw 1966, Wygnanski & Fiedler 1970). A simple measure of this sensitivity is provided by the variations of mixing-layer thickness $\theta(x)$ (Figure 16) and peak turbulence level (Figure 17) with streamwise distance.

In almost all experiments, the flow is made turbulent by tripping the boundary layer, and the initial Reynolds number Re_0 is usually of the order of 10^3 or less ($Re_0 = 240$ – 1000 in Oster et al. 1977, $Re_0 = 110$ – 450 in Hussain & Zedan 1978, $Re_0 = 210$ – 450 in Drubka 1981). As seen in Figure 16, the resulting turbulent shear layer is characterized by two distinct spreading rates, the shift from the initial value to the final higher value taking place at a normalized streamwise distance $Rx/\lambda_n \approx 10$. Nonetheless, in the same facility the asymptotic spreading rate of turbulent mixing layers ($R \neq 1$) is usually found to be much lower than the corresponding laminar value (Oster et al. 1977, Browand & Latigo 1979). The situation is more confusing in jets ($R = 1$): spreading rates are either enhanced (Batt et al. 1970, Oster et al. 1977) in a half-jet or reduced (Drubka 1981) in a circular jet by tripping the boundary layer.

In a mixing layer with laminar upstream conditions, the peak turbulence

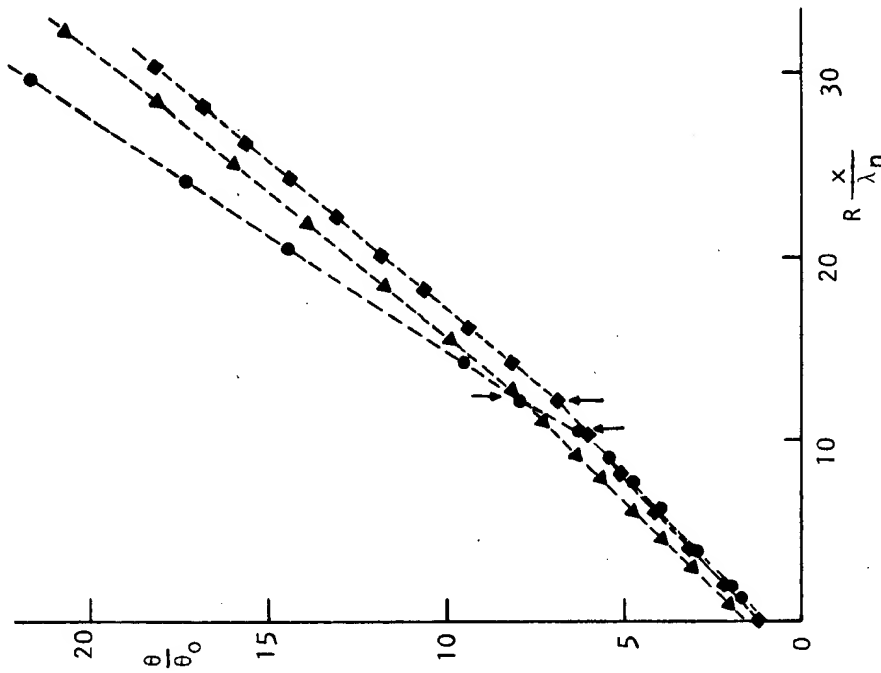


Figure 16 Variation of momentum thickness with downstream distance in the case of a turbulent boundary layer. ● $R = 1$, Foss (1977); ▲ $R = 1$, Hussain & Zedan (1978); ■ $R = 0.7$, Browand & Latigo (1979).

intensity $u'_p/\Delta U$ or u'_p/U_j increases along x (see Figure 17) and reaches a maximum around the first merging station. As a result of the small-scale transition, it eventually settles farther downstream to an asymptotic value characteristic of "fully developed" turbulent mixing layers. The peak fluctuation intensity of a turbulent boundary layer at $x = 0$ relaxes monotonically to approximately the same constant value as in the laminar boundary-layer case, but there is no overshoot (Bradshaw 1966, Hussain & Zedan 1978, Browand & Latigo 1979, Drubka 1981). It is interesting to note that for both laminar and turbulent initial conditions the asymptotic turbulence level is reached at the same streamwise station $Rx/\lambda_n \approx 10$,

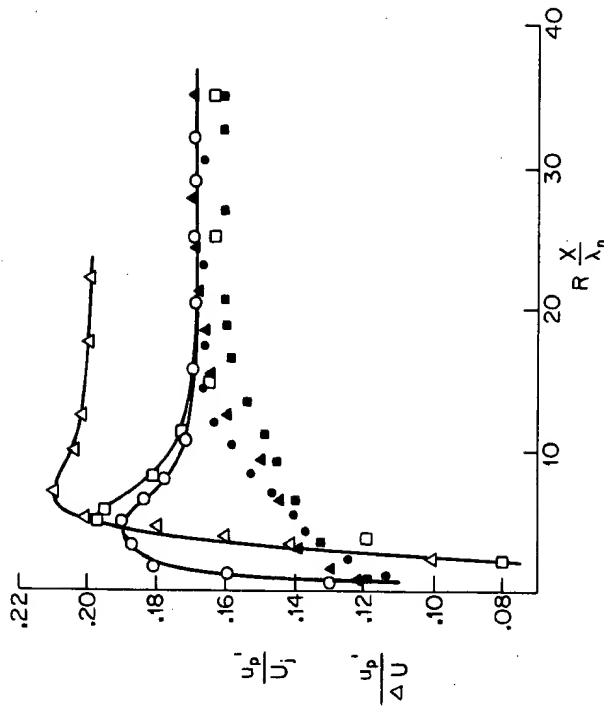


Figure 17 Peak turbulence level versus downstream distance in the case of a laminar or turbulent boundary layer. ○ $R = 1$, laminar boundary layer, ● turbulent boundary layer, arbitrary units (Bradshaw 1966); ▲ $R = 1$, turbulent boundary layer (Hussain & Zedan 1978); □ $R = 0.7$, laminar boundary layer, ■ $R = 0.7$, turbulent boundary layer (Browand & Latigo 1979); △ $R = 1$, laminar boundary layer (Jimenez et al. 1979).

which also coincides approximately with the breaking point in the spreading rates of Figure 16. Note also that in both cases the local Reynolds number at that same station is about 2.7×10^3 ($Re = 3.7 \times 10^3$ in Foss 1977, $Re = 1.6-3.1 \times 10^3$ in Hussain & Zedan 1978, $Re = 6.8 \times 10^3$ in Browand & Latigo 1979) and of the same order of magnitude as the small-scale transition Reynolds number for an initially laminar shear layer (Section 2.6).

Thus, it appears that laminar and turbulent boundary layers take the same distance downstream of the trailing edge to reach a self-similar state characteristic of turbulent shear layers (compare Figures 13 and 17). However, since the spreading rates differ, the concept of a single universal asymptotic state does not seem to apply. As an additional cautionary statement, we add that the measurements and even trends of several experiments do not agree with each other. The root cause of such discrepancies might very well lie in the long-lasting effect of the particular initial conditions prevailing in different facilities, as is discussed in Section 4.7.

4. SENSITIVITY TO ARTIFICIAL EXCITATION

4.1 Methods of Excitation

According to Sections 2.3 and 2.5, sequential mergings of coherent spanwise rolls are believed to be responsible for most of the entrainment into the shear layer and for the occurrence of small-scale transition. Hence, in order to manipulate most effectively the development of the flow, imposed excitations should as a first requirement be *spatially coherent* along the span.

Forcing is usually applied in two ways: mechanically with a ribbon or an oscillating flap, or acoustically by means of loudspeakers. In experiments conducted at low Mach numbers, the mismatch between the speed of sound and the phase speed of instability waves is large, and the only manner in which acoustic waves can effectively feed energy into the fluctuating vorticity field is at the trailing edge (Morkovin & Paranjape 1971). In high-speed flows, however, the shear layer can directly be excited acoustically without the mediation of a splitter plate (Tam 1978). Mechanical forcing acts in a more straightforward way: a large portion of the input energy is converted into instability waves.

The acoustic excitation frequencies commonly used in experiments are such that the acoustic wavelength is much larger than the typical spanwise extent of the test section. In other words, the criterion of spatial coherence is easily met in the acoustic forcing technique. Furthermore, loudspeakers can cover a wide range of frequencies from 20 Hz to 20 kHz. In contrast, the use of vibrating ribbons is limited to frequencies of the order of 100 Hz. In many experiments, sinusoidal acoustic excitations are therefore often preferred as a means of forcing.

4.2 Trailing-Edge Receptivity

Under this name, we include the class of mechanisms that at low Mach numbers govern the conversion of acoustic excitations into vortical instability waves at the sharp trailing edge of the splitter plate (Morkovin & Paranjape 1971). Since these issues have recently been reviewed by Crighton (1981) in the context of aeroacoustics (see also the forthcoming survey by the same author in Volume 17 of this series), the present discussion need not be exhaustive.

The rate at which vorticity is shed from the splitter plate, i.e. the magnitude of the initial instability wave in the shear layer, is primarily determined mathematically by *postulating* that an *unsteady Kutta condition* applies at the trailing edge ($x = 0$). According to this condition, a vortical instability wave should be added to the forced acoustic field of such magnitude as to keep pressure and velocity bounded at the trailing edge.

Theoretical investigations of this question have been limited to low Strouhal numbers $St_0 = f\theta_0/U \ll 1$, in which case the instability wavelength is much larger than the shear-layer thickness and the mean flow can be approximated by a vortex sheet. The first linear inviscid study was conducted by Orszag & Crow (1970) for the case of the eigenfunction only, i.e. without forcing. Daniels (1978) has performed a detailed asymptotic analysis of the same eigenfunction problem, which indicates that the Kutta condition is indeed applicable to unsteady trailing-edge flows. Under very specific scaling assumptions, the multilayered inner viscous flow derived by Daniels in the immediate vicinity of the trailing edge is found to match with the inviscid solution of Orszag & Crow that satisfies the full Kutta condition. As emphasized by Crighton (1981), the experiments of Bechert &

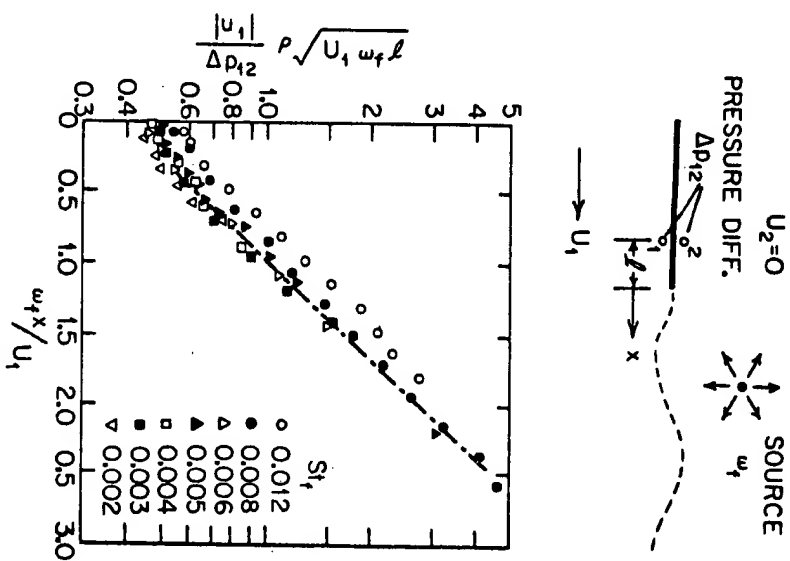


Figure 18 Mixing-layer receptivity close to the trailing edge: instability-wave evolutions with downstream distance (from Bechert 1983). The mixing layer is forced acoustically at a frequency $\omega_t = 2\pi f$. $R = 1$. — — — Semi-infinite vortex sheet analysis. Points refer to experiments.

Pfizenmaier (1975) have confirmed that the measured shape of the dividing streamline issuing from the trailing edge is consistent both with the Kutta condition and with Daniel's analysis. The unsteady flow leaves the splitter plate tangentially, so that the pressure gradient on the deflected streamline approaches zero at the trailing edge. More specifically, the dividing streamline has a shape of the form $y \sim x^{3/2}$ in the inviscid region and $y \sim x^{1/3}$ in the inner viscous region when only one stream is present ($R = 1$).

The efficiency of the trailing-edge conversion mechanism has been studied extensively in connection with the jet-noise problem. Bechert (1980), among others, has investigated the coupling effects arising between an incident acoustic wave traveling down a circular nozzle and instability waves on the jet shear layers. At low Helmholtz numbers, $f_1 D/a_0 \ll 1$ (a_0 is the speed of sound), the acoustic power radiated into the far-field was measured to be as much as 20 db below the net acoustic power transmitted down the nozzle. Since no significant reflected waves were detectable, most of the incident energy at low Helmholtz numbers was converted into vortical waves. Furthermore, a low-Mach-number cylindrical vortex-sheet model predicted very satisfactorily the total attenuation experienced by acoustic waves as a result of the conversion process.

Bechert (1983) has recently examined theoretically and experimentally the receptivity of a semi-infinite vortex sheet to a sound excitation of frequency f_1 (see also Bechert & Michel 1975). An elegant analytical model, valid for small amplitudes, small Strouhal number, and small Mach number, is applied to the flow configuration shown in Figure 18. The spatially growing instability waves propagating along the vortex sheet are found to be influenced by the trailing edge in a near-field region of the order of one hydrodynamic wavelength $\lambda_t \equiv U/f_1$. The parameter Δp_{12} , which denotes the pressure difference across the plate a distance l from the edge, provides a convenient reference level to characterize the acoustic excitation. Thus, in order to relate the flow response to the imposed sound field, Bechert suggests scaling the magnitude $|u_1|$ of the streamwise fluctuating velocity on the flow side of the layer as $|u_1| \rho \sqrt{U_1 \omega_t l / \Delta p_{12}}$. A comparison between the theory and carefully conducted experiments is displayed in Figure 18. The agreement is excellent at low Strouhal numbers St . At higher St , however, the stability characteristics of the true finite-thickness mixing layer are no longer approximated by the vortex-sheet model, and the theory breaks down.

Most of our present understanding of trailing-edge receptivity is limited to small amplitudes, small Mach numbers, and small Strouhal numbers, where the Kutta condition is applicable. The assumption of small Strouhal numbers is particularly restrictive, since it excludes the natural frequency of

free shear layers. Crighton (1981) suggests that in such a case local separation might occur and the Kutta condition would break down.

4.3 Mode Competition

One of the recurring themes in this review has been the interpretation of the dynamics of orderly structures in terms of a collection of single-frequency instability waves. The order of magnitude of the amplification rates seems to be well predicted by linear stability analysis (Section 2.1) and, in certain cases (Gaster et al. 1983), the total gain in amplitude is satisfactorily obtained from linear slowly diverging flow theories. In general situations, however, different frequency components not only extract energy from the mean flow, but they also exchange energy with one another through a variety of nonlinear interaction mechanisms (Sections 2.2–2.4). The downstream development of coherent structures is therefore “dictated” by a continuing nonlinear mode competition taking place in Fourier space between a finite number of waves. The important stages of the competition can, for instance, be visualized as in Figures 3 and 19. We now briefly mention some consequences of this phenomenon before giving a more complete discussion in the next few sections.

Mode competition most simply arises between an artificially generated single-frequency wave and natural broadband background noise, as shown by Freymuth (1966) and Miksad (1972). The presence of the monochromatic excitation suppresses the broadband component and leads to a very organized train of vortical structures. Single-frequency forcing can also considerably delay the appearance of another discrete frequency component (for instance, the naturally excited subharmonic $f/2$, as shown in Figure 3). Similarly, when a shear layer is forced at two frequencies (Miksad 1973), the respective equilibration levels of each wave differ markedly from those for single-frequency excitation. They are also greatly dependent on the initial wave amplitudes.

The spatial evolution of the flow therefore depends on the frequency, amplitude, and phase of each forced spectral component. Available experimental data do not presently cover the entire range of forcing parameter space, and in the next sections we separately consider the effects of frequency, amplitude, and phase, although such a separation is clearly not justified.

4.4 Forcing Frequency

The sensitivity of shear layers to initial conditions is most readily illustrated by the effects of a varying excitation frequency f_1 (Ho & Huang 1982). The initial *vortex-formation frequency* f_r is seen to correspond to that

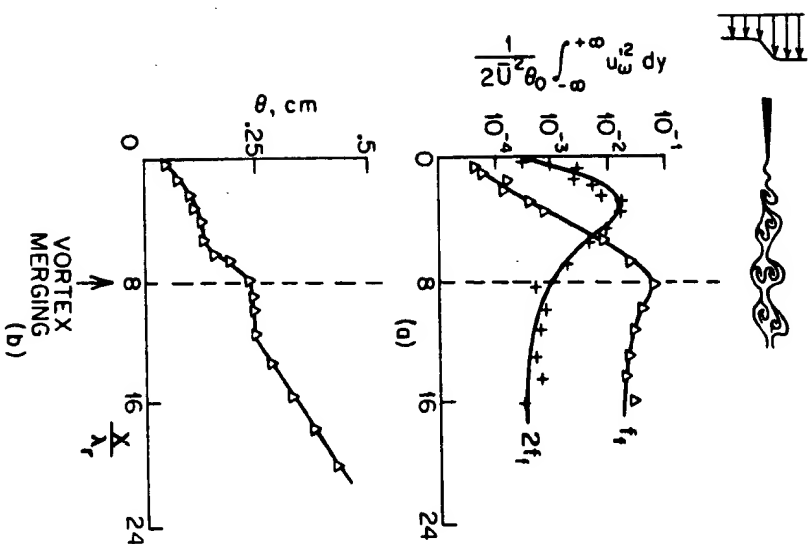


Figure 19 Evolution of (a) spectral components and (b) momentum thickness versus downstream distance (from Ho & Huang 1982). $f_n/4 < f_1 \leq f_n/2$; $R = 0.31$; $\lambda_f = 24$.

particular harmonic of the forcing frequency f_1 that is nearest to but smaller than f_n . In the range $(1/2)f_n < f_1 < 2f_n$, f_1 is found to be equal to f_n and vortices form at the forcing frequency. The downstream evolution of the corresponding spectral components is shown in Figure 3. The higher initial level of the fundamental f_1 temporarily suppresses the growth of the subharmonic $f_n/2$, and vortex pairing is delayed. When $(1/3)f_n < f_1 < (1/2)f_n$, the response frequency f_1 jumps to the first harmonic $2f_1$ closest to the natural frequency f_n (Figure 19). In other words, the excitation becomes the first subharmonic of the initial vortex passage frequency f_1 ; neighboring vortices are laterally displaced and subsequently wrap around each other to form a single structure. In contrast with the previous case, vortex pairing is promoted. Similarly, further reductions in the forcing

frequency f_1 lead to successive frequency-locking stages in which f_1 becomes the second and third subharmonic of f_n . Subharmonic forcing can thereby result in the simultaneous coalescence of as many as three or four vortices. Consequently, the shear-layer spreading rate can be either enhanced by promoting multiple-vortex amalgamations, or reduced by delaying them. *Mixing layers can be manipulated effectively with very low forcing levels, 0.01–0.1% of the average velocity \bar{U} , provided that the excitation is applied at the proper frequency.*

The dynamics of the spanwise vortices is intimately related to the amplitude evolution of the instability waves, as illustrated in Figures 3 and 19. For instance, in the range $(1/3)f_n < f_1 < (1/2)f_n$, the roll-up process is completed at the station where the component $f_1 = 2f_1$ reaches its peak amplitude. As the wave of frequency f_1 amplifies, vortices are displaced until they become aligned perpendicular to the stream. This location coincides with the maximum level of the subharmonic f_1 , where the local Strouhal number $f_1\theta/\bar{U}$ becomes neutrally stable. The pairing of vortices is thereby directly related to the development of the subharmonic. Similar arguments can be made in the other modes of excitation.

At forcing frequencies much lower than f_n , say, less than one tenth of f_n , and at high forcing amplitudes, many small vortices of streamwise spacing \bar{U}/f_n are observed to roll into large-scale structures on the downstream side of the long-wave crests. The small vortices lying on the upstream side of the crest are stretched by the resulting strain and constitute the braids of the large structures. In other cases, short instability waves of frequency f_n propagate on the long wave and directly form large vortices without going through the small-vortex stage. Variations in the flow pattern depend on the relative frequencies, amplitudes, and phases of the forced long wave and the naturally excited short wave. At any rate, a train of large vortices is formed at the low frequency f_1 . This qualitatively new type of dynamical process was identified by Ho & Nosseir (1981) as a *collective interaction*. The original forced-jet experiments of Crow & Champagne (1971) belong to this regime, the excitation frequency f_1 being of the order of the preferred jet frequency $f_n \ll f_n$. It is also interesting to note that the vortex simulations of Aref & Siggia (1980) give qualitatively the same picture: clusters of small vortices agglomerate to produce large-scale structures.

A similar phenomenon occurs in the experimental study of turbulent mixing layers conducted by Oster & Wygnanski (1982). Under a low-frequency excitation, the momentum thickness is initially found to increase sharply as a result of the collective interaction process. Farther downstream, θ reaches a plateau and finally resumes its linear growth. In the region of constant thickness, the *Reynolds stresses* ($-\overline{uv}$) become negative across the entire shear layer, as illustrated in Figure 20. Thus, there

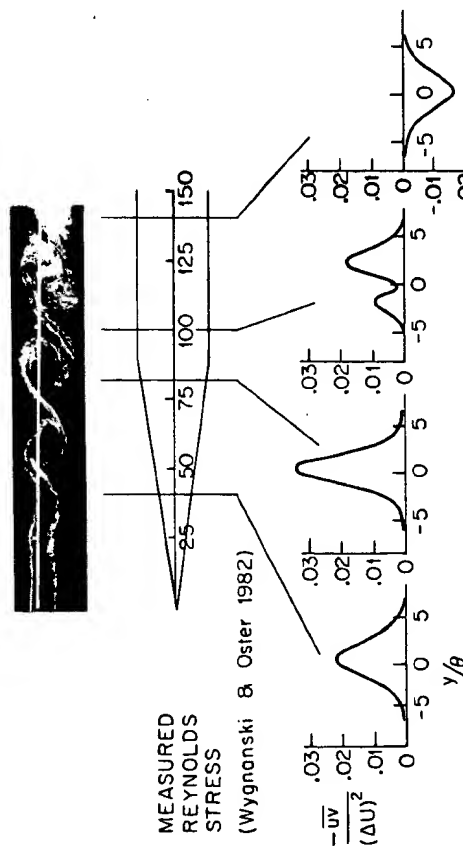


Figure 20 Evolution of Reynolds-stress cross-stream distribution with downstream distance in a forced turbulent mixing layer (from Oster & Wygnanski 1982 and Browand & Ho 1983). $f_t \ll f_n$. The measurements were performed at $R = 0.25$, but the visualization refers to $R = 0.43$. Comparison is only qualitative.

is in this part of the flow a transfer of energy from the fluctuations back to the mean flow, a characteristic behavior that has been confirmed numerically by Riley & Metcalfe (1980). Browand & Ho (1983) have given a simple kinematic explanation of the process by examining the orientation changes of elliptically shaped vortices, or *vortex nutation* in the terminology of Zabusky & Deem (1971). When the vortical structures are tilted as in Figure 21a, the corresponding streamwise and cross-stream velocity components generate a positive Reynolds stress and energy is extracted from the mean flow by the fluctuating field. The situation is reversed when the angle of inclination is as illustrated in Figure 21b. The reader may check from Figure 20 that this interpretation is indeed consistent. In the absence of vortex pairing, periodic exchanges of energy between the mean flow field and the fluctuating vorticity field can arise, as demonstrated by the numerical investigation of Brachet & Orszag (1983). From the preceding argument, this energy transfer is associated with the periodic nutation of the vortices. Furthermore, nonlinear stability analyses indicate that finite-amplitude periodic oscillations are possible close to the neutral Strouhal number (Benney & Maslowe 1975, Huerre 1977) and for the most amplified wave (Miura & Sato 1978). Note that the kinematic argument is also applicable to vortex-pairing events: according to Figure 19, the major axis of the elliptically shaped vorticity distribution rotates through the vertical during pairing and changes from the top configuration to the bottom config-

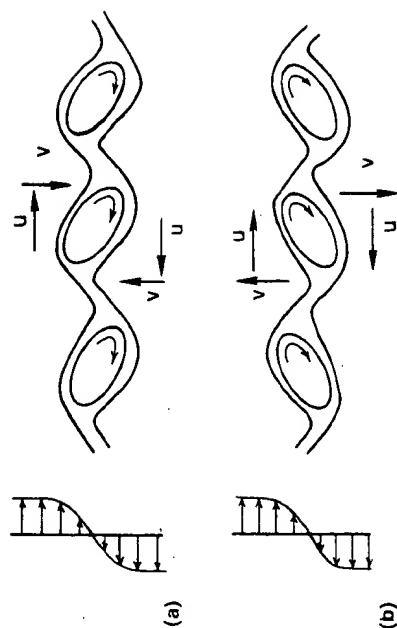


Figure 21 Mechanics of vortex nutation (from Browand & Ho 1983).

ation in Figure 21. Consequently, the energy transfer is reversed at that streamwise station, and the subharmonic energy goes through a maximum. This observation is in full agreement with the change of sign in the Reynolds-stress distribution calculated in the course of an amalgamation by Aref & Siggia (1980).

4.5 Forcing Level

The formation and mergings of vortices are known to occur at the peaks of the fundamental component and its subharmonics. Thus, by varying the excitation intensity at a given frequency f_t , one may expect to alter the evolution of the orderly structures. Unfortunately, too few measurements have been made to allow us to make any definite statements regarding the effects of forcing level. In the experiments of Laufer & Zhang (1983), a jet is forced close to the natural frequency f_n at very low levels, with u'/U_j estimated to be of order 10^{-7} . The peak of the fundamental is found to remain relatively constant with increasing excitation level, the resulting decrease in gain indicating the presence of nonlinear effects. In contrast, the subharmonic $f_t/2$ develops in a linear manner with a constant gain. The application of *low-level forcing* leads to a more organized flow evolution, but the locations of successive mergings appear to be insensitive to the excitation intensity. The measurements of Freymuth (1966), also conducted in a jet and at the same forcing frequency $f_t \sim f_n$, give some indication of the response at *higher forcing* levels, of the order of 10^{-4} . As seen from Figure 22, the location of the peak of f_n moves upstream, and its maximum amplitude saturates to a constant level with increasing forcing level. It can be inferred from the flow visualizations of Ho & Huang (1982) that under subharmonic forcing the location of vortex pairing, and hence the peak of

f_n also tends to be displaced upstream. In contrast with the high sensitivity of the flow to excitation frequency, adjustments in forcing level do not provide an efficient way to shift merging locations. As an example, note that in jets the initial amplitude at $f_i = f_n/2$ needs to be increased by a factor of 37 in order to move the vortex-pairing location one wavelength λ_n upstream. *Very high excitation levels* of the order of 17% have been applied to circular jets by Reynolds & Bouchard (1981): vortex rings then keep their identity and roll around each other three or four times before merging into a single structure. At very low frequencies, $f_i \ll f_n$, comparatively higher initial amplitude levels are necessary to force the mixing layer into a collective interaction regime. Such large perturbations ($u/U_j = 10^{-2}$ in Crow & Champagne 1971, 10^{-3} in Moore 1977, 10^{-2} in Oster & Wygnanski 1982) are required to offset the small amplification rates prevailing in the low-Strouhal-number range. The forced wave may thereby dominate the evolution of the flow, offering yet another example of mode competition between the two frequencies f_i and f_n . Furthermore, the formation of the large vortices can be shifted upstream by increasing the forcing level, just as in the higher-frequency case of Figure 22.

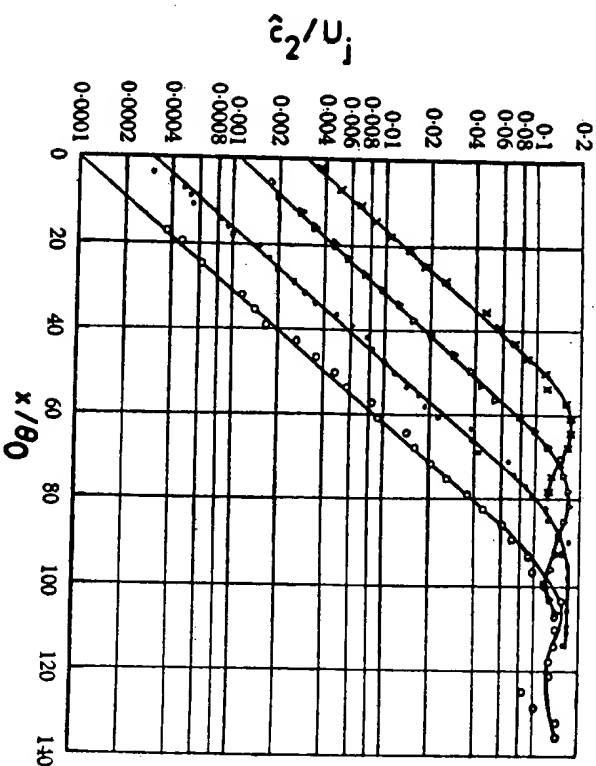


Figure 22. Evolution of wave amplitude with downstream distance for different forcing levels (from Freymuth 1966). C_2 is the peak of the eigenfunction. $f_i = 0.74f_n$; $R = 1$. \circ 70 dB; \bullet 80 dB; \triangle 90 dB; \times 100 dB.

4.6 Relative Phase of Frequency Components

The phase difference β between the fundamental f_n and its subharmonic $f_n/2$ affects not only the amplification rate of the subharmonic (Figure 6a), but also the nature of the vortex interaction (Figure 7). In mixing layers forced at both frequencies (Zhang et al. 1983), measured subharmonic growth rates are found to decrease by as much as 30% when β is varied between 0 and π . This observation is in qualitative agreement with the models of Kelly (1967) and Niktiopoulos & Liu (1982) mentioned in Sections 2.2 and 2.3. Furthermore, according to the simulations of Patnaik et al. (1976) and Riley & Metcalfe (1980), a vortex-pairing interaction occurs for all values of β except those close to π . When both waves are in phase ($\beta = 0$), the interaction involves two vortices of equal size; but as β is increased, one structure becomes thinner than the other during the pairing process (see Figure 7b). Finally, in the antiphase case ($\beta = \pi$), pairing is replaced by a shredding interaction (Figure 7c). We note that shredding seldom takes place in mixing layers excited in antiphase at f_n and $f_n/2$ (Zhang et al. 1983). It is observed instead that merging events are no longer localized as for other values of β . Ambient background noise possibly detunes the effective phase difference away from π , which precludes shredding and results instead in randomly distributed merging locations.

4.7 Facility Forcing

The measurements of characteristic flow properties that have been repeatedly taken in the past few decades in various facilities are found to differ by factors greatly exceeding experimental uncertainty. A scatter as large as 100% can exist among different estimates of the spreading rate (Brown & Roshko 1974, Oster & Wygnanski 1982), the jet-mode Strouhal number (Petersen 1978), or the initial shear-layer Strouhal number (Hussain & Zedan 1978). Facility-related parameters that might contribute to these discrepancies are the intensity and the scale of turbulence in the initial boundary layer (Batt et al. 1970, Oster et al. 1977, Hussain & Zedan 1978, Browand & Latigo 1979, Drubka 1981), the perturbations generated by the fan blades (Fiedler & Thies 1978), free-stream turbulence (Pui & Gartshore 1979), and organ-pipe resonances (Gaster 1971, Fiedler & Thies 1978).

Wind tunnels contain potential acoustic resonators, such as turbulence manipulators (honeycombs, straws, etc.; Way et al. 1973) or the system formed by the stagnation chamber, the contraction, and the test section. Infinitesimal acoustic perturbations present in any facility may then trigger a cavity resonance with a harmonic content in the unstable frequency range of the initial shear layer. According to Gutmark & Ho (1983), disturbance

levels as low as 10^{-5} can generate, within a certain range of velocities, 100% changes in the spreading rate, shear-layer Strouhal number, and preferred Strouhal number. The sensitivity of mixing layers to initial conditions is such that experimentalists will have to live with the many extraneous perturbations existing in individual flow facilities. "Natural" mixing layers are by nature excited flows.

4.8 Sources of Randomness

The application of a well-defined excitation is known to provide as one of its main advantages an unambiguous phase reference. In other words, the evolution of the flow downstream of the trailing edge is locked in phase with the forcing signal. Vortex interactions take place at fixed streamwise locations, and measurements taken at a fixed point in space can easily be related to a specific stage in the dynamics of the vorticity field. In this manner, a well-designed forcing experiment may unfold the main mechanisms governing the development of mixing layers. However, since a small level of forcing can significantly alter the flow, care should be exercised in making quantitative comparisons between different naturally or artificially excited mixing layers.

It should be emphasized that, even in the presence of forcing, the temporal evolution of the flow does not remain phase-locked indefinitely far downstream. It is usually observed that absolute control of the flow by forcing is limited to the first few vortex amalgamations. In certain jet experiments (Kibens 1980, Drubka 1981), the shear-layer natural frequency f_a is chosen as a multiple of the preferred frequency f_p of the form $f_a = 2^3 f_p$, so that exactly three pairings take place between the nozzle lip and the tip of the potential core. In such a case, initial phase information is preserved until the third vortex amalgamation, which is probably due to the presence of a feedback loop (see Section 5.1). At any rate, forcing is much more effective in permanently altering the asymptotic spreading rate of free shear layers than it is in phase-locking the flow very far downstream.

It is tempting to conjecture that the loss of phase reference experienced by the vortical structures during their evolution is related in some manner to the intrinsic chaotic behavior displayed by certain deterministic dynamical systems (see, for instance, Lanford 1982). In this context, Aref (1983) has recently emphasized that the motion of an initially periodic row of finite vortices is expected to display a gradual loss of phase coherence. The amplification of infinitesimal disturbances destroys the periodicity, in the sense that pairing events are no longer in phase along the row. Alternatively, from the point of view of wave theory, one can speculate that the phenomenon is similar to the onset of phase turbulence encountered in particular nonlinear amplitude evolution equations (Kuramoto 1978). This

term denotes a class of motions in which the loss of periodicity can primarily be ascribed to chaotic behavior in the phase of the waves but not in their amplitude. In any case, the self-generated loss of phase reference inherent in the dynamics of large-scale structures will result in a broadband spectrum in the low-frequency range.

Two additional factors contribute to the observed noise. The small-scale transition discussed in Section 2.6 is another intrinsic process linked to pairing events; it is responsible for the emergence of a continuous spectrum at high frequencies. Finally, the ambient background noise constitutes an obvious external source of random fluctuations. We note that these three processes are likely to be coupled; for instance, small scales may induce high-frequency phase jitter in the dynamics of the orderly structures.

5. THE GLOBAL FEEDBACK EFFECT

In most of the dynamical processes discussed so far in this review, the shear layer has been assumed to develop in the streamwise direction according to the local conditions prevailing at every downstream station. In other words, we have considered the x -coordinate to be a timelike variable and have deliberately ignored any influence of the downstream flow on the upstream flow. Dimotakis & Brown (1976) have suggested, however, that the upstream influence from all downstream large-scale vortices can equally be felt at the trailing edge. According to their argument, the $1/x$ decrease of induced velocity expected from the Biot-Savart law is exactly compensated by a corresponding linear increase of the circulation of the vortices. Thus, the development of free shear layers should also be viewed globally by including long-range coupling effects between the trailing edge and the dominant flow events.

5.1 Feedback Mechanism

Laufer & Monkewitz (1980) have chosen in particular to consider the global feedback mechanism associated with the sudden change of circulation during merging interactions. Each vortex-pairing event along the stream is assumed to be linked to the trailing edge via a feedback loop, consisting of a downstream-propagating subharmonic instability wave and an upstream-propagating acoustic wave. Furthermore, according to Ho & Nosseir (1981), the phase difference between the two waves is necessarily of the form $2N\pi$, N an integer. If x_j denotes the location of the j th vortex merging, λ_j the corresponding subharmonic wavelength, and λ_a the acoustic wavelength, the following constraint must then be satisfied:

$$\frac{x_j}{\lambda_j} + \frac{x_j}{\lambda_a} = N. \quad (11)$$

In a low subsonic shear layer ($\lambda_j \ll \lambda_u$), the acoustic branch of the loop can be neglected, and vortex-merging stations are simply given by $x_j = \lambda_j N$. If P vortices are involved in each merging interaction, the wavelength λ_j is related to the initial instability wavelength $\lambda_i \equiv U/f_i$ by the relation $\lambda_j = P\lambda_i$, and vortex-merging locations are simply given by

$$x_j = NP\lambda_i. \quad (12)$$

As seen from Figure 23, this relation leads to excellent predictions in a jet forced in the $P = 2$ pairing mode, provided that one assumes $N = 2$.

It can be recalled from Section 2.3 that *local* linear stability arguments have been incorporated by Ho (1981) into a phenomenological evolution model of the mixing layer. An alternate *global* model can be constructed by exploiting instead the consequences of the feedback equation (12). As before, the thickness θ is assumed to increase by a factor 2 in the roll-up phase and by a factor P during each merging interaction, so that $\theta = 2P^j\theta_0$. The spreading rate is then deduced from (12) in the form

$$\frac{d\theta}{dx} = \frac{2}{N} \frac{f_i\theta_0}{U} = \frac{2}{N} \frac{St_i}{St_r}, \quad (13)$$

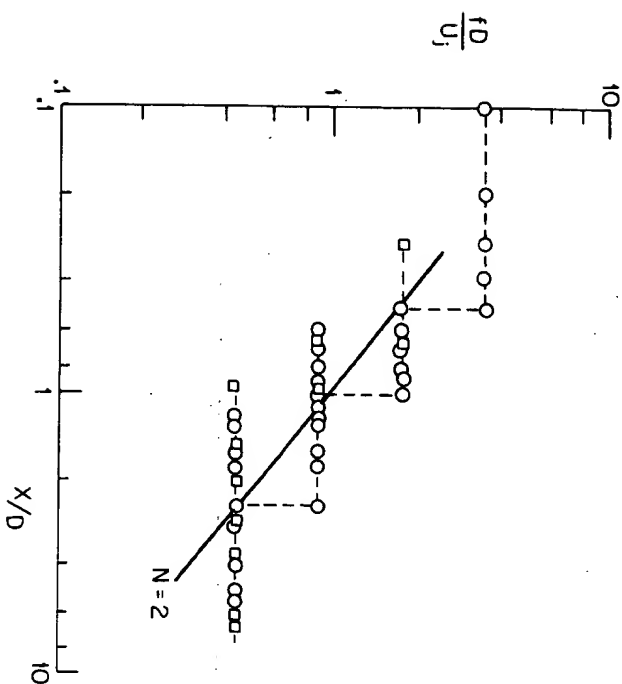


Figure 23. Evolution of vortex passage frequency in a forced jet (from Kibens 1980). $f_i \sim f_r$; $R = 1$. \circ measured in shear layers; \square measured on jet centerline. — Feedback equation (Laufer & Monkewitz 1980) with $N = 2$.

which the reader may compare with the scaling relation (9) obtained solely from local stability considerations. The dependence of N on the velocity ratio R must be inferred from experiments: according to Huang & Ho (1983), N falls in discrete steps from 5 to 2 as R increases between 0 and 1, the length of each step approximately covering an interval of 0.25 in R . Both relations (9) and (13) then lead to spreading-rate variations with R that are consistent with the measured data in Figure 15.

The importance of the feedback mechanism remains to be assessed, both experimentally and theoretically. Nonetheless, a few clues are already available. The feedback model (12) is the only one that correctly states that the distance to the first pairing event is the same as the distances between the first and second pairings, merging distances being doubled thereafter. In contrast with the local evolution approach, this particular prediction requires no information about the variations in the transverse-flow scale. Furthermore, experiments by Drubka (1981) indicate that pressure fluctuations at the outer edge of the initial shear layer are dominated by a strong first-subharmonic component. The first two pairings are indeed likely to be the most effective in exciting the shear layer, since they are spatially coherent. Finally, additional time scales are often found to be present in the unsteady flow field at the trailing edge. Such phenomena might be due to feedback from the end of the experimental apparatus (Dimotakis & Brown 1976) or, in the case of jets, to feedback from the preferred mode at the end of the potential core (Laufer & Monkewitz 1980, Monkewitz 1983).

5.2 Rescaled Shear Layer

The scaling relationships implied by the previous models may to some degree be tested by suitably renormalizing the downstream variations of momentum thickness under very different flow conditions. Guided by earlier linear stability arguments, we first rescale θ as a local Strouhal number $f_i\theta/\bar{U}$ at the forcing frequency f_i . A proper choice of streamwise coordinate is more ambiguous. Recall that the early evolution of mixing layers is dominated by vortex amalgamations that adjust the wavelength from λ_i to λ_r . According to the feedback equation (12), this process is completed at a downstream distance $N\lambda_r$. Thus, in order to obtain a unified picture of the region $0 < x < N\lambda_r$, the streamwise coordinate should be normalized as $x/N\lambda_r$. Such a scaling is illustrated in Figure 24 at different values of f_i and R . The increase of local Strouhal number in the range $0 < x/(N\lambda_r) < 1$ is followed by a plateau extending to approximately $x/(N\lambda_r) = 1.5$. Note that, as expected from stability considerations, the level of the plateau always coincides with the neutral Strouhal number 0.08 in Figure 2a. Farther downstream, linear spreading resumes at varying rates.

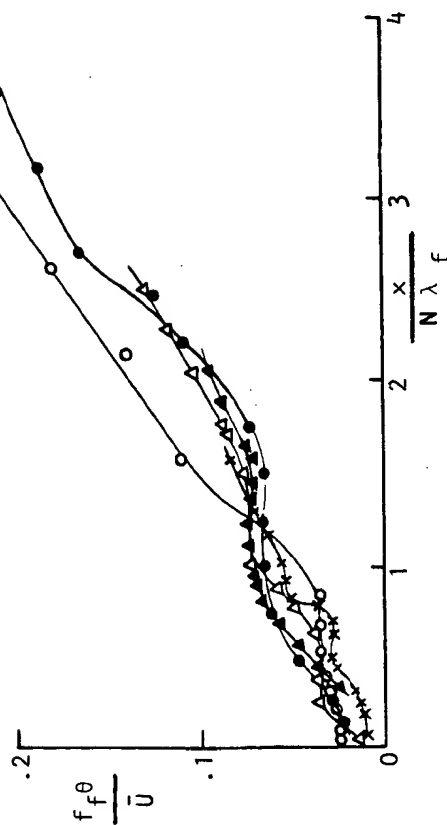


Figure 24 Rescaled free shear layer: variations of momentum thickness with rescaled downstream distance. \bullet $f_t = 0.65f_n$, Δ $f_t = 0.43f_n$, \times $f_t = 0.24f_n$; $R = 0.31$, $N = 4$ (Ho & Huang 1982). \blacktriangle $f_t \ll f_n$; $R = 0.25$, $N = 4$ (Oster & Wygnanski 1982). \circ $f_t = f_n$; $R = 1$, $N = 2$, natural forcing (Drubka 1981).

This normalization is not meant to imply the existence of a unique spreading profile; it simply illustrates the extent of the region controlled by artificial excitations. For comparison, a naturally forced mixing layer is also plotted in Figure 24. A similar collapse of experimental data would be obtained with the alternate streamwise coordinate Rx/λ_t resulting from the local evolution model.

6. PARTING REMARKS

In this review, we have deliberately avoided a detailed discussion of the random component of the motion, whether in the form of ambient noise or generated intrinsically in the dynamics of the large-scale structures. A new approach that would encompass both the random and non-random aspects of mixing layers but that would still be based on deterministic dynamics remains an ambitious but desirable goal.

ACKNOWLEDGMENTS

This work would not have been possible without the lively and stimulating research environment created by our friend John Laufer at USC. We are very grateful for his critical review of the manuscript, completed a few days before his untimely passing.

We wish to thank F. K. Browand and L. G. Redekopp for their helpful comments and their kind encouragement. We are also very much indebted to F. B. Hsiao, F. Munoz, and A. Nassiri for their help in preparing the draft.

The work was supported by the Office of Naval Research Contract N00014-77-C-0314 (CMH), the Air Force Office of Scientific Research Contract F49620-82-K-0019 (CMH), and the National Science Foundation Grant MEA-8120904 (PH).

Literature Cited

- Acton, E. 1976. The modelling of large eddies in a two-dimensional shear layer. *J. Fluid Mech.* 76: 561-92.
- Alper, A., Liu, J. T. C. 1978. On the interactions between large-scale structure and fine-grained turbulence in a free shear flow. II. The development of spatial interactions in the mean. *Proc. R. Soc. London Ser. A* 359: 497-523.
- Amesden, A. A., Harlow, F. H. 1964. Slip instability. *Phys. Fluids* 7: 327-34.
- Aref, H. 1983. Integrable, chaotic, and turbulent vortex motion in two-dimensional flows. *Ann. Rev. Fluid Mech.* 15: 343-89.
- Aref, H., Flinchem, E. P. 1983. Dynamics of a vortex filament in a shear flow. *J. Fluid Mech.* Submitted for publication.
- Aref, H., Siegala, E. D. 1980. Vortex dynamics of the two-dimensional turbulent shear layer. *J. Fluid Mech.* 100: 705-37.
- Ashurst, W. T. 1979. Numerical simulation of turbulent mixing layers via vortex dynamics. In *Turbulent Shear Flows I*, ed. F. Durst et al., pp. 402-13. Berlin/Heidelberg/New York: Springer.
- Batchelor, G. K., Gill, A. E. 1962. Analysis of the stability of axisymmetric jets. *J. Fluid Mech.* 14: 529-51.
- Batt, R. G., Kubota, T., Laufer, J. 1970. Experimental investigation of the effect of shear flow turbulence on a chemical reaction. *AIAA Pap. No. 70-721*.
- Bechert, D. W. 1980. Sound absorption caused by vorticity shedding demonstrated with a jet flow. *J. Sound Vib.* 70: 389-405.
- Bechert, D. W. 1983. A model of the excitation of large scale fluctuation in a shear layer. *AIAA Pap. No. 83-0724*.
- Bechert, D. W., Michel, U. 1975. The control of a thin free shear layer with and without a semi-infinite plate by a pulsating flow field. *Acustica* 33(5): 287-307.
- Bechert, D. W., Pfizenmaier, E. 1975. Optical compensation measurements on the unsteady exit condition at a nozzle discharge edge. *J. Fluid Mech.* 71: 123-44.
- Benney, D. J. 1961. A non-linear theory for oscillations in a parallel flow. *J. Fluid Mech.* 10: 209-36.
- Benney, D. J., Bergeron, R. F. 1969. A new class of nonlinear waves in parallel flows. *Stud. Appl. Math.* 48: 181-204.
- Benney, D. J., Lin, C. C. 1960. On the secondary motion induced by oscillations in a shear flow. *Phys. Fluids* 3: 636-57.
- Benney, D. J., Maslowe, S. A. 1975. The evolution in space and time of nonlinear waves in parallel shear flows. *Stud. Appl. Math.* 54: 181-205.
- Bernal, L. P. 1981. The coherent structure of turbulent mixing layers. I. Similarity of the primary vortex structure. II. Secondary streamwise vortex structure. PhD thesis. Calif. Inst. Technol., Pasadena.
- Beitchov, R., Criminale, W. O. 1967. Stability of Parallel Flows. New York/London: Academic.
- Beitchov, R., Szewczyk, A. 1963. Stability of a shear layer between parallel streams. *Phys. Fluids* 6(10): 1391-96.
- Brachet, M. E., Orszag, S. A. 1983. Secondary instability of free shear flows. *J. Fluid Mech.* Submitted for publication.
- Bradshaw, P. 1966. The effect of initial conditions on the development of a free shear layer. *J. Fluid Mech.* 26: 225-36.
- Breidenthal, R. 1981. Structure in turbulent mixing layers and wakes using a chemical reaction. *J. Fluid Mech.* 109: 1-24.
- Broadwell, J. E., Breidenthal, R. E. 1982. A simple model of mixing and chemical reaction in a turbulent shear layer. *J. Fluid Mech.* 125: 397-410.
- Browand, F. K. 1966. An experimental investigation of the instability of an incompressible separated shear layer. *J. Fluid Mech.* 26: 281-307.
- Browand, F. K., Ho, C. M. 1983. The mixing layer: an example of quasi-dimensional turbulence. *J. Méc. In press*.
- Browand, F. K., Latigo, B. O. 1979. Growth of the two-dimensional mixing layer from

- a turbulent and non-turbulent boundary layer. *Phys. Fluids* 22(6):1011-19
- Brownand, F. K., Laufer, J. 1975. The role of large scale structures in the initial development of circular jets. In *Turbulence in Liquids*, ed. J. L. Zakin, G. K. Patterson, pp. 33-44. Princeton, N.J.: Science
- Brownand, F. K., Troutt, T. R. 1980. A note on spanwise structure in the two-dimensional mixing layer. *J. Fluid Mech.* 97:771-81
- Brownand, F. K., Weidman, P. D. 1976. Large scales in the developing mixing layer. *J. Fluid Mech.* 76:127-44
- Brown, G. L., Rosko, A. 1974. On density effects and large structure in turbulent mixing layers. *J. Fluid Mech.* 64:775-816
- Cain, A. B., Reynolds, W. C., Ferziger, J. H. 1981. A three-dimensional simulation of transition and early turbulence in a time-developing mixing layer. *Intern. Rep. No. TF-14*, Stanford Univ., Calif.
- Canwell, B. J. 1981. Organized motion in turbulent flow. *Ann. Rev. Fluid Mech.* 13:457-515
- Cervantes de Gortari, J., Goldschmidt, V. W. 1981. The apparent flapping motion of a turbulent plane jet—further experimental results. *J. Fluids Eng.* 103:119-26
- Chandruska, C., Mehta, R. D., Weir, A. D., Bradshaw, P. 1978. Effect of free-stream turbulence on large structure in turbulent mixing layers. *J. Fluid Mech.* 85:693-704
- Christensen, J. P. 1973. Numerical simulation of hydrodynamics by the method of point vortices. *J. Comput. Phys.* 13:363-79
- Cohen, J., Gutmark, E., Wypianski, I. 1983. On modal distribution of coherent structures in a jet. *AIJA J.* Submitted for publication
- Corcos, G. M. 1979. The mixing layer: deterministic models of a turbulent flow. *Intern. Rep. No. FM-79-2*, Univ. Calif., Berkeley
- Corcos, G. M., Lin, S. J. 1983. Deterministic models of the shear layer. Part II: the origin of the three-dimensional motion. *J. Fluid Mech.* Submitted for publication
- Corcos, G. M., Sherman, F. S. 1976. Vorticity concentration and the dynamics of unstable free shear layers. *J. Fluid Mech.* 73:241-64
- Corcos, G. M., Sherman, F. S. 1983. The mixing layer: deterministic models of a turbulent flow. Introduction and Part I. The two-dimensional flow. *J. Fluid Mech.* Submitted for publication
- Cortisi, S. 1943. Investigations of flow in an axially symmetric heated jet of air. *NACA Aduis. Conf. Rep.* 3123
- Couet, B. 1979. Evolution of turbulence by three-dimensional numerical particle-vortex tracing. *Intern. Rep. SU-IPR No. 793*, Stanford Univ., Calif.
- Craik, A. D. D. 1971. Non-linear resonant instability in boundary layers. *J. Fluid Mech.* 50:393-413
- Craik, A. D. D. 1980. Nonlinear evolution and breakdown in unstable boundary layers. *J. Fluid Mech.* 99:247-65
- Crignion, D. G. 1981. Acoustics as a branch of fluid mechanics. *J. Fluid Mech.* 106:261-98
- Crignion, D. G., Gaster, M. 1976. Stability of slowly diverging jet flow. *J. Fluid Mech.* 77:397-413
- Crow, S. C., Champagne, F. H. 1971. Orderly structure in jet turbulence. *J. Fluid Mech.* 48:347-91
- Daniels, P. G. 1978. On the unsteady Kutta condition. *Q. J. Mech. Appl. Math.* 31:49-75
- Davis, R. E. 1969. On the high Reynolds number flow over a wavy boundary. *J. Fluid Mech.* 36:337-46
- Delcourt, B. A. G., Brown, G. L. 1979. The evolution and merging structure of a vortex sheet in an inviscid and viscous fluid modelled by a point vortex method. *Proc. Symp. Turbul. Shear Flows*, 2nd, pp. 14-35-40
- Dimotakis, P. E., Brown, G. L. 1976. The mixing layer at high Reynolds number: large-structure dynamics and entrainment. *J. Fluid Mech.* 78:535-60
- Drazin, P. G., Howard, L. N. 1966. Hydrodynamic stability of parallel flow of inviscid fluid. *Adv. Appl. Mech.* 9:1-89
- Drazin, P. G., Reid, W. H. 1981. *Hydrodynamic Stability*. Cambridge Univ. Press
- Drukka, R. E. 1981. *Instabilities in near field of turbulent jets and their dependence on initial conditions and Reynolds number*. PhD thesis, Ill. Inst. Technol., Chicago
- Fiedler, H. E., Thies, H. J. 1978. Some observations in a large two-dimensional shear layer. In *Structure and Mechanisms in Turbulence, Lecture Notes in Physics*, ed. H. E. Fiedler, 75:108-17. Berlin/Heidelberg/New York: Springer
- Fiedler, H. E., Drazin, B., Mensing, P., Rösger, T. 1981. Initiation, evolution and global consequences of coherent structures in turbulent shear flows. In *The Role of Coherent Structures in Modelling of Turbulence and Mixing, Lecture Notes in Physics*, ed. J. Jimenez, 136:219-51. Berlin/Heidelberg/New York: Springer
- Foss, J. 1977. The effects of the laminar/turbulent boundary layer states on the development of a plane mixing layer. *Proc. Symp. Turbul. Shear Flows*, 1st, pp. 11-33-42
- Feynman, R. 1966. On transition in a separated laminar boundary layer. *J. Fluid Mech.* 25:683-704
- Fuchs, H. V., Michel, U. 1977. Experimental evidence of turbulent source coherence affecting jet noise. *AIJA Pap. No. 77-1348*
- Gaster, M. 1962. A note on the relation between temporally-increasing and spatially-increasing disturbances in hydrodynamic stability. *J. Fluid Mech.* 14:222-24
- Gaster, M. 1971. Some observations on vortex shedding and acoustic resonances. *CP No. 1141*, Natl. Phys. Lab. Middlesex, Engl.
- Gaster, M., Kit, E., Wypianski, I. 1983. Large scale structures in a forced turbulent mixing layer. *J. Fluid Mech.* Submitted for publication
- Gatski, T. B., Liu, J. T. C. 1980. On the interactions between large-scale structures and fine-grained turbulence in a free shear layer. III. A numerical solution. *Philos. Trans. R. Soc. London* 293(1403):473-509
- Goldstein, M. E. 1984. Aeroacoustics of turbulent shear flows. *Ann. Rev. Fluid Mech.* 16:263-85
- Gutmark, E., Ho, C. M. 1983. On the preferred modes and the spreading rates of jets. *Phys. Fluids*. In press
- Haberman, R. 1972. Critical layers in parallel flows. *Stud. Appl. Math.* 51:139-61
- Herman, M. A., Jimenez, J. 1982. Computer analysis of a high-speed film of the plane turbulent mixing layer. *J. Fluid Mech.* 119:323-45
- Ho, C. M. 1981. Local and global dynamics of free shear layers. In *Numerical and Physical Aspects of Aerodynamic Flows*, ed. T. Cebeci, pp. 521-33. Berlin/Heidelberg/New York: Springer
- Ho, C. M., Hsiao, F. B. 1983. Evolution of coherent structures in a lip jet. In *Structure of Complex Turbulent Shear Layers*, ed. R. Dumas, L. Fulachier, pp. 121-36. Berlin/Heidelberg/New York: Springer
- Ho, C. M., Huang, L. S. 1982. Subharmonics and vortex merging in mixing layers. *J. Fluid Mech.* 119:443-73
- Ho, C. M., Nossier, N. S. 1981. Dynamics of an impinging jet. Part I. The feedback phenomenon. *J. Fluid Mech.* 105:119-42
- Huang, L. S., Ho, C. M. 1983. Small scale transition in two-dimensional mixing layer. In preparation
- Huerre, P. 1977. Nonlinear instability of free shear layers. In *Laminar-Turbulent Transition, AGARD CP No. 224*, pp. 5-1-12
- Huerre, P. 1980. The nonlinear stability of a free shear layer in the viscous critical layer regime. *Philos. Trans. R. Soc. London* 293(1408):643-75
- Huerre, P. 1983. Finite-amplitude evolution of mixing layers in the presence of solid boundaries. *J. Mec. In press*
- Huerre, P. 1984. Basic instability mechanisms in mixing layers. In preparation
- Huerre, P., Monkewitz, P. 1983. Absolute and convective instabilities in free shear layers. *J. Fluid Mech.* Submitted for publication
- Huerre, P., Redekopp, L. 1983. Nonlinear evolution equations and critical layers. *Lect. Appl. Math.* 20:79-96
- Huerre, P., Scott, J. F. 1980. Effects of critical layer structure on the nonlinear evolution of waves in free shear layers. *Proc. R. Soc. London Ser. A* 371:509-24
- Hussain, A. K. M. F., Reynolds, W. C. 1970. The mechanics of an organized wave in turbulent shear flow. *J. Fluid Mech.* 41:241-58
- Hussain, A. K. M. F., Zaman, K. B. M. Q. 1981. The "preferred mode" of the axisymmetric jet. *J. Fluid Mech.* 110:39-71
- Hussain, A. K. M. F., Zedan, M. F. 1978. Effects of the initial condition on the axisymmetric free shear layer: effects of the initial momentum thickness. *Phys. Fluids* 21(7):1100-12
- Jimenez, J. 1980. On the visual growth of a turbulent mixing layer. *J. Fluid Mech.* 96:447-60
- Jimenez, J., Martinez-Vel, R., Rebollo, M. 1979. On the origin and evolution of three-dimensional effects in the mixing layer. *Intern. Rep. DA-ERO 79-G-079*, Univ. Politéc. Madrid
- Kelly, R. E. 1967. On the stability of an inviscid shear layer which is periodic in space and time. *J. Fluid Mech.* 27:657-89
- Kelly, R. E. 1968. On the resonant interaction of neutral disturbances in two inviscid shear flows. *J. Fluid Mech.* 31:789-99
- Kibens, V. 1980. Discrete noise spectrum generated by an acoustically excited jet. *AIJA J.* 18:434-41
- Kibens, V. 1981. The limit of initial shear layer influence on jet development. *AIJA Pap. No. 81-1960*
- Konrad, J. H. 1976. An experimental investigation of mixing in two-dimensional turbulent shear flows with applications to diffusion-initiated chemical reactions. *Intern. Rep. CIT-8-PU*, Calif. Inst. Technol., Pasadena
- Kovaszny, L. S. G. 1970. The turbulent boundary layer. *Ann. Rev. Fluid Mech.* 2:95-112
- Kuramoto, Y. 1978. Diffusion-induced chaos in reaction systems. *Suppl. Prog. Theor. Phys.* 64:346-67
- Lamb, L. 1932. *Hydrodynamics*. New York: Dover
- Landford, O. E. III. 1982. The strange attractor theory of turbulence. *Ann. Rev. Fluid Mech.* 14:347-64
- Laufer, J. 1975. New trends in experimental turbulence research. *Ann. Rev. Fluid Mech.* 7:307-26

- Laufer, J. 1983. Deterministic and stochastic aspects of turbulence. *J. Appl. Mech.* In press.
- Laufer, J., Monkewitz, P. A. 1980. On turbulent jet flow in a new perspective. *AIAA Pap. No. 80-0962*.
- Laufer, J., Zhang, J. Q. 1983. Unsteady aspects of a low Mach number jet. *Phys. Fluids* 26:1740-50.
- Liepmann, H. W., Laufer, J. 1947. Investigation of free turbulent mixing. *NACA Tech. Note No. 1257*.
- Lin, C. C. 1955. *The Theory of Hydrodynamic Stability*. Cambridge Univ. Press.
- Lin, S. J. 1981. *The evolution of streamwise vorticity in the free shear layer*. PhD thesis. Univ. Calif., Berkeley.
- Lin, S. J., Corcos, G. M. 1983. The mixing layer: deterministic models of a turbulent flow. Part III: The effect of plane strain on the dynamics of streamwise vortices. *J. Fluid Mech.* Submitted for publication.
- Liu, J. T. C. 1981. Interaction between large-scale coherent structures and fine-grained turbulence in free shear flows. In *Transition and Turbulence*, pp. 167-214. New York/London: Academic.
- Liu, J. T. C., Merkle, L. 1976. On the interactions between large-scale structure and fine-grained turbulence on a free shear flow. I: The development of temporal interactions in the mean. *Proc. R. Soc. London Ser. A* 352:213-47.
- Lock, R. C. 1951. The velocity distribution in the laminar boundary layer between parallel streams. *Q. J. Mech.* 4:42-63.
- Lumley, J. L. 1978. Computational modeling of turbulent flows. *Adv. Appl. Mech.* 18:123-76.
- Lumley, J. L. 1981. Coherent structures in turbulence. In *Transition and Turbulence*, pp. 215-41. New York/London: Academic.
- Maslowe, S. A. 1977a. Weakly nonlinear stability of a viscous free shear layer. *J. Fluid Mech.* 79:689-702.
- Maslowe, S. A. 1977b. Weakly nonlinear stability theory of stratified shear flows. *Q. J. R. Meteorol. Soc.* 103:769-83.
- Maslowe, S. A. 1981. Shear flow instabilities and transition. In *Hydrodynamic Instabilities and the Transition to Turbulence*, ed. H. L. Swinney, J. P. Gollub, pp. 181-228. Berlin/Heidelberg/New York: Springer.
- Mattingly, G. E., Chang, C. C. 1974. Unstable waves on an axisymmetric jet column. *J. Fluid Mech.* 65:541-60.
- Michalke, A. 1964. On the inviscid instability of the hyperbolic tangent velocity profile. *J. Fluid Mech.* 19:543-56.
- Michalke, A. 1965a. Vortex formation in a free boundary layer according to stability theory. *J. Fluid Mech.* 22:371-83.
- Michalke, A. 1965b. On spatially growing disturbance in an inviscid shear layer. *J. Fluid Mech.* 23:521-44.
- Michalke, A. 1969. A note on spatially growing three-dimensional disturbances in a free shear layer. *J. Fluid Mech.* 38:765-67.
- Michalke, A. 1971. Instabilität eines Kompressiblen runden Freistrahls unter Berücksichtigung des Einflusses der Strahlengrenzschichtdicke. *Z. Flugwiss.* 19:319-28.
- Michalke, A. 1972. The instability of free shear layers. *Prog. Aerosp. Sci.* 12:213-39.
- Michalke, A., Hermann, G. 1982. On the inviscid instability of a circular jet with external flow. *J. Fluid Mech.* 114:343-59.
- Miksed, R. W. 1972. Experiments on the nonlinear stages of free shear layer transition. *J. Fluid Mech.* 56:695-719.
- Miksed, R. W. 1973. Experiments on nonlinear interactions in the transition of a free shear layer. *J. Fluid Mech.* 59:1-21.
- Miles, J. B., Shih, J. S. 1968. Similarity parameter for two-stream turbulent jet-mixing region. *AIAA J.* 6(7):1429-30.
- Mills, R. D. 1968. Numerical and experimental investigations of the shear layer between two parallel streams. *J. Fluid Mech.* 33:591-616.
- Miyura, A., Sato, T. 1978. Theory of vortex mutation and amplitude oscillation in an inviscid shear instability. *J. Fluid Mech.* 86:33-47.
- Monin, A. S., Yaglom, A. M. 1971. *Statistical Fluid Mechanics*, ed. J. L. Lumley, Vol. 1. Cambridge, Mass: MIT Press.
- Monin, A. S., Yaglom, A. M. 1975. *Statistical Fluid Mechanics*, ed. J. L. Lumley, Vol. 2. Cambridge, Mass: MIT Press.
- Monkewitz, P. A. 1982. On the effect of the phase difference between fundamental and subharmonic instability in a mixing layer. *Intern. Rep.*, Univ. Calif., Los Angeles.
- Monkewitz, P. A. 1983. On the nature of the amplitude modulation of jet shear layer instability waves. *Phys. Fluids*. In press.
- Monkewitz, P. A., Huerre, P. 1982. The influence of the velocity ratio on the spatial instability of mixing layers. *Phys. Fluids* 25:1137-43.
- Moore, C. J. 1977. The role of shear-layer instability waves in jet exhaust noise. *J. Fluid Mech.* 80:321-67.
- Moore, D. W., Saffman, P. G. 1975. The density of organized vortices in a turbulent mixing layer. *J. Fluid Mech.* 69:465-73.
- Morkovin, M. 1984. *Guide to Experiments on Instabilities and Laminar Turbulent Transition in Shear Layers*. New York: AIAA.
- Morkovin, M., Paranjape, S. V. 1971. Acoustic excitation of shear layers. *Z. Flugwiss.* 9:328-35.
- Morris, P. J. 1976. The spatial viscous instability of axisymmetric jets. *J. Fluid Mech.* 77:511-29.
- Niktopoulos, D. E. 1982. *Nonlinear interaction between two instability waves in a developing shear layer*. MS thesis. Brown Univ., Providence, R.I.
- Niktopoulos, D., Liu, J. T. C. 1982. Mode interactions in developing shear flows. *Bull. Am. Phys. Soc.* 27(9):1192.
- Orszag, S. A., Crow, S. C. 1970. Instability of a vortex sheet leaving a semi-infinite plate. *Stud. Appl. Math.* 49:167-81.
- Oster, D., Wygnanski, I. 1982. The forced mixing layer between parallel streams. *J. Fluid Mech.* 123:91-130.
- Oster, D., Wygnanski, I., Fiedler, H. E. 1977. Some preliminary observations on the effect of initial conditions on the structure of the two-dimensional turbulent mixing layer. In *Turbulence in Internal Flows*, ed. S. N. B. Murthy, pp. 67-87. Washington, DC: Hemisphere.
- Overman, E. A. II, Zabusky, N. J. 1982. Evolution and merger of isolated vortex structures. *Phys. Fluids* 25:1297-1305.
- Patel, R. P. 1973. An experimental study of a plane mixing layer. *AIAA J.* 11(1):67-71.
- Patnaik, P. C., Sherman, F. S., Corcos, G. M. 1976. A numerical simulation of Kelvin-Helmholtz waves of finite amplitude. *J. Fluid Mech.* 73:215-40.
- Petersen, R. A. 1978. Influence of wave dispersion on vortex pairing in a jet. *J. Fluid Mech.* 89:469-95.
- Pierrehumbert, R. T., Widnall, S. E. 1981. The structure of organized vortices in a free shear layer. *J. Fluid Mech.* 102:301-13.
- Pierrehumbert, R. T., Widnall, S. E. 1982. The two- and three-dimensional instabilities of a spatially periodic shear layer. *J. Fluid Mech.* 114:59-82.
- Plaschko, P. 1979. Helical instabilities of slowly divergent jets. *J. Fluid Mech.* 92:209-15.
- Pui, N. K. 1969. *The plane mixing layer between parallel streams*. MSc thesis. Univ. Br. Columbia, Vancouver.
- Pui, N. K., Gartshore, I. S. 1979. Measurements of the growth rate and structure in plane turbulent mixing layers. *J. Fluid Mech.* 91:111-30.
- Reichardt, H. 1942. *Gesetzmäßigkeiten der freien Turbulenz*. In *Schlichtung*, H. 1960. *Boundary Layer Theory*, pp. 599. New York: McGraw-Hill.
- Reynolds, W. C., Bouchard, E. E. 1981. The effect of forcing on the mixing-layer region of a round jet. In *Unsteady Turbulent Shear Flows*, ed. R. Michel, J. Cousteix, R. Houdeville, pp. 402-11. Berlin/Heidelberg/New York: Springer.
- Riley, J. J., Metcalfe, R. W. 1980. Direct numerical simulation of a perturbed turbulent mixing layer. *AIAA Pap. No. 80-0274*.
- Roberts, F. A., Dimotakis, P. E., Roshko, A. 1982. Kelvin-Helmholtz instability of superposed streams. In *Album of Fluid Motion*, ed. M. Van Dyke, p. 85. Stanford, Calif.: Parabolic.
- Rockwell, D. 1983. Oscillations of impinging shear layers. *AIAA J.* 21(5):645-64.
- Roshko, A. 1976. Structure of turbulent shear flows: a new look. *AIAA J.* 14(10):1349-57.
- Roshko, A. 1981. The plane mixing layer: flow visualization results and three dimensional effects. In *The Role of Coherent Structures in Modelling Turbulence and Mixing*, *Lecture Notes in Physics*, ed. J. Jimenez, 136:208-17. Berlin/Heidelberg/New York: Springer.
- Saffman, P. G., Baker, G. R. 1979. Vortex interactions. *Ann. Rev. Fluid Mech.* 11:95-122.
- Saffman, P. G., Szeto, R. 1981. Structure of a linear array of uniform vortices. *Stud. Appl. Math.* 65:223-48.
- Sato, H. 1956. Experimental investigation in the transition of laminar separated layer. *J. Phys. Soc. Jpn.* 11:702-9.
- Sato, H. 1959. Further investigation on the transition of two-dimensional separated layers at subsonic speed. *J. Phys. Soc. Jpn.* 14:1797-1810.
- Sato, H. 1960. The stability and transition of a two-dimensional jet. *J. Fluid Mech.* 7:53-80.
- Schade, H. 1964. Contribution to the non-linear stability theory of inviscid shear layers. *Phys. Fluids* 7:623-28.
- Spencer, B. W., Jones, B. G. 1971. Statistical investigation of pressure and velocity fields in the turbulent two-stream mixing layer. *AIAA Pap. No. 71-613*.
- Stewartson, K. 1974. Some aspects of non-linear stability theory. *Fluid Dyn. Trans.* 7:101-28.
- Stewartson, K. 1981. Marginally stable inviscid flows with critical layers. *IMA J. Appl. Math.* 27:133-75.
- Stuart, J. T. 1958. On the non-linear mechanics of hydrodynamic stability. *J. Fluid Mech.* 4:1-21.
- Stuart, J. T. 1962. Nonlinear effects in hydrodynamic stability. *Proc. Int. Congr. Appl. Mech.*, 10th, ed. F. Rolla, W. T. Koiter, pp. 63-97.
- Stuart, J. T. 1967. On finite amplitude oscillations in laminar mixing layers. *J. Fluid Mech.* 29:417-40.
- Stuart, J. T. 1971. Nonlinear stability theory. *Ann. Rev. Fluid Mech.* 3:347-70.
- Sunyach, M. 1971. *Contribution à l'étude des frontières d'écoulements turbulents libres*. DSc thesis. Univ. Claude-Bernard, Lyon.

- Takaki, R., Kovaszny, L. S. G. 1978. Statistical theory of vortex merger in the two-dimensional mixing layer. *Phys. Fluids* 21(2): 153-56.
- Tam, C. K. W. 1978. Excitation of instability waves in a two-dimensional shear layer by sound. *J. Fluid Mech.* 89: 357-71.
- Tam, C. K. W., Chen, K. C. 1979. A statistical model of turbulence in two-dimensional mixing layers. *J. Fluid Mech.* 92: 303-26.
- Tani, I. 1969. Boundary-layer transition. *Ann. Rev. Fluid Mech.* 1: 169-96.
- Thomas, A. S. W., Saric, W. S. 1981. Harmonic and subharmonic waves during boundary layer transition. *Bull. Am. Phys. Soc.* 26(9): 1252.
- Townsend, A. A. 1947. Measurements in the turbulent wake of a cylinder. *Proc. R. Soc. London Ser. A* 190: 551-61.
- Tso, J., Kovaszny, L. S. G., Hussain, A. K. M. F. 1981. Search for large-scale coherent structures in the nearly self-preserving region of a turbulent axisymmetric jet. *J. Fluids Eng.* 103: 503-8.
- Way, J. L., Nagib, H. M., Tan-atchat, J. 1973. On acoustic coupling in free-stream turbulence manipulators. *AIAA Pap.* No. 73-1015.
- Weissman, M. A. 1979. Nonlinear wave packets in the Kelvin-Helmholtz instability. *Philos. Trans. R. Soc. London Ser. A* 290: 639-85.
- Widnall, S. E., Bliss, D. B., Tsai, C. Y. 1974. The instability of short waves on a vortex ring. *J. Fluid Mech.* 66: 35-47.
- Wille, R. 1963. Beiträge zur Phänomenologie der Freistrahlen. *Z. Flugwiss.* 11: 222-33.
- Williams, D. R., Hama, F. R. 1980. Streaklines in a shear layer perturbed by two waves. *Phys. Fluids* 23: 442-47.
- Winant, C. D., Browand, F. K. 1974. Vortex pairing: the mechanism of turbulent mixing-layer growth at moderate Reynolds number. *J. Fluid Mech.* 63: 237-55.
- Wynanski, I., Fiedler, H. E. 1970. The two-dimensional mixing region. *J. Fluid Mech.* 41: 327-61.
- Wynanski, I., Oster, D., Fiedler, H., Dziomba, B. 1979. On the persistence of a quasi-two-dimensional eddy-structure in a turbulent mixing layer. *J. Fluid Mech.* 93: 325-35.
- Yule, A. J. 1972. Two-dimensional self-preserving turbulent mixing layers at different free stream velocity ratios. *Aeronaut. Res. Coun. R & M* 3683.
- Zabusky, N. J. 1981. Computational synergies and mathematical innovation. *J. Comput. Phys.* 43(2): 195-249.
- Zabusky, N. J., Deem, G. S. 1971. Dynamical evolution of two-dimensional unstable shear flows. *J. Fluid Mech.* 47: 353-79.
- Zhang, Y. Q., Ho, C. M., Monkewitz, P. A. 1983. The two-dimensional mixing layer with bi-modal excitation. In preparation.

SUBJECT INDEX

- A**
- Acoustic noise
vortex shedding and, 199, 201
- Aeroacoustics
turbulent shear flows and, 263-83
- Aerodynamic flow
computer simulation of, 338
- Aircraft efficiency
airfoil/wing design and, 338-40
- Mach number and, 337-38
- Airfoil design, 337-61
- compressible flow models
and, 342-44
- local supersonic flow fields
and, 346-47
- shock-free
direct method for, 351-55
- bodograph and inverse
methods for, 348-51
- methods for, 347-48
- shock-free flows and, 344-46
- Alkane-air detonations
propagation of, 332
- Alluvial-channel beds
secondary flow in, 179
- B**
- Blasius boundary layers
Tollmien-Schlichting waves
in, 390
- Blasius expansion
computer calculation of, 299
- Bluff bodies
fixed
vortex shedding and, 196-201
- flexibly mounted
equation of motion for, 203-5
- oscillations of, 202-3
- flow in wake of, 198
- oscillating, 195-219
- vortex shedding and, 201-16
- Boltzmann collision integral, 68
- Knudsen layers and, 93
- Monte Carlo method and, 71-72
- shock-wave problem and, 85
- Boltzmann equation
continuum-flow problems and, 80-81
- C**
- Centrifugal force
secondary flow in open-channel beds and, 179-81
- uniform curved flow in open-channel beds and, 182
- Chapman-Jouguet detonation
velocity, 316-17
- Chapman-Jouguet theory
equilibrium detonation states
and, 312
- Charney-Drazin theorems
wave action and, 35-36
- Circular cylinders
freely vibrating
vortex shedding and, 217-19
- Cnoidal waves
computer calculation of, 304
- Collision law
Boltzmann transport equations
and, 93-94
- Colloid suspensions
Brownian coagulation and, 250-51
- commercial applications of, 246
- DLVO theory and, 247-50
- flue dynamics and, 256-59
- heterocoagulation and, 256-59
- hydrodynamic interactions in, 250-56
- sedimentation and, 259
- shearing and, 251-55
- Colloids
microhydrodynamic processes
and, 245-46
- stability and coagulation in
shear fields, 245-60
- Compressible flow
airfoil/wing design and, 342-44
- computer-extended series and, 294-97
- Computer algebra
limitations of, 290
- Computer-extended series, 287-306
- analysis and improvement of, 291-94
- closed-form solutions and, 288-89
- compressible flows and, 294-97
- computer algebra and, 290
- numerical solutions and, 290-91
- potential flows and, 303-5
- singular perturbations and, 290
- viscous flows and, 297-303
- Condensation
Knudsen layers and, 92-93
- Couette flow
computer calculation of, 303
- Counterflow jets
attenuation measurements in
temperature gradients and, 144-45
- axial temperature measurements in, 145
- helium II and, 141-53
- second-sound attenuation in
calculation of, 147-50
- velocity-sensitive phase
measurements in, 150-52
- Creeping flow
computer calculation of, 297
- Critical energy

TC

17

4/30/01

strong-blast theory and, 328
and, 327-29
detonation initiation